

LEVEL

C

AGARD-CP-253

AGARD-CP-253

AGARD

ADVISORY GROUP FOR AEROSPACE RESEARCH & DEVELOPMENT

7 RUE ANCELLE 92200 NEUILLY SUR SEINE FRANCE

AD A073811

SEP 14 1973
RECEIVED

AGARD CONFERENCE PROCEEDINGS No. 253

**Models and Analogues for the Evaluation
of Human Biodynamic Response,
Performance and Protection**

This document has been approved
for distribution and sale; its
dissemination is encouraged

DDC FILE COPY

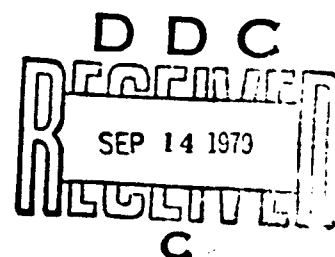
NORTH ATLANTIC TREATY ORGANIZATION



DISTRIBUTION AND AVAILABILITY
ON BACK COVER

BEST AVAILABLE COPY

NORTH ATLANTIC TREATY ORGANIZATION
ADVISORY GROUP FOR AEROSPACE RESEARCH AND DEVELOPMENT
(ORGANISATION DU TRAITE DE L'ATLANTIQUE NORD)



AGARD Conference Proceedings No.253

**MODELS AND ANALOGUES FOR THE EVALUATION OF
HUMAN BIODYNAMIC RESPONSE, PERFORMANCE AND PROTECTION.**

Edited by

Dr Ing. H. E. von Gierke
Director
Biodynamics & Bioengineering Division
6570th Aerospace Medical Research Laboratory (AFSC)
Wright-Patterson AFB
OH 45433
USA

This document has been approved
for public release and sale; its
distribution is unlimited.

Papers presented at the Aerospace Medical Panel's Specialists' Meeting held in
Paris, France, 6 - 10 November 1978.

BEST AVAILABLE COPY

THE MISSION OF AGARD

The mission of AGARD is to bring together the leading personalities of the NATO nations in the fields of science and technology relating to aerospace for the following purposes:

Exchanging of scientific and technical information;

Continuously stimulating advances in the aerospace sciences relevant to strengthening the common defence posture;

Improving the co-operation among member nations in aerospace research and development;

Providing scientific and technical advice and assistance to the North Atlantic Military Committee in the field of aerospace research and development;

Rendering scientific and technical assistance, as requested, to other NATO bodies and to member nations in connection with research and development problems in the aerospace field;

Providing assistance to member nations for the purpose of increasing their scientific and technical potential;

Recommending effective ways for the member nations to use their research and development capabilities for the common benefit of the NATO community.

The highest authority within AGARD is the National Delegates Board consisting of officially appointed senior representatives from each member nation. The mission of AGARD is carried out through the Panels which are composed of experts appointed by the National Delegates, the Consultant and Exchange Programme and the Aerospace Applications Studies Programme. The results of AGARD work are reported to the member nations and the NATO Authorities through the AGARD series of publications of which this is one.

Participation in AGARD activities is by invitation only and is normally limited to citizens of the NATO nations.

The content of this publication has been reproduced
directly from material supplied by AGARD or the authors.

Published June 1979

Copyright © AGARD 1979
All Rights Reserved

ISBN 92-835-0240-X



Printed by Technical Editing and Reproduction Ltd
Harford House, 7-9 Charlotte St, London, W1P 1HD

AEROSPACE MEDICAL PANEL

Panel Chairman: Médecin Général G.Perdriel, FAF
Panel Deputy Chairman: Air Commodore J.N.C.Cooke, RAF
Panel Executive: Lt Colonel F.Monesi, IAF

MEETING ORGANIZATION

Session Organizer: Dr Ing. H.E. von Gierke, US
Local Coordinator: Médecin Chef des Services J.Colin, FR

Accession For	
MTIS GRAAI	<input checked="checked" type="checkbox"/>
DDC TAB	<input type="checkbox"/>
Unannounced	<input type="checkbox"/>
Justification	
By _____	
Distribution/	
Availability Codes	
Dist	Avail and/or special
A	

SUMMARY

This volume contains the 30 presentations and related discussions presented at the AGARD Aerospace Medical Panel Specialists' Meeting on "Models and Analogues for the Evaluation of Human Biodynamic Response, Performance and Protection", held in Paris, France, 6-10 November 1978. The papers cover whole body kinematic models for the prediction of body motion, as well as spinal models, head-neck models and heat injury models for the prediction of internal stress and strain and injury probability under escape, crash and windblast conditions. Cardiovascular models are included to describe and explain human response to sustained acceleration and air combat maneuvers. Biodynamic models interpreting physiological and performance response as well as human operator control capability in vibration and roll motion environments are also presented. Operational injury analyses as well as laboratory human and animal response data are discussed as a basis for further model development and validation. Applications of the models include the prediction of body motions, physiological response and injury probability under biodynamic stress and the assistance in protective system, crashworthiness and cockpit design.

A technical evaluation by the editor summarizing the main findings, conclusions and recommendations completes the Proceedings.

PREFACE

The design of escape/crash protection systems has for many years relied on human, animal and dummy testing to evaluate escape systems, support and restraint systems, protective helmets and cockpit design. The recent growth of civilian interest in automotive crash safety has further intensified the need for optimized test procedures and quantitative injury prediction. The large investments required for this type of research and the rapid development of computer technology has led to the use of mathematical models to an increasing degree to explain test results, guide experiments, predict human response, reduce the need for hazardous human testing and interpret animal test results. Related biodynamic models describe biomechanic, physiological and performance response to sustained acceleration, air combat maneuvers, and multi-degree-of-freedom vibratory motion and buffeting inputs. Due to rapid progress in these fields, capabilities and limitations of the various analogues and models are not widely known and frequently are not appreciated.

As a consequence, the Aerospace Medical Panel decided to have at its 35th Meeting, 6-10 November 1978 in Paris, a specialists' meeting devoted to a comprehensive review of advances in model development, validation by response data and practical model applications. The results of the meeting provide authoritative guidance to the aerospace medical, human factors engineering and protection system design community on the proper use of animal, dummy and mathematical model data; they also suggest new avenues for future research and practical applications.

The discussions included with the papers have been edited by the Session Chairman based primarily on tape recordings and notes; they were not reviewed in final form by the discussants or the authors. The conclusions and recommendations in the editor's technical evaluation report summarize the various subjects brought up and discussed in the lively panel discussion concluding the symposium. An effort was made to include all points raised even if they might be considered of different degrees of importance.

Dr Ing. H.E. von Gierke
Editor

CONTENTS

	Page
PANEL AND MEETING OFFICERS	iii
SUMMARY by H.F. von Gierke	iv
PREFACE by H.E. von Gierke	v
TECHNICAL EVALUATION REPORT by H.F. von Gierke	viii
	Reference
PREDICTION OF WHOLE-BODY RESPONSE TO IMPACT FORCES IN FLIGHT ENVIRONMENTS by I.Kaleps	A1
PROCEDURES USED TO GENERATE INPUT DATA SETS FOR THE ARTICULATED TOTAL BODY MODEL FROM ANTHROPOMETRIC DATA by D.G.Leet	A2
CORRELATION OF MECHANISM OF EXTREMITY INJURY AND AERODYNAMIC FACTORS IN EJECTIONS FROM F-4 AIRCRAFT by S.P.Combs	A3
REFERENCE PARAMETERS FOR SHOCK INPUTS AND SHOCK TOLERANCE LIMITS by K.E.Meier-Dörnberg	A4
MULTIAXIS DYNAMIC RESPONSE OF THE HUMAN HEAD AND NECK TO IMPACT ACCELERATION by C.L.Ewing, D.J.Thomas and L.Lustick	A5
TRANSIENT INTRAVENTRICULAR CONDUCTION DEFECTS OBSERVED DURING EXPERIMENTAL IMPACT IN HUMAN SUBJECTS by P.L.Majewski, T.J.Borgman, Jr, D.J.Thomas and C.L.Ewing	A6
SIMULATION OF HEAD AND NECK RESPONSE TO -Gx and +Gz IMPACTS by A.I.King, S.S.Nakhla and N.K.Mital	A7
A THREE-DIMENSIONAL MATHEMATICAL ANALOGUE OF THE SPINE STRUCTURE: A COMPREHENSIVE APPROACH by M.M.Panjabi	A8
A THREE DIMENSIONAL DISCRETE ELEMENT DYNAMIC MODEL OF THE SPINE, HEAD AND TORSO by T.Belytschko and E.Privitzer	A9
APPLICATION OF BIODYNAMIC MODELS TO THE ANALYSIS OF F-16 CANOPY BIRDSTRIKE by L.J.Specker, N.S.Phillips and J.W.Brinley	A10
A FAILURE CRITERION FOR HUMAN, VERTEBRAL, CANCELLOUS BONE by M.J.Pearcy and J.H.Evans	A11
INJURY MECHANISMS ANALYSIS IN AIRCRAFT ACCIDENTS by I.R.Hill	A12
THE VALIDATION OF BIODYNAMIC MODELS by L.E.Kazarian and H.E. von Gierke	A13
FREQUENCY RESPONSE OF CARDIOVASCULAR REGULATIONS IN CANINES TO SINUSOIDAL ACCELERATION AT FREQUENCIES BELOW 1 Hz (BASIS FOR BIODYNAMIC MODELING) by C.F.Knapp, J.A.Marquis, J.M.Evans and D.R.Randall	A14

	Reference
MATHEMATICAL MODELING OF ARTERIAL OXYGEN SATURATION AND EYE-LEVEL BLOOD PRESSURE DURING +Gz STRESS by K.K.Gillingham and R.C.McNee	A15
UNSTEADY-STATE RESPONSE OF THE VASCULAR SYSTEM TO TRANSIENT AND SUSTAINED AEROSPACE ACCELERATION PROFILES by X.J.R.Avula and H.L.Oestreicher	A16
A HEAD INJURY MODEL by C.Ward	A17
POTENTIAL RELATIONSHIP BETWEEN HUMAN CENTRAL NERVOUS SYSTEM INJURY AND IMPACT FORCES BASED ON PRIMATE STUDIES by F.Unterharnscheidt and C.L.Ewing	A18
CORRELATION OF HEAD INJURY WITH MECHANICAL FORCES BASED ON HELMET DAMAGE DUPLICATION by B.Slobodnik	A19
THE EFFECT OF IMPACT ACCELERATION ON THE ELECTRICAL ACTIVITY OF THE BRAIN by M.S.Weiss and M.D.Berger	A20
A HUMAN BODY AND CREW STATION MODELLING SYSTEM FOR MOTION STUDIES by G.D.Frisch	A21
THE USE OF MATHEMATICAL MODELING IN CRASHWORTHY HELICOPTER SEATING SYSTEMS by G.T.Singley and J.L.Haley	A22
MAN, DUMMY, TEST VEHICLE: A COMPARISON OF TEST RESULTS FOR ESCAPE SYSTEMS WITH THE 3 DIFFERENT TEST METHODS by H.-D.Melzig, E.A.Bockemüller and U.Schmidt	A23
TENTATIVE D'ESTIMATION DES LESIONS POUVANT SURVENIR AU COURS D'UN CRASH D'HELICOPTERE GAZELLE SA 341 A PARTIR D'UNE ETUDE SUR MANNEQUINS par B.Vettes et R.Eckert	A24
PART I: THE USE OF A SPINAL ANALOGUE TO COMPARE HUMAN TOLERANCE OF REPEATED SHOCKS WITH TOLERANCE OF VIBRATION	
PART II: A CRITICAL LOOK AT BIODYNAMIC MODELLING IN RELATION TO SPECIFICATIONS FOR HUMAN TOLERANCE OF VIBRATION AND SHOCK by G.Allen	A25
THE RESPONSE OF A REALISTIC COMPUTER MODEL FOR SITTING HUMANS TO DIFFERENT TYPES OF SHOCKS by H.Mertens and L.Vogt	A26
SOME HUMAN RESPONSES TO REPEATED +Gz PULSES by E.Hendler and D.C.Johanson	A27
THE BIODYNAMIC RESPONSE OF THE HUMAN BODY AND ITS APPLICATION TO STANDARDS by M.J.Griffin, C.H.Lewis, K.C.Parsons and E.M.Whitham	A28
PROGRESS IN MEASURING AND MODELING THE EFFECTS OF LOW FREQUENCY VIBRATION ON PERFORMANCE by H.R.Jex and R.E.Magdaleno	A29
THE APPLICATION OF CONTROL THEORY TO THE INVESTIGATION OF ROLL MOTION EFFECTS ON HUMAN OPERATOR PERFORMANCE by A.M.Junker and W.H.Levison	A30

TECHNICAL EVALUATION REPORT

by

Henning E. von Gierke
Director, Biodynamics and Bioengineering Division
Aerospace Medical Research Laboratory
Wright-Patterson AFB, Ohio 45433
USA

SUMMARY OF THE COMMUNICATIONS

In response to the Aerospace Medical Panel's invitation for submission of papers on the general subject of biodynamic models as outlined in the theme, a large number of papers was submitted by academic, industry, government and military research organizations from four NATO countries. In spite of the fact that the time for this Session A was extended to last for two full days, or two thirds of the time of the 35th Aerospace Medical Panel Meeting, 6-10 November 1978 in Paris, not all papers submitted could be accepted. The final selection included 30 papers which promised to cover the whole broad spectrum of biodynamic models and their applications, and which were allotted different times for presentation and discussion depending upon their importance and relevancy to the theme. Several authors were asked to start with a short review of the field in addition to the presentation of new research results in order to assist in providing a complete review of the state of the art for all participants.

The session started with a review of the models designed to predict the site, severity and probability of injury under aircraft emergency escape and crash conditions. The articulated total body model, a kinematic model widely used, predicts gross motions of body segments and the forces applied to body surfaces (A1). The validity of the model predictions depends upon the anthropometric input data (A2) and the agreement of the injury predictions with operational accident data (A3). It was proposed that the limited accident and laboratory data available for model validation could be made more useful and easier to interpret through the adoption of standardized reference parameters for shock inputs and tolerance (A4). Tissue stress, strain and displacement relationships leading to internal injuries are analyzed by sophisticated spine, head and torso models, which model details of spinal architecture including static muscle action and tissue loads (A9, A8). The most vulnerable structure for many military emergency situations, the head-neck system, was discussed on the basis of a special model for this subsystem, (A7), for which probably the most extensive and precise biodynamic response data exist (A5) and for which well controlled primate experiments try to clarify the injury mechanism and identify the critical deformations (A18). The question of spinal injury model validation was addressed by reviewing available and reporting new data on human and animal vertebral body strength (A11, A13). The state of the art of the analysis of aircraft accident injury mechanisms and severity was also reviewed to indicate what type of data injury models must be able to predict and with what data they must be validated (A12).

Several papers dealt with the response of the cardiovascular system to impact (A6), vibration (A14) and sustained acceleration (A15, A16) and models of the circulatory system to describe or explain observed phenomena.

Head injury, as predicted by a head injury model (A17) and as operationally observed and correlated to the forces required for helmet damage (A19) was discussed and compared with currently used head injury criteria and severity indices. Subinjury changes in brain electrical activity observed in human impact tests were reported as further potential tolerance criteria to be used for model output responses (A20).

The various models discussed were applied in several papers to specific practical problems: G_z impact injury prediction (A26), canopy birdstrike problem analysis (A10), crew station design analysis (A21) and crashworthy helicopter design (A22). Differences between human and present day hardware dummy responses were demonstrated by escape system experiments and helicopter crash tests (A23, A24).

The final set of papers dealt with biodynamic models used to explain and predict human tolerance to vibration and repeated shock (A25) and with biodynamic and control theory models applied to modeling operator performance under linear and rotational vibration environments (A29, A30). New experimental data on human response were included in several papers as basis for the modeling efforts. Some papers concentrated on experimental data only as data input and for validation of present or future biodynamic models (A27, A28).

CONCLUSIONS AND RECOMMENDATIONS

The papers lead to the following conclusions and recommendations which were reinforced by comments during the meeting and during the concluding panel discussion:

- A large variety of mathematical biodynamic models of impressive complexity and capability have been developed. They each serve a useful purpose and have their practical application. The biodynamic models cover a whole spectrum of available technology.

They are an inseparable part or tool of all aspects of present-day biodynamic research.

- The use and application of these models differ with the problem at hand. In basic research they are frequently semiquantitative in nature and are primarily used to interpret and explain experimental findings and enable the experimenter to ask more intelligent questions. In exploratory research they become more quantitative and detailed; they allow extrapolations into unexplored areas; they help to reduce hazardous human experiments, reduce the need for animal data and allow interpretations with respect to human response; they save money and time. In the hardware development stage models should be sufficiently specific and quantitative to guide the systems designer and describe the system "man" in a language familiar to the engineer.

- It is unrealistic and counterproductive to hope for one "final" model to answer all practical questions. A whole hierarchy of models is needed and partly available to answer different problems and these will be modified and updated with time as research progresses. The danger of freezing too early on specific, quantitative models for hardware design is clearly recognized, since they cannot be updated as freely and easily. In spite of this the requirement and responsibility exists to provide to the design community the best guidance available at a particular point in time.

- Of the model applications presented the Articulated Total Body Model and the Head-Spine Injury Model appear to be closest to a possible transition to wider practical use for probability of injury prediction and protection system design for aircraft escape systems and crashworthiness. The unidirectional spinal injury prediction by means of the Dynamic Response Index (DRI), which served the design community in several countries well for the past 8 to 10 years, might be replaced by a general injury and specific spinal injury prediction capability for multidirectional impact.

- Prior to the recommendation of something like the Articulated Total Body Model and the Head-Spine Injury Model for general adoption by the Armed Services and for release to the design community, it is considered absolutely essential that a major validation effort be conducted with the best data available and that necessary response data which are not yet available be acquired. The final model response data must satisfy the following conditions:

- a. Biodynamic response of the models must be in general agreement with (1) sub-injury voluntary human impact tests for the various directions and (2) whole body impedance data and transmissibility measurements on human subjects on vibration tables for the frequency range of interest.

- b. Distribution and severity of injury prediction must be in agreement with (1) all relevant and properly analyzed aircraft and automobile accident and escape injury data available, (2) all properly conducted and interpreted cadaver injury tests on sleds and drop towers designed to fill gaps in operational injury experience and (3) all sub-system and tissue component tests on elements (such as vertebral body elastic properties and strength data) introduced as elements of the specific model.

- c. For exposure conditions, which for any reason cannot be validated by a. or b. above, injury predictions for properly adapted animal versions of the specific model must be in agreement with observed data with respect to injury mechanism, location and severity.

Proper validation of models should consider all quality data available in all three areas (a, b and c) outlined. Unfortunately, too often models are compared to limited or selected data only.

- Collection of data for model validation and the actual validation itself might deserve in the near future higher priority than the development of more sophisticated models. This is a formidable, labor intensive, task not to be underestimated. The collection of all relevant data in well-organized, easily accessible computerized biodynamic data banks, coordinated at national or international levels, is seen by many as the most valid and effective step toward the validation of present and future models.

- Several suggestions were made for more effective model validation. Among those were comments on more detailed, scientific evaluation of crash situations attempting to obtain quantitatively better supported force inputs to the human system by cockpit and seat deformation evaluation. Further standardization of accident pathology classification and accident/injury data collection were other items of concern. Other participants proposed "standard crash situations" or "standard escape maneuvers" to be used for all model validations to increase intra-model-comparability and computational efficiency. In many cases model validation requires additional tests or instrumentation channels in laboratory and field tests. Frequently for little additional cost valuable information for general application can be obtained from field tests and experiments which would be too costly for model validation per se. All biodynamic test data collection should be made as much as possible with model validation in mind or even guided by parallel model prediction.

- Although the need for more advanced, biodynamically realistic, anthropomorphic dummies for crash testing was stressed by several authors and discussants, no pay-off analysis as to the complexity, accuracy and costs desired for such a dummy was presented. Theoretical prediction capability appears to be closer at hand than hardware

realization of the model description of the human response.

- It is obvious that a whole family of models are needed depending upon the purpose and complexity of application. Simplification of some of the complex models discussed (e.g., the head-spine model) might be possible and would certainly be desirable for some of the applications (e.g., spinal injury prediction without detailed indication of injury location or mechanism). Enough data might be available soon for validation of such simplified models. More complicated models (e.g., to predict vision under vibration or to quantitate motion perception and control capability under biodynamic stress or under simulator conditions) might require considerably more biodynamic, physiological and performance data. If simplified models for specific applications are derived, their relationship to the more general models and their limits of validity and applicability should be well defined.

PREDICTION OF WHOLE-BODY RESPONSE TO IMPACT FORCES IN FLIGHT ENVIRONMENTS

by

Ints Kalens
Aerospace Medical Research Laboratory
Wright-Patterson Air Force Base, Ohio 45433
U.S.A.

SUMMARY

The general predictive and structural properties of human-body gross motion simulation models and their applicability to flight-associated problems is discussed. A specific application of such a model is demonstrated by the simulation of human response to whole-body- G_x impact and the comparison of the results with experimentally observed human responses to the same dynamic exposures. The simulations were performed using the Articulated Total Body (ATB) computer model based on rigid body mechanics and possessing a number of internal and external force and constraint options to reflect resistive forces within human joints and to allow the interaction of external configurational elements. Predicted data of limb motions, their accelerations and forces generated in the harness restraint system are compared with those obtained experimentally from acceleration transducers on the head and chest of human test subjects; tension measuring load cells for the harness system components and variously located sled on-board and stationary high-speed movie cameras. Discussion encompasses the model structure and its dynamic modeling capability; the general data input requirements; the specific set of data used for the G_x impact simulations; and some of the shortcomings and required improvements indicated by the present simulation.

INTRODUCTION

The use of biodynamic computer-based models for the prediction of human body response and injury resulting from impacts and abrupt accelerations typically encountered in various phases of flight operations is an accepted and necessary complementary research approach to direct experimentation with humans and animals. Considerable insight can be gained by a properly prepared and executed simulation of body dynamics concerning the resulting body motion, stresses developed within the body and interactions of the body segments with external structures.

These models can generally be separated into two categories: internal body structure and external gross motion body models. The first type deals with the detailed structure of various body subsystems; e.g. the head, thorax, spine, etc. and, provided with a specified input to the particular subsystem, will predict stresses, strains and localized deformations. The latter model category deals with overall body response and generally provides as output motion data of body segments and interactive forces between body segments and external structural elements. The present study describes the application of a model in this category.

The development of complex and detailed biodynamic models has been particularly rapid and successful during the last decade. This growth can mostly be attributed to the developments in computer technology including the development of sophisticated accessory software. This relatively new and powerful analysis capability has opened the door to the solution of analytical equations describing the complex and detailed mechanical structure of the human body. It has allowed the analysis of mechanisms and processes that in many cases had previously been known and postulated but could not be satisfactorily explored using classical mechanics methods because closed-form solutions did not exist and numerical solutions were too tedious.

This is particularly true of the gross motion simulation models of the body which are based on rigid body dynamics. The basic formulating equations for such models were already available in the 19th century and a number of treatises on this topic are discussed by Goldstein (1). While voluminous data have been generated on the theoretical aspects of such analyses, only solutions for relatively simple cases dealing mainly with a single body under various constraint conditions and applied forces have been successfully obtained. Current models applied in biodynamics have used the same formalism, usually either the Euler or Lagrange technique, to formulate equations describing chains of coupled rigid bodies, and with current computer-based analysis techniques solutions to such systems have become possible.

Models depicting the articulated, three-dimensional human body structure have been developed by a number of investigators. Among these are models described by Young (2); Robbins, Bennett and Bowman (3); Furusho and Yokoya (4); Huston, Hessel and Passerello (5,6); and Fleck, Butler and Vogel (7,8). The final system equations for all these models are quite similar in structure. Their main difference lies in the number of segments used to describe the body structure and the ease and flexibility of specifying input for a given dynamic event. A comparison of these factors as well as a number of other model features has been carried out by King (9).

The application of the gross motion simulation type of model is of particular interest to aviation medicine in the analysis of human body dynamic response during various phases of emergency escape from high-performance aircraft and restraint during aircraft crashes. The modeling technique has applicability to the analysis of body prepositioning either by active harness system forces or rapid changes in seat geometry prior to ejection, limb clearances during seat motion up the rails and limb flailing during windforce exposures. This type of model can also provide a method for analysis of the effectiveness of various harness systems for restraining the crewman during crashes and the effects of parachute opening shock transmitted through the harness system.

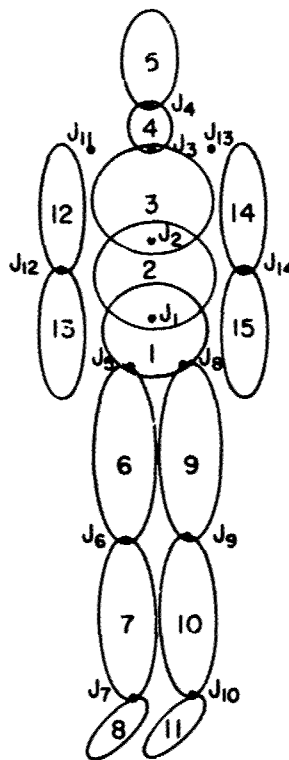
In general, this type of model can serve as a valuable design and evaluation tool in the development of new systems, and can contribute significantly to the prevention and reduction of presently occurring injuries.

MODEL DESCRIPTION

The model used in this study is based on rigid-body dynamics using Euler equations of motion with Lagrange-type constraints. The model was originally developed by Calson Corporation for the study of human-body and anthropometric dummy dynamics during automobile crashes for the United States Department of Transportation (DOT) (7,8). The formulation, however, was of sufficient generality to allow application of this model to problems involving whole-body articulated motion resulting from various types of impacts or other abrupt accelerations applied to the body. Modifications to the basic model were made to accommodate specific Air Force applications (10). Among these were the inclusion of a special joint force algorithm, a capability to apply aerodynamic forces to body segments as experienced during ejection from aircraft and improvements in the harness algorithm allowing simulation of complex restraint systems.

The specific model configuration applied in this study used 15 body segments. These consisted of the head, neck, upper torso, center torso, lower torso, upper arms, lower arms, upper legs, lower legs and feet. The lower arms were combinations of the forearms and hands. A schematic showing these segments and the numbering scheme used both for the segments and the interconnecting joints is shown in Fig. 1. The number of the segments used in simulating body response both in this and other studies has been dictated by the requirements of the particular event being simulated and the availability of individual segment data. For the present study, 15 segments were chosen, since it was felt that these would adequately represent the various differential motions of concern in a gross $-G_x$ body impact.

Since the body can be viewed as a chain link system having no closed loops, the choice of 15 segments resulted in 14 joints and a total of 48 degrees of freedom.



JOINT J CONNECTS SEGMENT N(J) WITH SEGMENT J+1

J =	1	2	3	4	5	6	7	8	9	10	11	12	13	14
N(J) =	1	2	3	4	1	6	7	1	9	10	3	12	3	14

Figure 1. Model segment and joint number scheme.

DATA FOR SPECIFIC SIMULATION

To simulate a specific dynamic event, considerable body descriptive data must be supplied for model input. These data include principal moments of inertia, mass, contact surface ellipsoid center and radii and joint locations for each segment, as well as segment interaction characteristics for segment-to-segment or configurational element contacts. Properties of joints must also be specified by identifying the type of joint (i.e., pin, ball and socket, etc.) and the torque properties across the joint as a function of relative adjacent segment rotational orientation. Additionally, the external dynamic environment to which the body is to be exposed must be defined.

The particular events chosen for simulation in this study consisted of three $-G_x$ impacts with 6, 8 and 10 g peak acceleration amplitudes respectively. The time histories of the accelerations are shown in Fig. 3 and were obtained from actual sled tests. All three tests were performed with the same subject, who weighed 217 lbs. and was just over 73 inches tall. On the basis of these two parameters, the subject was classified in the 95th percentile of the U.S. Air Force population according to the data compiled by Churchill (11). Using this classification and the body property generating program "GOOD" (12), a set of body segment weights, principal moments of inertia and joint locations were obtained. Specific anthropometric measurements obtained from the subject were used to refine the data using, in part, a procedure developed by Leet (13), which provides segment moment of inertia and centers of gravity from a set of anthropometric measurements, and a final data set was assembled. This data is presented in Table 1. The joint locations within the segments were obtained from program "GOOD" for a 95th percentile male and were used without modification.

The segment contact ellipsoid centers, located with respect to the segment centers of gravity, and the ellipsoid radii were obtained using the anthropometric data from the subject and a complementary graphics package used with the Articulated Total Body (ATR) Model. The graphics package provides a plot of the body contact ellipsoid structure as viewed from a specified direction and distance from the body. A frontal view of the body graphics display is shown in Fig. 4. By using photographs of the seated subject prior to impact, and overlaying these with corresponding body graphics generated from equivalent viewing positions, the respective segment contact ellipsoid radii and their centers were specified. The radii chosen for this particular series of simulations are listed in Table 2.

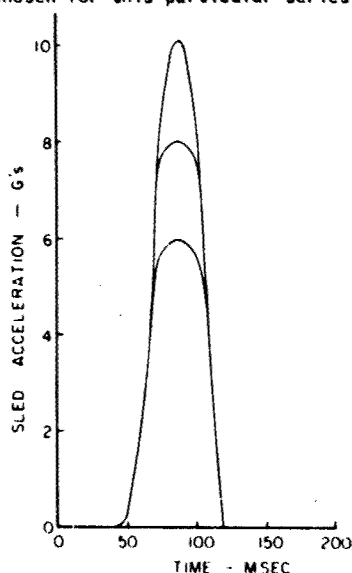


Figure 3. Six, eight and ten g peak acceleration inputs used for $-G_x$ sled impact simulations.

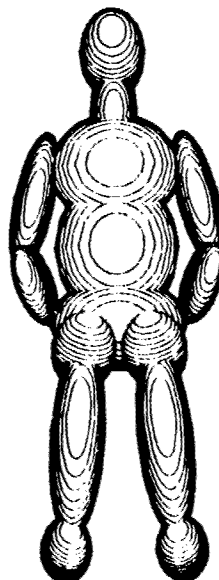


Figure 4. Computer graphics representation of body contact surfaces.

The simulation of harness and body interaction during the impact event required a geometric description of the harness, its placement on the body surface, and the specification of a common belt/segment elasticity. The common belt/segment elasticity is that obtained by assuming that the relative elasticities of the harness system and the body are coupled in series. A frontal view of the placement of the harness belts on the torso segments is shown in Fig. 5. These belt segments follow the contour of body contact surfaces and go through reference points (denoted by x's) defined on the surface of each segment.

The geometry of the harness system in the actual experiments is such that two belts are attached to the floor of the sled in a position such that when they are fastened together with a buckle across the lower abdomen of the seated subject they form approximately a 45° projected angle with the floor in the Z-X plane. (The coordinate system conventions employed in this study are such that X and Z axes lie in a plane parallel to the midsagittal plane, with Z positive downward, X positive forward and Y positive to the right of the subject.) The lateral placement of the tie-down points on the floor is slightly outside the hip width. Two other belt segments are attached to the buckle in front of the abdomen and extend upward across the shoulders. In the actual experiments, these two straps are tied together behind the subject and attach to one common point on the seat structure posterior to the neck. For the simulation, these two belt straps were attached separately to the seat back and posterior to the neck. The use of two tie-down points allowed the independent calculation of forces in each belt segment and also prevented the generation of large lateral forces from the belt segments in the

shoulder region. The initial length of each lap belt segment was 18.17 inches and each shoulder belt segment was 27.35 inches. The common belt/segment elastic characteristics were assumed to be linear with coefficients of 10,500 lbs. in/in and 7,300 lbs. in/in for the lap segment and shoulder segment respectively. These values were calculated from the experimentally observed belt loading curve widths and load times for the 10-g impact.

TABLE 1.a.
BODY SEGMENT WEIGHTS AND PRINCIPAL MOMENTS OF INERTIA

Segment Number N	Segment Name	Weight (lb.)	Segment Moment of Inertia (lb.-in.-sec ²)		
			X	Y	Z
1	Lower Torso	33.950	1.510	1.460	1.740
2	Center Torso	40.550	2.460	1.740	1.800
3	Upper Torso	26.000	1.190	.720	1.200
4	Neck	6.080	.024	.024	.020
5	Head	12.430	.200	.230	.140
6	R. Upper Leg	24.010	1.800	1.800	.490
7	R. Lower Leg	9.540	.650	.650	.070
8	R. Foot	3.310	.050	.050	.010
9	L. Upper Leg	24.010	1.800	1.800	.490
10	L. Lower Leg	9.540	.650	.650	.070
11	L. Foot	3.310	.050	.050	.010
12	R. Upper Arm	6.790	.170	.170	.032
13	R. Lower Arm	5.340	.310	.310	.017
14	L. Upper Arm	6.790	.170	.170	.032
15	L. Lower Arm	5.340	.310	.310	.017

TABLE 1.b.
JOINT LOCATIONS IN SEGMENT COORDINATE SYSTEMS

Joint Number J	Segment Number N	Joint Location in Segment (N) (in.)			Joint Location in Segment (J+1) (in.)		
		X	Y	Z	X	Y	Z
1	1	0.00	0.00	-3.85	0.00	0.00	3.85
2	2	0.00	0.00	-4.23	0.00	0.00	4.23
3	3	0.00	0.00	-2.82	0.00	0.00	2.82
4	4	0.00	0.00	-3.18	0.00	0.00	3.18
5	1	0.00	3.52	.92	0.00	0.00	-8.80
6	6	0.00	0.00	10.09	0.00	0.00	-7.93
7	7	0.00	0.00	9.05	1.68	0.00	-2.19
8	1	0.00	-3.52	.92	0.00	0.00	-8.80
9	9	0.00	0.00	10.09	0.00	0.00	-7.93
10	10	0.00	0.00	9.05	1.05	0.00	-2.19
11	3	0.00	7.28	-1.85	0.00	0.00	-5.44
12	12	0.00	0.00	5.58	0.00	0.00	-7.94
13	3	0.00	-7.28	-1.85	0.00	0.00	-5.44
14	14	0.00	0.00	5.58	0.00	0.00	-7.94

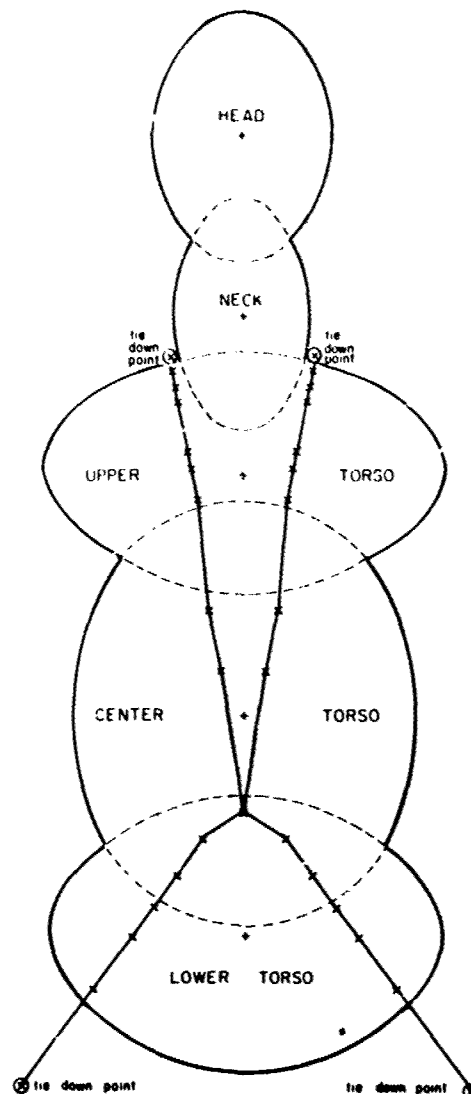


Figure 5. Body harness geometry used for $-G_x$ sled impact simulations.

With the current analysis scheme, the reference points are not allowed to migrate across the surface of the segment. This, of course, does not allow for consideration of belt lateral slippage effects. However, for the present set of impact events the loading on the body by the belt is mainly normal to the segment surface and tangential along the belt.

Other than through the harness system the only other localized force transfer to the body during the $-G_x$ impact event was through the seat pan, seat back and floor structures. The seat pan and back were of solid wood construction with polished surfaces to minimize tangential frictional forces. Similarly, the floor was also rigid and smooth, producing minimal sliding resistance on the feet.

Of these three interacting surfaces, only the seat pan interacted significantly with the body during the peak loading phase of the impact event. For the simulation of this interaction, the force-deflection characteristic shown in Fig. 6 was applied in a normal direction between the lower torso and upper legs and the seat pan. This characteristic produces a spring hardening or bottoming-out type of effect, since a small force will initially produce a relatively large deflection (.4 inches for 60 lbs.), but a much larger force is thereafter required to produce an equivalent deflection.

The same characteristic was used for both the foot/floor and the torso/seat back interactions; however, as indicated previously, neither of these interactions was of significance during the peak impact event.

The type of joints used were ball and socket except for the knees and elbows, where pin joints were used. Joint stops in terms of a flexure angle for the ball and socket joints and the single rotational angle for the pin joints were specified. For the present analysis, these joint stop values did not appear to be significant, except possibly for the elbow and knee, as the articulated limb motion observed in the experiments tended to be within the range of free joint motion. The joint stops for the elbow and knee were set at full extension for these joints.

TABLE 2
CONTACT ELLIPSOID SEMIAXES

Segment Number N	Contact Ellipsoid Semiaxes (in.)		
	X	Y	Z
1	5.05	7.49	4.39
2	4.80	6.14	7.49
3	4.91	6.99	4.12
4	2.52	2.52	4.83
5	4.07	3.20	4.83
6	3.43	3.43	12.77
7	2.52	2.52	10.62
8	1.68	2.14	5.54
9	3.43	3.43	12.77
10	2.52	2.52	10.62
11	1.68	2.14	5.54
12	2.27	2.27	7.71
13	1.98	1.98	10.07
14	2.27	2.27	7.71
15	1.98	1.98	10.07

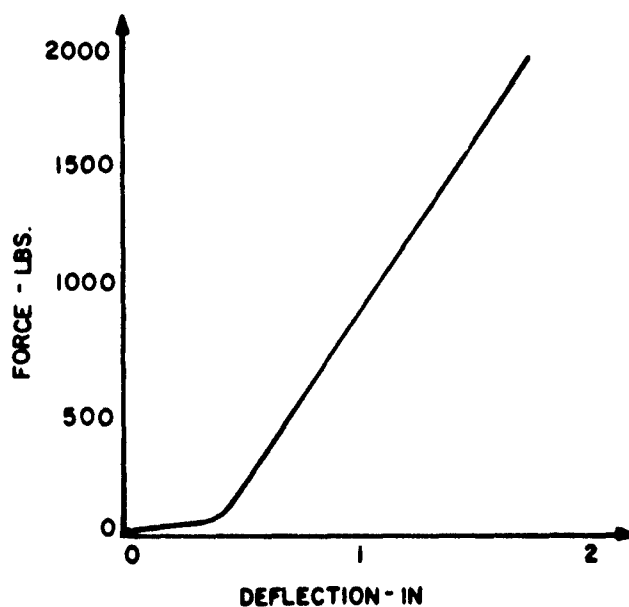


Figure 6. Force-deflection characteristic for body-seat pan interaction.

RESULTS

The data obtained from the simulations consisted of time histories of all segment linear and angular displacements, velocities and accelerations; the tensile belt forces of the harness system; and the contact forces generated and the points of contact between body segments and seat and floor surfaces. The experimental data available for purposes of comparison were accelerometer data from triaxial accelerometer packs mounted on the forehead and the chest; displacement data in the X-Z plane of fiducial marks on the hip, knee, shoulder, elbow, the head about an inch anterior to the tragus, and the lateral side of the triaxial accelerometer package on the forehead; and force data from transducers at two belt tie-down points on the floor and one in the seat back posterior to the subject's neck.

During these $-G_x$ impacts the force transmitted to the body was primarily through the harness system with a rather small component transmitted through the seat pan. This latter input consists of a normal component due to a 7° inclination of the seat from back to front and a tangential force component due to the friction between the subject and the seat surface. These forces, with the exception of the seat frictional forces which were taken as zero, were calculated using the model. Fig. 7 shows the forces obtained for the shoulder and lap belts from the simulation and the forces measured during the actual experiments. These curves show very close agreement, especially in view of the generally observed variability in the forces measured in the harness system during apparently identical sled impact events. A cursory review performed on about 60 $-G_x$ impact events indicated that at least a 10% variation may be expected in the peak harness loads observed under "identical" test conditions. Possibly additional constraints may be imposed to ensure more identical conditions between runs, but in the present study, compensation was not made for such factors as level of subject apprehension, small shifts in subject initial limb position and slightly varying harness positions on the pelvis. Even so, the level of loading observed in the shoulder belts decreased from about 600 lbs at 10 g's to 500 lbs at 8 g's and then to 400 lbs at 6 g's. The same level of decrease was observed in the simulation with peak values approximately 50 lbs higher. For the lap belt, an experimental peak load of slightly over 1000 lbs at 10 g's, 900 lbs at 8 g's and 500 lbs at 6 g's was observed. Simulated peak values were about 50 lbs lower at the 10-g and 8-g levels and 50 lbs greater at the 6-g level.

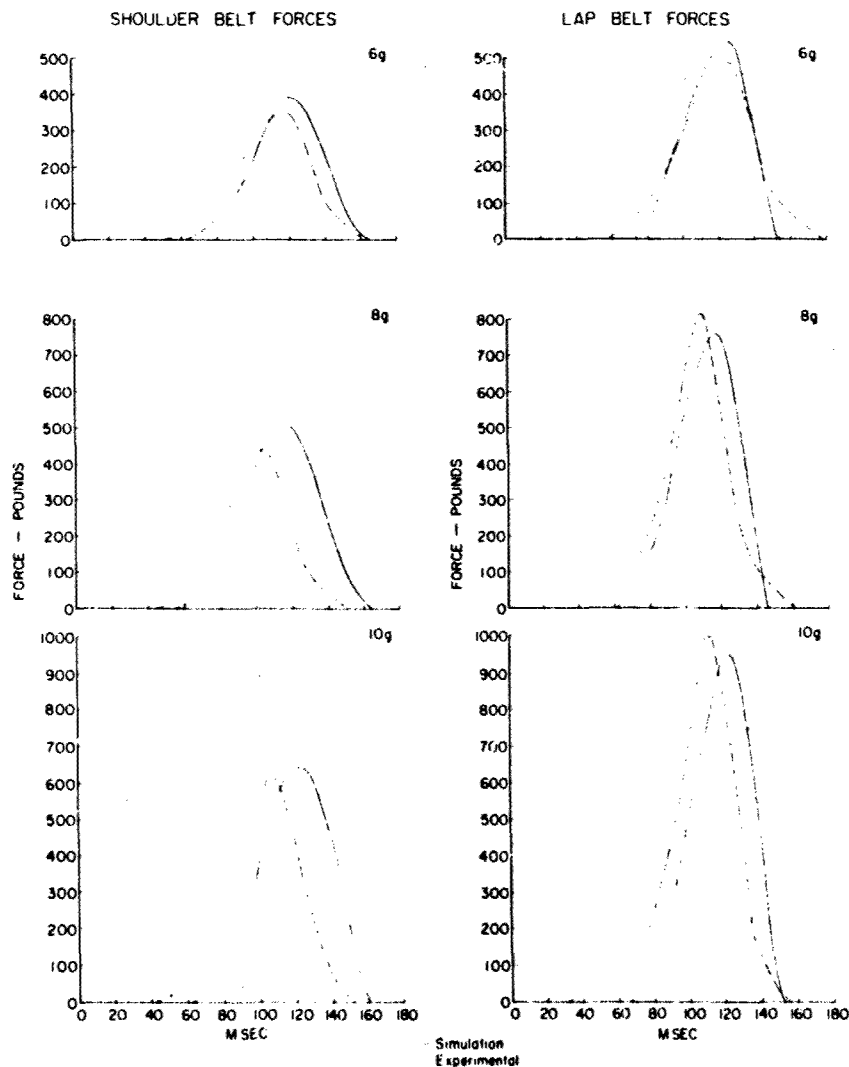


Figure 7. Comparison of simulated and experimental shoulder and lap-belt forces during $-G_x$ impacts.

Other factors of agreement which are of considerable importance in assessing the effect of these belt forces on the body are the times of peak load and the breadth of the loading curve. These factors can be related to the effective compliance of the harness/body interaction and the impulse transmitted to the body during the impact. The latter, in turn, may be used as a variable for correlation to probability of injury. Both the peak load times and the breadths of the loading curves show very good agreement between the measured and simulated results. The maximum difference in the times of peak load occurrence is about 10 msec and occurs at the higher g levels. At the 6- g load level the times for peak load are almost identical. The increase in the phase shift with increasing load levels may be attributable to the use of a linear force-deflection characteristic for the harness/body interaction where, in fact, the true characteristic is a nonlinear spring hardening type which at larger deflections exhibits a stiffer response and thus an earlier peak.

The normal forces of contact between the pelvis and upper legs for the 10- g simulation and the seat pan are shown in Fig. 8. The points of contact across which this force is transmitted initially shift forward in the seat as the body loads into the harness system. The total shift is about 2.5 inches.

This same shift is observed in Fig. 9, which shows the x-direction displacement of the lower torso (or pelvis) for the 10-, 8- and 6- g load levels for both the simulation and the actual impact events. Phase comparisons show very good agreement as maximum displacements occur at the same time. The predicted magnitude of displacement is, however, consistently greater than that observed from the experiments. The reason for this variation is most likely attributable to the deformation of the soft tissue surrounding and that encased by the pelvic structure. While the computer simulation provides predictions of the net motion of the center of mass of all these components, the experimentally measured data corresponds to the motion of a fiducial attached to lateral external tissue of the pelvis.

Although component accelerations of the head and chest were both calculated using the model and measured during the impact events, only comparisons of the resultant chest and head accelerations were made, since initial axes alignments between the simulated situation and the actual measurements could not be established. Comparisons were made for all three load levels, and it was found that the simulated and measured responses showed good agreement. The basic characteristics at all three load levels were the same, with no observed phase shifts. As expected, the resulting accelerations of the chest and head decrease with decrease in the applied external acceleration.

In Fig. 10 are shown the simulated and measured data for the 10- g input resultant chest acceleration. The agreement here is quite close, with a measured first peak acceleration of about 17 g 's and the corresponding simulated acceleration peak is about 16 g 's and occurs about five to ten milliseconds later than the measured peak. A second acceleration was observed to start at about 130 milliseconds and die out at about 180 milliseconds. This response was well predicted in the simulation as the plateau for this peak reached about 10 g 's in close agreement with the observed response. The higher frequency content of the measured response versus the simulated response may be explained by the interaction of the chest accelerometer package with the restraining harness shoulder straps as these slid tangentially across the chest during the impact event.

A comparison of the simulated and the measured head resultant acceleration for the 10- g input case is shown in Fig. 11. Similar responses, except for respectively lower amplitudes, were also observed for the 8- and 6- g inputs. A double peak occurs both for the experimental case and the simulation. The phase of both peaks is in very good agreement; however, the amplitude of the first peak in the simulation is only about half of that observed in the actual experiment (10 g 's versus 20 g 's). The second peak shows much better agreement, as practically the same amplitude of about 19 g 's is attained for both. While no clear answer is evident for the difference in amplitude for the first peak it should be pointed out that this model is not particularly suited for a detailed analysis of the complex articulated motion of the cervical spine which clearly contains several joints and does not in its present input parameter set account for pretensing of neck muscles or the voluntary or involuntary actions of these muscles during the impact event. Visual observations of head/neck response during the actual sled impact experiments tend to indicate that an active muscle input does occur and is a significant factor in head/neck response at the relatively low g levels (6 to 10 g 's) applied in these studies.

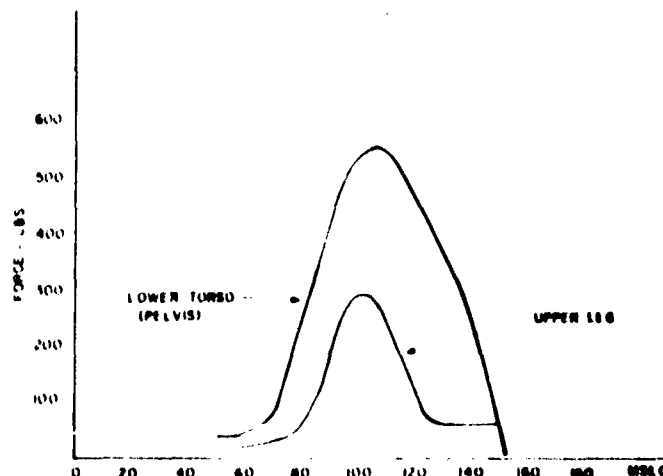


Figure 8. Predicted normal forces on the seat pan during 10- g peak - G_x impact.

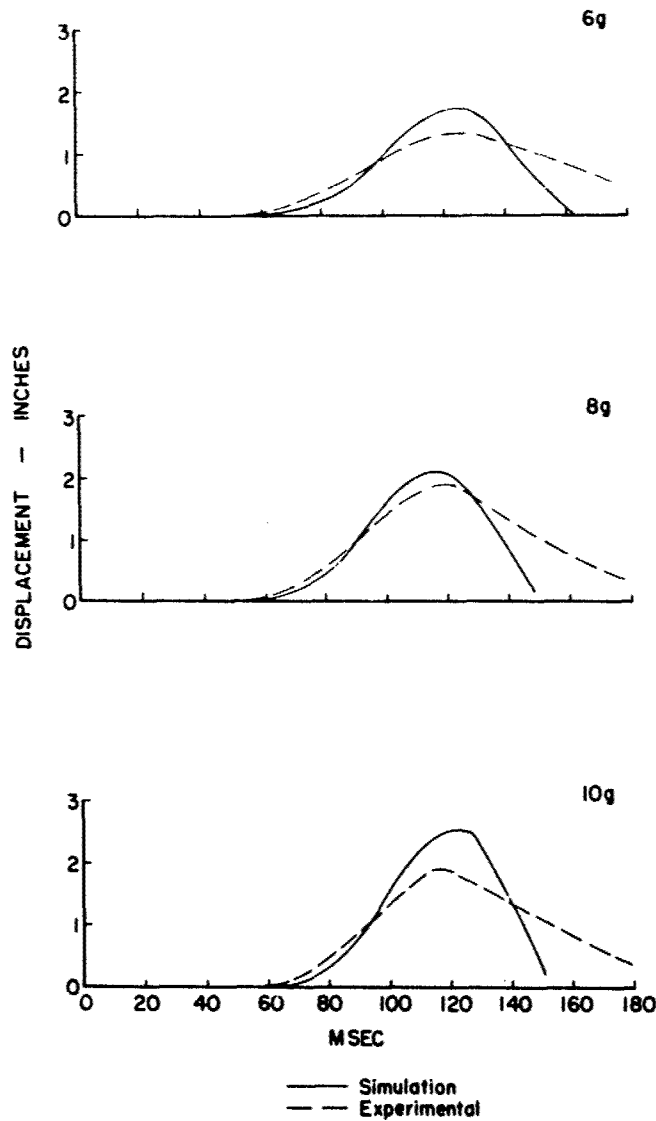


Figure 9. Comparison of simulated and experimental lower torso (pelvis) displacement tangent to seat pan surface.

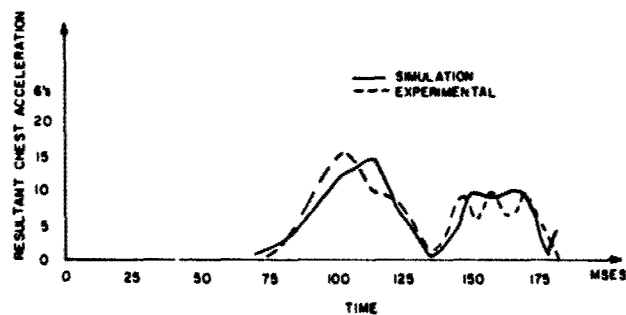


Figure 10. Comparison of simulated and experimental resultant chest acceleration during 10-g peak $-G_x$ impact.

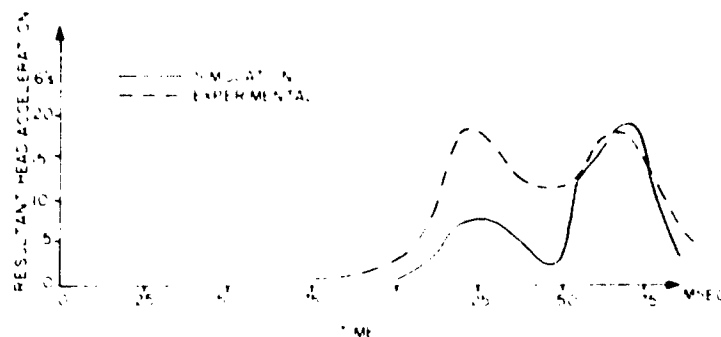


Figure 11. Comparison of simulated and experimental resultant head acceleration during 10-g peak $-G_x$ impact.

As indicated previously, the linear and angular displacements, velocities and accelerations of 15 body segments were calculated, and a number of additional variable displacements have been made. Most of these show good agreement with experimental data. Unfortunately the amount of experimental data available is considerably less than that provided by the computer model simulation, especially segment acceleration data and three-dimensional displacement data of segments. A particularly useful method for overcoming this deficiency is the time-sequenced comparisons of body positions during a dynamic event. An illustration of such a comparison is shown in Fig. 12, where lateral views of the body are compared at different times using the whole-body computer-generated graphics and high-speed films for the 10-g impact. Similar time-sequenced comparisons were also made for camera positions from the front and 45° from the y and x axes in the horizontal plane.

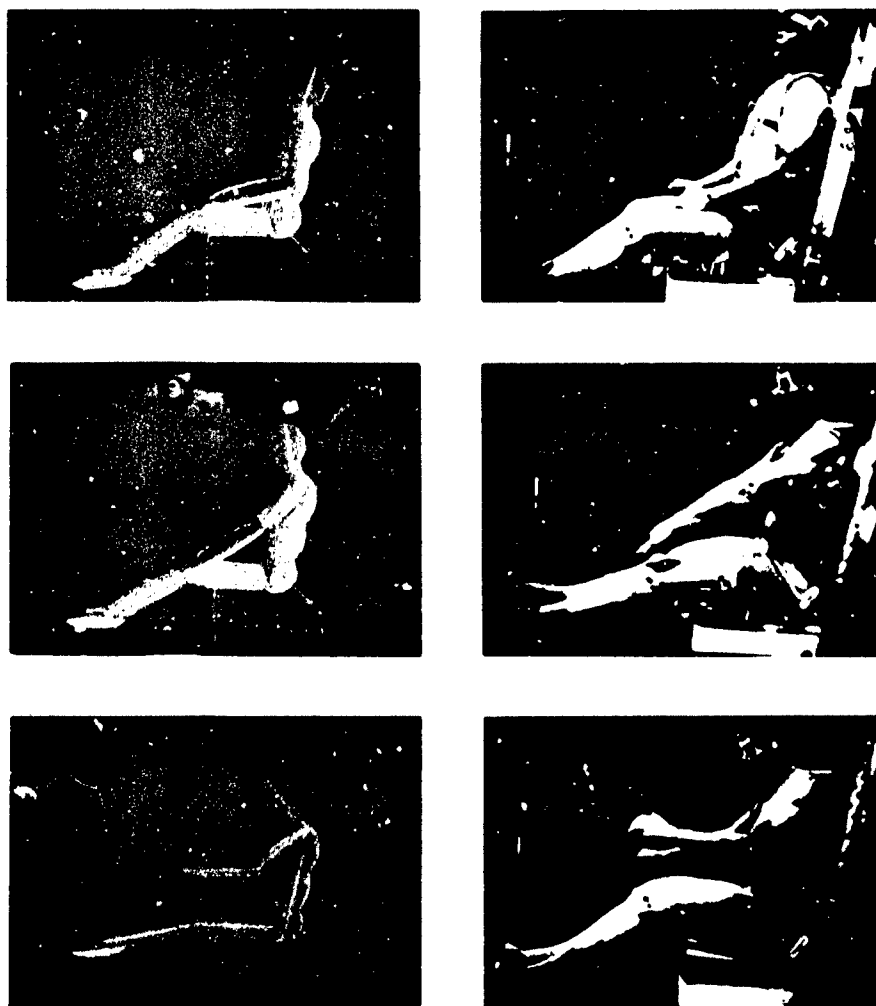


Figure 12. Comparison of simulated and experimental body motion from lateral view during 10-g peak $-G_x$ impact.

CONCLUSIONS

The objective of this report has been twofold: to present a methodology which can provide considerable insight into human body dynamics during whole body impacts and to demonstrate the application of this methodology. The methodology is, in effect, the use of a mathematically defined model of the articulated human body structure with appropriate parameters for body property description. The application of this model consisted of prescribing an initial body position and the subsequent dynamic environment to which the body was exposed.

On the basis of this study, certain conclusions may be drawn about the overall applicability of the Articulated Total Body (ATB) Model to impact problems in general and the $-G_x$ impact events in particular. This discussion is most easily pursued by reference to specific aspects of the current simulation study and then by an extension of these to more general applications.

It should be noted that not all variables predicted by the computer model are of practical interest, since many of them provide no useful insight into local stress concentrations and energy transfer cannot be directly measured and cannot be correlated to the occurrence of injury. No doubt as measurement techniques become more sophisticated, additional body dynamic variables will be considered. For the present, however, emphasis has been placed on the calculation of variables most easily comparable to ones measured during experimentation as well as those most applicable to injury probability prediction.

Thus the variables chosen for comparison have consisted of forces in the harness system which transfer most of the impact energy to the body, linear resultant accelerations of the head and chest, displacement of the lower torso and the three-dimensional displacements of all body segments. Contact forces between the subject and the seat pan were also calculated, but measured data were not available for comparison.

In all the data comparisons, agreement was very good with the exception of the head resultant acceleration. In some cases, even closer agreement could have been achieved by minor readjustments in some of the parameters. However, "fine tuning" of the model parameters was generally avoided, and no parameter changes in the model structure were made in the 10-, 8- and 6-g impact simulations.

The particular events chosen for simulation were well within the safe exposure range, with the most serious observed injuries being minor abrasions from the harness straps and occasional mild muscle strains. Also, the combination of load levels applied and harness geometry used resulted in limited limb motion during the impact. With the exception of the knee, none of the limbs approached their normal range of motion levels.

While this choice of simulation events was useful for demonstrating the predictive validity of the ATB Model for inertial segment response, it avoided the situations where relative limb rotations were large and significant internal joint torques were generated. The present model structure does provide for the application of such joint torques as a function of relative segment angular orientation. However, the joint data used are only approximate, and for cases of complex joint motion, especially into regions beyond the normal range of motion, response of the model is questionable. Presently a study is being carried out under the sponsorship of our laboratory to provide detailed, quantitative internal joint torque versus adjacent segment relative orientation data for the shoulder, elbow, hip, knee and ankle joints. This data will considerably improve the ATB Model's predictive capability for events involving large joint excursions.

The type of events simulated also allowed a potentially large dynamic response variation due to voluntary and involuntary muscle actions. This effect was felt to be particularly significant in the observed head response, and was reflected in the significant differences between the simulated and experimental head acceleration time histories. A more detailed analysis of the head response using the same model as employed in this study and including some of the effects of the active musculature has been carried out by Frisch (13,14).

The results of this study indicate that the ATB Model is a useful, predictive tool for the analysis of whole body articulated response to impact. It leaves little doubt that it provides a reliable, dynamic interpolative method for predicting changes in harness system loading on the body, accelerations of segments and interactive force levels between body segments and external system structural components for different impact loads. It also accurately provides predictions of body segment motions where internal joint torques are not significant or joints are not forced beyond normal motion envelopes.

Though model application to the simulation of the presently described $-G_x$ impacts has proven quite successful, several model improvements are currently being made and some programs are being carried out to refine the model data base. Among the improvements to the model structure are capabilities to allow lateral harness belt motion over the body surface, permit dissipation of energy in the harness body interaction and specify independent harness system and body segment compliances. Concurrent programs are being pursued to provide accurate data on the resistive torque properties of major human long-bone joints as functions of adjacent segment angular orientations, failure load levels for these same joints and more detailed data on human body segment mass distributions.

REFERENCES

1. Goldstein, H., Classical Mechanics, Addison-Wesley Pub. Co., 1959, pp 178-180.
2. Young, R.O., "A Three-Dimensional Mathematical Model of an Automobile Passenger," Texas Transportation Institute Research Report 140-2, 1970.
3. Robbins, D.H., R.O. Bennett, Jr. and B.M. Bowman, "User-Oriented Mathematical Crash Victim Simulator," Proceedings of the 16th Stapp Car Crash Conference, 1972, pp 128-148.
4. Furusho, H. and K. Yokoya, "Analysis of Occupant's Movement in Head-On Collision," Transactions of the Society of Automotive Engineers of Japan, No. 1, 1970, pp 145-155.
5. Huston, R.L., R. Hessel and C. Passerello, "A Three-Dimensional Vehicle-Man Model for Collision and High Acceleration Studies," Paper No. 740275, Society of Automotive Engineers, Inc., 1974.
6. Huston, R.L., C.E. Passerello, M.W. Harlow and J.M. Winnet, "The UCIN 3-D Aircraft-Occupant," Aircraft Crashworthiness, University Press of Virginia, 1975.
7. Fleck, J.T., F.E. Butler and S.L. Vogel, "An Improved Three Dimensional Computer Simulation of Motor Vehicle Crash Victims," Final Technical Report No. 70-5180-L-1, Calspan Corp., 1974, 4 vols.
8. Fleck, J.T., "Calspan Three-Dimensional Crash Victim Simulation Program," Aircraft Crashworthiness, University Press of Virginia, 1975.
9. King, A.I. and CCC.C. Chan, "Mathematical Modelling, Simulation and Experimental Testing of Biomechanical System Crash Response," J. Biomechanics, 1976, Vol. 9, pp 301-317.
10. Fleck, J.T. and F.E. Butler, "Development of an Improved Computer Model of the Human Body and Extremity Dynamics," AMRL-TR-75-14, 1975.
11. Churchill, E., P. Kikta and T. Churchill, "The Aerospace Medical Research Laboratory Data Bank Library," AMRL-TR-77-1, 1976.
12. Bartz, J.A. and C.R. Gianotti, "Computer Program to Generate Dimensional and Inertial Properties of the Human Body," Paper No. 73-11A-Bio-3, ASME Transactions, November 1973.
13. Leet, D.G., "Procedures Used to Generate Input Data Sets for the Articulated Total Body Model from Anthropometric Data," to be published in AGARD Proceedings of the 35th Aerospace Medical Panel Meeting held in Paris, France, November 1979.
14. Frisch, G.D. and C. Cooper, "Mathematical Modeling of the Head and Neck Response to -G_x Impact Acceleration (Minimum Articulation Requirements)," Aviation, Space and Environmental Medicine, January 1978, pp 196-204.
15. Frisch, G.D., L. D'Aulio and J. O'Rourke, "Mechanism of Head and Neck Response to -G_x Impact Acceleration. A Math Modeling Approach," Aviation, Space and Environmental Medicine, March 1977, pp 223-230.

DISCUSSION

HENRY JEX (USA)

Can your model be exercised to show the responses to more complex waveforms such as periodic motions (e.g., such as vibrations)?

AUTHOR'S REPLY

While the method of analysis used with the model is quite versatile for predicting response to practically any time-dependent input, its application to the prediction of body response to periodic forces, while possible, would be highly inefficient. The reason for this is that the model is highly nonlinear, and linear transform methods cannot be applied. The solutions must therefore be obtained by means of multiple integrations in the time domain. For periodic forces this generally leads to very long computer run times and exorbitant costs.

G. R. ALLEN (UK)

- (a) Should not damping in the joints be included in the model, or were its effects negligible?
- (b) For completeness, presumably elastic properties (mass-spring-damping) should be added to the model. Their absence could partly explain the discrepancy between experimental and theoretical head acceleration (Fig 11)?

AUTHOR'S REPLY

The model in its present form does account for damping and elastic properties of the joints. While the specification of these properties can no doubt be improved in all the joints - and will be as new data become available - the discrepancy between experimentally observed and theoretically predicted response for the head appears to be due to active pre-tensing of muscles in the cervical region by the subject prior to the impact, and the current model inadequacies in accounting for these muscle forces.

PROCEDURES USED TO GENERATE INPUT DATA SETS FOR
THE ARTICULATED TOTAL BODY MODEL FROM ANTHROPOMETRIC DATA

Duane G. Leet, Ph.D.
University of Dayton Research Institute
Dayton, Ohio 45469

1. INTRODUCTION

Protection of passengers from injury during vehicle and aircraft crashes and the protection of a crew from injury during aircraft ejection situations is one of the important design objectives of vehicle and aircraft design engineers. An increasingly important tool in evaluating the safety aspects of different designs is computer software simulation. Calspan Corporation has developed a particularly sophisticated class of these programs. The class includes the 3-D Crash Victim Simulator (CVS) Model, developed under DOT sponsorship (Fleck, et al, 1974), and the Articulated Total Body (ATB) Model, developed from the CVS Model under the sponsorship of the U.S. Air Force Aerospace Medical Research Laboratories (AMRL) specifically for application to aerospace-type problems (Fleck and Butler, 1975). These programs model the human (or laboratory animal) body as a multi-segment chained system. Currently 15 segments are defined: head, neck, upper arm (left and right), lower arm (left and right; includes the hand), upper torso (thoracic region), middle torso (viscera), lower torso (pelvic region), upper leg (left and right), lower leg (left and right), and foot (left and right). Figure 1 provides two views of a body on which standard body segment cut-planes have been marked. The actual body landmarks defining these cut-planes are described in Chandler, et al (1975).

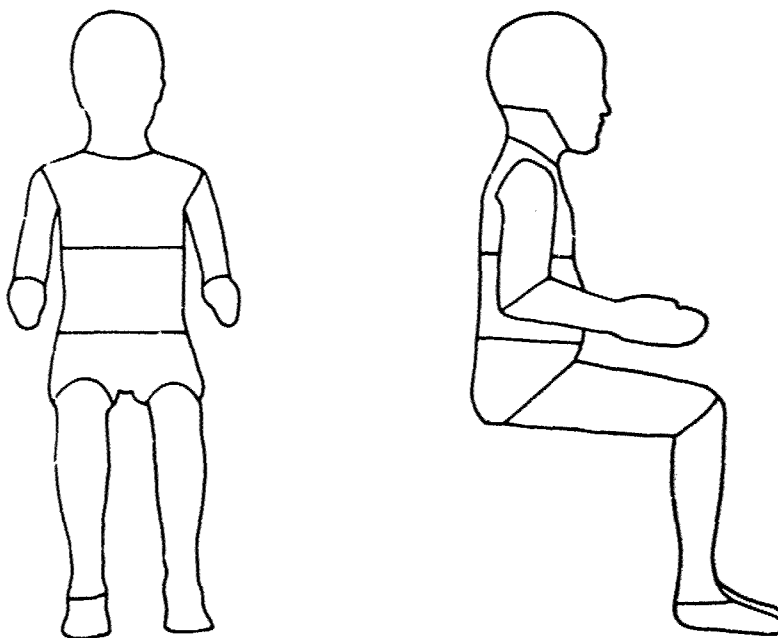


Figure 1. The Fifteen Body Segments Marked on (a) Front and (b) Right Side Views of a Six-Year-Old Child Manikin Developed From Anthropometric Data By Young, et al (1976).

Among the input data required on each segment are:

- inertial properties (mass, center of mass, principal moments, principal axes orientation).
- contact ellipsoid dimensions, axis origin with respect to the center of mass, and axes orientation with respect to the principal axes.
- joint locations with respect to the center of mass, and joint axes orientations (Each joint has two sets of axes, one for each segment associated with the joint. These axes are used to define torques at the joint.)
- various joint stiffness and friction constants.

In addition, data must be supplied to define the initial orientation of the body with respect to an external reference coordinate system. The environment (contact planes, restraint systems) must also be defined, as well as remaining initial conditions and the external stimuli to be applied to the system.

The program simulates the dynamics of body motion using a unique method that has been shown to be equivalent to the Lagrange method. Motion picture films of the dynamics can be produced through the use of plot packages supplied with the simulation program. The quality of the simulation is demonstrated in the paper in this session by Ints Kaleps.

The University of Dayton Research Institute, under the sponsorship of AMRL, is currently involved in a research program to develop input data sets for the ATB Model program. The next four sections of this paper provide a general background for the techniques we have developed to generate these input data sets from anthropometric data. The final section discusses the current state-of-the-art in implementing these techniques. The appendices provide some details on the techniques that have been developed.

2. TECHNIQUES USED TO GENERATE BODY SEGMENT INERTIAL DATA

There are two basic approaches used to obtain body segment inertial data. One approach is to perform actual pendulum-type measurements on cadaveric body segments. There have been only two significant studies performed in the U.S. on human cadavers using this approach, one by Chandler, et al (1975), which included data on all the body segments of six adult male cadavers, and the other by Walker, et al (1973), which emphasized the head and neck segments of 20 adult male cadavers. The second approach is to construct a geometric model of a body segment and compute the model's inertial properties. Data used to construct the models are from one of two sources: anthropometric or biostereometric measurements. We will be emphasizing techniques for constructing the geometric models from anthropometric data.

Previous body segment geometric models have been homogeneous ellipsoids, cylinders or frustrums of circular cones. [See, for example, Reynolds (1974).] We have developed the mathematics for a more general geometric shape shown in Figure 2. This segment model can have up to three parts. One of these parts is the right elliptical solid, which has these characteristics:

- It has two parallel elliptical end-planes. A z-axis is defined through the centroids of these end-planes and is normal to both planes.
- The end-planes and any other cross-section parallel to them are ellipses with centers on the z-axis and semiaxes in the xz- or yz-planes.

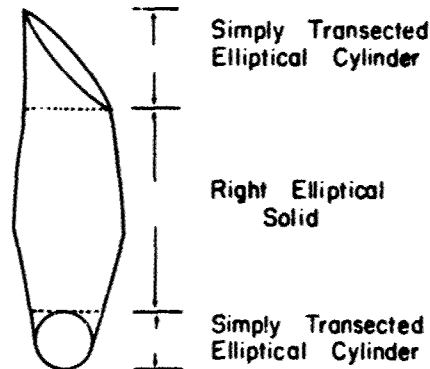


Figure 2. The General Geometric Model.

For our purposes, the shapes of the right elliptical solid is further restricted to those that can be defined by supplying the semiaxis values of the end-planes and a single cross-section somewhere between the end-planes. Although the other geometric models mentioned have the advantage of having existing closed-form expressions for their inertial properties, they are relatively poor approximations to actual body segment shapes when compared to the right elliptical solids described here.

The other parts of the segment model in Figure 2 are homogeneous simply-transected elliptical cylinders. A simply-transected elliptical cylinder is an elliptical cylinder that has been cut diagonally from the edge of one end-plane to the opposite edge of the other end-plane. In addition, if a coordinate system is defined with the z-axis passing through the centroids of the end-planes, the cut-plane is parallel to either the x-axis or the y-axis. In the segment model there can be one simply-transected elliptical cylinder at each end of the right elliptical solid.

To complete the specification of our body segment geometric model, we require that the z-axes of the three parts coincide and their xz- and yz-planes must line-up, although they need not coincide. (For example, the xz-plane of a simply-transected elliptical cylinder can line-up with the yz-plane of the right elliptical solid.)

The basic procedure for computing the inertial properties of a body segment using this model is:

1. Select one of the following models:
 - a. Right elliptical solid.
 - b. Simply-transected elliptical cylinder.
 - c. Right elliptical solid with a simply-transected elliptical cylinder at one end.
 - d. Right elliptical solid with simply-transected elliptical cylinders at each end.
2. Define the local coordinate system for each part and a coordinate system for the segment model as a whole.
3. If the model includes a right elliptical solid:
 - a. Identify the proximal, mid, and distal planes.
 - b. Determine the semiaxes for these planes and the distances between them.
 - c. Determine the density.
 - d. Run the program MISEC2.
4. For each simply-transected elliptical cylinder:
 - a. Determine the base semiaxes and the height.
 - b. Run the program "Simply-Transected Elliptical Cylinders."
5. Combine the individual segment inertia properties using the program "Parallel Axis Theorem."
6. Obtain the segment principal moments and direction cosine matrix using an available eigenvalue and eigenvector program.

Step 2 requires that local coordinate systems be defined for each part of the segment. It is helpful to orient the segment to the rest of the body by defining proximal and distal ends for the segment as a whole and for each of its parts, with the distal end being furthest from the head. Assuming each part has a proximal end-plane, the origins of the local coordinate systems can be located at the distal end-plane centroids; otherwise, the origin can be located at the distal end-plane centroid. By convention, the orientation of a segment's positive z-axis is along the cylindrical axis, from the proximal end to the distal end. The positive orientation of a segment's y-axis should be right lateral (out the right side). It follows that the positive orientation of a segment's x-axis should be anterior (out the front).

The MISEC2 program in Step 3d is a very fast interactive FORTRAN program written to compute the inertial properties of the homogeneous right elliptical solid (Leet, 1978a). The program approximates the solid as a stack of elliptical cylinders of varying semiaxes values, computes the inertial properties of each cylinder, computes the center of mass of the solid as a whole, and then used the parallel axis theorem to shift the individual cylinder's center of rotation to the solid's center of mass, where they are appropriately summed to provide the solid's moments of inertia about its center of mass.

The closed-form expressions for the inertial properties of a simply-transected elliptical cylinder, developed in Leet (1978b), are summarized in Appendix B. A convenient HP-97 Calculator program "Simply-Transected Elliptical Cylinders" has been written that computes these properties with respect to various axis orientations.

The HP-97 program "Parallel Axis Theorem" mentioned in Step 5 has been documented in Leet (1978d).

Appendix A specifies the anthropometric data required for each of the body segments in order to use the above procedure.

The head and neck body segments are special shapes and we have developed special procedures for them. Previously, the geometric model used for the head was either a homogeneous sphere or ellipsoid. Anthropometric measurements were made of the head's length, width, and depth, and approximate ellipsoid defined. The principal moments were computed from the closed-form expressions. The principal axes are naturally coincident with the geometric axes.

We have developed a novel procedure to obtain the head's principal moments of inertia and principal axes. This procedure is outlined in the following steps:

1. Determine these head measurements:
 - a. Head length (measured from the middle of the forehead¹, just above the eyebrows, to the middle of the back of the head).
 - b. Head breadth (the maximum breadth of the head).
 - c. Head height (the distance from the chin to the top of the head, in a vertical direction).
 - d. Mass (Homogeneity is still assumed.).
2. Obtain a direction cosine matrix defining the principal axes orientation with respect to a standard local axis system, and the coefficients of the linear equations relating the principal moments computed from the ellipsoid model to the true principal moment values.
3. Use the program "Moments of Inertia of a Rotated Ellipsoid" to compute the principal moments of the head.

¹Precise anthropometric terminology exists for all locations mentioned; it can be obtained from the author. It is felt that more common, albeit less precise, terminology is more appropriate for this paper.

The mass in Step 1 can be determined by obtaining the volume value by emersion and multiplying it by a density representative of the class of humans being modeled. For example, Chandler, et al (1975) have determined that the average density for the head segments of six adult male cadavers was 1.056 (SD = .020).

The direction cosine matrix mentioned in Step 2, which defines the orientation of the principal axes, has been determined for the adult male from the Chandler data (Leet, 1978c). This matrix is

$$\begin{bmatrix} 0.6484 & 0.0000 & -0.7613 \\ 0.0000 & 1.0000 & 0.0000 \\ 0.7613 & 0.0000 & 0.6484 \end{bmatrix}$$

The standard local reference system used has its origin at the head's center of mass, with the positive x-axis in the forward direction (It exits the head at about a point midway between the eyes at the level of the eyebrows.), positive y-axis to the right, and positive z-axis straight down, all with the head level and eyes straight ahead. (The technical terminology is "head oriented in the Frankfort Plane.") The direction cosine matrix specifies that the principal x-axis is rotated 49.6° counterclockwise about the local reference y-axis; this axis exits the head at about the top of the forehead. (The temptation was to say at the hairline, but that, unfortunately, can be too misleading.) The positive principal z-axis, therefore, exits the head approximately through the mouth.

The "Moments of Inertia of a Rotated Ellipsoid" program, which is documented in Leet (1978c), uses the three specified head dimensions to define an ellipsoid whose axes are oriented parallel to the local reference axes and centered at the geometric center of the head. It then uses the direction cosine matrix to define a new ellipsoid whose axes are centered at the geometric center, but oriented parallel to the principal axes. The semiaxis lengths for this ellipsoid are taken as the distances from the origins to the intersection of the principal axes with the first ellipsoid. The principal moments of the new ellipsoid are then calculated.

$$I_{xx}^*, 10^3 \text{ g-cm}^2$$

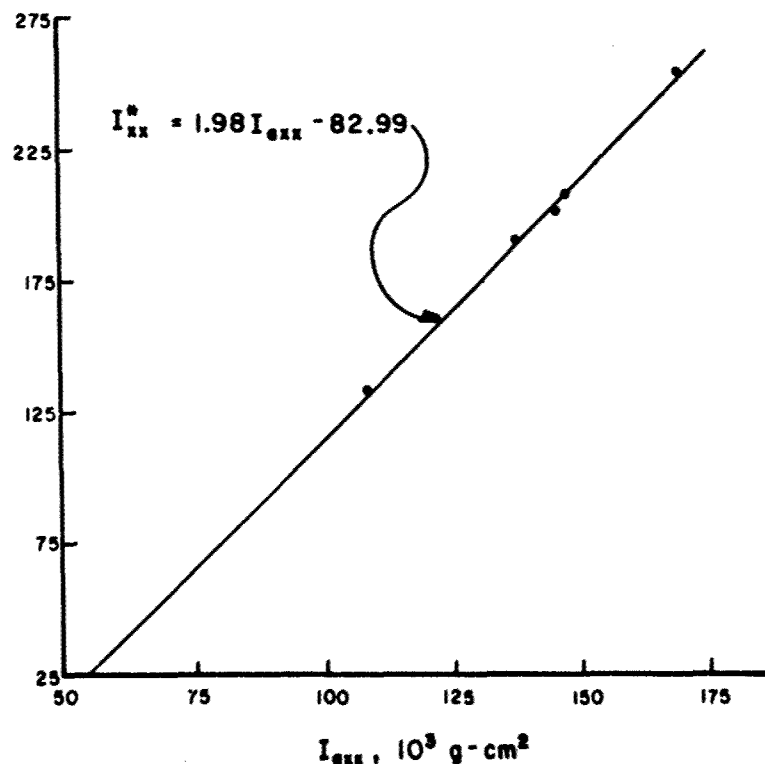


Figure 3. The Head's I_{axx} Principal Moment, Computed Using Rotated Ellipsoid Geometric Model, Compared to the Experimentally Determined Principal Moment, I_{xx}^* .

The principal moments obtained by applying this procedure to the six cadaver heads of the Chandler data were linearly correlated with the empirically determined principal moments. There was a high degree of correlation, as can be seen in Figures 3 through 5,

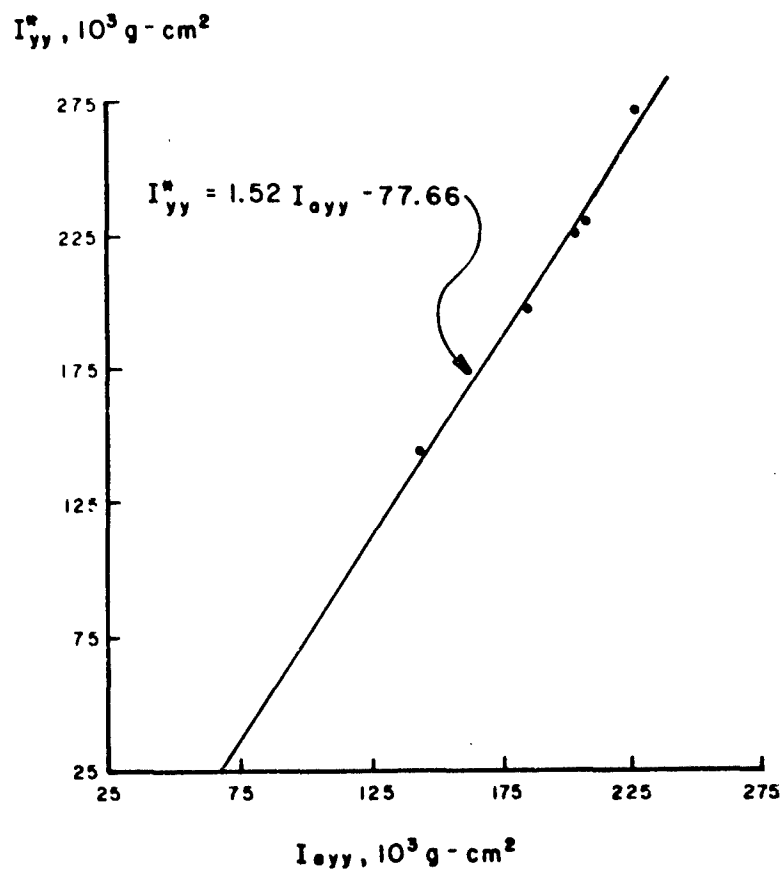


Figure 4. The Head's I_{yy}^* Principal Moment, Computed Using the Rotated Ellipsoid Geometric Model, Compared to the Experimentally Determined Principal Moment, I_{oyy} .

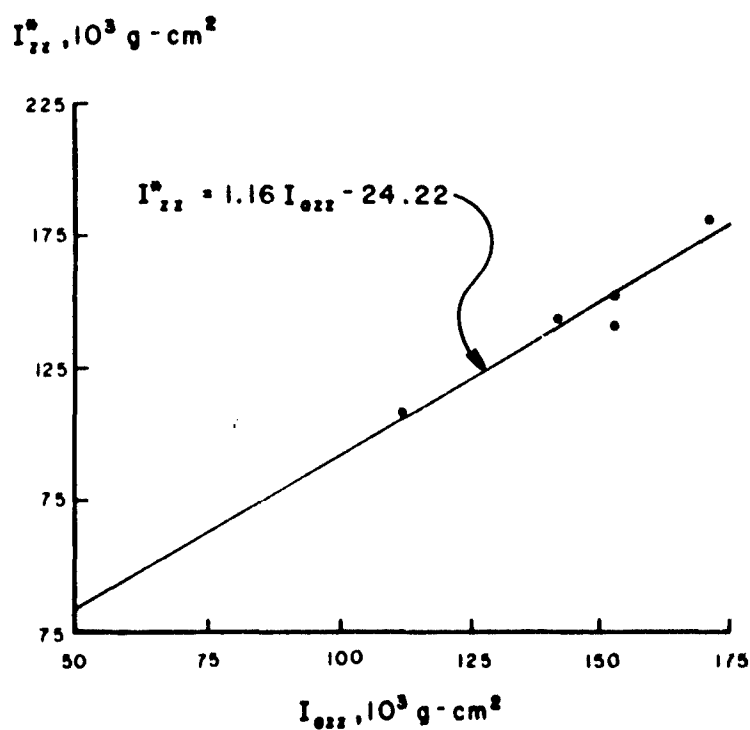


Figure 5. The I_{zz}^* Principal Moment, Computed Using the Rotated Ellipsoid Geometric Model, Compared to the Experimentally Determined Principal Moment, I_{ozz} .

with the equations being:

$$\begin{aligned} I_{xx}^* &= 1.9 I_{axx} - 82.99 & (r^2 &= 0.99) \\ I_{yy}^* &= 1.52 I_{ayy} - 77.66 & (r^2 &= 0.99) \\ I_{zz}^* &= 1.16 I_{azz} - 24.22 & (r^2 &= 0.92) \end{aligned}$$

(The experimentally determined moments are I^* and the computed moments are I_a .) It is the coefficients of these equations that are referred to in Step 2. The "Moments of Inertia of a Rotated Ellipsoid" program has the capability of performing these linear transformations.

The only inertial properties of the head not yet discussed is the center of mass. At present we know of no technique for determining the center of mass of the head from anthropometric data. Edward Becker (1973), at the Naval Aerospace Medical Research Laboratory, has shown that for adult male cadavers, at least, there is only a relatively small variability in the location of the head's center of mass about a mean value of 13 mm in the +x-direction and 21 mm in the -z-direction from the ear hole and midway between the ears.

The neck segment is a complex geometric shape, as shown in side view in Figure 6a. There are two cut-planes between the head and the neck: One is parallel to the Frankfort Plane, passing from the back of the head along the base of the skull to a point just behind the ear; the other is parallel to the body reference y-axis and runs from the point just behind the ear (on the mastoid) tangent to the upper portion of the Adam's apple and out the front of the neck. The cut-plane between the neck and the upper torso is parallel to the body reference y-axis and passes through the vertebral landmark at the lower back of the neck called the cervicale and a point just above where the two collar bones meet (the suprasternale).

The neck segment has been modeled as a three part solid: two simply-transected elliptical semicylinders with the surface curve removed on top of a right elliptical cylinder (Figure 6b). Figure 6c is a perspective view of a simply-transected elliptical semicylinder with the surface curve removed. In words, a semicylinder is a cylinder that has been bisected along its long, or z-y axis, the cut-plane being parallel to either the x- or y-axis. "Simply-transected" means that the semicylinder is cut by a plane that is parallel to the same axis as the bisecting cut-plane and runs from the bisecting cut-plane at one end-plane to the opposite side of the other cut-plane. The remaining part of the description specifies that the bisecting cut-plane is part of the solid. The part that is removed is the part containing the cylinder's surface curve.

A FORTRAN program has been written that uses the anthropometric data on the neck listed in Appendix A to compute the inertial properties of the solid with respect to a coordinate system with origin at the center of mass and axes in the same directions as the head reference system (Leet, 1978e). The program uses the inertial properties of the simply-transected elliptical semicylinder with the surface curve removed, which are summarized in Appendix C, the inertial properties of an elliptical cylinder, the parallel axis theorem, and some geometric relationships to determine the model's inertial properties.

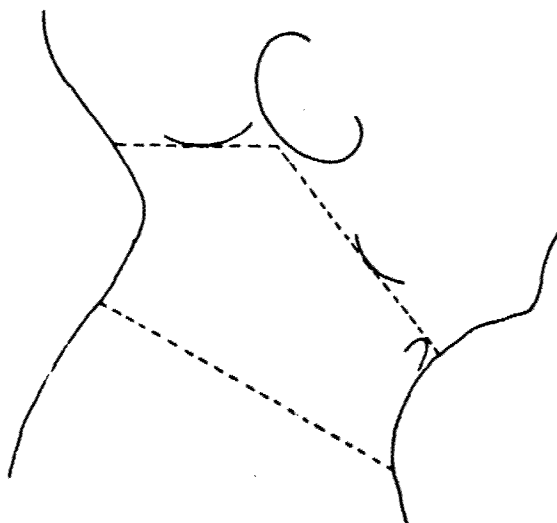


Figure 6a. Side View of the Neck Segment.

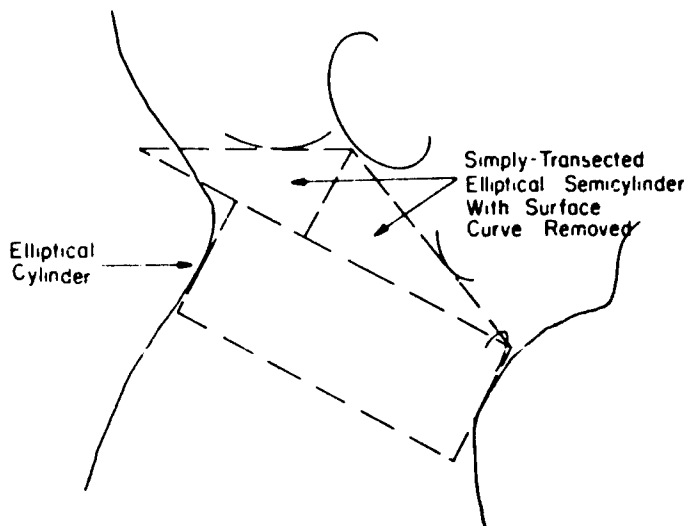


Figure 6b. Side View of the Three-Part Neck Geometric Model.

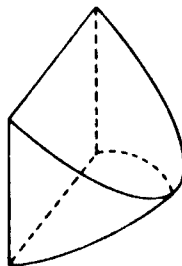


Figure 6c. Perspective View of a Simply-Transected Elliptical Semicylinder with the Surface Curve Removed.

3. TECHNIQUES USED TO ESTIMATE JOINT LOCATIONS

The body segments in the ATB Model are connected at joints to form the total body. The location of each segment's joints must be defined with respect to the segment's principal axes. In general, the segment's cut-planes are so defined that their centroids are the joint loci.² Therefore, the inertia computation process outlined above provides the necessary information to determine the joint locations. However, there are some exceptions. The head-neck joint is located at the mid-point of the line connecting the mastoids (the bone behind the ear). To locate this point with respect to the head's center of mass, anthropometric data must be available relating the center of mass to the mastoids. The neck modeling procedure provided information on this joint's location in the neck.

The neck has a second joint, the upper torso-neck joint. Assuming that it is located the same distance from the back of the neck as the head-neck joint, the coordinates of this joint in the neck can be obtained from the neck modeling procedure. The coordinates of the joint with respect to the centroid of the cut-plane between the neck and upper torso can also be determined. These coordinates can be transferred to the upper torso to provide the joint's location in the upper torso.

The shoulder joints are located using values from the upper arm and upper torso models. The joint is assumed to be one-third the distance from the top of the shoulder (acromion) to the arm pit (axilla), measured from the acromion. (This fraction is the subject of some controversy.)

The upper torso-mid torso and mid torso-lower torso joint locations are computed using a formula developed by Liu and Wickstrom (1973). With the standard local reference axis system having the positive x-axis forward, the positive y-axis to the right, and the positive z-axis down, the distance in the -x-direction from the center of mass is given by $a_0 + a_1 (W / H * Y)$, where a_0 and a_1 are regression coefficients computed by the authors for each vertebral level, W is the body weight, H is the body height, and Y is the width of the body at the joint location.

² It is recognized that there is a continuing controversy over rules that locate joints from external landmarks. This issue can not be addressed in this short summary; the results in this paper reflect the latest thinking.

The upper torso-mid torso joint is located at about the level of the T7 vertebra. The -x-distance can be computed by averaging the values obtained from the Liu and Wickstrom formula for the T6, T7, and T8 vertebrae. The mid-torso-lower torso joint is located at about the level of the L3 vertebra. The -x-distance can be computed by averaging the values obtained from the Liu and Wickstrom formula for the L3, L3, and L4 vertebrae. To complete the coordinate definitions: the y-coordinates for both points are zero; the z-coordinates can be obtained from the geometric models of the segments.

Specifications of the hip joint locations requires the geometric model of the lower torso and the anthropometric measurements bispinous breadth (the point of the hip bone in the lower abdomen), which is used to compute the y-coordinate (bispinous breadth/2), the trochanterion height (the hollow on the side of the hip), which is used to compute the z-coordinate, and the trochanterion-to-seat-back distance, which is used to compute the x-coordinate. [In the geometric model calculations, the center of mass is defined with respect to the top end-plane centroid. Knowledge of the vertical distance from the end-plane, which is the ilio-cristale height (the very top of the hip bone), to the trochanterion is enough to define the z-coordinate.]

4. TECHNIQUES USED TO ESTIMATE SEGMENT CONTACT ELLIPSOIDS

The surfaces of the body model are described by the surfaces of ellipsoidal shapes for individual body segments. The present state-of-the-art provides no algorithm for generating the dimensions of these contact ellipsoids; instead, the following set of heuristics is offered. But first it should be pointed out that the segment inertia ellipsoids are independent of the contact ellipsoids. The objective of the contact ellipsoid construction is to provide a surface description for contact force interactions and to generate a representative body shape for graphic display.

The technique used is to work from side and front view photographs of a person representative of the class of individuals being modeled. The person should be in this standard sitting position: the head is oriented in the Frankfort Plane, the upper arms are vertical with the palms in, the lower arms are horizontal, the lower legs are vertical, and the feet are flat on the floor. The objective here is to position the axes of the body segments parallel to the body reference axes. The outline of the body should be clearly visible in the photographs, and scales close to the body mid-planes should be included.

The body outline and scale are traced on graph paper. The segment cut-planes are drawn on these figures, along with the segment principal axes at the center of mass. At the present time the contact ellipsoid semiaxes are parallel to the principal axes (The ATB Model program has the option of reorienting the contact ellipsoid semiaxes, but to date this reorientation has not been required.). The intersections of the segment principal axes with the extreme edges of the segment are used, along with a compass, to locate a first estimate of the contact ellipsoid origins. The coordinates of the origins with respect to the segment principal axes and the semiaxes lengths are supplied to the ATB Model program. This program is run for zero simulation time, followed by a body ellipsoid outline plot program to obtain plots of the initial position of the total body in its environment. Inspection of these plots usually suggested adjustments to the contact ellipsoid dimensions or origin locations.

There is a definite "art" to these heuristics. Furthermore, the interactive process consumes a comparatively large amount of computer resources and time. Therefore, contact ellipsoid determination is a prime candidate for future procedural improvements.

5. TECHNIQUES USED TO DEFINE BODY AND JOINT AXES ORIENTATION

The body orientation in the environment is defined in the ATB Model program by specifying the orientation of the segment principal axes with respect to an inertial reference system and the location of the lower torso segment's center of mass. This is a straightforward procedure.

Two coordinate systems must be defined for each joint, one in each segment associated with the joint. Their relative orientations are used to determine the torque at the joint. A manual procedure, one that sets the usual initial condition of zero joint torque has been developed and an automated approach using an interactive computer program is under development.

The required input data for this program are the direction angles of each segment with respect to the segment's local reference system and the angles of certain body segments with respect to the inertial reference system. (Generally, only one direction angle per segment is required.) The program leads the user through the required input data by asking simple, completely unambiguous questions. It generates an annotated card deck that can be used directly in the ATB Model program input data deck plus a detailed listing in the same format as is generated by the ATB Model program.

6. CONCLUDING REMARKS

The obvious temptation for any programmer is to create one large interactive program that incorporates all the techniques developed so far, plus techniques that permit easy definition of the environment and contact ellipsoids, perhaps under light-pen or cursor control. Indeed, we are investigating the cost-effectiveness of such a program.

The new techniques we have described have had limited testing and use. We are hoping that publication of these techniques at this time will lead to further testing of them, along with the communication to us of any needed improvements.

Our research program will have an impact on the sciences of anthropometry and anatomy in a couple of ways. First, the geometric models we have developed require some new anthropometric measurements. We have been working closely with experts in these fields to insure that the desired measurements are practical and appropriately defined. Second, if more accurate geometric models of body segments are required, improvement will most likely be made by defining density distributions within segments. No such data currently exist.

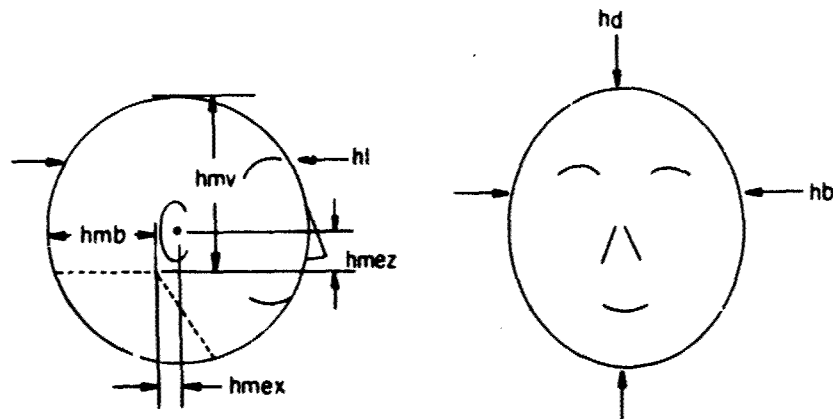
REFERENCES

1. Becker, E.B. (1973), "Measurement of Mass Distribution Parameters of Anatomical Segments", Sixteenth Stapp Car Crash Conference, Society of Automotive Engineers, Inc., New York, New York.
2. Chandler, R.E., C.E. Clauser, J.T. McConville, H.M. Reynolds, and J.W. Young (1975), "Investigation of Inertial Properties of the Human Body", AMRL-TR-74-137, Aerospace Medical Research Laboratory, Wright-Patterson Air Force Base, Ohio.
3. Fleck, J.T., F.E. Butler, and S.L. Vogel (1974), "An Improved Three-Dimensional Computer Simulation of Motor Vehicle Crash Victims, Volume I Engineering Manual, Volume II Model Validation, Volume III User's Manual, and Volume IV Programmer's Manual", Technical Report No. 2Q-5180-L-1, Calspan Corporation, Buffalo, New York.
4. Fleck, J.T. and F.E. Butler, "Development of an Improved Computer Model of the Human Body and Extremity Dynamics (1975)", AMRL-TR-75-14, Aerospace Medical Research Laboratory, Wright-Patterson Air Force Base, Ohio.
5. Leet, D.G. (1978a), "MISEC2: An Interactive FORTRAN Program That Computes the Inertia Properties of a Homogeneous Right Elliptical Solid", UDR-TR-78-26, University of Dayton Research Institute, Dayton, Ohio, 45469.
6. Leet, D.G. (1978b), "The Inertial Properties of a Simply-Transected Elliptical Cylinder", UDR-TR-78-94, University of Dayton Research Institute, Dayton, Ohio, 45469.
7. Leet, D.G. (1978c), "Estimating Moments of Inertia of the Head From Standard Anthropometric Data", UDR-TR-78-28, University of Dayton Research Institute, Dayton, Ohio, 45469.
8. Leet, D.G. (1978d), "An HP-97 Program That Computes the Inertia Properties of a Segmented, Rigid, Homogeneous Solid From the Inertia Properties of Its Parts", UDR-TR-78-29, University of Dayton Research Institute, Dayton, Ohio, 45469.
9. Leet, D.G. (1978e), "Estimating the Inertial Properties of the Neck From Anthropometric Data", UDR-TR-78-95, University of Dayton Research Institute, Dayton, Ohio, 45469.
10. Liu, Y.K. and J.K. Wickstrom (1973), "Estimation of the Inertial Property Distribution of the Human Torso From Segmented Cadaveric Data", in Perspectives in Biomedical Engineering, R.M. Kenedi (ed.), MacMillan New York, New York.
11. Reynolds, Herbert M. (1974), "Measurement of the Inertial Properties of the Segmented Savannah Baboon", Ph.D. Thesis, Southern Methodist University.

APPENDIX A: GEOMETRIC MODELS OF BODY SEGMENTS AND THEIR ANTHROPOMETRIC DATA REQUIREMENTS

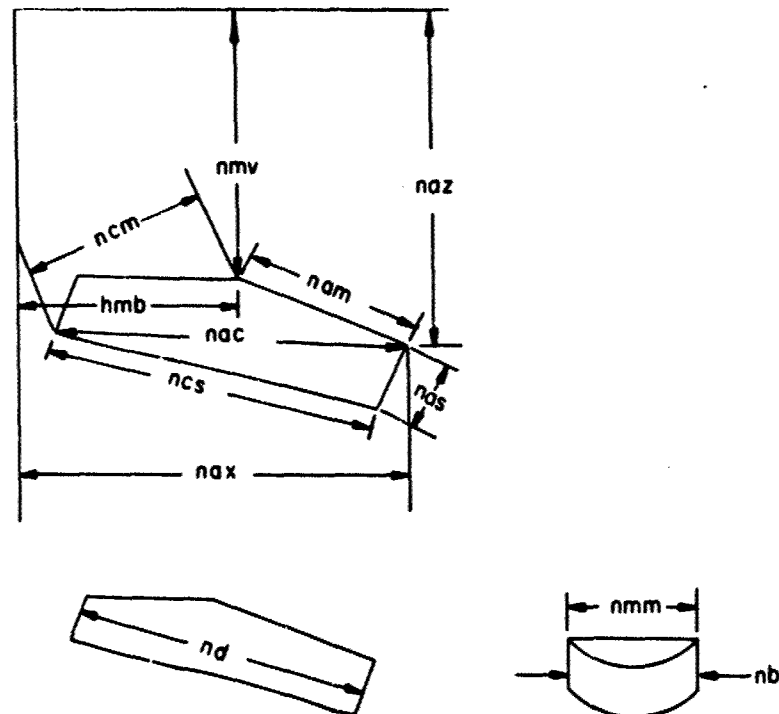
A.1 THE HEAD ANTHROPOMETRIC DATA

1. Head Length, hl
2. Head Depth (height), hd
3. Head Breadth, hb
4. Head, mastoid-to-vertex vertical distance, hmv
5. Head, mastoid-to-back-of head horizontal distance, hmb
6. Head, mastoid-to-ear hole distance (x- and z-coordinates), (hmex, hmez)



A.2 THE NECK ANTHROPOMETRIC DATA

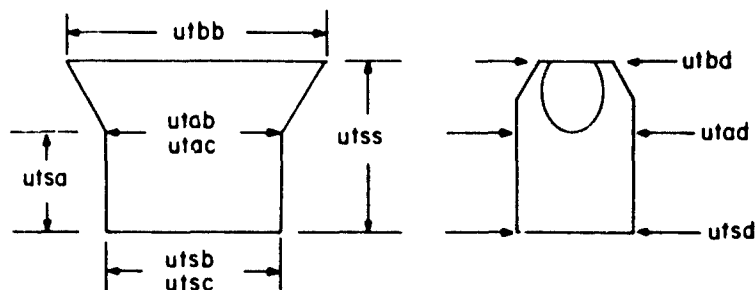
1. Head, mastoid-to-vertex vertical distance, nmv
2. Head, mastoid-to-back-of head horizontal distance, nmb
3. Adam's apple-to-wall distance, nax
4. Adam's apple to vertex vertical distance, naz
5. Cervicale-to-suprasternale distance, ncs
6. Cervicale-to-Adam's apple distance, nac
7. Cervicale-to-mastoid distance, projection on the midsagittal plane, ncm
8. Mastoid to Adam's apple distance, projection on the midsagittal plane, nam
9. Suprasternale to Adam's apple distance, nas
10. Mid-neck depth, nd
11. Mid-neck breadth, nb
12. Mastoid-to-mastoid distance, nmm



A.3 THE UPPER TORSO ANTHROPOMETRIC DATA

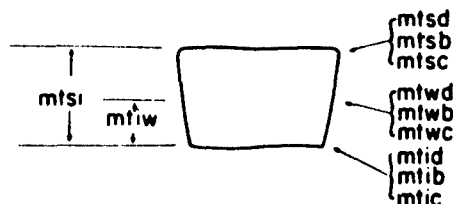
1. Biacromial Breadth, utbb
2. Horizontal depth at suprasternale, utbd
3. Depth at axilla level, utad
4. Breadth at axilla level, utab
5. Circumference at axilla level, utac
6. Depth at substernum level, utsd
7. Breadth at substernum level, utsb
8. Circumference at substernum level, utsc
9. Substernum-to-axilla distance, vertical, utsa

10. Substernum-to-acromion, vertical distance, utss
11. Volume of body to distal cut-plane of neck, utvn



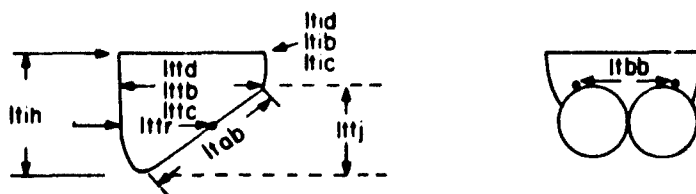
A.4 THE MIDDLE TORSO ANTHROPOMETRIC DATA

1. Substernum-to-iliocristale distance, mtsi
2. Iliocristale-to-waist (at navel) distance, mtiw
3. Depth at substernum, mtsd
4. Breadth at substernum, mtsb
5. Circumference at substernum, mtsc
6. Depth at waist (navel), mtwd
7. Breadth at waist (navel), mtwb
8. Circumference at waist (navel), mtwc
9. Depth at ilioeristale level, mtid
10. Breadth at ilioeristale level, mtib
11. Circumference at ilioeristale level, mtic
12. Volume from feet to substernum level, vfs



A.5 THE LOWER TORSO ANTHROPOMETRIC DATA

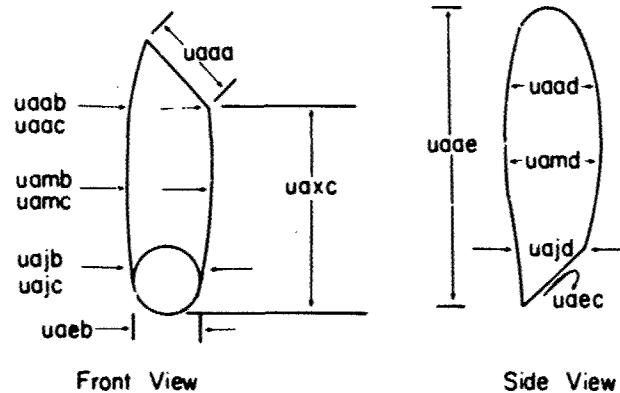
1. Thigh-abdominal junction height, lttj
2. Iliocristale height, ltih
3. Depth at ilioeristale level, ltid
4. Breadth at ilioeristale level, ltib
5. Circumference at ilioeristale level, ltic
6. Depth at thigh-abdominal junction level, lttid
7. Breadth at thigh-abdominal junction level, lttb
8. Circumference at thigh-abdominal junction level, lttc
9. Trochanterion height, ltth
10. Trochanterion-to-back distance, lttr
11. Bispineous breadth, ltbb
12. Length of the line from the thigh-abdominal junction through trochanterion to the buttock point, ltab
13. Volume from ilioeristale level down, ltv



A.6 THE UPPER ARM ANTHROPOMETRIC DATA

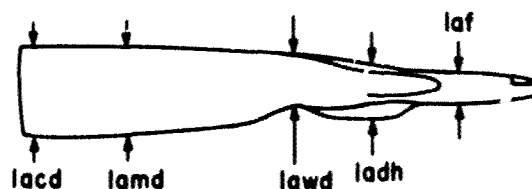
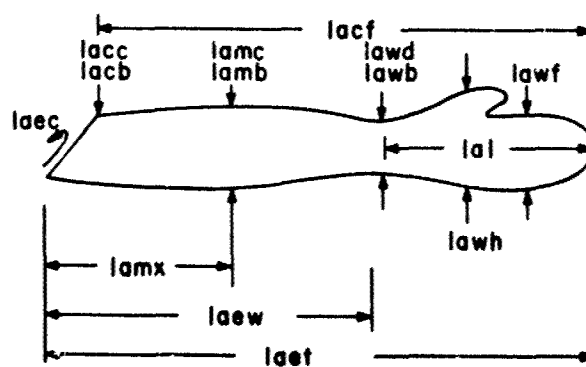
1. Acromion-to-elbow, uaae
2. Axilla-to-elbow, uaxe
3. Depth of upper arm at level of axilla, uaad
4. Breadth of upper arm at level of axilla, uaab
5. Circumference of upper arm at level of axilla, uaac
6. Depth of upper arm midway between acromion and elbow, uamd
7. Breadth of upper arm midway between acromion and elbow, uamb
8. Circumference of upper arm midway between acromion and elbow, uame

9. Depth of upper arm at level of lower arm-upper arm junction (inside elbow), uajd
10. Breadth of upper arm at level of lower arm-upper arm junction (inside elbow), uajb
11. Circumference of upper arm at level of lower arm-upper arm junction (inside elbow), uajc
12. Axilla-to-acromion length, uaaa
13. Breadth at elbow, uaeb
14. Circumference at elbow, uaec
15. Upper arm-lower arm volume to axilla-acromion line, vual



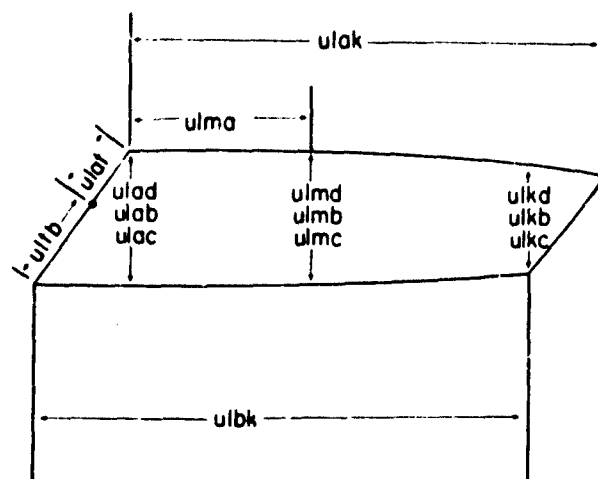
A.7 THE LOWER ARM-HAND ANTHROPOMETRIC DATA

1. Elbow-to-finger tip length, laet
2. Width of 4 fingers held tightly together, lawf
3. Depth of thickest finger at second joint, laf
4. Width of hand and thumb together, lawh
5. Maximum depth of hand, ladh
6. Depth of wrist, lawd
7. Breadth at wrist, lawb
8. Circumference at wrist, lawd
9. Hand length to wrist, lai
10. Elbow-to-wrist length, laew
11. Depth lower arm at maximum circumference, lamd
12. Breadth lower arm at maximum circumference, lamb
13. Circumference lower arm at maximum circumference, lamc
14. Elbow to lower arm maximum circumference distance, lamx
15. Depth of lower arm at arm crease, lacd
16. Breadth of lower arm at arm crease, lach
17. Circumference of lower arm at arm crease, lacc
18. Elbow circumference, laec
19. Length of lower arm from crease to finger tip, lacf
20. Volume of lower arm-hand segment, lavh



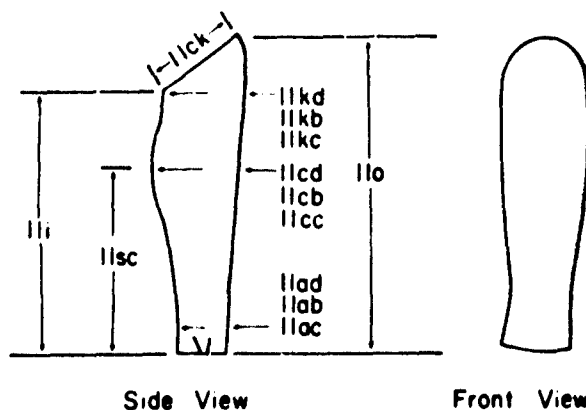
A.8 THE UPPER LEG ANTHROPOMETRIC DATA

1. Abdomen-thigh junction to mid kneecap distance, ulak
2. Buttocks point to crease at back of knee (The buttocks point is located by extending a line from the abdomen-thigh junction through the trochanterion point to the surface of the buttocks.), ulbk
3. Depth of leg at level of the crease at the back of the knee, ulkd
4. Breadth of leg at level of the crease at the back of the knee, ulkb
5. Circumference of leg at level of the crease at the back of the knee, ulkc
6. Depth of leg at mid-thigh, ulmd
7. Breadth of leg at mid-thigh, ulmb
8. Circumference of leg at mid-thigh, ulmc
9. Depth of leg at abdomen-thigh junction, ulad
10. Breadth of leg at abdomen-thigh junction, ulab
11. Circumference of leg at abdomen-thigh junction, ulac
12. Abdomen-thigh junction to trochanterion, ulat
13. Trochanterion to buttocks point, ultb
14. Location of mid-thigh measurements to abdomen-thigh junction, ulma
15. Volume of leg and foot (Submerge to line connecting abdomen-thigh junction and trochanterion.), lv



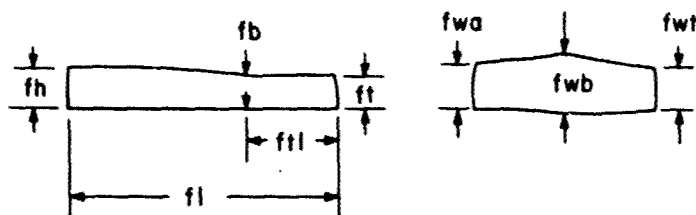
A.9 THE LOWER LEG ANTHROPOMETRIC DATA

1. Crease at back of knee to sphyrion (lower leg inside length), lli
2. Mid-kneecap to sphyrion (lower leg outside length), llo
3. Depth of leg at level of the crease at the back of the knee, llkd
4. Breadth of leg at level of the crease at the back of the knee, llkb
5. Circumference of leg at level of the crease at the back of the knee, llkc
6. Crease at the back of the knee to mid-kneecap distance, llck
7. Depth of leg at maximum calf circumference, llcd
8. Breadth of leg at maximum calf circumference, llcb
9. Circumference of leg at maximum calf circumference, llcc
10. Sphyrion to level where maximum calf circumference measurements were made, llsc
11. Depth of ankle at minimum circumference, llad
12. Breadth of ankle at minimum circumference, llab
13. Circumference of ankle at minimum circumference, llac
14. Volume of lower leg (submerge to line connecting crease at back of knee with the mid-kneecap), llv



A.10 THE FOOT

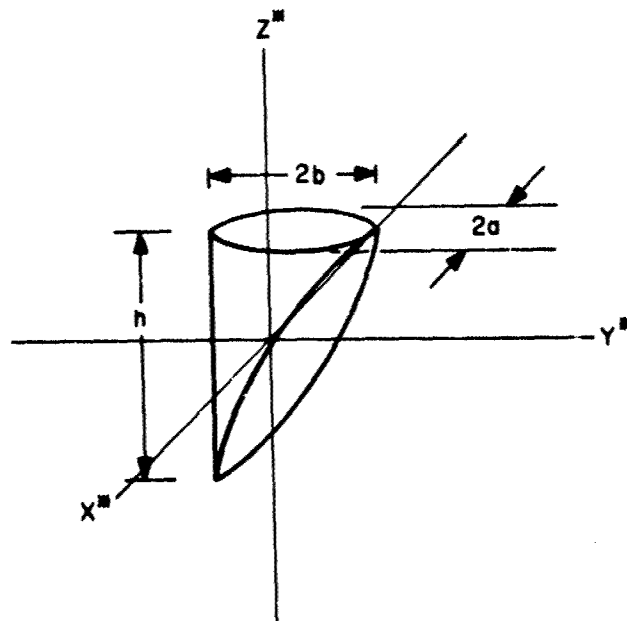
1. Heel-to-toe length (maximum foot length), fl
2. Sphyrion height, fh
3. Foot height at ball of foot, fb
4. Big toe height at nail, ft
5. Distance from distal point of big toe to point where fb measurement was made, ftl
6. Width of foot at tip of toes, fwl
7. Width of foot at ball of foot, fwb
8. Width of ankle just below sphyrion, fwa
9. Volume of foot (submerged to sphyrion), fv



APPENDIX B: INERTIAL PROPERTIES OF A SIMPLY-TRANSECTED ELLIPTICAL CYLINDER

Property	Value ¹
V	$\frac{\pi}{2}abh$
CM_x	0
CM_y	$-\frac{b}{4}$
CM_z	$\frac{3}{16}h$
I_{xx}^*	$\frac{\pi}{1536}abh (144b^2 + 37h^2)$
I_{yy}^*	$\frac{\pi}{1536}abh (192a^2 + 37h^2)$
I_{zz}^*	$\frac{\pi}{32}abh (4a^2 + 3b^2)$
I_{xy}^*	0
I_{xz}^*	0
I_{yz}^*	$-(\frac{1}{12} + \frac{3\pi}{128})ab^2h^2$

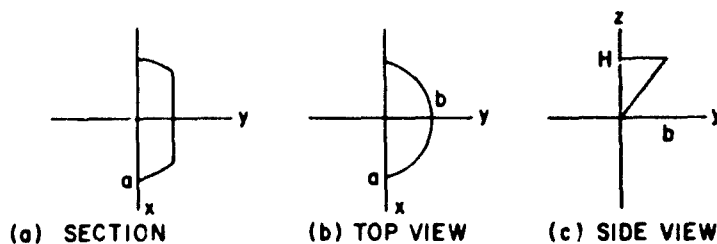
¹The density is implied in all moment values.



APPENDIX C: INERTIAL PROPERTIES OF A SIMPLY-TRANSECTED ELLIPTICAL SEMICYLINDER WITH THE SURFACE CURVE REMOVED

Property	Value ¹
Volume	$abH(\frac{\pi}{2} - \frac{2}{3})$
CM_x	0
CM_y	$\frac{b}{4} \frac{(16 - 3\pi)}{(3\pi - 4)}$
CM_z	$\frac{9\pi H}{8(3\pi - 4)}$
I_{xx}	$\frac{ab^3H}{2}(\frac{\pi}{4} - \frac{8}{15}) + \frac{abH^3}{3}(\frac{\pi}{2} - \frac{4}{15})$
I_{yy}	$\frac{a^3bH}{2}(\frac{\pi}{4} - \frac{4}{15}) + \frac{ab^3H}{3}(\frac{\pi}{2} - \frac{4}{15})$
I_{zz}	$\frac{a^3bH}{2}(\frac{\pi}{4} - \frac{4}{15}) + \frac{ab^3H}{2}(\frac{\pi}{4} - \frac{8}{15})$
I_{xy}	0
I_{xz}	0
I_{yz}	$-\frac{ab^2H}{5}$

¹The density is implied in all moment values.



ACKNOWLEDGMENTS

The research reported in this paper covers work performed under contract F33615-75-C-5054 and F33615-78-C-0504, sponsored by the 6570th Aerospace Medical Research Laboratory, Aerospace Medical Division, Air Force Systems Command, Wright-Patterson Air Force Base, Ohio. The author acknowledges the contributions of AMRL's Mr. Ints Kaleps.

CORRELATION OF MECHANISM OF EXTREMITY INJURY AND AERODYNAMIC FACTORS IN EJECTIONS FROM F-4 AIRCRAFT

Steven P. Combs, Major, USAF
Aerospace Medical Research Laboratory
Aerospace Medical Division
Air Force Systems Command
Wright-Patterson Air Force Base, Ohio 45433

A retrospective study of F-4 ejections from 1967-77 revealed extremity injuries during the ejection sequence in 43 of 399 ejections for an injury rate of 10.8%. Of the 43 ejections there were 95 extremity injuries. The injuries were divided into two groups: Severe and Minimal. Severe injuries consisted of fractures, dislocations, ligamentous tears and nerve palseys. There were 61 severe injuries. Minimal injuries consisted of contusions, lacerations, minor sprains. There were 34 minimal injuries. The 61 severe injuries were divided into 39 upper extremity injuries and 22 lower extremity injuries. The majority of the severe upper extremity injuries involved the proximal joints and the majority of the severe lower extremity injuries involved the distal joints. When the windblast/windflail injuries were compared to the various variables correlation was seen with the Knots Indicated Airspeed (KIAS), aircraft attitude and aircraft type. The incident of extremity injury increases with increased airspeed, a nose down attitude, and decreases in the RF-4C aircraft configuration.

The problem of extremity injury during emergency escape in the open seat ejection has been a continuing one and has received considerable attention over the past decade. Reports by Fryer and Payne, and by Hawker have shown extremity injury rates resulting from wind flail forces to range from 7% to 9%. The extremity injury rate under combat conditions has risen to 25%. Based upon these data, it was decided that a retrospective study should be conducted on F-4 ejectees. Its purpose was to: (a) identify the musculoskeletal regions most susceptible to windblast/windflail forces, (b) identify the modes and severity of trauma, and (c) speculate on the biomechanics of motion required to produce the injury mode observed. Initially, all the accident reports that listed an extremity injury for F-4 ejections at the Air Force Inspection and Safety Center, Norton AFB, CA, were carefully reviewed with respect to aircrew/seat anthropometry, aerodynamic conditions, ejection seat type, and the site, type, and time of occurrence of injury during the ejection sequence.

The anthropometric data consisted of the aircrewmembers' height, weight, age, trunk height, sitting height, leg length, knee-buttock length, and shoulder diameter; aerodynamic data culled included Knots Indicated Airspeed (KIAS), aircraft attitude, altitude AGL and/or MSL, and aircraft type. The ejection seat data consisted of ejection seat type, history of modification, inertia reel type, restraint harness type, mode of ejection initiation, and seat and body position at ejection. The injury data consisted of the type and location of the injury, the number of days grounded and hospitalized, and the results of any radiographs taken. The reports were also screened for severity of parachute opening shock, parachute oscillations, landing terrain, and previous ejections or emergency parachute jumps.

These preliminary findings indicated that of the 399 noncombat F-4 ejections for this time period, there were 43 ejectees who sustained long bone and/or joint trauma that could be attributed to emergency escape sequence. These statistics did not include injuries that were ascribable to parachute landing kinematics. Based upon these data, the extremity injury rate for the decade under study was 10.8%.

Letters were written to the respective medical centers, and post-ejection radiographs and clinical records were retrieved. Based upon clinical and radiographic materials, the injuries were classified as either severe or minimal injuries. Severe injuries were identified as long bone fractures and dislocations, ligamentous injuries, and nerve palseys. The ligamentous injuries were those requiring either surgical repair or prolonged immobilization over one week including meniscal tears. The nerve palseys were either permanent or the temporary ones that lasted more than one day. The severe injuries required more than one week loss from duty. The minimal injuries included: (1) contusions with or without bruising that required no immobilization and resolved in 2 days, (2) lacerations which did not include tendons, major arteries, motor nerves, or compound fractures, (3) sprains (a ligamentous injury that does not cause discontinuity of the ligament) which required no more immobilization than an elastic bandage and did not prevent the aircrewmembers from returning to duty.

In all, there were 95 extremity injuries recorded for the 43 ejections studied. Of these, 61 were identified as severe injuries and 34 were minimal injuries. The severe injuries could be further broken down into 39 injuries of the upper extremity and 22 injuries of the lower extremity.

The severe upper extremity injuries consisted of 25 shoulder, 9 elbow, 3 forearm, and 2 hand injuries. These were attributable to the following forcing functions with respect to the ejection sequence with injury number listed in parenthesis: (a) retraction [1], (b) rocket catapult ignition [6], (c) windblast and windflail [32].

A single retraction injury was found. It consisted of a fracture of the midshaft of the clavicle that was the result of the inertia reel forces during the retraction sequence of the restraint harness shoulder strap.

The six injuries occurring during rocket catapult ignition are listed along with their mechanisms of injury:

- (1) Midshaft ulnar fracture caused by a blow to the ulnar side of the forearm most likely the result of violent contact with sill.
- (2 & 3) A transverse fracture of the humerus with a median nerve palsey caused by a blow to the midarm by the cockpit sill secondary to a midair collision.

- (4) A compound midforearm fracture caused by the arm striking the idler push-pull rods during an inadvertent ejection.
- (5) An ulnar styloid fracture caused by a blow to the dorsal ulnar side of the wrist by the console.
- (6) Intraarticular thumb metacarpalphalangeal (MCP) joint fracture caused by a blow to the ulnar side of the distal thumb due to forceful interaction with the throttle.

The 32 windblast/windflail injuries are listed below with the mechanism of injury:

- (1) 3rd, 4th, and 5th metacarpal fractures caused by the arm flailing and striking either the seat or personnel equipment.
- (2 & 3) Fractured ulnar coronoid process and median nerve palsy secondary to elbow hyperextension.
- (4) Posterior elbow dislocation caused by hyperextension of the elbow.
- (5-8) Posterior elbow dislocation and proximal ulnar fracture caused by hyperextension of the elbow.
- (9 & 10) Humeral supracondylar fracture caused by hyperextension of the elbow.
- (11) Midshaft humeral fracture caused by abduction of the arm and striking the seat or from violent muscular contraction in an attempt to control the arm.
- (12-17) Proximal humeral fractures: i.e., greater tuberosity or humeral neck fractures, with tears of the long head of the biceps tendon or median nerve palsy caused by hyperabduction of the arm.
- (18) Shoulder dislocation, an anterior subglenoid type, caused by hyperabduction of the arm.
- (19-26) Shoulder dislocation with proximal humeral fracture caused by hyperabduction of the arm.
- (27-29) Glenoid fractures associated with dislocated shoulders which were spontaneously reduced, caused by hyperabduction of the arm with or without external rotation of the arm.
- (30-32) Scapular fractures of the spine and neck caused by a blow to the scapula or by hyperabduction of the arm.

From this review, it is apparent that the severe upper extremity injuries were proximal involving the elbow and shoulder. The elbow severe windflail injuries occurred secondary to the hyperextension of the elbow. The shoulder severe windflail injuries occurred secondary to hyperabduction of the shoulder.

The 22 severe injuries of the lower extremities consisted of 2 ankle, 7 calf, 10 knee, 2 thigh, and 1 hip injury. These could also be classified by when they occurred during the ejection sequence: retraction (4), seat ejection (3), and windflail (15).

The four injuries occurring during retraction are listed with their mechanism of injury:

- (1-4) Spiral fractures of the proximal fibula caused by a blow to the fibular head by dual leg garter configuration.

The three injuries occurring during seat ejections are listed with mechanism of injury:

- (1 & 2) Tibial plateau fracture with transverse fibular fracture occurring from a blow to the lateral side of the knee secondary to a midair collision.
- (3) A compound tibial-fibular fracture caused by entanglement of the WSO's (Weapons Systems Operator) foot and leg in the pilot's deployed parachute.

The fifteen injuries occurring during windflail are listed with their mechanism of injury:

- (1) Lateral subtalar dislocation with fracture of the anterior calcaneal facet caused by external rotation of the foot.
- (2) Medial malleolar fracture caused by external rotation and eversion of the foot.
- (3 & 4) Compound comminuted tibial fibular fracture caused by external rotational forces applied to the foot and calf.
- (5 & 6) Internal derangement of the knee, a nebulous diagnosis but usually a torn meniscus, anterior cruciate ligament, medial collateral ligament or capsule, subsequently diagnosed as a torn medial collateral ligament with the mechanism of injury being external rotation of the foot and calf.
- (7-10) Medial collateral ligament tears caused by external rotation of the foot and calf, which may also be accompanied by a valgus moment of the foot and calf.
- (11) Medial collateral ligament and anterior cruciate ligament tear caused by a forced external rotation-valgus moment of the foot and calf.
- (12) Knee dislocation with a torn medial meniscus and medial collateral ligament caused by a violent external rotation force applied to the foot and calf.

(13 & 14) Comminuted fractures of the midshaft of the femur most likely caused by torque applied to the distal femoral shaft.

(15) Posterior rim of the acetabulum fracture that could result from a direct blow to the knee with the hip flexed to 90° or by marked external rotation of the leg forcing the femoral head against the posterior rim of the acetabulum.

From reviewing the mechanism of severe windfall injuries of the lower extremity, all are the result of excessive external rotation.

The majority of the ejections involved the Martin-Baker H7 seat (34 of 43). The rest (9 of 43) involved the Martin-Baker H5 ejection seat. The severe windfall injury rate for the ejections studied from these two seats is 45.5% for the H5 and 47.1% for the H7.

A review of the anthropometric data shows no significant difference between the minimal and severe windfall injury groups for all parameters studied.

A comparison of the KIAS (Knots Indicated Airspeed) between the severe windfall group and the minimal injury group revealed an average KIAS of 403 knots for the severe group and 310 knots for the minimal injury group.

In analyzing the severe injury group, it was noted that the majority (94%) occurred in a nose down attitude as compared to 54% for the minimal injury group. If the attitude of +10° nose down is considered, the severe injury group rate was 92% as compared to only 14% for the minimal injury group. Examination of the two ejections that compromise this 14% for the minimal injury group revealed: (1) an YRF-4C modified aircraft with a large CRT display and console present with the ejection occurring at 10° nose down at 550 KIAS by the WSO after an ejection by the pilot (a reversal of the normal ejection sequence) at 20° nose up at 600 KIAS, and (2) an RF-4C at 10° nose down but flying at only 150 KIAS. The study of these ejections helps highlight the fact that ejections of 10° or greater nose down at KIAS over 200 knots will most likely result in extremity injury.

A comparison of aircraft types showed that the RF-4C group had only a 35% severe extremity injury rate while the rest of the F-4 C, D, E's has a 76% severe extremity injury rate. Since the ejection and restraint systems, aircrewmen and aerodynamic factors are comparable for both groups, the difference is most likely the reconnaissance configuration of the RF-4C, especially the longer nose and anterior oblique camera blister.

From this study it can be seen that the majority of extremity injuries are windfall injuries (77%). The windfall injuries occur at the higher speeds 403 knots as compared to 310 knots, in a nose down attitude 92% as compared to 14%, and more frequently in F-4C, D, E aircraft 76% as compared to the RF-4C 35%.

The mechanism of injury in the windfall injuries was one of hyperextension of the elbows, hyperabduction of the shoulders, and external rotation with or without valgus moment in the legs.

REFERENCES

- Fryer, D.L.: "Operational Experience with British Ejection Seats, a Survey of Medical Aspects," Flying Personnel Research Committee, FPRC/1166, 1961.
- Payne, Peter R., and Fred W. Hawker: "USAF Experience of Flail Injury for Non-Combat Ejections in the Period 1964-1970," AMRL-TR-72-11, Aerospace Medical Research Laboratory, AMD, AFSC, USAF, 1974.

DISCUSSION

D. H. REID, CDR, USN (USA)

What accounts for the significantly greater number of ejection injuries in the USAF RF-4 vice F-4 version? In the absence of ejection system and/or aerodynamic explanation for this first question, could there be an "operational," i.e., flight profile, reason for more injuries in RF vice F versions of F-4 aircraft?

AUTHOR'S REPLY

No real explanation or rationale can be offered. The restraint systems are the same, the crewmen are essentially the same. The speeds and the attitude are the same. The only difference is that the reconnaissance configuration has a somewhat longer nose. You have some blisters for the cameras, larger ducts along the sides to run the heat exchangers. I don't know of any windtunnel studies that tell you the difference of the air flow over the canopy. We've gone to the manufacturer and they can't tell us. They can tell us what happens out on the wings, but they can't tell us what happens in the area of the cockpit.

D. H. Reid, CDR, USN (USA)

I suggest that this may be chance observation not related to escape system or aerodynamic peculiarity between F-4 and RF-4 A/C.

G. R. ALLEN (UK)

To meet the chairman's plea for input/injury data, would it be possible to correlate estimated input aerodynamic and acceleration (ejection) loads with injury?

AUTHOR'S REPLY

The determination when the injuries occurred during the ejection sequence was done from reviewing the accident reports and listening to the aircrew man's description of when he thought he first experienced pain or the injury. In analysis of the injury itself, certain types of injuries are almost exclusively wind flail whereas other types have to come almost directly from a blow. Those usually are during seat firing sequence or from mid-air collision where he was either thrown against the side of the cockpit or had his hand on the stick and got inadvertently ejected. Only in this way can you correlate the injuries with a certain phase of the ejection sequence and the estimated force inputs.

Reference Parameters for Shock Inputs and Shock Tolerance Limits

Dr.-Ing. K.E. Meier-Dörnberg
Institut für Mechanik
Technische Hochschule
D 6100 DARMSTADT
Federal Republic of Germany

A B S T R A C T

Wherever acceptable limits of shock, parameters of design or test conditions must be established, it is necessary to reduce both the data of the applied shocks and the properties of the affected systems to only a few relevant mechanical quantities.

The proposed kind of data reduction which leads to coherent presentation of input and tolerance data, shall define a way of comparing the various design methods to sum up the numerous research results.

1. Properties of an applied shock (the Shock Polygon).
Approximate solutions of the Duhamel Integral (in the time domain) and the Laplace Transform (in the frequency domain) lead to simple relations between time histories, Fourier and response spectra and show that a given shock can be approximated by a set of step functions. On this level of approximation, a set of step values defines an equivalent class of shocks as well as generalized Fourier and response spectra and thus should be used as basic reference parameters. The form of presentation and quality of approximation will be discussed.
2. Shock relevant properties of a system (the Exposure Polygon).
The characteristic and determining property of a system is its shock exposure boundary. With regard to all types of shocks it is a multiparametrical envelope area, but it can be well approximated by a set of different tolerable step loadings. Each tolerable step loading defines a significant quality of the system such as the static or step load capacity, the energy capacity or the deflection ability. The effect of damping, nonlinearities and plasticity will be discussed under different tolerance criteria.

As further examples, some severity criteria, models and methods which are used to describe head or whole body tolerance (e.g. HIC, SI, DRI) will be compared with research data by means of the established reference parameters in order to discuss their mechanical meaning and suitable range of application.

The indicated reference parameters may be used in two levels of application,

1. as generalized research results or safety requirements.
The proposed reference parameters themselves are approximate solutions of a shock problem. They represent the lowest level of approximation, i.e. the highest grade of data reduction which remains meaningful;
2. as reference parameters.
In more detailed or sophisticated researches they may be used as reference parameters for uniform data presentation, because they expose the most significant characteristics of a shock problem.

1. INTRODUCTION

The success of data reduction depends highly on the quality of the chosen reference parameters and the form of data presentation.

We know that many important research results were and are lost by inadequate or misleading interpretation.

The method of data reduction has to consider two main objects:

- it must allow easy comparison of various test and computation results and thus facilitate interdisciplinary cooperation;
- it must be easy in handling but expose the most significant mechanical features of the whole problem.

The proposed method is based upon the wellknown practice used in control techniques and system analysis but is adapted and extended for the purpose of single shock events in nonlinear systems. Experiences and methods in other fields have also been considered, e.g.

shock isolation and design
shock testing and measurement
dimensions analysis and modelling techniques
structural blast or earthquake research
packaging and transportation problems.

The main intentions are:

1. Evaluation and definition of system relevant input quantities and of input relevant system properties as reference parameters.
2. Uniform plotting of the various deduced shock data as input values, exposure limits, safety requirements, test and design parameters, standard Fourier and response spectra in terms of the defined reference parameters.

Obviously there are three different ways or possibilities to reduce the variety of parameters:

- a) Reduction of the given input shock pattern to only few significant values.
- b) Reduction of the real object to a simple mathematical or structural model.
- c) Evaluation of input relevant properties of the affected system.

Each single way should be checked or supported by the two other ways. Such a cross-checking can plainly be facilitated by using the indicated reference parameters.

REMARK

In this paper the input quantities are described in terms of a translational motion of some defined input point of the system, see chapter 2. This is only a matter of easier interpretation and of course no restriction. Other physical quantities can be treated in the same way or be reduced to parameters that have the chosen dimensions, e.g. the ratio of a force and a reference mass is an acceleration, the ratio of a pressure impulse and a mass distribution is a velocity, etc.

2. DEFINITIONS

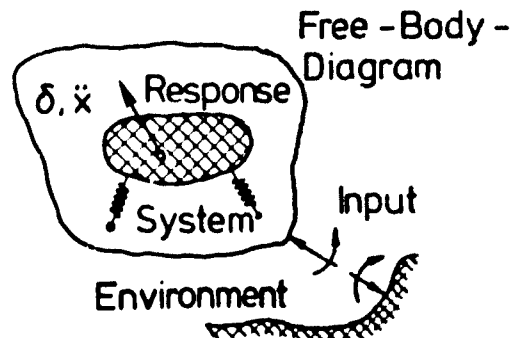
First, we will try to clarify some definitions and terms which sometimes are used in a not well defined and therefore misleading way:

System

A system must clearly be determined by a "free-body diagram" which separates what we call system and what environment. The chosen border depends on the kind of problem and the aim of evaluation. Intrinsic properties of the system are its physical features (material; resilience, damping, plasticity of components; size; weight, etc.)

Input

All kinds of interaction between system and environment (e.g. forces, moments, pressures, motions). In order to identi-



fy a specified input, it is sometimes necessary to include supporting devices or resilient contact areas as parts of the system.

Response

All reactions of the system or its parts, e.g. stress, strain, inner forces, injuries, fracture, absolute or relative displacements and their derivatives.

Tolerance criteria

Tolerance limits of one or more response quantities, e.g. tolerable stress, tolerable deformation, injury level, fragility limit or other performance or comfort criteria.

Input dependent system properties

(usually called dynamic system properties)

Relations between an actual response value with reference to a specified input value in the frequency or time domain, e.g. transfer functions, step responses, dynamic load factor, response to a specific shock input.

Criteria related system properties

Limits of tolerable input values with reference to a specified tolerable response quantity, e.g. performance or exposure limit boundaries, iso-damage curves.

Especially the "criteria related properties" which are the most important statements in biomechanical applications need a distinct identification of the system, the kind of input and tolerance criterion to avoid misunderstandings. A very simple example may illustrate it.

Example: Collision of a resilient support and a rigid mass

a) The free-body diagram includes the mass and all resilient components

a) System:

mass m
linear spring k
natural frequency $\omega = \sqrt{k/m}$

b) Input:

velocity step

c) Response:

half-sine pulse

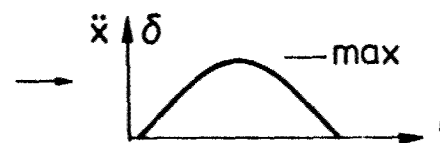
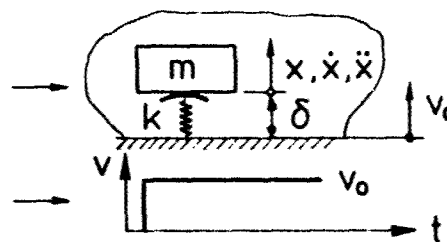
e.g. maximum deformation $\delta_{\max} = v_0/\omega$,
absolute acceleration $\ddot{x}_{\max} = v_0 \omega$
total velocity change $\Delta \dot{x} = 2 v_0$

d) Tolerance criterium:

e.g. tolerable acceleration \ddot{x}_{tol}

e) Performance limit:

tolerable input quantity $v_{0 \text{ tol}} = \ddot{x}_{\text{tol}}/\omega$



b) Free-body diagram excludes all resilient components

a) System:

mass m

b) Input:

must be specified, e.g.
half-sine force pulse $F(t)$

c) Response:

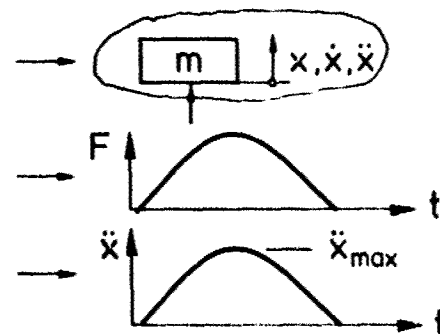
e.g. absolute acceleration $\ddot{x} = F/m$

d) Tolerance criterion:

tolerable absolute acceleration \ddot{x}_{tol}

e) Performance limit:

tolerable input force $F_{\text{tol}} = m \ddot{x}_{\text{tol}}$



3. FORMAT OF DATA PRESENTATION (the Shock Net)

The mechanical problems we have to deal with, have predominantly a multiplicative character, for instance relations between acceleration - velocity - or displacement amplitudes and frequency of a harmonic motion, or integral transformations from the time to the frequency domain. Therefore, it is evident to use logarithmic graphs. Figure 3 shows a graph of the suggested type. It is the wellknown multi-scaled logarithmic net that already has found widespread application in the field of vibration and control techniques but has been adapted and completed for shock problems by some additional scales. In the following chapters we will see that these multiplicative connections will lead to approximate relations between values of time functions and their Fourier or response spectrum without further calculation and that they provide an overall view whether an input shock exceeds a given exposure boundary or meets a specified test requirement. The scales are:

- Abscissa:**
inverted time axis, dimensions s^{-1} , for spectral angular frequencies ω (s^{-1}), natural angular frequencies $\omega(s^{-1})$, equivalent durations $t_{eq}(s)$ so that scale $\omega = \text{scale } \omega = \text{scale } 1/t_{eq}$. Furthermore, a 2π shifted scale for frequencies $f = \omega/2\pi$ (Hz) or natural periods $T = 1/f$ may be provided for convenience.
- Ordinate:**
velocity axis, dimensions m/s, scaled for spectral modulus $A(\omega)$ of acceleration histories $a(t)$, maximum velocities or total velocity changes of shock inputs v_{max} ; velocity response amplitudes $\dot{\phi}$ or tolerable velocities v_{tol} .
- Angled scales for the corresponding displacement values s , dimension (m); acceleration values a , dimension m/s^2 ; and jerk values j , dimension m/s^3 .**

EXAMPLES:

- A harmonic motion is represented by a point on the graph exhibiting the various amplitudes and frequency $\hat{s} \omega = \dot{\phi} = \hat{s}/\omega = \hat{j}/\omega^2$.
- A rectangular acceleration pulse is represented by the intersection of the velocity, acceleration and duration scales $v = a \cdot t$, i.e., each intersection of two lines represents an (equivalent) rectangular pulse.

4. CHARACTERISTIC FEATURES OF SHOCK FUNCTIONS (the Shock Polygon)

4.1 The family of simple shock functions.

The time integrals and derivatives of a pulse function form a family of basic shock functions. Let us take for example an acceleration pulse $a(t)$ and its integrals and derivatives as illustrated in Fig. 1.

We see that for instance a velocity step can be represented either by a jerk double pulse or an acceleration pulse or a displacement rise.

This family can be expanded to other dimensions. Figure 2 shows for instance a similarly structured group of time functions which all have the dimension of acceleration $a(t)$. Further the Laplace transform $A(\omega)$ of these functions is plotted in Fig. 2 where $A(\omega)$ is the modulus, and the spectral angular frequency ω is the Laplace operator.

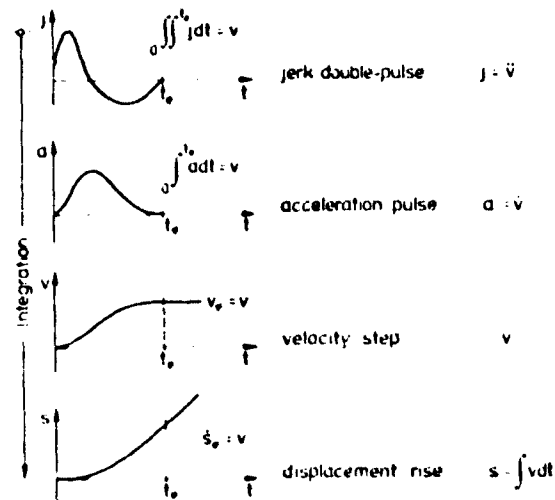


Fig. 1 A group of identical shocks

Ideal shock functions $t_e \rightarrow 0$.

In the special case of ideal shock functions, $t_e \rightarrow 0$, the following exact relations exist:

Time domain		Frequency domain	
		Modulus	Phase
double pulse $a(t)$	displacement step s	$A(\omega) = s/\omega$	$\phi(\omega) = \pi/2$
pulse $a(t)$	velocity step v	$A(\omega) = v$	$\phi(\omega) = 0$
step $a(t)$	acceleration step a	$A(\omega) = a/\omega$	$\phi(\omega) = -\pi/2$
rise $a(t)$	jerk step j	$A(\omega) = j/\omega^2$	$\phi(\omega) = -\pi$

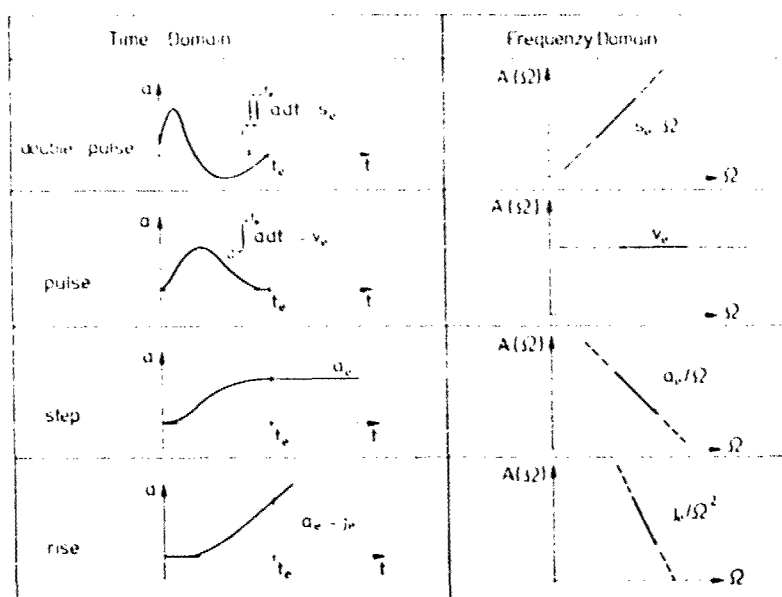


Fig. 2 A family of shock functions $a(t)$ and their spectral moduli $A(\Omega)$

We see: In the special case $t_e = 0$, the various functions $a(t)$ are represented by straight infinite lines in the logarithmic frequency net. If we use the proposed format with ordinate scales $A(\Omega)$, v and angled scales for a , s , j , each of these lines represents both the step values (time domain) and their spectral moduli and thus the exact solution of the Fourier or Laplace transform.

More general shock functions $t_e \neq 0$.

Now we will study time and frequency relations of more general functions.

For all shock functions (functions having only values in the positive time range) Fourier and Laplace transform are identical when basing on the specific definition

$$X(\Omega) = \int_0^\infty x(t) e^{-i\Omega t} dt = \int_0^\infty x(t) e^{-pt} dt$$

where Ω is the spectral angular frequency and (the imaginary part of) the Laplace operator $p = i\Omega$, respectively.

Using the limit theorems of Laplace theory we find the asymptotic modulus values if $x(0)$ and $x(\infty)$ exist

$$\lim_{p \rightarrow \infty} [p X(p)] = \lim_{t \rightarrow 0} [x(t)]$$

$$\lim_{p \rightarrow 0} [p X(p)] = \lim_{t \rightarrow \infty} [x(t)]$$

Taking for example the shock function $a(t)$ of Fig. 3, these asymptotic relations can be applied to the derivative j , because $j(0) = j_{\max}$, and to the double integral s , because $s(\infty) = s_{\max}$ with the resultant asymptotes [1,2]

$$\Omega \rightarrow \infty : \Omega J(\Omega) = j_{\max}$$

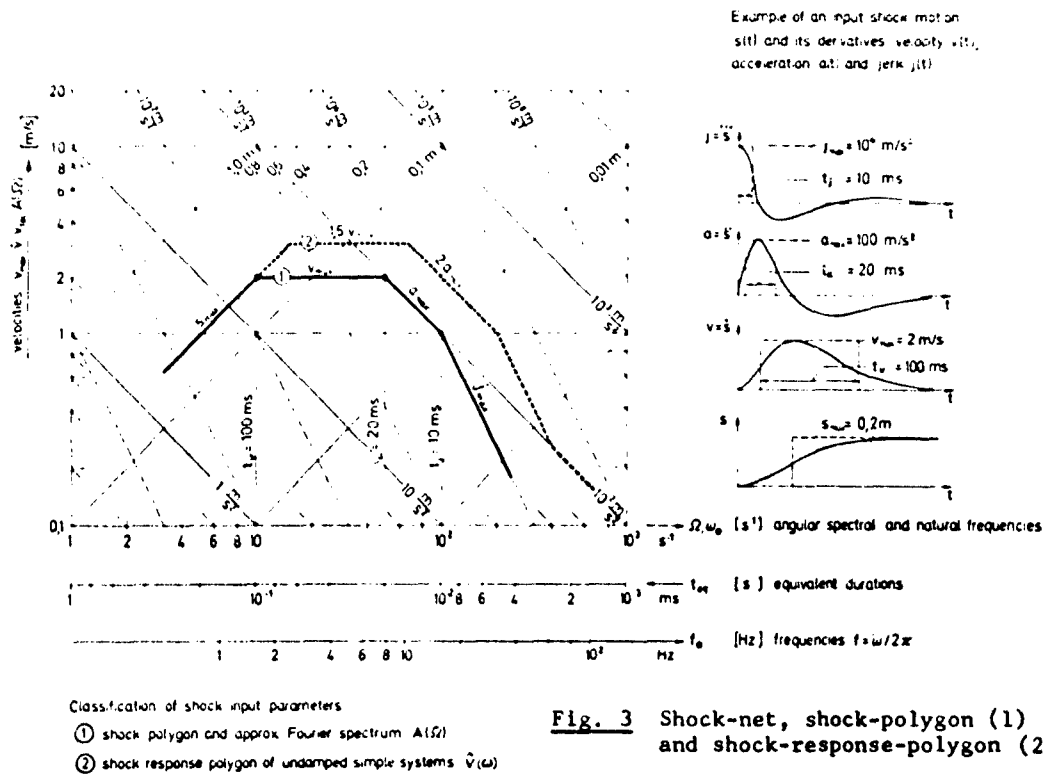
$$\Omega \rightarrow 0 : \Omega S(\Omega) = s_{\max}$$

Because $J(\Omega) = \Omega A(\Omega)$ and $S(\Omega) = A(\Omega)/\Omega^2$, the final results are the asymptotic modulus values $A(\Omega)$

$$\Omega \rightarrow \infty : A(\Omega) = j_{\max}/\Omega$$

$$\Omega \rightarrow 0 : A(\Omega) = s_{\max} \cdot \Omega$$

as lines j_{\max} and s_{\max} in the proposed format.



Approximations in the medium frequency range in setting $t_j \rightarrow 0$ and $t_a \rightarrow 0$ are:

$$t_j \rightarrow 0 : A(\Omega) = a_{\max}/\Omega$$

$$t_a \rightarrow 0 : A(\Omega) = v_{\max}.$$

The polygon, Fig.3, line (1), which is formed by the values s_{\max} , v_{\max} , a_{\max} and j_{\max} of a given function $a(t)$ is therefore an approximate solution of the Fourier transform $a(t) \leftrightarrow A(\Omega)$. Let us call it the SHOCK POLYGON.

The intersections of this polygon exhibit very informative relations between a time function and its spectrum. The ratios of two maximum values of two successive time functions define certain time values which may be defined as equivalent durations, e.g.

$$\text{equivl. duration of (positive) jerk} \quad t_j = \frac{a_{\max}}{j_{\max}},$$

$$\text{equivl. duration of (positive) acceleration} \quad t_a = \frac{v_{\max}}{a_{\max}},$$

$$\text{equivl. duration of (positive) velocity} \quad t_v = \frac{s_{\max}}{v_{\max}}.$$

They represent the duration of an area equivalent rectangular pulse.

The polygon intersections in the frequency domain exhibit another group of relations.

$$\text{corner frequency } \Omega_j = \frac{j_{\max}}{a_{\max}}$$

$$\text{corner frequency } \Omega_a = \frac{a_{\max}}{v_{\max}}$$

$$\text{corner frequency } \Omega_v = \frac{v_{\max}}{s_{\max}}.$$

The above definitions establish a close connection between the time and frequency domain

$$t_j = \frac{1}{\Omega_j}, \quad t_a = \frac{1}{\Omega_a}, \quad t_v = \frac{1}{\Omega_v},$$

which lead to the stated interrelation between the abscissa scales $\Omega_{eq} = 1/t_{eq}$.

Besides, the corner frequencies or equivalent durations mark per se the validity range of approximation in which a shock function can be replaced alternatively by an acceleration, velocity or displacement step.

The approximation of a Fourier spectrum by the maximum values of time derivatives is very close for all functions with one discontinuity, for example all combinations of e-functions without time lags (phase minimum functions). It gradually becomes less precise for rougher or more oscillating histories.

4.2 Construction of an upper spectrum limitation.

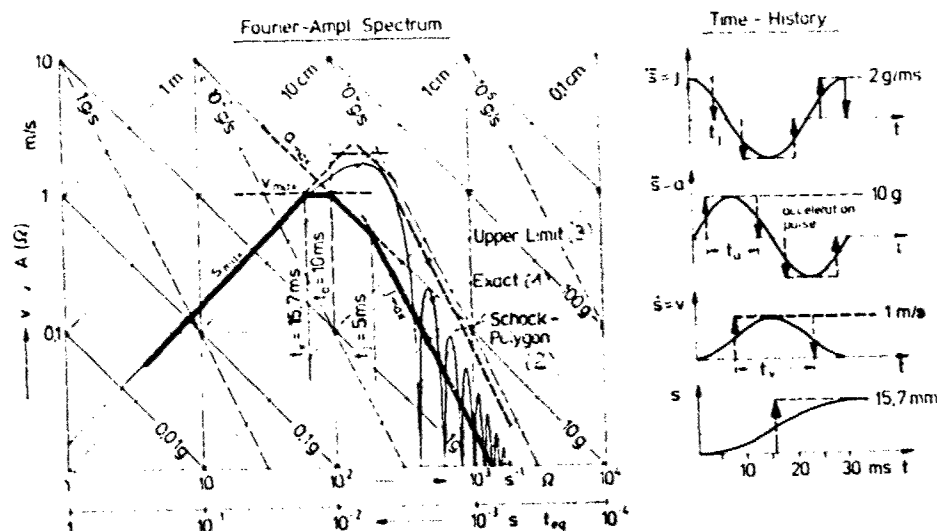


Fig. 4 Double-sine acceleration pulse $a(t)$, its exact Fourier spectrum (1), its shock polygon (2) and the upper limits of spectral values (3)

The upper limits of a spectrum may be of special interest for acoustics and structural design work where linear, small-damped systems have to be investigated. In contrast, mean spectral values which are represented by the shock polygon are more significant for safety or statistical performance applications.

The upper limit of a spectral modulus can be found by summing up all changes (ups and downs) of the time function instead of using the simple maxima values. Figure 4 shows as an example a double-sine acceleration pulse, its exact Fourier spectrum, the shock polygon formed by the simple maxima s_{\max} , v_{\max} , a_{\max} , j_{\max} , and the upper limit formed by the sums s_{\max} , $2v_{\max}$, $4a_{\max}$, $8j_{\max}$. (More information and examples in [1]).

4.3 Valuation of the deduced reference parameters.

We must ascertain now that the deduced reference parameters not only exhibit plain relations between time functions and their spectra but that they are also relevant input parameters with respect to system responses or tolerance limits.

The convolution integral

Linear system analyses, using approximate solutions of the Duhamel or convolution integral lead directly to the same result and show that the exhibited maxima of a shock input and its derivatives are predominant and response relevant values of a shock input [3].

Shock response spectra

The so-called response spectra are simply pointwise diagrams of specified response values of an ensemble of equal systems by varying their natural frequency. Response spectra thus are another kind to describe an input shock. Otherwise expressed the applied shock is weighted (filtered) by a specific type of systems.

The simplest response spectrum is that of the oscillatory parts of the residual response of an undamped simple linear system.

A comparison of the Fourier spectrum with this residual response spectrum by means of the Fourier integral, [2],

$$A(\Omega) = \int_0^{te} a(t) e^{-i\Omega t} dt$$

and the convolution integral

$$\phi = \omega \delta = \int_0^t a(t) \sin \omega(t-\tau) d\tau / \max$$

confirms the well-known similarity of both solutions. The corresponding values are

spectral modulus and velocity response amplitude
 $A(\Omega) \leftrightarrow \phi$,

spectral angular frequency and natural system frequency
 $\Omega \leftrightarrow \omega$.

Conclusion: In the proposed format of the shock net, where scale Ω = scale ω , and scale $A(\Omega)$ = scale ϕ , the Fourier spectrum and this residual response spectrum have exactly the same curve thus, the shock polygon is not only an approximation to the Fourier spectrum but also to this response spectrum.

4.4 Relations between response spectra and exposure limit boundaries.

In linear systems the relation between a maximax response spectrum and the corresponding exposure limit boundary is evident. Both solutions are merely inverse interpretations of the same problem.

A maximax response spectrum exhibits the maximum response values of a set of equal systems excited by one specific shock input as function of the system frequency ω . Figure 5a shows the max. acceleration response \ddot{x}_{\max} of damped linear simple systems (ω) to a double-sine acceleration input which is defined by the value v_{\max} and the equivalent duration t_a .

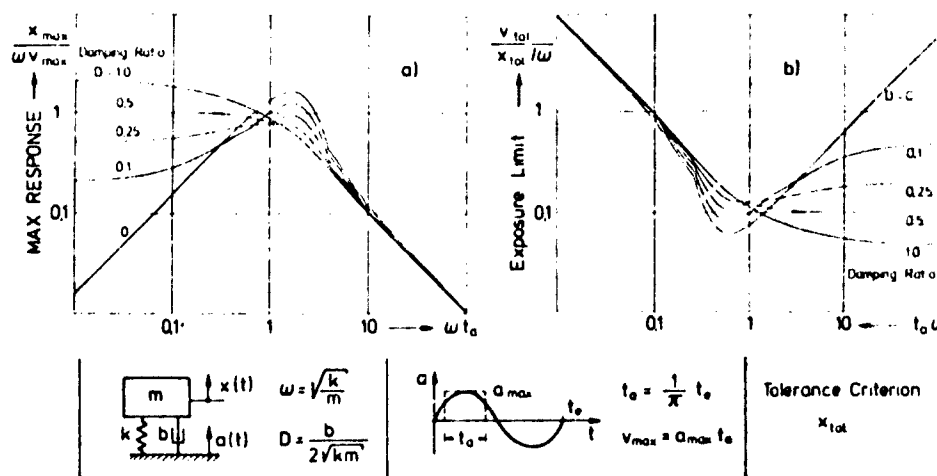


Fig. 5 Equivalence of response spectra a) and exposure limit boundaries b) in linear systems

An exposure limit boundary exhibits the limit values of a set of equally shaped input shocks which excite a specified tolerable response value of the given system as function of the shock durations. Figure 5b shows the input tolerance values v_{tol} of all double-sine input shocks of various equivalent durations t_a . The tolerance criterion is the tolerable system response \ddot{x}_{tol} .

For linear systems and logarithmic plotting the two results in Fig. 5a, b are reciprocal congruent curves.

In linear systems the approximate response spectrum and the exposure boundary respectively can easily be developed from the shock polygon by calculating the various step responses, i.e. weighting each polygon range by a corresponding "load" factor.

Figure 3 line (2) shows the standard "shock spectrum" for relative displacement and absolute acceleration of single-degree-of-freedom systems with small or no damping as

used in the field of shock testing and isolation. The weighting factors are $1 s_{\max}$; $1,5 v_{\max}$ and $2 a_{\max}$ up to $\omega = 2/t_j$.

In nonlinear systems a response spectrum is meaningless and not defined. Yet the exposure boundary which is a significant system property, remains meaningful. (See chapter 5.)

4.3 Summary and instructions.

The quantifying of an input shock relies on a suitable assessment of typical peak values of a shock function and its appropriate derivatives and integrals, e.g. max. displacement, velocity, acceleration, and jerk if applicable, see Figure 3. The peak values are plotted as lines parallel to the appropriate axes on the SHOCK NET. (See chapter 3.) They form the SHOCK POLYGON from which several important relations can be deduced as under:

- (a) The time coordinates of the intersections indicate the equivalent pulse durations, e.g.
 - equiv. jerk pulse duration (or rise-time of the acceleration pulse) $t_j = a_{\max}/j_{\max}$
 - equiv. acceleration pulse duration $t_a = v_{\max}/a_{\max}$
 - equiv. velocity pulse duration $t_v = s_{\max}/v_{\max}$
- (b) The shock polygon approximates a given shock by a couple of step functions, e.g. an acceleration step a_{\max} , a velocity step v_{\max} , and a displacement step s_{\max} . The intersections indicate the validity range of approximation.
- (c) The shock polygon is an approximation to the modulus of the Fourier spectrum $A(\omega)$ of the acceleration $a(t)$, i.e. it approximates the Fourier transform of $a(t)$. Thus it is a generalized Fourier spectrum.
- (d) It also approximates the residual response spectrum of undamped single-degree-of-freedom systems with natural angular frequencies ω . The responding vibration amplitudes ξ ; $\dot{\xi}$ or $\ddot{\xi}$ can be read off the corresponding scales for displacement, velocity or acceleration.

Notes. The approximate relations b), c), d) fit well for all shocks with only one discontinuity, they gradually become less precise for rough, oscillating histories. To obtain suitable peak values, the shock pattern may be smoothed or filtered with regard to the frequency range of interest.

If some of the values, e.g. j_{\max} , a_{\max} or s_{\max} are not known (or are infinite), the polygon reduces to a straight line, e.g. v_{\max} which indicates that all other values are assumed to be infinite.

Shocks having the same shock polygon, have approximately the same frequency content but may differ more or less in phase characteristics. The remaining additional information of an actual pulse shape has only second-order quality.

In the case of transient vibrations (e.g. earthquake motions) the generalized Fourier spectrum of a polygonal type is a shock polygon and thus defines the basic parameters of an equivalent shock.

Independent of the application of the relations b) - d) the defined peak values and equivalent durations should be used as descriptive shock parameters.

Generalized (approximate) response diagrams can be obtained from the shock polygon by calculating the various step responses of the specific type of systems (e.g. damped, undamped) and the response of interest (e.g. max. relative displacement, absolute acceleration). A generalized shock response diagram, thus originates in the polygon by weighting each range. It may be called SHOCK RESPONSE POLYGON.

5. CRITERIA RELATED SYSTEM PROPERTIES (the Exposure Polygon).

The ensemble of shock inputs of the same pattern (e.g. all double-sine acceleration pulses, Fig. 5b) affecting the same response value (e.g. a tolerable relative displacement or stress) form a specific exposure limit boundary. Each specific tolerance criterion creates another special limit boundary.

In general, the exposure limit boundary for a specific system with one criterion considering all various types of shock inputs is a multi-parametrical envelope area which can be obtained by means of modelling techniques or numerous series of shock tests.

A useful approximation which reduces the envelope area to a simple line, is the envelope of all tolerable shock groups represented by their shock polygons. As further approxi-

mation, which represents the highest grade of meaningful data reduction, this boundary can be approximated by a polygonal line, see Figure 6, which may be called the EXPOSURE POLYGON.

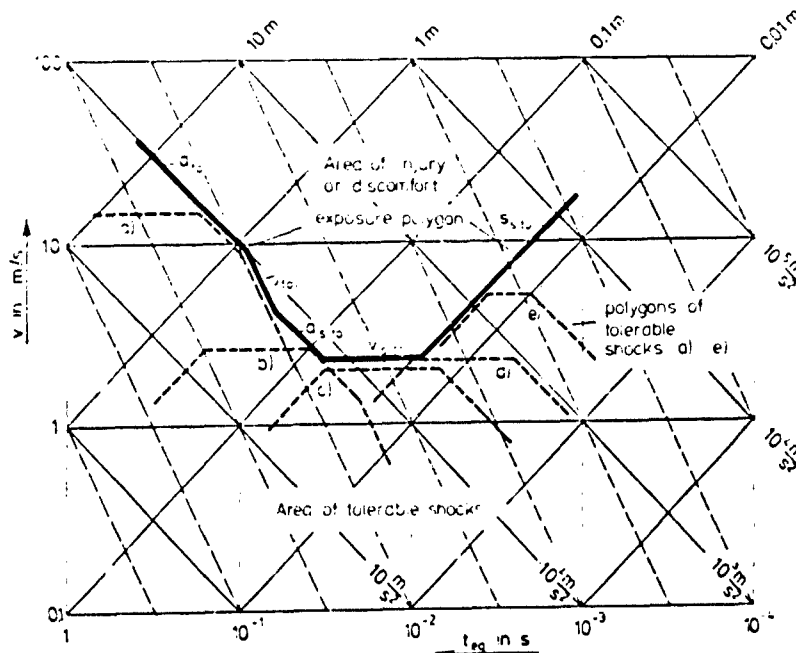


Fig. 6 Definition and elements of the exposure polygon

The exposure polygon requires the following shock relevant properties of the affected system; see Figure 7 as an example:

- a) Steady acceleration limit a_{tol} (static load capacity):
the asymptotic value for tolerable long-duration shocks with low jerk values ($j_{max} \rightarrow 0$).
- b) Acceleration step limit, a_s tol:
the value of the tolerable acceleration step (sudden applied load, $j_{max} \rightarrow \infty$) which is related to the steady acceleration limit by means of the dynamic load factor $DLF(\omega) = a_{tol}/a_s$ tol. The transition range from the steady acceleration limit a_{tol} to the acceleration step limit a_s tol is given by the tolerable jerk j_{tol} or the rise-time t_j^* which is approximately $t_j^* = 10/\omega$.
- γ) Velocity step limit v_s tol:
the shock tolerance for relatively short acceleration pulses which is related to the energy capacity or the wave resistance of the system.
- δ) Displacement step limit s_s tol:
the shock tolerance value in the case of sudden displacement changes which is related to the deflection ability of the system. In viscous damped or continuous systems s_{tol} is zero.

The shock exposure polygon applies approximately to all types of shock, and thus is a shock relevant property of the system and its tolerance criterion.

Figure 7 shows as an example exposure polygons of the spinal injury model [5,6]. The chosen tolerance criteria are

- a) tolerable deflection $\delta_{tol} = 0.36; 1.1; 3.6$ cm
resp. $DRI = 1; 3; 6$ g
- b) tolerable absolute acceleration $\ddot{x}_{tol} = 10; 30; 100$ m/s²

The most simple computations of step responses are carried out in [3]. Figure 7 may give us some basic information on the behavior of the system and the influence of the chosen criteria:

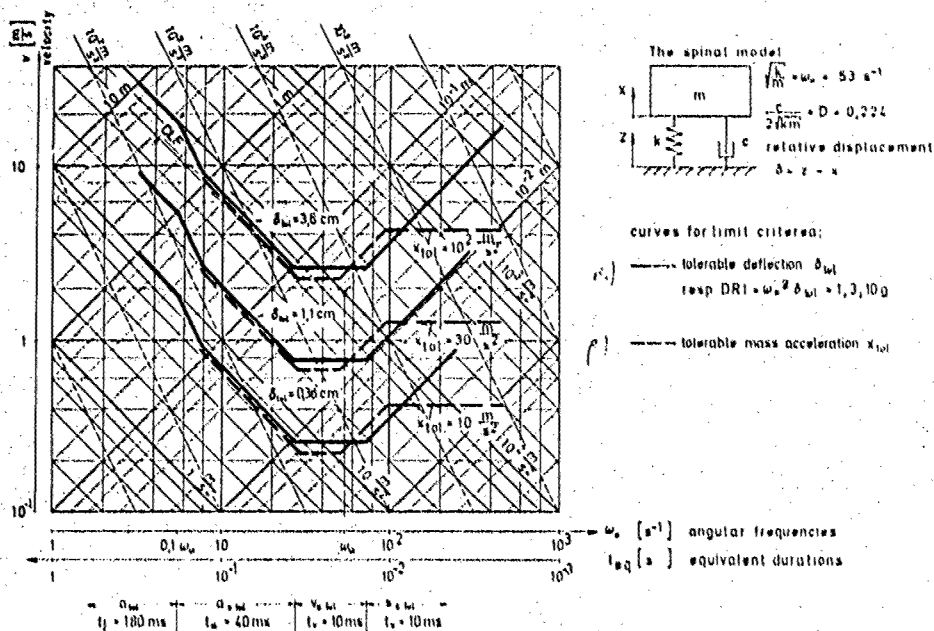


Fig. 7 Exposure polygons of the spinal model

- the intersection of lines a_{tol} and s_{tol} has the abscissa value ω_0 .
- in the range of short duration (double) pulses $t_v < 10$ ms, the different criteria δ_{tol} and \ddot{x}_{tol} lead to obviously different limits because of the system damping. In the range $t_v > 10$ ms the influence of the damping force is likewise small;
- long duration pulses with small jerk values or long rise-times $t_j < 180$ ms respectively can be treated as static loads;
- in the range $t_j > 180$ ms = $10/\omega_0$ the "overshoot" increases and reaches the value of the dynamic load factor of about 1.4 for sudden acceleration rise;
- the pulse duration $t_a = 40$ ms = $1.4/\omega_0$ separates the quasistatic and impulsive load range;
- the value $v_{s\ tol}$ represents the energy capacity E of the system according to $E_{tol} = m v^2/2$;
- the comparison of Fig. 5b and Fig. 7 will explain more clearly the influence of system damping with regard to the acceleration criterion \ddot{x}_{tol} .

SUMMARY AND INSTRUCTIONS.

The exposure polygon as an approximate tolerance boundary is a useful tool in orientation and planning for more detailed theoretical or experimental studies. It defines typical criteria related system properties and the range of their relevance;

- static load capacity ($t_j > 10/\omega_0$)
- step load capacity ($t_a > 1/\omega_0$)
- impulse load capacity ($t_a < 1/\omega_0$)
- deflection ability ($t_v < 1/\omega_0$)
- dynamic load factor ($1 < \omega_0 t_j < 10$)

In linear systems the term ω_0 represents the lowest system frequency, in nonlinear systems an equivalent corner frequency.

In damped or degressive nonlinear systems (e.g. elastic-plastic restraint) the influence of the actual pulse shape is still less than in undamped linear systems, [3].

Experts experienced in harmonic system response and "Bode-diagrams", will recognize at once the relationship between the tolerable step loads which form the exposure polygon and the driving point mobility, where the real part of mobility relates to the tolerable velocity step and the imaginary parts (real parts of compliance and inverse apparent mass) are comparable with the displacement and acceleration step respectively. Thus the transition from vibration to shock problems can easier be understood when the same kind of representation will be used in both areas.

The proposed criteria related system properties are easy to calculate or to determine by test because they are simply step responses. They furnish the basic information for the shock resistance of the system.

6. EXAMPLES AND REMARKS.

6.1 Total or Equivalent Pulse-Durations

Some authors, [7,8] for example, use the total pulse duration T and the peak acceleration a_{\max} as reference parameters for comparing the effect of shocks, see Fig. 8.a. When using the equivalent pulse duration t_e instead of T (Fig. 8.b), the curves shift together in the short duration range, and the influence of the actual pulse shape turns out to be less important. The resultant curves only differ noticeably in the long duration range because the rise-times $t_r = a_{\max}/j_{\max}$ of both pulses are quite different. The difference would disappear almost completely if the comparison of various pulses would be based on the proposed reference parameters including the jerk j_{\max} , see Fig. 12 and the displacement s_{\max} , if applicable.

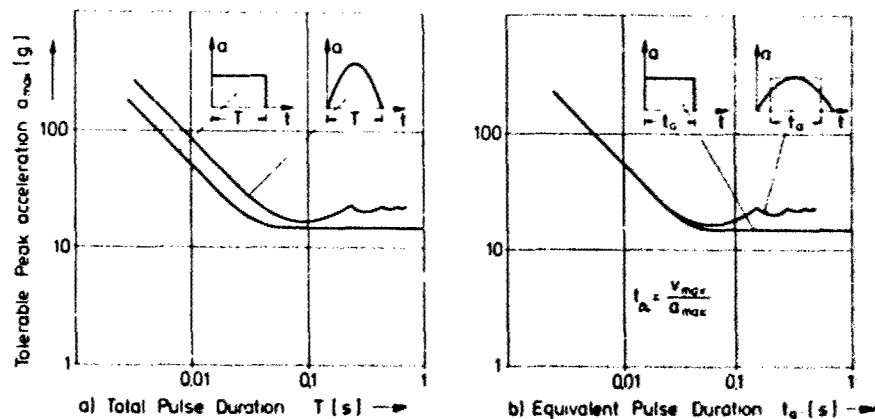


Fig. 8 Significance of reference parameters in comparing exposure limits

6.2 Shock Performance of Ski-bindings

Own researches in shock performance of safety ski-bindings [3,9] may serve as a further example. The problem was broken down into two groups of problems.

- Evaluation of the steadiness (respectively dive) limit boundary of the skier against horizontal shocks in frontal and cross direction in order to specify the necessary shock performance of the ski-binding. I. e. the binding has to stay closed as far as the skier can master the situation, to avoid mis-releasing.
 - The shock performance boundaries of various ski-bindings at different adjustment levels.
- a) Steadiness to frontal shocks.

In order to reduce the number of volunteer shock tests and to avoid risky ranges, static tests were performed at first. Figure 9 shows the test situation: a man standing in fixed ski-shoes was pulled forward by a horizontal force at the height of the reduced body mass. Figure 10 represents the obtained average load deflection curve of several tests with one volunteer. As tolerance criterion in the static and dynamic tests served the maximum tolerable deflection $\delta_{tol} = 0.6$ m of the body.

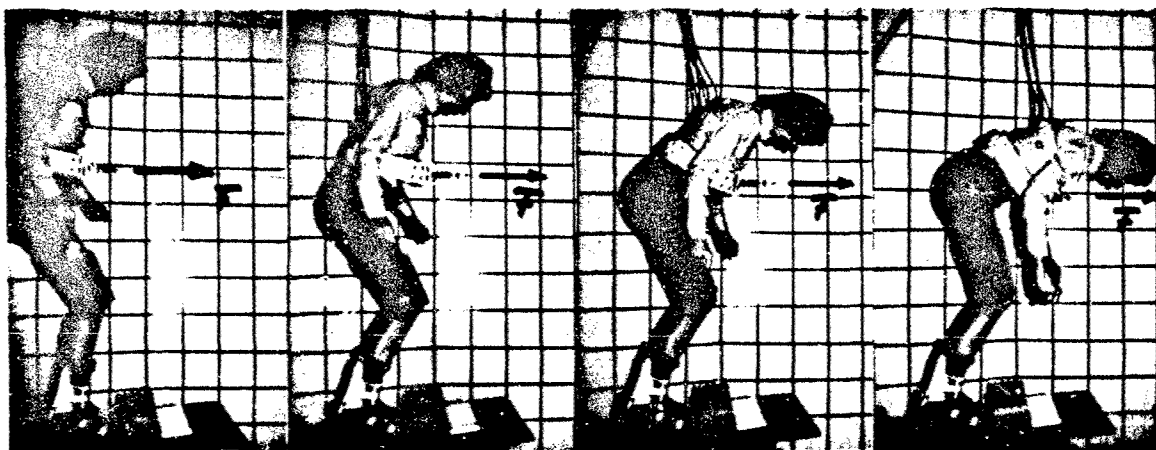


Fig. 9 Static load-deflection test of a man in fixed ski-shoes

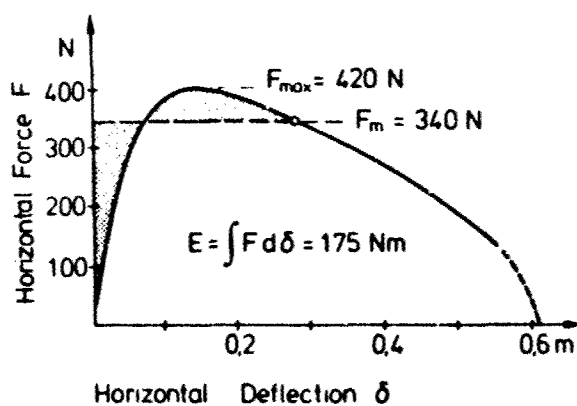
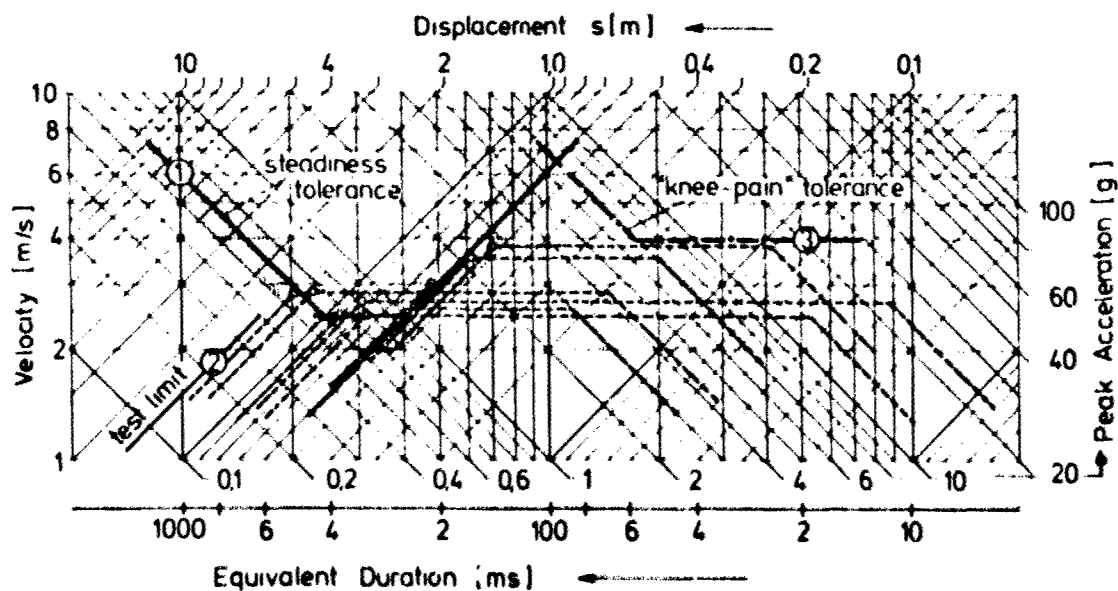


Fig. 10 Load-deflection-curve obtained in the static test (Fig. 9)

Fig. 11 Steadiness of a standing man to horizontal shock motions obtained by static tests and its verification by shock tests



Assuming a test equivalent reduced mass $m = 56$ kg of about 80 % of the man's weight, the exposure polygon values could be calculated from the static test result:

$$\text{acceleration step limit } a_{s \text{ tol}} = F_m/m = 0.6 \text{ g}$$

$$\text{velocity step limit } v_{s \text{ tol}} = \sqrt{2E/m} = 2.5 \text{ m/s}$$

$$\text{displacement step limit } s_{s \text{ tol}} = \delta_{\text{tol}} = 0.6 \text{ m}$$

The obtained step values are plotted in Figure 11, line (1) as exposure polygon. To verify or adjust this "static" exposure polygon only few shock tests need be performed. Some shocks which met the criterion s_{tol} are plotted in Figure 11 as shock polygons. Although the shapes of the used pulses were varied, the shape had no significant influence on the result.

Line (2) in Figure 11 indicates the displacement capacity of the test equipment of 1.5 m and thus the upper limit of equivalent velocity durations t_v of about 500 ms which could be produced. In the range of short duration double pulses with high accelerations and velocities but tolerable displacement values quite another tolerance boundary was reached which is characterized by the "volunteer knee or leg pain" tolerance criterion, line (3). The "knee pain" tolerance limit depends highly on the flexibility of the ski-shoes.

b) Shock performance of ski-bindings.

In frontal direction the required shock performance of the ski-binding depends greatly on the flexibility of the ski-shoes so that a performance requirement for the binding itself cannot be specified. According to Figure 11, line (1) the flexibility of shoe plus binding should be at least constructed so as to match a velocity step of about 3 m/s without mis-releasing and without reaching the "knee pain" or leg fracture tolerance, (9).

In cross direction, however, the steadiness limit of the skier turned out to be the only significant shock performance requirement for the binding itself which was found to be an input velocity step of 2 m/s, (2).

6.3 MEAN ACCELERATIONS AND TOTAL VELOCITY CHANGES.

Investigators in the field of crash test and car safety research are accustomed to use total velocity change Δv and mean acceleration a_{mean} as reference parameters in order to define a crash situation. This kind of problems deals with pulse functions only having "one side" values which of course essentially reduces the variety of parameters.

The original mechanical quantities turn out to be the response of the system "car", i.e. the total velocity change $\Delta x = x_2 - x_1$ and the deformation δ of the crash zone. (See chapter 2.) The calculations

$$\begin{aligned} \text{mean acceleration } a_{\text{mean}} &= \Delta \dot{x}^2 / 2\delta \\ \text{and total pulse duration } T &= 2\delta / \Delta \dot{x} \end{aligned}$$

are only a transformation to some other plain values (input to system "cell"), but provide no additional information. Of course, if no other information is available, for instance in collision case studies, the approximation of the actual shock input by a rectangular pulse is near at hand but as speculative as any other assumption.

If additional data can be obtained, e.g. acceleration histories in field tests or load deflection curves of the crashing components they should be carried out at least to provide the peak acceleration (or a kind of shock crest factor $a_{\text{max}}/a_{\text{mean}}$) or jerk, if applicable, as minimum additional information.

In many papers, e.g. [10], the collected whole body or head tolerance data are presented as plots of tolerable mean accelerations versus velocity change. Disadvantages of such a presentation are for instance:

- the effect of jerk or acceleration rise-time cannot well be incorporated,
- the asymptote of the exposure boundary for long duration acceleration pulses relies on system relevant smoothed peak values and not on mean values,
- double pulse (displacement step) effects cannot be presented,
- relations between shock and vibration thresholds cannot be developed.

6.4 SINGLE NUMBER TOLERANCE INDICES.

Single number tolerance criteria if not related to a well defined model or test situation need to be handled and applied with caution. Two wellknown representatives are the

Gadd Severity Index GSI

and the slightly modified

Head Injury Criterion HIC.

The single number weighting of problem so multiparametrical, is an extensive data reduction and consequently leads to a substantial loss of basic information. Let us try to value the mechanical relevance of these quantities by means of the shock net and the proposed reference parameters. Figure 12 presents some "one side" acceleration pulses having equal equivalent rise-times t_j , durations t_a , and the corresponding GSI and HIC values.

When using the proposed reference parameters the GSI and HIC valuations differ obviously not very much and the influence of the pulse shape is remarkably small. Figure 13 even accentuates this statement: the influence of GSI weighting indeed turns out to be a narrow band of about 1 dB. Furthermore, Fig. 13 exhibits the original idea and quality of the GSI to be an overall human tolerance limit including blackout phenomena at long duration accelerations as well as skull fracture in the short duration range. The weighting exponent 2.5 of acceleration has no other background or intention as to produce the inclination 1:0,6 of an overall fitting line.

6.5 HEAD TOLERANCE TO FRONTAL SHOCK

No other special shock tolerance problem seems to yield more secondary papers than the head injury problem, and with this the confusion increases. Let us make another attempt.

The head injury criterion HIC for instance sometimes is understood to be

- the evaluation of input quantities, in other words an input tolerance limit
- a true tolerance criterion, i.e. a specified tolerable response value. (Definitions see chapter 2.)

If b) applies, a clear specification of the nature and location of the response value must be stated or a specified model be constructed. The relation between a) and b) is the transfer function from a given input point to the point of measurement. It may enlarge or attenuate the input quantity depending on whether the input load has a more static or more impulsive character.

If a) applies, the acceleration history of the contact area between head and (ductile) target must be measured and evaluated. Now we will try to compare some data of head tolerance to frontal shock by using the proposed shock net and the reference parameters.

Figure 14 illustrates the various attempts to substitute the Wayne-State Tolerance-Curve by simple models. A fifth model was added by the author. Because no other information about the "Wayne-State pulse shape" is available and because the tolerance curve is presented by insignificant mean acceleration values, a special pulse shape had to be assumed. Obviously, the assumption for determining the parameters and tolerance criteria of almost all models was a triangular pulse. Figure 14 shows the deduced model parameters, the chosen tolerance criteria and further in the last line the corresponding exposure polygon values.

More original skull fracture data are listed below:

Lissner 1960

Free fall tests, 50% skull fracture, tolerable velocity step $v_{tol} = 5 \text{ m/s}$
measured accelerations (responses?) $\ddot{x}_{max} = 176 \pm 210 \text{ g}$

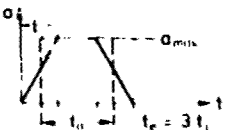
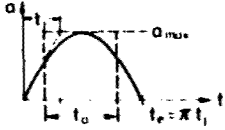
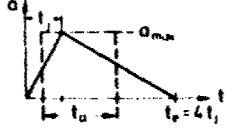
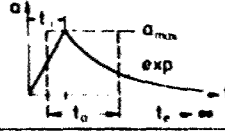
Shocks with equal parameters $a_{max} = v_{max} = j_{max}$	Gadd - Severity - Index $GSI = \int_0^{t_a} \left(\frac{a}{g}\right)^{2.5} dt$	Head Injury Criterion $HIC = \left[\frac{1}{\Delta t} \int_{t_1}^{t_2} \ddot{x} dt \right]^{2.5} \Delta t$
	$GSI = \left[0.9 \frac{a_{max}}{g} \right]^{2.5} t_a$	$HIC = \left[0.87 \frac{a_{max}}{g} \right]^{2.5} t_a$
	$GSI = \left[0.88 \frac{a_{max}}{g} \right]^{2.5} t_a$	$HIC = \left[0.84 \frac{a_{max}}{g} \right]^{2.5} t_a$
	$GSI = \left[0.8 \frac{a_{max}}{g} \right]^{2.5} t_a$	$HIC = \left[0.76 \frac{a_{max}}{g} \right]^{2.5} t_a$
	$GSI = \left[0.72 \frac{a_{max}}{g} \right]^{2.5} t_a$	$HIC = \left[0.66 \frac{a_{max}}{g} \right]^{2.5} t_a$

Fig. 12 Comparison of GSI and HIC valuations by means of the proposed reference parameters

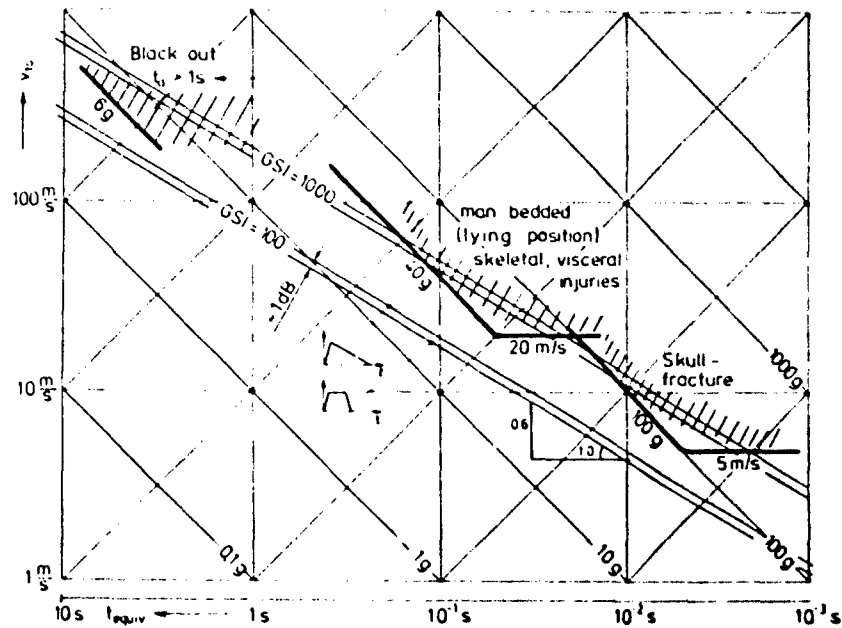


Fig. 13 Origin and intention of GSI valuations

Author	Wayne State Tolerance Curve H R Lissner 1962	JTI J. - Tolerance Index A. Stohr 1966	HBM Revised Brain Model W R S Fan 1972	EOI Effective Displace- ment Index I. Brinn 1970	MSC Mean Strain Criterion R L Stalnaker 1970	MD 1978
System Properties	 $a_{100} = 100g$ $T = 10ms$	 $\omega_0 = 635 s^{-1}$ (100 Hz) $D = 1.0$	 $\omega_0 = 175 s^{-1}$ (28 Hz) $D = 0.4$	 $\omega_0 = 462 s^{-1}$ (77 Hz) $D = 0.7$	 $m_1 = 0.27 kg$ $m_2 = 4.54 kg$ $b = 0.76 N/mm$ $c = 0.25 Ns/mm$	 $\omega_0 = 460 s^{-1}$ (73 Hz) $D = 0.3$
Tolerance-Injury Criterion	50% skull fracture ($a_{100} = 150g$)	fat deformation $\delta_{100} = 2.35 mm$	fat deformation $\delta_{100} = 32 mm$	fat deformation $\delta_{100} = 3.8 mm$	fat strain $\epsilon_{100} = 8.1\%$ ($\delta_{100} = 0.9 mm$)	fat deformation $\delta_{100} = 6.5 mm$ or fat acceleration $a_{100} = 150g$
Shock limits polygon values	$v_{100} = 4.2 m/s$ $a_{100} = 100g$	$v_{100} = 4.2 m/s$ $a_{100} = 95g$	$v_{100} = 9.3 m/s$ $a_{100} = 74g$	$v_{100} = 4.1 m/s$ $a_{100} = 84g$	$v_{100} = 1.25 m/s$ $a_{100} = 87g$	$v_{100} = 4.2 m/s$ $a_{100} = 100g$

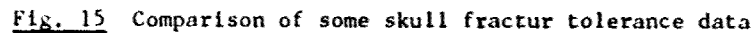
Fig. 14 Wayne-State head tolerance curve and its substitutions by simple models

v. Gierke, Goldmann 1961 [8].
Energy capacity of skull 50 - 75 Nm,
Assuming an equivalent mass of 5 kg,
the tolerable velocity step is $v_{tol} = 4.5 \div 5.5 m/s$

Swearingen 1967
Tolerable input force 10 kN
measured tolerable accelerations (response?) $\ddot{x}_{tol} = 200 g$

Daniel, Patrik 1975:
Tolerable acceleration (responses?) $\ddot{x}_{tol} = 165 g$

Let us discuss these data with the use of Figure 15. It shows the Wayne-State Curve, represented by tolerable input peak accelerations having the polygon values $a_{tol} = 100 g$ and $v_{tol} = 4.2 m/s$. The tolerable velocity step seems to be well confirmed by the above



Most of the reported tolerable accelerations likely are response values and thus a kind of steady acceleration limit. Assuming a dynamic load factor for step accelerations of 1.5 and the transition from the step to the steady acceleration limit in the jerk range of 5 g/ms, the exposure polygon may be represented by the values

velocity step limit $v_{s, \text{tol}} = 4,2 \text{ m/s}$

The intention of this chapter is not to produce new head exposure limits, but to indicate how existing data may be compared in order to check their qualities and PERMISSIBLE ranges of application.

REFERENCES

- [1] Meier-Dörnberg, K.E.: "Die Beschreibung von Stoßvorgängen durch ihre Zeitfunktionen, Fourier- und Schockspektren". VDI-Bericht Nr. 135, VDI-Verlag 1969
- [2] Klotter, K.: "Schwingungslehre", Band I A, Neuauflage, Springer-Verlag 1978
- [3] Meier-Dörnberg, K.E.: "Kenngrößen für Schockeinwirkungen und Schockverträglichkeitsgrenzen", VDI-Bericht Nr. 210, VDI-Verlag Düsseldorf 1973
- [4] Meier-Dörnberg, K.E.: "Das Schockpolygon und das Verträglichkeitspolygon, eine Basis zur Bewertung von Stoßeinwirkungen und Verträglichkeitsgrenzen", VDI-Bericht Nr. 221, VDI-Verlag 1974
- [5] Payne, P.R.: "Working Paper for the Experts of ISO TC 108 SC 4, Aug. 76
- [6] Allan, G.R.: "Ride Quality and International Standard ISO - 2631, NASA T MX 3295, Nov. 1975
- [7] Pyne, G.R.: "Optimizations of Human Restraint Systems for Short Period Accelerations" ASME Paper No. 63 - WA - 277
- [8] v. Gierke, H. and D.E. Goldmann: "Effects of Shock and Vibration on Man". Mc Graw-Hill 1961 and 1978, Shock and Vibration Handbook
- [9] Meier-Dörnberg, K.E. and W. Stamm: "Sicherheits-Skibindung und Standsicherheit" Diplomarbeit am Institut für Mechanik, Technische Hochschule Darmstadt, Okt. 1978
- [10] Hirsch, A.E.: "Man's Response to Shock Motions". ASME Paper No. 63 - WA - 283, 1964

SYMBOLS

Input quantities (time functions)

s ; v ; a ; j ; displacement; velocity; acceleration; jerk values or histories.

Spectral values (transformations of input values)

Ω ; $i\Omega$; p spectral angular frequencies, Laplace or Fourier operator

Ω_v ; Ω_a ; Ω_j spectral corner frequencies (see chapter 4.1)

$A(\Omega)$; $V(\Omega)$ spectral moduli (capital letters) of time functions $a(t)$, $v(t)$.

Time values (used to describe input time functions)

t_e ; T total pulse durations (e = end)

t_v ; t_a ; t_j equivalent durations of (positive) velocity; acceleration; jerk-pulses (see chapter 4.1)

Response quantities

x , \dot{x} , \ddot{x} absolute response values, e.g. displacement, velocity and acceleration.

δ , $\Delta\dot{x}$ relative displacement, total velocity change in a system.

System properties

m ; k ; b parameters of a simple linear system: mass, stiffness, damping resistance.

$\omega = \sqrt{k/m}$ natural angular frequency

$D = b/2m\omega$ damping ratio

ω_c corner frequency in nonlinear or complex systems.

Indices

ϕ ; δ amplitudes in harmonic vibrations

v_{max} ; \ddot{x}_{max} maximum or peak input or response values

\ddot{x}_{tol} ; δ_{tol} tolerable response values, tolerance criteria

a_{tol} ; v_{tol} tolerance limits, maximum tolerable input quantities

$a_{s\ tol}$; $v_{s\ tol}$ tolerable step inputs (exposure polygon)

MULTIAXIS DYNAMIC RESPONSE OF THE HUMAN HEAD AND NECK TO IMPACT ACCELERATION

C. L. Ewing
D. J. Thomas
L. Lustick

Naval Aerospace Medical Research Laboratory Detachment
P. O. Box 29407
New Orleans, Louisiana 70189

SUMMARY

The protection of man against crashes requires the development of protective mechanical systems which must be evaluated in the design phase and in preproduction and production testing to determine their efficacy. Such testing requires the use of validated mathematical models or other valid analogs that have the appropriate human dynamic response to peak acceleration, direction of acceleration, rate of onset of acceleration, duration at peak acceleration and initial position of body segments including the range of human anthropometry. The impact acceleration event associated with crashes has a time duration of less than one second and usually less than 200 ms. From 1974 through October 1978, 80 volunteers have undergone approximately 2000 impact acceleration experiments. The complete kinematic response of the head and the first thoracic vertebral body (T_1) was measured over the range of variables required for human analog development.

The relationships of the kinematic variables are graphically presented and statistically analyzed. A previously suggested head and neck model for two-dimensional response is evaluated. The approaches and constraints for a three-dimensional model are evaluated. Anthropometric effects on the dynamic response are presented. The data base serves as a basis for the validation of human surrogate head and neck response to $-X$ and $+Y$ acceleration.

INTRODUCTION

Evaluation of candidate human protective devices against impact acceleration requires human simulation by such analogs as cadavers, anthropomorphic dummies, mathematical models and various primates. The human analog is required because man cannot tolerate the extreme impact forces against which such systems are designed to afford protection. All human analog testing and data derived therefrom suffers from one principal defect. Its correspondence to man cannot be quantitatively established, largely because of the almost complete absence of quantitative human dynamic response data and human injury criteria. As a consequence, dummies are designed to reproduce static rather than dynamic anthropometric measurements. An alternative, the use of volunteers to test protective systems is dangerous, expensive and difficult to interpret. If a subject is not used as his own control, variance between subjects makes comparisons difficult. Adjustments of certain protective restraint systems are a very large factor in their ability to protect, but are difficult to reproduce for crash test, even for the same subject. Obviously, a volunteer can not be used for the testing of higher levels of operation of a protective system due to excessive risk of injury.

Development of a valid analog would result in the capability to reproduce man's dynamic response. Such an analog does not exist today. Its development requires determination of the following:

1. Mass, center of mass location and principal moments of inertia data of the important body segments. Some of these data are available (1, 2, 3, 4, 5, 6).
2. Functional relationships between those body segments in the dynamic environment. The goal is to be able to predict dynamic response of a given segment, given the input accelerations to that segment.
3. Deformation characteristics of critical anatomical segments which interact with the restraint system.
4. Injury criteria from appropriately scaled human surrogates.

An experimental approach using volunteers and non-human primates was adopted in order to resolve these difficulties of protective equipment evaluation. The approach is as follows:

1. Measure the dynamic and physiological response of critical rigid body segments of volunteer subjects undergoing linear impact acceleration experiments within the limits of volunteer tolerance. Independent variables are the peak acceleration, rate of onset, duration, direction and the initial condition of the anatomical segments.
2. Measure the same responses for non-human primates up to the comparable levels of human exposure to determine the between species differences of dynamic and physiological response.
3. Measure the pathological response of non-human primates at levels of permanent injury.
4. Develop the specifications for a human analog and construct appropriate anthropomorphic test devices. This would include the means to measure the responses in the dummy and the criteria of injury to be applied to the response data.

The measured dynamic relation between anatomical segments is independent of restraint, provided that no restraint is used between the two anatomical points where the measurements are taken. Data measured this way are subject to general use. Innovation of reliable means to mount instrumentation to anatomical segments and to interpret the data between runs, between subjects and between species is required in order to accomplish the effort. This has been accomplished on volunteers at the head, T_1 and the pelvis, with limited comparison between investigators (7, 8, 9, 10, 11, 12, 13, 14, 15). The means for calibrating and processing the data have also been developed and

reported (16, 17, 18). This paper summarizes the head and neck response data for -X and +Y impact experiments. Transducer mounts for impact experiments must achieve 1) reproducibility of placement between runs; 2) lack of spurious movement of the transducer relative to the man; 3) results which could be related to the human population rather than to the individual alone; 4) location of the transducers relative to anatomical coordinate systems. The experiments must include repeated runs on a single instrumented individual to determine the repeatability of any data collected, as well as to assess between subject variation. The various requirements for coordinate system documentation and conventions in three-dimensions have been presented (19, 20, 21, 22).

The majority of pre-1967 instrumentation effort usually has been directed toward the vehicle. Instrumentation of Stapp's experiments was limited because of the state-of-the-art of inertial measurement transducers. These deficiencies included accelerometers, rate gyroscopes and the means to attach the transducers to the anatomy. In those experiments, Stapp noted that head-mounted transducers mounted on a helmet or a "bite-plate" could not give useable results (23).

A joint Army-Navy-Wayne State University project was initiated in 1966 at the Naval Aerospace Medical Institute, Pensacola, Florida, to make these measurements using U. S. Army enlisted volunteers. This program is continuing at the Naval Aerospace Medical Research Laboratory Detachment (NAMRLD), New Orleans, Louisiana, using U. S. Navy enlisted volunteers.

Dynamic response of the head and neck to experimentally applied impact acceleration was the first subject of the study. Previous studies (23, 24) have demonstrated the difficulties inherent in measuring accelerations and displacements of the head and neck, as referenced to the seat. One difficulty has been in the means of generating the input acceleration. Many studies have been performed by acceleration facilities in which an initial acceleration was given, followed by an almost constant velocity phase with a deceleration of less than 0.5G, followed by a shaped terminal deceleration pulse. One disadvantage of such an accelerator is the necessity for establishing a condition of zero dynamic response prior to entry into the deceleration phase. If the head and neck were responding to the initial acceleration or subsequent velocity decay at the time of initiation of the input acceleration, an artifact would be introduced into the measured response to the deceleration pulse. Another disadvantage is that physiological data collected during an experiment cannot be related to a single pulse, but instead are related to a series of pulses. It would appear less difficult to determine the effect of a single pulse if the experimental pulse were induced with the subject at both inertial and physiological rest.

Additional difficulty lies in the complexity of the forces acting simultaneously on the anatomy. The sled moves away from the pelvis in the direction of acceleration, but the pelvic restraint which couples the man to the seat transmits the acceleration to the pelvis and thus to the torso. The torso then attempts to rotate around the restrained pelvis in the mid-sagittal plane but is prevented from doing so by the shoulder restraint harness. Both the pelvic and shoulder harnesses stretch in response to the dynamic load of the subject. A reversal of torso trajectory then occurs, resulting in the torso being forced down and back. Concurrently, the torso is being moved through space with the acceleration vehicle. The head and neck also respond by rotating through space about a center of rotation in the neck or neck-torso junction area. Schulman, et. al., have shown that the neck is capable of considerable stretch (24). Therefore, displacements of the head as measured from a seat reference point are difficult to interpret due to the complexity of motion of the entire sled-torso-head system. The experimental methods adopted for the data presented in this report attempt to avoid these difficulties.

EXPERIMENTAL DESIGN

A total of 15 U.S. Army volunteers were used for measurement of the two-dimensional mid-sagittal plane response to -X (chest to back) impact acceleration during 236 experiments on the WHAM II accelerator at Wayne State University (7, 8, 10). Sixty-five U.S. Navy enlisted volunteers were used on the HYGEE impact accelerator at NAMRLD. The three-dimensional response of the head and neck was measured for 563 -X experiments and 731 +Y (right to left shoulder) experiments. The volunteers ranged from the 3rd to the 96th percentile of sitting height relative to the U.S. naval aviator population (25). The anthropometry on all subjects was measured by Clauser and Kennedy (26, 27).

The experimental data base analyzed in this paper is derived from four subsets of data, summarized as follows:

Direction	Number of Subjects	Number of Experiments	Sled Acceleration Range (G)	Number of Experimental Sled Profile Conditions	Number of Experimental Initial Conditions
-X	10	75	6, 10, 15	3	1
-X	13	100	6, 10	1	4
+Y	5	85	2 through 11	3	1
+Y	6	100	2 through 7	1	4

The experimental sled conditions for the first group are high onset long duration (HOLD), high onset short duration (HOSD), and low onset long duration (LOLD) for the sled acceleration profile as shown for 15G, Figure 1.

LX0875	ACXXOS = (X)	H00035	0.	HOLD	0.0
LX1038	ACXXOS = (+)	H00035	0.	LOLD	0.0
LX1132	ACXXOS = (.)	H00035	0.	HOSD	0.0

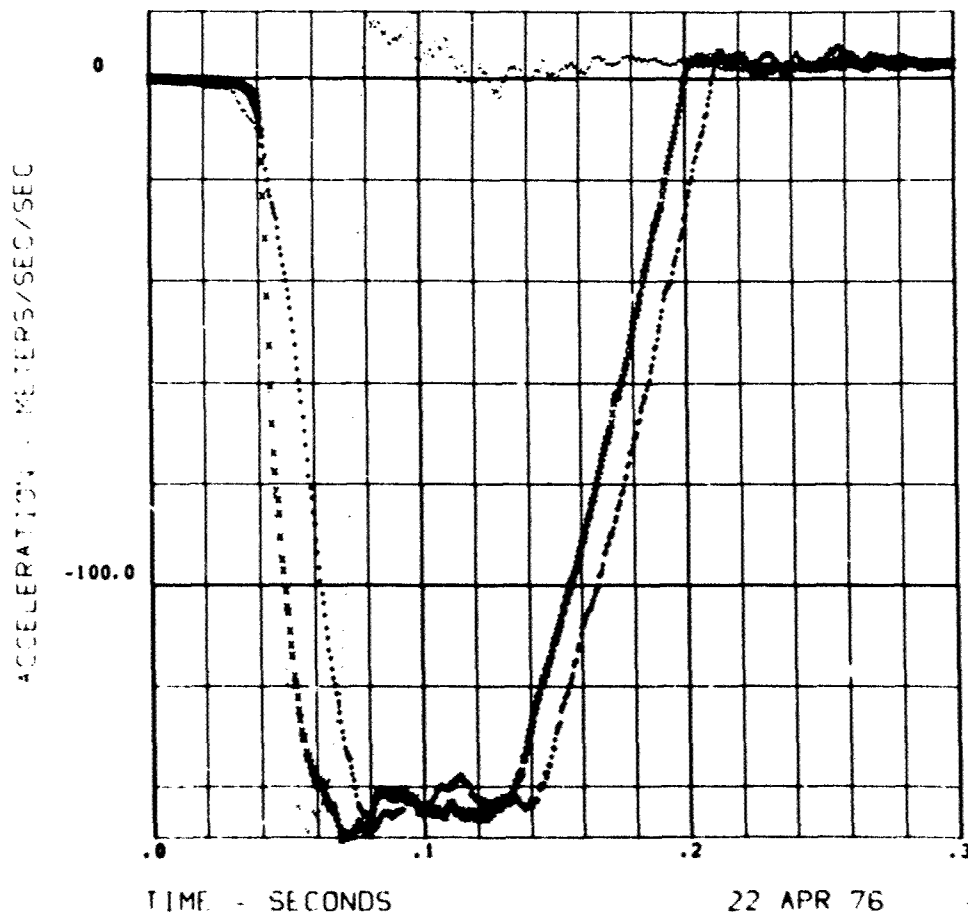


Figure 1 - Typical Sled Acceleration Profiles, 15G, -X Experiments

The initial condition was neck up/chin up (NUCU). The experimental initial conditions of the head and neck anatomy for the second group are NUCU, neck up/chin down (NUCD), neck forward/chin up (NFCU) and neck forward/chin down (NFCD), with HOLD sled acceleration profile. The third group of runs used the three sled conditions HOLD, HOSD and LOLD with the NUCU initial condition. Average sled profiles at 7G are shown for this group in Figure 2. The fourth group used four initial conditions of the head and neck, NUCU, head tilted right (HTRT), head tilted left (HTLT) and head down (HDWN), with the HOLD sled acceleration profile. Overlap of subjects and experiments is reported among the four groups. Consideration of the effect of the anthropomorphic variable of sitting height was examined from a set of eight experiments involving six U.S. Army volunteers on the WHAM II.

RUN NO.	SYM. PLOTTED	SUBJECT	SLED ACC.	ONSET
H0SD07	ACXXOS = (X)	AVERG	70.3	8261.
L0LD07	ACXXOS = (+)	AVERG	70.1	1618.
H0LD07	ACXXOS = (D)	AVERG	69.3	5957.

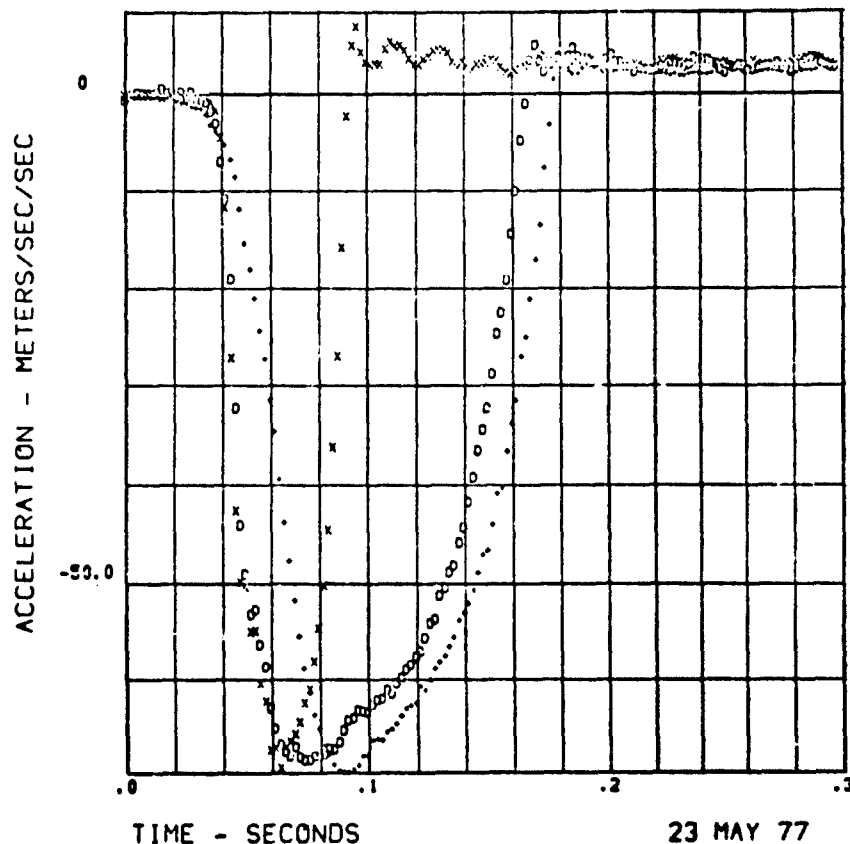


Figure 2 - Average Sled Acceleration Profile (7G)

EXPERIMENTAL METHODS

SUBJECTS - The details of the procedures and results of solicitation and evaluation of volunteers for impact and vibration acceleration stress experiments have been reported (28). Of 1,277 prospective naval volunteers, only 63 (4.9%) were qualified and only 44 (3.4%) successfully completed the experimental program as of 1977.

SLED ACCELERATION PROFILES - A Bendix HYG[®] pneumatically driven 0.340m diameter accelerator is used at NAMRLD to accelerate an approximately 1.2m by 3.7m sled of 1669 kg mass. This is rail mounted on twelve Delrin AF[®] pucks. The acceleration stroke is limited to 1.52m and sled mounted brakes are not used. The effective drag is about 0.2G, the sled is allowed to coast to a stop, and total rail length is 213m.

At Wayne State University the WHAM II accelerator (29) was used at the acceleration end of the track. The end of the experimental conditions of interest occurred when dynamic response was substantially completed. This occurred in every instance prior to the end of the initial acceleration pulse. The sled achieved a peak velocity which remained relatively constant until the sled brakes were activated. Sled braking produced a smooth 2G deceleration until zero sled velocity was attained. Accelerator pulse shape for each run was triangular with a long decay. Only two-dimensional instrumentation was used (7, 8, 10).

RESTRAINT - At NAMRLD, the subjects are restrained for -X experiments in a nominally upright position by shoulder straps, a lap belt and an inverted V pelvic strap tied to the lap belt. The thrust vector is nominally directed from chest to back. Upper arm and wrist restraints are used to prevent flailing during all higher level -X impact acceleration experiments. The same pelvic and torso restraint was applied during +Y experiments. The thrust vector of the sled was nominally directed from the right to the left shoulder and the subject was positioned snugly against a lightly padded wooden board against the right shoulder to limit the upper torso motion. In all experiments, a loose safety belt around the chest was also employed.

EXPERIMENTAL MEASUREMENTS - The dynamic parameters of interest presented in this paper were derived from measurements using six piezoresistive accelerometers mounted on a T shaped plate at the mouth and six accelerometers mounted on a T-plate at the spinous process of T₁. The configuration of the accelerometers on the T-plate and the error propagation associated with this method for determining linear displacement, velocity, acceleration and angular orientation, angular velocity and angular acceleration components of a rigid body have been described (16). The cinephotographic system and the two rate gyroscopes used to validate this measurement system have been described (17).

The standard geometry of the T-plate is illustrated in Figure 3, showing the position and orientation of the accelerometers.

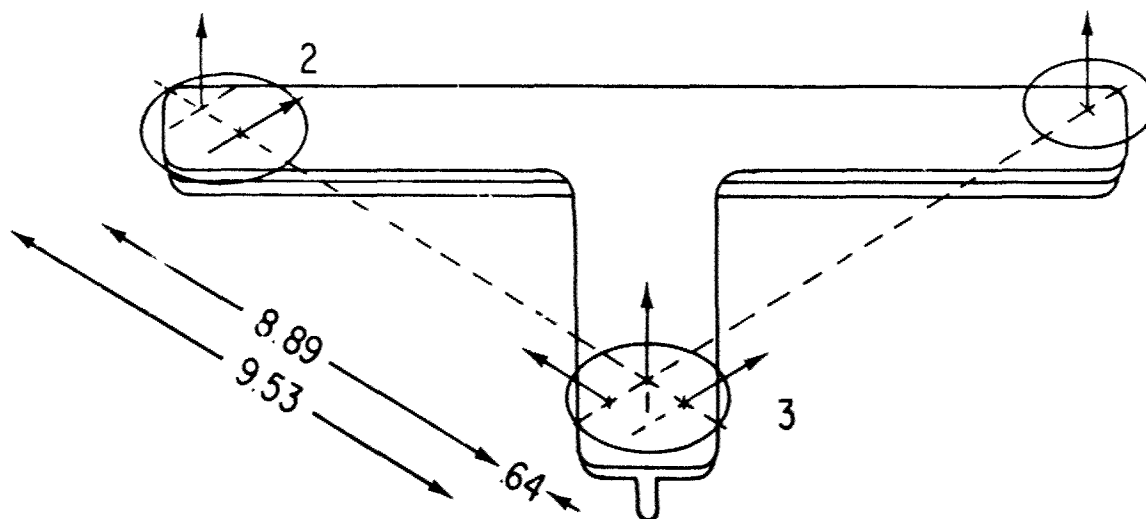


Figure 3 - 6 Accelerometer System 3-2-1 Configuration

The output of each accelerometer was hardwired to an EAI-Pacer 600[®] hybrid computer, digitized at 2000 samples per second and stored on magnetic disk in real time. The calibration information is available in the computer memory prior to the run and carried with the accelerometer data. Within minutes after each experiment the digital data are scaled, reconverted to analog form and plotted on a cathode ray tube for validation by comparison with a scaled light beam oscillographic plot of the data, independently generated at the time of the run. In addition, a two axis rate gyroscope is mounted on the head mount and on the T₁ mount. The data from these gyroscopes were used as an independent measurement of two components of the angular velocity of the head and of the neck.

Cinephotographic coverage of the event is provided by two sled-mounted, pin-registered 16mm, 500 frame per second cameras, Milliken DBM 50[®] or DBM 55[®], situated orthogonally to each other at approximately one meter from the subject. These cameras are equipped with 12.5mm Kinoptic[®] lenses at f4. Each camera has a 140 degree shutter and is equipped to print ten digits of the time of day at time of shutter opening resolved to 0.1 ms along the frame edge as well as serial IRIG B timing along the opposite edge. One hundred foot rolls of Kodak 2479 RAR[®] film are used.

Lighting is provided by four sled-mounted General Electric[®] 4582 lamps mounted in pairs at each of the camera sites. One camera was mounted to the right of the subject with lens axis approximately normal to the mid-sagittal plane of the subject. The other one was mounted in front of the subject. Photographic targets on the T₁ instrumentation mounts as well as the sled-mounted target remained in the field of view of the lateral camera. Targets on the mouth mount instrumentation were in the field of view of both cameras. There was an additional overhead camera for the +Y experiments. The T₁ mount displacement was constrained to the mid-sagittal plane and was measured relative to the sled coordinate system for -X experiments. The three dimensional motion of T₁ mount was measured for +Y experiments. The mouth mount displacement can be measured in three dimensions relative to the sled.

In order to compare subjects at similar points in the anatomy, it is required to define a head anatomical coordinate system and a T₁ anatomical coordinate system (19, 20, 21, 22). These anthropometric coordinate systems are related to the instrumentation coordinate systems by three-dimensional x-ray anthropometry on each subject (18). The basic reference frame for the entire series of experiments is fixed to the laboratory. This is established by first defining a sled coordinate system in which the origin is a benchmark permanently machined into the sled structure. The +X axis is parallel but in the opposite direction to the thrust vector of the accelerator. The +Z axis is parallel to gravity and positive

upward and the +Y axis is established so that the XYZ axes form an orthogonal right hand triad. All coordinate systems used in this study are right handed where X, Y and Z axes are taken in that order.

The dependent variables presented in this report for -X experiments are defined as follows:

- (a) Angular velocity (RHBOXS) (RM20XS) is the component along the +Y head anatomical coordinate system relative to the laboratory reference coordinate system. For -X experiments there is no significant X or Z angular velocity.
- (b) Angular acceleration (QHBOXS) is the +Y component along the +Y head anatomical coordinate system relative to the laboratory reference coordinate system. For -X experiments there is no significant X or Z angular acceleration.
- (c) Resultant acceleration (AAXXZS) is the magnitude of the linear acceleration at the head anatomical coordinate system origin relative to the laboratory reference system origin computed from the components along the X and Z axes of the laboratory reference coordinate system. For -X experiments the Y component of acceleration is not significant.
- (d) Horizontal acceleration (ANXXOS) (ATXXOS) at T_1 is the acceleration component of the T_1 anatomical coordinate system origin relative to the laboratory reference coordinate system along the +X axis of the laboratory reference coordinate system.
- (e) Sled acceleration (ACXXOS) is the acceleration of the sled along the X component of the laboratory coordinate system. The laboratory Y and Z components of acceleration are negligible for -X experiments.

Many of the -X experiments presented in this analysis were conducted with a mouth mount that had a resonant frequency which contaminated the output data. Spectral analyses of accelerometer data were run to determine the frequencies at which the mouth mount resonance occurred. A linear filter, consisting of two second order notch filters (ratio of two second order polynomials), and a second order low pass filter were selected to attenuate the mouth mount resonance across subjects, without significantly affecting the derived parameters. The accelerometer data were shifted to account for the delays associated with the filtering process. To establish that this filter did not alter the output variables significantly, runs without a mouth mount resonance were analyzed with no filter and with the filter, described previously. No significant changes in the output variables were observed when the filter was used on mouth mount data known to be free of resonances. This study is interested in the average effects of onset and duration over subjects and the subjects were pooled in subsequent regression analyses. In order to determine the general response of subjects to onset and duration, an alignment program was used to line up the variables of all runs in each of the nine experimental conditions defined by onset, duration (HOSD, LOLD and HOLD) and peak sled acceleration. The average profiles for each variable of interest were calculated for each experimental condition and comparison plots of these average profiles were made at each of the three nominal G levels. The alignment program was designed to shift the signal vector representing the time profile of the variable, so that in the time window of interest, the average correlation between all the vectors in a group was maximized. This is consistent with a minimum mean square departure of the normalized signal vectors from the average. The average profiles determined prove to be a good method to observe subtle shape differences in the time profiles of the variables of interest. The average profiles were shifted so that the peak values for each variable were approximately consistent with the average time at which the peak occurred for that condition.

The sled acceleration is fixed in the -X laboratory direction. In the +Y experiments the orientation of the subject on the sled is such that the sled acceleration is in the +Y anatomical direction.

The dependent variables for +Y experiments presented in this report are named and defined as follows:

- a. RHACXS (RHOXS) - Resultant Angular Velocity is the resultant of the head angular velocity about the head anatomical X and Z axes. The component of angular velocity about the anatomical Y axis (pitching of the head) is not significant for these +Y experiments.
- b. QHACXS (QHOOXS) - Resultant Angular Acceleration is the resultant of the head angular acceleration about the head anatomical X and Z axes. The component of angular acceleration about the anatomical Y axis is not significant for these +Y experiments.
- c. AAOXS - Resultant Linear Acceleration is the magnitude of the head linear acceleration at the origin of the head anatomical coordinate system relative to the laboratory reference coordinate system.
- d. ANXXOS - Horizontal acceleration at T_1 is the acceleration component of the T_1 anatomical coordinate system origin relative to the laboratory reference coordinate system along the +X axis of the laboratory reference coordinate system.
- e. ACXXOS - Sled acceleration is the acceleration of the sled along the X component of the laboratory coordinate system. The laboratory Y and Z components of acceleration are negligible.
- f. RANGLE - Direction of angular velocity vector is defined as the arc tangent of the component of head angular velocity about the head anatomical Z axis divided by the head angular velocity about the head anatomical X axis. The component of head angular velocity about the head anatomical Y axis is not significant for these +Y impact runs.

For all experiments, the time on all plots is relative to a time called data processing time zero established as 40 milliseconds prior to first motion of the sled. First motion of the sled is determined by the best straight line fit to the rising portion of the sled acceleration profile between 20 and 50 percent of peak sled acceleration. The extrapolation of this line to its intercept with the time axis establishes time of first motion. Rate of onset is defined as the slope on the rising portion of the acceleration profile between 20 and 50 percent of peak sled acceleration, and duration is defined as the time spent above 75 percent of peak sled acceleration.

Analysis of +Y experiments is directed toward the evaluation of the average effects of onset and duration over subjects. Data from five subjects were pooled to obtain average profiles of parameters of interest as well as for purposes

of subsequent regression analysis on peak values of interest. The average profile for each variable of interest was calculated for each experimental condition and compared. The average profile for each condition was obtained by averaging across subjects using first motion as determined from the sled profile to align the profiles of the subjects' response. The variations in time at which peak values of head and T_1 response measurements occurred were small enough across subjects so that the average profiles were an excellent summary of the replications.

In this study, the relationship of head peak angular acceleration, head peak angular velocity, head peak resultant acceleration and T_1 peak horizontal acceleration to sled onset, duration and peak acceleration were of particular interest for all experiments. For each variable of interest, the peaks were read manually from the variable profile. The first positive major peak was used for the parameters of head angular acceleration, angular velocity and resultant linear acceleration. These first peaks were ordinarily found to be the largest for these runs with the exception that the angular acceleration for one subject was characterized by two peaks of almost equal value. An unambiguous first peak was found to be more difficult to define for the horizontal linear acceleration at T_1 . The first peak was always negative and was usually followed by a relatively sharp decrease in magnitude followed by a series of lesser peaks. The first peak was selected as the peak value as long as the decrease subsequent to it was of sufficient magnitude. However, if the decrease was minor and the continuing part of the curve fit in well with its antecedent, the second peak was selected.

The peak values of the parameters of interest were regressed on the three parameters defining the sled profile. A stepwise, multiple linear regression analysis was used in which parameters were eliminated on the basis of an F test if found to be not significant at the five percent level. In addition, regression of head kinematic variables on peak horizontal linear acceleration at the T_1 anatomical origin was also obtained. Previous attempts to define equivalent onset and duration parameters for the horizontal acceleration at T_1 were only partially successful and were not attempted in this study.

INITIAL CONDITIONS - The effects of initial conditions for $-X$ and $+Y$ experiments were evaluated in the HOLD sled acceleration condition. The initial conditions during $-X$ experiments were established from photography. The photo data from four targets on the T_1 mount and four targets on the mouth mount from the lateral camera were only used to obtain the initial conditions. This was done by analyzing 15 frames, approximately 2 msec apart, prior to first motion of the sled to verify that there was little head or neck motion prior to this condition. The initial values are consistent with the position and orientation data at first motion.

The least square fit of initial conditions was obtained and was consistent with the photo data and consistent with the constraint that the anatomical origins were only allowed to be moved in the laboratory X and Z directions. The rotation was only about the laboratory Y axis. This constraint is consistent with the established finding that motion of the head and neck was limited to the mid-sagittal plane for $-X$ experiments.

The neck angle illustrated in Figure 4 was calculated from the coordinates of the head anatomical and T_1 anatomical origin locations at first sled motion. The head angle, also shown in Figure 4, comes directly from the photo data.

For all $+Y$ runs the subject is seated upright in a chair so that the sled thrust vector is nominally in the direction from the right to the left shoulder, and the gravity vector is downward from the head through the subject's seat. Therefore, the initial nominal orientation of the head anatomical and the T_1 anatomical coordinate system is such that the anatomical $+X$ is nearly along the laboratory $+Y$ and the anatomical $+Y$ is parallel with the laboratory $-X$ as shown in Figure 5.



Figure 4 - Illustration of the Initial Conditions of Head Angle and Neck Angle for $-X$ Experiments

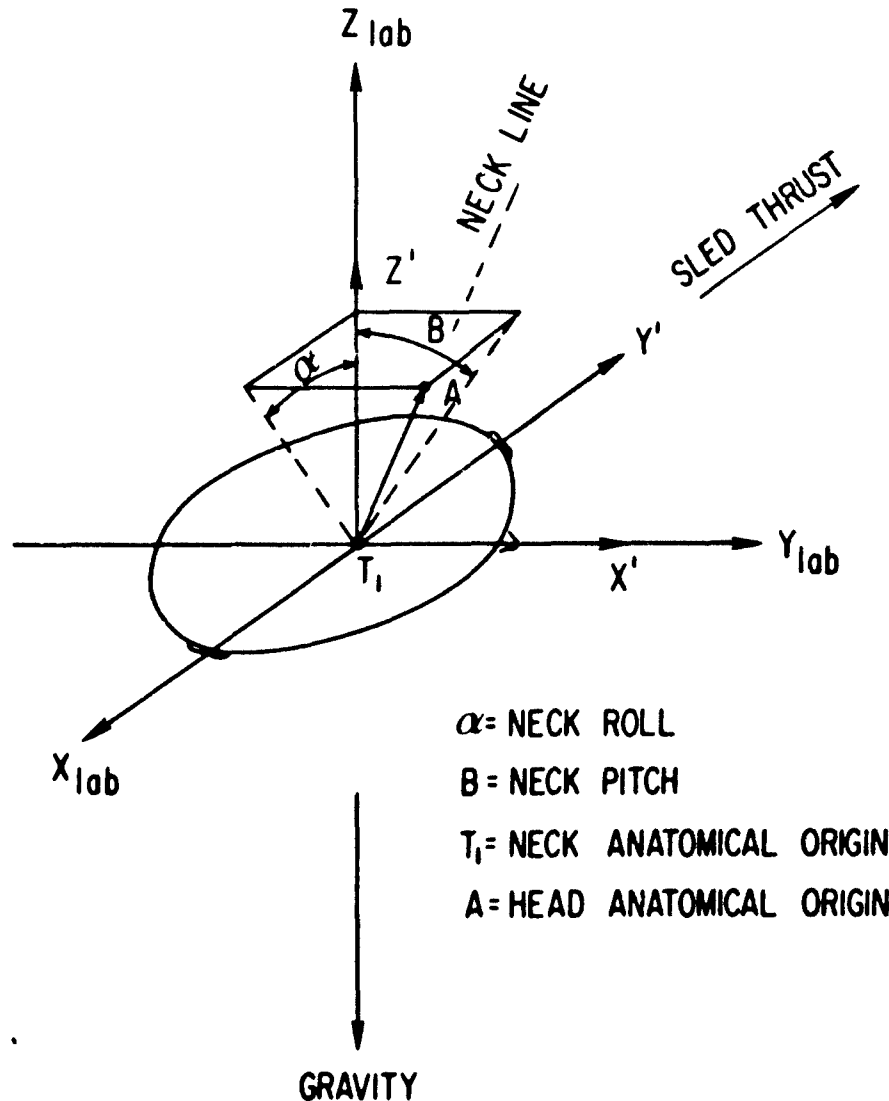


Figure 5 - Illustration of Initial Condition Variables for +Y Experiments

Photography is used again to measure the initial position of the head and T_1 in three dimensions. The initial conditions of the neck link and the head are defined relative to a coordinate system with the Y' axis directed along the sled thrust vector. The Z' axis is directed upward in the opposite direction to the gravity vector, and the X' axis is directed so that X' , Y' , Z' form a right hand orthogonal coordinate system. This coordinate system and its orientation relative to the laboratory coordinate system is relative to the origin of the coordinate system for T_1 . The neck line is defined by a length from T_1 to A and two angles, as shown in Figure 5. The initial orientation of the head anatomical coordinate system is defined by three Euler angles. Assuming that the head anatomical X , Y , Z coordinate system is aligned with the X' , Y' , Z' system in Figure 5, then Euler 1 is a rotation about the head anatomical X axis (roll), Euler 2 is a rotation about the carried head Y anatomical axis (pitch) and Euler 3 is a rotation about the carried head Z anatomical axis (yaw).

RESULTS

Figure 1 presents the typical sled acceleration profiles for 15G, -X experiments for the three conditions of onset and duration. The characteristic shape of HOLD profile was used for initial condition -X experiments. Figure 2 presents the average sled acceleration profiles for 7G, +Y experiments. Again, HOLD profile was used for the initial condition, +Y experiments. Every attempt was made to hold the sled acceleration shape constant for the specified condition regardless of initial condition or orientation of subject on the sled.

Figures 6a, 6b, 6c and 6d are comparisons of the average horizontal acceleration at T_1 anatomical origin, head angular acceleration and velocity about the head anatomical Y axis and the resultant (X and Z components) acceleration of the head for 15G, -X experiments. The comparison is for the three sled acceleration profiles HOLD, HOSD and LOLD. The average time profiles of the horizontal acceleration at the T_1 anatomical origin are considered to be the main driving input for the

head and neck dynamic response. Independent of condition or G level, the form of these curves, including peak structure and time latencies, is very similar. The form of the T_1 curve most likely reflects the restraint torso interaction dynamic response. The first peak value for the HOLD and HOSD conditions is higher than the peak for the low onset condition (LOLD) at all G levels. The high onset results in a higher first peak acceleration at T_1 . The duration has marked effect on the level of acceleration subsequent to the first peak at all G levels.

An important observation concerning the horizontal acceleration at T_1 profiles is that the differences in onset for the HOLD and HOSD conditions, when compared with the LOLD condition, do not reflect the differences implied by the onset of the sled profiles. To verify this, an onset rate was defined for the T_1 profile as the average slope in the 20 to 50 percent region of the peak acceleration at T_1 . The onset thus defined was found to be extremely variable. On an average basis it was found that the onset for the LOLD condition was approximately equal to that of the sled, whereas the onset thus defined for the HOLD and HOSD conditions was about one-half the value expected. The angular acceleration profiles are similar in shape for the three conditions but the HOLD condition has the highest peak and the LOLD has the lowest peak value for 6, 10, 15G, as shown for 15G in Figure 6b. The HOSD condition is intermediate between the other two conditions.

LOLD	ANXXOS = (X)	15.	0.0
HOSD	ANXXOS = (+)	15.	0.0
HOLD	ANXXOS = (O)	15.	0.0

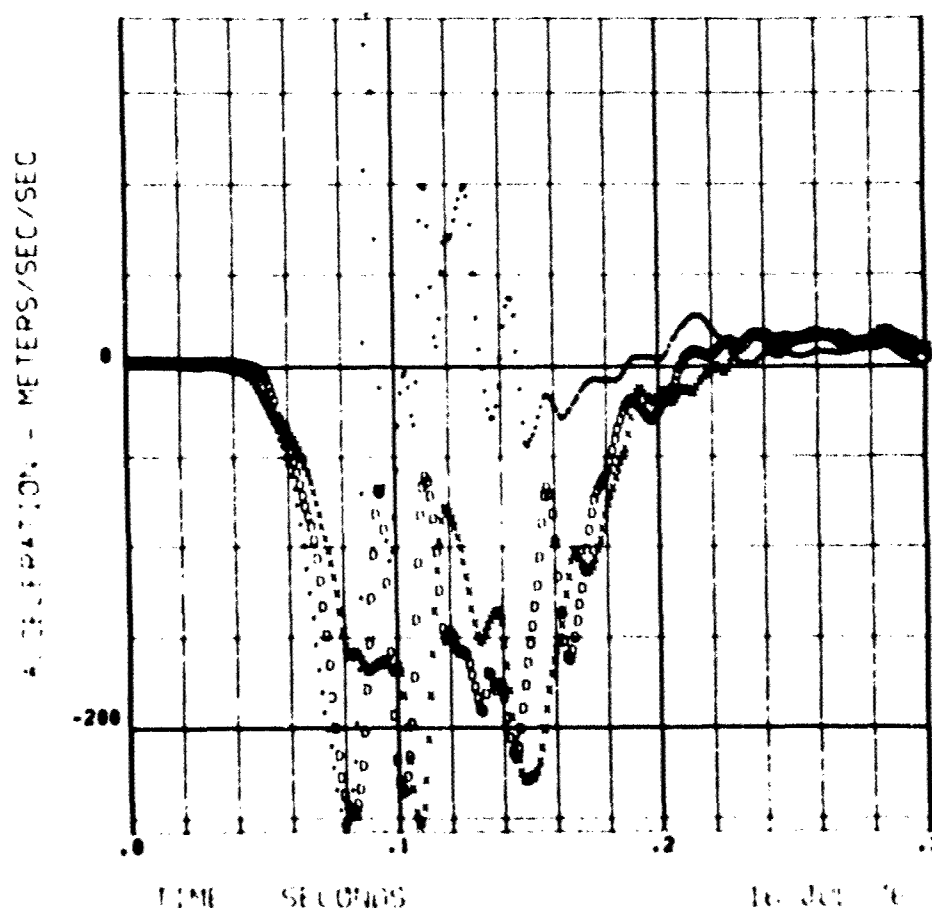


Figure 6a - Comparison of Horizontal Linear Acceleration Profiles at $T_1/15G$, -X Experiments

Although the peaks are significantly different at 6 and 10G peak sled accelerations, there is little difference between the HOSD and LOLD condition at 15G. In addition to the peak differences, the profiles for the HOLD and HOSD conditions are more peaked than for the LOLD condition. The width or duration of the HOSD condition is significantly less than that of either HOLD or LOLD condition. The width or duration of the LOLD condition is somewhat greater than the HOLD condition. In general, increasing onset and duration both tend to increase the peak value of angular acceleration.

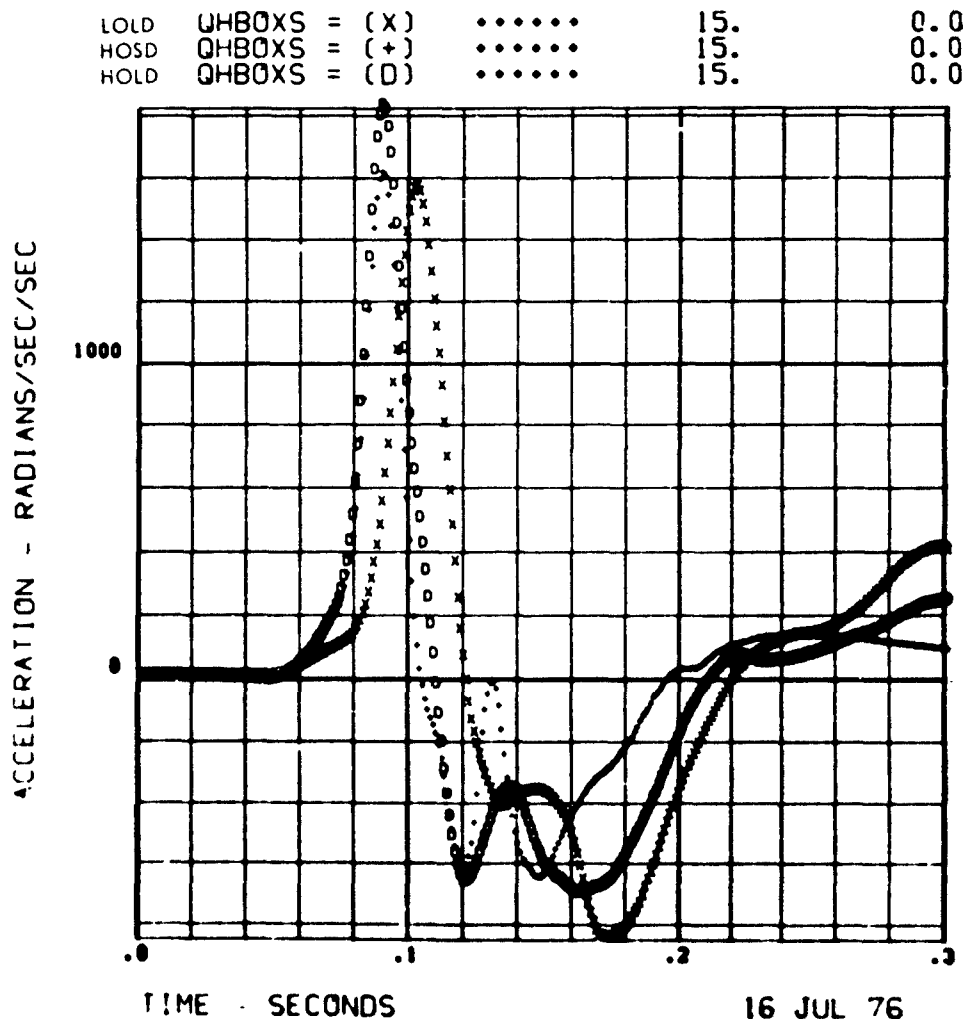


Figure 6b - Comparison of Average Head Angular Acceleration Profiles/15G, -X Experiments

The average angular velocity profiles for the three conditions of this study were compared at 6, 10 and 15G peak sled acceleration, respectively. The 15G condition is shown in Figure 6c. The runs with long duration, independent of onset, have a significantly larger peak angular velocity than the short duration run (HOSD). Comparing the HOLD and LOLD conditions, only a slight difference in peak values is observed. However, the HOLD condition has a more peaked profile in and around its maximum value, followed by a plateau which eventually blends in and follows the LOLD profile. This suggests that the major effect on peak angular velocity is duration, with a lesser effect due to onset resulting in the peakedness of the profile around its maximum value. The peakedness of the HOSD condition is similar to that of the HOLD condition, but the width of the profile for the HOSD condition is significantly less than that for the conditions with the longer durations. The curves suggest that the HOLD condition is an addition of a rather large effect due to duration and a smaller effect due to onset. The above comments are in general correct at all three G levels, however, the peakedness difference between the HOLD and LOLD conditions seems to become less pronounced as G level increases. This is consistent with the fact that in this study the onset conditions were increasing with G level, and hence, at 15G even the onset for the LOLD condition was high.

Comparison of the resultant linear acceleration at the head anatomical origin for the three conditions at 6, 10 and 15G peak sled acceleration was done, and is shown for 15G in Figure 6d. In general, for all conditions and G levels, this profile is characterized by two dominant peaks. The HOLD condition has significantly higher peak values than either the LOLD or the HOSD condition. The two peak values for the long duration runs are approximately the same magnitude and spaced apart about the same time. The second peak for the HOSD condition is much attenuated (attenuation increasing with G level), and the time interval between these peaks for this condition is much shorter than that for the long duration condition. There are both onset and duration effects on the first peak of this variable. The time at which the second peak occurs should make it almost solely dependent on duration, but it also seems to be affected by onset. This is perhaps due to the effect that onset has on the T_1 acceleration peak structure at this time, as a result of restraint system torso interaction dynamics.

LOLD	RHBOXS = (X)	15.	0.0
HOSD	RHBOXS = (+)	15.	0.0
HOLD	RHBOXS = (D)	15.	0.0

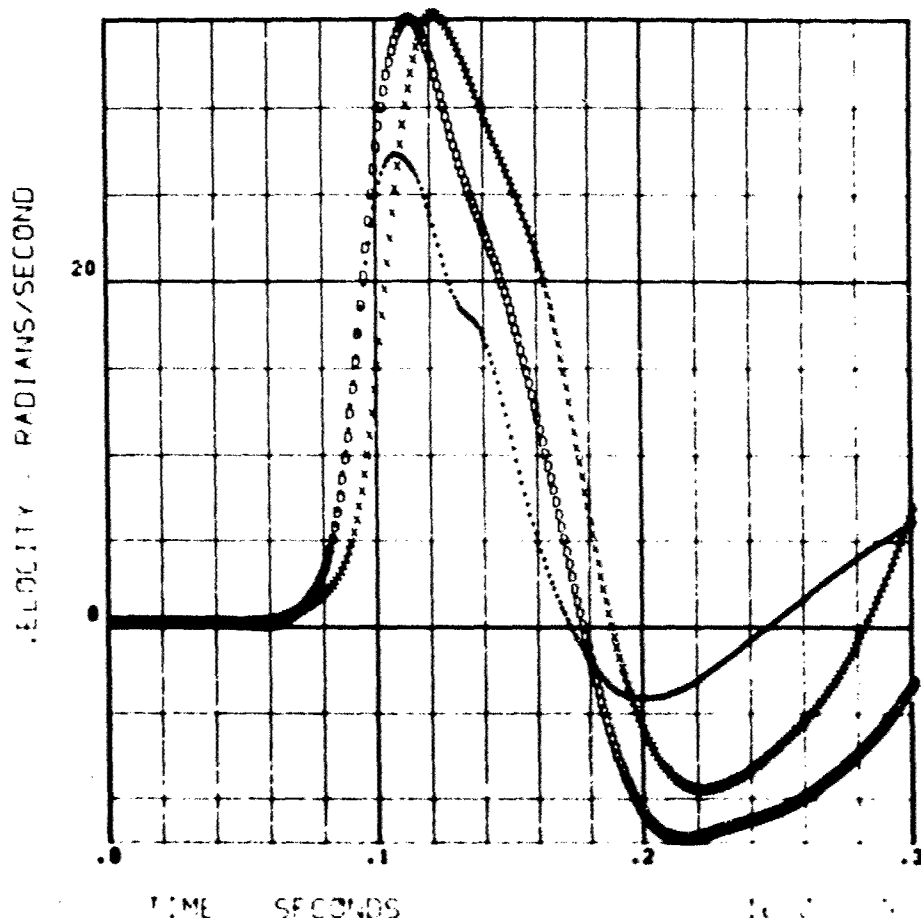


Figure 6c - Comparison of Average Head Angular Velocity Profiles/15G, -X Experiments

A characteristic sequence of events independent of G level and onset duration conditions is invariably the peak sled acceleration followed successively by peak horizontal acceleration at T_1 , peak angular acceleration of the head and peak angular velocity. The first peak of resultant acceleration occurs at about the same time as peak angular acceleration in most experiments.

Since restraint system dynamics vary, it is desirable to relate the results of this study to parameters defined from the acceleration profiles measured at T_1 , rather than the sled. The sled profile can be characterized well by peak sled acceleration, rate of onset and duration. The input at T_1 has a more complicated structure due to head feedback and torso restraint dynamic characteristics. The T_1 profile was characterized by using the three parameters extracted from the T_1 horizontal acceleration profiles: 1) the magnitude of the first peak, 2) onset, defined as the slope of the T_1 profile between 20 and 50 percent of the first peak value, and 3) duration, defined as the velocity in the horizontal direction at 140 milliseconds divided by 75 percent of the peak magnitude. The peak magnitude and onset are defined similarly to the corresponding definitions on the sled profile. The rationale for defining duration in this manner, is an attempt to define a single parameter which reflects in general the duration of the average acceleration of the T_1 profile in a time window where all the peaks of interest have occurred. The data for all subjects and all G levels were pooled and a multiple step-wise regression was performed on each output variable using parameters defined from the sled profile or parameters defined from the horizontal acceleration profile at T_1 .

IOLD AAXXZS = (X) 15. 0.0
 HOSED AAXXZS = (+) 15. 0.0
 HOLD AAXXZS = (0) 15. 0.0

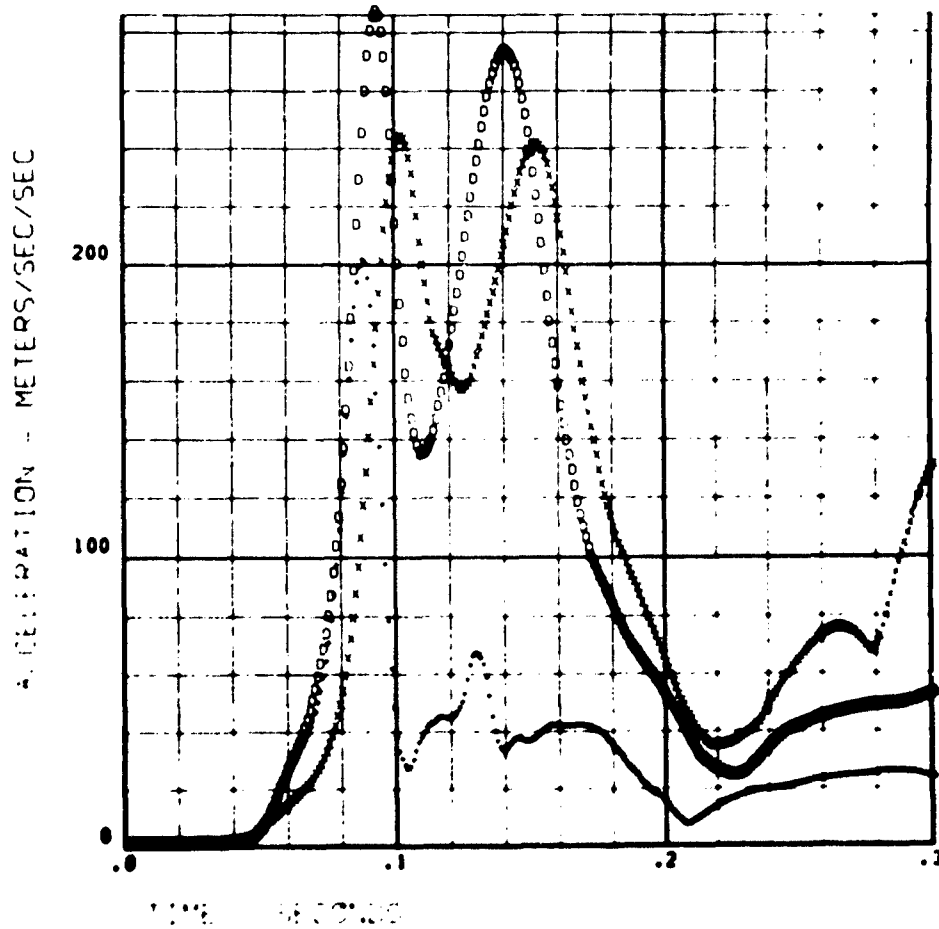


Figure 6d - Comparison of Average Head Resultant Acceleration Profiles/15G, -X Experiments

INDEP. VAR. DEP. VAR.	REGRESSION ON SLED PARAMETERS					REGRESSION ON T ₁ PARAMETERS				
	CONSTANT	PEAK SLED ACCEL.	SLED ONSET	SLED DUR.	STD. DEV.	CONSTANT	1ST PEAK HORIZ. ACCEL. AT T ₁	ONSET T ₁	DUR. T ₁	STD. DEV.
ANG. ACCEL.	- 543	12.1	.0197	1807	246		5.6		2090	332
ANG. VEL.	- 6.54	.23		63.7	2.55		.09		135	4.6
RESULTANT LINEAR ACCEL.	- 87.8	1.99		482	36	- 58	.95		1077	38
HORIZ. ACCEL. AT T ₁		1.25	.0039		47					

UNITS OF COEFFICIENTS CONSISTENT WITH:

ANGLE - RADIANS
 LENGTH - METERS
 TIME - SEC.

Table 1 - Regression Coefficients for the Effect of HOLD, HOSED and IOLD, -X Experiments

Table I presents the coefficients found significant at the five percent level for each dependent variable based on regression on sled defined parameters and parameters characterizing the horizontal acceleration profile at T_1 . The standard deviation in the residuals for each dependent variable is also shown. In order to better understand the mechanism by which onset and duration affect peak dynamic parameters of interest on the head, a model of the head and neck was exercised to see to what extent the horizontal acceleration profile at T_1 explained the effects observed. The model consists of a hinge point at T_1 , and a neck link coupled to a head link with a hinge point. The driving input to the model used in this study was the average horizontal acceleration profile at T_1 . Details of this analysis have been previously reported (30).

If one linearizes the differential equations of the model and neglects torso neck interaction and damping terms, the peak angular acceleration of the head is found to depend on two terms. The rate of extension of the head on the neck at the instant of head/neck spring constant discontinuity is the extension velocity. The first, and apparently major term is proportional to this extension velocity, at the extension corresponding to the spring constant discontinuity, the natural frequency of the head/neck interaction and a combination of model parameters involving the lengths of the neck and head link and radius of gyration of the head. The second term is dependent on duration or the average acceleration level at T_1 subsequent to the extension angle discontinuity in the head/neck spring constant.

The natural frequency of the head/neck interaction consistent with the model parameters is 18.6 Hz. If the first term is the leading factor, the maximum angular acceleration will occur in one-fourth cycle of the head/neck period, or approximately 13 milliseconds. This was found to be the time interval which occurs between the extension angle discontinuity in spring constant and the peak angular acceleration at all G levels in all conditions. This explains in the model the correlation of extension velocity with peak angular acceleration. Since the model is in reasonable agreement with the data in the relative effects of onset and duration, it suggests the importance of extension velocity in the data as well.

It is interesting to note that this same linear analysis indicates that peak angular acceleration may have a subject dependent parameter approximately proportional to the square root of the spring constant, times the neck length, divided by the head moment of inertia. If the spring constant can be assumed proportional to the strength measurements of the neck, it will be interesting in a future study to correlate this parameter with peak angular acceleration. This is particularly significant since preliminary analysis of the effect of sitting height on dynamic response runs conducted on the response of six U.S. Army volunteers to -X impact acceleration showed no significant relationships (as shown in Table II).

Table II - Selected Physical Anthropometric Data on Test Subjects

Subject No.	Sitting Height		Percentile ^b	Weight	
	cm	(in) ^a		kg	(lb)
010	97.8	(38.5)	96	80.2	(176.5)
007	97.8	(38.5)	96	70.2	(154.5)
003	92.5	(36.4)	53	71.6	(157.5)
016	91.9	(36.2)	47	75.7	(166.5)
009	89.2	(35.1)	17	70.7	(155.6)
013	88.4	(34.8)	12	60.8	(133.7)

^a From Clauser (26)

^b From NAEC-ACEL Report 533 (25)

The correlation coefficients relating both the mouth mount peak resultant accelerations and mouth mount peak angular velocities to the sitting heights of the six subjects for the selected runs did not demonstrate a significant relationship at the p-0.05 level. A correlation coefficient of 0.811 would be required to establish significance at the p-0.05 level with only six subjects for any given run. The inclusion of data from additional subjects would make it possible to demonstrate a significant relationship with a lesser correlation coefficient value, if any relationship does indeed exist. However, no relationship was established between mouth mount peak resultant linear acceleration or mouth mount peak angular velocity and subject sitting height. Therefore, the contribution of anthropometric variables to the between subject variability in dynamic response remains unknown.

Variation of the initial condition of the head and neck for the -X experiments has further important effects on the dynamic responses. The NUCU, NUCD and NFCU condition effects on variable peaks can be represented by a linear regression model, as shown in Table III. However, the NFCD condition induces such major changes in the response, that a simple statistical model is unable to explain the results.

Table III - Regression Constants Pooled 6 and 10G Runs for Condition
NFCU, NUCD, and NUCU, -X Experiments

DEPENDENT VARIABLE	INDEPENDENT VARIABLES					STD. DEVIATION OF DEPEND. VARIABLE
	CONSTANT	P.S.A.	ATX	NECK ANGLE	HEAD ANGLE	
E	-	2.53		-.111	-.152	2.90
	-	.0718		.0200	.0315	
E°	- 241.0	135.0		-7.04	-5.43	224.4
	111.9	12.39		1.66	2.45	
R	- 53.2	22.42		-	-	26.4
	12.24	1.44		-	-	
E	9.46			.793	-.108	3.84
	1.40			.0782	.0283	
E°	231.0			-43.9	-7.01	259.1
	93.8			5.23	1.90	
R	-			9.02	-	31.0
	-			.232	-	
ATX	5.19	2.36		-	-	2.81
	1.30	.153		-	-	

REGRESS. COEF.
ST'D DEVIATION

Comparison of the T_1 horizontal acceleration shows little difference between NFCU and NUCU for 10G experiments (Figure 7). The initial condition effect is best shown in Figure 8, wherein the head angular velocity is markedly attenuated in the NFCU portion. In general, the closer the alignment of the head and neck long axis to the acceleration stroke, the lesser the

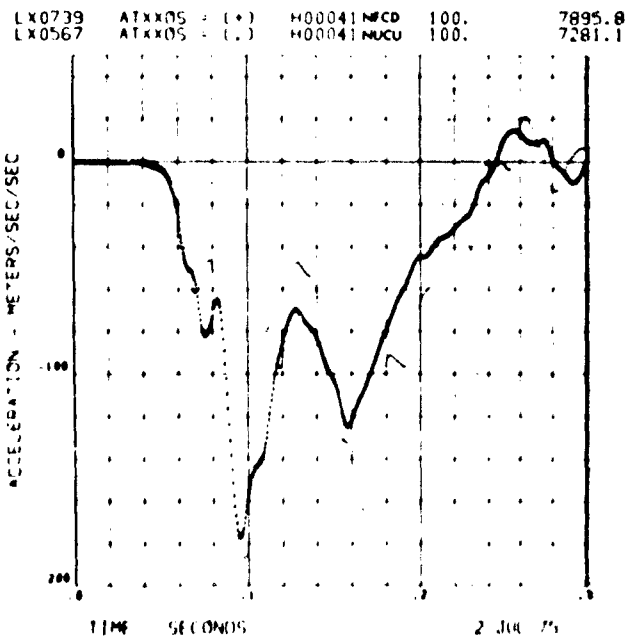


Figure 7 - Comparison of Horizontal Acceleration at T_1 Origin for NUCU
Versus NFCU Initial Conditions, 10G, -X Experiments

LX0739 RM20XS = (+) H00041 NFCD 100. 7895.8
 LX0567 RM20XS = (.) H00041 NUCU 100. 7281.1

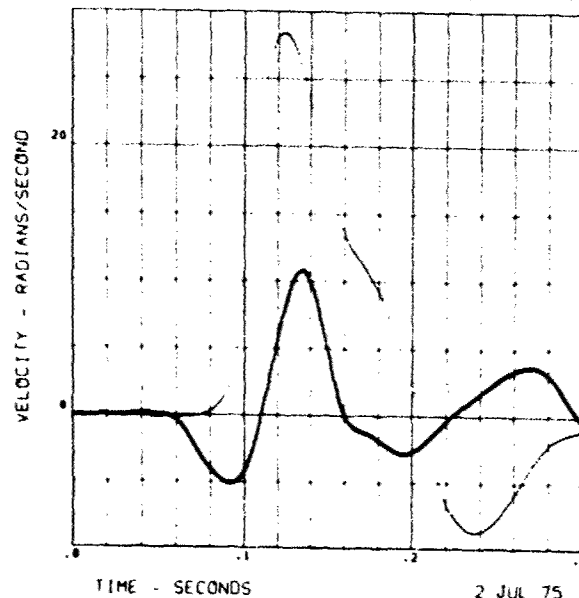


Figure 8 - Comparison of Angular Velocity for NUCU Versus NFCD Initial Conditions, 10G, -X Experiments

RUN NO.	SYM.	PLOTTED	SUBJECT	SLED ACC.	ONSET
H0SD07	ANXXOS = (X)	AVERG	70.3	8059.	
L0LD07	ANXXOS = (+)	AVERG	70.1	1618.	
H0LD07	ANXXOS = (D)	AVERG	69.3	5957.	

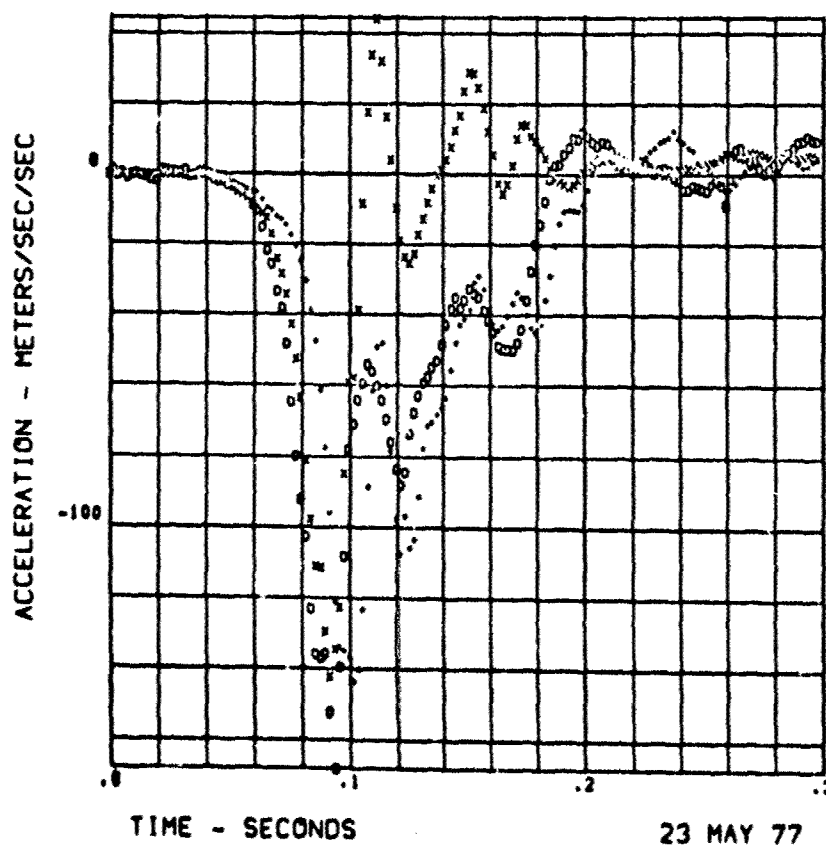


Figure 9a - Average Profiles of Horizontal Acceleration at T₁ Anatomical Origin, 7G +Y Experiments

The results of the +Y experiments and the effect of sled acceleration variables of peak, onset and duration are presented in the same way as for the -X experiments. Important similarities were found. The 7G average profiles for horizontal acceleration at the T₁ anatomical origin (ANXXOS), resultant head angular acceleration (QHACXS), resultant head angular velocity (RHACXS) and resultant linear acceleration of the head (AAOXOS) are presented in Figures 9a, 9b, 9c, and 9d. Each figure shows the comparison of the average profile for the three conditions defined by onset and duration. Observation of Figure 9a indicates that the profile structure for horizontal acceleration at T₁ is very similar for each of the conditions. Corresponding peaks can be found for each condition and it is possible to observe the impulse response of the restraint torso dynamic system. As to be expected, the latency for the first peak for the LOLD condition relative to that for the HOSD and HOLD condition can be observed in the plots for all the variables in Figures 9a, 9b, 9c and 9d. The magnitude of the HOLD condition is greatest with little difference between the HOSD and LOLD conditions.

RUN NO.	SYM. PLOTTED	SUBJECT	SLED ACC.	ONSET
HOSD07	QHACXS = (X)	AVERG	70.3	8261.
LOLD07	QHACXS = (+)	AVERG	70.1	1818.
HOLD07	QHACXS = (O)	AVERG	69.3	5957.

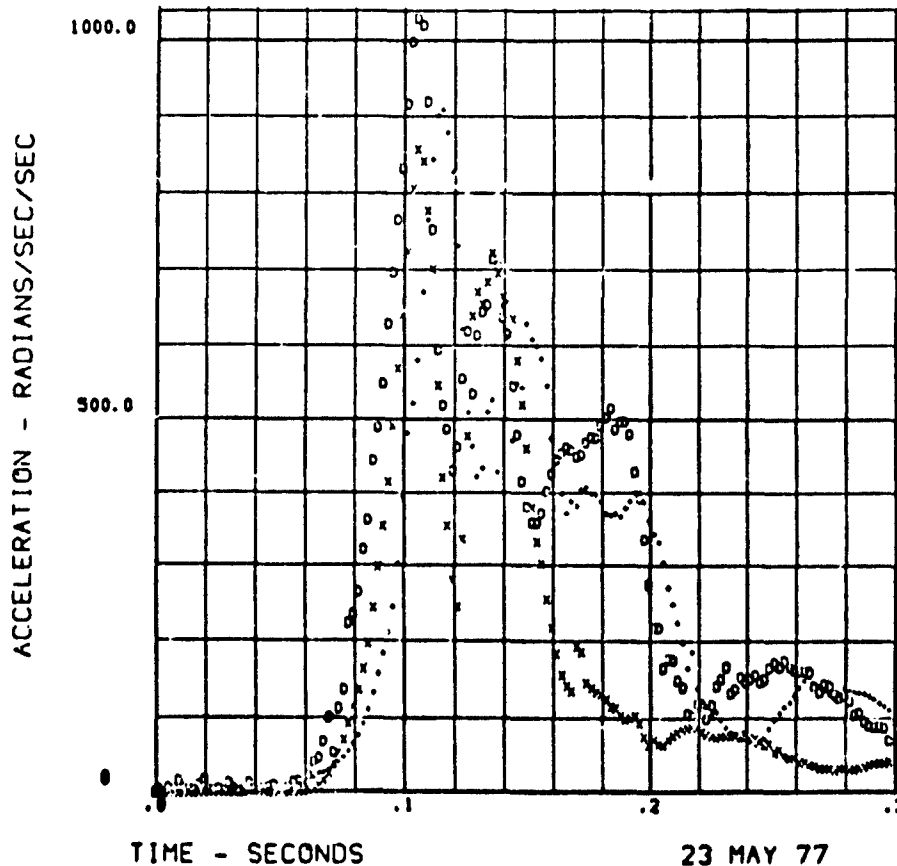


Figure 9b - Average Head Angular Acceleration Profile, 7G, +Y Experiments

The magnitude of the head angular acceleration for the HOLD condition is greatest with little difference between the HOSD and LOLD condition. The magnitude of the second peak (maximum angular deceleration) is a large percentage of the magnitude of the first peak and on individual runs is often as great as the first peak. This effect seems to be subject dependent and is most pronounced for one particular subject who was quite short and muscular. Semiquantitatively, the magnitude of the peak head angular deceleration, (second peak) relative to the peak head angular acceleration, (first peak) is greater for +Y experiments than for -X experiments. The peak angular velocity for HOLD is the greatest, with the LOLD condition a close second and the HOSD condition significantly less than either of the previous conditions (Figure 9c).

RUN NO.	SYM. PLOTTED	SUBJECT	SLED ACC.	ONSET
HOSD07	RHACXS = (X)	AVERG	70.3	8261.
LOLD07	RHACXS = (+)	AVERG	70.1	1618.
HOLD07	RHACXS = (O)	AVERG	69.3	5957.

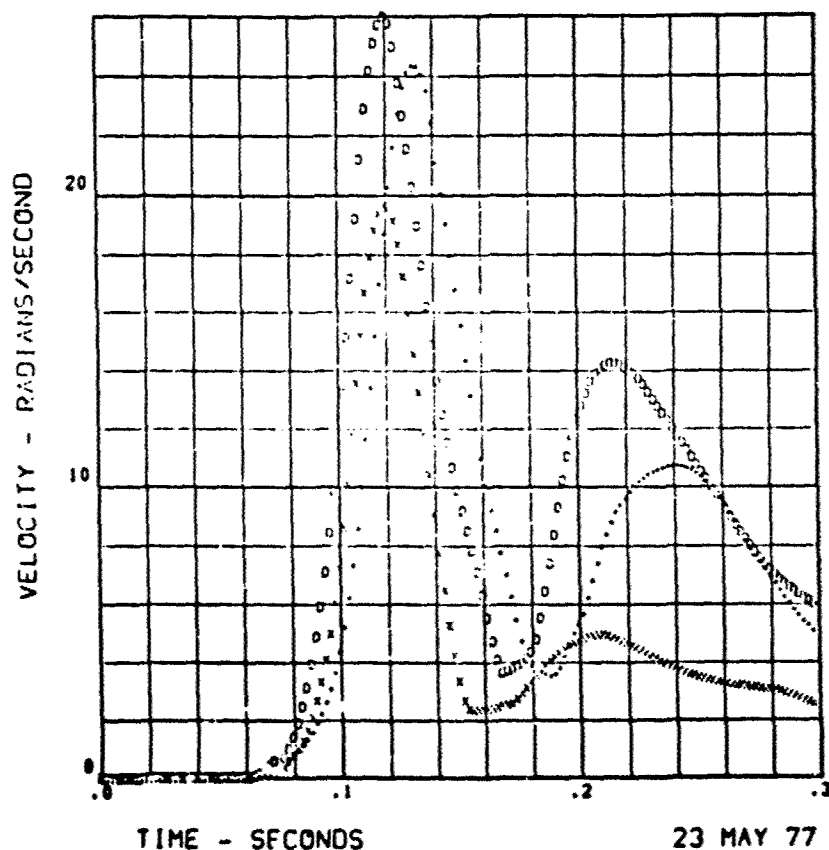


Figure 9c - Average Head Angular Velocity, 7G, +Y Experiments

The resultant head linear acceleration, Figure 9d, is a bimodal curve and very similar in structure, independent of onset duration condition. There is little difference in the magnitude of the first peak for HOLD and LOLD conditions, but both are significantly greater than the corresponding peak for the HOSD condition. Allowing for the fact that in this study resultant head angular acceleration and velocity are presented, instead of the single component of the -X study the profiles for +Y are very similar to those for -X (11).

RUN NO.	SYM. PLOTTED	SUBJECT	SLED ACC.	ONSET
HOSD07	AAOXOS = (X)	AVERG	70.3	8261.
LOLD07	AAOXOS = (+)	AVERG	70.1	1618.
HOLD07	AAOXOS = (D)	AVERG	69.3	5957.

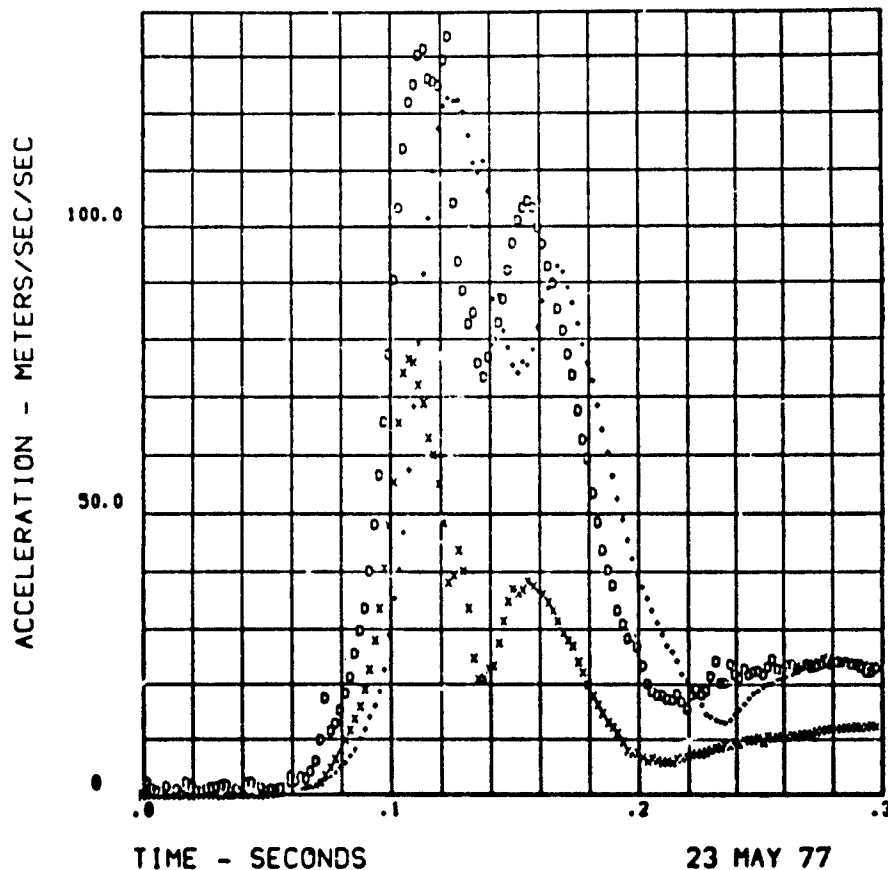


Figure 9d - Average Resultant Linear Acceleration at Head Anatomical Origin, 7G, +Y Experiments

The average peak value of head angular acceleration, angular velocity and resultant linear acceleration have been analyzed for -X and +Y experiments in relation to peak sled and T_1 acceleration. Figures 10 and 11 illustrate the relation for peak head angular acceleration, peak sled and T_1 acceleration respectively. The dashed line on each figure is the regression line obtained from pooling +Y data for all subjects and all conditions in the peak sled acceleration range from 2 to 8G. Data beyond this point were not used in the regression because many of the curves appeared to require non-linear regression models. Figure 10 shows the higher angular acceleration relative to sled acceleration for the +Y experiments. On the other hand, in Figure 11, the peak head angular acceleration is plotted versus the T_1 peak horizontal acceleration and the difference between the +Y and -X experiments disappears. The higher head angular accelerations seen in the +Y study are undoubtedly the result of higher acceleration at T_1 for the same sled acceleration. The coupling of sled forces to the upper torso of the subject, through the lightly padded rigid board, contact with the subject's right shoulder, as well as the different transmission paths through the torso, are responsible for this increased T_1 linear acceleration in the +Y runs. For -X experiments the only significant component of angular acceleration and angular velocity is around an axis which is normal to the mid-sagittal plane. In contrast to this, analysis of the +Y experiments show that the components around the anatomical X and Z axes (roll and yaw, respectively) were both significant. Therefore, the resultants of the angular acceleration and of the angular velocity around these two axes have been used in the +Y study. The similarity in shape of the components of angular velocity around the anatomical X and Z axes suggests that perhaps the direction of the angular velocity remained constant during most of the angular travel of the head.

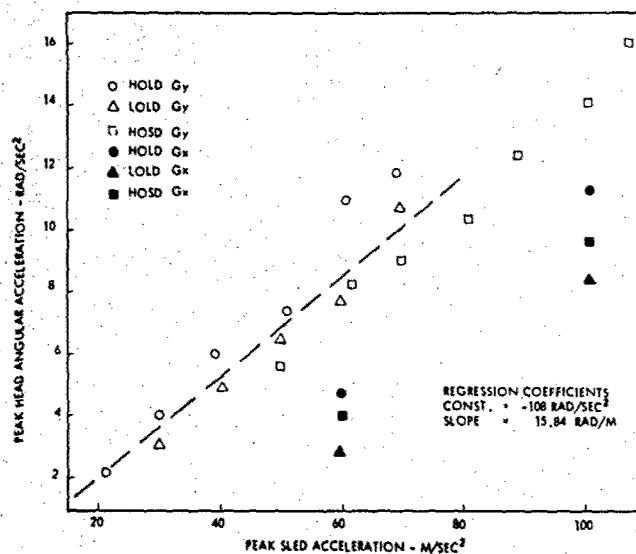
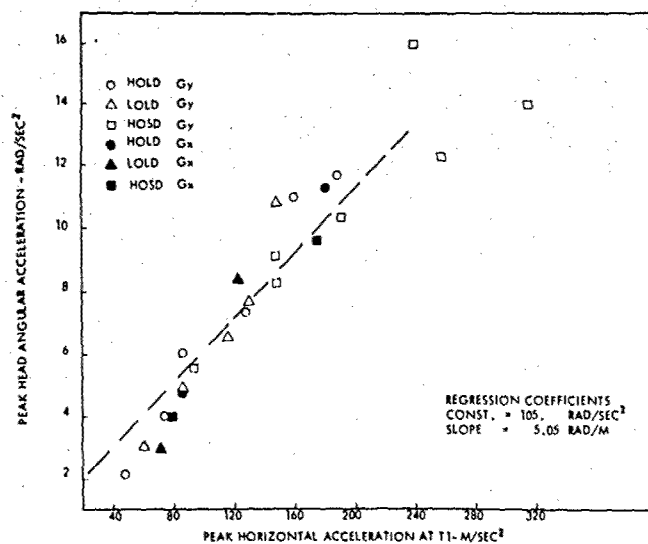


Figure 10 - Peak Head Angular Acceleration Versus Peak Sled Acceleration

Figure 11 - Peak Head Angular Acceleration Versus Peak Acceleration at T₁

RUN NO. SYM. PLOTTED SUBJECT SLED ACC. ONSET
 LX1594 RANGLE = (0) H00065 69.6 6847.
 CX5 (0)

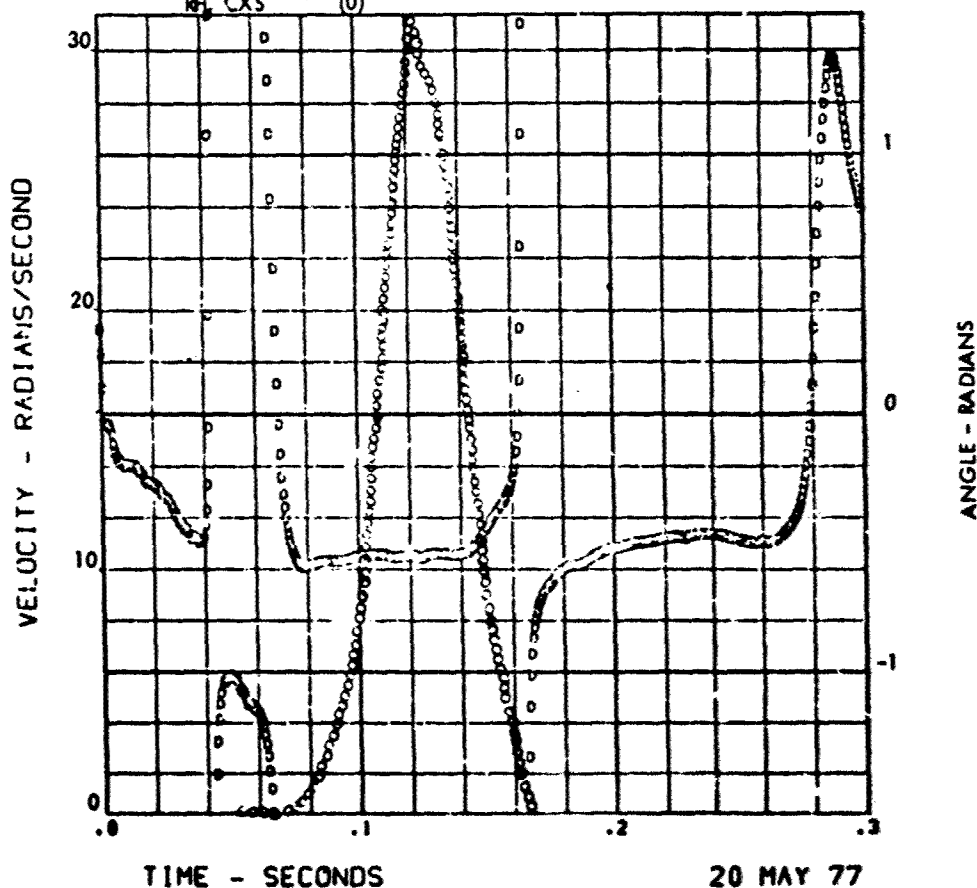


Figure 12 - Resultant and Direction of Angular Velocity Vector, 7G, HOLD, +Y Experiment

Figure 12 is a plot of the direction of the angular velocity in the head anatomy superimposed on the resultant angular velocity. As can be seen from this figure, the angle made by the angular velocity vector in the head anatomy is constant over the time where the angular velocity is appreciable. Although this figure is for a particular run in this study, it is indicative of most of the runs in the study independent of conditions of G level. The angular velocity vector is in the mid-sagittal plane between the +X and -Z anatomical axes and makes an angle of approximately 0.6 radians with the +X axis. The angle is approximately constant across the subjects used for the analysis and across the G levels. It is consistent in both value and variability with a direction approximately normal to a neck line for the neck up/chin up (NUCU) initial condition. These results, together with observation of photographic data have reinforced the idea that for these +Y runs the head rotates around a direction fixed in the laboratory and oriented approximately normal to the neck line defined between the T₁ anatomical origin and the head anatomical origin. The above result has far reaching implications regarding the degrees of freedom required in a head/neck model for the +Y data base. A model with a hinge between the head and neck link oriented as described above and located to best fit the displacement data of the head relative to T₁ should be effective in representing the +Y data base over much of the angular travel of the head.

Finally, it is important to consider the effects of initial condition of the head and neck for +Y experiments. Previous analysis of initial condition effect of the Euler angles head orientation and the direction of neck line relative to the laboratory for the four conditions of NUCU, HTLT, HTRT and HDWN have been presented (15).

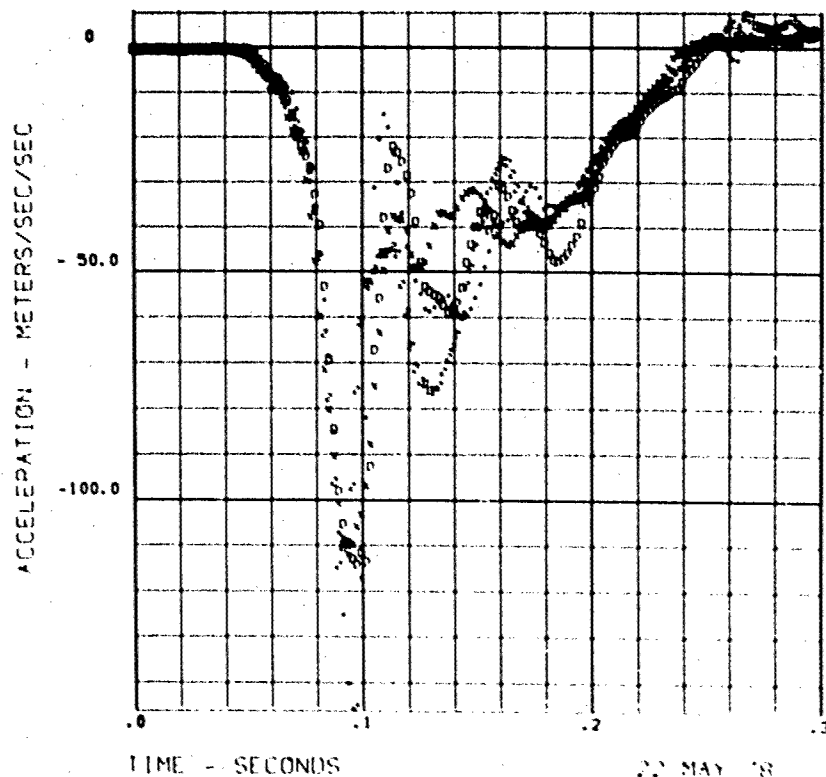
Observations of Table IV where all the initial conditions are pooled, indicate that a positive Euler 1 angle (head roll to right) reduces the angular acceleration by 9.7 rad/sec² per degree and the angular velocity by 0.22 rad/sec per degree. Neck roll to the right, on the other hand, increases the angular acceleration and angular velocity by 8.4 rad/sec² per degree and 0.18 rad/sec per degree respectively. Hence, head tilted to the right relative to the neck magnifies the decrease in angular acceleration and angular velocity. The linear acceleration at the head anatomical origin increases with neck roll to the right (0.73m/sec² per degree). The head angular acceleration and velocity also increase with increased neck pitch angle (2.74 rad/sec² per degree and 0.073 rad/sec per degree, respectively). The horizontal acceleration at T₁ decreases with head roll to the right and increases with neck roll to the right.

Coeff. Dep. Variable	Const. Units of Dep. Var.	PSA m/sec ²	ANXXOS m/sec ²	Euler 1 Deg.	Neck Roll Deg.	Euler 2 Deg.	Neck Pitch Deg.	Std Dev. Units of Dep. Var.	Condition
QHOXS rad/sec ²	112.0	--	-3.84	-9.70	+8.4	Insign.	2.74	169.0	All G levels NUCU, HTLT, HTRT, HDWN
RHOXS rad/sec	7.38	--	-0.072	-0.22	0.18	Insign.	0.073	3.85	"
AAOXOS m/sec ²	41.1	--	-0.33	Insign.	0.73	Insign.	Insign.	20.7	"
ANXXOS m/sec ²	50.7	-3.51	--	-1.68	2.84	Insign.	Insign.	53.7	"

Table IV Linear Regression Analysis of Initial Condition Effect for +Y Experiments

Figure 13 shows that T_1 acceleration is minimally affected. Figure 14 shows the marked decrease in head angular velocity for HTRT condition. This is the same effect as for -X experiments which is a decrease in the magnitude of the dynamic response when the head and neck long axis is initially aligned along the acceleration axis. For all conditions, except HDWN, there is a constant direction in the anatomy and laboratory about which the head and neck rotate. However, for the HDWN condition such constant direction does not exist, implying the need for a full three-dimensional model.

RUN NO.	SYM. PLOTTED	SUBJECT	DELTA-1	ACC.	ONSET
HTRT05	ANXXOS = (2)	AVERG	.0020	50.2	4769.
HTLT05	ANXXOS = (X)	AVERG	.0020	50.1	5797.
HDWN05	ANXXOS = (+)	AVERG	.0020	50.0	4875.
NUCU05	ANXXOS = (D)	AVERG	.0020	49.5	4203.

Figure 13 - Average Horizontal Acceleration at T_1 for Various Initial Conditions, 5G, +Y Experiments

RUN NO.	SYM.	PLOTTED	SUBJECT	DELTA-T	ACC.	ONSET
HTRT05	RH00XS	= (2)	AVERG	.0020	50.2	4769.
HTLT05	RH00XS	= (X)	AVERG	.0020	50.1	5797.
HDWN05	RH00XS	= (+)	AVERG	.0020	50.0	4875.
NUCU05	RH00XS	= (D)	AVERG	.0020	49.5	4203.

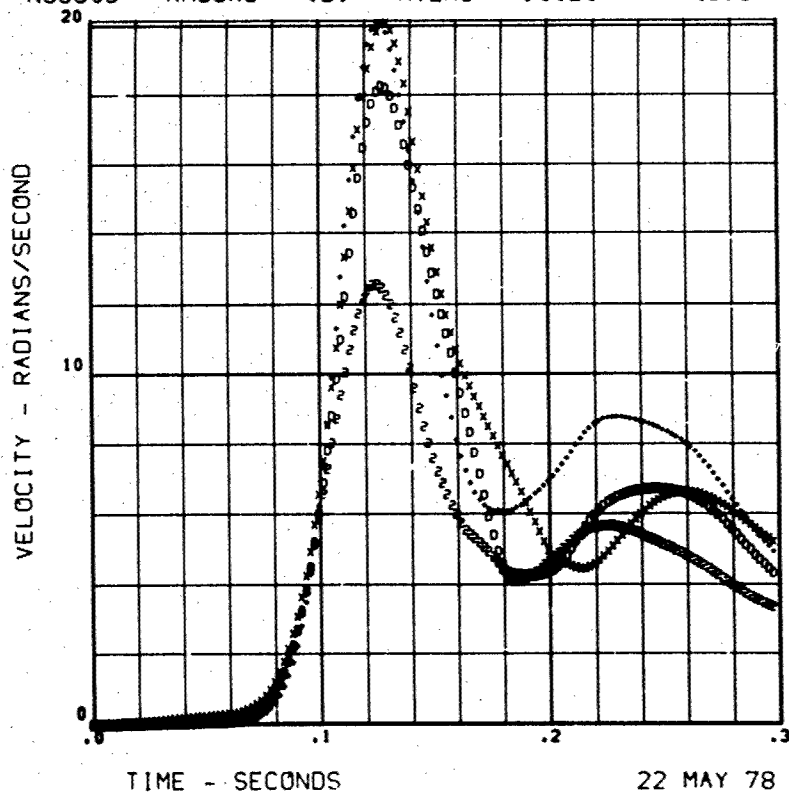


Figure 14 - Average Head Angular Velocity for Various Initial Conditions, 5G, +Y Experiments

CONCLUSIONS

1. Peak head angular acceleration, head angular velocity and head linear acceleration are variously affected by changes in peak sled acceleration, duration and rate of onset for -X and +Y experiments.
2. These effects are mediated through the peak and the duration of linear acceleration at T_1 along the laboratory -X axis (direction of accelerator stroke). The T_1 acceleration explains the differences in head amplitude responses in the -X and +Y experiments.
3. Computations from formerly developed head/neck model for the -X direction (mid-sagittal plane response) indicate the following:
 - (a) The model is consistent with the data in the relative effects of onset and duration.
 - (b) The model head angular acceleration correlates well with the extension angular velocity (head link relative to neck link) at the extension limit assumed in the model.
 - (c) Peak angular acceleration should have a subject dependent parameter proportional to the square root of the product of the head neck compliance and neck length divided by the head moment of inertia. However, a method of measuring neck compliance, neck length and head moment of inertia in a human volunteer has not been satisfactorily validated.

4. For the +Y runs, the head rotates around an axis with a fixed orientation in the mid-sagittal plane approximately normal to the neck line defined as a line between the T₁ anatomical origin and the head anatomical origin. The variation of this axis orientation with subject initial condition will be developed in future experimental studies. Incorporating this constraint into a +Y head/neck model should greatly simplify modeling efforts.
5. Analysis of the initial condition effects for -X and +Y experiments disclosed an effect on peak response related to parameters of the initial conditions. Appropriate regression models describe this effect except for the extreme initial conditions where the head and neck long axis is aligned with the acceleration stroke axis.
6. All conditions can be approximated by a two dimensional model, except the head response in +Y experiments, head down initial condition.
7. Despite inferences that anthropomorphic variables explain between subject variability, appropriate variables have not been identified.
8. Any modeling effort or anthropomorphic dummy design and evaluation effort must reproduce these findings in order to be valid.

ACKNOWLEDGEMENTS

Major funding and support for this work was provided by the Bureau of Medicine and Surgery, the Naval Medical Research and Development Command and the Office of Naval Research.

Volunteer subjects are recruited, evaluated and employed in accordance with procedures specified in Secretary of the Navy Instruction 3900.39 and Bureau of Medicine and Surgery Instruction 3900.6 which are based on voluntary informed consent, and meet or exceed the most stringent provisions of all prevailing national and international guidelines.

Opinions or conclusions contained in this report are those of the authors and do not necessarily reflect the views or the endorsement of the Navy Department.

Trade names of materials or products of commercial or nongovernment organizations are cited only where essential to precision in describing research procedures or evaluation of results. Their use does not constitute official endorsement or approval of such commercial hardware or software.

The authors wish to express their appreciation to the entire staff of the NAMRL Detachment, in particular Elke Lewis for editorial assistance. Special acknowledgement goes to the volunteer subjects without whom this research would be impossible.

REFERENCES

1. W. T. Dempster, "Space Requirements of the Seated Operator", Wright Air Development Center, WADC TR 55-159. Wright-Patterson Air Force Base, Ohio, 1955.
2. W. Braune, O. Fischer, J. Amar, and W. T. Dempster, "Human Mechanics - Four Monographs Abridged", Wright Patterson Aerospace Medical Division, AMRL-TDR-63-123, Wright-Patterson Air Force Base, Ohio, December 1963.
3. K. Fujikawa, The center of gravity in parts of the human body, *Okajimas Folia anat. jap*, 39:117-126, 1963.
4. E. E. Clauser, J. T. Mc Conville, and J. W. Young, "Weight, Volume and Center of Mass Segments of the Human Body", AMRL TR-69-70, Wright-Patterson Air Force Base, Ohio, 1969.
5. L. Walker, Jr., E. H. Harris, and U. Pontius, "Mass, Volume, Center of Mass, and Mass Moment of Inertia of Head and Neck of Human Body", Paper 730985, Proceedings of Seventeenth Stapp Car Crash Conference. New York: Society of Automotive Engineers, Inc., 1973.
6. E. B. Becker, "Measurement of Mass Distribution Parameters of Anatomical Segments." Paper 720964, Proceedings of Sixteenth Stapp Car Crash Conference, P-45. New York: Society of Automotive Engineers, Inc., 1972.
7. C. L. Ewing, D. J. Thomas, G. W. Beeler, L. M. Patrick, and D. B. Gillis, "Dynamic Response of the Head and Neck of the Living Human to $-G_x$ Impact Acceleration." Paper 680792, Proceedings of Twelfth Stapp Car Crash Conference, P-26. New York: Society of Automotive Engineers, Inc., 1968.
8. C. L. Ewing, D. J. Thomas, L. M. Patrick, G. W. Beeler, and M. J. Smith, "Living Human Dynamic Response to $-G_x$ Impact Acceleration. II. Accelerations Measured on the Head and Neck." Paper 690817, Proceedings of Thirteenth Stapp Car Crash Conference, P-28. New York: Society of Automotive Engineers, Inc., 1969.
9. H. J. Mertz and L. M. Patrick, "Strength and Response of the Human Neck." Paper 710855, Proceedings of Fifteenth Stapp Car Crash Conference, P-39. New York: Society of Automotive Engineers, Inc., 1971.
10. C. L. Ewing and D. J. Thomas, "Human Head and Neck Response to Impact Acceleration." Naval Aerospace Medical Research Laboratory Detachment, New Orleans, Monograph 21 August 1972.
11. C. L. Ewing and D. J. Thomas, "Torque versus Angular Displacement Response of Human Head to $-G_x$ Impact Acceleration", Proceedings, Seventeenth Stapp Car Crash Conference, Society of Automotive Engineers, 400 Commonwealth Drive, Warrendale, PA, 1973.
12. C. L. Ewing, D. J. Thomas, L. Lustick, W. H. Muzzy III, G. Willems and P. L. Majewski, "The Effect of Duration, Rate of Onset and Peak Sled Acceleration on the Dynamic Response of the Human Head and Neck", Proceedings, Twentieth Stapp Car Crash Conference, Society of Automotive Engineers, Inc., 400 Commonwealth Drive, Warrendale, PA, 1976.
13. C. L. Ewing, D. J. Thomas, L. Lustick, E. Becker, G. Willems and W. H. Muzzy III, "The Effects of the Initial Position of the Head and Neck on the Dynamic Response of the Human Head and Neck to $-G_x$ Impact Acceleration", Proceedings, Nineteenth Stapp Car Crash Conference, Society of Automotive Engineers, Inc., 400 Commonwealth Drive, Warrendale, PA, 1975.
14. C. L. Ewing, D. J. Thomas, L. Lustick, W. H. Muzzy III, G. Willems and P. L. Majewski, "Dynamic Response of Human Head and Neck to $+G_y$ Impact Acceleration", Proceedings, Twenty-First Stapp Car Crash Conference, Society of Automotive Engineers, Inc., 400 Commonwealth Drive, Warrendale, PA, 1975.
15. C. L. Ewing, D. J. Thomas, L. Lustick, W. H. Muzzy III, G. C. Willems and P. L. Majewski, "Effect of Initial Position on the Human Head and Neck Response to $+Y$ Impact Acceleration", Proceedings, Twenty-Second Stapp Car Crash Conference, Society of Automotive Engineers, Inc., 400 Commonwealth Drive, Warrendale, PA, 1978.
16. E. Becker and G. Willems, "An Experimental Validated 3-D Inertial Tracking Package for Application in Biodynamic Research", Proceedings, Nineteenth Stapp Car Crash Conference, Society of Automotive Engineers, Inc., 400 Commonwealth Drive, Warrendale, PA, 1975.
17. E. Becker, "A Photographic Data System for Determination of 3-Dimensional Effects of Multiaxis Impact Acceleration on Living Humans", Proceedings, Society of Photo-Optical Instrumentation Engineers, V. 57, Box 1146, Palos Verdes Estates, CA 90274, 1975.
18. E. Becker, "Stereoradiographic Measurements for Anatomically Mounted Instruments", Proceedings, Twentieth Stapp Car Crash Conference, Society of Automotive Engineers, Inc., 400 Commonwealth Drive, Warrendale, PA, 1977.
19. D. J. Thomas, and C. L. Ewing, "Theoretical Mechanics for Expressing Impact Accelerative Response of Human Beings," AGARD Conference No. 88 on Linear Acceleration of Impact Type, Oporto, Portugal, 1971.

20. D. J. Thomas, "Specialized Anthropometry Requirements for Protective Equipment Evaluation", AGARD Conference Proceeding No. 110, Current Status in Aerospace Medicine, Glasgow, Scotland, 1972.
21. D. J. Thomas, D. H. Robbins, R. H. Eppinger, A. I. King, and R. P. Hubbard, "Guidelines for the Comparison of Human and Human Analogue Biomechanical Data." Report of an Ad-Hoc Committee, December, 1974.
22. D. J. Thomas, D. H. Robbins, R. H. Eppinger, A. I. King, R. P. Hubbard, and H. M. Reynolds, "Guidelines for the Comparison of Human and Human Analogue Biomechanical Data", 2nd Annual Report of an Ad-Hoc Committee, November 19, 1975.
23. J. P. Stapp, Human Exposure to Linear Acceleration. Part 2. The Forward Facing Position and the Development of a Crash Harness. WADC TR-5915. Part 2. Wright-Patterson Air Force Base, Ohio, Wright Air Development Center. 1951.
24. M. Schulman, G. T. Critz, F. M. Highly, and E. Hendler, Determination of Human Tolerance to Negative Impact Acceleration. NAEC-ACEL 510. Philadelphia, PA, Naval Air Engineering Center, Aerospace Crew Equipment Laboratory, 1963.
25. E. C. Gifford, J. R. Provost, and J. Lazo, "Anthropometry of Naval Aviators, 1964." NAEC-ACEL Report 533, Naval Air Engineering Center, Aerospace Crew Equipment Laboratory, Philadelphia, PA. 1965.
26. C. Clauser, "An inquiry into the Ranges of Values Existing in the U. S. Navy Acceleration Study." 6570th Aerospace Medical Research Laboratory, Wright-Patterson Air Force Base, Ohio, June 17, 1969. Unpublished.
27. C. Clauser and K. Kennedy, "An Inquiry into the Ranges of Values Existing in the U. S. Navy Acceleration Study." 6570th Aerospace Medical Research Laboratory, Wright-Patterson Air Force Base, Ohio, April 1975, Unpublished.
28. D. J. Thomas, P. L. Majewski, C. L. Ewing, and N. S. Gilbert, "Medical Qualifications Procedures for Hazardous-Duty Aeromedical Research", AGARD Conference Proceedings
29. L. M. Patrick, D. J. Van Kirk, and G. W. Nyquist, Vehicle Acceleration Crash Simulator. Proceedings of the Twelfth Stapp Car Crash Conference. New York, Society of Automotive Engineers, Inc., 1968, pp. 402-423.
30. E. B. Becker, "Preliminary Discussion of an Approach to Modeling Living Human Head and Neck Response to $-G_x$ Impact Acceleration." Human Impact Response, Ed. W. F. King and H. J. Mertz, New York: Plenum Press, pp. 321-329, 1973.

DISCUSSION

DR. GILLINGHAM (USA)

Did you instruct your subjects to relax during the test, or were they allowed to brace themselves for the impact?

AUTHOR'S REPLY

The only instructions given to the subject is to position themselves in their initial conditions, which they can view through a closed circuit TV, which looks at them from the front and the side. That's how we maintain repeatability of initial conditions. There was no effort to have them either relax or to brace. Now in the use of human volunteer subjects, regardless of what you tell them, the best you can hope for is, that they will hold those initial conditions, because after the first experiment they become very, very experienced. The learning curve is practically infinitely fast. It is a demanding stressful situation. The subjects have different approaches to how they will handle themselves and how they try to condition themselves to the situation. They are very, very successful in holding their initial conditions as we can check on repeatability from subject to subject. The important point is that regardless of what they're doing, the between subject variability is not very much. The characteristic shape of the curve is there on every single run; some amplitude differences between subjects we think may be due to anthropometric variables. We see no learning at all. The reason is we start them at very low levels and basically they're experienced at the second run because of the drama of the event.

H. R. JEX (USA)

1. The size of the accelerometer packages, and especially the distance of its components from the centers of rotation of the head suggests that its moment-of-inertia might significantly affect the motion of the head. (a) What is the ratio of sensor-package inertia to isolated head inertia (e.g., about the ear-hole axis)? (b) How does this effect the data (e.g., could the mass and inertia of the sensor package be added to Dr. King's model to compare the calculated effects?) (c) How are the data corrected for these effects?
2. Within the time-to-peak accelerations of the head (or of maximum stresses in the neck tissues) is there any evidence of active neuromuscular control or reflexes? (not just open-loop neuromuscular compliance and damping)

AUTHOR'S REPLY

1. We have the weights on each of these individual mounts. I don't remember what they are off-hand, but it is about 12-oz., as I recall, that is the mounting systems plus the accelerometers plus the T plate. How much the inertia is due to the wires is hard to speculate. But that is a constant relatively constant from subject to subject so it constitutes a data base. There is no way to get the measurements without adding something on. The only way, to get at that problem would be to add more weight to see what the effect is between the low weight condition and the higher weight condition. Then you could extrapolate back. But we haven't done that.
2. The effects of the rate of onset and changing the rate of onset on the sled is fairly complex. One of the interesting things that happens is that the difference between high onset and low onset for the sled as reflected in the rate of onset at T_1 is very little. In other words T_1 simply doesn't respond to any major extent to the input. I believe this has to do with the restraint-torso interaction. In some way you can only drive this system up to a certain rate of onset. This is discussed somewhat in the paper. We don't see much of an onset effect, but we believe this is because we just can't drive it through the T_1 .

DR. VON GIERKE (USA)

To what extent is in the Y impact tests the input to T_1 influenced by the restraint system? It looked in the movies as if a 2-dimensional response is already to some extent in the upper torso.

AUTHOR'S REPLY

The T_1 responses were significant only along the X-axis regardless of whether it was a Y experiment or X experiment. You got primarily a unidimensional acceleration. The accelerations along the off axis were very small relative to that peak and do not improve the quality of the regression. So essentially, you have a unidirectional input at T_1 . As far as the restraint systems are concerned they have markedly different effects at T_1 .

DR. VON GIERKE (USA)

I think the input to T_1 is influenced by the dynamics of the upper torso below T_1 . I assume this could only be proven by animal experiments where you would have the upper torso in a complete cast for example, but as long as you have deformation of the spine below T_1 from torso dynamics you have some input into T_1 .

AUTHOR'S REPLY

That's absolutely correct. Not only is the input to T_1 dependent upon the chest, it is dependent upon the restraint system itself. And we didn't know what we would get at T_1 at any given experiment. That is why we used T_1 as the basic input to the head, because we couldn't predict what would go into the head without that T_1 data.

DR. MEIER-DORNBERG (GERMANY)

Why are the input sled histories only varied in such a small range? e.g., velocity range 1:4; rise time 1:2. It doesn't cover enough "decades" as to establish ISO-tolerance limits or tolerance (comfort) criteria. Why does the evaluation only tend to produce response histories to special input motions? More interesting are the limits of tolerance inputs which meet a specified criterion (tolerable response value).

AUTHOR'S REPLY

(Requested first slide) There is a marked difference in duration of the acceleration pulse. There is a difference in the rate of onset between the two curves of approximately 2 to 1. At the present time that's a constraint in the particular accelerator pin combination that we have at the laboratory. This can be modified. You can go to triangular pulses or whatever, but for this series the constraint was taken as the widest dispersion we could get with the particular pin and a particular sled acceleration. That was the only reason for that limitation, but it is a factor of 2 to 1 variation. But it is not a restriction; we can do other experiments.

TRANSIENT INTRAVENTRICULAR CONDUCTION DEFECTS OBSERVED DURING EXPERIMENTAL IMPACT IN HUMAN SUBJECTS

P. L. Majewski
T. J. Borgman, Jr.
D. J. Thomas
C. L. Ewing

Naval Aerospace Medical Research Laboratory Detachment
P. O. Box 29407
New Orleans, Louisiana 70189

SUMMARY

The Naval Aerospace Medical Research Laboratory Detachment (NAMRLD), New Orleans, Louisiana has been engaged in impact acceleration research utilizing normal human volunteer subjects since 1974. Of 1,282 human impact experiments, 923 have been completed using electrocardiographic monitoring. Four episodes of transient intraventricular conduction disturbances have been observed. Details of these events are presented and discussed relative to previous clinical and experimental investigations.

INTRODUCTION

Unexpected instances of transient intraventricular conduction defects in trauma victims have been noted occasionally over the past three decades when electrocardiograms were obtained after injury. Most of these conduction defects were associated with severe, nonpenetrating trauma, not only to the heart, but also to the thorax and other regions (1,2,3). A few of the reported episodes were not associated with other known injuries but represented isolated cardiac conduction disturbances following blunt chest trauma (4,5). During 923 experiments conducted at NAMRLD, four episodes of transient bundle branch block were observed following the exposure of human volunteer subjects to impact acceleration.

The principal research activity of NAMRLD is the investigation of the biodynamics of impact acceleration. A sophisticated impact acceleration bioengineering research facility has been built and professionally staffed. This research effort utilizes human subjects and subhuman primates, and has been in progress since 1974. Electrocardiographic monitoring of the experimental subjects is an integral, essential component of the research investigations. The goal of the research is the representation of the dynamic response of the human head, neck, and torso to impact acceleration by a mathematical model derived from an analysis of, and validated by, human dynamic response data.

MATERIALS AND METHODS

A. The Human Subjects - The volunteer human research subjects are recruited, evaluated, and undergo experimentation in strict accordance with procedures specified by the Secretary of the Navy. In addition, the experiments are approved by the Protection of Human Subjects Committee of the Naval Aerospace and Regional Medical Center, Pensacola, Florida, as required by the United States Navy, Bureau of Medicine and Surgery. Each volunteer subject is fully informed regarding the nature and risks of the experiments. Because of their performance as experimental subjects utilized in experimental acceleration or deceleration devices, they are entitled to hazardous duty pay. Before being accepted, a prospective experimental subject must undergo a detailed evaluation. The qualification standards applied to the volunteers are more stringent than the normal medical qualification standards for military service or even for other categories of experimental stress duty. The medical examination is designed to uncover the most likely physical defects and abnormalities prevalent in a young adult male population. The determination of existing defects, abnormalities, and physiological status establishes the baseline condition to which all subsequent examinations are referred. A subject with any defect which increases the risk of experimentation to him as compared to a subject without the defect is considered disqualified.

This multidisciplinary examination employs specialists in cardiology, orthopedics, radiology, neurology, dentistry, ophthalmology, otolaryngology, psychiatry, clinical psychology, acoustical physiology, vestibular physiology, physiological optics, and other specialty areas as required in individual cases. The primary examination, performed by the cardiologist, consists of a general medical history with system review; a complete physical examination; a standard 12-lead electrocardiogram with the subject fasting and resting; a graded maximum stress test utilizing the Bruce protocol (6); a Frank vectorcardiogram (VCG) (7); pulmonary ventilation studies; echocardiogram if a murmur is found; an SMA-19 blood biochemical profile, a hemogram with coagulation studies; and a urinalysis. A complete dental evaluation with full mouth x-rays is performed in order to ascertain the adequacy of dental support for the specialized stainless steel maxillary mouth mount used to collect acceleration data during the experiments. To screen for latent seizure activity, a baseline electroencephalogram is obtained and interpreted by a neurologist. Visual acuity testing, manifest refraction, tonometry in indicated subjects, visual field mapping, and fundus photography are done under the supervision of an ophthalmologist. Ear, nose, and throat evaluation, including indirect laryngoscopy, is done by an otolaryngologist. Following the ear, nose, and throat evaluation and after the cleansing of the external auditory canals, a detailed audiometric evaluation is obtained. A comprehensive musculoskeletal evaluation including review of skull and complete spine x-rays is performed by an orthopedic surgeon. These x-rays, and anterior-posterior and lateral chest x-rays are reviewed by a radiologist. Extensive testing and interviewing are done by the clinical psychologist and psychiatrist. Detailed evaluation of the vestibular system is performed by utilizing a variety of specialized examinations developed by the Naval Aerospace Medical Research Laboratory (NAMRL), Pensacola, Florida. The data from this series of

medical evaluations are reviewed by the NAMRLD medical staff, and each abnormality is carefully considered. The significance of each abnormality with regard to the fitness of each prospective volunteer is carefully judged. Only those volunteers considered not to be at excess risk are then permitted to become experimental subjects. Of all those who initially express an interest in the research program, only about 5% are actually chosen (8).

B. The Accelerator - The impact experiments are conducted on a 20,000 kilopascal (3,000 psi), 1,000,000 newton (255,000 lb) thrust, nitrogen gas powered horizontal linear accelerator. The accelerator consists of a gas operated piston which pushes against the sled, a movable platform, which rests upon two parallel machined steel flat rails 213m long. During an experiment, the volunteer subject is seated in an adjustable chair and fitted with a lap belt-inverted V pelvic restraint and a bilateral shoulder harness restraint. A loosely fitting chest safety strap is also employed. The restraint system is progressively tightened during the pre-run preparation phase in order to minimize unwanted movement by the subject during impact. However, the head and neck are unrestrained. In addition to the chair, the sled also carries inertial and physiologic instrumentation, signal conditioning amplifiers, several high speed cine cameras for photographic data collection, and an array of high intensity lights. Acceleration-time data collected from accelerometer packages located at the mouth and the posterior spinous process of the first thoracic vertebra, are processed by a hybrid computer system and permanently stored on digital magnetic tape which is used for computerized data analysis.

C. The Physiologic Data Collection System - The physiologic data collection system utilizes an eight-electrode harness, signal conditioning amplifiers, an FM transmitter-receiver telemetry package, an instrumentation quality analog magnetic tape recorder, a pen recorder, and oscilloscope monitors. The frequency response of the entire system is flat from 0.1 Hz to 80 Hz, down 4 dB at 0.05 Hz and down 1 dB at 100 Hz. Signal to noise ratio on tape is 55 dB and 80 dB on the pen recorder.

Although the electrode placement is in accordance with the system described by Frank, slight modifications have been made to accommodate the anatomic mount placed at the first thoracic vertebra. Electrodes at locations I, E, C, A, and M have been placed in agreement with Frank. H has been shifted from the posterior neck to the spinous process of the third thoracic vertebra. Lead F has been shifted from the left leg to the midline of the mid-sacrum. The common reference electrode (ground) has been shifted from the right leg to the left iliac crest (Figure 1). The electrodes are of the active variety. The skin is prepared by vigorous scrubbing with an acetone moistened sponge. The electrode surface is sparingly coated with a conductive cream and the electrode is placed in the proper anatomic location. The electrode, along with a loop of wire to provide strain relief, is covered with an adhesive backed pad. The individual electrode wire leads are cabled together and attached to the sled mounted amplifier-FM transmitter package by a single connector. The transmitting antenna is sled mounted and located approximately 6 cm from the receiving antenna which runs the entire length of the track. The received FM multiplex signal is conducted by shielded cable to the control room where the electrocardiographic data are appropriately demodulated and stored on analog magnetic tape. The three VCG channels are also written out by a pen recorder and displayed on oscilloscope monitors.

The vectorcardiographic data are collected within an anatomic coordinate system based on the three-axis Cartesian system utilizing the right hand rule. This system was chosen to assure conformity with the other laboratory coordinate systems. The anterior-posterior lead pair is termed X, the left-right pair is termed Y, and the superior-inferior pair is termed Z. Anterior, left, and superior are positive in polarity. Therefore, the NAMRLD channels X, Y, Z correspond to Frank -Z, X, -Y and approximate the standard leads V2, I, -aVf respectively (Figure 2).

D. Experimental Protocol and Procedure - Each subject is informed one day in advance of his scheduled run. On the day of the experiment, each subject is interviewed by the physician assigned to monitor the experiment. The interview consists of a standardized review of systems and a review of any medical problems that may have occurred since the subject's last impact exposure. The results of the interview are entered on a coded form which is later processed for automated data retrieval. Following the history taking, a physical examination including urinalysis is performed and recorded on a separate coded form. The use of these checklist forms serves two purposes: 1) to assure uniformity and completeness by different staff physicians and 2) to facilitate automatic data processing. Upon completion of the impact experiment, a post-experiment history and a physical are obtained in similar manner. Therefore, each subject is under continuous medical surveillance before, during, and after every exposure to impact.

Following the pre-experiment physical examination, the qualified subject is fitted with electrodes if electrocardiographic data collection is planned. Such collection has been routine on all acceleration exposures in the -X vector at or above 110m/s^2 (11G). Since 1976, with the beginning of lateral impact acceleration experiments in the -Y vector, the VCG has been obtained on all experiments. The subject walks to the sled, the restraint system is fitted, and the anatomic mounts are applied. A baseline VCG is recorded for 2 minutes with the subject fully restrained immediately preceding the experimental exposure to impact acceleration. The immediate post-impact VCG data collection period commences with the impact stroke and lasts 3 minutes. The subject is then released from the restraints, and the anatomic mounts and the associated inertial instrumentation are removed. The subject remains seated while the sled is returned to its starting point on the track, and a second 3-minute post-experimental VCG is obtained. Afterwards, the subject is escorted from the sled and undergoes the post-run examination by the physician monitor. The entire experimental protocol for the subject lasts 15 minutes and approximately 8 minutes of electrocardiographic data are obtained.

A physician is present during the entire experimental sequence. He has the sole responsibility for the health and safety of the human subject and consequently has the authority to terminate any experiment at any time and for any reason. Both the volunteer subject and the medical monitor have abort devices. These switches must be kept closed continuously or else the experimental sequence will automatically be halted. Oscilloscope monitors provide a continuous display of the VCG. A hard copy of the VCG is provided by the pen recorder, and is reviewed by the medical monitor immediately after the experiment. These records are also reviewed on a routine basis by an internist. Immediate review by the internist may be requested if abnormalities are suspected during the initial review.

Subjects have been exposed to peak sled impact accelerations ranging from 30 m/s^2 to 150 m/s^2 (3 to 15G) to date. The majority of experiments have been conducted with the accelerator mechanically configured to produce, at any chosen peak sled acceleration level, the maximum duration at that peak measured as the time above 75% of peak, about 100 milliseconds, and the maximum possible rate of onset of acceleration to reach that peak. The rate of onset varies with the peak sled acceleration and ranges from approximately $3,000 \text{ m/s}^3$ (300 G/s) to $20,000 \text{ m/s}^3$ (2,000 G/s). Other configurations are possible and have been used in selected experiments.

Over the past 4 years, 651 human impact experiments at the NAMRLD have been conducted in the -X vector, that is, the acceleration is transmitted chest-to-back with the subject seated in the sled mounted chair facing opposite the direction of sled travel. At the time of impact, the unrestrained head and neck are forced towards the chest as the sled is pushed away by the accelerator piston. The test acceleration from onset to offset is of short duration, about 250 milliseconds, and is initially applied to the sled at rest. At the end of the applied acceleration stroke, the sled coasts to a gradual stop under a constant drag of 2.5 m/s^2 (0.25G). End stroke velocities of 17.5 m/s (40 mph) with a total travel of 55 m were achieved for 150 m/s^2 (15G) sled peak acceleration, the highest human impact levels administered at this facility. In addition to the -X vector experiments, 818 lateral impact experiments in the +Y vector have been conducted since 1976. In the +Y experiments, the acceleration is transmitted from right to left, and the unrestrained head and neck move towards the right shoulder.

RESULTS

From January 1974 until 21 February 1978, 923 impact acceleration experiments utilizing human volunteers with electrocardiographic monitoring have been conducted. This represents 72% of the 1,282 inertially instrumented human impact experiments conducted at NAMRLD during this period. Out of 550 inertially instrumented -X impact experiments, 194 (35%) have been monitored with the VCG, and 729 out of 732 inertially instrumented +Y impact experiments (99%) have been similarly monitored. Three instances of clearly identifiable right bundle branch block and a solitary instance of an incomplete left bundle branch block have been observed. One right bundle branch block was seen in a +Y impact experiment, the rest were seen in the -X experiments. The duration of the conduction disturbances ranged from 2 to 10 complexes, 1.5 to 6 seconds, and were recorded on at least two of the three VCG channels. The first three episodes, that is, the two right bundle branch blocks and the solitary left ventricular conduction delay, occurred with the accelerator configured for the maximum rate of onset of acceleration and the maximum duration at the peak acceleration in the -X vector direction. The final episode of right bundle branch block occurred in the +Y vector in a 100 m/s^2 (10G) high rate of onset, short duration accelerator configuration.

In addition to these three episodes clearly identified as right bundle branch block, there have been 42 other instances of single complexes resembling right bundle branch block recorded immediately after the impact stroke. These latter instances could not be defined with certainty because differentiation from solitary premature ventricular contractions with a right bundle branch block pattern was impossible. Several episodes of transient right bundle branch block have been recently observed in a chimpanzee following +Y lateral impact acceleration exposures at levels comparable to the human exposures conducted at this facility. Similarly, right bundle branch block has been observed in a rhesus monkey undergoing -X accelerations at quite high levels. These observations in the subhuman primate have not yet been reported.

The first episode of transient right bundle branch block was observed in Subject 35. The acceleration parameters are shown in Table I. The VCG is shown in Figure 3. The Y channel presents the most clearly identifiable complexes, characteristic of right bundle branch block. Channels X and Z confirm the diagnosis. The conduction delay persisted for 2 seconds following impact and involved four complexes. The electrocardiogram then returned to the pre-impact baseline pattern. A premature atrial contraction was seen following the right bundle branch block complexes; similar premature contractions were also evident in the baseline period immediately preceding the impact event. The subject had no symptoms referable to the cardiovascular system and noted nothing unusual about this experiment. This subject had participated in 19 experiments during the prior 6 months and had previously experienced accelerations up to 103 m/s^2 (10G) without incident.

Because of the conduction disturbance, serial 12 lead electrocardiograms were taken daily for the next 3 days. These were normal and unchanged in comparison with his qualification electrocardiogram. The subject was referred to NAMRL, Pensacola, Florida, where he was fully reevaluated 7 weeks later. He remained asymptomatic during the interval. The reevaluation examination was identical to his initial qualification cardiovascular examination but also included echocardiography which had previously not been available. No evidence of cardiac pathology was found. The subject was advised of the examination results, and with the concurrence of the medical staffs, chose to continue in the experimental protocol. After returning to the experimental impact program, he subsequently underwent 16 acceleration exposures during the next 9 months. His highest peak sled acceleration level was 150.2 m/s^2 (15G) and no cardiac abnormalities were detected during any of the 16 experiments. After a total of 16 months in the impact program, he was transferred to another assignment to continue his naval career.

The second episode of transient right bundle branch block was observed in Subject 50. The acceleration parameters are in Table I. The VCG is shown in Figure 4. The Y channel again presents the clearest identifiable complexes characteristic of right bundle branch block. The complexes which can be identified in the X channel confirm the diagnosis. In this instance, the conduction delay persisted for approximately 6 seconds and included 10 complexes. A normal sinus mechanism was present with a rate of 130 beats per minute. Unlike the previous episode of right bundle branch block, the return to a normal intra-ventricular conduction mechanism took place over two or three complexes rather than immediately returning to the baseline pattern. As in the previous case, this subject remained asymptomatic and noted nothing unusual about the run. His previous impact experience extended over 8 months and included nine experimental exposures up to 99.8 m/s^2 (10G). A standard 12 lead electrocardiogram was obtained 2 hours post impact. This tracing revealed minimal ST segment elevation in the anterior precordial leads. The consulting internist recommended immediate hospitalization, and the subject was admitted to a coronary care unit in New Orleans. He was closely observed over the next 72 hours. Serial electrocardiograms demonstrated that the initial ST and T wave abnormalities gradually returned to normal. Cardiac enzyme analysis did not reveal any significant change, however creatine phosphokinase isoenzyme analysis was not available. No treatment other than bed rest

was employed. On the third post-impact day, he was transferred to the Naval Hospital, Pensacola, Florida, for further observation. Normal electrocardiograms were obtained on several occasions. The subject was discharged after 14 days to limited activity and with a diagnosis of cardiac contusion. Three months later, he was returned to NAMRL, Pensacola, Florida, and a complete reevaluation was performed. This study included standard and vector electrocardiography, the Bruce graded stress test, and echocardiography. All results of these studies were normal and unchanged in comparison with his initial qualification examination. After this reevaluation, he was assigned to unlimited duty in the U.S. Navy, but was not permitted to return to an active experimental subject status. His total impact acceleration experience consisted of 10 experiments.

The third observed intraventricular conduction defect occurred in Subject 42. The acceleration parameters are in Table I. The VCG is shown in Figure 5. The first identifiable complexes post impact are seen only in the X and Y channels. The Z channel was not satisfactorily recorded. In the X channel, the S wave deepens with an associated loss of the S wave in the Y channel. There is a slight prolongation of the QRS interval. Definite changes in the ST segment and in the T wave are demonstrated. Even though these changes suggest the diagnosis of a left anterior hemi-block, the initial evaluation of the VCG did not yield the proper identification. Again, the subject remained asymptomatic and did not notice anything unusual about the run. He was exposed to a 130.4 m/s^2 (13G) impact experiment the following day without any identifiable change in the VCG. Two weeks later during a routine review of the VCG, the internist made the correct diagnosis. A review of the VCG which was taken on the day after the incomplete bundle branch block occurred, suggested that no significant lasting change occurred. The subject's prior experience encompassed 23 impact exposures over 9 months, with a maximum sled peak acceleration of 114.2 m/s^2 (11G). He was exposed an additional five times in the next 4 weeks to impact with the highest peak sled acceleration of 152.1 m/s^2 (15G) with no abnormalities noted on the VCG. After 1 year in the impact program, he departed to continue his naval career elsewhere.

The last observed right bundle branch block occurred in Subject 81 during a +Y lateral impact experiment. The acceleration parameters are in Table I. Note that in this experiment both the vector and the accelerator configuration were different from those in the other three episodes. The VCG is shown in Figure 6. All three channels were adequately recorded, however, the bundle branch block is best demonstrated in channels X and Y. The two complexes that immediately follow impact clearly show the right bundle branch block. The return to normal is abrupt. Like all the others, this subject was entirely asymptomatic. Serial post-experiment 12 lead electrocardiograms were normal and unchanged compared to his qualification electrocardiogram. Unlike the earlier three cases, creatine phosphokinase isoenzyme determinations were done twice - one set immediately after the post-experiment physical examination, and the second set 18 hours later. No change was noted in the second set compared to the first "control" set. Prior to the right bundle branch block episode, this subject had experienced 21 impact experiments including both one 10G and one 11G experiment with the same accelerator profile, i.e., high rate of onset and short duration at peak. Subsequent to the intraventricular conduction defect episode, Subject 81 was exposed to a total of 15 additional lateral impact experiments with no recurrence of the bundle branch block.

DISCUSSION AND CONCLUSION

Although nonpenetrating cardiac lesions have been recognized for a long time, recently more attention has been focused on the frequency of cardiac trauma caused by blunt injury. A substantial variety of injuries may result, ranging from electrophysiologic disturbances to chamber rupture (9,10). In 1937, Kissane, Fidler, and Koons observed transient bundle branch blocks in dogs which underwent experimental blunt chest trauma (11). In 1968, Louhimo utilized calibrated weights to produce blunt chest trauma in rabbits, and demonstrated, among other cardiac disturbances, transient intraventricular conduction defects (12). Several clinicians have reported episodes of bundle branch block of a transitory nature following a variety of impact events (1,3,5). It is difficult to compare our observations with previous research since in our experiments there was no direct blow to the chest. Stapp and Taylor (Personal Communication) conducted impact acceleration experiments with human volunteer subjects in 1963 at Holloman Air Force Base, New Mexico and observed no evidence of intraventricular conduction disturbances despite continuous cardiac monitoring. The conduction abnormalities presented here represent events recorded during experimental human exposures to impact accelerations wherein the acceleration applied to the subject as measured at the first thoracic vertebra is known precisely. These forces are thought to be well within human impact tolerance levels.

The etiology of the intraventricular conduction defects reported here is unknown. The volunteer subjects in each of these four cases had a normal cardiovascular system prior to impact, and there is no evidence to suggest any permanent functional changes related to the impact. Increased right ventricular chamber pressure coincidental with the acceleration stroke is a possible mechanism, but would not explain the left ventricular conduction abnormality nor changes suggestive of myocardial contusion. In the last case especially, the subject had been exposed to virtually identical acceleration profiles almost one month prior to the one in which the conduction defect was observed. Although the numbers are too small to be statistically significant, three conduction defects have been seen in 194 -X impact experiments but only one has been seen in 729 +Y lateral impact experiments, suggesting a possible vector dependency.

In the animal experiments referred to earlier, right bundle branch block was produced in a chimpanzee exposed to +Y lateral impact each and every time he was accelerated to and above 120 m/s^2 (12G). This same animal subject did not show any intraventricular conduction disturbances when subjected to -Y impact at similar levels, further suggesting vector dependency.

In a clinical setting, the detection of an isolated asymptomatic intraventricular conduction defect following blunt chest trauma is rarely, if ever, seen. In reviewing the available literature regarding transient conduction defects, all patients had either obvious physical findings or were symptomatic to suggest the ordering of an electrocardiogram. Many persons who remain asymptomatic after exposure to forces similar to those reported here will not consult a physician, and therefore, if a conduction defect or other electrocardiographic changes are transiently present, they will not be discovered. The experimental setting described in this report offers a unique opportunity for studying such fleeting abnormalities.

The chimpanzee is an excellent human surrogate in which to observe impact-induced electrocardiographic changes, and future experiments have been planned in an effort to define the causative mechanisms involved. The important questions are: 1) Is right bundle branch block related in a dose response way to the acceleration applied to the subject, and 2) Is right bundle branch block premonitory of additional problems at a higher level, i.e., permanent block? Therefore, by utilizing the subhuman primate, it should be possible to develop a predictive injury model and to delineate the natural history of impact-induced intraventricular conduction defects.

REFERENCES

1. Jones, J. W., Hewitt, R. L., Drapanas, T.: Cardiac Contusion: A Capricious Syndrome. *Annals of Surgery*, 181:567-574, 1975.
2. Parmley, L. F., Manion, W. C., Mattingly, T. W.: Nonpenetrating Traumatic Injury of the Heart. *Circulation*, 18:371-396, 1958.
3. DeMuth, W. E., Jr., Bave, A. E., Odom, J. A.: Contusions of the Heart. *Journal of Trauma*, 7:443-455, 1967.
4. Rankin, T. J., Patterson, J. W.: Transient Intraventricular Block in Cardiac Contusion. *American Heart Journal*, 43:103-107, 1952.
5. Ferre, G. A., Steward, W. D.: Cardiac Contusion. *Clinical Orthopedics and Related Research*, 53:123-130, 1967.
6. Bruce, R. A., Rowell, L. B., Blackmon, J. R., Doan, A.: Cardiovascular Function Tests. *Heart Bulletin*, 14:9-14, 1965.
7. Frank E.: An Accurate, Clinically Practical System for Spatial Vectorcardiography. *Circulation*, 13:737-749, 1956.
8. Thomas, D. J., Majewski, P. L., Ewing, C. L., Gilbert, N. S.: Medical Qualification Procedures for Hazardous-Duty Aeromedical Research. AGARD: Aerospace Medical Panel Specialists Meeting, London, U.K., 24-28 October 1977.
9. Liedtke, A. J., DeMuth, W. E., Jr.: Nonpenetrating Cardiac Injuries: A Collective Review. *American Heart Journal*, 86:687-697, 1973.
10. Symbas, P. N.: Contusion of the Heart, Chapter 5, in Traumatic Injuries of the Heart and Great Vessels. Springfield, Charles C. Thomas, 1972, pp. 37-52.
11. Kissane, R. W., Fidler, R. S., Koons, R. A.: Electrocardiographic Changes Following External Chest Injury to Dogs. *Annals of Internal Medicine*, 2:907-935, 1937.
12. Lohimo, I.: Heart Injury after Blunt Thoracic Trauma. *Acta Chirurgia Scandinavica*, (Supplement 380), 1:1-60, 1968.

SUBJECT	VECTOR	PEAK SLED ACCELERATION	RATE OF ONSET	DURATION	VELOCITY CHANGE
35	-X	111.3 m/s ² (11G)	8841 m/s ³ (884G/s)	0.1088 s	14.16 m/s (31.6 mph)
50	-X	126.8 m/s ² (13G)	13001 m/s ³ (1300G/s)	0.1006 s	15.28 m/s (34.2 mph)
42	-X	121.0 m/s ² (12G)	10234 m/s ³ (1023G/s)	0.1078 s	15.06 m/s (33.7 mph)
81	-Y	100.5 m/s ² (10G)	12024 m/s ³ (1202G/s)	0.0292 s	3.28 m/s (7.3 mph)

TABLE I

SLED INERTIAL PARAMETERS

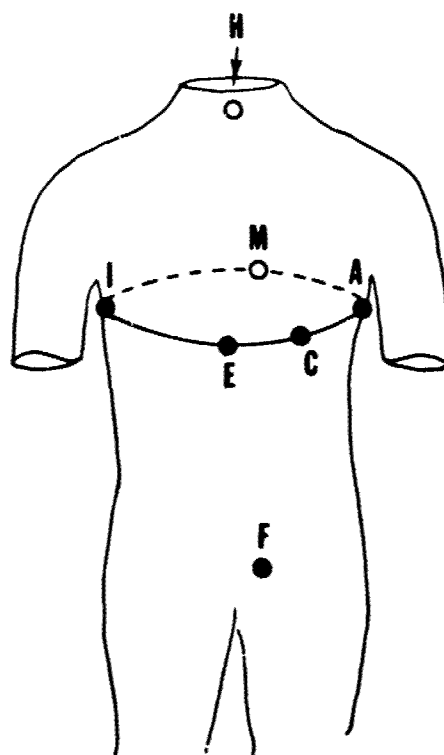


Figure 1 VCG Electrode Placement

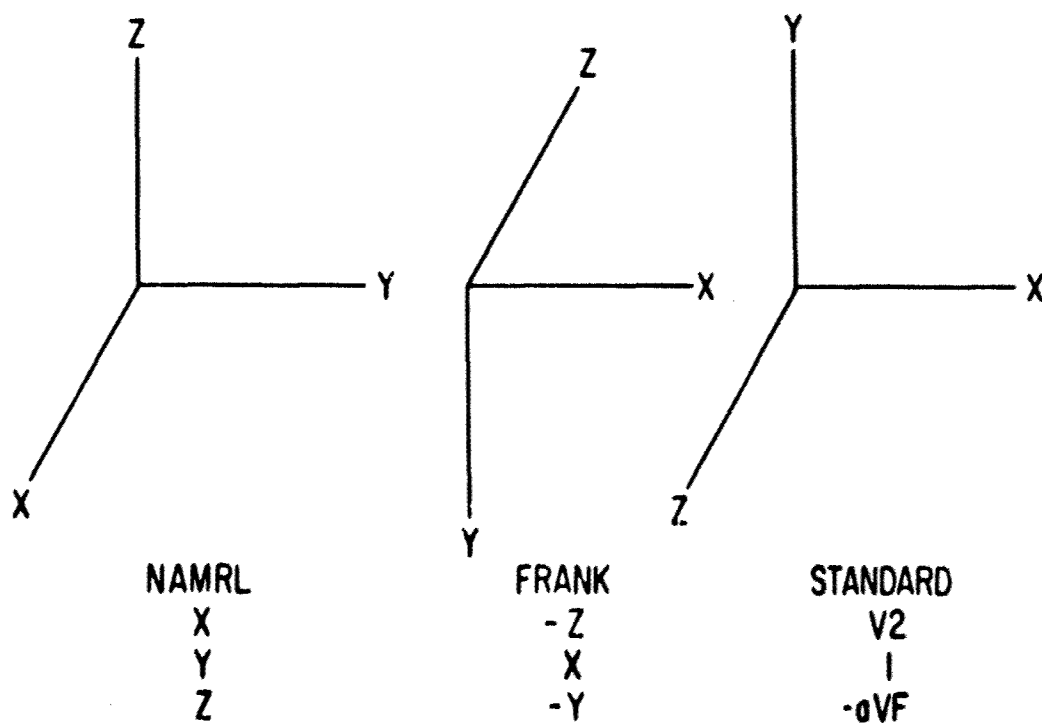


Figure 2 Physiologic Coordinate Systems Comparison

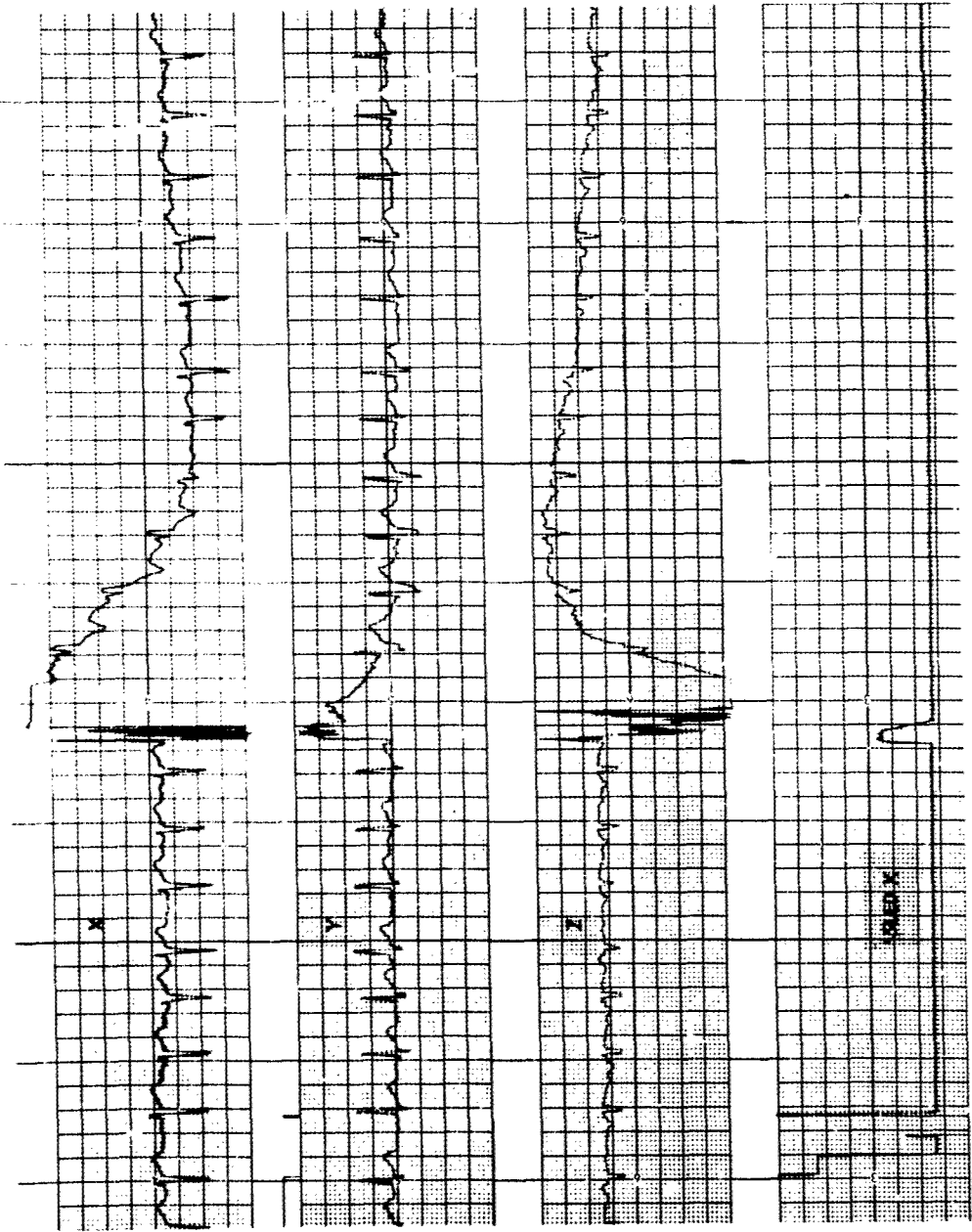


Figure 3 Right Bundle Branch Block - Subject 35

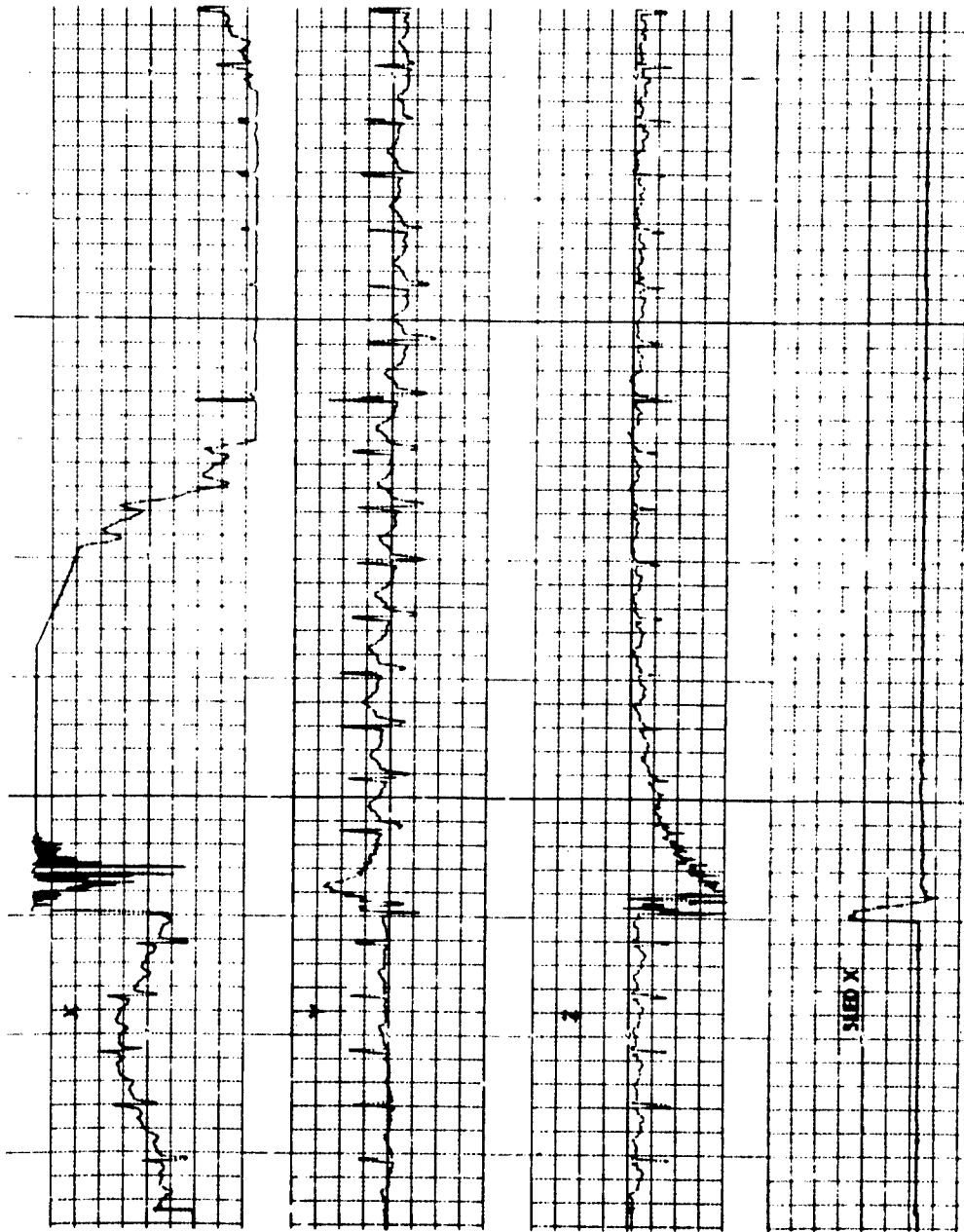


Figure 4 Right Bundle Branch Block - Subject 50

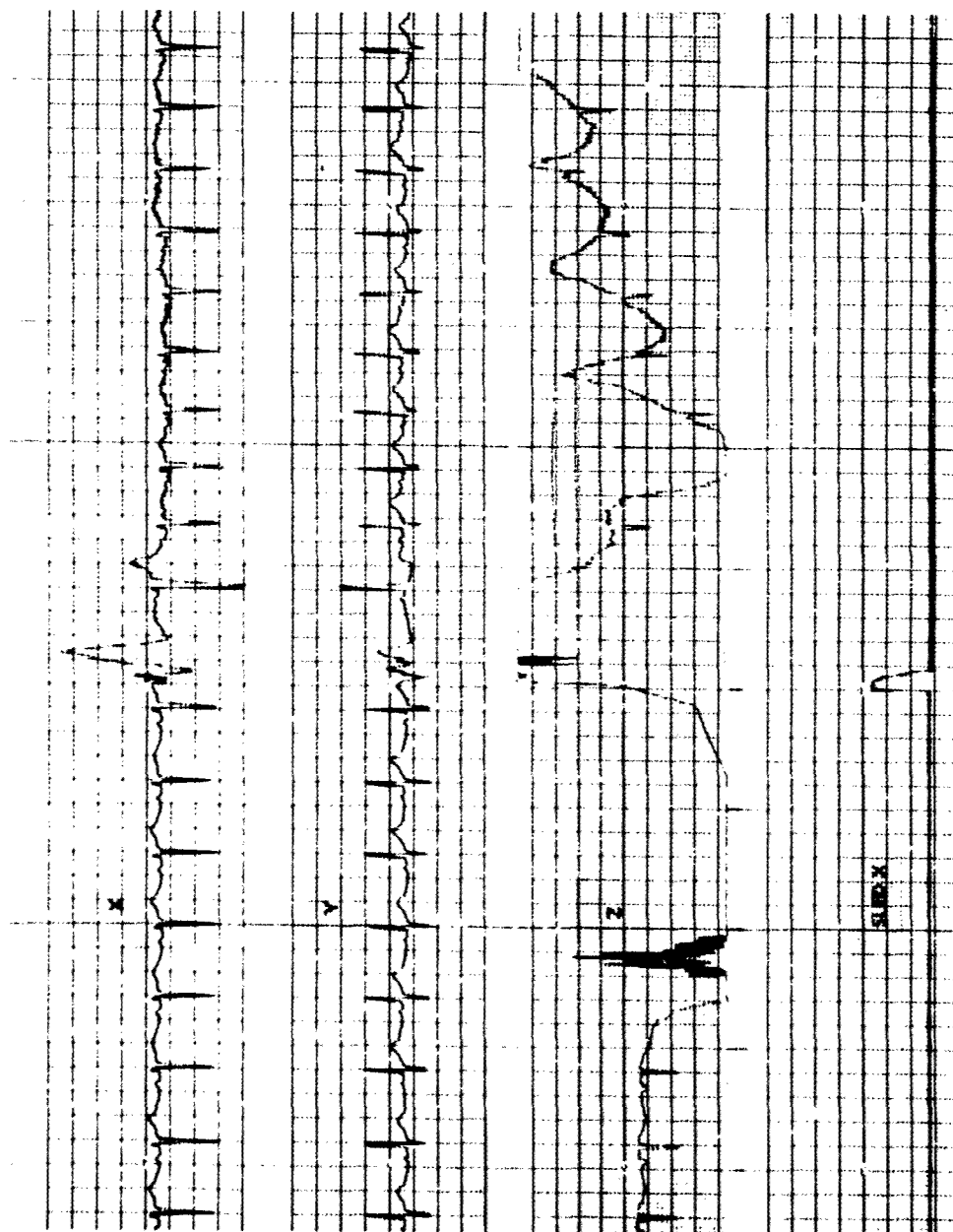


Figure 5 Incomplete Left Bundle Branch: Block - Subject 42

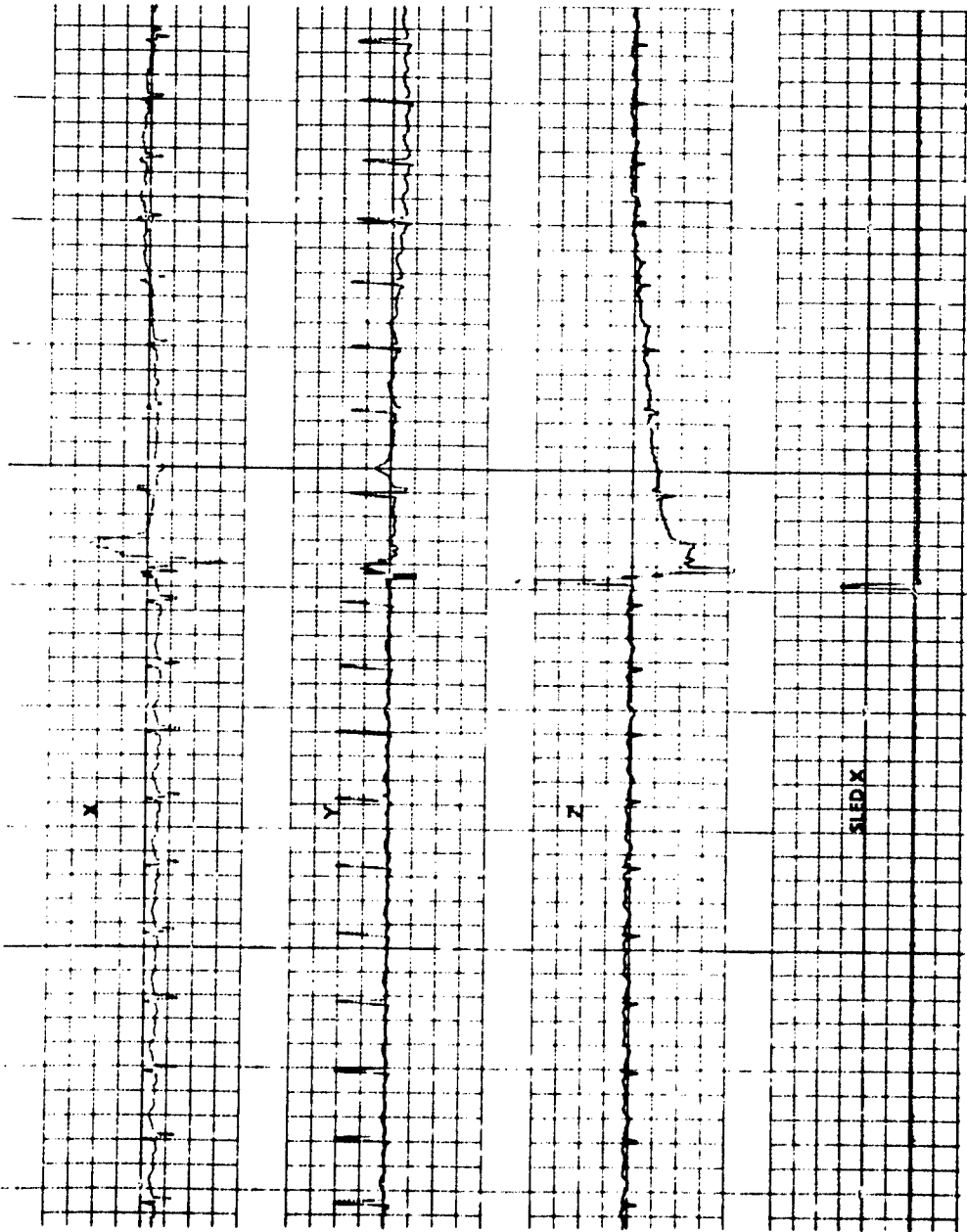


Figure 6 Right Bundle Branch Block - Subject 81

DISCUSSION

COL. C. KNAPP (USA)

Have you tried to correlate this finding with anyone that has ever had significant chest trauma or has been restrained in say an aircraft or vehicular accident? Looking for hemi-block or development of acquired right bundle branch block?

AUTHOR'S REPLY

The literature review on the subject that you're alluding to is included in the paper. There is, in the medical literature very little information that relates to this observation. If you review the literature about myocardial-contusion the statement is present that myocardial-contusion does not exist in the asymptomatic patient and we have seen it here in the totally asymptomatic patient. There's some work that was produced out of Tulane University (Ref. 1) that pointed to the incidence in clinical practice of myocardial damage in automobile accidents.

COL. C. KNAPP (USA)

One last question: Will you be monitoring these subjects for any period of time epidemiologically to see if ten years from now they developed anything?

AUTHOR'S REPLY

We hope to.

DR. D. THOMAS (USA)

I've one point of clarification with regard to the monitoring of people for a long time. The only subject that we have had the opportunity to follow for a long time period after exposure to impact acceleration experiments is Dr. J. P. Stapp. Having sustained far more acceleration than we could ever expose our subjects to - I think he had over 20 high g exposures, one as high as 40 g's - he has been extensively evaluated by Dr. Mitchell at Pensacola, Florida, and is in good health. Other than that his gourmet habits have added to his girth, he is a very healthy, alert and productive individual. He is over 65 years of age now. No evidence of myocardial problems at all.

SIMULATION OF HEAD AND NECK RESPONSE TO -G_x AND +G_z IMPACTS

by

A. I. King, S. S. Nakhla and N. K. Mital

Wayne State University
Bioengineering Center
Detroit, Michigan 48202
U.S.A.

SUMMARY

A two-dimensional mathematical model of the spine was exercised to identify mechanisms of neck injury due to hyperflexion. Loss of pilots due to ditching at sea was one of the motivations for this study. It was found that helmets have the potential of increasing injury severity particularly during a combined +G_z and -G_x impact, with the pulses coincident in time. The four parameters that are potentially injurious are neck shear, chin-chest contact force, odontoid process excursion into the spinal canal and spinal cord stretch.

1. INTRODUCTION

Hyperextension injuries of the neck have been extensively studied as a result of the common 'whiplash' syndrome. However, neck injuries due to head motion are not restricted to this mechanism. Ewing and Inomas (1) have conducted studies on head and neck kinematics during hyperflexion, using living human volunteers. Mertz and Patrick (2) have used both volunteers and cadavers to establish the strength and response of the human neck. They provided a response envelope for both flexion and extension. Hyperflexion injuries of the neck have been sustained by automobile crash victims involved in frontal collisions (-G_x acceleration), as reported by Patrick and Andersson (3). The problem of ditching fatalities was reported by Wolff et al (4). Navy pilots who miss the carrier deck and ditch in full view of the carrier were unable to eject and were lost along with the aircraft. They were apparently concussed although there was no evidence of direct head impact with the aircraft interior. In addition, protective helmets were worn. This is a cursory review of the neck injury problem and points to the need for a deeper understanding of the mechanisms involved and the eventual establishment of a set of injury criteria for the neck.

This paper is concerned with a parametric study of neck response using a validated mathematical model of the head and spinal column developed by Tennyson and King (5). The purpose of the investigation is to quantify certain kinematic and kinetic variables which can cause injury to the central nervous system (CNS) but are not currently identifiable from experimental studies using other forms of human surrogates. One of the principal variables is the helmet which increases the mass and mass moment of inertia of the head and is not usually worn by civilians involved in automobile accidents. The effects of a combined +G_z and -G_x impact were analyzed using a triangular 10-g pulse for each direction of impact. The relative time of occurrence of the 2 peak acceleration was varied to demonstrate differences in response. The principal dependent variables of this study are neck shear and moment, head linear and angular acceleration and displacement, odontoid process motion into the spinal canal, stretch of the cervical cord and chin-chest contact force.

2. MATHEMATICAL MODELS OF THE SPINE

In a recent survey of mathematical models simulating impact of biomechanical systems, King and Chou (6) cited a variety of lumped and discrete parameter models as well as continuum models of the spine. Developments subsequent to this survey include the introduction of three dimensional models by Schwer (7) and the simulation of muscular response. Huston and Advani (8) proposed a head and neck model which consisted of the head, 7 cervical vertebrae and the torso. It was validated against experimental data obtained by Ewing and Thomas (1) who subjected human volunteers to -G_x acceleration impacts on a horizontal sled. The correlation was very good. Muscle action was included in the model but neuromuscular delay was not properly simulated. There was no muscle force for the first 100 ms and thereafter it was an instantaneous function of stretch and stretch rate. Pontius and Liu (9) formulated a head and neck neuro-muscular model from the model by Orne and Liu (10). The muscle configuration consisted of active elements between adjacent vertebrae and there were no muscles which spanned more than one disc space. Muscle force was assumed to be function of stretch only and the delay was simulated properly by storing the stretch information for a predetermined delay period of 40 to 80 ms. There was also a muscle activation level to simulate a tensed or relaxed state. The model was exercised to simulate a mild 'whiplash' but model results were not compared with any experimental data.

Tennyson and King (5) proposed a biodynamic model of the spine to simulate the action of the spinal musculature on a discrete parameter vertebral column model conceptually similar to the one developed by Prasad and King (11). It is, thus, a two-dimensional model which can simulate motion of the head, the pelvis and the 24 vertebrae in the mid-sagittal plane. Each segment was treated as a rigid body and was assigned to carry a portion of the torso weight which was eccentric with respect to the centerline of the spine. The rigid bodies assumed a trapezoidal shape and were arranged to simulate the spinal curvatures as closely as possible. The dual load path through the spinal column was modelled by

elements. The disc is an elastic element capable of simultaneously resisting axial and shear loads and bending moments. The posterior vertebral structure (facets) was taken to be a spring element which could transmit axial and shear forces. Auxiliary forces were added to the appropriate vertebrae to simulate external contact forces, such as loads due to the shoulder harness, the lap belt and the seat back. It was also possible to simulate chin-chest contact.

The principal muscles represented in the model are the postero-lateral musculature of the spine. These include the deep musculature which is divided into three longitudinal muscle masses, each comprising many overlapping fascicles. The deepest and most medial muscle group is the transversospinalis system, consisting of the interspinalis, rotatores, multifidus, spinalis, semi-spinalis and semispinalis capitis. The longissimus system is lateral to the transversospinalis system and consists of overlapping fascicles extending from all the vertebrae to the head. The longissimus thoracis and lumborum are the strongest muscles of the trunk having their origin at the iliac crest of the pelvis and insertions in all the lumbar and thoracic vertebrae. The longissimus cervicis and capitis are continuations of the longissimus thoracis, having their insertions in the cervical vertebrae and on the mastoid part of the temporal bone. The iliocostalis system is lateral most with its caudal fascicles originating on the ilium and cranial fascicles extending to the seventh cervical vertebra.

The following assumptions were made in the development of muscle model:

- (a) All load transmitting (passive) elements in the posterior structure of the spine including the passive component of muscle were included in the facet model. That is, in compression the 'facet' represented facet joint and spinous process interaction. In tension, the facet model simulated the action of the facet joints, spinous ligaments and passive muscle components.
- (b) The active mode elements for force generators linked vertebra to vertebra posteriorly and were essentially in parallel with the facets.
- (c) The muscle contractile force was taken to be a linear function of stretch and stretch rate.
- (d) The transversospinalis system was represented by the active elements which linked adjacent vertebra.
- (e) The longissimus and iliocostalis systems were represented by a 'linked' muscle system with an insertion at every vertebral level and the head. The contractile force was based on a summation of the activity in the individual active elements. This muscle system was anchored inferiorly in the pelvis.
- (f) A numerical scheme was developed to store the activity of each contractile element for subsequent recall so that a variable neural time delay of up to 100 ms could be simulated.
- (g) As the predominant passive response of the spinal column was one of flexion during $-G_x$ acceleration, only the extensor half of the spinal musculature was modelled.
- (h) Muscular tetany was represented by setting a maximum allowable force developable by any particular muscle.
- (i) Neural activity was confined to the 'stretch reflex' phenomenon and the v -efferent effect remained constant.

It was shown by Tennyson and King (5) that this model simulated very well the head and neck response of a living human subject who was subjected to a $-G_x$ acceleration of 8.1 g. The data were acquired by Ewing and Thomas (1) and the input pulse was sled acceleration, necessitating the use of the entire spine in the model. In a second paper by Tennyson and King (12), it was exercised to reproduce a $-G_x$ acceleration of 5.7 g on the same subject to demonstrate its repeatability. For the same model constants and spinal geometry, the results of the model agreed well with experimental data. Due to the lack of flexors in the neck, the results are only valid for the first 240 ms during which most of the injury would have occurred. Furthermore, this model was validated against cadaveric data for $+G_z$ acceleration by Prasad and King (11), using a version with no muscular response.

This model possesses sufficient flexibility for the parametric study outlined above. The input data set was modified to accept a helmeted head and the model was used to simulate a ditching impact involving a combined $+G_z$ and $-G_x$ acceleration. The peak g-level was restricted to 10 g so as not to overwhelm completely the muscular response of the model.

The weight of the helmet was assumed to be 13.3 N (3 lb) and the combined mass moment of inertia about the lateral centroidal axis was computed to be $11.55 \times 10^{-3} \text{ kg-m}^2$ (164.18 lb-s²/in) by assuming that the helmet to be a spherical shell. The corresponding mass moment of inertia for the head above was taken to be $7.66 \times 10^{-3} \text{ kg-m}^2$ (108.81 lb-s²/in). The shift in the center of gravity due to the helmet was 12.7 mm anteriorly. Several runs were also made with a cephalad shift of 12.7 mm.

3. RESULTS

The input pulse for a combined $+G_z$ and $-G_x$ impact is shown in Figure 1. The simulation

started 20 ms before onset of acceleration and the peaks of the triangular pulses were assumed to occur simultaneously (Case 1) or one peak preceded the other by 50 ms. (Cases 2 and 3). The magnitude of both peaks was 10 g and the duration of each pulse was 200 ms. The rate onset was 200 g/s. The three impact conditions are identified as follows:

Case No.	Symbol	Condition
1	TOGETHER	Simultaneous $+G_z$ and $-G_x$ impact
2	Z THEN X	$+G_z$ impact occurring 50 ms before the $-G_x$ impact
3	X THEN Z	$-G_x$ impact occurring 50 ms before the $+G_z$ impact

The subject was assumed to be in a seated position restrained by a full military harness consisting of a lap belt and an inverted-Y shoulder belt. The pelvis was subjected to the impact pulse shown in Figure 1 and the resulting response of the head and neck is analyzed for possible injury mechanisms. The helmet is assumed to cause a 12.7 mm anterior shift of the head center of gravity.

Figure 2 through 4 show spinal kinematics for a helmeted head for the 3 impact conditions. They show the initial spinal shape (dotted line) and that for extreme forward flexion at the time indicated on the figure (solid line), describing qualitatively the extent of the vertical and horizontal displacement of the head as well as that of its rotation relative to T1 or the inertial reference frame. The corresponding spinal shapes for the case without a helmet are shown in Figures 5 through 7. It is seen that maximum hyperflexion is attained in Case 3, with or without a helmet.

Quantitative data are provided in terms of time history plots of the various parameters that can produce injury. A set of 8 plots for the case of simultaneous $+G_z$ and $-G_x$ peaks (Case 1) is shown in Figure 8 through 15. In each figure, the effect of the helmet is demonstrated. The peak value for disc shear at C1/C2 is doubled due to the helmet, as shown in Figure 8. There is a double contact of the chin with the chest, as shown in Figure 9. The increase in chin-chest force due to the helmet is approximately 30%. Figure 10 shows the vertical acceleration of the head relative to the inertial reference frame. The large positive values coincide with chin-chest contact and the increase in peak acceleration is also approximately 30%. In view of the fact that the helmet causes an increase in the mass moment of inertia of the head, the angular acceleration of the head is reduced when a helmet is worn. This is shown in Figure 11. The horizontal displacement of the head is not affected by the helmet as shown in Figure 12 but the vertical displacement is substantially increased as shown in Figure 13. Since the magnitude of head acceleration is relatively low, other causes of concussion are examined. Fielding (13) has stated that the motion of the odontoid process into the spinal canal is a possible cause for spinal cord injury. Figure 14 shows the extent of this excursion. It is less than 3 mm without the helmet and over 6 mm with the helmet. Another possible source of injury to the CNS is spinal cord stretch which was demonstrated in cats by Friede (14). Figure 15 compares the occurrence of the peaks for the $+G_z$ and $-G_x$ acceleration appears to cause a large percentage increase in disc shear, chin-chest contact force, vertical head acceleration, vertical head displacement odontoid process motion and spinal cord stretch. For the other two cases in which the peaks are separated by a 50-ms duration, the increase in the quantities are less pronounced or non-existent. When the $-G_x$ acceleration peak precedes that of the $+G_z$ acceleration (Case 3), there is very little change in disc shear at C1/C2 (Figure 16), chin-chest contact force (Figure 17), odontoid process motion (Figure 18) and cervical cord stretch (Figure 19). The corresponding curves for Case 2, in which the $+G_z$ acceleration pulse precedes the $-G_x$ pulse by 50 ms, are shown in Figures 20 through 23. The helmet causes a slight increase in these parameters.

The three impact cases can also be compared simultaneously. Figures 24 and 25 show cervical cord stretch for the helmeted and unhelmeted head respectively. It is most severe in Case 1 with helmet and in Case 2 without helmet. The corresponding curves for odontoid process motion are shown in Figures 26 and 27. The displacement is most pronounced for Case 1 with or without helmet.

Table 1 summarizes the peak values of 11 parameters for all 3 impact cases, with and without helmet. The disc and facet shear force are at the level of C1/C2. The rotation of the head is with respect to T1 and the negative sign represents a relative clockwise rotation. All maximum values given in this table occurred at or before 240 ms of simulation.

If the combined center of gravity of the head and helmet was assumed to be shifted caudally by 12.7 mm, the change in injury parameters was surprisingly less severe, as shown in Table 2. For Case 1, there was an increase in head rotation with respect to T1 in comparison with the corresponding value for an anterior shift in the center of gravity. Head displacement also increased but all other values were lower. In the other 2 cases, there was also more head rotation but the other parameters were not altered significantly in comparison with the corresponding values in Table 1. For the helmeted head, conditions are generally most severe for Case 1 when the 2 pulses are coincident. However, the chin-chest contact force is highest in Case 2 and spinal cord stretch is the largest in Case 3.

4. DISCUSSION AND CONCLUSIONS

Spinal cord injury has been identified as a possible cause of concussion when there is no direct head impact. The involvement of the CNS precludes the use of human volunteers or cadaveric subjects. Anthropomorphic and species differences render the results of animal testing somewhat uncertain. An attempt has been made to demonstrate possible mechanisms of

injury using the mathematical model as a human surrogate. The model has been validated against human volunteer and cadaveric data and is expected to yield reasonable results. However, its results are always subject to experimental verification.

A comparison of 3 impact cases with and without helmet was made using a 2-dimensional model of the spine. The same model constants were used for all runs and changes in response could be considered as more reliable than absolute values. The combined $+G_z$ and $-G_x$ impact acceleration pulse was used primarily to simulate a ditching at sea, during which it is possible to have the pulses occur simultaneously or one before the other. A hypothetical profile was selected and a rather low peak acceleration was assumed so as not to overwhelm completely all passive muscular response.

In general, the helmet increased the disc and facet shear forces, resulting in an increased displacement of the odontoid process into the spinal canal. There was also a general increase in spinal cord stretch, chin-chest contact force and head displacement. Head angular acceleration showed a significant decrease. Conditions were most severe when the $+G_z$ and $-G_x$ pulses coincided in time and when the helmet was worn. Spinal cord stretch was over 40 mm with or without helmet for Case 3, in which the $-G_x$ pulse preceded the $+G_z$ pulse. The corresponding values for Case 2 were much lower.

An anterior shift of 12.7 mm in the center of gravity due to the helmet is apparently less desirable than a cephalad shift of the same magnitude. There was less stretch in the cervical cord and the maximum displacement of the odontoid process was approximately the same for all 3 cases with helmet.

In conclusion, this parametric study has identified some possible mechanisms of injury to the cord during hyperflexion of the neck. It has also facilitated future experimental studies by pointing out the conditions that are likely to be most hazardous. The helmet has the potential of increasing injury severity, particularly when the two pulses are coincident in time. The four parameters which are potentially injurious are neck shear, chin-chest contact force, displacement of the odontoid process and spinal cord stretch. They are of higher magnitude for an anterior shift of the head center of gravity in comparison with a cephalad shift of the same magnitude (12.7 mm). This result contradicts intuition and should be verified experimentally.

5. REFERENCES

1. Ewing, C.L. and Thomas, D.J., "Human Head and Neck Response to Impact Acceleration," Naval Aerospace Medical Research Laboratory, NAMRL Monograph 21, August, 1972.
2. Mertz, H.J. and Patrick, L.M., "Strength and Response of the Human Neck," Proc. 15th Stapp Car Crash Conference, SAE, Warrendale, SAE Paper No. 710855, pp. 207-255, 1971.
3. Patrick, L.M. and Andersson, A., "Three-Point Harness Accident and Laboratory Data Comparison," Proc. 18th Stapp Car Crash Conference, SAE Warrendale, SAE Paper No. 741181, pp 201-282, 1974.
4. Wolff, J. et al., "Development of a Method for Evaluating Means for Reducing Impact Injuries to Pilots in Aircraft Accidents," Technical Report No. 69-68-7, Final Report by Serendipity Associates, 1968.
5. Tennyson, S.A. and King, A.I., "A Biodynamic Model of the Human Spinal Column," SAE Transactions, pp 2430-2443, 1976.
6. King, A.I. and Chou, C.C., "Mathematical Modelling, Simulation and Experimental Testing of Biomechanical System Crash Response", J. of Biomech. Vol 9, pp 301-318, 1976.
7. Schwer, L.E., "A Three-Dimensional Large Displacement Transient Analysis of the Human Spine and Torso," Ph.D. Thesis, University of Illinois, Chicago, 1976.
8. Huston, J.C. and Advani, S.H., "Three-Dimensional Model of the Human Head and Neck for Automobile Biodynamic Response to Impact", in Mathematical Modeling Biodynamic Response to Impact, SAE Publication No. SP-412, pp 9-20, 1976.
9. Pontius, U.R. and Liu, Y.K., "Neuromuscular Cervical Spine Model for Whiplash", in Mathematical Modeling Biodynamic Response to Impact, SAE Publication No. SP-412, pp 21-30, 1976.
10. Orne, D. and Liu, Y.K., "Mathematical Model of Spinal Response to Impact", J. of Biomech., Vol. 4, pp 49-72, 1970.
11. Prasad, P. and King, A.I., "An Experimentally Validated Dynamic Model of the Spine, J. of Appl. Mech., Vol. 41, pp 546-550, 1974.
12. Tennyson, S.A. and King, A.I., "Mathematical Models of the Spine," Proc. 1st International Conf. on Mathematical Modeling, Ed. by X.J.R. Avula, U. of Missouri-Rolla, Vol. II, pp 977-985, 1977.
13. Fielding, W., Recorded Statement made at Head and Neck Injury Workshop sponsored by the National Motor Vehicle Safety Council, held in Washington, D.C., 1977.

14. Friede, R.L., "Specific Cord Damage at the Atlas Level as a Pathogenic Mechanism in Cerebral Concussion," J. of Neuropathology and Experimental Neurology, Vol. 19, pp 266-279, 1960.

6. ACKNOWLEDGMENT

This research was supported in part by ONR Contract No. N00014-75-C-1015.

Table 1 - Summary of Peak Values For Anterior Shift of C. G.

Case No. Symbol Parameter	1 TOGETHER		2 Z THEN X		3 X THEN Z	
	W/O Helmet	W/Helmet	W/O Helmet	W/Helmet	W/O Helmet	W/Helmet
Disc. Shear @C1/C2 (N)	399	868	358	409	234	262
Facet Shear @C1/C2 (N)	361	814	357	424	226	260
Chin-Chest Force (n)	2733	3534	3533	3795	3315	3437
Head Vert. Accel (g)	44.5	58.4	57.4	40.6	56.3	48.3
Head Horiz. Accel (g)	45.8	37.4	33.5	33.1	27.1	16.3
Head Ang. Accel (Rad/s ²)	5267	3922	5369	4745	4538	3236
Head Horiz. Disp. (mm)	201	208	185	190	209	211
Head Vert. Disp. (mm)	172	191	200	192	186	187
Odontoid Disp. (mm)	2.9	6.2	2.6	3.1	1.8	2.0
Cord Stretch (mm)	36.4	43.3	29.4	33.4	41.0	40.6
Head Rot. (deg)	-77.5	-73.4	-68.9	-65.6	-69.1	-65.0
(with respect to T1)						

Table 2 - Summary of Peak Values For Caudal Shift of C. G.

Case No. Symbol Parameter	1 TOGETHER		2 Z THEN X		3 X THEN Z	
	W/O Helmet	W/Helmet	W/O Helmet	W/Helmet	W/O Helmet	W/Helmet
Disc. Shear @C1/C2 (N)	399	854	358	527	234	249
Facet Shear @C1/C2 (N)	361	797	357	486	226	245
Chin-Chest Force (n)	2733	2881	3533	3874	3315	3079
Head Vert. Accel (g)	44.5	51.2	57.4	40.2	56.3	46.2
Head Horiz. Accel (g)	45.8	42.4	33.5	40.8	27.1	15.7
Head Ang. Accel (Rad/s ²)	5267	3653	5369	3905	4538	3022
Head Horiz. Disp. (mm)	201	216	185	202	209	221
Head Vert. Disp. (mm)	172	209	200	171	186	201
Odontoid Disp. (mm)	2.9	5.2	2.6	3.8	1.8	2.3
Cord Stretch (mm)	36.4	38.2	29.4	28.6	41.0	39.4
Head Rot. (deg)	-77.5	-83.6	-68.9	-74.3	-69.1	-77.7
(with respect to T1)						

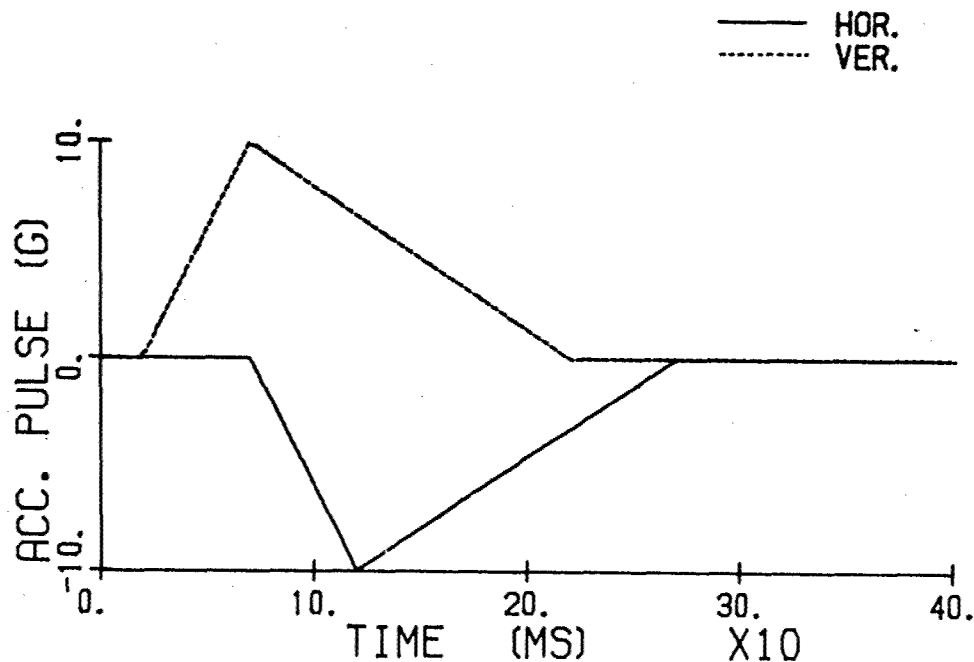


Fig. 1 Combined +G_z and -G_x Input Pulses (Case 2 shown)

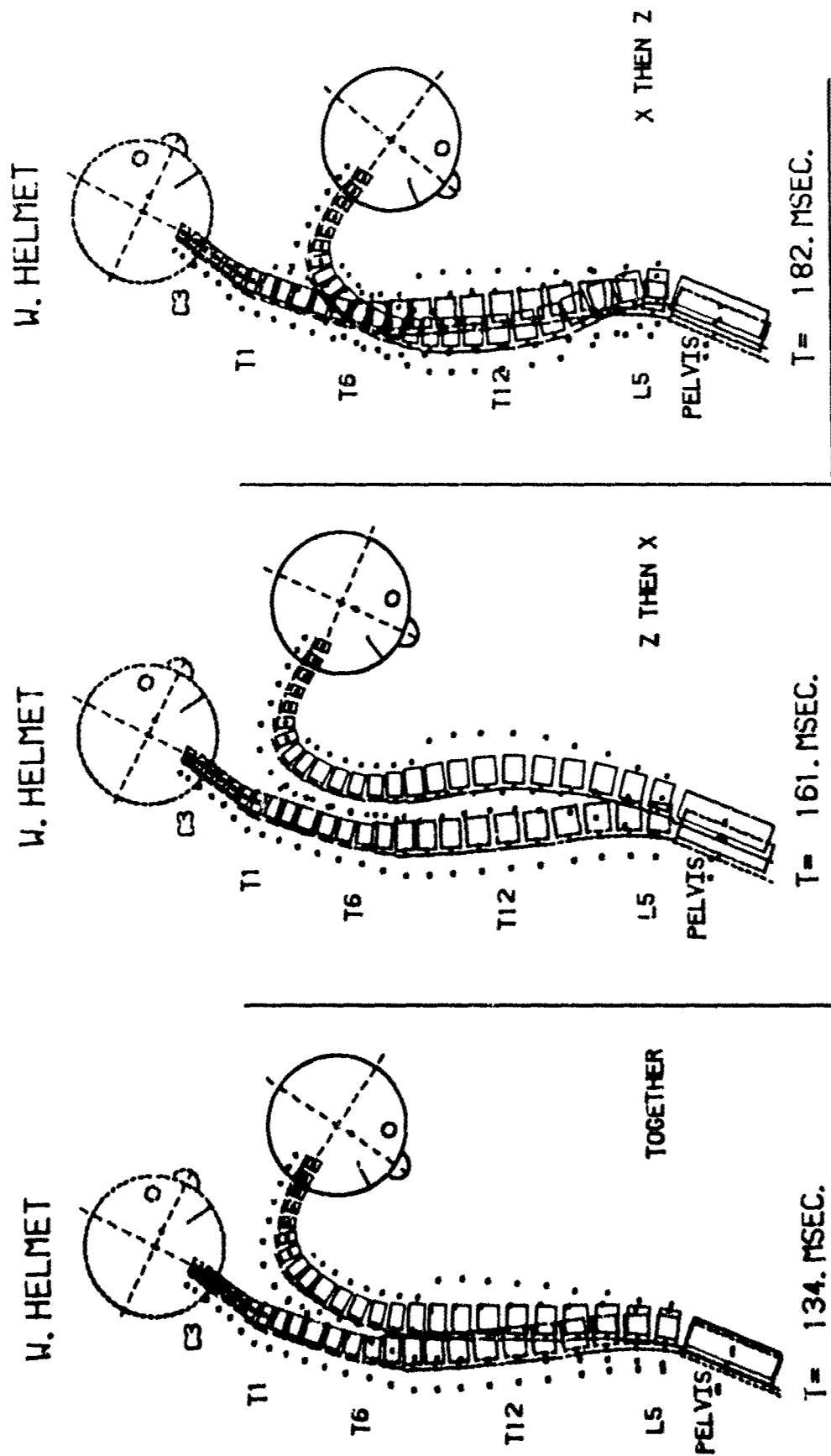
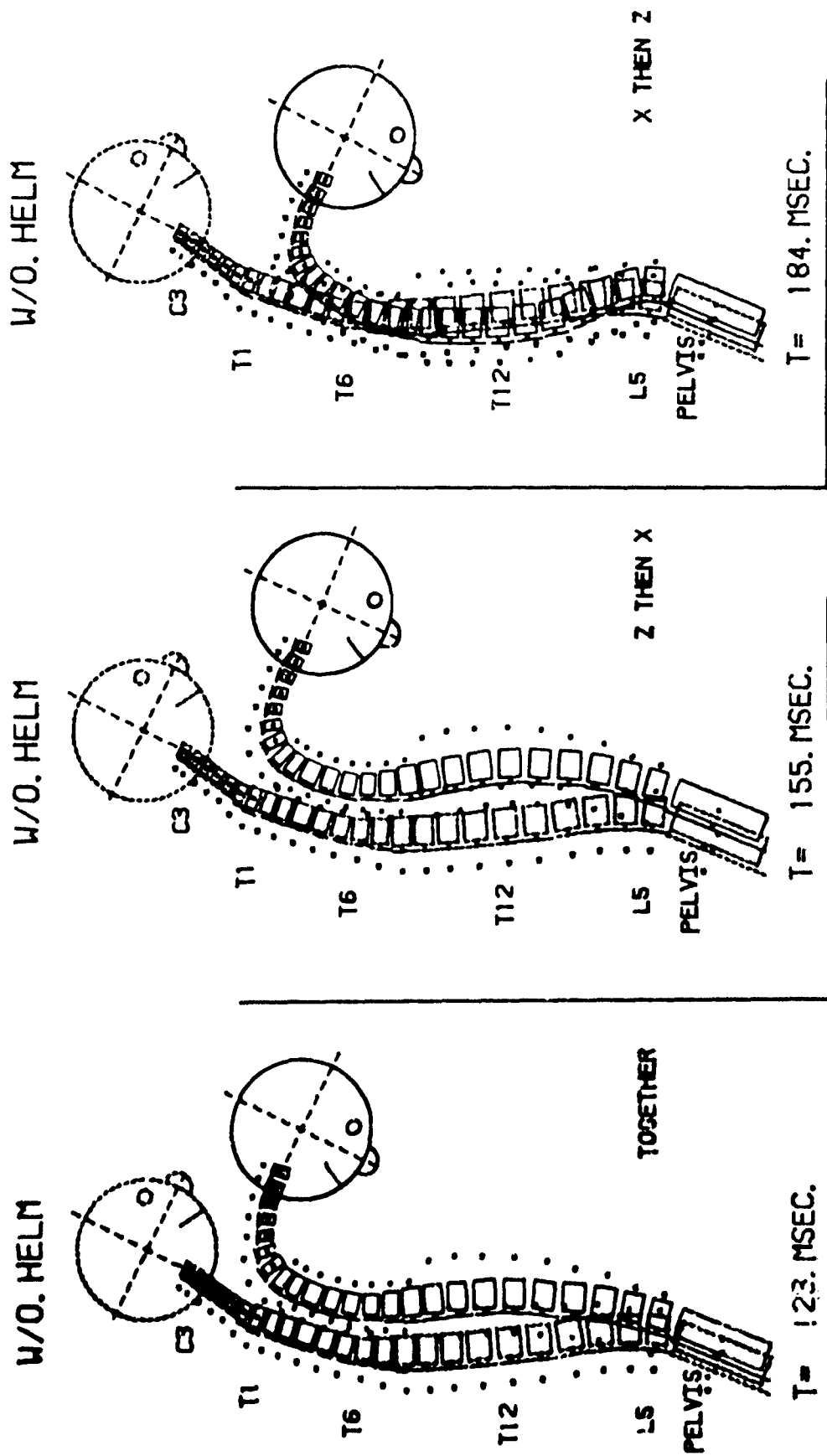


Fig. 2 Spinal Kinematics with Helmet, Case 1

Fig. 3 Spinal Kinematics with Helmet, Case 2

Fig. 4 Spinal Kinematics with Helmet, Case 3



5 Spinal Kinematics Without Helmet, Case 1 Fig.6 Spinal Kinematics Without Helmet, (Case 2 Fig.7 Spinal Kinematics Without Helmet)

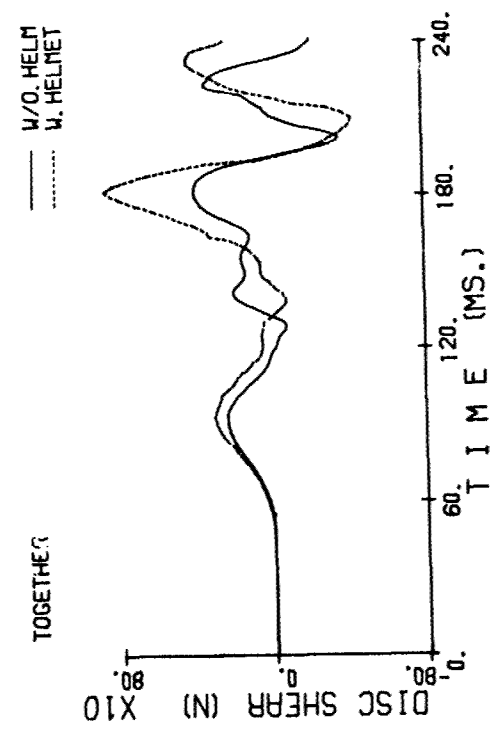


Fig. 8 Disc Shear Force at C1/C2, with and without Helmet, Case 1

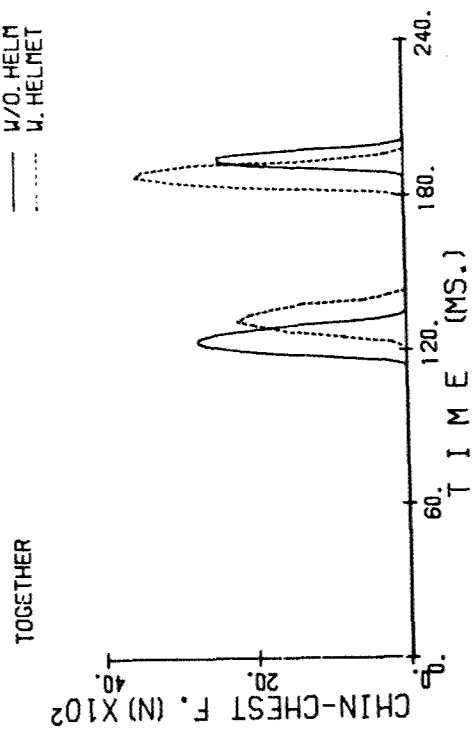


Fig. 9 Chin-Chest Contact Force, with & Without Helmet, Case 1

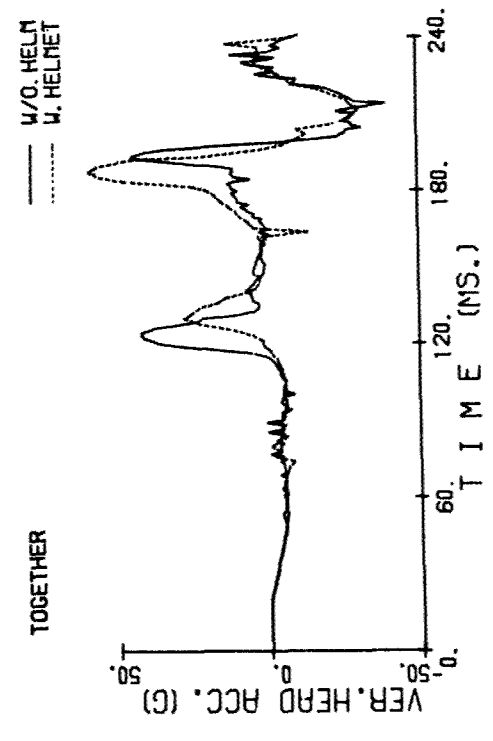


Fig. 10 Vertical Acceleration of the Head, with & Without Helmet, Case 1

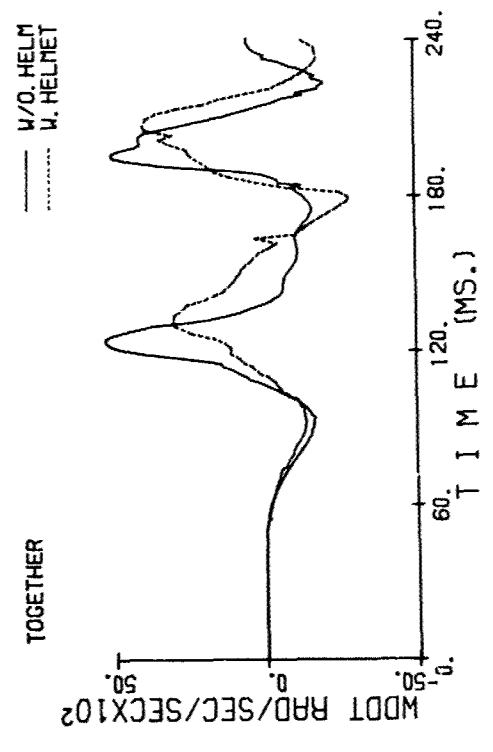


Fig. 11 Angular Acceleration of the Head, with & Without Helmet, Case 1

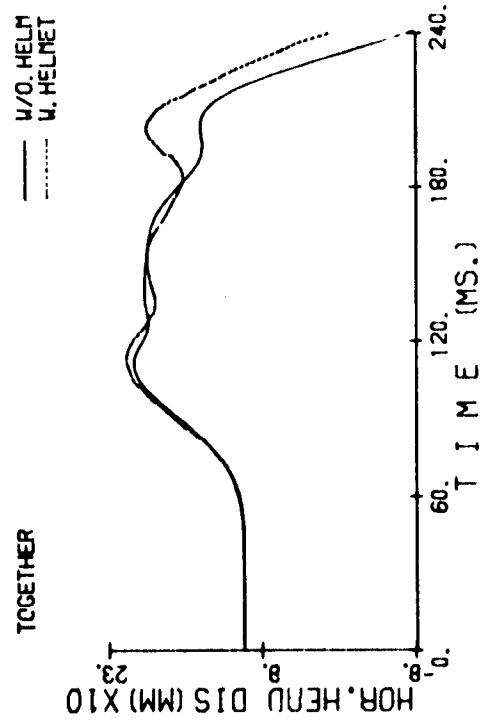


Fig. 12 Horizontal Displacement of the Head, with & without Helmet, Case 1

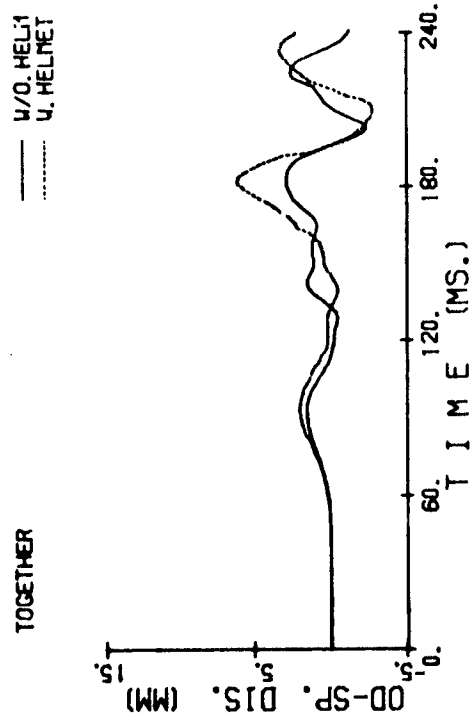


Fig. 14 Odontoid Process Displacement into the Spinal Canal, with & without Helmet, Case 1

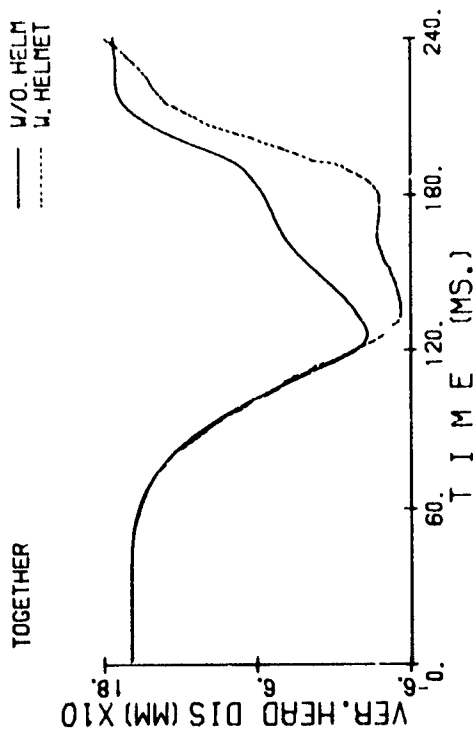


Fig. 13 Vertical Displacement of the Head, with & without Helmet, Case 1

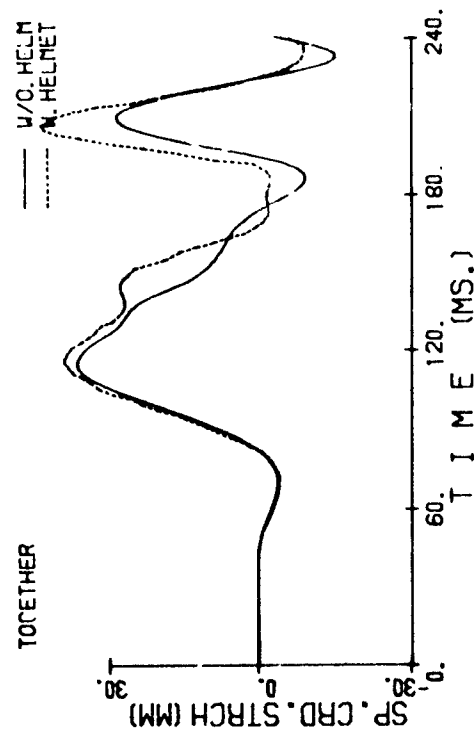


Fig. 15 Spinal Cord Stretch, with & without Helmet, Case 1

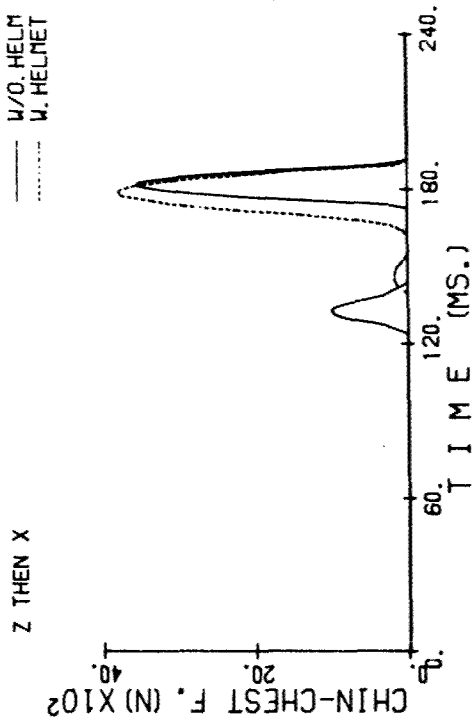


Fig. 16 Disc Shear Force at C1/C2, with & without Helmet, Case 2

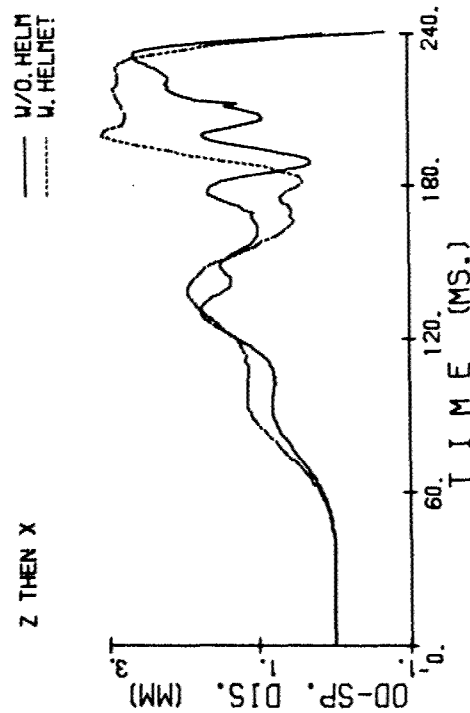


Fig. 17 Chin-Chest Contact Force, with & without Helmet, Case 2

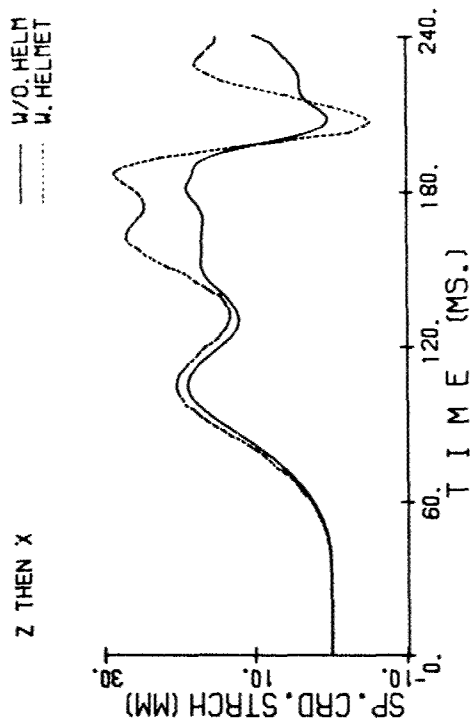


Fig. 18 Odontoid Process Displacement into the Spinal Canal with & without Helmet, Case 2

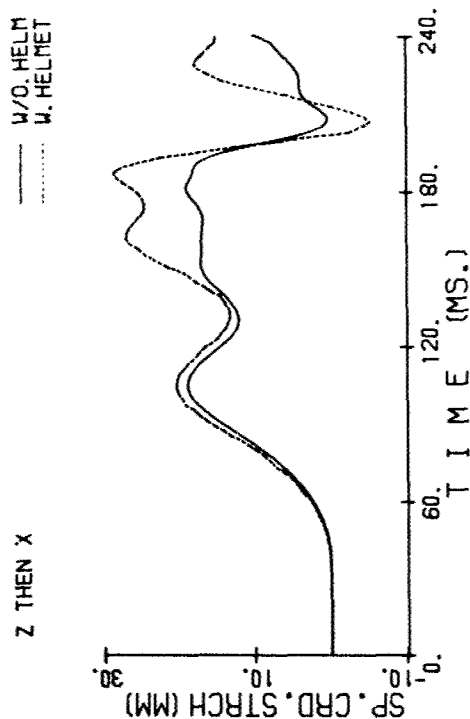


Fig. 19 Spinal Cord Stretch, with & without Helmet, Case 2

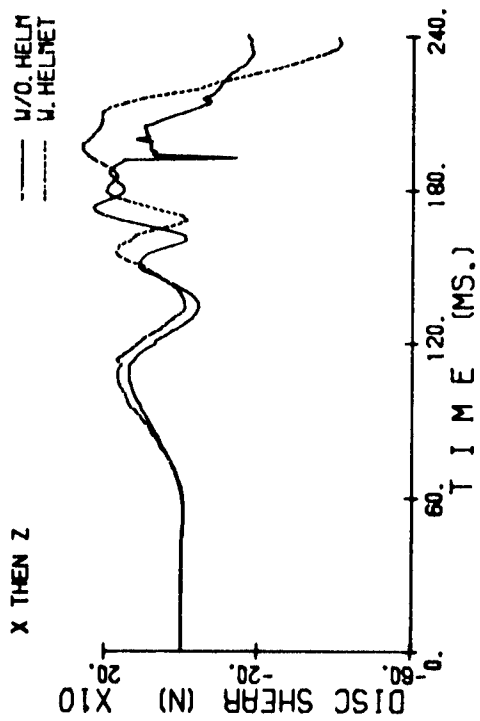


Fig. 20 Disc Shear Force at C1/C2, with & without Helmet, Case 3

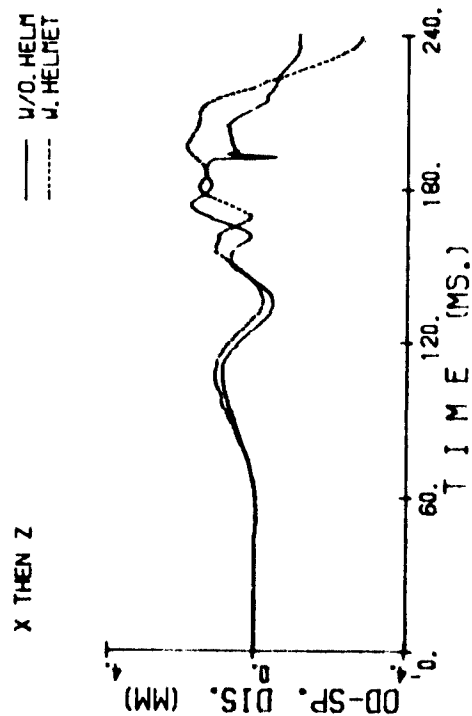


Fig. 22 Odontoid Process Displacement into the Spinal Canal, with & without Helmet, Case 3

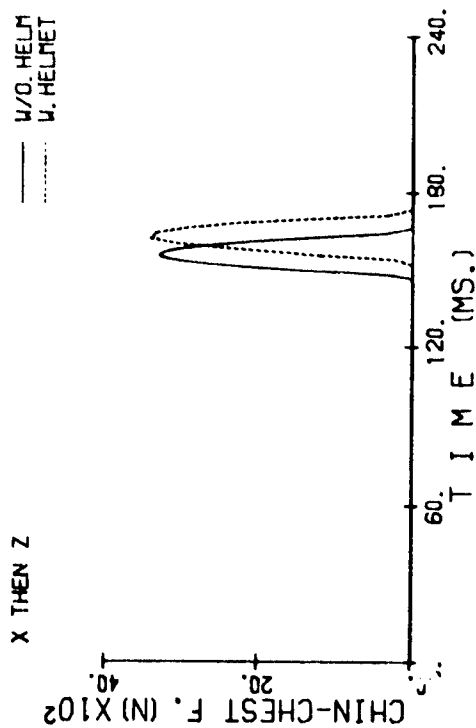


Fig. 21 Chin-Chest Contact Force, with & without Helmet, Case 3

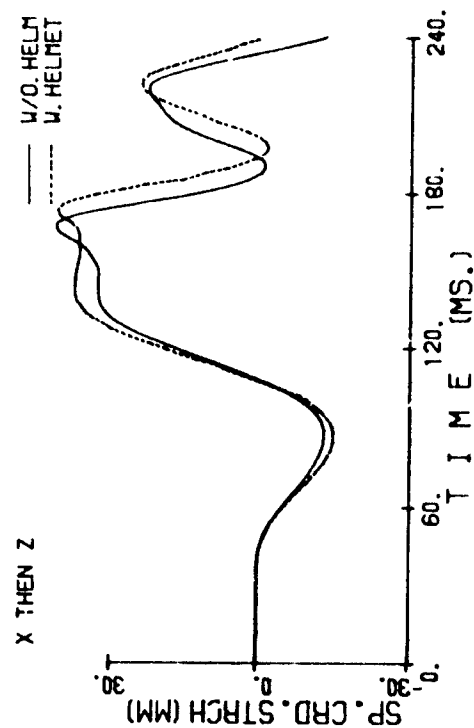


Fig. 23 Spinal Cord Stretch, with & without Helmet, Case 3

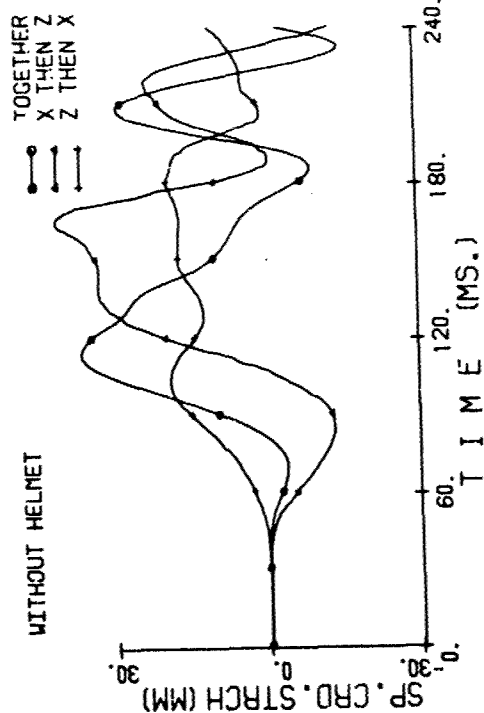


Fig. 25 Spinal Cord Stretch without Helmet, Cases 1 through 3

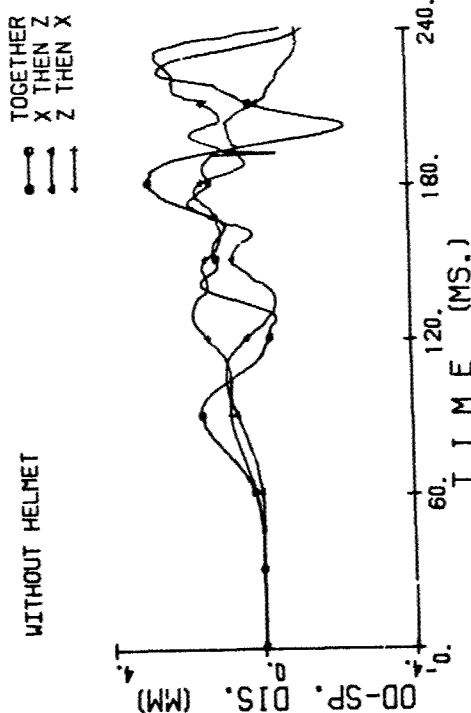


Fig. 27 Odontoid Process Displacement into the Spinal Canal without Helmet, Cases 1 through 3

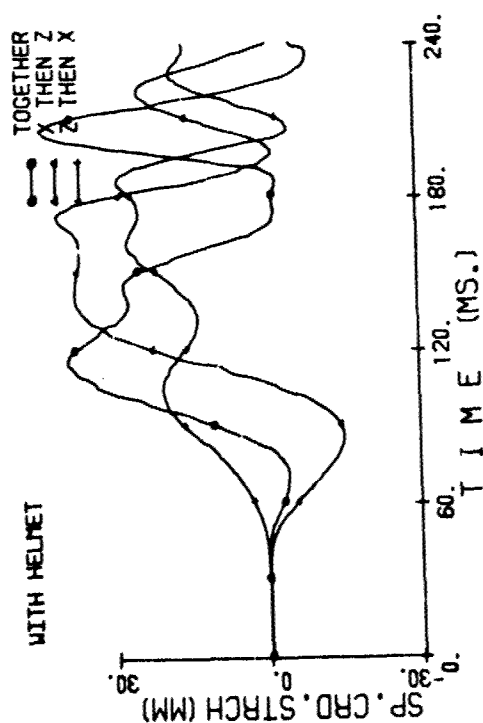


Fig. 24 Spinal Cord Stretch with Helmet, Cases 1 through 3

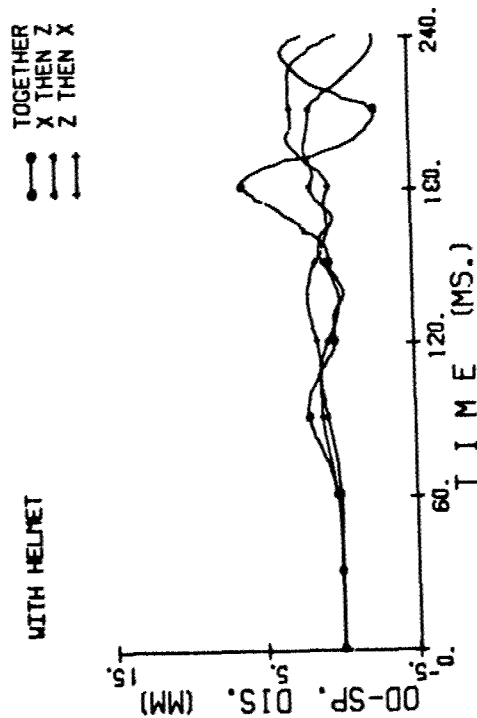


Fig. 26 Odontoid Process Displacement into the Spinal Canal with Helmet, Cases 1 through 3

DISCUSSION

COL. C. KNAPP (USA)

What was the total added helmet weight?

AUTHOR'S REPLY

1.36 kilograms.

COL. C. KNAPP (USA)

Are you willing to make an estimate, what would happen if the CG was lateral instead of sublateral inferior in opposed torquing?

AUTHOR'S REPLY

We have some helmets with visually coupled systems that have a significant lateral loading. This problem we have to refer to Dr. Belytschko's 3-dimensional model.

DR. MEIER-DORNBERG (FRG)

Have you all established some tolerance criteria for your model for instance tolerable deflection or yield or something else? Or have you only computed some response values?

AUTHOR'S REPLY

We are in the process of trying to establish tolerance criteria. We have not yet done it.

A THREE-DIMENSIONAL MATHEMATICAL ANALOGUE OF THE SPINE STRUCTURE A COMPREHENSIVE APPROACH

Manohar M. Panjabi, Dr. Tech.
Engineering Laboratory for Musculoskeletal Diseases
Section of Orthopaedic Surgery
Yale Medical School
New Haven, CT 06510
U.S.A.

SUMMARY

Mathematical analogues of the human spine structure are important tools in the understanding of the mechanism of injury and its prevention and treatment. The analogue may be thought of as having two parts: a set of governing equations, also called the mathematical model, and the physical properties data of the human spine. The comprehensive approach presented here stresses the need for simultaneous development of both of these constituents.

The human spine is viewed as a collection of functional spinal units, each unit consisting of two adjacent vertebrae and the interconnecting soft tissue. Mathematically this unit of the spine is modelled as two rigid bodies connected by a single deformable link. The latter is a three-dimensional three-element viscoelastic solid. Experimental techniques have been developed which provide the physical properties of the human functional spinal units in three-dimensional space. Such data is being made available now. These properties incorporated into a three-dimensional mathematical model will provide, for the first time, a mathematical analogue of the spine which is entirely based upon experimentally derived spine data.

LIST OF SYMBOLS

C	- damping matrix
K	- stiffness matrix
M	- inertia matrix
d	- displacement vector
f	- force vector
q	- load vector
r	- translation vector
u	- position vector, body coordinate system
v	- position vector, global coordinate system
μ	- moment vector
ϕ	- rotation vector
a,b,c	- axes of the spring coordinate system
i	- arbitrary body
k	- arbitrary spring
l,m,n	- axes of the global coordinate system
x,y,z	- axes of the body coordinate system
.	- derivative with respect to time

I. INTRODUCTION

Mathematical analogues of the human spine structure are important tools in the understanding of the mechanism of injury and its prevention and treatment. The usefulness of an analogue depends upon the accuracy with which it can predict the behavior of the spine structure for a given set of stimuli. The mathematical model may be of the continuous or of the discrete-parameter type. This discussion is limited to the latter. A review of the literature may be found in Belytschko et al (1973,¹), Panjabi (1973,¹³) and King and Chou (1976,⁵).

Latham (1957,⁷) is generally credited for having proposed the first discrete-parameter type mathematical model involving the human spine. The first continuous model was utilized by Hess and Lombard (1958,²). There has been a continuous progress from the simple one-degree-of-freedom uniaxial model of Latham to quite sophisticated multiple degree-of-freedom three-dimensional models of the present day, Schultz et al (1972,¹⁵), Belytschko et al (1973,¹) and Panjabi (1973,¹³).

One of the major difficulties in the use of these spine models has been the assignment of values to the stiffness and damping coefficients of the deformable elements. Hess and Lombard were aware of this difficulty and they devised a solution to the problem of the missing data of the physical properties of the human spine. "The values of the mechanical properties of the human body (spine) are unknown.... There exists, however, another possibility, an indirect procedure, which may be called "model fitting". In this procedure use is made of data showing the response of the human body (torso) to a certain applied acceleration, the values of these parameters are varied until the response of the model is as nearly as possible the same as that of the torso, and in this way the model is fitted to the data."* Unfortunately this "solu-

*Hess and Lombard (1958,²). Words in parentheses are ours.

tion" with some modifications has been often used ever since.

The basic assumption underlying this "solution" is that the matching of the model behavior with the experimental behavior in a set of given situations somehow validates the model for all other situations. This is quite convenient, but is not necessarily true.

We believe a better and more accurate solution lies not in finding a shortcut of "model fitting", but in making progress on two fronts simultaneously: 1) determining the mechanical properties of the human spine under physiological loading environments that are as close to *in vivo* situation as possible and 2) developing mathematical models that are capable of incorporating the experimentally obtained physical properties of the spine.

The purpose of this paper is to present some details of the above approach and to document the progress that has been made.

II. A COMPREHENSIVE APPROACH

A mathematical analogue may be thought of as having two constituents, namely a set of governing equations (the mathematical model) and the physical properties data of the spine it incorporates. The approach presented here is comprehensive in the sense that the two constituents have evolved simultaneously and are related to each other.

A. The Mathematical Model

1. General Considerations

The human spine has 24 vertebrae that articulate with each other and with the head and sacrum on either end, thus constituting 25 articulating joints, Figure 1. Each of these joints may be considered as a unit of the bony and ligamentous spine. Thus, we may define the functional spinal unit (FSU), with the exception of the occiput-C1 and L5-S1 articulations, as a basic unit of the spine consisting of two adjacent vertebrae and the interconnecting tissues, namely a disc, nine ligaments and two facet joints, Figure 2.

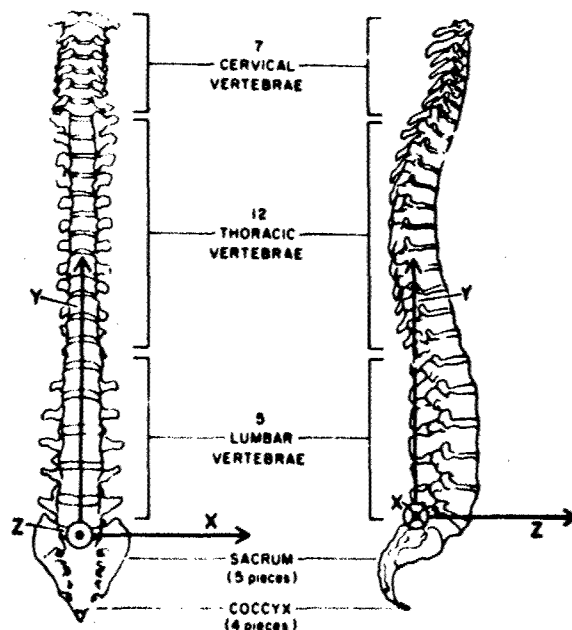


Figure 1. Anatomy of the human bony and ligamentous spine.

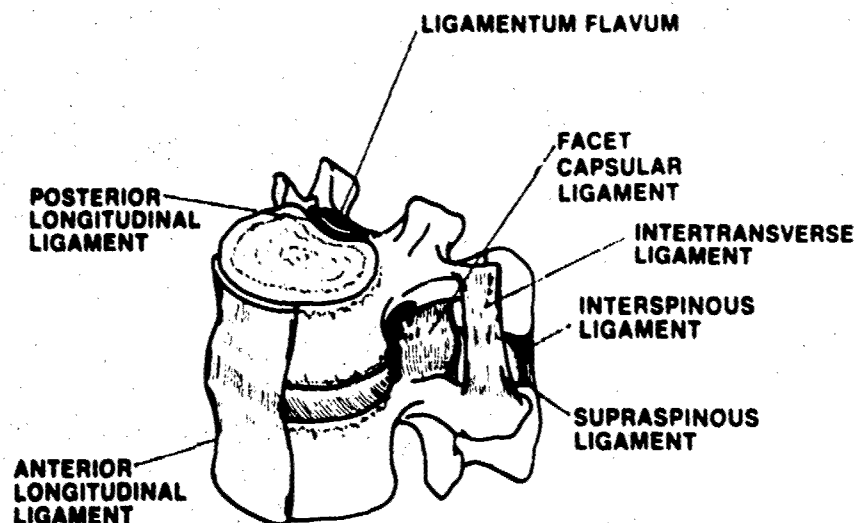


Figure 2. Anatomy of the functional spinal unit (FSU) or the motion segment.

The human spine is idealized as a collection of functional spinal units connected in a serial manner. Each of the FSU is mathematically modelled as a single three-dimensional three-element deformable link connecting two rigid bodies at their centers. The deformable link represents the three-dimensional viscoelastic characteristics of the intact FSU, i.e. the disc, ligaments, facet joints and a vertebra. One of the ways this concept can be illustrated is shown in Figure 3.

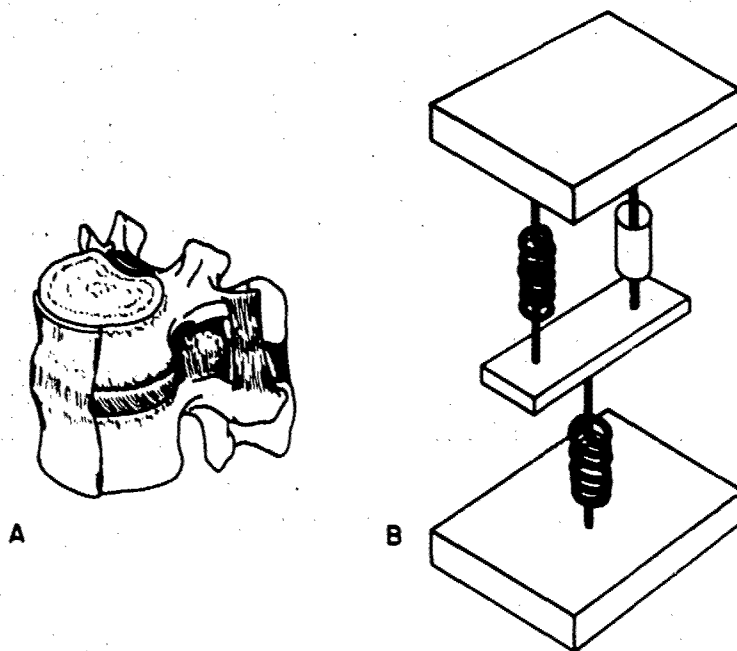


Figure 3. A. Functional Spinal Unit (FSU) or a motion segment of the spine consists of two vertebrae and the interconnecting tissues. B. Conceptual representation of the viscoelastic characteristics of the FSU by a three-dimensional three-element deformable link connecting the centers of the two rigid bodies.

2. Defining the Structure

Three types of right-hand cartesian coordinate systems are used to define the spine structure, Figure 4. The global system, lmn , is conveniently orientated and fixed to the ground. It defines the centers of gravity (c.g.) of all the rigid bodies and the orientations of the other coordinate systems. Local body coordinate systems xyz_i are fixed in space at the centers of gravity of the rigid bodies and are orientated along the principal axes of inertia of each of the bodies. The deformable viscoelastic links are

sequentially numbered. The k th deformable link has the k th local coordinate system $(abc)_k$. The orientation of the system is such that the a_k -axis is parallel to the line joining the two ends of the k th deformable link and with its positive direction towards the body with the higher number.

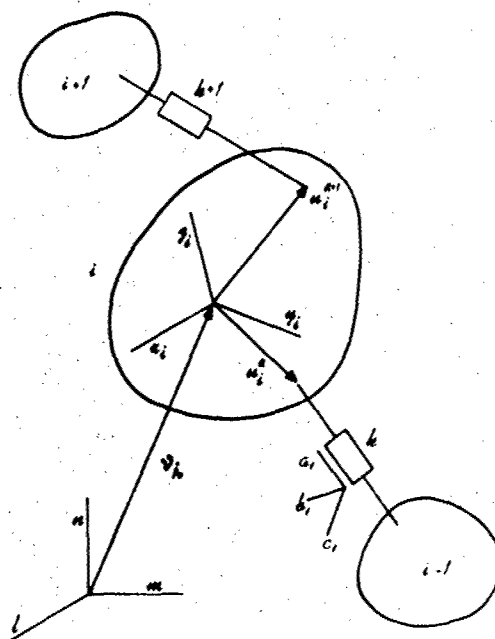


Figure 4. The system of defining the spine structure is shown. The rigid bodies, $i-1, i, i+1$, etc., representing the vertebrae, are connected by three-dimensional deformable links, $k, k+1$, etc., representing the viscoelastic characteristics of the functional spinal unit.

The center of gravity of the i th body is defined by a position vector v_i in the global coordinate system (lmn) while the point of attachment of the k th deformable link is defined by u_k^i in local body coordinate system $(xyz)_i$.

3. System Governing Equations of Motion

The system governing equations of motion in the inertia coordinate systems $(xyz)_i$ are

$$M\ddot{d} + C\dot{d} + Kd = q \quad (1)$$

where d and q are $6n \times 1$ system displacement and load vectors respectively. M , C and K are $6n \times 6n$ system inertia, damping and stiffness matrices respectively. Letter n stands for the number of rigid bodies in the system. The system vectors d and q are defined by a set of subvectors of displacement and load, d_i and q_i , for each body and in the respective local inertia systems. Thus,

$$d = [d_1 \ d_2 \ \dots \ d_i \ \dots \ d_n]^T, \text{ and}$$

$$q = [q_1 \ q_2 \ \dots \ q_i \ \dots \ q_n]^T.$$

The subvectors, in turn, are defined by their components

$$d_i = [r_x \ r_y \ r_z \ \phi_x \ \phi_y \ \phi_z]_i^T,$$

$$q_i = [f_x \ f_y \ f_z \ u_x \ u_y \ u_z]_i^T$$

where r , ϕ , f and u are respectively translation, rotation, force and moment vectors. Further details of this method are given elsewhere, Panjabi (1973,13).

B. Physical Properties

1. The Rigid Bodies

The masses and moments of inertias have been documented by Liu and Wickstrom (1973,⁸).

2. The Deformable Links

Although it will be ideal to have the mechanical properties of each of the FSU obtained in the *in vivo* situation, it is not feasible for practical reasons. The mechanical behavior of a structure requires the documentation of both the applied loads and the displacements produced. Although the displacements can be measured with a good deal of accuracy, there is no method yet that can precisely measure the loads applied to a FSU in an *in vivo* situation. The *in vitro* experiments done on fresh cadaveric material provide a reasonable alternative.

The physical properties of the human spine cadavers have been studied since the days of Messerer (1880, 10) who determined the crush strength of the vertebrae. Until 1970, most of the loads utilized were compressive with a few exceptions. A sudden increase in our knowledge was provided by Markolf (1970, 9) who determined the load-displacement curves of FSU under compression, tension, shear, flexion, extension, lateral bending and torsion. However, he neither included preloads nor did he measure the coupled motions in his experiments. The preloads are the loads applied to the FSU in situ when the person is standing in anatomic position. It has been documented that such loads are present in vivo and that they are of considerable magnitude, Nachemson and Morris (1964, 11). The coupled motions are the components of motion that occur in directions other than the direction of the applied load. In contrast, the motions in the directions of the applied load are called the main motions. It has been shown in the later sections of this paper that both the preloads and the coupled motions are important for a complete documentation of the physical characteristics of the spine.

The above discussion has been concerned with the elastic properties of the spine only. For complete characterization damping properties are equally important. However, very little is known about these properties of the spine except under compression loading. Virgin (1951, 16) and Hirsch and Nachemson (1954, 3) were probably the first to report their observations of the phenomena of hysteresis and creep respectively, both of which involve the damping properties of the spine. Most recently Kazarian (1975, 4) has done extensive compression creep testing on functional spinal units and has shown that the damping properties of the disc vary with the grade of disc degeneration.

Returning to the elastic properties, it may be observed that much more precise information has become available now; although the absence of the application of the preloads and the measurements of the coupled motions has remained, except in the studies to be described here. A short theoretical discussion given below provides a basis for a systematic determination of the physical properties of the functional spinal unit. For greater details one may consult other sources, Krag (1975, 6), Panjabi et al (1976, 14) and Panjabi (1977, 12).

a. Theoretical Basis

Let us place the origin of a three-dimensional coordinate system at the center of the body of the upper vertebra of a functional spinal unit and orient it as shown in Figure 5. A load vector, applied to the center of the vertebra, has six components, i.e. three forces along and three moments about the three axes. Similarly, the displacement vector of the center of the upper vertebra has six components, i.e. three translations along and three angulations about the three axes of the coordinate system. The complete description of the behavior of a FSU can be obtained by applying all the load components, one at a time, and measuring all the displacement components for each load application.

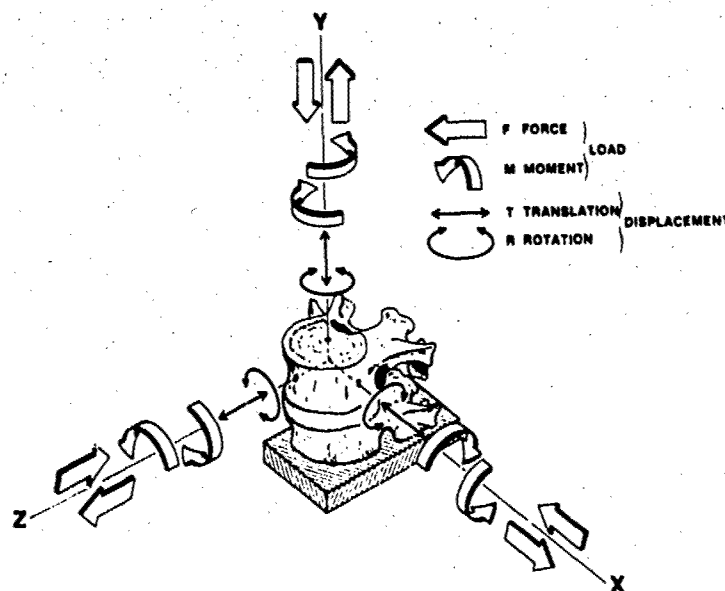
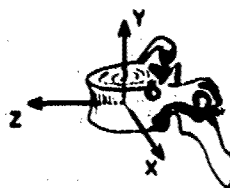


Figure 5. A three-dimensional coordinate system is located with its origin at the center of the vertebral body of the upper vertebra of a functional spinal unit. The axes are oriented as shown. Twelve components of load vector are depicted by broad arrows while the six displacement components are shown by thin arrows.

The loads may be applied in the positive as well as the negative directions. Because the behavior of a spinal functional unit must be assumed to be different in the positive and negative directions (for example, axial compression and tension), we may consider the load vector to have 12 components -- six positive and six negative. These load and displacement components are depicted in Figure 5.

Theoretically, any one load component may produce all the six displacement components. Thus, if all 12 load components are applied one at a time, there will be a total of 72 load displacement curves. The foregoing description is depicted in Figure 6. Horizontally we have arranged the 12 load components, from the force of $+F_x$ to the moment $-M_z$. Vertically we have arranged the six displacement components, from

lateral translation $\pm T_x$ to lateral angulation $\pm A_z$. Thus, a total of 72 load-displacement curves, each represented by a square in Figure 6, are required to document completely the elastic mechanical behavior of a single functional spinal unit.



F = FORCE
M = MOMENT
T = TRANSLATION
A = ANGULATION

	$+F_x$	$+F_y$	$+F_z$	$-F_x$	$-F_y$	$-F_z$	$+M_x$	$+M_y$	$+M_z$	$-M_x$	$-M_y$	$-M_z$
$\pm T_x$	<input type="checkbox"/>	<input type="checkbox"/>	<input type="checkbox"/>	<input type="checkbox"/>	<input type="checkbox"/>	<input type="checkbox"/>	<input type="checkbox"/>	<input type="checkbox"/>	<input type="checkbox"/>	<input type="checkbox"/>	<input type="checkbox"/>	<input type="checkbox"/>
$\pm T_y$	<input type="checkbox"/>	<input type="checkbox"/>	<input type="checkbox"/>	<input type="checkbox"/>	<input type="checkbox"/>	<input type="checkbox"/>	<input type="checkbox"/>	<input type="checkbox"/>	<input type="checkbox"/>	<input type="checkbox"/>	<input type="checkbox"/>	<input type="checkbox"/>
$\pm T_z$	<input type="checkbox"/>	<input type="checkbox"/>	<input type="checkbox"/>	<input type="checkbox"/>	<input type="checkbox"/>	<input type="checkbox"/>	<input type="checkbox"/>	<input type="checkbox"/>	<input type="checkbox"/>	<input type="checkbox"/>	<input type="checkbox"/>	<input type="checkbox"/>
$\pm A_x$	<input type="checkbox"/>	<input type="checkbox"/>	<input type="checkbox"/>	<input type="checkbox"/>	<input type="checkbox"/>	<input type="checkbox"/>	<input type="checkbox"/>	<input type="checkbox"/>	<input type="checkbox"/>	<input type="checkbox"/>	<input type="checkbox"/>	<input type="checkbox"/>
$\pm A_y$	<input type="checkbox"/>	<input type="checkbox"/>	<input type="checkbox"/>	<input type="checkbox"/>	<input type="checkbox"/>	<input type="checkbox"/>	<input type="checkbox"/>	<input type="checkbox"/>	<input type="checkbox"/>	<input type="checkbox"/>	<input type="checkbox"/>	<input type="checkbox"/>
$\pm A_z$	<input type="checkbox"/>	<input type="checkbox"/>	<input type="checkbox"/>	<input type="checkbox"/>	<input type="checkbox"/>	<input type="checkbox"/>	<input type="checkbox"/>	<input type="checkbox"/>	<input type="checkbox"/>	<input type="checkbox"/>	<input type="checkbox"/>	<input type="checkbox"/>

Figure 6. Twelve load components ($+F_x$ to $-M_z$) are arranged horizontally. Six displacement components ($\pm T_x$ to $\pm A_z$) are arranged vertically. Application of any load component to the functional spinal unit may produce all the six displacement components. Each of the 72 squares represents a load-displacement curve.

b. Three-Dimensional Studies

The foregoing experimental ideas were incorporated into two studies in our laboratory, with the purpose of determining complete three-dimensional elastic behavior of the spine. In the first study of the thoracic spine, Panjabi et al (1976,¹⁴), certain simplifications were made. The spine was assumed to have bilateral symmetry and no preloads were included. A suitable physiological environment of 20° C. and 100% humidity was utilized to maintain the physical characteristics of the spine during testing. Further, all the twelve load components were utilized and three displacement components (one main and two coupled) were measured for each load application. To eliminate the effect of creep, the displacement readings were taken after three minutes of load application.

The second study, done on lumbar motion segments, incorporated two additional features as compared to the thoracic study. Firstly, we modified the measuring techniques so that instead of three, we were able to measure all six displacement components simultaneously, thus fulfilling the requirements for a complete description. Secondly, we incorporated physiologic axial compressive preloads to bring the in vitro experimental conditions closer to the in vivo situation. As mentioned earlier, the presence of such a compressive preload in vivo has been well documented by Nachemson and Morris (1964,¹¹). The lumbar spine study conducted by Krag (1975,⁶) is not yet complete, and we present here a sample of the load displacement curves taken from his thesis.

Figure 7 shows the resulting three translational and three rotational components of the motion at the center of the upper vertebral body when the load component $+M_z$ (right lateral bending) is applied to it with zero preload. We observe the following. The most dominant motion is the main motion, i.e. the lateral bending as denoted by the load-displacement curve marked A_z . The other five curves describe the coupled motions. The behavior is nonlinear, with the spine becoming less flexible as higher loads are applied.

The physical properties of the spine are seen to be significantly altered by preloads in the physical range. This is exemplified in Figure 8 where results of applying left lateral shear $+F_x$ to the lumbar functional spinal unit are shown without and with 1000 N of preload. Again, there are six load-displacement curves. Lateral shear deformation (T_x) is the main motion while the other five are the coupled motions, e.g. A_z angulation about the Z-axis. It is interesting to note that addition of the preload of 1000 N changes the shape of nearly all the six load-displacement curves. In the example shown, all the curves indicate softening of the spine segment with the addition of the preload. In some of the other examples, not shown here, the spine segments were observed to harden and in some there were mixed results. Details of these results are given elsewhere, Panjabi et al (1976,¹⁴).

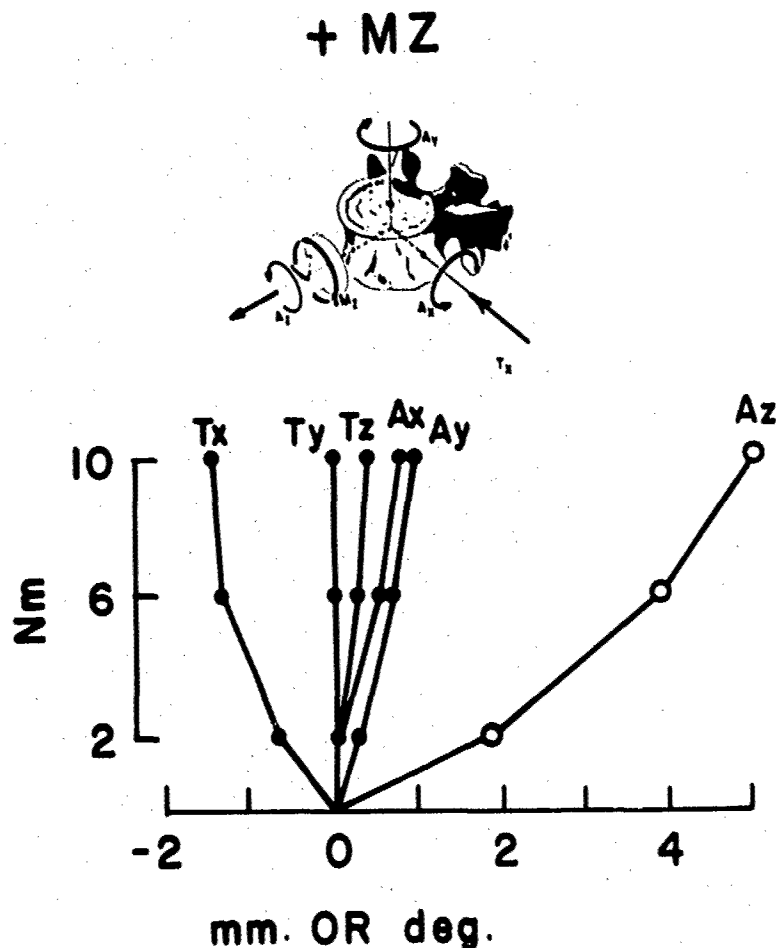


Figure 7. Six load displacement curves for the center of the upper vertebral body of a lumbar functional spinal unit subjected to a single load: right lateral bending moment $+M_z$. The applied moment is on the ordinate, while the translations T_x , T_y and T_z in millimeters and angulations A_x , A_y and A_z in degrees are on the abscissa. The lateral angulation A_z curve represents the main motion while the remaining five curves depict the coupled motions.

DISCUSSION

An analogue may be defined as something that resembles something else, because of certain specified characteristics, but is not the same. Thus, it follows that the characteristics of the "something else" must be known and taken into consideration before the "something" can be constructed. The quality of a mathematical analogue of the human spine is, therefore, dependent upon the quality of the spine physical properties data that it incorporates. Development of the analogue requires a simultaneous development of the techniques of mathematical modelling as well as the determination of the physical characteristics of the human spine. The two go hand in hand.

Thus, the mathematical analogue has two constituents, namely the mathematical part that sets up the governing equation, and the physical data part that characterizes the real spine behavior. Although they are quite different, there is nonetheless a reciprocal relationship between the two. The mathematical part must be able to incorporate the real physical data while, on the other hand, it should be experimentally feasible to provide the physical data required by the mathematical part. Although great progress has been made in construction of the mathematical models and much data has been obtained concerning the physical properties of the human spine, yet the two have developed more or less independently and at different rates. In our opinion, the progress in the determination of the physical data of the spine has lagged far behind that of the mathematical model.

Some of the recent mathematical models have broken down the functional spinal unit into its several elements, namely a disc, nine ligaments and two facet joints. Thus, to simulate the human spine in these mathematical models, physical properties of each of these spinal elements are required for each level of the spine. This kind of elemental data may be difficult to obtain without violating the spine integrity. A good example is the capsular ligaments which completely enclose the facet articulations. To obtain their physical properties, the facet articulation must be destroyed without destroying the capsular ligaments: not an easy task. Such an approach in mathematical modelling, we believe, is unrealistic as it does not recognize the special anatomy of the human spine.

The approach presented here circumvents the above difficulties. The physical properties data required is not for the individual elements, e.g. ligaments, disc and facet joints, but of the intact functional spinal unit. The experimentally obtained three-dimensional physical properties data of such spinal

units are being made available. The mathematical model presented has the capability to incorporate such data.

We have shown that the load displacement characteristics of the spinal unit are complex. They are not only nonlinear, but are intrinsically coupled. Further, they are affected by the preload (the load due to the weight of the body parts above it). The significant magnitude of the preload effect makes the previous data obtained without the preload much less useful. A realistic analogue of the spine must take into account the above considerations.

The mathematical analogue presented here provides a comprehensive approach. It has the potential of simulating the real situation with high fidelity. However, the physical properties necessary for functioning of the model are only now becoming available. We hope to present the results in the near future.

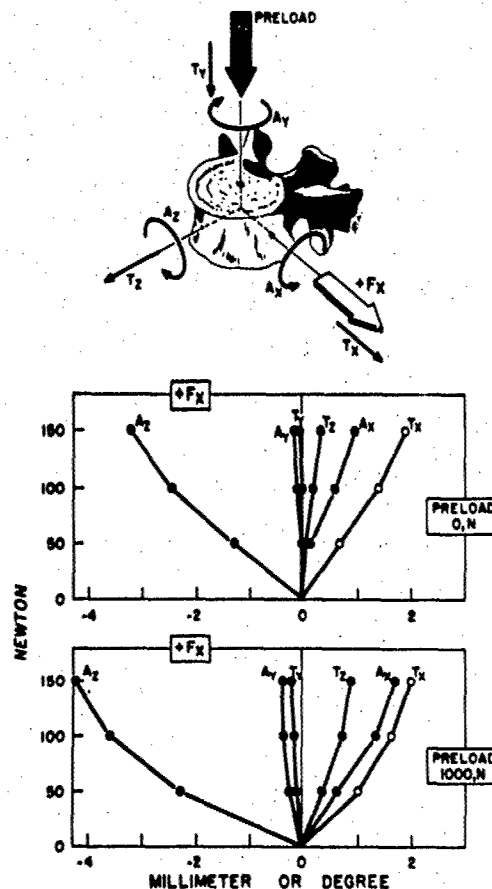


Figure 8. Coupled as well as main motion load-displacement curves for a physiologic lateral force $+F_x$ and two preloads 0 and 1000 N. The lateral force produced all the six motions T_x to A_z . Note the change due to 1000 N preload. Open circle curves are the main motion curves and the filled-in circle curves are the coupled motion curves.

REFERENCES

1. Belytschko, T.B., Andriacchi, T.P., Schultz, A.B. and Galante, J.O.: Analog Studies of Forces in the Human Spine: Computational Techniques. *J. Biomech.* 6, 361-371, 1973.
2. Hess, J.L. and Lombard, C.F.: Theoretical Investigations of Dynamic Response of Man to High Vertical Accelerations. *J. Aviation Med.* 29, 66-75, 1958.
3. Hirsch, C. and Nachemson, A.: A New Observation on the Mechanical Behavior of Lumbar Discs. *Acta Orthop. Scand.* 23, 254-283, 1954.
4. Kazarian, L.E.: Creep Characteristics of the Human Spinal Column. *Orthopaedic Clinics of North America* 6 (1), 1975.
5. King, A.I. and Chou, C.C.: Mathematical Modelling, Simulation and Experimental Testing of Biomechanical System Crash Response. *J. Biomech.* 9, 301-317, 1976.
6. Krag, M.H.: Three-Dimensional Flexibility Measurements of Preloaded Human Vertebral Motion Segments. M.D. Thesis, Yale University School of Medicine, New Haven, CT, 1975.

7. Latham, F.: A Study in Body Ballistics: Seat Ejection. Proc. R. Soc. B-147, 1957.
8. Liu, Y.K. and Wickstrom, J.K.: Estimation of Inertial Property Distribution of the Human Torso From Segmented Cadaveric Data. Perspectives in Biomedical Engineering, 1975.
9. Markolf, K.L.: Stiffness and Damping Characteristics of the Thoracic Lumbar Spine. Proceedings of the Workshop on Bioengineering Approaches to the Problems of the Spine, N.I.H., 1970, 89-142.
10. Messerer, O.: Über Elasticität und Festigkeit der Menschlichen Knochen. Stuttgart, J.G. Cotta'schen Buchhandlung, 1880.
11. Nachemson, A. and Morris, J.M.: In Vivo Measurements of Intradiscal Pressure. J. Bone and Joint Surg. 46, 1077, 1964.
12. Panjabi, M.M.: Experimental Determination of Spinal Motion Segment Behavior. Orthopaedic Clinics of North America, 8 (1), 169-180, 1977.
13. Panjabi, M.M.: Three-Dimensional Mathematical Model of the Human Spine Structure. J. Biomech. 6, 671-680, 1973.
14. Panjabi, M.M., Brand, R.A. and White, A.A.: Three-Dimensional Flexibility and Stiffness Properties of the Human Thoracic Spine. J. Biomech. 9, 185-192, 1976.
15. Schultz, A.B., LaRocca, H., Galante, J.O. and Andriacchi, T.P.: A Study of Geometrical Relationships in Scoliotic Spines. J. Biomech. 5, 409-420, 1972.
16. Virgin, W.: Experimental Investigations Into Physical Properties of Intervertebral Disc. J. Bone and Joint Surg., 33B, 607, 1951.

ACKNOWLEDGEMENTS

Support from N.I.H. Grant 1 R01 AM/GM 21869-01 and RCDA 1 K04 AM-00299-01A1 AFY is thankfully acknowledged. Thanks are also due to Drs. Martin Krag and Noshir Langrana for many valuable suggestions and to Mary Carroll for help with the editing.

DISCUSSION

DR. BELYTSCHKO (USA)

I noticed that you described your model by a system of linear equations $M \ddot{d} + C \dot{d} + Kd = q$ and treated your rotations by $\theta_{x1}, \theta_{y1}, \theta_{z1}$ which is applicable only to small rotations. Are you implying that nonlinear effects, such as those due to nonlinear materials or large displacements, are unimportant in the spine?

AUTHOR'S REPLY

We know that most of the equations that you must consider are nonlinear to start with, but when it comes to solving them certain approximations must be made. The intent of this paper was not to present a method for solving specific equations, but rather to present a comprehensive approach which stresses the simultaneous development of model structure and mechanisms and the physical properties of the system being modeled.

DR. D. J. THOMAS (USA)

What is your criterion of "good agreement" between the model and any experiment to validate the model?

AUTHOR'S REPLY

I do not address this question in my paper.

A THREE DIMENSIONAL DISCRETE ELEMENT DYNAMIC MODEL OF THE SPINE HEAD AND TORSO

by

Ted Belytschko

Department of Civil Engineering
Northwestern University
Evanston, Illinois 60201
U. S. A.

and

Eberhart Privitzer
Stanford Research Institute
Menlo Park, California 94025
U. S. A.

SUMMARY

A three dimensional, discrete model of the human spine, head and torso is described. This model is an evolution of earlier discrete models which are reviewed and discussed. The anatomy is modeled by a collection of rigid bodies, which represent skeletal segments such as the vertebrae, pelvis, and ribs, interconnected by deformable elements, which represent ligaments, cartilagenous joints, viscera and connective tissues. The model has been validated by comparing its impedance to measurements on human volunteers. The principal feature of this model is the generality of its formulation which enables it to be applied to a wide variety of impact situations. Simulations are reported for a vertical ejection, a pre-ejection alignment and bird impact on a canopy. A postprocessor has been developed which interprets the complex time history output in terms of injury potential.

INTRODUCTION AND REVIEW OF LITERATURE

Because of the difficulties of studying impact environments experimentally, considerable effort has been devoted over the past thirty years to the development of models of various components of the human body. In the study of pilot safety, attention has focused on the spine, head and neck. Models ranging in complexity from one degree of freedom models of the spine to multidegree of freedom models which represent the individual vertebrae have been developed.

Mathematical models of the spine have evolved into two general classes: continuum and discrete models. The term continuum here refers to models where the spine is treated as homogeneous, requiring the determination of extrapolated material properties representing the composite behavior of the intervertebral discs and the vertebrae. In the discrete models, the individual vertebrae are modeled as rigid bodies interconnected by the discs and the various spinal ligaments. This allows for the direct utilization of the disc and ligament properties.

Latham [1] is generally cited as the first to develop a mathematical model for describing the dynamic response of the spine to $+G_z$ acceleration. His model consisted of two rigid masses, one representing the body and the other the ejection seat interconnected by a spring. It was developed to study the dynamic overshoot of the body when seat cushions of varying resiliency were placed between the pilot and the ejection seat.

Payne [2] also developed a one degree of freedom model of the spine. The head and upper torso were modeled as a single rigid mass and the spine as a spring with a dashpot in parallel. The stiffness of this spring was determined by matching the natural frequency of the model to the average frequency of the dominant peak of experimentally measured driving point impedances. This model was subsequently extensively correlated with injury data to develop the dynamic response index (DRI) model. It has provided a very useful tool for evaluating the safety of a pilot in an axial (G_z) acceleration environment when the non-axial (flexural) response is small.

In an effort to simulate more complex situations, Toth [3] developed the first model in which individual vertebrae and discs were idealized. It consisted of rigid masses representing vertebrae T11 through L5 and the pelvis, interconnected by springs and dampers representing the intervertebral discs.

Orne and Liu [4] subsequently developed a similar model for the entire thoracolumbar spine. They included the axial, shear, and bending resistance of the discs and modeled each vertebrae as a rigid body with three degrees of freedom (two translations and one rotation). Spinal curvature and variations of disc stiffness with vertebral level were treated. The force-deflection characteristics of the intervertebral discs were modeled with a three parameter viscoelastic relationship. Orne and Liu introduced the concept of modeling the inertial properties of the torso by assigning to each vertebral level the inertial properties of the associated torso segment. The eccentricity (distance between the vertebral mass center and the mass center of the entire torso segment) of the mass center for each motion segment (vertebral level) was included. Interaction of the spine with the torso, ejection seat or a restraint system were not considered. Failure to represent these interactions in a large displacement formulation results in unrealistic deformation of the spinal column and may invalidate the force distributions predicted by the model.

Payne and Band [5] developed a one dimensional, four degree of freedom model of a seated man. It consisted of rigid masses representing the head, upper torso, abdominal viscera and the pelvis, interconnected by springs and dampers. A spring and damper were included to represent the elastic and viscous properties of the buttocks. The stiffnesses of this model were chosen so that the model's frequency content reflected the average frequencies at which peaks occur in experimentally obtained impedances of seated humans. This model was restricted to axial motion only.

Moffat [6] developed a continuum model which included both axial and bending response. The formulation was restricted to small displacements. Continuum models have the advantage of permitting the use of fewer degrees of freedom for the spine than in models that represent the individual vertebrae. On the other hand, they require an extrapolation of the material properties representing the intervertebral discs and vertebrae and also the interpretation of continuous response variables in terms of actual forces in these discrete anatomical segments.

The discrete Orne and Liu [4] model was modified by Prasad and King [7] to include the articular facet interaction. The motivation for this was to model a secondary path of load transmission along the spinal column which is provided by the actions of the articular facets as determined by the experimental work of Prasad, et al [8]. The interaction of the articular facets was modeled by two springs, one limiting relative rotations and the other limiting the relative sliding of adjacent vertebrae. The properties of the articular facet elements appear to have been chosen rather arbitrarily, since no reference was made as to how the axial stiffnesses were determined and no values for the rotational stiffnesses were given. An important feature of their model was its validation by comparison of certain response forces with cadaver drop tower tests. Though such limited comparisons certainly do not constitute a complete validation, they serve an important purpose.

The models described up to this point were restricted to one or two dimensional behavior and, in general, had not considered interaction of the spine with other portions of the torso such as the rib cage and viscera.

The first three dimensional head-spine model was developed by Belytschko, et al [9], who developed several models of varying complexity. The basic model was the isolated ligamentous spine model, consisting of rigid bodies representing the head, vertebrae T1 through L5 and the pelvis interconnected by deformable elements representing the intervertebral discs and the various connective tissues. Interaction between the spine and the torso was modeled with a secondary column of beam elements representing the action of the viscera-abdominal wall system in the lumbar region and the rib cage in the thoracic region.

The complete spine model of Belytschko, et al consisted of the ligamentous spine model plus detailed representations of the cervical spine, the rib cage and the viscera. The cervical spine model consisted of rigid bodies representing vertebrae C2 through C7 and interconnected by deformable elements representing the intervertebral discs. The actions of the articular facets were modeled with hydrodynamic elements, which were able to reproduce the kinematic actions of the articular facets in three dimensions more effectively than spring elements. The viscera were modeled with hydrodynamic elements stacked in series between the pelvis and the bottom of rib pair 10 (the rib pair connected to vertebra T10). By including the interaction of the spine with the torso and the seat and restraint system, they were able to employ their model to investigate the behavior of the spine in situations involving substantial bending.

A major difficulty in the development of discrete, multidegree of freedom models such as that of Orne and Liu, Prasad and King and Belytschko, et al is the large amount of data that is needed to characterize the numerous elements of the model. Furthermore, in spite of their complexity, these models still involve substantial idealizations of the human body, as exemplified in the single segment mass approximations of Orne and Liu. It is imperative, therefore, that models of such complexity be validated by comparisons with experimental observations on complete body response in dynamic environments.

One source of dynamic body response data are measurements of human volunteer impedances. Major contributions to our knowledge of the impedance of human subjects were made by Coermann, et al [10], [11] and Vogt, et al [12]. Coermann, et al determined the impedances of sitting and standing subjects by shake table induced vertical ($+G_z$) vibrations through a frequency range of 1 to 19 Hz. He found a major resonance at 5 Hz.

Resonances in the displacement response of the abdominal viscera were also studied by Coermann, et al. This was accomplished by placing the subject in a supine position on a shake table and subjecting him to longitudinal harmonic vibrations through a frequency range of 1 to 15 Hz. Motion of the skeleton was suppressed by using metal brackets at the head, shoulders, and feet to clamp the subject to the table. Resonances in the abdominal wall displacements were found to occur typically between 3 and 4 Hz. Restricting the mobility of the abdomen resulted in a shift of the abdominal wall displacement peak to between 6 and 7 Hz.

Vogt, et al [12] measured the impedances of ten male subjects who were seated in a slightly erect posture and loosely restrained. Vogt, et al also considered impedances under sustained accelerations of $+2 G_z$ and $+3 G_z$. These sustained accelerations were induced via a centrifuge. The application of the sustained accelerations allowed for the observation of the change in the impedance when exposed to a preload, thus indicating the effects of the nonlinear stiffness of the tissues. These results exhibit a shift in the resonance to a higher frequency and an increase in impedance magnitude when the G loading is increased from normal gravity.

The important characteristic of the results reported by Coermann, et al and Vogt, et al is the major peak which occurs in the neighborhood of 5 Hz for the impedances of seated human subjects under normal gravity. Second and third peaks, both considerably smaller than the first, generally occur in the vicinity of 10 to 11 Hz and 14 Hz, respectively. These second and third peaks are not always reported. The peaks in the impedance curves indicate the vertical excitation frequencies at which the maximum energy is transferred to the body. Coermann, et al suggest that the 5 Hz peak is caused by resonant motion of the upper torso in connection with the bending elasticity of the pelvis and spine, and that the 10 to 11 Hz peak is probably attributable to another elasticity of the pelvis.

Vykukal [13] exposed four subjects in a semi-supine position to a vertical acceleration of $\pm 0.4G$ in a frequency range from 2 1/2 to 20 Hz, combined with a linear acceleration of 1, 2, and 4 G. The mechanical impedance of each subject was recorded. He observed that for the higher linear accelerations, the stiffness increased, the damping increased, and the overall impedance magnitude increased. The resonances at higher frequencies became more predominant in magnitude because of increased coupling of the body systems when subjected to a high G environment.

Woods [14] reported transmissibilities for longitudinal and lateral vibrations of three subjects in the frequency range of 1 to 10 Hz. Results are also reported for the effect of random vertical and lateral vibrations. All of the transmissibility curves for the sinusoidal, longitudinal oscillations had a peak between 4 to 6 Hz. A major peak in the transmissibility curve for the sinusoidal lateral oscillations occurred at 1.5 Hz.

The impedance characteristics of the complex, multidegree-of-freedom models ([4], [7], [9]) were not reported. However, Belytschko, et al [9] reported modal analyses of their models: for the ligamentous spine with head and pelvis but no separate elements for the viscera and buttocks they found a lowest natural frequency of 17 Hz when restricted to axial motion. This is considerably higher than the average frequency, 5 Hz, at which the dominant peaks of experimentally determined impedances occur. Because this disparity is far greater than that which would result from any possible error in the stiffness or inertial properties of the model, they suggested that the 5 Hz peaks in experimentally determined impedance curves cannot represent an axial response of the spine.

In this paper, the impedance of a modified Belytschko, et al [9] model will be examined. It is shown that the impedance of this model duplicates the experimentally determined impedance quite well and that the resonance at 5 Hz results from a combination of three factors: the seat-body mode, the flexural response of the spine and the axial response of the viscera. The model will then be used to simulate several situations of interest in pilot safety: ejection, pre-ejection alignment, and head impact resulting from bird-strike on the canopy.

DESCRIPTIONS OF MODELS

The models represent the human body by a collection of rigid bodies interconnected by deformable elements. The rigid bodies are used for the modeling of bones while the deformable elements are used to model ligaments, muscles and connective tissues. The treatment of bones as rigid bodies is preferable from both the viewpoint of numerics and modeling, for the stiffness of bones is usually orders of magnitudes greater than that of connective tissue, so that if both are modeled as deformable the resulting numerical problem is poorly conditioned. However, long slender bones, such as ribs, may be modeled as deformable. The deformable elements may also be used to model entities external to the body, such as restraint systems and harnesses.

For purposes of describing the models, it is worthwhile to distinguish between the following:

- 1) The computer-based method of solution, or mathematical model, which is a rather general system for the treatment of the dynamics of collections of rigid bodies interconnected by deformable elements, and
- 2) The specific models of the spine, torso, and ejection system, which constitute a data base for the computer system.

The analytical procedure is basically a matrix structural technique which serves as a versatile framework for constructing the equations of motion. The program enables these equations of motion to be integrated in time by either explicit or implicit techniques, or analyzed by modal procedures, which give the natural frequencies and modes of the model; details may be found in Belytschko et al [9]. The formulation is completely three dimensional and treats arbitrarily large rotations and displacements of the rigid bodies. However, the deformation of some of the elements is restricted to be moderately small. Material properties may be linear or nonlinear and viscous forces are included.

The following mathematical elements are used in the model:

- 1) Rigid bodies, which are used to represent skeletal segments, and may be interconnected by deformable elements connected to any point on the rigid body;
- 2) Spring elements, which have stiffness only against axial deformation, and are used to represent ligaments and harness restraints;
- 3) Beam elements, which have bending, torsional, and axial stiffness, and which are used to model intervertebral discs;
- 4) Hydrodynamic elements, which are governed by pressure-volume laws;
- 5) Elastic surfaces which provide a simplified model of seat surfaces; and
- 6) Plate elements, which can be used to represent deformable elements within the pilot's environment, such as the canopy.

For purposes of illustrating how the mathematical model is used to represent the pilot's anatomy, we will describe two representative models used in these studies. The first model consists of the isolated thoracolumbar spine, the cervical spine, the head, the rib cage and viscera, and the seatback and restraint system. In the second model, the rib cage and viscera are replaced by a series of beams parallel to the spine, which represent the stiffness of the torso. This simplification is made to save computer costs. Lateral and anterior-posterior views of the complex model are shown in Fig. 1; only the rigid bodies representing skeletal segments are shown.

In the thoracolumbar spine, each pair of vertebrae is connected by seven spring elements and one beam element. The intervertebral disc is represented by a beam element, which joins the geometrical centers of the endplates of each pair of adjacent vertebrae. The spring elements represent the following ligaments and connective tissues: the pair of spring elements which connect the transverse process tips represent the intertransverse ligaments; one spring element, which connects the spinous process tips, represents the intra- and supra-spinous ligaments; a pair of elements which connect posterior points on the vertebral bodies, represent the ligamenta flava; two spring elements are used to represent the articular facets. The latter are short, stiff elements and are primarily intended to represent the kinematic constraints resulting from the facets. All of these elements interconnect secondary nodes on the rigid body. The data given in Schultz et al [15] was used for these stiffnesses.

In the cervical spine, adjacent vertebrae are connected only by elements representing the disc, the interspinous ligaments, and the articular facets. The discs are represented by beam elements, the ligaments by spring elements, the articular facets by hydrodynamic elements. The triangular endplates of the

hydrodynamic element may be seen in Fig. 1. Because these elements have resistance primarily through a line joining the centroids of the two opposing triangular facets, these elements are more effective in representing the directional properties of articular facets than spring elements. The use of these elements for the representation of facets would also be desirable in the lumbar and thoracic spines, but the procurement of data for the location of the facet planes in these portions of the spine has not been completed.

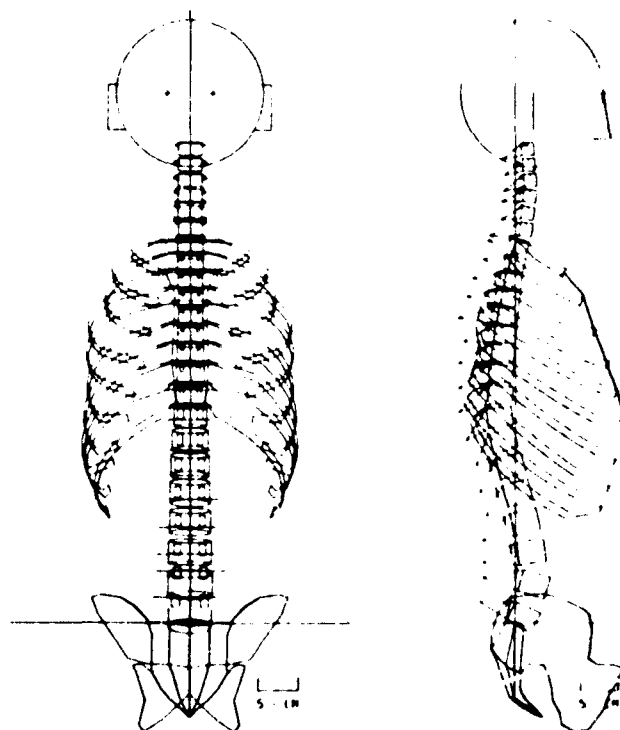


Figure 1 Frontal and sagittal plane views of complete head-spine model.

Each of the ribs is modeled as a rigid body, and connected to two vertebrae by means of these deformable elements, which represent the costo-vertebral joint. These deformable elements have been chosen so that the directional properties of the joint are represented and an axis of great rotational flexibility is included. The ribs are connected to the sternum through the costosternal joint by a deformable element, which represents the deformability of the costal cartilage. Data for this rib cage model is taken from Andriacchi et al [16].

The abdominal cavity and viscera are represented by hydrodynamic elements stacked in series between the pelvis and level T10, thus treating the overall behavior of the viscera as a compressible medium. In the actual viscera, the contents are almost incompressible and the wave motion is mainly governed by the interaction of the walls of the torso and its contents. In response to a compressive load, the contents would move vertically and laterally, stretching the abdominal walls. The mechanism of wave propagation through the viscera by an interaction of the membrane lining and the hydrodynamic contents has been studied by Torvik [17]. He derived relationships for both large deformations of the membrane and nonlinear membrane response. For small-deflection linear membrane response, he gives the standard water hammer formula for wave speed

$$c = \sqrt{\frac{E_m t}{2r\rho}} \quad (1)$$

where E_m is Young's modulus for the membrane wall, t the thickness of the wall, r its radius and ρ the density of the fluid; in this instance, the viscera. This formula neglects the compressibility of the viscera. Belytschko, et al [18] let $E = 6 \times 10^7$ dynes/cm², $t = 1$ cm, $r = 10$ cm and obtained a value of $c = 1700$ cm/sec.

The force deflection relation of the viscera here is taken to be

$$F = K_1(1 + K_2 \delta^2)(\delta + a\delta^3) \quad (2)$$

$$K_1 = AE_v \quad (3)$$

where

A = cross-sectional area of viscera (800 cm²)

E_v = effective Young's modulus of viscera at zero axial strain

K_1 = linear stiffness

K_2 = cubic stiffness

- α = damping parameter
 δ = axial strain, which is given by elongation divided by the original length
 $\dot{\delta}$ = axial strain rate

The linear stiffness was chosen by matching Coermann's [11] observed resonance in the visceral wall abdominal system of 3 to 4 Hz. This yielded a value of $K_1 = 8 \times 10^7$ dynes and corresponds to an effective Young's modulus of 10^5 dynes/cm². The cubic stiffness coefficient K_2 was chosen to be 640. At an axial strain of $\delta = 0.1$, which is typical in ejections, the resulting linearized stiffness is 6×10^8 and the effective Young's modulus is 7.4×10^5 dynes/cm². This corresponds to a wavespeed in the viscera of about 400 cm/sec. This is significantly below the value reported by Belytschko, et al [18], but presently our understanding of the cubic part of the response is quite limited. However, a cubic component is quite necessary if the low amplitude response and ejection response is to be simulated properly; as will be shown subsequently, failure to ascribe sufficient stiffness to the viscera results in dynamic buckling of the spine in ejection simulations. It is interesting to observe that ejection simulations with both the previous high value of E and the present law show only small differences in responses; evidently, the loose coupling of the viscera and spine causes the viscera to take up the same amount of force regardless of its precise stress-strain law.

The visceral elements are connected through rigid bodies to ribs T10. This implies that the whole axial load in the abdominal cavity is transferred to the rib cage; no axial load transfer to the interior of the thoracic cavity is assumed.

The head is a single rigid body joined to C2 by a beam element (C1 was not included in the model). The helmet can be assumed to be rigidly connected to the head or can be attached to the head by means of spring elements.

The seatback is a plane surface, which is vertically aligned and the bottom of the seat is horizontal. The seat constrains the motion of the rigid bodies only when they come in contact. A cubic force deflection law with damping of the following form was used:

$$F = (k_1 + k_2 \dot{d}^2) (d + \alpha \dot{d}) \quad (4)$$

where

d = distance of penetration into the seat

\dot{d} = velocity of penetration into the seat

k_1 and k_2 = linear and cubic stiffness

α = damping parameter

A value of 6.6×10^7 dyne/cm was used for k_1 , a value of 3 for k_2 . The restraint systems were modeled by linear springs.

The detailed data for the complex model is given in Refs. [9] and [18]. We will here only give the data for the simplified model, isolated ligamentous spine with viscera (ILSV), which is shown in Fig. 2. This model is identical to the complex model except that: (1) the cervical spine is replaced by a single beam element; (2) the hydrodynamic elements for the viscera are replaced by a series of springs interconnected to the vertebrae as shown; (3) the rib cage is replaced by a single series of beam elements which represent the flexural resistance of the rib cage.

The stiffnesses of the elements are given in Table 1, the inertial data in Table 2. The inertial properties are based on the work of Liu and Wickstrom [19], who measured the masses, mass moments of inertia, and centroids of the segments of frozen cadavers. For the purpose of this model, the mass of each segment must be subdivided among the vertebral bodies and the viscera in the levels L1 to L5, and between the ribs and vertebral bodies in the thoracic region. Therefore, the cross-sectional illustrations of Eycleshymer and Schoemaker [20] were used to estimate the ratio of the area of the viscera to the total cross-sectional area in levels L1 to L5. The total mass measured by Liu and Wickstrom was then apportioned between the vertebrae and viscera according to the ratio of their areas.

TABLE 1. ISOLATED LIGAMENOUS SPINE WITH VISCERA (ILSV) INERTIAL DATA

Vertebral Level	Translational	Rotational Mass (gm - cm ² x 10 ⁵) [*]		
	Mass (gm x 10 ³)	\bar{I}_{xx}	\bar{I}_{yy}	\bar{I}_{zz}
Vertebral Inertial Data				
Pelvis	16.200	12.800	20.000	19.300
L5	0.466	0.044	0.054	0.083
L4	0.562	0.042	0.096	0.123
L3	0.433	0.027	0.006	0.086
L2	0.342	0.018	0.067	0.080
L1	0.284	0.014	0.050	0.059
T12	0.333	0.014	0.032	0.035
T11	0.318	0.012	0.029	0.033
T10	1.352	0.603	1.129	1.648
T9	1.417	0.616	1.230	1.716
T8	1.326	0.554	1.208	1.670
T7	1.308	0.535	1.219	1.659
T6	1.193	0.443	1.162	1.546
T5	1.175	0.383	1.151	1.490
T4	1.064	0.314	1.060	1.354
T3	1.160	0.288	1.174	1.422

TABLE 1. (Continued)
ISOLATED LIGAMENTOUS SPINE WITH
VISCERA (ILSV) INERTIAL DATA

T2	1.074	0.208	1.029	1.230
T1	1.359	0.075	0.518	1.716
Head	5.612	4.479	4.044	3.385
Visceral Inertial Data				
S1	1.708	0.100	0.100	0.100
L5	1.744	0.590	1.741	2.114
L4	1.625	0.485	1.608	1.887
L3	1.720	0.442	1.616	1.837
L2	1.670	0.537	1.628	1.931
L1	1.676	0.556	1.519	1.916
T12	1.341	0.476	1.277	1.671
T11	1.282	0.490	1.201	1.704

* Rotational masses about body axes \bar{x} , \bar{y} , \bar{z} which coincide with the principle axes of inertia.

TABLE 2. ISOLATED LIGAMENTOUS SPINE WITH
VISCERA (ILSV) STIFFNESS DATA

Disc Level	Axial Stiffness dyne/cm x 10 ⁹	Torsional Stiffness dyne-cm x 10 ⁹	Bending Stiffness dyne-cm x 10 ⁹	Visceral Stiffness dyne/cm x 10 ⁷
S1-L5	1.10	0.90	0.70	1.29
L5-L4	1.40	1.10	0.80	1.68
L4-L3	1.50	1.20	0.90	1.64
L3-L2	1.50	1.20	0.90	1.91
L2-L1	1.60	1.20	0.90	2.24
L1-T12	1.80	1.00	0.90	2.42
T12-T11	1.50	0.80	1.00	2.62
T11-T10	1.50	0.70	1.20	2.86
T10-T9	1.50	0.70	1.10	
T9-T8	1.50	0.60	1.10	
T8-T7	1.50	0.60	1.00	
T7-T6	1.80	0.60	1.00	
T6-T5	1.90	0.60	1.00	
T5-T4	2.10	0.60	1.00	
T4-T3	1.50	0.40	0.60	
T3-T2	1.20	0.30	0.40	
T2-T1	0.70	0.20	0.20	
Neck	0.14	0.52	0.69	

All ligament and facet axial stiffnesses = 115×10^7 dyne/cm

Pelvis-S1 visceral element stiffness = 0.92×10^7 dyne/cm

All viscera-vertebra interconnecting element stiffnesses = 1.0×10^6 dyne/cm

Vertebral Level	Coordinates of Center of Inferior End Plate		Vertebral Body Height (cm)	Intervertebral Disc Height (cm)
	y (cm)	z (cm)		
L5	1.800	2.020	2.392	1.859
L4	1.100	5.700	2.636	1.354
L3	1.000	9.550	2.751	1.223
L2	1.331	13.450	2.792	1.173
L1	2.142	17.150	2.726	0.996
T12	3.003	20.590	2.567	0.822
T11	3.382	23.680	2.433	0.645
T10	4.194	26.500	2.298	0.477
T9	4.849	29.240	2.146	0.460
T8	4.638	31.830	2.073	0.459
T7	4.580	34.300	2.019	0.404
T6	4.250	36.610	1.990	0.314
T5	3.990	38.850	1.957	0.266
T4	3.690	41.000	1.902	0.214
T3	3.350	43.150	1.850	0.274
T2	2.920	45.260	1.790	0.306
T1	2.410	47.440	1.648	0.448

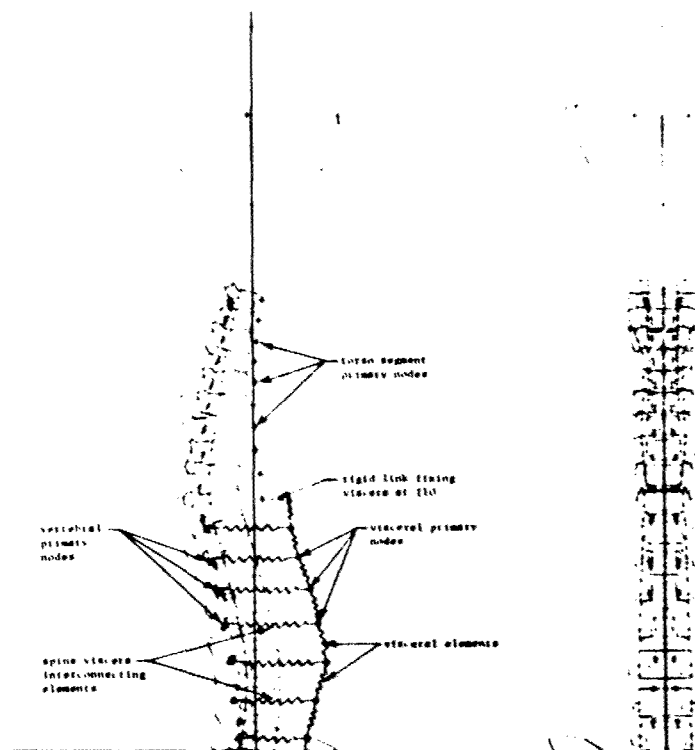


Figure 2 Frontal and sagittal plan views of simplified isolated ligamentous spine with viscera (ILSV).

The ILSV damping parameters were set as follows: the visceral damping parameters were based on 30% damping of the lowest visceral mode (5.5 Hz); the spine longitudinal damping parameters were based on 20% damping of the lowest spine axial mode (13.17 Hz) and the spine flexural damping parameters were based on 15% damping of the 5.5 Hz spine bending mode.

IMPEDANCE OF MODEL

The impedance is here defined as the modulus of $Z(j\omega)$ where

$$Z(j\omega) = \frac{F(j\omega)}{V(j\omega)} \quad j = \sqrt{-1} \quad (5)$$

and ω is the frequency, F the Fourier transform of the driving force and V the transform of the velocity of the driving point.

The impedances of the models were determined as follows:

- 1) a unit step velocity is prescribed at either the buttocks or the seat
- 2) the response of the model is computed, including the driving force necessary to maintain the unit step velocity
- 3) the Fourier transform $F(j\omega)$ of the driving force is computed by a Fast Fourier transform.

The Fourier transform of the step velocity input can analytically be shown to be

$$V(j\omega) = \frac{1}{j\omega} \quad (6)$$

Hence once $F(j\omega)$ is determined numerically, the impedance of the system can then be found. In order to obtain an accurate Fourier transform of the driving force, the simulation had to be run sufficiently long so that most of the oscillatory response was damped out. This entailed simulations on the order of 1.00 second in duration, which would be prohibitively expensive for the complete spine model. Therefore, the ILSV was used for the impedance studies.

When the model was driven at the pelvis, the effect of the pelvic mass does not appear in the numerical response because its acceleration is an impulse. Therefore, in determining impedances at the pelvic mass, the pelvic mass was considered in series with the remainder of the model, and its mass impedance was simply added to the impedance of the rest of the model.

Figure 3 shows the impedance of the ILSV model when driven at the pelvis, as compared to the experimental results of Vogt, et al [12]. The ILSV impedance exhibits peaks at 6.0 Hz and 13.4 Hz, compared to the experimental peaks of 4.9 Hz and 13.5 Hz. However, the magnitudes of the peaks and the shapes of the computed and experimental results differ substantially.

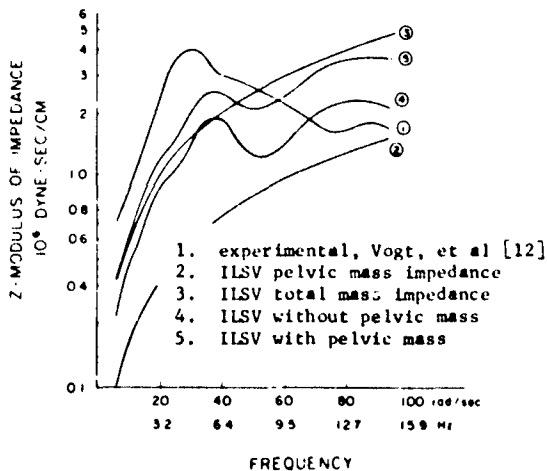


Figure 3 Impedance of ILSV model driven at pelvis.

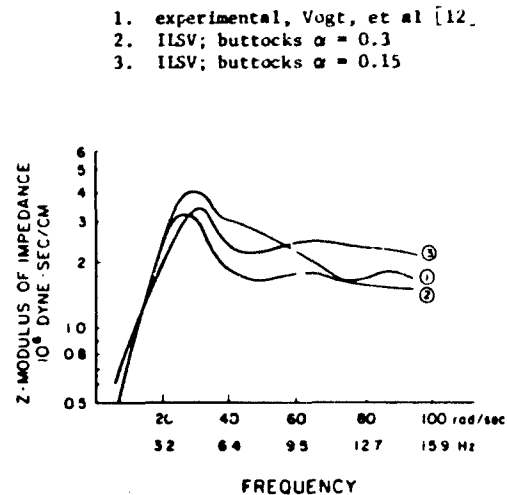


Figure 4 Impedance of ILSV model driven at a seat with two damping parameters.

Figure 4 shows the impedance of the ILSV model when driven at a seat, with a stiffness as given by Eq. (4); damping ratios of 0.30 and 0.15 were used. It can be seen by comparing Figs. 3 and 4 that the seat has a pronounced effect on the impedance. The first peak has shifted to 4.8 Hz, which agrees very well with the experimental curve. The mode associated with this frequency is dominated by rigid body motion of the body relative to the seat; it is called the steatopygic mode. The second peak is diminished severely by the introduction of the seat, although a small "bump" is still apparent in the 10 Hz domain; this "bump" appears to correspond to the excitation of the axial mode of the spine. It cannot be said whether this bump bears any relation to the experimentally observed peak at 13.5 Hz.

In order to gain further insight into the impedance of the model, we have shown in Fig. 5 the impedances of only the spine, the viscera, and the combined spine and viscera when constrained to axial motion. It can be seen that the viscera exhibits a peak at about 5.0 Hz, while the spine alone exhibits a peak at 10 Hz. Although not shown in Fig. 5, we have found when lateral vibrations of the spine model are allowed,

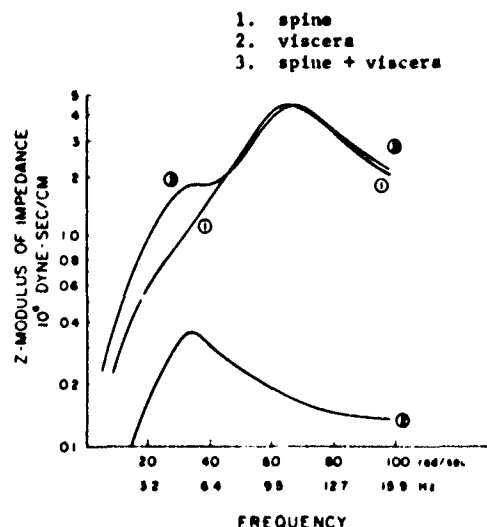


Figure 5 Impedance of ILSV subsystems when restricted to axial motion.

its impedance is increased in the 3 to 10 Hz domain because this part of its spectrum is rich in flexural modes. This can also be seen by comparing curve 5 of Fig. 3 with curve 3 of Fig. 5; which are identical except for the absence of the lateral constraint in the former. In the latter, the impedance in the 5 Hz domain is significantly smaller.

It can thus be concluded that the 5 Hz peak that is experimentally observed in human impedance measurements results from a combination of the steatopygic mode, the visceral resonance, and the flexural response of the spine. The ILSV model developed here duplicates the experimental impedance quite well; however, any inferences about the validity of the model because of the good comparison must be guarded because the impedance of the experimental results is dominated by the steatopygic mode, so that the effects of other subsystems are severely masked.

SIMULATION RESULTS

To illustrate some applications of this model, four simulations are reported: 1) a set of ejection simulations; 2) a pre-ejection alignment with a shoulder harness; 3) a horizontal acceleration simulation representative of frontal crash and 4) a head impact resulting from bird-strike on a canopy.

In most of the ejection simulations the simplified model (ILSV) was used for parametric studies; the complex model was only used to verify specific cases and to tune the stiffness of the parallel elements representing the torso. The first set of results are for simple, vertical ejection, which is a symmetric problem and, therefore, could have been studied with a two-dimensional model. Three cases were considered:

- 1) Vertical ejection with a slow rate of onset,
- 2) Vertical ejection with a rapid rate of onset, and
- 3) Ejection at a 30° angle with a rapid rate of onset.

In all of the simulations, the maximum accele-

ration was 10 G and was maintained constant for 80 milliseconds. In the slow onset, the maximum acceleration is reached in 40 milliseconds with an onset rate of 250 G/s, while in the rapid onset, maximum acceleration is attained in 14 milliseconds with an onset rate of 714 G/s.

The orientation of the ejection seat with respect to the direction of the acceleration vector is an important consideration in the ejection problem. By reclining the seat so that the acceleration vector has a slight anterior component with respect to the axis of the spine, two beneficial effects are introduced: 1) the acceleration component along the axis of the spine is reduced, and 2) the resulting anterior component of the acceleration provides support for the spine by forcing the seatback against the torso. In an ejection at a 30° angle with a peak acceleration of 10 G, 8.66 G is along the axis of the spine and the anterior component is 5 G.

Table 3 compares the maximum lumbar forces in the three simulations. The forces for the rapid onset at a 30° angle and the slow onset at a 0° angle are of similar magnitudes, while the rapid onset vertical ejection exhibits generally higher force levels. This similarity can be attributed to a reduction in the effective inertial forces in both simulations. In the slow onset simulation, the effective inertial force is reduced by the decrease in dynamic magnification. In the rapid onset at 30° , a similar reduction in inertial force results from the action of the seatback, which supports part of the inertial load.

The maximum acceleration of the head was 19.07 G at 60 milliseconds for the rapid onset, 18.03 G at 72 milliseconds for the slow onset. Thus the model predicts, as expected, that slower rates of onset reduce the dynamic magnification of axial loads and accelerations and reduce the overall bending response of the spine, though for these rates of onset the dynamic magnification is quite large. The deformation of the complete model for the 10 G slow onset vertical ejection is illustrated in Fig. 6. It can be seen that the ejection causes significant additional curvature in the lower thoracic and lumbar spines.

TABLE 3. COMPARISON OF MAXIMUM AXIAL FORCE AND MOMENT FOR THREE VERTICAL EJECTIONS

	Axial Force 10^3 Newtons			Moment Newton-Meters		
	30° Rapid Onset	0° Slow Onset	0° Rapid Onset	30° Rapid Onset	0° Slow Onset	0° Rapid Onset
Disc Level						
L5-L4	-3.50	-3.96	-4.27	9.33	8.18	9.40
L4-L3	-3.39	-3.91	-4.24	9.49	10.47	11.19
L3-L2	-3.26	-3.69	-4.03	9.26	10.03	11.11
L2-L1	-3.03	-3.09	-3.68	7.29	7.74	9.56
L1-T12	-2.89	-3.01	-3.32	-10.52	-9.06	-11.11

The importance of the visceral representation is indicated by an ejection simulation of an isolated spine model without viscera as shown in Fig. 7. As can be seen, the spine buckles dramatically, which is quite contrary to what is observed experimentally. However, the theoretical consistency of these results becomes quite clear if one considers that Lucas and Bresler [21] have experimentally shown the static buckling load of the isolated, ligamentous spine to be 20 to 100 Newtons. The 10 G environment results in axial loads of about 4500 Newtons, and the duration is on the order of 200 milliseconds. Hence, it is not unexpected that the isolated spine will buckle in this environment. Therefore, if a model is to have the capability of treating large deflections, it must include the viscera and rib cage, which increase the flexural stability of the torso.

To illustrate the application of the model to another class of problems, we will briefly describe some preejection alignment studies. In some ejection systems, prior to the application of the vertical force, the pilot is pulled back by the shoulder belt. There is some concern that this increases the curvature of the spine and that it may predispose the pilot to injuries. In addition, the stresses caused by preejection alignment are of concern.

Figure 8 shows the response of the model to a preejection reel load: the belt load increases linearly to 740 Newtons in 100 milliseconds and drops back to zero by 200 milliseconds. The belt force is applied to the spine through a shoulder model depicted in Fig. 9. The shoulders are here represented by rigid bodies that interact with the inertial reel belt. The forces are transmitted from the pair of shoulder rigid bodies by 6 beam elements which are connected to vertebrae T1, T2 and T3. In this simulation, T1 was initially 6 inches (15 cm) forward from the seat. The magnitude of the loads experienced by the spine is indicated in Fig. 10, which shows the injury potential diagram for this simulation. This diagram reflects the stresses in the cortical bone at each vertebral level arising from the combination of the maximum moment and axial force during the simulation. It can be seen that the stresses arising from preejection alignment alone are quite moderate compared to the tolerance of the vertebrae and hence are not likely to cause vertebral body failure; details of this injury potential analysis may be found in Belytschko and Privity [22].

The response of the model to horizontal accelerations is shown in Fig. 11. Here, the model was given an initial horizontal velocity of 1340 cm/sec in the anterior direction, and the pelvis was then subjected to an acceleration of 67,000 cm/sec² (68.3 G). The pelvis was constrained from rotation in the sagittal plane in a simple effort to simulate a lap belt restraint, although the elasticity of the restraint belt was not included in this simulation.

In the simulation, an axial expansion wave travels up the spine at 3000 cm/sec, which is about the same wave speed exhibited in ejection simulations. Peak tensile axial forces ranged from 6.84×10^8 dynes at the L5-S level to 4.165×10^8 at the T3-T2 level. As can be seen from Fig. 11, the lateral displacement is somewhat exaggerated in its final configuration. This is attributed to two shortcomings of the model:

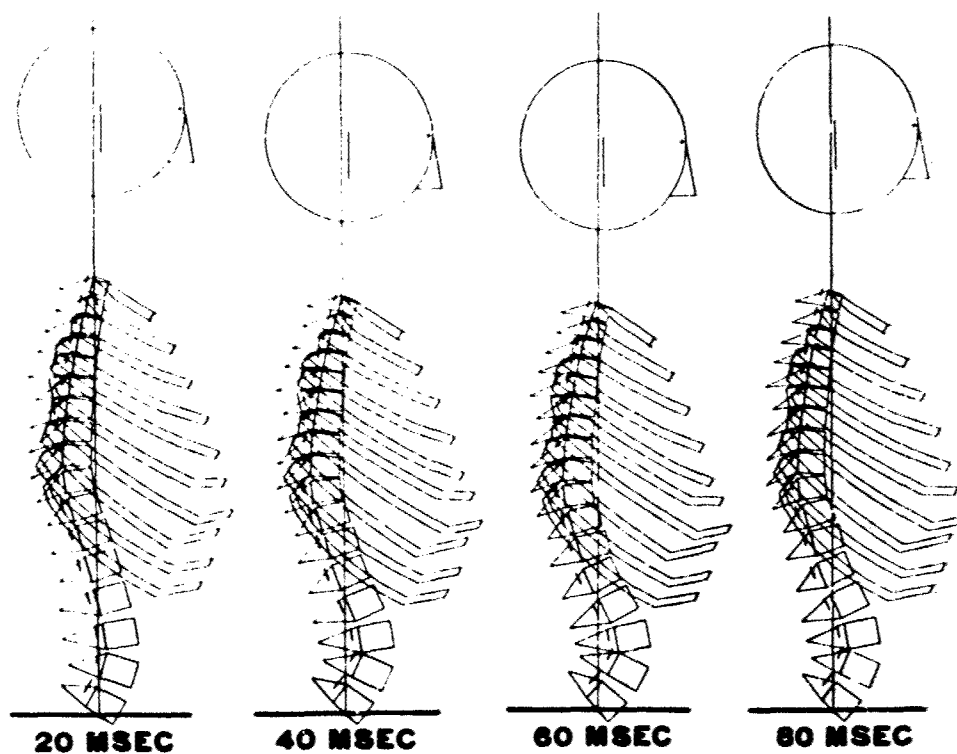


Figure 6 Response of complete spine model in 10 G ejection simulation.

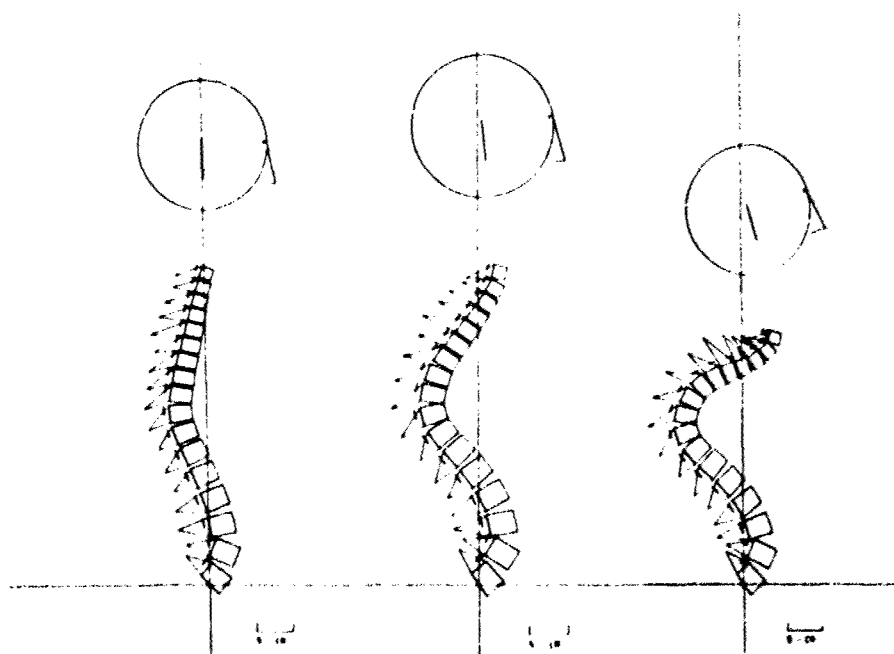


Figure 7 Response of an isolated ligamentous spine without viscera in a 10 G ejection simulation.

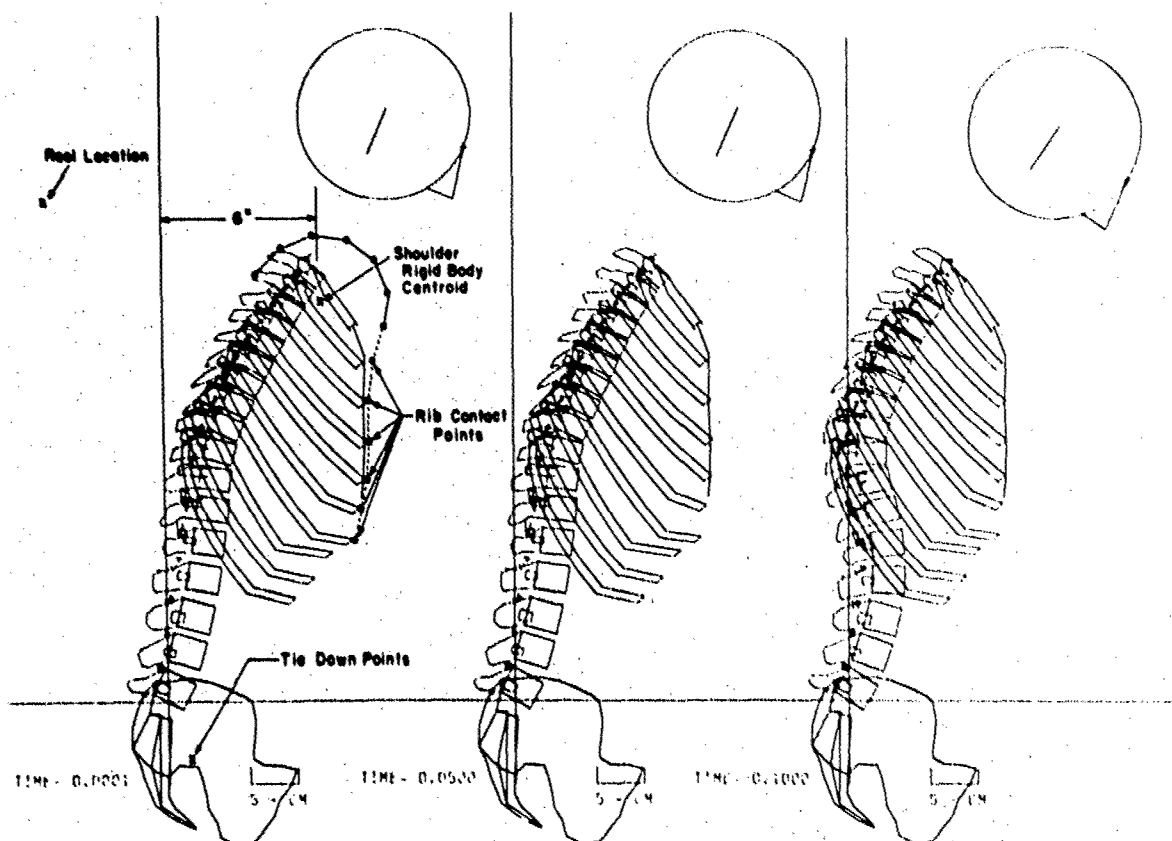


Figure 8 Simulation of a pre-ejection alignment, showing configuration of model at 0, 50 and 100 milliseconds.

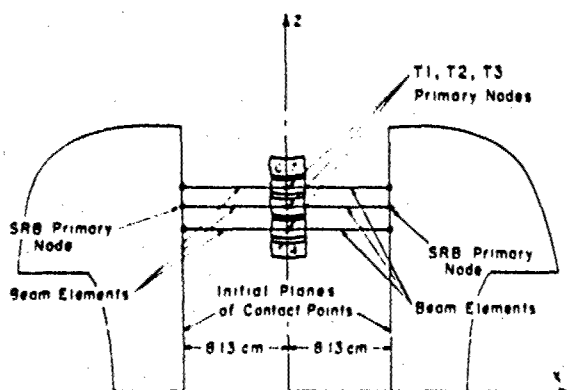


Figure 9 Model of shoulder and its interconnection to the spine.

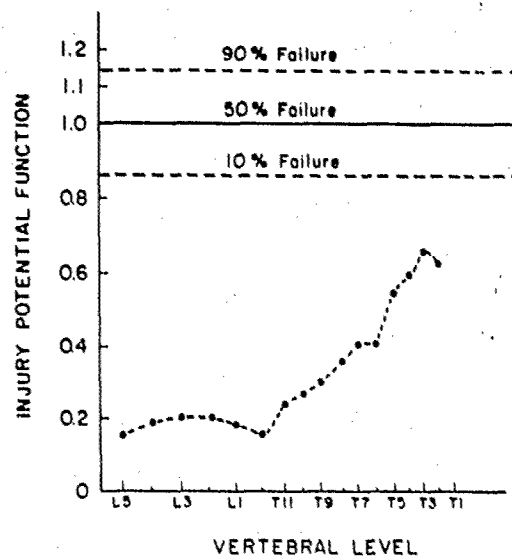


Figure 10 Injury potential diagram for a pre-ejection alignment simulation.

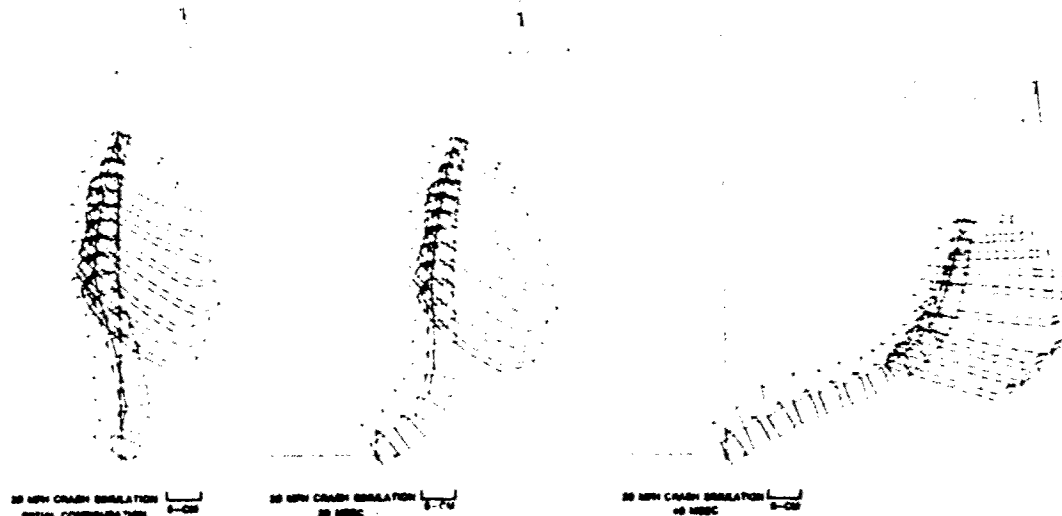


Figure 11 Simulation of frontal crash with a horizontal acceleration of 68.3 G.

1) the rotational stiffness of the costo-vertebral joints appears to be too low and 2) the tensile behavior of the membrane walls is not included in the model. However, with these refinements in the model it should become feasible to study horizontal impact.

Figure 12 illustrates a simulation we are now in the process of studying: bird strike on a canopy resulting in impact with the pilot's head. The top part of the figure shows the response of the flexible canopy to the impact of a 1800 gm bird with a horizontal velocity of 75,000 cm/sec. The canopy is here modeled by plate elements, which can treat both geometric and material nonlinearities. As can be seen from Fig. 12, the bird strike results in severe deformation of the canopy and in contact between the canopy and the pilot's helmet. The response of the pilot is also depicted in Fig. 12. The impulse imparted to the head is quite sensitive to its location relative to the canopy.

CONCLUSIONS

The three-dimensional simulation model for the dynamic response of the human body described here has the potential for examining a wide variety of dynamic environments. It has been partially validated by checking its vertical driving point impedance against experimental measurements; however, these impedance results are heavily dominated by the static pygic mode, so that other modes of verification, particularly for impulsive loads in other directions, are needed.

Efforts are now underway to develop similar models for nonhuman primates so that more extensive validation of the basic modeling concepts can be undertaken. Unfortunately, cadaver data for motion segments of nonhuman primates is presently less complete than that for humans. Since nonhuman primate experiments are essential if complex models of this type are to be validated, the acquisition of this data is critical.

As can be seen from the simulations reported here, considerable development in modeling technology is also needed if simulations with significant nonaxial characteristics are to be successful. The interaction of the spine with the viscera, ribs and abdominal walls play a significant role in these responses. Therefore, a good understanding of these interaction effects is essential.

Sometimes, these aspects can be avoided entirely by the use of articulated rigid body models. It would be quite desirable in the future to link deformable element models such as this one with articulated rigid body models so that the impulsive portions of a simulation can be treated by the deformable element model, the large, rigid body motions by the articulated models. By linking models appropriately in this manner, the simulation of a large number of crashworthiness tolerance problems may become feasible.

REFERENCES

- 1) Latham, F., "A Study in Body Ballistics: Seat Ejection", Proceedings of the Royal Society 147, Series b, p. 121, 1957.
- 2) Payne, P. R., "The Dynamics of Human Restraint Systems, Impact Acceleration Stress," National Academy of Sciences, National Research Council, Publication No. 977, Washington, D.C., 1961.
- 3) Toth, R., "Multiplying Degree of Freedom, Nonlinear Spinal Model," Proc. of 15th Annual Conference on

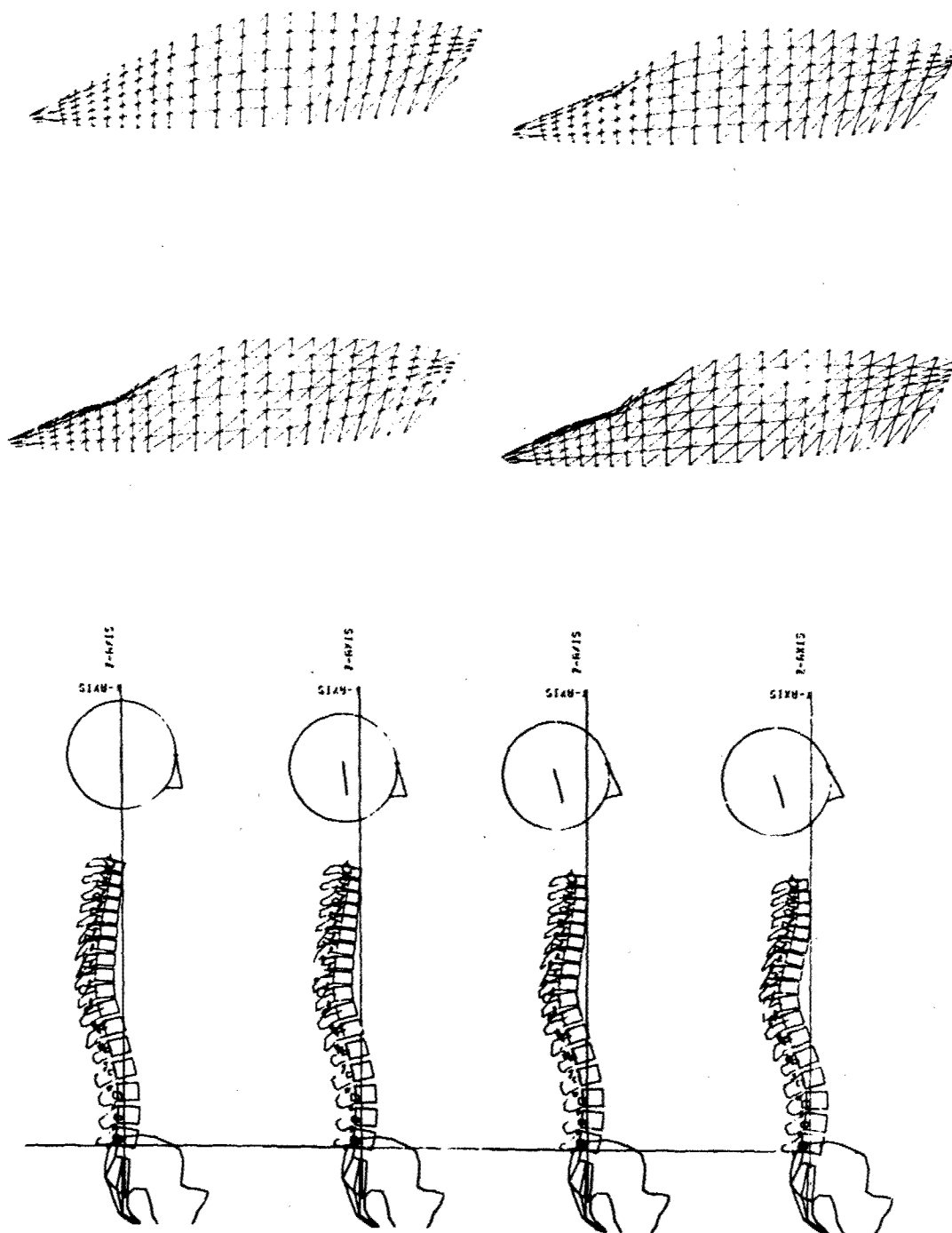


Figure 12 Simulation of bird strike on canopy and resulting canopy impact with head of pilot; top views show canopy at 1.5, 3.0 and 4.5 milliseconds, bottom views the response of spine model after impact.

Engineering in Medicine and Biology 8, 1966.

- 4) Orne, D. and Liu, Y. K., "A Mathematical Model of Spinal Response to Impact", J. of Biomechanics, 4, pp. 49-71, 1970.
- 5) Payne, P. R. and Band, E. G. U., "A Four Degree-of-Freedom Lumped Parameter Model of the Seated Human Body", Wyle Laboratories, Payne Division Working Paper No. 59101-6.
- 6) Mottatt, C. A., Advani, S. H. and Lin, C., "Analytical and Experimental Investigations of Human Spine Flexure", American Society of Mechanical Engineers, Division of Biomechanical and Human Factors, 71-WA/BHF-7, November 1971.
- 7) Prasad, P. and King, A. I., "An Experimentally Validated Dynamic Model of the Spine", J. Appl. Mech., pp. 546-550, 1974.
- 8) Prasad, P., King, A. I., and Ewing, C. L., "The Role of the Articular Facets During +G Acceleration", Bioengineering Division of the American Society of Mechanical Engineers, 73-WAM/Bio 31st, November 1973.
- 9) Belytschko, T., Schwer, L. and Schultz, A. B., "A Model for Analytic Investigation of Three-Dimensional Head-Spine Dynamics", University of Illinois at Chicago, Report to Aerospace Medical Research Laboratory, Wright-Patterson Air Force Base, AMRL-TR-76-10, 1976.
- 10) Coermann, R. R., "The Mechanical Impedance of the Human Body in the Sitting and Standing Position and its Significance for the Subjective Tolerance to Vibrations", presented at the Third Biophysical Society Meeting, Pittsburgh, Pennsylvania, 1959.
- 11) Coermann, R. R., Ziegenruecker, G. H., A. L. and von Gierke, H. E., "The Passive Dynamic Mechanical Properties of the Human Thorax-Abdomen System and of the Whole Body System", Aerospace Magazine, 1960.
- 12) Vogt, H. L., Coermann, R. R., and Fust, H. D., "Mechanical Impedance of the Sitting Human under Sustained Acceleration", Aerospace Medicine, 39, 1968.
- 13) Vykukal, H. C., "Dynamic Response of the Human Body when Combined with Various Magnitudes of Linear Acceleration", Aerospace Medicine, 39, 1968.
- 14) Woods, A. G., "Human Response to Low Frequency Sinusoidal and Random Vibration", Aircraft Engineering, 39, 1967.
- 15) Schultz, A., Belytschko, T. B., Andriacchi, T. P. and Galante, J. O., "Analog Studies of Forces in the Human Spine: Mechanical Properties and Motion Segment Behavior", J. Biomechanics 6, pp. 373-383, 1973.
- 16) Andriacchi, T., Schultz, A., Belytschko, T. and Galante, J. O., "A Model for Studies of Mechanical Interactions Between the Human Spine and Rib Cage", J. Biomechanics 7, 497-507, 1974.
- 17) Torvik, P. J., "An Analysis of Pressure Wave Generated in Seated Spinal Impact," Symp. on Biodynamic Models and Their Applications, Dayton, Ohio, October, 1970.
- 18) Belytschko, T., Schwer, L. and Privitzer, E., "Theory and Application of a Three-Dimensional Model of the Human Spine", Aviation, Space and Environmental Medicine, pp. 158-165, January, 1968.
- 19) Liu, Y. K. and Wickstrom, J. K., "Estimation of the Inertial Property Distribution of the Human Torso from Segmented Cadaveric Data", Perspectives in Biomedical Eng., 1973.
- 20) Eycleshymer, A. C. and Schoemaker, D. M., "A Cross-Section Anatomy", Meredith Corporation, 1970.
- 21) Lucas, D. and Bresler, B., "Stability of the Ligamentous Spine", Biomechanics Laboratory Report 40, University of California at San Francisco, 1961.
- 22) Belytschko, T. and Privitzer, E., "Refinement and Validation of a Three-Dimensional Head-Spine Model", Report AMRL-TR-78-7.

ACKNOWLEDGMENT

This research was sponsored by the Aerospace Medical Research Laboratory under Air Force Contracts US AFSC F33615-76-C-0506 and F33615-78-C-0523. We would also like to express our thanks to I. Kaleps and A. B. Schultz for their advice and support.

DISCUSSION

G. R. ALLEN (UK)

Your model was aimed at impact studies. Could it be used in principle for response to whole body vertical vibration?

AUTHOR'S REPLY

The impedance results described were a demonstration of the model's capability for vibration exposures response predictions. We have also tried to validate our model response with transmissibility data, but have found that the data available for comparison tends to be very erratic. For example, we tried to use data by Woods that was in a very low frequency range and found that this data was so affected by seat cushion properties and instrumentation that the data was not reproducible, and we could thus not define corresponding simulation conditions.

DR. EWING (USA)

It seems like everybody seizes upon the question of voluntary muscle response as with questions such as: Do people tense their muscles? How big of an affect does this have? Would you have the same effect if you were asleep? How much is it possible to alter the response if voluntary muscle tensing could not occur? With our experiments that are verified by two other investigators in different laboratories at 3 g a man with strong muscles can prevent a dynamic response in the -x vector. At 4 g the same thing, at 5 g maybe 1 out of 10 can prevent the dynamic response, at 6 g they are all identical, there is no strong difference.

AUTHOR'S REPLY

I am not saying that the active response of the muscles is necessarily what invalidates models of this type in long-time simulations; rather, it is the passive contribution of muscles and other soft tissues which are of importance in long-term response and which are not accounted for properly. You would get a similar difference if you took an exhumed spine, which is essentially what these models are with the rib cage attached, and compared the response of these to experiments on an actual human body at 20 g.

APPLICATION OF BIODYNAMIC MODELS TO THE ANALYSIS OF F-16 CANOPY BIRDSTRIKE

Lawrence J. Specker*
Norman S. Phillips**
James W. Brinkley*

*Aerospace Medical Research Laboratory
Aerospace Medical Division
Air Force Systems Division
Wright-Patterson Air Force Base, Ohio 45433

**University of Dayton Research Institute
300 College Park Avenue
Dayton, Ohio 45469

The bird impact problem has become especially critical for the new generation of aircraft canopies such as the monolithic windshield/canopy of the F-16. It was required that the canopy be capable of withstanding the impact of a four-pound bird while the aircraft is flying at 350 KEAS. Canopy failure modes identified by testing were fragmentation, penetration and deflection of the canopy material. Of special concern to the Aerospace Medical Research Laboratory were the significant deflections observed as a traveling wave in the canopy material. Biomedical design and evaluation criteria have not been available to apply to this problem. In order to evaluate the degree of crew protection provided by various canopy designs, a research approach was developed that uses mathematical models of the human kinematic and injury response to extrapolate from data acquired in the laboratory to this highly unusual impact environment. The approach included simultaneous efforts to measure the unique impact stresses and to select and use existing biodynamic models to evaluate the effectiveness of each new canopy design.

Thirty-eight birdstrike tests were completed by the USAF during the period of March-August 1977. High speed film data were analyzed from the F-16 birdstrike test program to quantitatively define the deflection motion as a function of the initial test conditions. Crewmember position studies indicated probable head contact with the canopy surface during birdstrike at comfortable seating positions. Helmet size and crewmember size were shown to have a negligible effect on increasing clearance between helmet and canopy. A specially instrumented head-neck apparatus was designed and used in the test program to measure the accelerations of the head and the impact forces and moments at the head and neck. The acceleration data from the head-neck test apparatus were used as input to a head injury severity prediction model to determine the level of injury sustained by the pilot. The force data were compared to known injury force levels. A second approach involved the use of the photometric data to describe the response shape and velocity of the canopy and inertial properties associated with the impact as a driving input to a computer model of the helmeted crewman to further evaluate the crewman response to birdstrike.

INTRODUCTION

Operational statistics compiled during the period of 1963 through 1972 indicate that a total of 3,548 bird/aircraft impacts were recorded by the USAF. Four hundred and fifteen of these incidents (11.7%) involved impact of the windshield/canopy area of the aircraft. Bird impact occurring in the windshield/canopy area of the F/B-111 aircraft has resulted in the loss of five of the six US aircraft lost due to birdstrike. One Australian F-111 aircraft has been lost due to a bird impact on the windshield/canopy area. These statistics have been of considerable concern to the USAF and action has been taken to increase the degree of crew protection provided by the windshield/canopy materials. Although the initial efforts have been focused on the F/B-111 problem, the research has more recently been broadened to study other aircraft systems where unique impact problems might exist.

The latest production USAF aircraft, the F-16, uses an integrated windshield/canopy constructed of a monolithic, polycarbonate material which eliminates the need for the conventional metal windshield frame and thereby increases the visual field of the pilot. To provide birdstrike protection, the canopy is designed to plastically deform to absorb the impact energy. Unfortunately, under certain conditions the bird impact may be severe enough to cause the canopy materials to deform into the space occupied by the pilot. The resulting impact between the canopy and the pilot may cause serious or even fatal injury. Therefore, the goal of the F-16 canopy development program has been to provide a canopy capable of withstanding the impact of a 1.8 kg bird and protecting the pilot from canopy impact while the aircraft is flying at a velocity of 350 KEAS.

Biomedical design and evaluation criteria have not been available to apply to this unique problem. The Aerospace Medical Research Laboratory (AMRL) of the USAF was asked to provide the F-16 Systems Program Office with criteria by which the birdstrike resistance of the canopy could be assessed. The ultimate objective of the research effort has been to provide aeromedical design criteria that can be generally applied during the development and evaluation of new aircraft canopy designs for both current and future aircraft. However, the emphasis of this paper is on the effort that has been accomplished within the cost and schedule constraints of the F-16 canopy development program.

It was clear that proven measuring techniques and established biodynamic models had to be used to remain within the F-16 program constraints. Furthermore, the injury criteria had to be comprehensive enough to describe levels of injury ranging from short period disruption of the pilot psychomotor performance capability to frank major injury such as skull fracture.

Initial efforts were devoted to an investigation of available bird impact testing techniques. Test methods used to impact aircraft canopies were reviewed with the primary emphasis placed on evaluation of existing measurement techniques, description of their limitations and the potential for their improvement. Measurement of the canopy response was found to be best accomplished by use of high-speed motion picture photography although the accuracy of this technique left much to be desired.

Measurement of the response of the impacted crewmember was a major problem. The initial experimental efforts accomplished by airframe contractors utilized anthropometric dummies or specially instrumented headforms. The data collected from tests with the anthropometric dummies were of little value since the dynamic response properties of the dummies were unknown and the instrumentation within the dummies was very limited. The special headform devices were similarly unacceptable since these devices contained elastic structural elements of unknown dynamic response characteristics and the instrumentation had also been limited. Furthermore, the headform device could not simulate the interaction between the head-neck system and the torso dynamics. To partially resolve this problem, a specially instrumented and calibrated headform was designed by AMRL. This device is instrumented with accelerometers to measure the acceleration of the headform. The impact forces and moments reacted through the neck of the head-neck system are measured by an array of six force cells. This device is shown in Figure 1. An approach was still required to determine the interaction between the head, neck and torso. Moreover, an approach was required to analyze existing canopy test data and to provide a design tool to analytically evaluate the influence of factors such as pilot position, helmet thickness, etc.

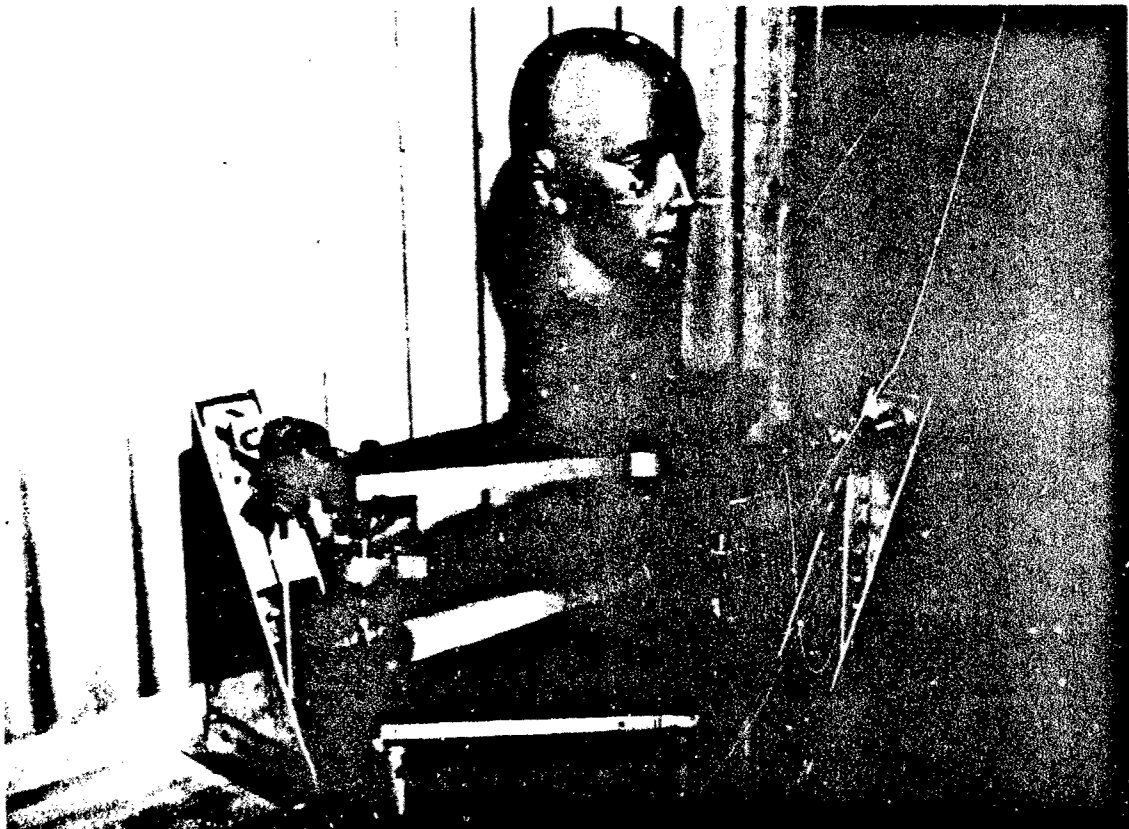


Figure 1. Instrumented Head-Neck Apparatus

In order to establish an analytical procedure to evaluate the effects of the impacting canopy on the crewmember, five candidate approaches were reviewed. These were:

1. Characterization of the aircraft canopy and crewmember in terms of finite element models.
2. Use of a chain model similar to the three dimensional Calspan model to represent the human body. The canopy deformation wave impacting the crewman would be represented as a geometric object.
3. The canopy, the head-neck inertial response characteristics and the injury response of the crewmember would all be represented by lumped parameter models.
4. Acceleration, forces and moments measured by the instrumented headform device would be evaluated using waveform evaluation methods such as the Gadd Severity Index (SI) and the Head Impact Criteria.
5. Measurements made with the instrumented headform device would be compared to available human tolerance data collected under specific test conditions.

Each of the candidates, of course, had specific advantages and disadvantages. The finite element modeling approach was attractive from a long range point of view since the Air Force Flight Dynamics Laboratory was sponsoring a research effort to model the aircraft canopy using this technique. Nevertheless, the approach was complex and human impact response models of this type were nowhere near the point of validation with experimental data and correlation with impact tolerance limits. The chain modeling approach offered many advantages; the most pronounced of these being availability, some validation with human impact experimental results, and the relative ease with which the computer program could be modified to meet the objectives of this program. Its primary disadvantage was that it could not be used to determine if injury limits had been exceeded. The modified three dimensional Calspan model, a chain model used by AMRL, hereafter referred to as the Articulated Total Body Model (ATBM), was available and could be used to predict whole body inertial and kinematic responses.

Lumped parameter modeling approaches were approached with caution. From the standpoint of biomedical applications, they are often oversimplifications of human body subsystems and injury responses. Nevertheless, the lumped parameter model referred to as the Maximum Strain Criteria (MSC) head injury model developed by Stalnaker was available and had several especially attractive features. First, relatively large amounts of human and animal experimental data had been used to develop the model parameters. Second, the model could be used to calculate levels of injury which had been correlated with experimental pathology. Additionally, the model had been developed specifically for the study of the effect of direct impact to the head for cases of both frontal and lateral impact.

Waveform evaluation methods were considered initially and had, in fact, been used to analyze some of the early birdstrike data collected during the development of a new F-111 canopy; however, these methods presented extreme limitations in the F-16 application. The most critical limitation was the fact that the available systems such as the Gadd SI method evaluate the effect of the impact in terms of an absolute limit, an SI of 1,000, which is assumed to be related to occurrence of linear skull fracture. The authors are not aware of any attempt to correlate the SI with other levels of injury.

The empirical approach offered no advantages and was included in the study for completeness only.

The selected approach was a combination of several of the candidate approaches. Briefly, the approach included:

1. Use of the ATBM to calculate the dynamic inertial and kinematic response of the human body.
2. Modification of the ATBM to include an analog of the flight helmet which could be used to determine the effect of the helmet shell and liner on the transmission of impact forces to the human head.
3. Analysis of photometric data collected during birdstrike tests to develop impact forcing functions to be used to calculate the response of the ATBM.
4. Use of the ATBM head acceleration-time history to drive the MSC head injury model and thereby determine strain level.
5. Measurement of the forces, moments and accelerations at the center of gravity (CG) of the head and neck using a specially instrumented headform for comparison with the calculated head and neck response of the ATBM.
6. Use of ATBM calculations, validated with the experimental measurements, were then related to injury criteria describing rotational, and translational acceleration and velocity limits and head-neck forces and moment limits.

This approach was the most likely to be able to evaluate the influence of the interrelationships of parameters such as the initial position of the crewman's head, bird size, bird impact velocity, canopy

response characteristics, and helmet liner thickness upon the overall estimate of injury severity. The paths that were followed in pursuit of this technical approach are shown in Figure 2. The highlights of the research efforts that were accomplished are summarized in the following text.

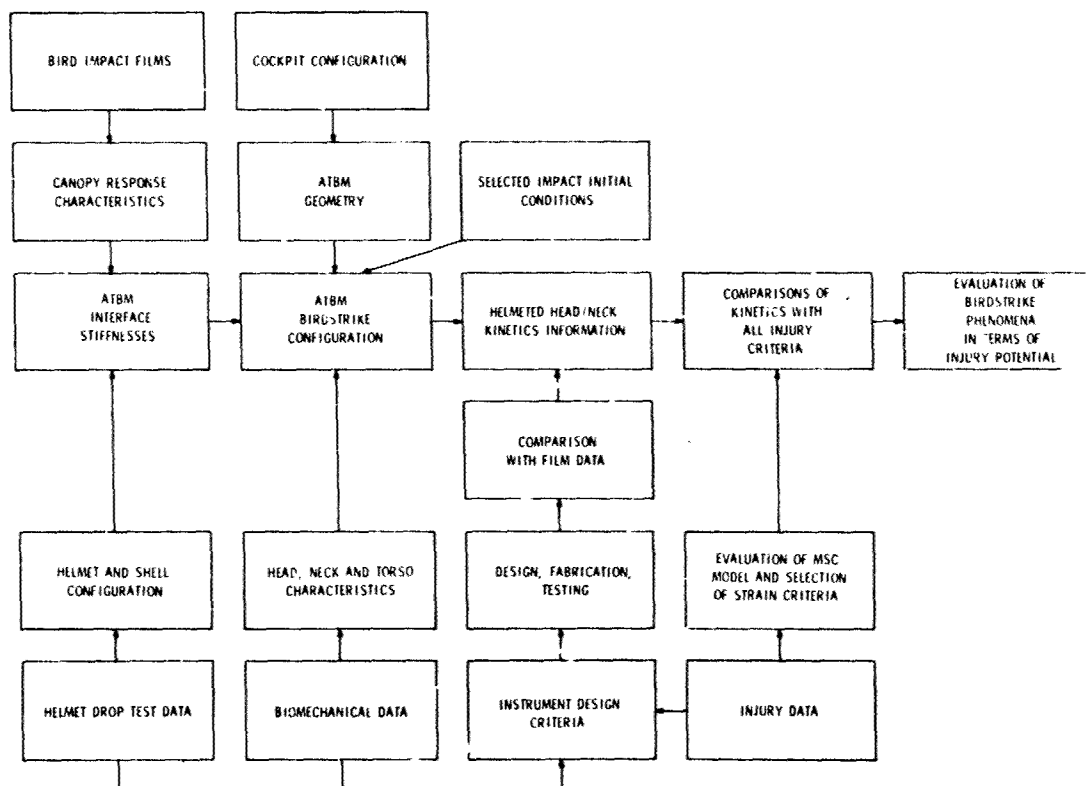


FIGURE 2 FLOW DIAGRAM OF TECHNICAL APPROACH

DESCRIPTION OF CANOPY RESPONSE

The first objective of the analytical effort was the development of the quantitative description of the characteristics of the aircraft canopy at the point of impact with the crewmember's helmet. The parameters necessary for analysis were canopy curvature, velocity and compliance. Data collected during 38 tests conducted for the F-16A alternate canopy design program at the Arnold Engineering Development Center and at the General Dynamics Corporation were made available for analysis. These data consisted of high-speed motion picture films collected during the bird impact tests. The tests were conducted with bird masses of approximately .9, 1.4 and 1.8 kg impacting the canopy at velocities ranging from 123 to 363 knots. Figure 3 shows the F-16 canopy with the head and neck test apparatus in place prior to impact tests.



Figure 3. F-16 Canopy Test Fixture with Head-Neck Apparatus in Place

Using photometric analysis techniques, the value of the maximum canopy deflection was determined and the average wavespeed from the point of maximum deflections to the head location was calculated. The results are plotted in Figures 4 and 5. The displacements that are plotted in Figure 4 are those of the interior of the canopy relative to the original undeformed canopy center line as seen in a side view. The plot of maximum amplitude appears to be bilinear whereas the amplitude of the deformation measured with respect to aircraft station 140.0, the vertical axis on which the design point of the pilot's eye is located, is nearly linear with kinetic energy. The maximum amplitude of the canopy deformation was greater than 12.7 cm at large energy levels for even the thickest canopy that was tested.

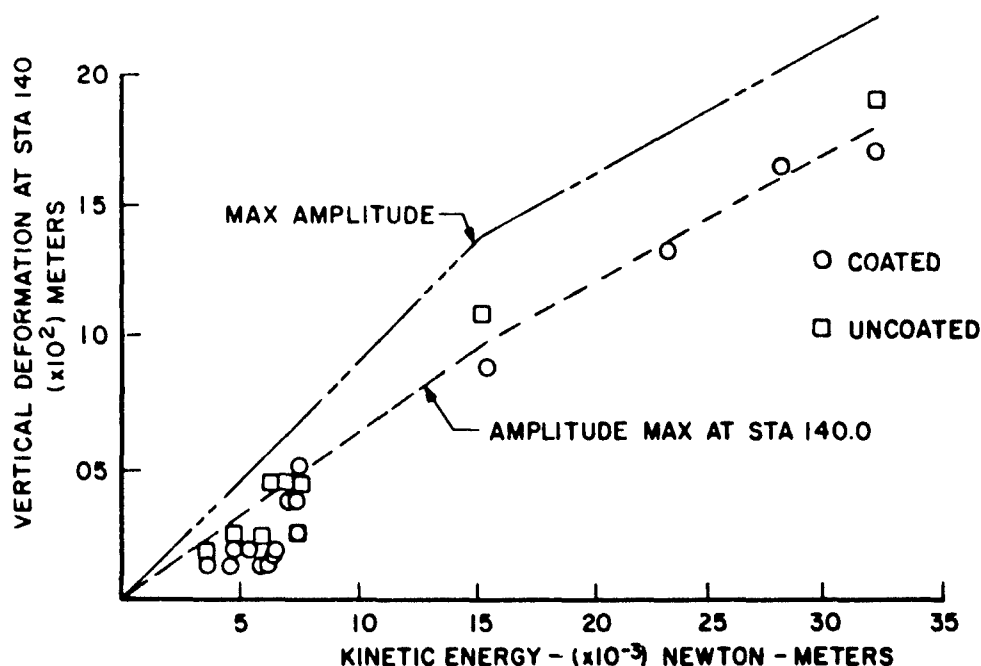


Figure 4. Vertical Deformation at Sta 140.0 vs Kinetic Energy of Bird for 1.27 cm Thickness

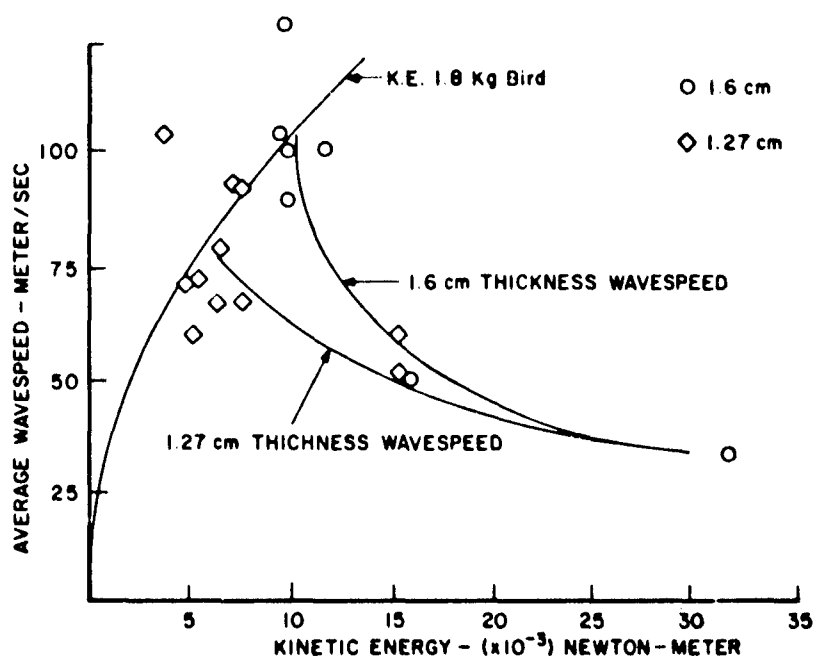


Figure 5. Wavespeed vs K.E.

Figure 5 indicates that the speed of the canopy deformation wave may decrease with increased kinetic energy. This is attributed to the fact that at higher impact velocities the bird is disintegrated in a very short period of time. The impact is, therefore, impulsive in nature and permits the canopy to respond in a free-vibration mode rather than as a forced response as exists at lower impact speeds. At the highest impact speeds, the canopy deformation wave is traveling at less than one-fifth the impact speed of the bird.

A further purpose of the analysis was to determine the compliance of the canopy. Published data collected by impacting birds against instrumented plates provided an approximate means of estimating the peak force and waveform associated with the impact. A study of the motion picture films revealed that the maximum normal deformation of the canopy, as a function of time, could be well approximated by a half-sine pulse. Having the impact forcing function and assuming that the output was indicative of the response of a simple spring-mass system, it was possible to calculate the stiffness and the inertia of a model which would duplicate the observed impact and response.

Based upon cockpit drawings of the F-16 as well as data available on seat adjustment, visual requirements and anthropometric data, analyses were conducted to establish the location of the aircrewman relative to the canopy and selected design eye points. The results were presented in terms of envelopes of helmet volume as functions of aircrewman size and seat location.

DEFINITION OF HELMET PROPERTIES

The stiffness of the helmet was determined by a series of impact tests using standard HGU-22/P helmets with foam and fitting pad liners. Accelerations measured within the metal headform used for these tests were doubly integrated to obtain deformations across the helmet shell and liner as a function of time. These data were plotted to create the force-displacement curves shown in Figure 6. These indicate a slight difference in the form of the curve due to the location of the point of impact, and due to the shape of the anvil on which the headform was impacted. The curve shown in Figure 7 was used to describe the force displacement curve of the helmet liner. From the data that were available, it was assumed that the liner thickness could be described as varying from 2.5 cm at the brow to 3.2 cm at the crown.

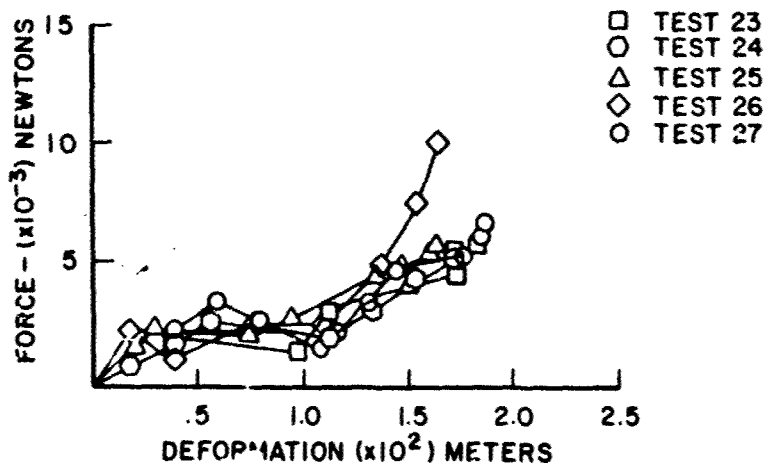


Figure 6. Force Deformation Curves from Drop Tests on HGU-22/P, with Fitting Pads, Helmet Impact Velocity of 3.99 Meter/Sec onto Flat Anvil

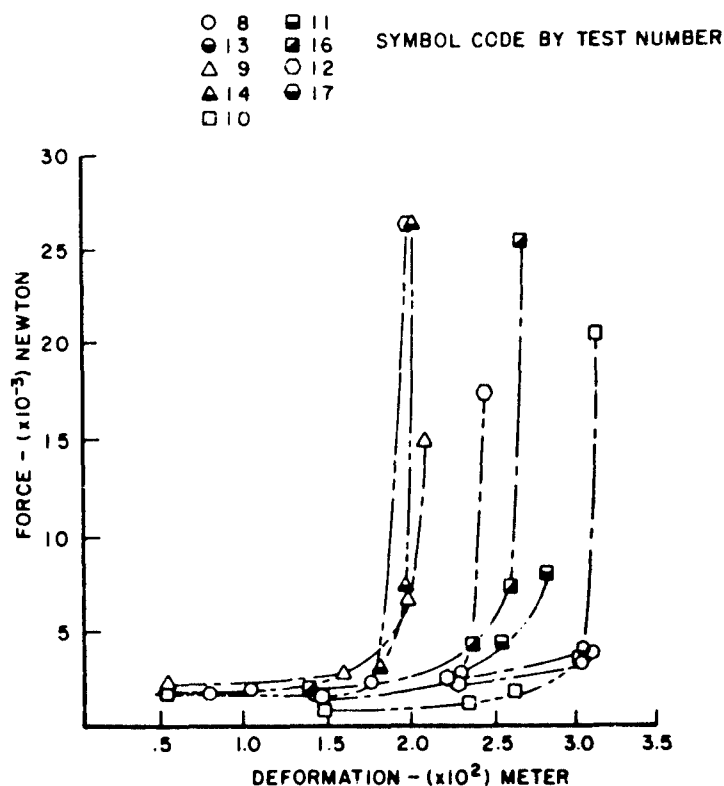


Figure 7. Force Deformation Curves from Drop Test Data on HGU-22/P Styrofoam, Insulite & Foam Helmets Impact Velocities of 4.95 & 5.15 Meter/Sec

HEAD AND NECK CHARACTERISTICS

The ATBM of the human can only duplicate the response of the human body to impact if the proper input coefficients are specified. During the initial phase of the analysis, the ATBM was configured to reflect the response of a 95th percentile anthropometric dummy. As published biomechanical data became available, the coefficients used were compared with those developed to match human responses. The report of Schneider, et al, was particularly applicable since coefficients for an analytical model of the human head and neck had been developed to duplicate the head kinematics of 18 subjects. Furthermore, the coefficients were for a model having similar body segments and joints as the ATBM. The coefficients developed by Schneider were compared with those being used at AMRL and it was found that the differences were negligible. Hence, the values of stiffness and damping for the joints, mass and mass moments of inertia for the segments are in agreement with those known to duplicate observed head and neck response.

INJURY LIMITS AND INJURY MODEL

Many sources of injury criteria were reviewed to establish parameter value limits that could be used in the injury model. Many investigators have published results related to particular parameters such as head acceleration, head velocity change, or head rotational velocities. But selecting the MSC model as a means of evaluating the effect of waveform dictated the need to select a particular strain as a limit. Additionally, strain values were required to be assigned to specific injury scale levels as appropriate to the birdstrike application.

Stalnaker's work was analyzed to determine an acceptable strain level as indicative of concussion. The original strain value of .0061 cm/cm was selected based upon experimental data collected at an injury scale level of 3, "marginal as to whether injury is reversible (i.e., results in permanent disability of function or structure)." This injury level was obviously too severe for the F-16 application. The data were reviewed and the procedure established by Stalnaker was followed to determine a strain level comparable to an injury scale value of 1, "no injury-minor injury." By using the "no injury" data, finding appropriate scaling parameters, and then relating the scale value to strain, a value of .0022 was determined. A plot of constant value strain at .0022 is shown in Figure 8 with the values of .0061 and .00329. It was realized that a strain of .0022 would create extremely severe restrictions on the acceleration environment permitted. The strain level for no injury is too conservative and that for marginal injuries, too severe.

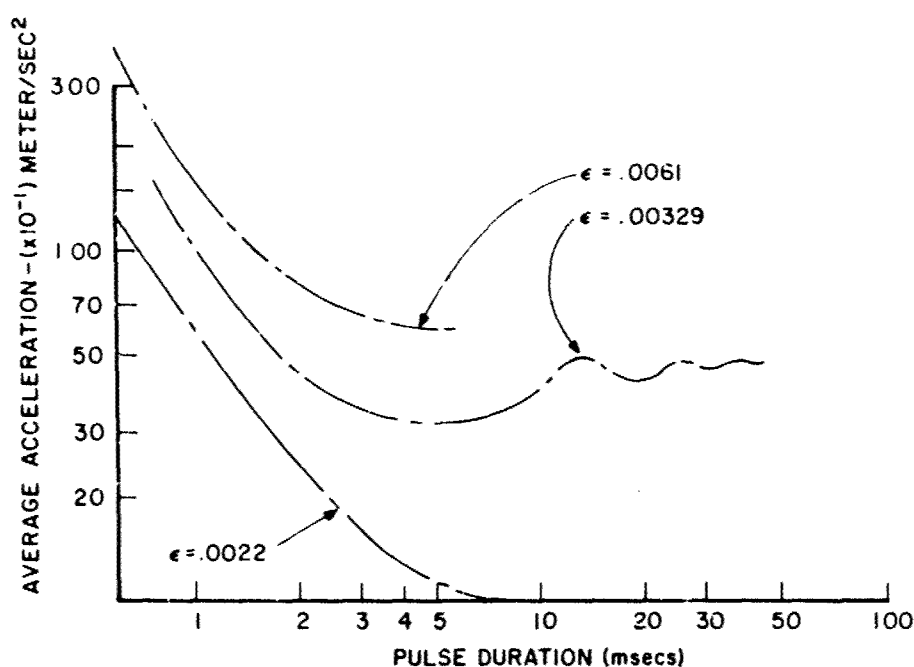


Figure 8. MSC Variations

Data were collected from many sources to relate measured injury to a parameter which could be related to translational acceleration and plotted upon the existing MSC tolerance curves. Data were available from head impact experiments, whole body experiments, and theoretical studies. The criteria for injury ranged from skull fracture to brain shear stress and normal pressure. All results were related to the deceleration pulse which created the "injury" and were plotted on Figure 9. The plotted points indicate that indeed above a strain of .0061, all points were considered "injurious." All points below .0022 are "noninjurious." Consequently, it was necessary to establish some level between the two which could be acceptable. The value selected was .00329 for two reasons. First, the only points of intolerable head response that are below that strain limit are those generated by theoretical models, not experimental data. The points above the limit are points of observed skull fracture. Secondly, the strain value of .00329 was originally established by Stalnaker and McElhaney using the Eiband point (a rectangular pulse of 50 G and 45 milliseconds) as the "survival" acceleration pulse.

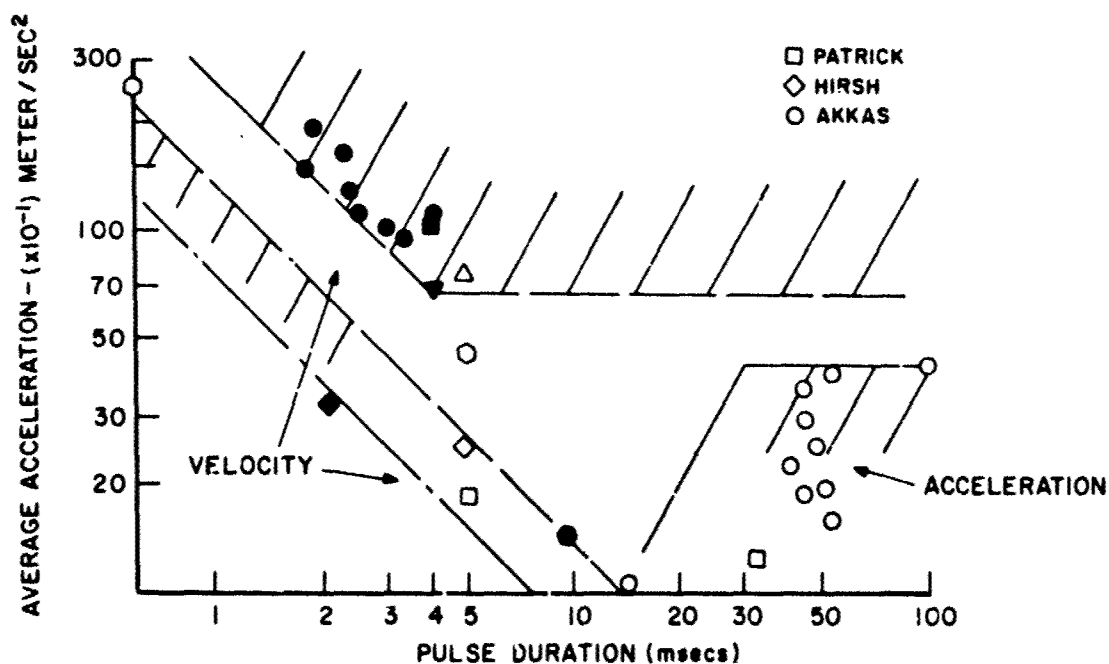


Figure 9. Compilation of Translational Data with Approximate Boundaries for Tolerable Response

The value of strain selected and the models evolved from measured data establish tolerance curves for both longitudinal and lateral head impacts. These are shown in Figure 10. Both assume that injury is related to an 'idealized strain between "model" elements of skull and brain, and that limiting brain strain is independent of the direction of impact.

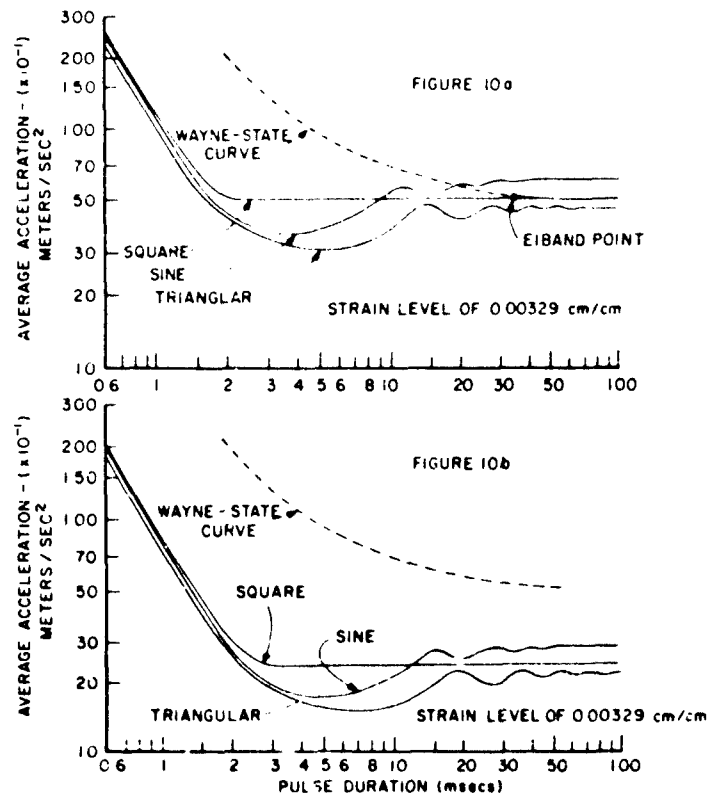


Figure 10. Maximum Strain Criterion Curve for Human Lateral Head Impact

INCORPORATION OF CHARACTERISTICS INTO AN ATBM REPRESENTATION

Use of the ATBM requires that all body segment joints, impact surfaces, and their mutual stiffnesses be defined. The canopy was described as a deformation wave traveling at a given speed and angle to the horizontal. This was duplicated by having the occupant translating forward and the canopy deformation wave moving upward at the time of impact. The location of the deformation wave was established by specifying a particular interference between a nondeforming sphere and helmet shell. Since the shell was of a fixed radius in the sagittal plane, and the direction of the deformation wave was specified, the location of the center of gravity of the deformation wave was established such that the deformation wave and helmet touched at the beginning of each computer run. The maximum interference between the two identifies the computer run being examined.

The stiffness required for analysis was constructed by assuming that the characteristics of deformation wave and shell act in series. The two stiffnesses generate one force-displacement curve which was entered into the computer program. This dictates the kinetic response between the canopy deformation wave and the helmet shell.

The shell was duplicated by an ellipsoid having the curvature of a helmet and separated from the head by a varying liner thickness. The head used had inertial properties indicative of a 95th percentile aircrewman, and had head-neck and neck-torso elasticity and damping coefficients comparable to those developed by Schneider. The torso was that of the 95th percentile individual.

RESULTS OF ANALYSIS

Many computer runs were made to study the response of the helmeted head to selected inputs. Before the model of the canopy had been evolved, empirical data were available in terms of displacement of the canopy normal to its centerline as a function of applied force at the impact point. For the 1.6 cm thick canopy, the apparent stiffness was approximately 1.09×10^6 N/m. This value was used with the helmet test data to generate a force-displacement curve. Runs were made using this stiffness to determine the crewman's response in terms of injury criteria parameters.

The calculated outputs from the computer runs provide several interesting results. First, theoretical interference and computed crush or displacement do differ significantly at large input values of interference. Secondly, injury criteria values versus crush indicate that the differences do not significantly alter the interpretation of tolerability. That is, if a birdstrike results in a canopy deformation wave that would create 3.2 cm of interference, the resulting crush is nearly the same.

Tabulated results clearly show that any interference of greater than the least values computed, is excessive. There is little doubt that the kinematics of the head due to helmet crush depths of greater than 3.2 cm are intolerable. The question then becomes one of examining the responses at crush depths of nearly 2.5 cm.

For the two birdstrikes at 3 cm of interference, the acceleration waveforms were used as inputs to the MSC model to compute the longitudinal strain. This can be easily accomplished manually since the MSC model is a lightly damped (damping ratio of 0.028) system and the peak strain occurs in the first 3 milliseconds. The response of a lightly damped single degree of freedom system to a linear acceleration change is a relatively simple expression containing the period and natural frequency of the model as well as the acceleration rate and skull reference length. The waveforms examined were approximated by line segments and the strain of each segment was summed using superposition to calculate the maximum strain.

For the waveforms selected, the strain value is .003 cm/cm which is, according to the current criteria, tolerable. Examination of the greater crush depth waveforms makes it apparent that the other listed would greatly exceed the tolerable strain.

Other aspects of the birdstrike phenomena that were examined using the model were the effects of the presence of a helmet visor and a headrest. Both were merely extensions of the developed model. For the visor, it was necessary to conduct laboratory experiments to measure the force displacement characteristics at many points. With this information, the stiffness at the impact point was then generated by combining the stiffness of the canopy, helmet and visor.

The longitudinal acceleration of the head as modified by the visor is seen in Figure 11. This is indicative of the response due to 3 cm interference with a stiff canopy. Although the presence of the visor has reduced the peak value of the acceleration, the calculated strain for both has the same magnitude. The increase in interference is apparently offset by the softness of the visor.

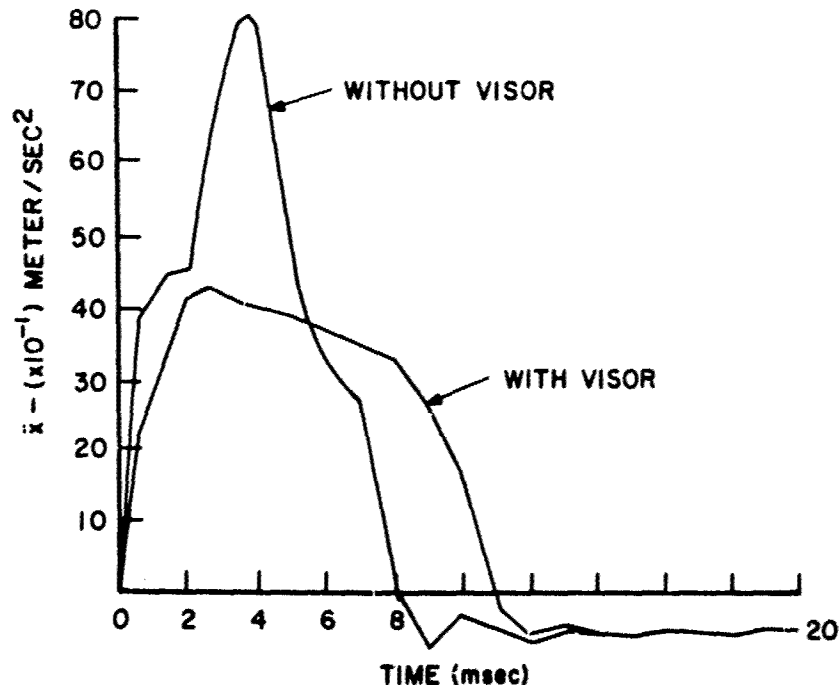


Figure 11. Head Acceleration Generated with and without Visor

The results that are presented are always related to original interference. This was done so that the applicability of the results would not be restricted. No effort was made to relate the interference to clearance within the F-16 canopy. This was done so that the results could be used to go first from injury to interference and then clearance. If an impact is tolerable, and the interference is 3 cm, then one can return to a cockpit drawing with selected percentiles of men at selected seat positions, and determine

what the acceptable clearance would be. For example, during a study of crew position for the F-16, crewmen head positions were established for analysis purposes for 5th, 50th and 95th percentile air-crewman seated at low, mid and upper seat position. The head positions were established by placing an anthropometric model in the seat and attempting to locate the crewman in the most comfortable position based upon head tilt and back support. With seat adjusted full up, the helmet position is such that an interference of 3 cm would require a deflection of about 4.6 cm for a 1.6 cm thick canopy. If another position were selected as being critical, the interference can be added to the helmet shell location and the depth of deflection established.

SUMMARY OF EFFORT

The purpose of the effort was to develop an analytical model of the birdstrike phenomena. As such, the model had to reflect the characteristics of the canopy, helmet, head and headrest as they influence one another. It was not sufficient to just have a model of each and subject them to selected impacts. The model had to reflect the interaction between all elements. Additionally, it was desired to be able to compare the kinetic outputs of the model with injury criteria parameters and have some means of overcoming the problem of acceleration waveform evaluation. The purpose of the effort was achieved in that the ATBM model in conjunction with the MSC model was used to simulate the total birdstrike process.

The ATBM model has the capability to reflect the kinetic process studied if adequate information is available. Specifically, test data are needed to establish the compliance, speed and direction of the canopy deflection. Also needed are force displacement measurements from the helmet impact tests and headrest tests. These, in conjunction with biomechanical data for the inertial, elastic and viscous characteristics of the human, can provide a realistic means of studying the overall system response from both a kinetic and injury potential viewpoint.

BIBLIOGRAPHY

- Advani, S. H. and Owings, R. P., "Structural Modeling of Human Head," Journal of the Engineering Mechanics Division, American Society of Civil Engineers, Vol 101, 1975, pp 257-266.
- Akkas, N., "Effects of Pulse Duration on Head Injury," Journal of Engineering Mechanics Division, American Society of Civil Engineers, Vol 103, 1977, pp 35-50.
- Becker, E. B., "Preliminary Discussion of an Approach to Modeling Living Human Head and Neck to -Gx Impact Acceleration," Human Impact Response, pp 321-329. Edited by W. F. King and H. J. Mertz, Plenum Publishing Corporation.
- Bishop, P. J., "Head Protection in Sports with Particular Application to Ice Hockey," Ergonomics, July 1967, pp 451-464.
- Bycroft, G. N., "Mathematical Model of a Head Subjected to Angular Acceleration," Journal of Biomechanics, Vol 6, 1973, pp 487-496.
- Ewing, C. L., "Injury Criteria and Human Tolerance for the Neck," Aircraft Crashworthiness, pp 141-152. Edited by K. Saczalski, et al, University Press of Virginia, 1975.
- Ewing, C. L. and Thomas, D. J., "Torque Versus Angular Displacement Response Human Head to -Gx Impact Acceleration," Proceedings of the Seventeenth Stapp Car Crash Conference, pp 309-342, 1974.
- Glaister, D. H., Evaluation of Aircrew Protective Helmets Worn During Crashes and Ejections, FPRC/1330, May 1974.
- Goldsmith, W., "Construction Helmet Response Under Severe Impact," Journal of the Construction Division, American Society of Civil Engineers, Vol 101, 1975, pp 335-343.
- Hickling, R. and Wenner, M. L., "Mathematical Model of a Head Subjected to an Axisymmetric Impact," Journal of Biomechanics, Vol 6, 1973, pp 115-132.
- Hirsch, A. E., "Current Problems in Head Protection," Head Injury Conference Proceeding, pp 37-40. Edited by W. F. Caveness and A. E. Walker, J. B. Tippincott, 1966.
- Hodgson, V. R., et al, "Fracture Behavior of the Skull Frontal Bone to Cylindrical Surfaces," Proceedings of 14th Stapp Car Crash Conference, Society of Automotive Engineers, New York, 1970, pp 341-355.
- Hodgson, V. R. and Thomas, L. M., "Breaking Strength of the Human Skull Versus Impact Surface Curvature," Department of Transportation HS-801 002, November 1973.
- Hodgson, V. R. and Thomas, L. M., "Head Injury Tolerance," Aircraft Crashworthiness, pp 175-196. Edited by K. Saczalski, et al, University Press of Virginia, 1975.

- Hughes, T. R., et al, "Numerical Prediction of Head/Helmet System Response," Measurement and Prediction of Structural and Biodynamic Crash-Impact Response, American Society of Civil Engineers, 1976, pp 151-165.
- Jemian, W. A. and Liu, N. H., "Computer Modeling of the Body-Head-Helmet System," United States Army Aeromedical Research Laboratory Report No. 76-13, February 1976.
- Kazarian, L. E. and Graves, G. A., "Human Vertebral Centrum," Spine, Vol 2, pp 1-14, March 1977.
- Liu, Y. K., et al, "Angular Acceleration of Viscoelastic, (Kelvin), Material in a Rigid Spherical Shell - A Rotational Model," Journal of Biomechanics, Vol 8, 1975, pp 285-292.
- Liu, Y. K. and Chandran, K. B., "Packare Cushioning for the Human Head," Journal of Applied Mechanics, September 1975.
- Melvin, J. W., et al, "Human Head and Knee Tolerance to Localized Pressure," International Automobile Safety Compendium, Society of Automotive Engineers, New York, 1970, Paper 690477, pp 39.
- Nahum, A. M., et al, "Impact Tolerances of the Skull and Face," Proceedings of the 12th Stapp Car Crash Conference, pp 303-316, 1968.
- Ommaya, A. K. and Hirsch, A. E., "Tolerance for Cerebral Concussion from Head Impact and Whiplash in Primates," Journal of Biomechanics, Vol 4, 1971, pp 13-23.
- Patrick, L. M. and Sato, T. B., "Methods of Establishing Human Tolerance Levels: Cadaver and Animal Research and Clinical Observations," Impact Injury and Crash Protection, pp 259-274. Edited by E. S. Gurdjian, et al, Charles C. Thomas, 1970.
- Patrick, L. M. and Grime, G., "Applications of Human Tolerance Data to Protective Systems," Impact Injury and Crash Protection, pp 444-473. Edited by E. S. Gurdjian, et al, Charles C. Thomas, 1970.
- Payne, P. R., "Some Aspects of Biodynamic Modeling for Aircraft Escape Systems," In Symposium on Biodynamic Models and Their Applications, AMRL-TR-71-29 (AD 739 501), Aerospace Medical Research Laboratory, Wright-Patterson AFB, Ohio, December 1971, pp 233-336.
- Rayne, J. M., Dynamic Behavior of Crash Helmets, C. P. No. 1202, 1972.
- Robbins, D. H., Snyder, R. G., and Roberts, V. L., Injury Criteria Model for Restraint System Effectiveness Evaluation, Department of Transportation HS-800 499, April 1971.
- Saczalski, K. J. and Richardson, E. Q., "Nonlinear Numerical Prediction of Human Head/Helmet Crash Impact Response," Aviation Space and Environmental Medicine, Vol 49, pp 114-119, January 1978.
- Stalnaker, R., et al, "A Mechanical Impedance Model for Head Injury," In Symposium on Biodynamic Models and Their Applications, AMRL-TR-71-29 (AD 739 501), Aerospace Medical Research Laboratory, Wright-Patterson AFB, Ohio, December 1971, pp 905-931.
- Stapp, J. P., "Voluntary Human Tolerance Levels," Impact Injury and Crash Protection, pp 308-349. Edited by E. S. Gurdjian, et al, Charles E. Thomas, 1970.

A FAILURE CRITERION FOR HUMAN, VERTEBRAL, CANCELLOUS BONE

by

M. J. Percy, J. H. Evans
 Bioengineering Unit, Wolfson Centre
 University of Strathclyde
 106 Rottenrow
 Glasgow
 Scotland

SUMMARY

The published data on the mechanical properties of cancellous bone was found to be an inadequate base from which to predict the mechanical tolerance of vertebral cancellous bone as no information is available on the behaviour in shear. In order to define a realistic criterion of failure, the compression and shear characteristics of human, vertebral, cancellous bone were investigated. To produce shear, torsion tests were used and the atmospheric environment during the tests was controlled to simulate physiological conditions. A rational mathematical characterisation of the bone was developed to enable a realistic failure criterion to be established, encompassing the large biological variation of the results. The mechanical characteristics of the bone are complex but an elementary consideration of anisotropy led to a characterisation that would appear to be sufficient. In order to produce a more definitive mathematical characterisation more detailed investigation of the structure of vertebral cancellous bone and its anisotropy must be conducted, but it is doubtful whether this will produce more practically pertinent information.

SYMBOLS

τ - shear stress
 τ_y - shear stress at yield
 γ - shear strain
 γ_y - shear strain at yield
 σ - normal stress
 σ_y - normal stress at yield
 ϵ - normal strain
 u - strain energy per unit volume

INTRODUCTION

In life, vertebral bodies are subject to complex loading patterns. The compressive forces transmitted through the end plates are compounded by shear forces resulting from translation and rotation of neighbouring bodies. Mechanical failure of vertebra, although not uncommon, is not readily predictable, but its consequences can be catastrophic.

Over the past 100 years some of the mechanical characteristics of human vertebrae have been extensively investigated; in particular the compressive and tensile properties of the bone have received much attention and both Evans, F.G. ⁽¹⁾ and Yamada, H. ⁽²⁾ have produced excellent reviews of this work. In contrast, the only reference to the shear properties of cancellous bone in the literature appears to be the torsional study of Sonada, T. ⁽³⁾ who obtained values for the breaking moment of intact vertebral bodies.

Much of this work has been conducted on intact vertebral bodies and the results cannot be directly related to the cancellous bone within the bodies because of the cortical bone which encases them.

The experiments which have been conducted on purely cancellous bone from human vertebrae show clear evidence of topographic differences in the compressive strength. However, there is a wide variation in published values which is probably attributable in part to the differing experimental techniques employed.

The accumulated data is an insufficient base from which to predict the mechanical tolerance of cancellous bone.

In order to define a realistic criterion of failure, an investigation was initiated into the compressive and shear characteristics of cancellous bone and their topographic variation.

The shear characteristics were studied by means of torsion tests because this method produces simply distributed, homogeneous shear without the complication of compressive forces which could be introduced by other methods.

PREPARATION OF THE SPECIMENS

In order to conduct tests on fresh specimens of bone, sections of lumbar spine consisting of two or more vertebrae were obtained from routine post mortems within a few hours of death. If not used immediately for experimentation, the specimens were stored at approximately -20°C . There is evidence that storage at this temperature does not substantially affect the mechanical properties of bone ⁽⁴⁾.

For torsion tests a single vertebrae was first separated from the vertebral column and the neural arch was removed leaving just the centrum.

A central rectangular block of bone was then separated out and divided into 16 specimens of approximate dimensions 10 mm x 10 mm x 15 mm (Fig. 1).

Each specimen was then cemented into brass mounting cups with bone cement (Acrlite-Microtech Type A). Brass cups were used to conduct heat away from the specimens as the bone cement cured. Before the cement had completely cured, the alignment of the mounting cups was checked by positioning the specimen in a jig which was subsequently used to machine them. The specimens were rotated in the jig and machined to a regular cylindrical section using a special tool. The tool has the ends of the cutting edges radiused in order to produce the specimen shape required to reduce stress concentrations occurring at the ends of the specimens (Fig. 2).

The apparatus used for the machining had to be specially made to comply with local safety regulations concerning the handling of human tissues. The machining jig was built to allow the specimens to be rotated whilst providing support for the mounting cups to reduce bending stresses during the machining process.

A very slow speed of machining was used as there is evidence that slow machining of wet specimens of bone does not significantly change their mechanical properties (2).

The specimen dimensions were a compromise, the upper limit on size being dictated by the body dimensions. The lower limit for the diameter of the specimens was dependent on the maximum trabecular spacing of the bone which appeared to be of the order of 1 mm. The length of the specimen was chosen to reduce end effects from the torsion test and allow heat from the bone cement to be dissipated without affecting that part of the specimen under test.

For these reasons the specimen size was chosen as:-

Test section 5 mm in length x 5 mm diameter
Whole length 15 mm (see Fig. 2)

For the compression tests, cylindrical specimens (10 mm diam. x 10 mm) were removed from the central block, cemented onto brass cups and allowed to set with the end faces of the cups parallel in an attempt to produce a uniform stress distribution during the tests.

TEST CONDITIONS AND PROCEDURES

Throughout the preparation and testing procedures, great care was taken to ensure that the bone specimens were maintained in a high humidity environment.

The preparation could not be undertaken inside the available controlled environment chamber, and so whenever the specimens were not being handled they were kept in individual plastic bottles, which prevented them from losing moisture. Prior to test the bottles were kept in the environment chamber so as to maintain their temperature close to 37°C.

In order to simulate physiological conditions, the testing procedures were conducted in the chamber which maintained an atmosphere of saturated water vapour at 37°C \pm 1°C. It was not possible to measure 100% relative humidity but the electronic hygrometer used consistently measured 99% + r.h.

To discover whether the chamber was effective at preventing fluid exchange to and from the specimens, initial tests were conducted to investigate the weight change of specimens left in the chamber.

Specimens, initially at room temperature, put into the chamber at 99% + relative humidity and 37°C \pm 1°C gained approximately 2% of their initial weight due to condensation, but reached an equilibrium after 10 minutes. No further change was then recorded after another hour in the chamber.

A specimen which had been allowed to equilibrate thermally in a plastic bottle first, showed no change of weight at all within the first 30 minutes exposure in the chamber.

To produce measurable torsion in a specimen using a conventional tension test machine (Instron TTDM), a test rig was designed to translate the linear motion into pure rotation applied to the specimen, without significant deformation of the rig itself.

For the torsion tests, prepared specimens were put into the controlled environment chamber inside plastic bottles for at least 10 minutes in order to allow them to reach the temperature in the chamber. They were then positioned in the test rig and taken to failure in torsion at a strain rate of 0.03 rad/min.

For the compression tests, after temperature equilibration, the cylindrical specimens were taken to failure in the Instron test machine at a strain rate of 0.05/min.

RESULTS

The shear stress and strain at yield was calculated for each specimen from every vertebral sample. The only apparent topographic differences were that the shear stresses at yield were generally lower for the superior (top) half than for the inferior (bottom) half of the vertebral bodies. This is demonstrated in Fig. 3, where the mean values for the shear stress are plotted against the mean values for shear strain for all the specimens from the top and bottom positions respectively.

The mean values for shear stress at yield, shear strain at yield and an approximate shear modulus for the top and bottom sections of each vertebral body, are shown in Table 1.

Combining the overall mean value for the top and bottom, gives working values of

Shear strength at failure	= 0.689 MPa
Shear strain at failure	= 0.101 Rad
Approximate shear modulus	= 8.982 MPa Rad ⁻¹

The results for the compression tests showed a mean maximum compressive strength of

1.377 MPa for the top section, and
1.974 MPa for the bottom section

giving an overall mean of

1.676 MPa.

The latter results are in general agreement with other published data^(5, 6)

THEORY AND DISCUSSION

In order to use the experimental results to produce a realistic criterion of failure, it is necessary to examine rational mathematical characterisations of the cancellous bone.

To calculate shear stresses and shear strains for this initial analysis, principles of mechanics for elastic, isotropic and homogeneous materials were used. It has been stated that for all practical purposes trabecular bone behaves elastically (7,8). However, it is neither isotropic nor homogeneous. The measured range of shear stress at yield was 0.128 - 2.654 MPa and this amount of biological variation is an indication that the approximations assumed in using simple mechanics formulae may be acceptable when determining a usable value for failure of the bone. However, it must be emphasised that for any design value used the safety factor must also reflect this variability.

The consideration of classical failure criteria leads initially to the Maximum shear stress or Tresca criterion⁽⁹⁾. This theory assumes that yielding begins when the maximum shear stress in the material becomes equal to the maximum shear stress at the yield point in a simple uniaxial tension test. The maximum shear stress in the material is equal to half the difference between the maximum and minimum principal stresses.

The next stage of sophistication is to consider the strain energy of deformation (shear strain energy or Maxwell Mises Hencky) criterion.

For a simple uniaxial tensile test

$$U = \frac{1}{2} (\epsilon_1 \sigma_1 + \epsilon_2 \sigma_2 + \epsilon_3 \sigma_3)$$

where the suffices refer to the principal three-dimensional directions (see Timoshenko⁽⁹⁾).

It is usual to divide the strain energy into two parts:- that resulting from volume change (hydrostatic or dilatational) and that resulting from deformation or distortion. In general, materials can withstand very large hydrostatic forces and it is reasonable to consider the component producing distortion alone for a failure criterion.

This produces a distortion energy criterion of

$$(\sigma_1 - \sigma_2)^2 + (\sigma_2 - \sigma_3)^2 + (\sigma_1 - \sigma_3)^2 = K$$

where K is a constant.

For a simple uniaxial test $K = 2\sigma_y^2$

For a two-dimensional stress field $\sigma_3 = 0$

$$\text{Thus } \sigma_1^2 - \sigma_1\sigma_2 + \sigma_2^2 = \sigma_y^2$$

For combined axial compression and torsion it can be shown that

$$\sigma^2 + 3\tau^2 = \sigma_y^2 \quad (1)$$

The experimental results conform to this criterion in part of their range for the plane of stress investigated.

The next stage of complication involves some consideration of the anisotropy of the bone. There is some evidence that the trabecular structure consists of laminae strengthened with struts⁽¹⁰⁾. From theories of anisotropic materials^(11,12) it can be shown that for a unidirectional laminar, symmetrical in the 2-3 plane with fibres in the 1 direction, and with plane stress in the 1-2 plane

$$\frac{\sigma_1^2}{\sigma_{1Y}^2} - \frac{\sigma_1 \sigma_2}{\sigma_{1Y}^2} + \frac{\sigma_2^2}{\sigma_{2Y}^2} + \frac{\tau_{12}^2}{\tau_{12Y}^2} = 1 \quad (\text{Tsai-Hill criterion})$$

With the wide range of values obtained experimentally, it is reasonable to assume $\sigma_{1Y} = \sigma_{2Y}$ in order to deduce a usable criterion.

This gives
$$\sigma_1^2 - \sigma_1 \sigma_2 + \sigma_2^2 + \frac{\tau_{12}^2 \sigma_Y^2}{\tau_Y^2} = \sigma_Y^2$$

From equation (1) for combined compression and torsion

$$\sigma_1^2 - \sigma_1 \sigma_2 + \sigma_2^2 = \sigma^2 + 3\tau^2$$

Thus
$$\sigma^2 + (3 + \frac{\sigma_Y^2}{\tau_Y^2})\tau^2 = \sigma_Y^2 \quad (2)$$

If the overall mean values for τ_Y and σ_Y are used

$$\frac{\sigma_Y^2}{\tau_Y^2} = \frac{1.68^2}{0.7^2} = 5.76$$

then equation (2) becomes

$$\sigma^2 + 8.76\tau^2 = \sigma_Y^2 \quad (3)$$

(Compare equation (3) with equation (1)).

This equation gives a better correlation with the range of experimental results.

It is obvious that the mechanics of the bone are complex.

Before a more definitive mathematical characterisation can be attempted, more detailed investigations of the structure of cancellous bone and its anisotropy must be conducted. However, in predicting the quasi-static load bearing capacity of cancellous bone within the body, the rational approach set out above would appear to be sufficient.

REFERENCES

1. Evans, F.G. Mechanical Properties of Bone. Charles C. Thomas Publisher, Illinois, 1973.
2. Yamada, H. Strength of Biological Materials. The Williams and Wilkins Company, Baltimore, 1970.
3. Sonada, T. Studies on the Strength for Compression, Tension and Torsion of the Human Vertebral Column. J. Kyoto Pref. Med. Univ. 71, 1962 pp. 659-702.
4. Sedlin, E.D. and Hirsch, C. Factors Affecting the Determination of the Physical Properties of Femoral Cortical Bone. Acta Orthop. Scand. 37, 1966, pp. 29-48.
5. Galante, J., Rostoker, W., Ray, R.D. Physical Properties of Trabecular Bone. Calif. Tissue Res. 5, 1970, pp. 273-276.
6. Yokoo, S. Compression Test of the Cancellous Bone. J. Kyoto Pref. Med. Univ. 53(3), 1952, pp. 273-276.
7. Pugh, J.W., Rose, R.M., Radin, E.L. Elastic and Viscoelastic Properties of Trabecular Bone - Dependence on Structure. J. Biomechanics 6(5), 1973 p. 475.
8. Sedlin, E.D. A Rheologic Model for Cortical Bone. A Study of the Physical Properties of Human Femoral Samples. Acta Orthop. Scand. Supp. 83, 1965, p.36.
9. Timoshenko, S. Elements of Strength of Materials. Van Nostrand Reinhold Company, 1968 pp. 183 and 313-320.
10. Pugh, J.W., Rose, R.M., Radin, E.L. Structural Model for the Mechanical Behaviour of Trabecular Bone. J. Biomechanics 6(6) 1973, pp. 657-670.
11. Jones, R.M. Mechanics of Composite Materials. McGraw-Hill Book Company, 1975 pp. 31-84
12. Tsai, S.W., Wu, E.M. A General Theory of Strength for Anisotropic Materials. J. Composite Materials, 1971 pp. 58-80.

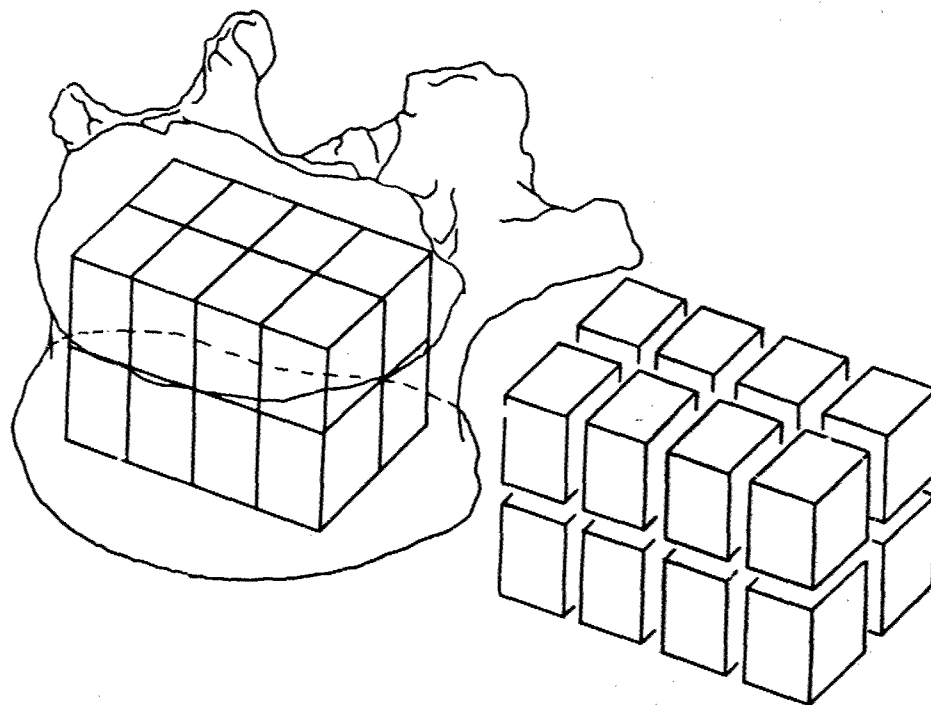


Fig. 1 Separation of bone specimens from the vertebral body

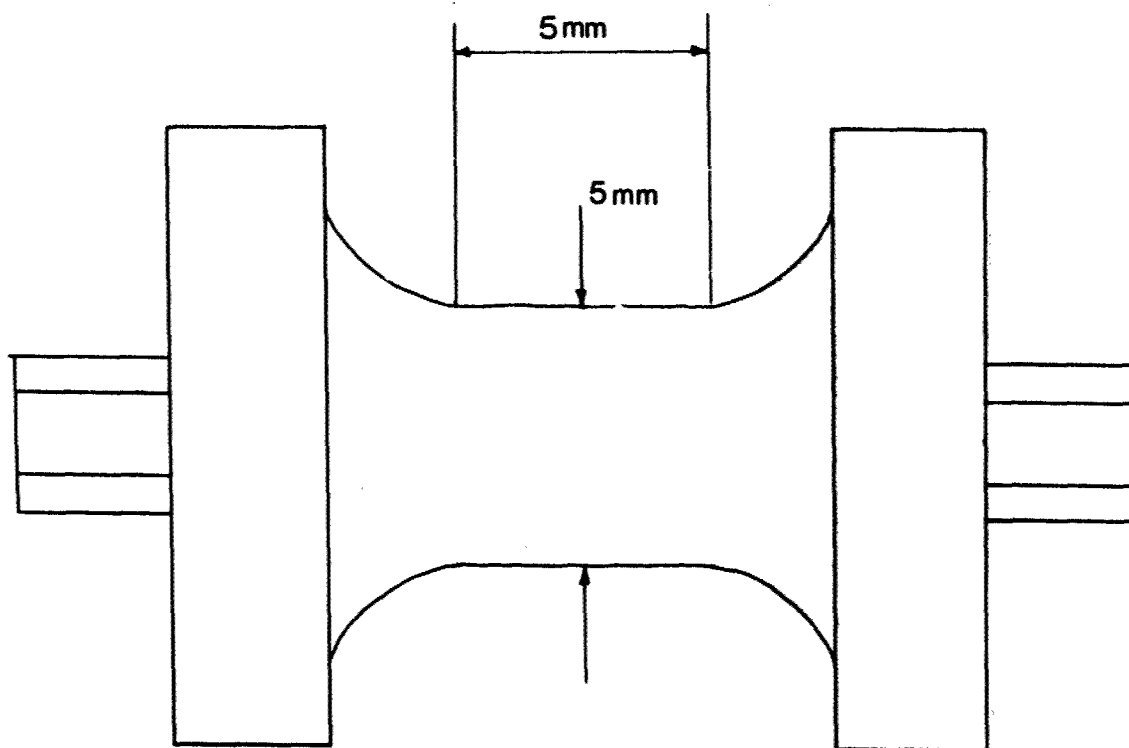


Fig. 2 Dimensions and shape of the prepared specimens

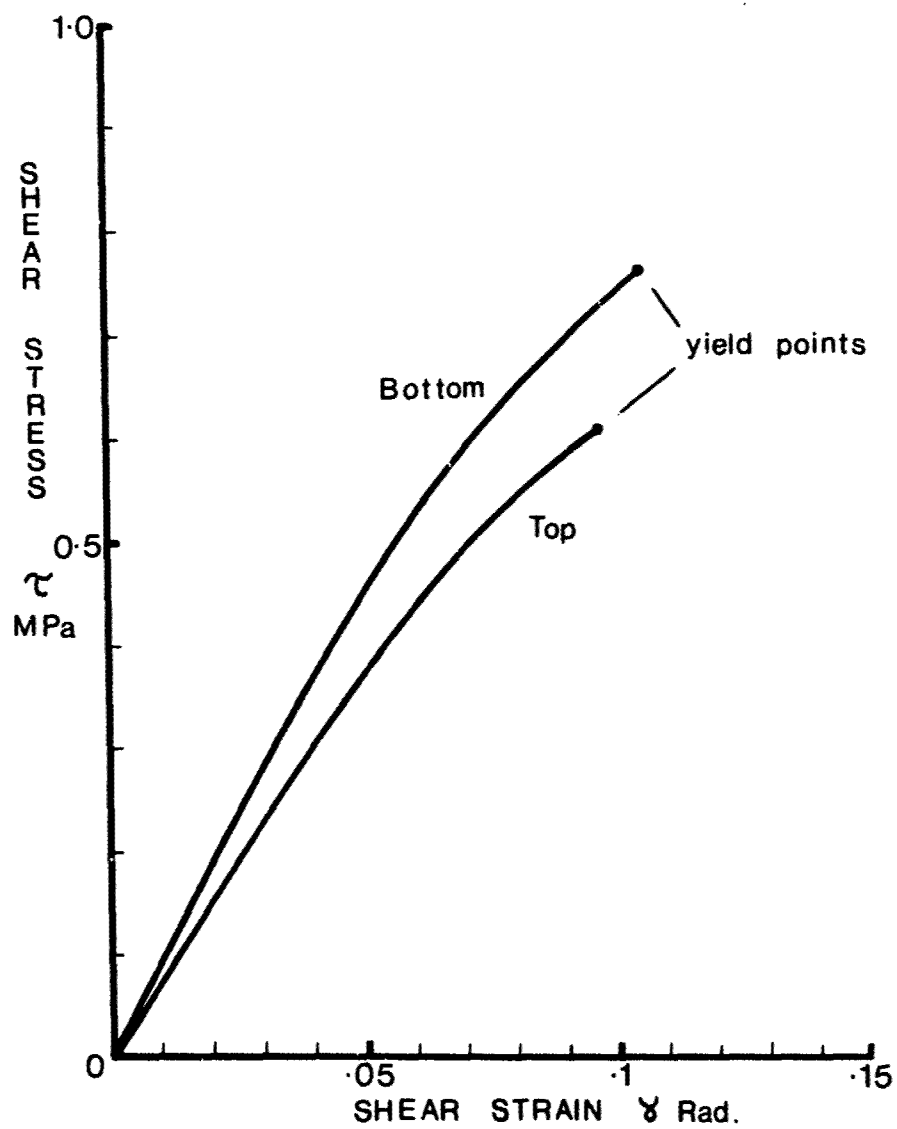


Fig. 3 Representative plot of the mean shear stresses at yield, showing the difference between specimens from the Top (superior) and Bottom (inferior) sections of the vertebrae.

TOP							
	Vertebra	Age	Sex	τ_y MPa	Range τ_y MPa	γ_y Rad	Shear Mod. MPa Rad ⁻¹
	L4	61	M	1.036	1.431 - 0.815	0.086	17.652
	L4	60	M	0.649	1.183 - 0.128	0.093	7.555
	L5	60	M	0.548	0.807 - 0.384	0.088	6.705
	L3	73	M	0.442	0.767 - 0.208	0.095	5.206
	L2	73	M	0.388	0.592 - 0.320	0.112	4.430
	L5	56	F	0.615	0.815 - 0.352	0.105	6.714
Overall means				0.613		0.097	8.077
BOTTOM							
	L4	61	M	1.633	2.654 - 1.095	0.084	27.935
	L4	60	M	0.769	1.023 - 0.512	0.150	6.143
	L5	60	M	0.747	1.071 - 0.512	0.117	8.736
	L1	68	F	0.914	1.374 - 0.400	0.080	12.555
	L4	56	F	0.555	0.711 - 0.400	0.108	5.643
	L2	56	F	0.328	0.448 - 0.232	0.093	4.366
	L3	56	F	0.386	0.496 - 0.232	0.105	4.172
	L4	42	F	0.783	1.191 - 0.520	0.101	9.545
Overall means				0.764		0.105	9.887

Table 1. Mean values of shear stress and strain at yield and shear modulus for individual vertebrae. Specimens from the superior (Top) and inferior (Bottom) portions of the vertebrae are tabulated separately.

INJURY MECHANISMS ANALYSIS IN AIRCRAFT ACCIDENTS

BY

SQN LDR I R HILL

ROYAL AIR FORCE INSTITUTE OF PATHOLOGY AND TROPICAL MEDICINE

HALTON, AYLESBURY BUCKINGHAMSHIRE, ENGLAND

SUMMARY

The type and severity of injury seen in aircraft accidents is influenced by many factors. Assessments of the ways in which injuries are produced must be broadly based, taking into account the various aspects of aircraft accidents. A simple analysis of 30 fatal aircraft accidents, some of which were survivable shows that the basic mechanisms of injury are common to many different accidents. This type of analysis facilitates the identification of problem areas quickly and accurately and should be of value to accident investigators and research workers. Survivable accidents and those in which the degree of injury in fatalities is only moderate, provide the richest sources of utilisable data.

INTRODUCTION

Accident-injury research is a relatively new science, encompassing many disciplines which has grown up out of the need to reduce death and injury from trauma. Aerospace pathology is an established branch of this study, having pioneered many of the techniques used.

Trauma is the fastest growing and most costly medical problem in the world today. Bull and London (1) estimated that in the United Kingdom 18,000 people died annually as a result of accidents, and that the number of Hospital admissions was increasing annually by 6%; double the rate for any other condition. In 1970 the total annual cost in the UK for accidents was £1000 million. By 1977 road traffic accidents alone cost £1289 million. The fact that trauma is predominantly the prerogative of the young and middle-aged makes attempts to reduce its effects all the more important.

Because aircraft accidents are complex events and their effects are dramatic, their investigation demands the use of an integrated team of experts from a wide variety of disciplines. Hitherto the bias of the medical investigation has depended upon the particular needs and interests of those involved. Thus in the past considerable attention has been paid to safety equipment in the United Kingdom, whereas in Canada a more pathophysiological approach was used. Presently there is a growing awareness amongst many investigators, that a more fundamentally biodynamic approach should be used. Only in this way can useful recommendations be made. The production of injuries must be seen in the light of the whole crash sequence, and the results of laboratory investigations considered before reaching conclusions.

This paper presents a review of some of the present knowledge on injury production and discusses these principles in the light of a numerical analysis of a number of accidents investigated by this department. Thus it is hoped that the value of this type of approach will be realised.

METHODS

In an attempt to identify the principle mechanisms of injury, and to isolate potentially hazardous features, a mathematical analysis was performed on thirty randomly selected fatal aircraft accidents. Each of the accidents had been investigated previously by a member of the Department of Aviation Pathology at RAF Halton. The aircraft types ranged from a Hang-Glider to a commercial airliner, thus representing most types of flying, though most of them were light aircraft. This bias would be expected because this type of operation provides the bulk of the department's workload. The accidents were divided into two groups, either survivable or non-survivable. A survivable accident being defined as one in which there were survivors and or, the degree of destruction of the airframe was so slight as to permit survival. In each case the individual investigators assessment of survivability was accepted.

The autopsy reports of fatalities and the description of the injuries sustained by survivors were then examined in detail. Points were then awarded according to the schedule in Table 1, for injuries sustained in 44 bodily regions (Table 2). Only the most severe injury in each area was scored, thus a compound fracture of the femur would be scored, but grazes in the thigh would be ignored. The total score for each victim of every accident was then totalled. This injury score was then compared with

the degree of airframe destruction and the victims placed into three groups according to the overall extent of their injuries.

The results so obtained are discussed in relation to the known principles of crash dynamics and biodynamics and recommendations are made for the analysis of the data accumulated from future accidents, so that it will be of maximum use to research workers and aircraft designers.

<u>Points</u>	<u>Degree of Injury</u>
0	Nil
1	Mild
2	Moderate
3	Severe
4	Fatal

Table 1 - Injury Severity Coding

1. General external examination.
2. Limbs - each long bone rated separately.
3. Thoracic skeleton.
4. Thoracic viscera rated separately.
5. Abdominal viscera rated separately.
6. Head and contents rated separately.
7. Pelvis and each area of spine rated separately.

Table 2 - Areas Scored

RESULTS

The results of the mathematical analysis of injury severity are contained within Tables 3 - 8.

Number of accidents studied	30
Number of survivable accidents	12
Number of non-survivable accidents	18
Total number of casualties	30
Total number of fatalities	101
Number fatalities in survivable accidents	20

Table 3 - Breakdown of the material studied

<u>Points Awarded</u>	<u>Number of Casualties</u>
1	7
2	10
3	5
4	6
5	1
6	-
7	-
8	-
9	-
10	-
11	1

Table 4 - The severity of injury sustained by survivors

<u>Points Awarded</u>	<u>Number of Casualties</u>
0-9	1
10-19	7
20-29	10
30-39	9
40-49	8
50-59	8
60-69	8
70-79	9
80-89	16
90-99	3
100-109	5
110-119	1
120-129	6
130-139	1
140-149	3
150-159	4
160-169	-
170-179	2

Table 5 - The severity of injury sustained by fatalities

<u>Score</u>	<u>Cause of Death</u>
8	Drowning
15	Head Injury
15	Head Injury
16	Head Injury
17	Concussion - Drowning
17	Head Injury
19	Head Injury
19	Head Injury
20	Head Injury
22	Head Injury
22	Concussion - Drowning
25	Asphyxia
22	Asphyxia
28	Concussion - Drowning
28	Multiple Injuries
30	Head Injury
31	Respiratory failure - Head injury
37	Head Injury
50	Head Injury - Burning
84	Head Injury

Table 6 - Injury severity score and cause of death
in the fatalities occurring in survivable
accidents

<u>Degree of Injury</u>	<u>Range of Points</u>	<u>Number of Victims</u>	<u>Total Score</u>	<u>Average Score</u>
Mild	1-11	31	90	2.9
Moderate	12-54	39	1305	33.5
Massive	55+	61	5869	96.2

Table 7 - Degree of injury and average scores in each group

1. Ejection.
2. Compression by Airframe.
3. Penetrating Injuries.
4. Inadequate restraint including seat failure.
5. Incorrect usage of restraint.
6. Poor design features - (fuel tanks.
(fascia.
7. Inadequate escape mechanisms.

Table 8 - Principle causes of injuries

DISCUSSION

It is readily apparent from a study of the literature, that the correlation between individual research projects on the biomechanics of impact and actual crash studies, that there are grave difficulties in relating the one with the other. In some instances comparisons between the results of different institutions, carrying out research into the same projects is not possible (2). Because of this and because of complaints that the quality of clinicopathological information made available to research workers is often inadequate (3), I have reviewed some of the basic principles on the mechanism of injury production in aircraft accidents. Theoretically the observations made in any kind of transport accident should be readily transferable. If we consider the pattern of injuries seen in road traffic accidents (4) and compare these with the predominant sites of injury in aircraft accidents, then it can be seen that they are similar. This is not a surprising observation, because the body has only a limited range of response to trauma, thus a fractured femur sustained in a road traffic accident is the same as one seen in the victims of air crashes.

Injury to the human body is a response to the release of energy resulting from a reaction between the tissues and various physico-chemical agents. Thus either a morphologically apparent wound, a pathophysiological imbalance or both is produced. The degree of response and the subsequent outcome will depend upon a wide variety of factors, (5, 6, 7, 8, 9, 10). The human body is a complex range of heterogenous tissues in the solid, liquid and gaseous phases. They each manifest varying degrees of elasticity, viscosity and plasticity, as well as reacting non-isotropically. They are arranged upon a skeleton which acts like a damped system of levers and links. Because the body can, and does, act as an open kinetic system, in which the joints have a wide range of movement, injuries may be produced at sites distant from the point of impact. Each joint acts as a fulcrum so that forces may accumulate along the shafts of long bones, and where these aggregates exceed the local stress tolerance, they produce injuries. This usually occurs at points of weakness such as the insertion of tendons and ligaments or around congenital defects. In these circumstances they are all acting as stress raisers, and forming a focus for the accumulation of force.

Though fire and toxic fumes may be potent causes of death in aircraft accidents, we are primarily concerned with mechanical forces. The manner in which these are generated in aircraft accidents has and is being studied extensively, (11, 12). From a study of these reports, and the proceedings of conferences such as Stapp and IRCOBI, it is possible to conclude that the most important features are:

1. The velocity of the aircraft.
2. The angle of strike.
3. The nature of the surface struck.
4. The structural characteristics of the aircraft.
5. The site at which the forces are measured.

It is obvious that velocity is fundamental to the outcome of an accident. High velocity impacts are associated with massive injury, including total disintegration of the airframe and its occupants, such as was seen in the THY DC 10 accident. Though it is possible to design structures capable of withstanding intense physical forces, their ability to fly would be questionable. Consequently design is aimed at the minimum injury level, which is alleged to be an adequate compromise. Though accurate assessments of impact speed are not available, the general impression gained from this and other studies of aircraft accidents is, that it is the middle range of speeds, from about 50 to 150 Kts, where the picture is far from clear. One of the problems is that we are not dealing with a simple single deceleration in every accident. Thus in one of the survivable accidents reviewed the speed prior to impact was calculated to be 95 Kts. The only force produced was along the longitudinal axis of the aircraft, the impact angle being less than 3 degrees, increasing this angle produces a linear magnification of the horizontal forces until such time as the airframe begins to crush. This is a particularly important observation because in most accidents there is a significant angle of impact. This was seen in this series, and studies conducted by NASA suggest that the 40° stall: spin incident is particularly common in light aircraft crashes.

Perhaps the most important attenuating features in these circumstances are the configuration and strength of the airframe. Pressurised hulls are stronger than unpressurised versions, because they have to withstand the pressure differential. The presence of engine nacelles and fuel tanks on wings may produce high crash forces, which can tear the cabin apart if they are mounted high up on the fuselage. Low-mounted wings of similar design can plough into the earth producing slewing, giving rise to sharp deceleration peaks which may increase the load applied to individual victims by as much as two thirds. Moving the wings towards the tail produces a long "nose" section which can buckle and fold over on itself.

Thus the number, magnitude, direction and the qualities of the decelerative forces applied during an aircraft accident are highly variable. They must be considered in the analysis of injuries if the results are to mean anything. By applying our knowledge about these factors, it is possible to show that the most likely sources of impact injury in aircraft accidents are:

1. Being crushed within a collapsing airframe.
2. The absence or failure of restraint.
3. Entrapment within the wreckage.
4. Injuries associated with escape.
5. Being struck by loose objects.
6. Explosive decompression.

The crushing of victims within a collapsing airframe is typically a feature of high velocity impacts. Characteristically the injuries are severe, ranging from total fragmentation to extensive soft tissue and skeletal damage. A high proportion of limb amputations is seen and the whole body looks as though it has been crushed. Perineal splitting, with or without herniation of viscera and wide fracture dislocations of the sacro-iliac joints is synonymous with vertical deceleration.

Entrapment within the wreckage is a rather different problem, with potentially equally serious sequelae (13) being responsible for many deaths in otherwise survivable situations. The victims are trapped either because the exits are jammed due to distortion, or lack of maintenance, or they sustain injuries which render them immobile. In two accidents, not analysed in this study, which were investigated by this department, these features were well documented. Both were accompanied by fire, which was the immediate cause of death of many of those who were killed. In the first case the seats concerted and a bar at the bottom of the seat caused fractures of the tibiae and fibulae in many of the victims, thus they were unable to get to the emergency exits, many of which were unused. In the second incident only 5 people died out of a total of 127. They were all trapped by fire near an inoperable exit. Thirty-eight people sustained minor injuries as a result of falls during egress.

Injuries associated with restraint systems have been the subject of considerable debate, some of which has been as ill-informed as it was ill-advised. Antagonists frequently attribute injuries to the safety belt without any acknowledgement of the fact that without them the extent and severity of damage would have been greatly increased. Restraint systems may be adequate or inadequate. Snyder(13) reports an author who suggests that we have 40G people sitting in 20G passenger aircraft riding on 9G seats. Restraint may fail at the following sites:

1. The belt itself.
2. Its attachments.
3. The seat mounting.
4. A combination of the above.

Failure occurs either because the forces involved are excessive, the materials and design are defective or the tolerance limits are inadequate. Failure to wear a safety belt cannot rightly be concluded to be an

example of failure, but the effects are the same, for lower impact forces. Cesari and Ramet (14) reviewed some of the literature and studied the effects of this problem in road traffic accidents. They found that the risk of dying after being ejected from a car was six times greater than if the victims stayed within the vehicle. In addition it is generally accepted that the risk of severe injury is greater in unbelted than in belted victims.

Behrens et al (15), found that malfunction of seat belts in cars produced a distinct pattern of injury. The most seriously affected regions in descending order of severity were the head, thorax and pelvis/abdomen. Typically they found ruptures of the thoracic and abdominal viscera. They also showed that the overall severity of injury increased with the degree of vehicle deformation, and incorrect usage of the seat belt. Nielsen et al (16) showed that when the angle of impact in road traffic accidents exceeds 40°, then the shoulder component of lap and diagonal belts slips out. Up to this point such a restraint system reduces the imparted impact forces by 20 to 30%. If the seat is stiff then chest, lower abdominal and gluteal lesions predominate, whereas soft seating is associated with higher incidences of back, knee and head injuries.

The patterns of injuries associated with failure or inadequacy of restraint are essentially the same. Individual injuries are severe, penetrating lesions are common and there is often diaphragm rupture. Multiple injuries are found in nearly every case. There are usually a number of impacts and trace marks may be found on the body, in the wreckage and on the ground.

The foregoing discussion outlines the principle sources of injury in aircraft accidents. Explosive decompression and ejection are rather special problems, and the latter has been the subject of many reviews. Explosive decompression is well tolerated by man, therefore it is rarely fatal by itself. The classical sign is rupture of the eardrum without fracture of the base of the skull.

The actual method of injury in various organs has been widely reviewed by Gurdjian et al (17) and more latterly by Rotondo (18). The essential problem which we have to solve is how are we to assess the mechanisms? To do it effectively requires a painstaking systematic approach to every detail of each accident. The following features of each injury must be fully noted:

1. The type of injury.
2. Its location.
3. Its general appearance.
4. Its extent.
5. Its direction.
6. Its severity.

It is the last of these criteria which can provide perhaps the greatest single clue to the aetiology in this situation.

After an accident the only direct evidence of its severity is the degree of damage to the aircraft and its occupants. Any method chosen to analyse these features should be simple to use and universally applicable. Data thus accumulated should be of considerable value to research workers in constructing experimental models, and it should include clinical as well as pathological information if the full value is to be realised.

A variety of methods of assessing vehicle deformation have been suggested. The first of the systems was designed by the Cornell Aeronautical Laboratory in 1964. Subsequently various refinements were produced, but the basic system remains the same, and this is really the comparison of photographs of wreckage against a series of "standardised accidents". McKay (19) and Ashton et al (20) amongst many others have reviewed their usage. Lynch (21) discussed the use of the Calpan measurement system in aircraft accidents. Thus far none of the schemes have found routine use in the investigation of aircraft accidents. This is perhaps a little shortsighted, though the accusation that one would expect injuries to be more severe in badly crushed vehicles is impossible to refute, nor would it be desirable to do so. However, it is in those grey areas exemplified in the accidents analysed above, when people die in survivable accidents, that such studies may reveal hazards.

The analysis of injury severity has probably been practised throughout the history of medicine, but it was not until comparatively recently that workers tried numerical assessments. De Haven and his colleagues produced the first research orientated scale, later modifications of which are available (22). Like nearly every other system it has serious shortcomings. The comparison of multiple injuries and their quantification is hard, this is because there is some variation in the numerical values assigned to different injuries.

Towards the end of 1968 a Committee was set up by the American Medical Association to review this problem. In 1971 and 1972 they published a system based on one first used by the General Motors Corporation. It is extremely complicated and difficult to use, but it has nevertheless found quite wide acceptance by road traffic accident workers. It incorporates assessments of prognosis, energy dissipation and other factors such as possible disability. Its subjectivity is readily admitted and its

shortcomings in the assessment of fatality are only too obvious. Probably the most serious problems are associated with the overall assessment of injury which uses the highest scores in the worst affected areas. Thus if a victim had a fractured pelvis and a fractured femur only the former would count. Baker (23) has published an interesting review of the system and a variety of other workers have applied complex statistical analysis to assess prognosis using this method.

It is obvious from this brief survey of the available systems that none of them are ideal. Thus the system used is proposed. Its advantages are:

1. It is easy to use.
2. No complex reference manual is needed.
3. It can be used to study individual regions or the whole body.
4. It is not time consuming.
5. It is comprehensible.

One of the real benefits of numerical analysis of injuries is that it easily highlights those accidents in which there may be some remediable problem. Thus in crashes where the crash forces are catastrophically high and massive injuries ensue, the provision of even better safety equipment would be valueless for survival, additionally improvement in aircraft crash-worthiness would not help the victims. However, where moderate injury is concerned this is a different matter.

In this series of accidents- quite by chance- the principle primary cause of injury was restraint failure. In the pilots who were injured they either flexed forwards over a lap belt, had shoulder straps loosely fastened or had made unauthorised modifications to the seat. In one instance a small pilot had put a loose cushion behind his back, which slipped out at impact. Break up of the floor and on the attachments of the seat to the cabin floor accentuated the injuries. In one instance amongst some of the passengers inadequate seat mountings were the sole cause of the injuries sustained. Thus despite previous exhortations by this organisation and many research workers restraint is still poor.

Pathologically the most interesting group of victims are those who died in survivable accidents, only 1 died of multiple injuries. In this instance the victim was in the most deformed part of the aircraft. The presence of a high proportion of fatal head injuries is of considerable concern. The proximity of the fascia and seats to one another means that there is little if any chance of occupants not hitting one or the other at impact. The surprising finding here was the almost total absence of serious neck injury, which would normally be expected as the head was arrested and the remainder of the body went forward. It must therefore be assumed that the trunk was stopped at the same time by hitting either seat backs or other parts of the aircraft, thus accounting for the thoracic injuries. Injuries to limbs were not on the whole severe, they can be accounted for by compression against failing seats and by limited flailing. Of the 4 people who drowned, 3 had concussion and one was unable to free himself from his hang glider because he was not equipped to do so.

It can also be shown that occupants who are flung clear of the aircraft are more likely to suffer serious injury; particularly to the head, than those who are retained in their seats. Finally children tend to do better than adults. In the one accident where there were a significant number of children their overall score was 55 as against 87 for the adults. This is probably because they are more relaxed, and certainly as the age of the children approached puberty they began to behave more like adults in their response to trauma. Relaxation has been advanced as a working hypothesis to account for this phenomenon here, just as it is said to account for the survivals in high free falls seen in some grossly intoxicated persons.

CONCLUSIONS

This is a lengthy summary of basic principles in injury causation as applied to aircraft accidents, illustrated by reference to 30 crashes investigated by us, of which 12 were survivable. To analyse injury mechanisms successfully the following protocol should be followed:

1. An analysis of the crash dynamics.
2. An estimation of vehicle deformation.
3. A full description of each injury.
4. An assessment of injury severity.

From the study outlined above the following conclusions can be made:

1. Serious or fatal head injury is the single most serious problem in aircraft accidents, particularly in light aircraft.
2. There is a wide margin in injury severity between survivors and fatalities.
3. Restraint systems are still inadequate, especially for passengers.

4. The severity of injury is increased by:
 - a. "Ejection" from the aircraft.
 - b. Severe damage to the airframe.
 - c. Poor design features such as badly sited fuel tanks.
5. The principle method of serious injury is forward flexion over a lap belt.
6. Mathematical scoring of injuries makes more accurate analysis of accidents a feasible proposition.

REFERENCES

1. Bull J. P. and London P. S. (1970)
In Modern Trends In Accident Surgery and Medicine (Ed by London) - 2. 1 - 10
Butterworths - London
2. Wanderer U. , Bloedorn A. , Appel H. (1977)
Results of West European Accident Investigation Programmes
Proceedings of the Third International Conference on Impact Trauma
1 - 18
3. Hirsch A. (1977)
Personal Communication
4. Gogler E. (1965)
Road Accidents - Documenta Geigy - Series Chirurgica - Geigy Manchester
5. Gillies J. A. (1965)
A Textbook of Aviation Physiology. Pergamon - Oxford
6. Stapp J. P. (1971)
Biodynamics of Impact
Agard Graph CP - 88 Linear Accelerations
7. Krefft S. (1971)
Aircraft Accident Injuries and Aircraft Accident Reconstruction.
Agard Graph CP - 88 Linear Acceleration
8. Snyder R. G. (1970)
Man's Survivability of Extreme Forces In Free-Fall Impact
Agard Graph CP - 88 Linear Acceleration
9. King W. F. and Mertz H. J. (1971)
Human Impact Response - Plenum - New York
10. Gurdjian E. S. (1975)
Impact Head Injury. Charles C. Thomas, Springfield USA
11. Preston G. M. and Moser J. C. (1956)
"Crash Loads". In Conference on Airplane Crash Impact Loads. National Advisory Committee
for Aeronautics, Washington DC.
12. Snyder R. G. (1975)
Crashworthiness Investigation of General Aviation Accidents
Society of Automotive Engineers (750537)
13. Snyder R. G. (1976)
Advanced Techniques in Crash Impact Protection and Emergency Egress from Air Transport
Aircraft
Agard Ag - 221
14. Cesari D. and Ramet M. (1977)
Study of In Field Roll Over Accidents and Comparison with Roll Over Crash Tests. Proceedings
of the Third International Conference on Impact Trauma 19 - 28
15. Behrens S. , Suren E. G. , Gotzen L. and Stuert G. (1977)
Injury Patterns Caused by Seat Belts
Proceedings of the Third International Conference on Impact Trauma 80 - 92

16. Nielsen H. V. , Weeth R. and Eriksen (1977)
Lesions in Belted Car Riders from Oblique and Lateral Impacts
Proceedings of the Third International Conference on Impact Trauma
17. Gurdjian E. S. , Lange W. A. , Patrick L. A. and Thomas I. M. (1970)
Impact Injury and Crash Protection. Charles C. Thomas, Springfield, USA
18. Rotondo G. (1976)
Midico-Legal Problems of Flight Accidents Investigation. Agard CP-190
Recent Experience/Advances in Aviation Pathology
19. McKay G. M. (1970)
A Vehicle Deformation Index
Accident Investigation Workshop - NATO Brussels
20. Ashton S. J. , Hardy J. L. G. , and McKay G. M. (1973)
The Use of the Vehicle Deformation Index and Collision Speed Assessments
Proceedings International Accident Workshop. NATO - Brussels
P 85 - 102
21. Lynch J. P.
Application of the Calspan Scene Measurement System to the Investigation of Aircraft Accidents
Aviation Space and Environmental Medicine
46 - 1257 - 1259
22. Mason J. K. , Reals W. J. (1973)
Aerospace Pathology
College of American Pathologists Foundation - Chicago USA
23. Baker S. P. , O'Neill B. , Hasson W. , and Long W. B. (1974)
The Injury Severity Score. Jnl Trauma. 14, 3, 187 - 196

DISCUSSION

DR. H. VON GIERKE (USA)

Are you familiar with proposals for standardization of accident analysis and autopsy protocols which are studied by the US Department of Transportation and are proposed by various committees?

AUTHOR'S REPLY

I've seen some of the information which has been published on this and certainly some of it would seem to be applicable to the aircraft accident situation. I am not too sure how far they intend to take these various proposals because they are quite lengthy. The only ones I've seen required something like 20-30 pages of information to be filled in. Some of this information didn't seem to be entirely relevant.

DR. H. VON GIERKE (USA)

Relevant to the aircraft situation?

AUTHOR'S REPLY

Yes.

DR. H. VON GIERKE (USA)

Certainly the procedure would have to be adapted to the air accident situation. It is so far only developed for the surface transportation accidents. But do you feel that for the aircraft accident investigation a similar procedure should be developed and perhaps internationally agreed upon among the AGARD countries?

AUTHOR'S REPLY

Certainly the American, Canadian and British organizations have a more or less standard way of going about these investigations. But we don't include all this material that I was discussing today.

THE VALIDATION OF BIODYNAMIC MODELS

Leon E. Kazarian
 Henning E. von Gierke
 Biodynamics and Bioengineering Division
 Aerospace Medical Research Laboratory
 Wright-Patterson Air Force Base, Dayton Ohio 45433

To predict human dynamic response and injury in mechanical force environments, assessments and extrapolations are usually based on mathematical biodynamic models developed from anatomical geometry and tissue properties and validated by accident data and subinjury human dynamics. The shortcoming of this approach is the scarcity and frequent inaccessibility of human tissue properties and strength data, the limited, hard-to-interpret accident data and frequently undefined injury mechanisms. To overcome these problems, various animal species have been used as human surrogates: tissue properties as well as injury mechanisms are more easily studied in controlled tests. Unfortunately, the differences in anatomy and tissue properties make direct use and quantitative interpretation of the animal data of doubtful value. The solution appears to be in the establishment and detailed quantitative experimental validation of mathematical animal models which then in turn can be used to assist in the validation of the human models into the injury range, and to provide confidence into the procedures used.

Three-dimensional discrete element dynamic models of the axial skeletal system have recently been developed for man, the chimpanzee, baboon and rhesus monkey. This paper describes the anatomical differences which formed the basis for the different models and analyzes the hard and soft tissue components constituting the deformable elements of the systems. Best available estimates are presented for the dynamic and strength properties of some elements; for other elements more exact data from recent refined measurements on human as well as animal components are discussed. Various approaches and suggestions for compilation of biodynamic response data are included. Gaps in present day knowledge are identified, which must be filled to make these sophisticated theoretical biodynamic models of maximum quantitative usefulness in injury explanation, prediction and prevention.

INTRODUCTION

Human injury tolerance data are necessary to formulate injury assessment criteria to evaluate a measured or predicted impact or acceleration time history in terms of its injury producing potential. An example is that of an aircrewman required to eject from a disabled aircraft using an ejection seat. The ejection seat imparts a mechanical force, the effect of which is dependent upon both amplitude and duration of exposure. Injury assessment of such mechanical impacts to the human system find application in guidelines for the design and development of ejection seats.

Over the past three decades, biodynamicists have been called upon to state in quantitative terms how a given forcing function will effect various elements of the human musculoskeletal system. This problem requires a thorough understanding of the static and dynamic strength properties of biological tissues, organs and body segments along with a mathematical insight into the mechanisms underlying energy transmission and attenuation, response characteristics and modes of failures. The most obvious realization of this requirement is an appropriate mathematical model. Numerous theoretical models have been created to specifically ascertain the variation of risks as well as the likelihood of spinal trauma to high transient, caudocephalad accelerations. Most of these modeling efforts are far ahead of the detailed quantitative, dynamic and strength measurements required to make the models useful. Few if any of these models have been quantitatively validated to give satisfactory confidence into their validity or ranges of their applicability. Human injury data and subinjury laboratory response data allow only limited testing of the models validity. To assist the validation of human models into the injury range animal models based on equivalent assumptions to the human model have been developed and their quantitative validation through well-planned and instrumented experiments appear easier achievable.

This paper is concerned with the biological data required for developing and validating an axial musculoskeletal computer model of subhuman primates that in turn can be used to support the validation of a human response model and assist in predicting human tolerance. Comparisons will be made between the various validation approaches. The shortcomings and advantages of the various types of biodynamic data presently collected and available are delineated. Comparative whole body primate spinal impact tolerance curves are presented. Some physical constants for subhuman primate tissue are given, and areas where additional data are required to validate a subhuman primate model are identified.

DATA BASE ON HUMAN BIODYNAMIC RESPONSE

Human Tolerance - In biodynamic research five basic techniques are used to assist in defining human tolerance: (1) controlled tests using human volunteers at subinjury exposure levels, (2) human cadaver research, involving whole body, regional anatomy and component strength analysis, (3) operational/clinical accident and injury observations, (4) live animal investigations to extend experimental results up to and beyond injury threshold exposure levels, (5) animal cadavers, involving specific biomechanical tests on regional anatomy, and various hard and soft tissue elements. Each of these methods contributes to our overall knowledge of biodynamics although each presents problems and imperfections of itself. None of these approaches is comprehensive and even together they do not provide real world preciseness. Nevertheless, the discrete use of these techniques in concert, provides the best available means of addressing human tolerance criteria. Reviews of human impact tolerance have been published by Snyder (1970) and Eiband (1959).

If biodynamic models are being used to explain or predict human biodynamic response, tolerance limits

or injury probability the same techniques and types of data must be used to validate the model, i.e., to establish its validity and accuracy. The following brief description and comparison of the different types of data concentrates primarily on the contribution of animal data to the solution of the overall problem.

Human Volunteers - Most laboratory investigations using human volunteers are conducted under optimal conditions, under the control of the subject and a medical monitor. The restraint system is ideally situated and/or tightened in contrast to most operational situations and prior to impact exposure the test subject is optimally positioned. Subjects are initiated and conditioned at low force levels. The force values are gradually increased in successive experiments to a level where the volunteer becomes either apprehensive of the environment, experiences discomfort or pain and at will, terminates the experiment.

The precise methods for extrapolating voluntary exposure values to injury levels are uncertain. Often times there is no relationship between pain at the limit of voluntary exposure, and the trauma to be expected at the higher acceleration exposure levels. As a result, a precise method for establishing a quantitative relationship between voluntary exposure levels and injury levels of various degrees is nonexistent. Tolerance envelopes developed from these conditions may not be representative of the general aircrew population - or even of the subjects tested when impacted under different environmental conditions. It may be assumed that the voluntary subinjury tolerance levels provide a conservative value indicating a lower threshold limit for the population at risk. Human volunteer impact investigations have been conducted by Ewing (1978), Stapp (1961, 1970), and others.

In addition to human volunteer impact tests, data on the steady state vibration response of human subjects in various positions and with various restraints are useful for model validation purposes. The large body of data on human driving point impedance and transmissibility must be matched by a realistic model.

Human Cadaveric Research - Human cadavers have been experimentally utilized in very few whole body impact experiments. The cadaver has both advantages and limitations. Morphologically, the cadaver is an identical model to the "live subject." Using the cadaver, musculoskeletal injury levels, the mechanisms and severity of trauma may be comparatively assessed for a variety of acceleration time histories. Energy transmission and attenuation pathways as a function of torso position may in general, be qualitatively identified. However, since the cadaver is no longer a functioning biological system, injury to soft tissue, hollow and parenchymatous organs can only be inferred. Muscle tonus no longer exists, and as a result, energy transmission and attenuation pathways, both in hard and soft tissues, cannot be precisely defined. The skeletal system is, in general, least affected by the "live" versus cadaver change in system properties. The interpretation of such tests involves considerable analysis of and insight into the processes and pathways throughout the musculoskeletal system. Human whole body impact experiments have been conducted by King (1965), Prasad (1974), Tennyson (1977) and others.

A comparatively large and growing number of investigations have been conducted dealing with the tissue strength properties of the human spinal column, e.g., the intervertebral joint (Lin, Liu and Ray, 1978; Galante, 1967; Kazarian, 1975; Kulak, 1976; Markolf, 1972; Nachemson, 1960; Brown, Hansen, Yorra, 1957; Hirsch, 1957), the vertebral body (Furst, 1940; Hartman, 1974; Hakim and King, 1977; Kazarian and Graves, 1977; Messerer, 1880; Ruff, 1950; Yamada, 1970), the ribs, rib cage and sternum (Andriacchi, 1974; Agostoni, et al, 1966; Schultz, 1974 a and b).

In Figure (1) the ultimate breaking strength for isolated human vertebral bodies is summarized based upon the experimental data reported by Messerer (1880), Gazulov (1966), Yamada (1970), and Kazarian (to be published). The data clearly show an increase in vertebral body strength between T₁ and L₅. The strain rate sensitivity of the vertebral body to axial compressive load is clearly shown in the studies of Kazarian. There are two different strain rates: 8.89×10^{-1} meters/second and 8.89×10^{-5} meters/second.

Operational Accident Analysis - Accident investigations are primarily conducted for the detection of malfunctions, statistical analysis and aircraft/ejection seat systems improvements rather than injury analysis and human threshold tolerance values. Individual accident reports usually contain some description of the musculoskeletal trauma sustained. However, for the most part, accident reports fail to identify the precise nature, degree of severity, sequence and mechanics of trauma, mechanisms of cumulative pathology of exposure to the impact environment. The operational injury data collected can rarely be correlated quantitatively to the environment. Therefore, accident reports are of only limited values, although recent efforts to establish large scale injury banks (such as that for the automotive crash field) might provide more meaningful injury analysis possibilities.

DATA BASE ON ANIMAL RESPONSE

Experimental Animals - To date, much of our knowledge of the injury mechanics, and of the acute and chronic effects of various degrees of injury has been derived from animal experimentation. Subhuman primates provide a good functional model which may closely simulate the response characteristics of man. This review limits itself to data on subhuman primates.

Data regarding static and dynamic range of motion, kinetic response to various force inputs with various support and restraint systems can be collected by subjecting primates to subinjury tests throughout the range of interest. However, the use of animals for identifying injury threshold levels also present problems. A major problem involves extrapolation of animal data to the human case. There exist many morphologic similarities and differences between primates. Examples of such differences include the vertebral column formula, segmental inertial properties, kinesiological aspects, muscle/bone mass, muscle origin, insertion and innervation, all of which are not directly comparable to man. The anesthesia usually used in animal experiments is another factor modifying animal response compared to the real world event. On the other hand, much knowledge can be learned from primate studies which include, injury threshold, the mechanics and sequence of injuries, time course degenerative diseases, and the role of mechanical instability on future impact situations.

Whole Body Animal Tests - A number of uniaxial longitudinal spinal investigations have been conducted using the squirrel monkey, rhesus monkey, baboon and chimpanzee. The objective of these tests was to identify spinal injury potential based upon a rectangular deceleration time history. In addition, the level, frequency, severity and type of vertebral body trauma was radiographically documented, then compared to necropsy findings. Stable anterior wedge compression fractures at the level of the transregional articular facet joint was the primary injury mode. It has been found that the restraint system may markedly influence the level and severity of trauma.

Based upon whole body animal investigations, the 50% probability of spinal injury curves shown in Figure (2) were generated. This figure compares the acceleration resulting in 50% probability of spinal injury versus time for a rectangular deceleration time history for the squirrel monkey, rhesus monkey, baboon, chimpanzee and man. The radiographic criteria for spinal trauma on this curve is set at 10% loss in vertebral body height, (Kazarian, 1970). Some data on rhesus monkey driving point impedance and transmissibility are available, but more complete data on baboons and chimpanzees are highly desirable (Slonim and Kazarian, to be published).

ANIMAL CADAVERIC RESPONSE

Animal Component Tests - The primary component characteristics required once a geometric morphological model of a species has been derived are the elastic and damping properties of the material and its strength characteristics. Restricting ourselves again to the primate models, new data in this area became recently available.

Uniaxial compression tests have been conducted on vertebral centra excised from the rhesus monkey, baboon and man. Figure (3) is a composite load plot of vertebral centra at two different strain rates. The slow strain rate is 8.89×10^{-5} meters/second. The fast strain rate is 8.89×10^{-1} meters/second. The data clearly show that vertebral body strength is related to spinal position. The vertebral bodies in the thoracic spine are weaker than those of the lumbar spine. The strength of a vertebral body increases as strain rate increases. (An unexpected finding is the relationship of baboon vertebral body breaking strength to that of the rhesus monkey and man at high and low strain rates.) For the case of slow compressive loading, the vertebral centrum of the baboon is stronger than that of man. Its strength coincides more closely with the rhesus monkey at high loading rates. In comparison, at the high loading rates, mans vertebral body strength exceeds that of the baboon (Kazarian, to be published).

Stiffness - Figure (4) identifies the value of stiffness for the rhesus monkey, baboon and man. The correlation of stiffness with displacement rate is not as great in the baboon and rhesus monkey as it is in man. The stiffness values for baboons tend to be less than that of man, but significantly greater than those of the rhesus monkey.

Ultimate Load - Figure (5) compares the isolated vertebral body strength of the rhesus monkey, baboon, and man for three different strain rates. Comparative values and relationship of ultimate load to displacement rate and vertebral body position are shown. This figure clearly illustrates that ultimate load values are significantly higher in the baboon. The values of the rhesus monkey and human breaking strength are somewhat lower and similar to each other. The rate of change of load as a function of displacement rate is also greater in the baboon than in humans (which in turn, is greater than that of the rhesus monkey).

Deformation to Ultimate Load - The comparative values of deformation to ultimate load are shown in Figure (6). In man, the values of deformation to ultimate load are significantly influenced by displacement rate but not by position. The deformations from position groupings one and two are not significantly different, but those of the two other positions (three and four) were found to be significantly higher. The baboon clearly exhibited larger deformations to ultimate load than does the rhesus monkey, and the rhesus monkey in turn exhibited larger deformations than the tests on the human vertebra.

Energy to Ultimate Load - Figure (7) is a plot of the energy to ultimate load versus position and strain rate. The energy to ultimate load for the rhesus monkey and man both exhibited a significant correlation with displacement rate. The overall correlation is significantly greater for human vertebra than for the baboon, which is somewhat equivalent to that of the rhesus monkey. Significantly higher energy to ultimate load values were obtained from the baboon vertebra than from either the rhesus monkey or the human vertebral centra.

COMPARISON OF HEAD-SPINE MODELS OF PRIMATES

The Human Head-Spine Model - Static and dynamic models of the human axial skeletal system have been developed by numerous investigators. Static models have been aimed at understanding scoliosis and postural disturbances in the musculoskeletal system while dynamic models have attempted to provide insight into kinematic behavior and mechanisms of spinal trauma. Dynamic spinal response models were developed in the late 1950's and early 1960's. Hess and Lombard provided the basis of many continuum models while those of Latham (1957) and Payne (1971) were of the lumped parameter variety.

Liu and Murray (1966) proposed a model of the spinal column represented by a viscoelastic medium carrying a non-eccentric load. Toth (1966), Hopkins (1971), Kalepa (1971), Payne (1969) proposed models intended to simulate whole body response and that of the spinal column disregarding bending response. Due to the limited value of the lumped parameter models, Orne and Liu (1970) proposed a distributed parameter model which accounted for the effect of the eccentric loading and included spinal curvature. Based on earlier experimental work by Kazarian, L., Boyd, D., and von Glucke, H., (1971) it was learned that a dual load transmission, load attenuation corridor existed along the spinal column; one, through the vertebral centra, and the other through the posterior articular facet joints. Hence, a two-dimensional discrete parameter model of the spinal column was formulated by Prasad, which incorporated two distinct load transmission pathways. The model considered natural spinal curvature, the effects of flexion and eccentric inertial loading. Head and neck motions were simulated and their effects on the forces and moments with respect to the thoracic and lumbar spinal column were investigated for off-axis loading in the mid-sagittal plane (Prasad and King, 1974).

Belytschko and Privitzer, et al (1978) have developed a complex mathematical description of the axial skeletal system. The geometry of each vertebral body is considered. Each vertebral body is connected to the adjacent vertebral body by an intervertebral disk and spring elements. The intervertebral disk elements possess axial stiffness, stiffnesses for flexion and extension, lateral bending, torsion and shear. Seven spring elements representing the axial stiffnesses of the ligaments and other soft tissues of the ligamentous spine are attached as follows: one joining the tips of the spinous processes; two joining the right and left side tips of the transverse processes; two elements joining each pair of articular facets and two points joining on each side of the laminae to the base of the spinous processes of the superior vertebra. The rib cage and sternum are modeled as a rigid body, the actions of the intercostal tissues are represented by spring elements. The abdominal viscera are modeled by hydrodynamic elements stacked in series between the pelvis and 10th rib suggesting a third load transmission corridor.

The mass and moment of inertia of each element was estimated using the distribution of the mass of the whole body to the vertebral level. The physical constants were extracted from the literature or estimated. Herein lies the problem; there exists very little information on the physical constants of tissues under static and dynamic loading.

The Head-Spine Model for Rhesus Monkey, Baboon and Chimpanzee - Because of the difficulties discussed above in quantitatively validating a complete axial skeletal model for man, the experimental data collected for subhuman primates were integrated into a generalized model for each primate. It is anticipated that such an approach would enable the basic modeling procedure to be evaluated and to shed some light on "scaling" subhuman primate data to man. The methods used for obtaining geometrical, stiffness, and inertial data for the subhuman primate spinal models are summarized by Belytschko (1978).

The lateral and anterior skeletal system of the rhesus monkey is illustrated in Figure 8A. Belytschko's computer model is shown in Figure 8B.

The lateral and anterior skeletal system of the baboon is illustrated in Figure 9A. Belytschko's computer model is shown in Figure 9B. Mass data and head mass movements were extracted from Reynolds (1974).

The lateral and anterior skeletal system of the chimpanzee is illustrated in Figure 10A. Belytschko's computer model is shown in Figure 10B. The mass data was determined on the basis of measurements reported by Rholes and Fineg (1961).

Thoracic and Lumbar Spinal Column - The number of thoracic vertebrae varies in the different primate genera as well as in individual specimens of the same species. The rhesus has 12 thoracic vertebrae whereas the baboon possesses 13, the chimpanzee 13, and man 12. The geometry of the thoracic vertebrae, intervertebral disks, costovertebral joints and the geometry of the articular facet joints relative to each other need precise definitions. With respect to the latter, an examination of the direction of the articular processes reveals that a characteristic type of articular facet geometry is retained in the lumbar regions and is departed from in the thoracic region. This change in form from the lumbar-type process to a thoracic-type process probably indicates adaptation to different types of functional torso kinesiology.

It is of interest to notice the locality of this change with respect to the subhuman primates and man. While this change is usually determined in man by the location of the ribs, the rhesus monkey and baboon continue the lumbar type of vertebral body into the thoracic column. Characteristically, the macaque has seven lumbar vertebrae; however, if one considers the two or three caudal thoracic vertebrae which maintain similar general form as the lumbar vertebrae, the total may be eight to ten vertebrae. A similar analogy holds true for the baboon, which may have two or three caudal thoracic vertebrae, which also have a similar form as the lumbar vertebrae, bringing it to a total of eight to ten vertebrae. In the case of the chimpanzee, the total number of vertebrae with the same form as the lumbar vertebrae totals four to six. Likewise, in man this number equals five. The change occurs suddenly between the last two ribs; the lower articular process of approximately the eleventh thoracic vertebrae being the last to retain the lumbar-type process.

The location of this changeover in facet geometry was found to occur most frequently in the rhesus monkey and baboon between the ninth and tenth thoracic vertebra; in the chimpanzee it occurred at the level of the second and third lumbar vertebra. In man this changeover is a normal anatomical feature occurring most frequently in the region of the eleventh and twelfth thoracic vertebrae. The spinal region below the mortice displays more mobility than above the mortice.

Viewed anteriorly, the proportionate lengths of the spinal regions are not closely correlated with the number of vertebral segments within a particular region. For instance, the macaque has a shorter cervical length and a much longer lumbar region when compared with man. If the vertebral column is viewed posteriorly and its regions identified by the abrupt variations in the articular facet joint geometry, still a different modal number of vertebrae appears. Utilizing the distances between the corresponding articular facet joints of similar geometry, the tenth thoracic vertebra acts as a center of muscular motion toward that the adjacent spinous processes converge in the macaque and baboon, a point that varies in position (lower) when compared with the chimpanzee and man.

Below the level of this transregional vertebra the articular facet joints are nonaxial weight bearing, but react in torsional shear (horizontal rotation). At and above the level of the transitional vertebra, two energy transmission corridors exist: (1) the vertebral body centrum and (2) the articular facet joints. These transitional levels are the initial energy crossover points where the load transmission and distribution between the anterior and posterior spine changes, (Kazarian, in publication).

Thoracic Cage - The geometry of the thoracic cage is variable. Its relationship to the sternum, and thoracic cage requires further definition. The sterna display complex geometry and may be either long and slender or short and broad corresponding to the shape of the thorax. The intercostal portions of the sterna as a rule are separate. There may be a tendency toward fusion. The lengths of the sterna are also variable.

Pelves - The three primary pelvic elements, the ilium, ischium, and pubis do not meet in the center of the acetabulum, but in a point situated more ventrally. Mid-sagittal sacral curvature, length-width proportions and the height of the mid-sagittal curvature are proportionally different. The geometry of the pelvis varies as does the load transmission pathways to the lumbar spine.

The primate model must also consider musculoskeletal interactions during and following mechanical excitation. The role of the various primary muscle groups must be identified using electromyographic signals. Although a relationship has not been established between the EMG signal level and force, the feasibility of using EMG signals for the measurement of muscular response is required.

To accurately model the primate, additional data are required depending on the degree of complexity and types of answers desired. The type of data necessary include, but are not limited to, the following categories: (1) gross anatomy, (2) static and dynamic tissue property data, (3) regional anatomical/biomechanical investigations. In Table I available data and gross anatomy and missing gaps are identified. The geometry and mass distribution of the head must be defined in a manner that allows comparative studies and analysis. The geometry of the cervical vertebrae, intervertebral disks and their kinesiological and kinematic relationships with respect to the skull and C7 requires in-depth investigation.

Table II identifies the geometry and strength measurements of axial skeletal system components required for the model.

Table III identifies the regional anatomy/biomechanical investigation required for complete validation of a primate model.

THE VALIDATION OF MODELS

The foregoing review of the biological data required and available for the design of primate biodynamic models and for their subsequent validation by various testing techniques is by no means exhaustive or complete. References are given on a few selected subjects only since otherwise each subarea would have been too voluminous and it was felt, that the main message of the paper would be clear to the biodynamic research community without belaboring the details. It became obvious after previous conferences on biodynamic models, and it appears again to be one of the most important conclusions to be drawn from the program of this meeting, that the definition of the validity, accuracy and of the limits of applicability of our complex biodynamic models is one of the biggest jobs which confronts this research area. So far, no serious attempt has been made to collect all valid experimental test results available, which could - no, must be in an effort to validate a biodynamic model of a human subject for body motion and/or injury prediction in mechanical stress environments. It has been proposed before, that a Biodynamic Data Bank coordinated at the National and International level should be considered for the collection of such data (von Gierke, 1978). In the USA, a National Academy of Sciences Committee has been established to look into the feasibility of such a data bank and to make recommendations regarding its scope, ground rules and organization.

The general philosophy presented in this paper with respect to the various test data required and the conviction that only the simultaneous application of all test methods possible will enable us to validate convincingly the complex models envisioned, determines our Laboratory's approach to this most challenging basic problem in biodynamics. We emphasized in our review the animal models and the anatomical, geometric, elasticity and strength data required, because it provided us the opportunity to present some of the newer data obtained by our program designed to collect systematically some of the missing data. This emphasis should not be interpreted as this animal component characteristics data base having any priority over accumulation of the human data base. Nor does it imply that the component tests are more important than the subinjury whole body human and animal C_x , C_y , C_z and off-axis impact tests required or the animal injury tests in all the axes mentioned, or the human and animal transmissibility and driving point impedance data, which are already partly available. Our emphasis on tissue component data was only guided by the fact that we think we made some advances in this area and completed some kind of analysis of what is available and what is needed. To review in detail each of the data bases available and desirable for validation would have been clearly beyond the scope of a single paper.

In summary, the requirements for biodynamic data from ten test areas reflect our thinking and broad laboratory program in support of model validation. We need: (1) human subinjury impact response data, (2) human steady state transmissibility and impedance data, (3) human operational and accident data (aircraft and automotive), (4) human whole body cadaveric data, (5) human component characteristics data, (6) animal subinjury impact response data, (7) animal steady state transmissibility and impedance data, (8) animal impact injury data, (9) animal whole body cadaver impact data, (10) animal component characteristic data.

In addition, we need the anatomical/morphological data material on each species. To fill the gaps in each of these areas our approach to data collection might benefit from better organized collection, storage and retrieval capability of all data. Many data, which we think are missing, might be stored somewhere, accessible only to a few or with unknown accuracy or experimental background. To a large extent our experimental programs should be oriented to fill the gaps in the data required for model validation. Our experiments should be guided by the models we have. Only in this way can we hope to have, in the foreseeable future, the next generation of realistic, validated biodynamic models, which can be used with confidence by human factors and design engineers outside the biodynamics research community.

1. Snyder, R. G., Society of Automotive Engineers, "Human Impact Tolerance," 1970, SAE Paper 700398.
2. Eiband, A. M., National Aeronautics and Space Administration, "Human Tolerance to Rapidly Applied Acceleration: A Survey of the Literature," 1959, NASA Memo No. 5-19-59E.
3. Ewing, C.; Thomas, D., AGARD-NATO-PARIS, FR., "Dynamic Response of the Living Human Head and Neck to Experimental Impact Acceleration: A Review Published in Symposium Proceeding - Models and Analogues for the Evaluation of Human Biodynamic Response, Performance and Protection," AGARD-CPP-253
4. Stapp, J. P., "Human Tolerance to Severe Abrupt Acceleration. "Gravitational Stress in Aerospace Medicine," Boston, Little Brown and Co., 1961, pp 165-188.
5. Stapp, J. P., "Voluntary Human Tolerance Levels. Impact Injury and Crash Protection." Springfield, Charles C. Thomas, 1970, pp 308-349.
6. King, A. I.; Prasad, P.; Ewing, C. "Mechanism of Spinal Injury Due to Caudocephalad Acceleration," Orthopaedic Clinics of North American, Vol 6, No. 1, 1975.
7. Prasad, P.; King, A. I.; Ewing, C. L.; "The Role of Articular Facets During +G_z Acceleration," J. of Applied Mechanics, Vol 41, No. 2, 1974, pp 231-326.
8. Tennyson, S.; Mital, N. K.; King, A. I., "Electromyographic Signals of Spinal Musculature During +G_z Impact Acceleration," Orthopaedic Clinics of North American, Vol 8, No. 1, 1977, pp 97 - 119.
9. Lin, H. S.; Liu, Y. K.; Ray, G.; Nikravesh, "Systems Identification for Material Properties of the Intervertebral Joint," J. Biomechanics, Vol II, 1978, pp 1 - 14.
10. Galante, J. O., "Tensile Properties of the Human Lumbar Annulus Fibrosis," Acta Orthop. Scand., Supple. 100, 1967.
11. Kazarian, L. E., "Creep Characteristics of the Human Spinal Column," 1975, Orthopaedic Clinics of North America, 6:1, pp 3 - 18.
12. Kulak, R. F.; Belytschko, T.; Schultz, A.; Galante, J., "Nonlinear behavior of the Human Intervertebral Disk Under Axial Load," J. Biomechanics, Vol 9, 1976, pp 377 - 396.
13. Markolf, K., "Deformation of the Thoracolumbar Intervertebral Joints in Response to External Loads," J. Bone Jnt Surgery, 54A, 1972, pp 511 - 533.
14. Nachemson, A., "Lumbar Intradiscal Pressure," Acta Orthop. Scand., Supple. 43, 1960, pp 1 - 104.
15. Brown, T.; Hansen, R. J.; Yorra, A., "Some Mechanical Tests on the Lumbosacral Spine with Particular Reference to the Intervertebral Disk," J. Bone Jnt Surg., 39A, 1957, pp 1135 - 1164.
16. Hirsch, C.; Nachemson, A.; "New Observations on the Mechanical Behavior of Lumbar Disc," 23, 1953, pp 254 - 283.
17. Furst, W., "The Force to Crush Vertebrae," Psychiatri Quart, 14-397-402, 1940.
18. Hartman, W., "Deformation and Failure of Spinal Materials," Exp. Mech., 14, 1974, pp 98 - 107.
19. Hakin, N. S., Wayne State University, "An Experimental Study and Finite Element Analysis of the Mechanical Response of a Vertebra," Ph.D. Dissertation, 1976.
20. Kazarian, L.; Graves, G., "Compressive Strength Characteristics of the Human Vertebral Centrum," SPINE, Vol 2, No 1, March 77, pp 1 - 14.
21. Messerer, O., "Uber Elastizitat Und Festigkeit Der Menschlichen Knochen," 1880, Verlag Der J. G. Cotta'schen Buchhandlung, Stuttgart, Germany.
22. Ruff, S., The Surgeon General, U.S. Air Force, "Brief Acceleration Less Than One Second, German Aviation Medicine - World War II," 1950, pp 584.
23. Yamada, H., STRENGTH OF BIOLOGICAL MATERIALS, Baltimore, Williams and Williams, 1970.
24. Andriacchi, T.; Schultz, A.; Belytschko, T.; Galante, J., "A Model For Studies of Mechanical Interactions Between the Human Spine and Rib Cage," J. Biomechanics, Vol 7, 1974, pp 497 - 507.
25. Agostoni, E.; Mognoni, G.; Torri, G.; Miserocchi, G., "Forces Deforming the Rib Cage," Resp. Physiol., Vol 2, 1966, pp 105 - 117.
26. Schultz, A.; Benson, Hirsch, C.; "Force Deformation Properties of Human Ribs," J. Biomechanics, Vol 7, 1974A, pp 303 - 309.
27. Schultz, A.; Benson, D.; Hirsch, C., "Force Deformation Properties of Human Costo-Sternal and Costo-Vertebral Articulations," J. Biomechanics, Vol 7, 1974B, pp 311 - 318.
28. Gazulov, S.A.; Korshen, Y.; Skrupnik, V. G.; Sushkov, Y.N.; "Issledovaniye Prochnosti Pozvonkov Cheloveka Na Szhatiye," Arkh Gistol Embriol 43-51, 1966.

29. Yamada, H., STRENGTH OF BIOLOGICAL MATERIALS, Baltimore, Williams and Wilkins, 1970.
30. Kazarian, L., "Comparative Compressive Strength Characteristics of Thoracic and Lumbar Vertebral Centra," to be published.
31. Kazarian, L.; Hahn, J.; von Gierke, H., Fourteenth Stapp Car Crash Conference, "Biomechanics of the Vertebral Column and Internal Organ Response to Seated Spinal Impact in the Rhesus Monkey," SAE Paper 700898.
32. Slonim, A.; Kazarian, L., "Transmissibility Investigations and Spinal Column Acceleration"
33. Hess, J.; Lombard, C., "Theoretical Investigations of Dynamic Response of Man to High Vertical Accelerations," Aviation Medicine, 1958, pp 66 - 75.
34. Latham, F., Proceedings of the Royal Society, "A Study of Body Ballistics: Ejection Seat," 1957, B-147, pp 121.
35. Payne, P., Symposium on Biodynamic Models and Their Applications, Wright-Patterson Air Force Base, Ohio, "The Human Spine - A Critical Review of Existing Dynamic Data in Relation to Aircraft Systems," 1971, AMRL TR-71-29-9.
36. Liu, Y.K.; Murray, J., Editor - Y. C. Fung, "A Theoretical Study of the Effect of Impulse on the Human Torso Biomechanics," 1966, pp 167 - 186.
37. Toth, R., Proceedings of the 19th Annual Conference on Engineering and Medicine in Biology, "Multiple Degree of Freedom Non-Linear Spinal Model," Vol A, 1966, pp 102.
38. Hopkins, G. R., Symposium on Biodynamic Models and Their Applications, Aerospace Medical Research Laboratory, Wright-Patterson Air Force Base, Ohio, "Non-Linear Lumped Parameter Mathematical Model of Dynamic Response to the Human Body," 1971, AMRL-TR-71-29, pp 649 - 699.
39. Kaleps, I.; von Gierke, H. E.; Weis, E. B., Symposium on Biodynamic Models and Their Applications, Aerospace Medical Research Laboratory, Wright-Patterson Air Force Base, Ohio, "A Five Degree Of Freedom Mathematical Model of the Body," 1971, AMRL-TR-71-29, pp 211-231.
40. Payne, P.R.; Band, E. G. U., Wyle Laboratories, Payne Division Working Paper No. 59101-6, "A Four Degree-of-Freedom Lumped Parameter Model of the Seated Human Body," 1969.
41. Orne, D.; Liu, Y. K., "A Mathematical Model of Spinal Response to Impact," J. Biomechanics, Vol 4, pp 49 - 71.
42. Kazarian, L.; Royd, D.; von Gierke, H., "The Dynamic Biomechanical Nature of Spinal Fractures and Articular Facet Derangement," 1971, AMRL-71-17, Wright-Patterson Air Force Base, Ohio.
43. Prasad, P.; King, A. I., "An Experimentally Validated Dynamic Model of the Spine," J. Appl. Mech., 1974, pp 546 - 550.
44. Belyachko, T.; Privitzer, E., Aerospace Medical Research Laboratories, Wright-Patterson Air Force Base, Ohio, "Refinement and Validation of a Three-Dimensional Head-Spine Model," TR-78-7, 1978.
45. Reynolds, H. M.; Thesis, Southern Methodist University, "Measurement of the Inertial Properties of the Segmented Savannah Baboon," 1974.
46. Rohles, Jr., F. H.; Fineg, J., Aerospace Medical Research Laboratories, Wright-Patterson Air Force Base, Ohio, "Cross-Body Measurements of the Young Chimpanzee," 1961, AMRL Tech. Report MCD-TDR-61-36, Holloman, Air Force Base, New Mexico.
47. von Gierke, H. E., "Biodynamics Symposium Summary - Aviation Space and Environmental Medicine," Vol 49, No. 1. January 1978.

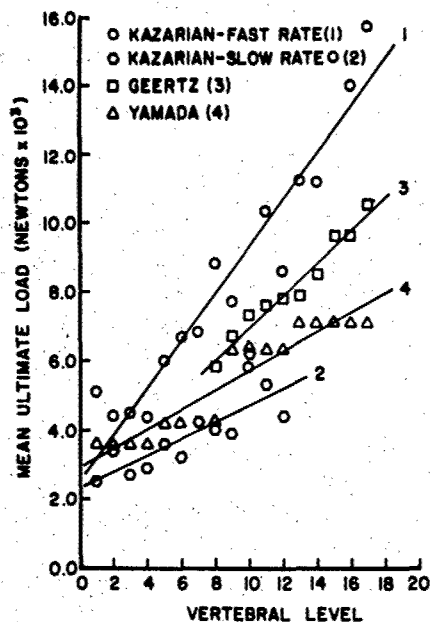


Figure 1 - Comparative breaking strength for isolated human vertebral elements between the T_1 L_5 vertebral body levels.

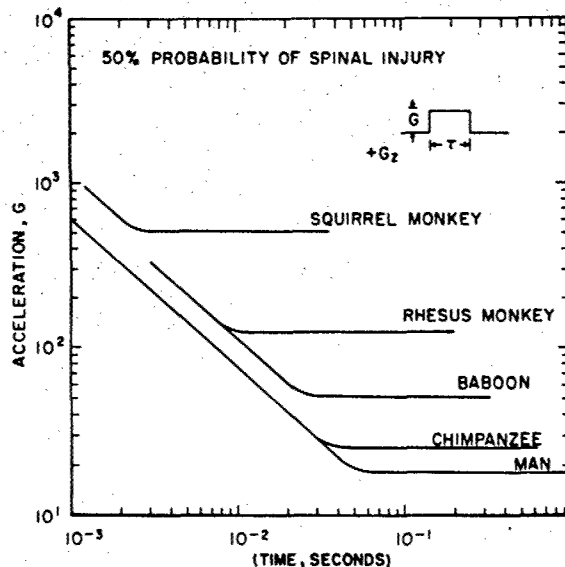


Figure 2 - Impact sensitivity curves for a rectangular deceleration time history for the rhesus monkey, baboon, chimpanzee and man. The logarithm of the peak acceleration and the logarithm of the pulse duration are plotted to obtain a straight line representation.

The scaling sensitivity curves relate only to the parameters of impact function and spinal injury for identical support and restraint systems, body posture and other factors. These curves imply geometrically similar structures which appear to be formed of similar materials (but of different size and strength), dynamically respond in a similar manner (inversely proportional to size) and insinuate that subhuman primates have a spinal injury threshold which can be accurately described by an interspecies impact sensitivity curve. In this figure, the lines at the left of the graphs, which angle down at 45° represent a regime in which the change in velocity governs the peak force in the vertebral column, while the horizontal lines extending to the right of the graph represent the regime in which the peak acceleration force is the governing factor. Vertebral body fracture patterns and modes vary within both regimes.

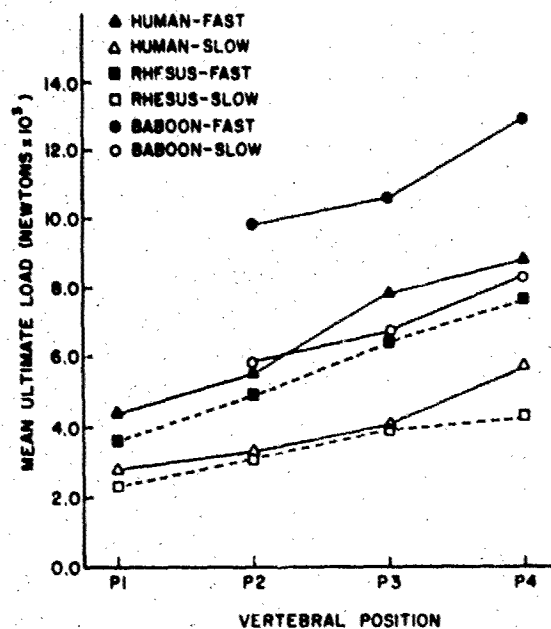


Figure 3 - Composite plot of rhesus, baboon and human vertebral centra subjected to uniform axial compressive load at two different strain rates. The slow strain rate is 8.89×10^{-5} meters/second while the fast strain rate is 8.89×10^{-1} meters/second. Note the unexpected finding in the comparative strength characteristics between the baboon at the slow and fast compression rates to human and rhesus monkey vertebrae.

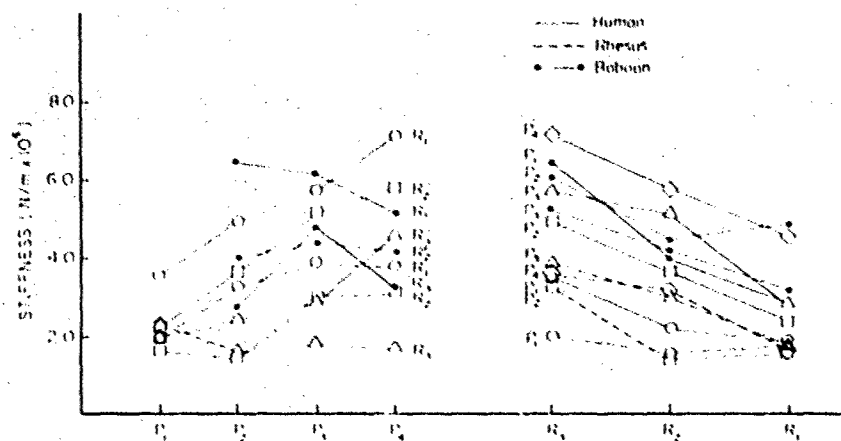


Figure 4 - Stiffness for position by displacement rate combinations

where $P_1 = T_1 - T_2 - T_3$

$P_2 = T_4 - T_5 - T_6$

$P_3 = T_7 - T_8 - T_9$

$P_4 = T_{10} - T_{11} - T_{12}$

and $R_1 = 8.89 \times 10^{-5}$ m/s

$R_2 = 8.89 \times 10^{-3}$ m/s

$R_3 = 8.89 \times 10^{-1}$ m/s

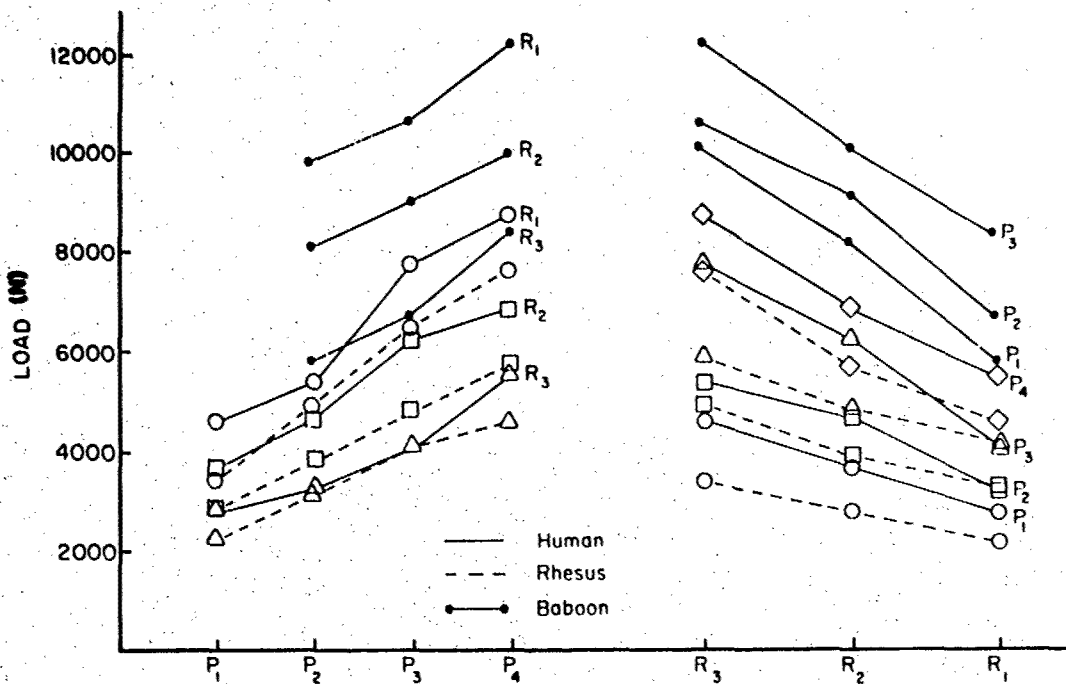


Figure 5 - Average ultimate load (Newton's) for position by displacement rate combinations where $P_1 = T_1-T_2-T_3$

$$P_2 = T_4-T_5-T_6$$

$$P_3 = T_7-T_8-T_9$$

$$P_4 = T_{10}-T_{11}-T_{12}$$

and $R_1 = 8.89 \times 10^{-5} \text{ m/s}$

$$R_2 = 8.89 \times 10^{-3} \text{ m/s}$$

$$R_3 = 8.89 \times 10^{-1} \text{ m/s}$$

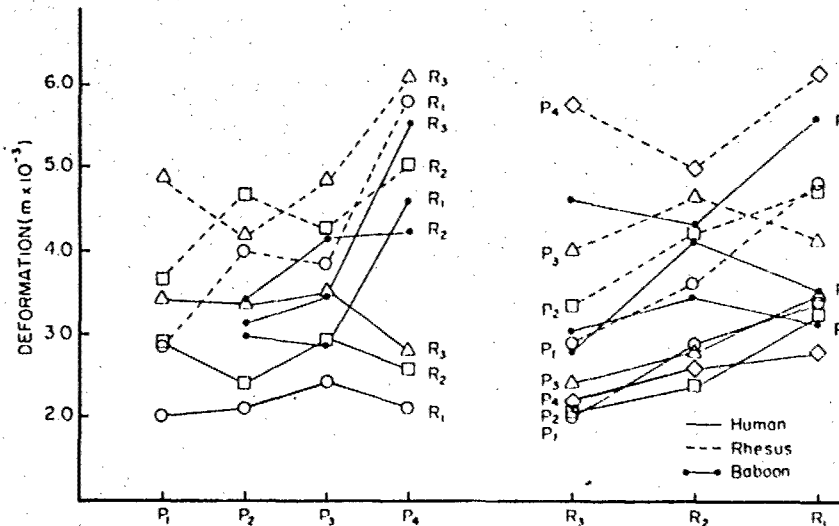


Figure 6 - Average deformation to ultimate load for position by displacement rate combinations - P and R are defined in Figure 5.

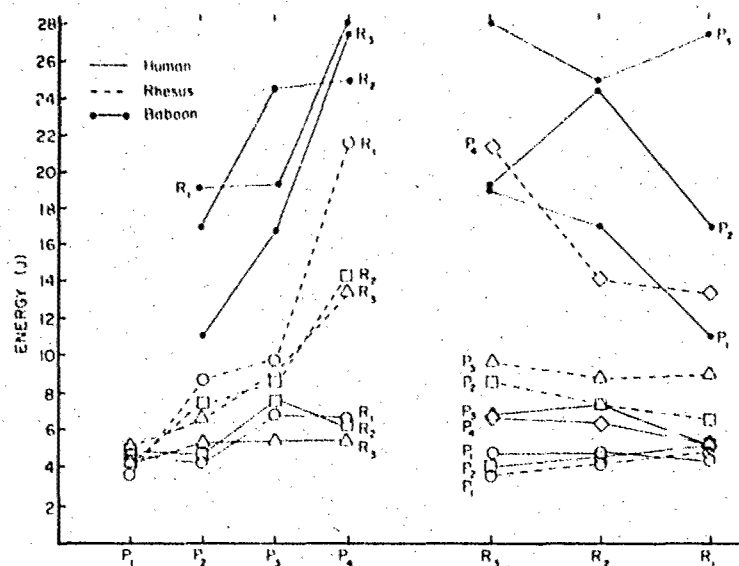


Figure 7 - Average energy to ultimate load for position by displacement rate combinations. Values of P and R are defined in Figure 5.

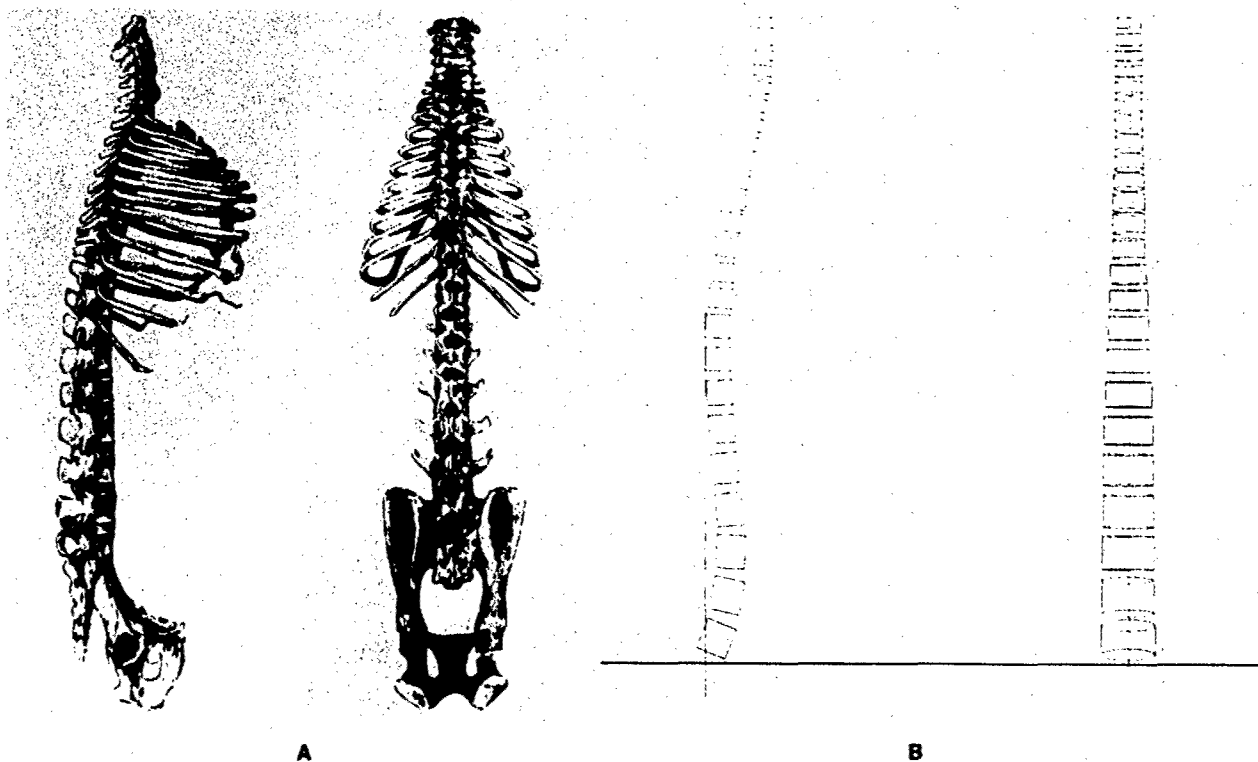


Figure 8 - Lateral and anterior skeletal system (8A) of the rhesus monkey compared to computer model (8B)

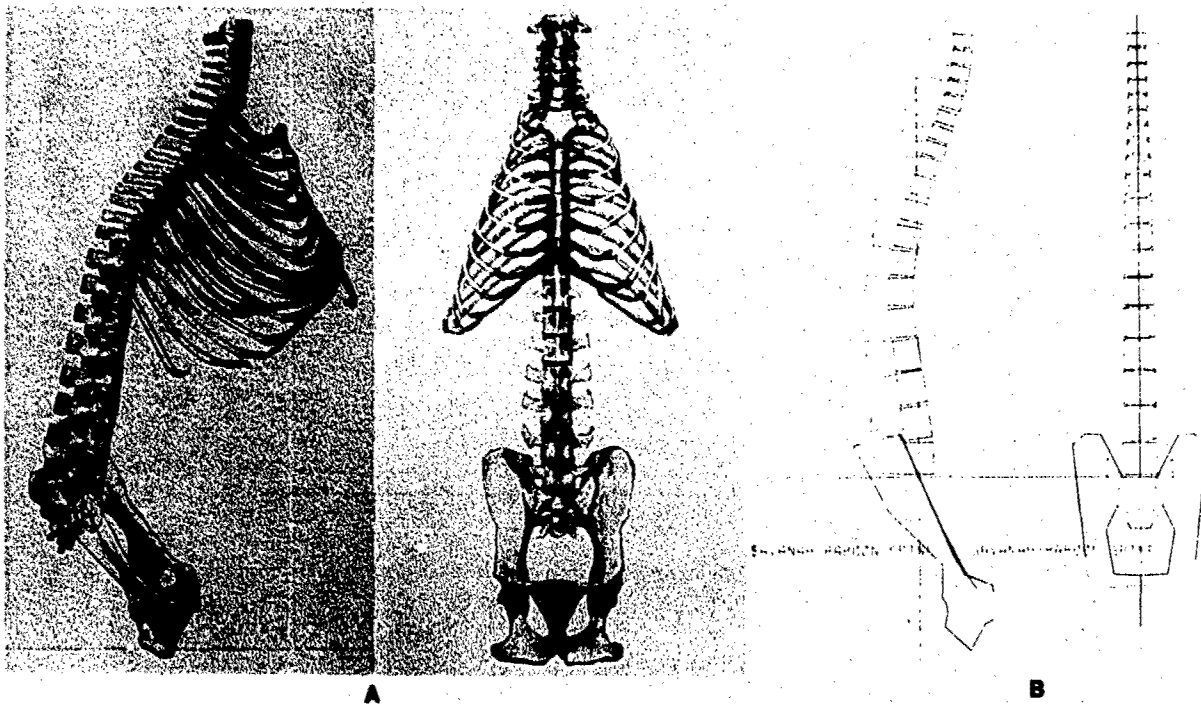


Figure 9 - Lateral and anterior view of the baboon skeletal system (9A) compared to computer model (9B)

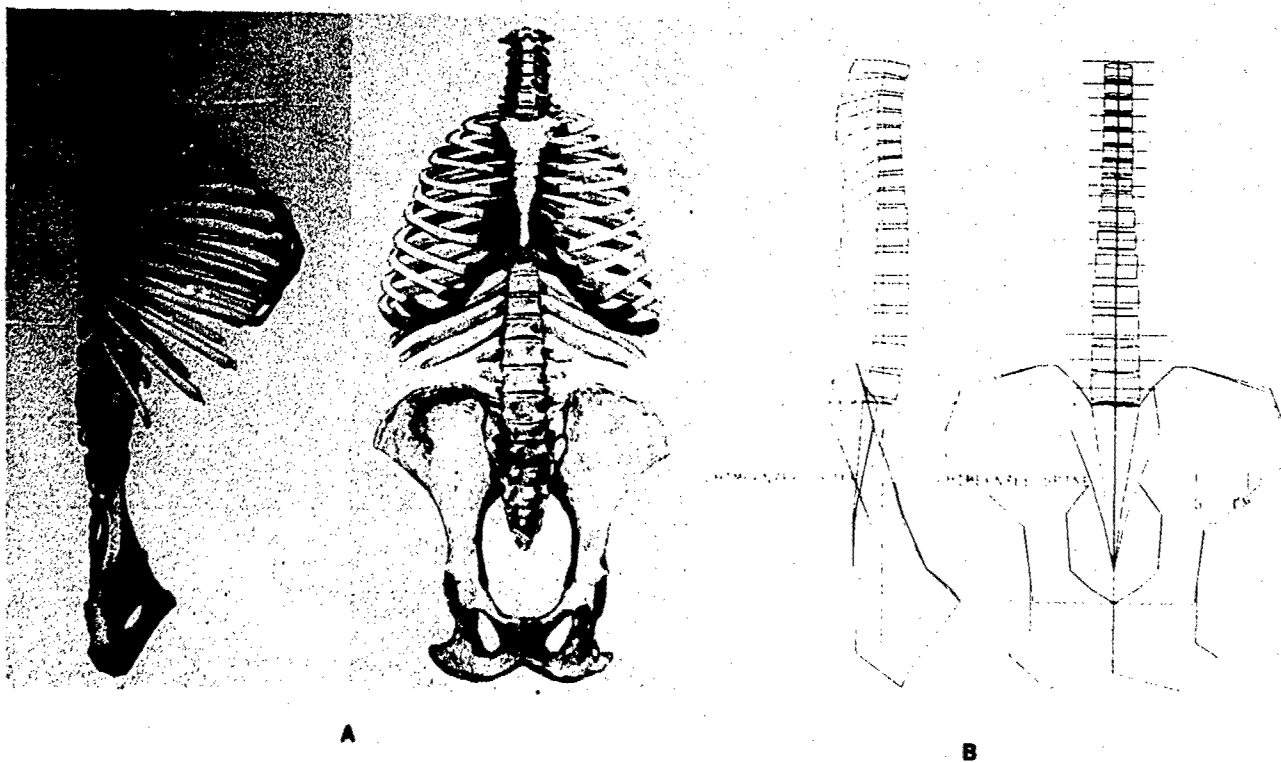


Figure 10 - Lateral and anterior view of skeletal system of chimpanzee (10A) compared to computer model (10B)

GROSS ANATOMY

OSTEOLOGY	REQUIREMENTS
<u>AXIAL SKELETON</u>	
SKULL	— INERTIAL PROPERTIES
VERTEBRAL COLUMN	RANGE OF MOTION
BONY THORAX	RANGE OF MOTION
PELVIS	GEOMETRY
<u>BACK</u>	
BACK/SHOULDER	DIMENSIONS/
BACK MUSCLES	DIMENSIONS
SUBOCCIPITAL REGION	MUSCLE/BONE MAPS
<u>THORAX</u>	
THORACIC WALL I	
SUPERFICIAL MUSCULATURE	MUSCLE/BONE MAPS
DEEP MUSCULATURE	DIMENSIONS
THORACIC WALL II	
INTRINSIC THORACIC MUSCULATURE	
THORACIC WALL III	
TRANSVERSE THORACIC MUSCULATURE	
<u>ABDOMEN</u>	
ABDOMINAL MUSCULATURE	DIMENSIONS
ABDOMINAL VISCERA	MUSCLE/BONE MAPS
<u>PELVIS</u>	
PELVIS/LUMBAR SPINE	GEOMETRY
	MUSCLE/BONE MAPS

Table I - Type of gross anatomical data required on the rhesus monkey, baboon, and chimpanzee

GEOMETRIC / STRENGTH REQUIREMENTS

COMPONENTS	GEOMETRY	REQUIREMENTS
* VERTEBRAL BODY	CENTRA	STRENGTH
	ARTICULAR FACETS	
* INTERVERTEBRAL DISK	GEOMETRY	STRENGTH
* VERTEBRAL BODY COMPLEX	STRENGTH	FAILURE MODES
LIGAMENTOUS STRENGTH	GEOMETRY	STRENGTH
REGIONAL SPINAL MECHANICS	GEOMETRY / RANGE OF MOTION	
* INTRADISCAL PRESSURE	PRESSURE	
* LIGAMENTOUS PRESTRESS	STRENGTH RELATIONS	
SKELETAL ATTACHMENT OF TRANSDUCERS		DEFINITION OF MUSCLE ACTION
IN VIVO MUSCLE FORCE MEASUREMENTS —		
THORAX	DEFLECTIONS, STRAINS, PRESSURE, FAILURE PROPERTIES, GROSS DEFORMATION	
ABDOMEN	DEFLECTIONS, STRAINS, PRESSURE	
PELVIS	GEOMETRY	

Table II - Identification of the axial skeletal system components and type of data required on the rhesus monkey, baboon, and chimpanzee - The asterisk (*) indicates efforts are currently underway.

REGIONAL ANATOMY BIOMECHANICAL INVESTIGATIONS

REGIONAL ANATOMY	REQUIREMENTS
HEAD/CERVICAL SPINE	RANGE OF MOTION — STRENGTH CHARACTERISTICS
THORAX	RANGE OF MOTION — RIB INTERACTION
AXIAL SKELETON	LOAD TRANSMISSION / ATTENUATION PATHWAYS <ol style="list-style-type: none"> 1. VERTEBRAL CENTRA 2. ARTICULAR FACETS 3. ABDOMINAL / THORACIC CAVITY
	RANGE OF MOTION GEOMETRIC / MATERIAL PROPERTIES
* IMPEDANCE	SPINAL COLUMN / INTRAABDOMINAL / INTRATHORACIC PRESSURE RELATIONSHIPS

Table III - Types of regional anatomical biomechanical investigation required to complete validation of the model. The asterisk (*) indicates investigations are currently underway.

Frequency Response of Cardiovascular Regulation in Canines
to Sinusoidal Acceleration at Frequencies Below 1 Hz
(Basis for Biodynamic Modeling)

C.F. Knapp, J.A. Marquis*, J.M. Evans, and D.R. Randall
Wenner-Gren Research Laboratory
University of Kentucky
Lexington, Kentucky 40506 U.S.A.

SUMMARY

Sinusoidal, whole body acceleration was used as a noninvasive forcing function to the cardiovascular system of unanesthetized, chronically instrumented canines to determine the low frequency (<1 Hz) dynamics of integrated barostatic cardiovascular regulation. Animals were restrained horizontally on an independently controlled, rotatable platform attached to the arm of a 15 m diameter centrifuge. With this centrifuge configuration, sinusoidal variations in spinal axis acceleration ($\pm 2 G_z$) were produced at frequencies from 0.008 to 0.25 Hz. Aortic pressure and flow, right and left ventricular pressure, heart rate and spinal axis acceleration were digitally sampled and filtered. Two additional variables, effective systemic vascular resistance and left ventricular stroke flow were also computed. The filtered data were then Fourier analyzed. The participation of neurally-mediated cardiac and vascular baroreflex mechanisms in the overall response was evaluated by comparing the subjects' responses in a reflexive (neurally active) and non-reflexive (neurally blocked) condition. Transfer functions were then derived to describe the passive acceleration-induced intravascular pressure disturbances and the control action of the major baroreflex mechanisms.

The dynamic (oscillatory) frequency response of the major cardiac and vascular baroreflex mechanisms was found to be limited primarily to the frequency range below 0.10 Hz. A comparison of the participation of cardiac and vascular mechanisms in the overall responses indicated that barostatic control is achieved principally via the systemic vascular mechanisms below 0.02 Hz, via the cardiac mechanisms from 0.04 to 0.10 Hz, and by the combined action of the two between 0.02 and 0.04 Hz.

INTRODUCTION

Certain aerial combat maneuvers and the flight of high speed, low altitude, terrain-following aircraft expose operational crews to dynamic acceleration environments with a significant frequency content below 1.0 Hz (19,20). Essential cardiovascular control may be significantly challenged by these dynamic, force-field environments which produce transient pressure, flow and volume disturbances to the cardiovascular system. The degree to which the barostatic control network is able to minimize these transient acceleration-induced disturbances is determined by the dynamic response characteristics and integrated function of the individual cardiac and vascular control mechanisms.

The majority of previous studies of neural barostatic cardiovascular regulation (6-18) using a Systems Analysis Approach (26-28) examined the response of specific control mechanisms to invasively-applied localized pressure, volume and/or flow disturbances using anesthetized animal preparations. Consequently, the application of the results to normal integrated barostatic control in unanesthetized animals, exposed to the global arterial and venous disturbances associated with whole body acceleration, is unclear.

Considerable research has also been conducted to quantify cardiovascular responses to whole-body acceleration. While responses to sustained acceleration (1,2,5) and time-dependent acceleration loadings above 1.0 Hz (whole body vibration) (21-23) have been extensively researched and documented, there is a very limited amount of information (24,25) available concerning responses to, and potential physiological hazards associated with, acceleration at frequencies below 1.0 Hz.

This lack of information concerning the low frequency (<1 Hz) dynamics of integrated barostatic cardiovascular regulation has hampered efforts to model human cardiovascular responses to time dependent acceleration loadings, in order to assess potential hazards to flight personnel. To alleviate this critical shortage of data, studies have been conducted using unanesthetized, chronically instrumented canines to quantify cardiovascular responses to whole body acceleration below 1 Hz, and to establish the frequency response characteristics of cardiovascular regulation in this region. Measurements from invasive instrumentation, possible only with this type of animal preparation, are vital for conducting realistic model studies and for identifying the meaningful variables for assessing acceleration-induced cardiovascular responses when noninvasive measurements are made on man.

The specific objectives of this research effort were to:

1. Quantify the pressure and flow disturbances produced by whole-body sinusoidal G_z acceleration as a function of acceleration frequency.
2. Quantify the reflex circulatory adjustments to these disturbances, emphasizing the participation and, hence, frequency response characteristics of the individual cardiac (heart rate and stroke volume) and vascular (resistance and capacitance) control mechanisms involved in these adjustments.
3. Determine the active (reflexive) versus passive (nonreflexive) response characteristics of the circulatory network, by studying the animals in a normal (reflexive) state and in a pharmacologically-blockaded (nonreflexive) state where the regulatory action of the major cardiovascular control mechanisms was inhibited.
4. Develop transfer functions encompassing the response characteristics of the major barostatic control mechanisms, based on this and previous work, which are suitable for inclusion in existing passive (nonreflexive) cardiovascular models (3).

* Currently with the Department of Mechanical Engineering, Tennessee Technological University, Cookeville, Tennessee, 38501.

EXPERIMENTAL DESIGN AND PROTOCOL

A. Chronically Instrumented Animal Preparation

Adult male and female mongrel dogs of 20 kg average weight were used in this study. Each dog was anesthetized with sodium penothal and prepared for sterile surgery. A left thoracotomy was performed and a left ventricular pressure gauge (Kongsberg Instruments), a right atrial cannula, and an aortic flow cuff on the ascending aorta (Zepeda Instruments) were implanted (4,41,45). Each animal was allowed at least four weeks of post-operative recovery prior to any experimental intervention. The principles of laboratory care as outlined by the National Society for Medical Research were rigorously observed.

On the day of the experiment, the animal was tranquilized with an intramuscular injection of Innovar Vet at 1.5 cc/20 kg. Piezoelectric manometer-tipped catheters (Millar PC 350, 5 French) were placed, under local anesthetic, in the right and left ventricles via small branches of a main femoral vein and artery respectively. One Millar gauge was used to calibrate the implanted Kongsberg gauge and then retracted into the aorta, just outside the aortic valve, to measure arterial pressure. The animal was maintained in a lightly tranquilized state for the duration of the experiment with hourly injections of Innovar (0.5 cc) administered through the right atrial cannula.

The measured physiological variables included aortic pressure and flow, left and right ventricular pressure, and heart rate (derived from left ventricular pressure).

B. Procedure For Autonomic Blockade

In order to delineate the neural and nonneural components of the measured cardiovascular responses to acceleration, a pharmacologically-induced total autonomic blockade was used to inhibit adrenergic and cholinergic efferent activity (Figure 1), thus removing normal reflex barostatic action. This approach was chosen because the use of pharmacological blocking agents has several advantages over other techniques in that 1) it is a standard procedure with many of its limitations well documented; 2) the effects of these agents are distributed throughout the system and do not have the uncertainty associated with attempts at total denervation; and 3) the use of these agents allows for repeated blocked and nonblocked studies on the same animal without compromising the integrity of the preparation.

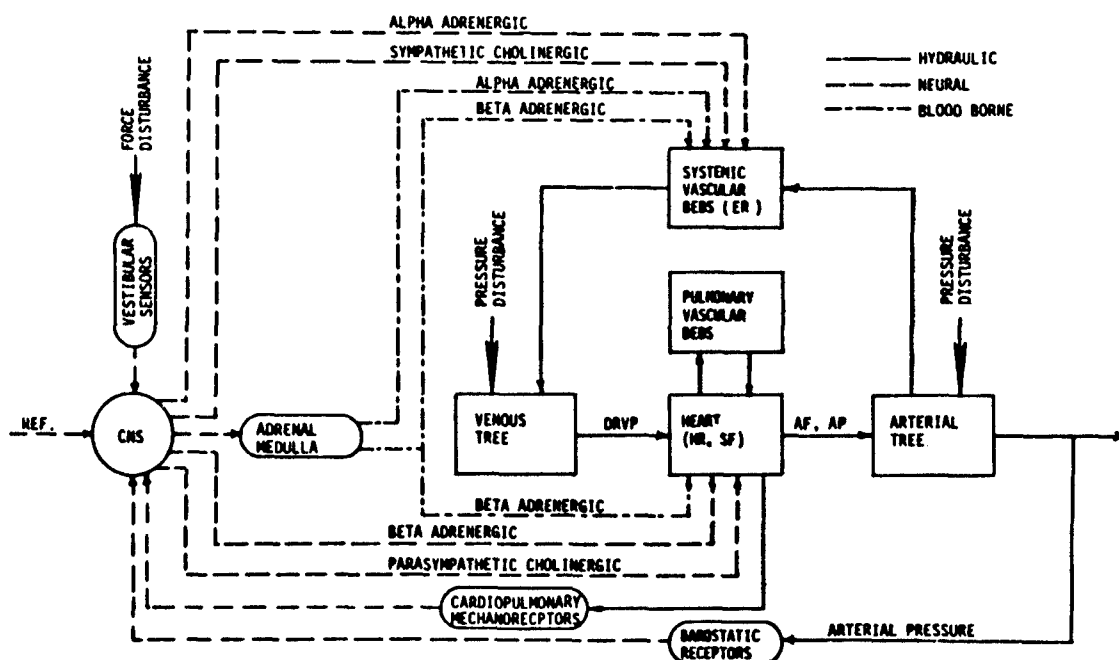


FIG. 1. SCHEMATIC OF THE BAROSTATIC CONTROL SYSTEM FOR RESPONSE TO ACCELERATION-INDUCED PRESSURE DISTURBANCES IN THE CARDIOVASCULAR SYSTEM.

Specifically, the total autonomic blockade consisted of the alpha adrenergic blocker, phenoxybenzamine (Dibenzylamine), at 20 to 30 mg/kg administered over an hour, followed by beta blockade with propranolol (Inderal) at 1 to 4 mg/kg over approximately ten minutes, followed by cholinergic blockade with atropine (Atropine Sulphate) at 0.1 to 0.4 mg/kg over approximately five minutes. The efficacy of the blockade was tested and verified by a comparison of systemic responses to specific agonists given prior to blockade, following blockade and then again at the conclusion of the blocked acceleration sequence. These consisted of a 50 µg/kg bolus of phenylephrine (Neosynephrine) to test the alpha blockade and a 0.5 µg/kg bolus of isoproterenol (Isuprel) to test the beta blockade. If heart rate showed evidence of parasympathetic activity (respiration rhythm), the atropine dosage was supplemented. This blockade and test procedure is discussed in greater detail elsewhere (34,35).

C. Centrifuge Facility

Low frequency acceleration loadings were produced by a modified 50 ft. (15.24m) diameter centrifuge shown in Figure 2. This system was used to produce sinusoidal acceleration below 1.0 Hz at $+2G_z$ ($1G = 9.806 \text{ m/sec}^2$). Mounted to the large arm of the centrifuge (Figure 2-a) is a platform (Figure 2-b) capable of rotation speeds from 0.005 to 11.5 rad/sec. The animal subject was restrained horizontally on this platform so that its center of rotation was approximately at heart level. With the large centrifuge arm rotating at an appropriate speed to produce the desired radial peak acceleration, an initiation of the platform rotation produces sinusoidal G_z (spinal axis) acceleration loadings. This configuration also produces sinusoidal G_y (lateral) acceleration 90° out of phase with that of G_z , and a $+1G_x$ acceleration vector due to Earth gravity. The exact time representations of the G_z and G_y acceleration loadings are given by (36):

$$G_z = [-\omega_R^2 R \cos(\omega_R t) - (\omega_R - \omega_P)^2 r]e_r \quad \text{and} \quad G_y = [-\omega_R^2 R \sin(\omega_R t)]e_p \quad [1]$$

where

R = the radial distance from the center of rotation of the large centrifuge arm to the center of rotation of the platform,

r = the radial distance from the center of rotation of the platform to an arbitrary point along the spinal axis of the animal,

ω_P = the rotational speed of the platform (determines the acceleration frequency),

e_r, e_p = unit vectors, with e_p perpendicular to e_r .

It should be noted that the G_z component of acceleration contains two terms. The first is the desired spinal axis sinusoid of constant amplitude. The second is a bias term representing a "dc offset" of this sinusoid due to the interactive effect of the rotation rates ω_R and ω_P , at various distances r along the spinal axis.

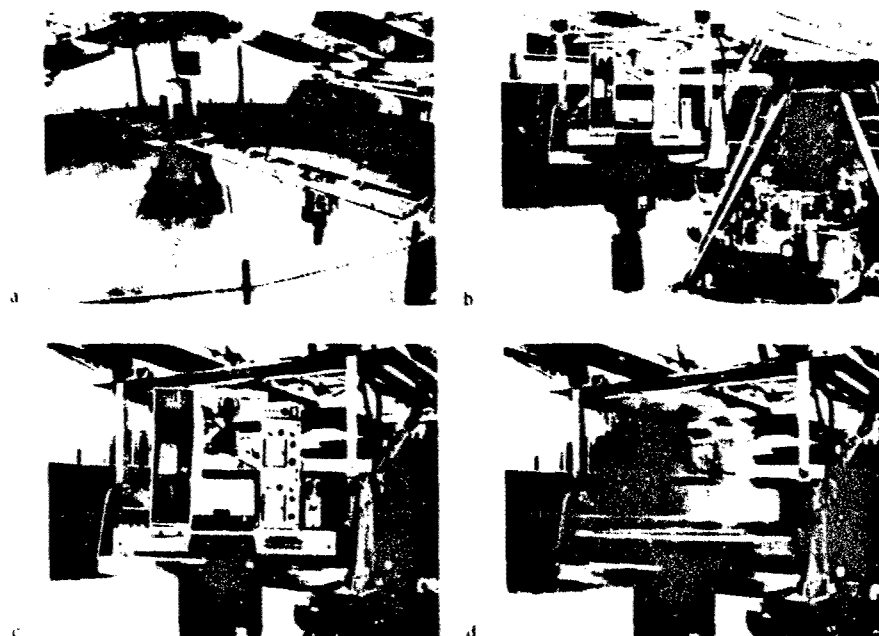


Fig. 2. Successive close-ups of the Wenner-Gren centrifuge modification:
 a. Rotating platform mounted on arm of conventional centrifuge
 b. Close-up detailing rotating platform with associated drive train
 c. Close-up detailing animal restraint (front view of rectangular box) with associated instrumentation on each side
 d. Time exposure of slowly rotating platform

away from the platform's center of rotation ($r=0$). This bias term can be minimized (or negated) by a proper choice of ω_R and ω_P , with the two being of opposite sign. In the present study $R = 6.10 \text{ m}$ and $\omega_R = 1.8 \text{ rad/sec}$, which yielded the desired $2G_z$ sinusoid with less than a $0.006 G/cm$ bias along the animal's spinal axis for acceleration frequencies from 0.005 to 0.25 Hz.

While cardiovascular responses to G_z and G_y sustained acceleration have been shown to be relatively small when compared to those of the G_x direction (1), their potential influence cannot be totally disregarded when interpreting data from these experiments.

All physiological signals from the animal and the G_z acceleration were conditioned and preamplified by electronics contained on the rotating platform (Figure 2-c), and then transmitted through two sets of slip rings (platform and centrifuge axes) and a long line interface to a remote location where they were monitored.

and recorded.

D. Acceleration Protocol

An acceleration amplitude of $\pm 2 G$ was chosen for this study for a number of reasons: It was felt that this acceleration level would represent a stress somewhat greater than that seen by the animal during normal physical activity, but less than that which might produce total circulatory collapse. The latter possibility was of particular concern during the blockaded runs, where the animal's compensatory mechanisms were purposely compromised. In addition, it was estimated that this acceleration level would generate intravascular pressure disturbances in the range of ± 10 -20 mm Hg, similar to the invasively-applied pressure stimulus used in previous studies.

On the day of experiment, after placement of the acute instrumentation, the animal was placed in the restraint couch and mounted on the rotating platform (Figure 2-c). The instrumentation leads were then connected and tested, and all signals were calibrated, thus readying the animal for the test series.

All variables were allowed to stabilize for a pre-acceleration control period. The test series then consisted of $\pm 2 G$, sinusoidal acceleration at discrete frequencies in the range from 0.005 to 0.25 Hz. The frequencies were run sequentially (low-to-high in most animals) without stopping, allowing from 3-4 min at the low frequencies and 1-2 min at the highest. It was found that this continuous frequency "sweep" minimized startling responses associated with centrifuge start up and shut down, thus enhancing the stability of responses at each frequency. A number of animals were run using random sequencing of the frequencies, and both low-to-high and high-to-low protocols, to determine the influence of these factors on the overall responses. The effect was minimal. At the conclusion of the frequency sweep the animal was allowed a suitable recovery period, during which all variables could return to pre-acceleration control levels. Next, the animals were tested to determine their pre-blockade response to the appropriate adrenergic agonists after which time the total blockade was implemented and a second post-blockade, pre-acceleration test made. The same control-test-recovery sequence used in the nonblocked run was then repeated. Finally, another test was made to verify the efficacy of the total blockade.

DATA ANALYSIS

During each experimental session, a continuous on-line magnetic tape record (Ampex FR-3020, 14 channel recorder) and a strip chart record (Beckman Type-RM Dynograph, 8 channel recorder) was made of the following variables: spinal axis acceleration (ACC), heart rate (HR), aortic pressure (AP) and flow (AF), right ventricular pressure (RVP), and left ventricular pressure (LVP). The HR variable was generated by a calibrated cardiostachometer (Beckman Type 9857B) triggered from the phasic LVP signal. The strip chart data was reviewed, off-line, to determine exact acceleration frequencies, and inclusive tape counts and record (time) lengths for each edited "window" of data to be digitally sampled and Fourier analyzed.

The sampling and Fourier analysis of the data were carried out on a Digital Equipment Corporation (DEC) PDP-11/10 minicomputer system, with the aid of the DEC LAB APPLICATIONS-II, V-3 library package and a number of user-written BASIC applications programs. Details of the analysis are reported elsewhere (4).

Representative phasic analog data shown in Figure 3 is presented in its digitally-filtered form in Figure 4.

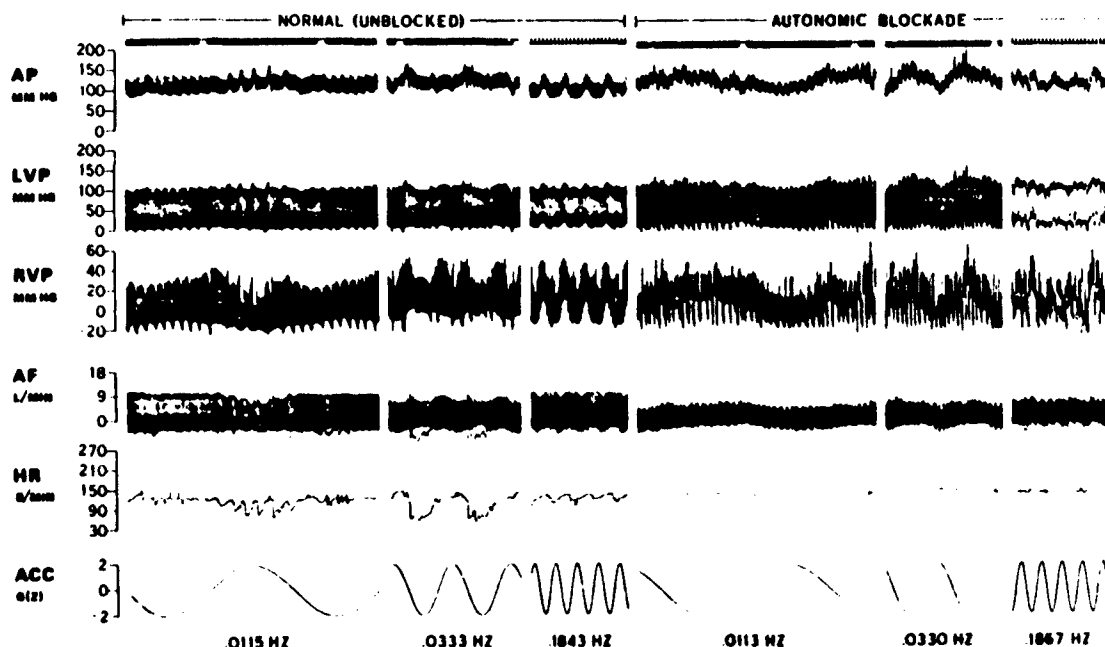


Fig. 3. Example of phasic cardiovascular data: The response of one animal in both a nonblocked and autonomically-blocked state at three acceleration frequencies, with one second event markers shown above the AP traces.

The purpose of filtering the sampled data was to avoid the phenomenon of spectral "aliasing" (37) in the compressed data, and hence in the Fourier analyzed results.

After filtering and compression the paired input (ACC) and output (AP, DRVP, AF, and HR) waveforms were Fourier analyzed using the SPARTA program from the LAB APPLICATIONS library. Two additional calculated output variables, effective systemic resistance $ER = (AP - DRVP)/AF$ and stroke flow $SF = AF/HR$ were also frequency analysed.

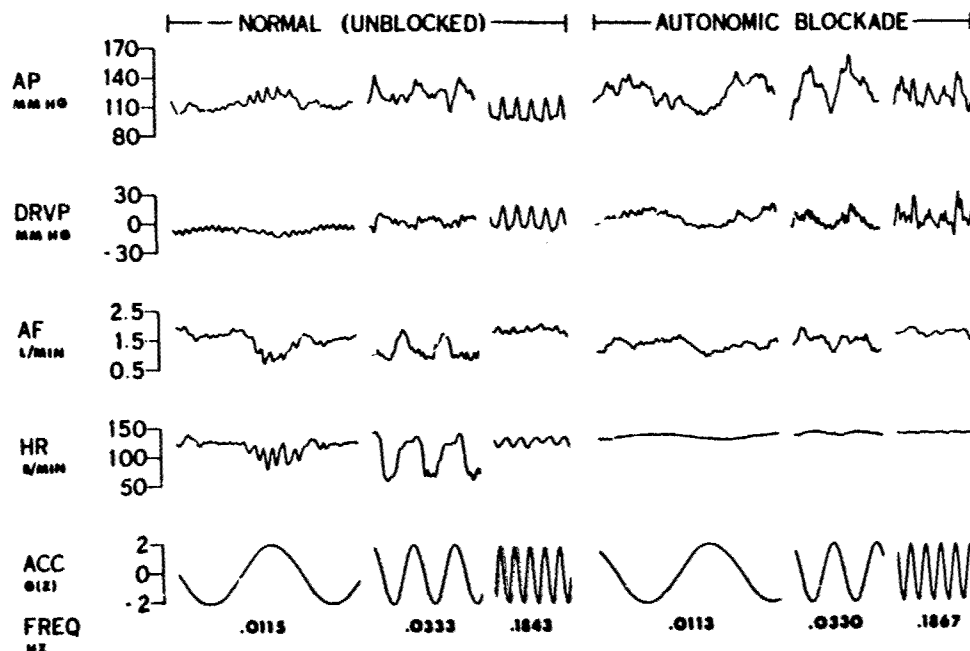


Fig. 4. Example of filtered cardiovascular data: The digitally-filtered representation of the phasic response data from the preceding Figure, for one animal in both a nonblocked and autonomically-blocked state at three acceleration frequencies.

The mean (nonoscillatory) response and amplitude/phase values of the first several harmonics (of the input acceleration frequency) were saved from the computed spectrum of each output variable. In specific cases, where predictable inaccuracies due to spectrum "leakage" or the digital filtering occurred in the data, suitable correction factors were applied. An example of the Fourier analyzed power spectra for the HR response of one subject to 0.008 - 0.65 Hz, $\pm 2G$, sinusoidal acceleration is shown in Figure 5, which is a composite plot of the individual amplitude spectrum for each discrete input frequency. While second and third harmonics of the input acceleration frequency can be seen, predominance of the first harmonic in the response is apparent.

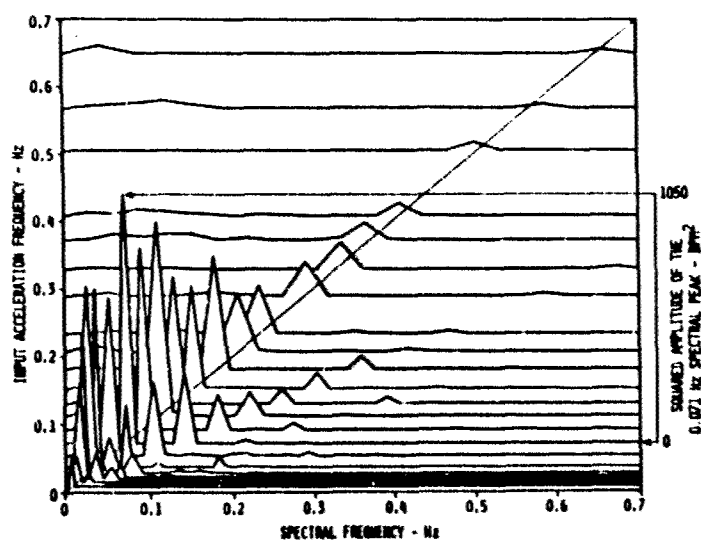


Fig. 5. Orthogonal (3-dimensional) representation of heart rate response versus spectral frequency, as a function of input acceleration frequency, for one nonblocked animal during exposure to 0.008 - 0.650 Hz, $\pm 2 G(z)$ sinusoidal acceleration.

C. Grouping of Data, Statistical Treatment

While the presentation of data for individual animals is appropriate to emphasize specific aspects of acceleration-induced cardiovascular responses, the presentation of group data is desirable in so far as it serves to demonstrate the similarity of responses of all animals, facilitate the comparison of nonblocked and autonomically-blocked responses, and the identification of frequency-dependent trends in the responses. Due principally to practical hardware limitations associated with the operation of the centrifuge facility, acceleration test frequencies were not matched exactly for individual subjects during the nonblocked and blocked runs, nor from one animal to the next. Consequently, for the presentation of group responses, the data are grouped into nine frequency ranges and averaged. The frequency ranges are given in Table 1, and have been selected so that each animal is represented within a given range for both the nonblocked and blocked runs. In cases where an individual subject was run at more than one test frequency within a frequency range, the subject's data were averaged. The data for all animals were then averaged and statistically compared, by frequency range, for both the nonblocked and blocked states, using an analysis of variance test called Treatments-By-Subjects Design (38). Completely Randomized Design was also used to check for carry-over effects from one treatment to the next, which is not tested for with the Treatments-By-Subjects Design. After the analysis of variance is satisfied, a t-Test for the Difference Among Several Means derived from Treatments -By-Subjects Design is used to determine which means differ from each other. In order not to violate the Probability Theory, all treatments are tested, as seen in Table 1. Table 1 is a comparison of group means of various cardiovascular response variables by frequency range, in the nonblocked versus blocked states, with levels of significance for the difference between means appropriately indicated.

Table 1.

STATISTICAL COMPARISON OF UNBLOCKED VERSUS AUTONOMICALLY BLOCKED GROUP MEANS of variables for nine frequency ranges; using a t-Test for Difference Among Several Means, with two-tailed alpha levels (derived from Treatment-By-Subjects Design, repeated measures on one factor). ^a The level of significance is as indicated, with blanks denoting a $P > .05$ (not significant).										
	.005 to .012 Hz	.012 to .021 Hz	.021 to .032 Hz	.032 to .052 Hz	.052 to .077 Hz	.077 to .110 Hz	.110 to .150 Hz	.150 to .200 Hz	.200 to .250 Hz	
AP mean amplitude	.01	.01	.001	.01	.01					
AP phase	.06	.01	.06	.06	.06	.06	.06	.06	.06	
DRVP mean amplitude	.06									
DRVP phase	.06									
ER mean amplitude	.001	.01	.001	.001	.01	.01				
ER phase			.06							
AF mean amplitude	.01		.06	.06	.06	.06	.06	.06	.06	
AF phase	.06	.01	.01	.001	.01	.01	.06	.06	.01	
HR mean amplitude										
HR phase ^b	.06	.06	.001	.001	.001	.001	.001	.001	.01	
SF mean amplitude	.001	.01	.01	.001	.01	.01	.001	.001	.001	
SF phase	.001	.01	.001	.001	.001	.01	.001	.001	.01	

^aRefer to text for further description^bAutonomically blocked phase values not available

RESULTS

Data from eight dogs were available for analysis. Since a comparison of nonblocked and blocked responses was a principal concern in this study, one subject was dropped from consideration due to loss of blockade during the experiments. Two other animals were dropped, because of malfunctioning pressure or flow instrumentation. The resulting group of five animals (hereafter referred to as the "group") consisted of two females and three males.

Both the graphical and verbal presentations will be based primarily on a comparison of the nonblocked and blocked group response of particular cardiovascular variables as a function of acceleration frequency. In addition, it should be noted that the data has not been normalized with respect to acceleration level (i.e., response value per G) since the acceleration input or forcing function was of a constant 2 G amplitude.

With reference to Figure 4 it can be seen that while the input function (ACC) is sinusoidal, the output responses (AP, DRVP, AF and HR) are definitely nonsinusoidal, implying a nonlinear input/output relationship. In cases where output oscillations are seen, however, they contain a major component at the same frequency as the input acceleration frequency. Thus the input/output relationship will be presented using a "describing function" technique (39); a frequency-response method for handling nonlinear systems.

The graphical representation of the response of each variable will generally include the following information for both the nonblocked and blocked tests: 1) mean value of the response for control and recovery periods (pre and post-acceleration respectively) and for the acceleration series, and 2) the amplitude and relative phase of the first (fundamental) Fourier component of the response, as a function of acceleration frequency (output lagging input denoted by positive phase angles). Dots above and below each data point indicated the range of the Standard Error of the Mean (SEM).

Since sinusoidal acceleration was the primary stimulus applied to the cardiovascular system, the response of the measured variables (AP, DRVP, AF and HR) and calculated variables (ER and SF) will be examined initially from the standpoint of their relationship to acceleration.

The response of the controlled variable, aortic pressure (AP) is shown in Figure 6. After the initiation of the acceleration run there is an overall stress response, indicated by a 10-30 mm Hg increase in AP mean. This increased pressure is maintained throughout the entire test series, at an almost constant level, and remains into the recovery period. Except for the pre-acceleration control period, there was no significant difference between blocked and non-blocked AP means. On the other hand, blocked AP amplitude has a significant frequency dependent response, with a peak of 18 mm Hg at 0.04 Hz, and a tendency toward reduced oscillations at higher frequencies. Viewing blocked AP amplitude as the passive acceleration-induced "open loop" input to the baroreceptors, and comparing these oscillations with the nonblocked AP amplitude response, it can be seen that reflex barostatic mechanisms are able to achieve a significant degree ($P > .01$) of reflex adjustment for frequencies up to about 0.08 Hz. Above this frequency there was no significant difference between non-blocked and blocked AP amplitude, indicating a lack of effective regulatory response. These features of the AP response are better illustrated in Figure 7, which shows the relative nonblocked/blocked response. Of special interest in Figure 7 is the relative AP amplitude which is equal to the (nonblocked/blocked) AP amplitudes from Figure 6. With a value of 1.0 denoting no compensatory regulation, relative AP amplitude indicates a 30-35% reflex adjustment of the passive (i.e., blocked) acceleration-induced pressure disturbances up to 0.07 Hz. Blocked AP phase (Figure 6) exhibits a definite frequency-dependent trend, but essentially lags acceleration by 180° , thus supporting the contention that the oscillatory blocked AP response represents a passively-produced (i.e., "Hydraulic") pressure disturbance within the cardiovascular system. Nonblocked AP phase was similar, but shifted by approximately $30-40^\circ$.

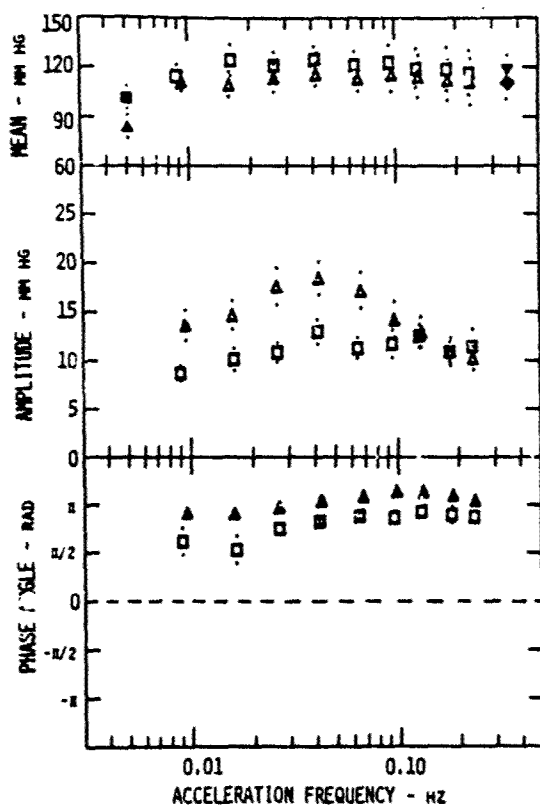


Fig. 6. AORTIC PRESSURE: mean, amplitude and phase of the first Fourier component with respect to acceleration (□ unblocked, Δ autonomic blockade, ■ control and ● recovery values; : SEM) for a group of 5 animals.

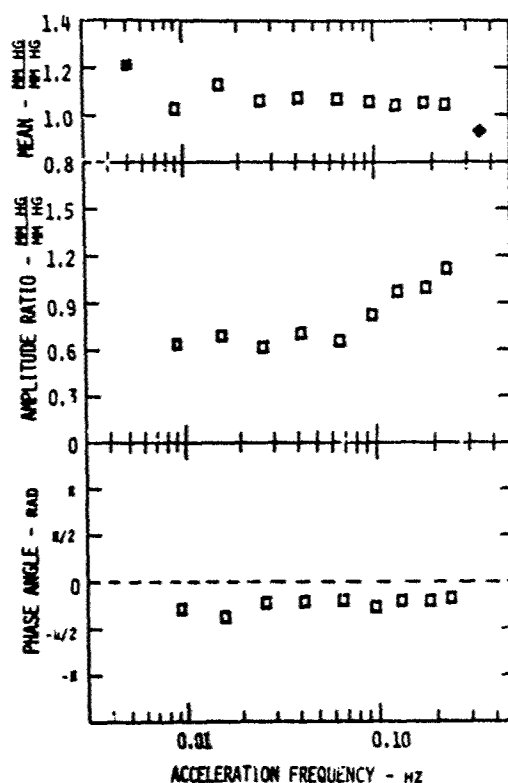


Fig. 7. RELATIVE UNBLOCKED/BLOCKED AORTIC PRESSURE RESPONSE: mean ratio, amplitude ratio and relative phase of the first Fourier components as a function of acceleration frequency, for a group of 5 animals (■ control and ● recovery values).

In contrast to AP, the response of diastolic right ventricular pressure (DRVP, which is roughly equivalent to central venous pressure) is essentially identical for both blocked and nonblocked cases, as Figure 8 shows. During the acceleration series there is a slight elevation (3-5 mm Hg) in DRVP mean from the control/recovery levels, which is probably indicative of an overall systemic pressor response, as was seen in AP mean. The response of DRVP amplitude ranges from 5 to 12 mm Hg, with an apparent (although not significant) trend toward greater oscillatory amplitudes at higher frequencies. Finally, there is a constant 180° lag of DRVP phase with respect to acceleration. These DRVP amplitude and phase data indicate that for the frequency range from 0.008 to 0.25 Hz, the venous system essentially responds to acceleration as a passive element in the circulatory network (i.e., is not a controlled variable). This is not to say, however, that the mean level of central venous pressure is not controlled (e.g., DRVP mean response), nor that venous pressure oscillations are not sensed and do not provide efferent information to the barostatic regulatory mechanisms.

Since the AP data (Figures 6 and 7) indicate some level of effective barostatic regulation, it is important to determine the participation of vascular and cardiac mechanisms in these responses. The first of these mechanisms, effective systemic resistance (ER), is shown in Figure 9. As noted previously, ER is a calculated variable, defined as $(AP-DRVP)/AF$, where AF is aortic flow. Consequently, while ER is not a rigorous measure of resistance on the peripheral vascular level, it does represent an index of the overall or composite level of systemic vascular (resistance) activity. The apparent pressor reflex noted in the rise of AP mean and DRVP mean during acceleration is also seen in the ER mean response for frequencies up to 0.04

Hz. At the onset of the acceleration run, ER mean goes from a control value of 40-50 mm Hg/(L/min) to approximately 65 mm Hg/(L/min) for both the blocked and nonblocked cases. The nonblocked and blocked values of ER mean are not significantly different during either the acceleration series or in the recovery period. Both are essentially constant (65-70 mm Hg/(L/min)) up to 0.04 Hz, with a decreasing trend at higher frequencies. Nonblocked ER amplitude and phase are highly frequency-dependent. The amplitude increases from about 8 mm Hg/(L/min) at 0.008 Hz to a maximum resonant peak of approximately 12 mm Hg/(L/min), followed by a decrease to a value around 4 mm Hg/(L/min) above 0.13 Hz. Nonblocked ER phase increases with acceleration frequency, from 0° at 0.008 Hz to about 150° at 0.065 Hz remaining $150-180^\circ$ out of phase with acceleration above 0.065 Hz. These nonblocked ER amplitude/phase data indicate roughly an underdamped second-order response. The blocked ER amplitude response is, however, essentially invariant with frequency (about 4 mm Hg/(L/min)) from 0.008 to 0.25 Hz, indicating that it may represent a nonreflexive baseline or residual level resulting from nonneural factors. Consequently, the difference between the nonblocked and blocked ER amplitude can be taken as the actual active baroreflex-mediated systemic vascular (resistance) response. Furthermore, these ER amplitude data indicate that the pharmacological blockade does in fact inhibit neurally-mediated systemic vascular activity.

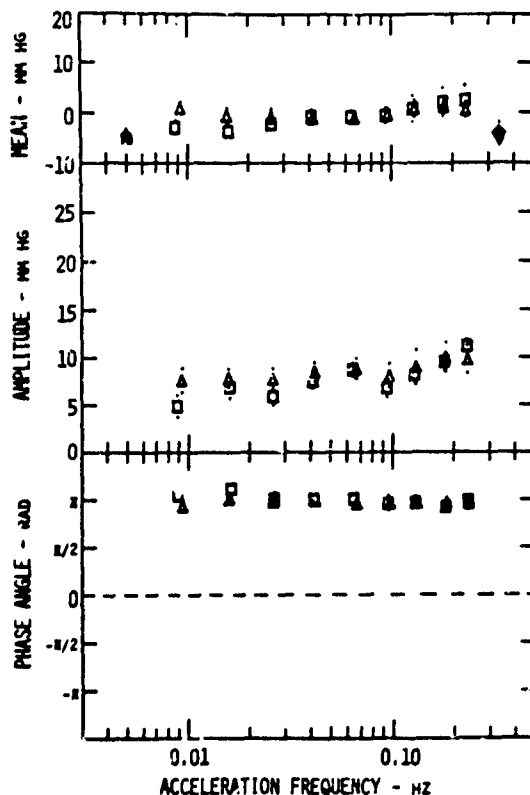


Fig. 8. DIASTOLIC RIGHT VENTRICULAR PRESSURE: mean, amplitude and phase of the first Fourier component with respect to acceleration (\square unblocked, \triangle autonomic blockade, \blacksquare control and \blacklozenge recovery values, \pm SEM) for a group of 5 animals.

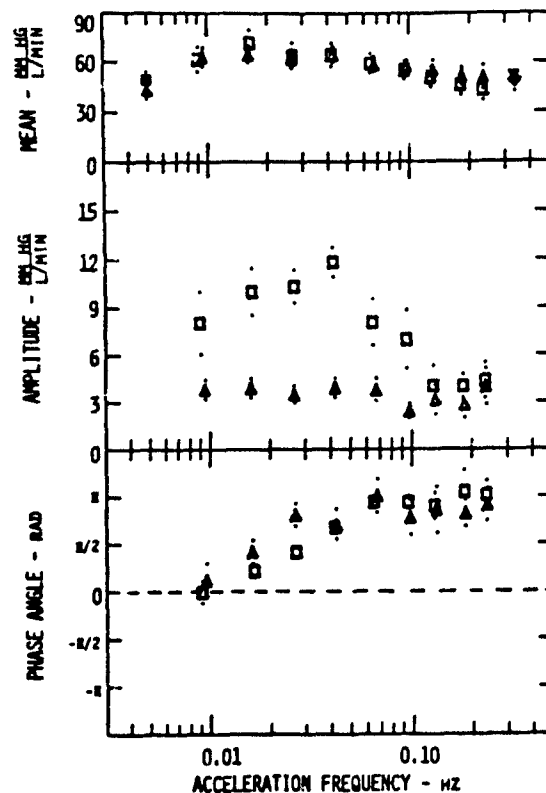


Fig. 9. EFFECTIVE SYSTEMIC RESISTANCE: mean, amplitude and phase of the first Fourier components with respect to acceleration (\square unblocked, \triangle autonomic blockade, \blacksquare control and \blacklozenge recovery values, \pm SEM) for a group of 5 animals.

The response of aortic flow (AF, equal to cardiac output minus coronary flow), the second determinant of AP is shown in Figure 10. There was a marginally significant difference ($P > .05$) between the nonblocked and blocked AF mean response during acceleration. In both cases AF mean tended to increase with higher acceleration frequencies. This trend in AF mean, along with the tendency of ER mean to decrease at higher frequencies (Figure 9), resulted in a more or less constant level of AP mean (Figure 6) throughout the entire frequency range. Control AF mean levels were equal to or slightly greater than the low frequency values (1.8-2.2 L/min), while the recovery levels reflected the larger, high frequency values (2.3-2.5 L/min). The nonblocked AF amplitude response was approximately twice the blocked response for frequencies above 0.02 Hz, demonstrating the effect of heart rate oscillations (an influence only in the nonblocked tests). At frequencies below 0.02 Hz there was no significant difference between non-blocked and blocked AF amplitude. Both the nonblocked and blocked AF oscillations were about 180° out of phase with acceleration in the low frequency range, and lagged progressively more at higher frequencies. The large difference between nonblocked and blocked AF phase in the range from 0.02 to 0.13 Hz is another consequence of heart rate oscillation, which occurred (only) during the nonblocked tests.

Since the behavior of AF responses during acceleration is directly determined by both heart rate and stroke volume changes, the response of these variables will be presented next. Heart rate (HR) is shown in Figure 11. The first feature of HR response to note is that the autonomic blockade did effectively inhibit reflex heart rate changes. Blocked HR mean was a constant 135 bpm (beats per minute) throughout the acceleration.

ation series, and for the control and recovery periods. Blocked HR amplitude was less than 3.5 bpm, so that blocked HR phase could not be calculated with accuracy, and is therefore not shown. Nonblocked HR mean increased from a resting, control level of 107 bpm to a relatively constant 120-125 bpm during the acceleration series, reflecting the overall pressor response seen in previous variables. Nonblocked HR amplitude is highly frequency-dependent, with relatively small oscillations of approximately 8 bpm at 0.008 Hz, increasing to a maximum of 22 bpm at 0.04-0.06 Hz, and then decreasing to 9 bpm at 0.23 Hz. At the same time, HR phase leads acceleration by approximately 90° at 0.008 Hz, then increases progressively with frequency through 0° at 0.05 Hz, to a maximum lag of 90° at 0.23 Hz. These amplitude/phase data suggest an underdamped second-order type of response.

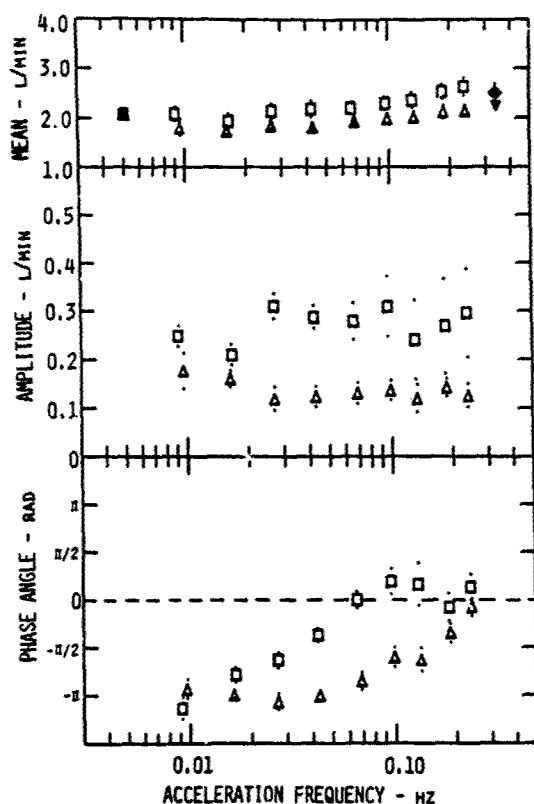


Fig. 10. AORTIC FLOW: mean, amplitude and phase of the first Fourier component with respect to acceleration (\square unblocked, Δ autonomic blockade, \blacksquare control and \blacktriangle recovery values, \pm SEM) for a group of 5 animals.

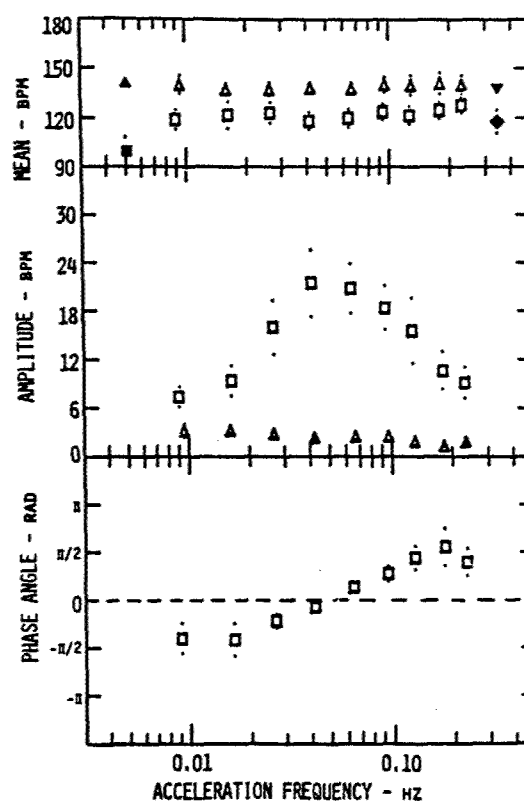


Fig. 11. HEART RATE: mean, amplitude and phase of the first Fourier component with respect to acceleration (\square unblocked, Δ autonomic blockade, \blacksquare control and \blacktriangle recovery values, \pm SEM) for a group of 5 animals.

Stroke flow (SF, approximately equal to left ventricular stroke volume) is shown in Figure 12. Nonblocked SF was consistently 5-7 ml/b greater than blocked SF for both the control and recovery periods, and during the acceleration series. Noting the reciprocal relationship between HR and SF, this was probably due largely to the higher blocked versus nonblocked HR means shown in Figure 11. Nonblocked and blocked SF mean both increased with frequency, approaching their control/recovery values at the high end of the frequency range. The low frequency decrease of SF mean from control/recovery levels is probably due to increased arterial output impedance (overall pressor response noted in AP mean and ER mean, Figures 9 and 6) at the lower end of the frequency range, while the high frequency recovery of SF mean reflects a relaxation of this pressor activity above 0.05 Hz. Due to the influence of nonblocked HR amplitude and the higher level of nonblocked SF mean, the nonblocked SF amplitude is roughly 2-3 times the response of blocked SF amplitude. Nonblocked SF amplitude shows a slight peaking behavior at about 0.04 Hz, within the frequency range where heart rate has maximal oscillations. On the other hand, blocked SF amplitude is essentially frequency-invariant from 0.008 to 0.23 Hz. There was no significant difference between nonblocked and blocked SF phase. Both were 180° out of phase at low frequencies, then showed a further lagging tendency with increasing frequency.

The data presented above indicate a significant neurally-mediated response of cardiac and vascular mechanisms during exposure to low frequency, whole body acceleration. It is important to recognize, however, that these reflex mechanisms are probably responding primarily to intravascular pressure/flow disturbances produced by the acceleration stress, not the acceleration itself (except for possible vestibular involvement [25,29], Fig. 1). Therefore, in order to model the barostatic reflex activity seen in the experimental data, the cardiac and vascular control mechanisms will be viewed primarily from the standpoint of pressure as the sensed, as well as the controlled variable. This will be done in the following section.

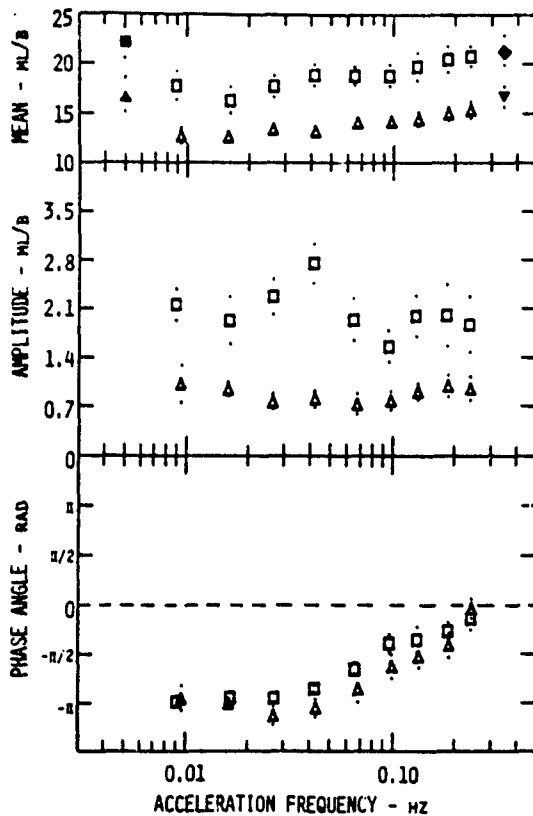


Fig. 12. STROKE FLOW: mean, amplitude and phase of the first Fourier component with respect to acceleration (□ unblocked, Δ autonomic blockade, ■ control and ● recovery values, \pm SEM) for a group of 5 animals.

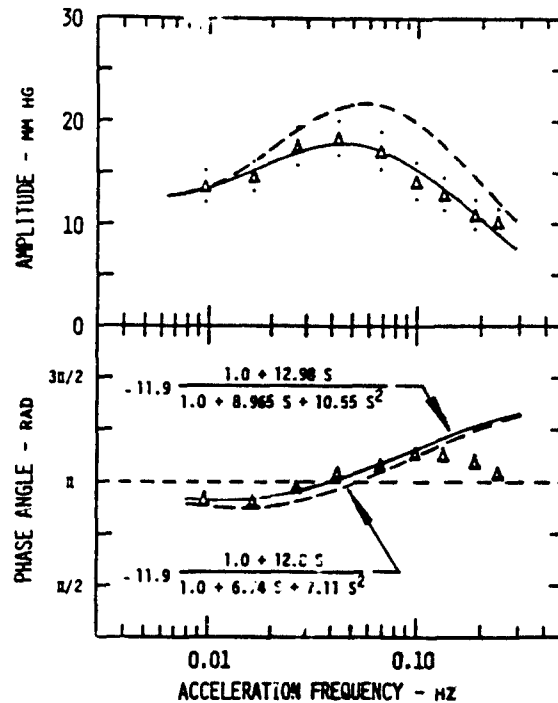


Fig. 13. AUTONOMICALLY BLOCKED AORTIC PRESSURE RESPONSE: — the author's single-zero double-pole transfer function fitted to the experimental Fourier amplitude and phase values (Δ , \pm SEM), and --- the single-zero double-pole acceleration-to blood pressure transfer function for humans from Gillingham [25].

RESPONSE MODELING

In addition to providing heretofore unavailable information about the low frequency dynamics of integrated barostatic cardiovascular regulation during exposure to a natural, noninvasively-applied stress, the results of these studies constitute a quantitative data base from which to mathematically model the major components of the baroreflex control network. The approach taken in this study was to derive empirical linear transfer function, using "describing function" techniques, to characterize the general reflex action of the major cardiac and vascular control components, within the context of normal integrated barostatic regulation. Although not part of the present work, it is intended that these transfer functions be incorporated into an existing passive circulatory model (3,40) which is part of an available simulation package (41), designed to run on a PDP-11/10 minicomputer system having limited core storage capabilities.

The transfer functions to be presented are generally of proportional or proportional-plus-derivative second-order form, with some having exponential transportation lag terms. Higher order terms were not included in the derived transfer functions for several reasons: 1) Most often the low frequency dynamics of the baroreflex mechanisms have been adequately modeled as first or second-order controllers, with input/output time lag terms in particular instances. In addition, the amplitude/phase data in the present study seem to reflect roughly a second-order type of response. Consequently, it was felt that higher order terms would not be necessary, to achieve a reasonable approximation of the experimental responses. 2) Also, the eventual incorporation of the transfer functions into a total cardiovascular model would be made somewhat more difficult by the addition of higher order terms.

A. Acceleration-Induced Pressure Disturbances

The first step is to develop a transfer function for the arterial pressure disturbances generated by whole body acceleration within the passive, nonreflexive cardiovascular system. These passively produced arterial pressure disturbances are given by the blocked AP amplitude/phase data in Figure 13, and are important because they represent: 1) the acceleration-to-arterial pressure response characteristics that must be realized in a passive, noncontrolled circulatory model before baroreflex components can be added, and 2) those pressure changes which the baroreflex mechanisms should act to minimize (i.e., the "open loop" input to the baroreceptors). These data were least squares fitted with an acceleration-to-arterial pressure transfer function of the form:

$$\frac{AP}{ACC}(s) = -5.05 \frac{(1.0 + 12.98s)}{1.0 + 8.965s + 10.55s^2}$$

[2]

where AP = blocked aortic (arterial) pressure
 ACC = input acceleration, of 2G amplitude
 s = complex quantity, $j\omega$
 ω = circular frequency rad/sec.

This proportional-plus-derivative, second order response indicates a highly damped (damping coefficient, $\xi = 2.76$) system with an undamped natural frequency of 0.049 Hz. Note that the leading gain term of the transfer function depicted in Figure 13 is twice that given by Equation 2, reflecting the 2G acceleration amplitude employed in the present study.

Although the blocked AP response represents the pressure disturbance generated by whole body acceleration within the passive noncontrolled arterial system and is, therefore, an approximation of the open loop input to the baroreceptors, it was not the input seen by the baroreceptors during the nonblocked acceleration tests. In the nonblocked tests, since the barostatic regulatory mechanisms are functioning in a closed loop integrated fashion, the input to the baroreceptors is more properly approximated by the nonblocked AP response. As a result, the derivation of transfer functions for baroreflex action of the individual cardiac and vascular control mechanisms was approached from the standpoint of nonblocked AP response as the input variable.

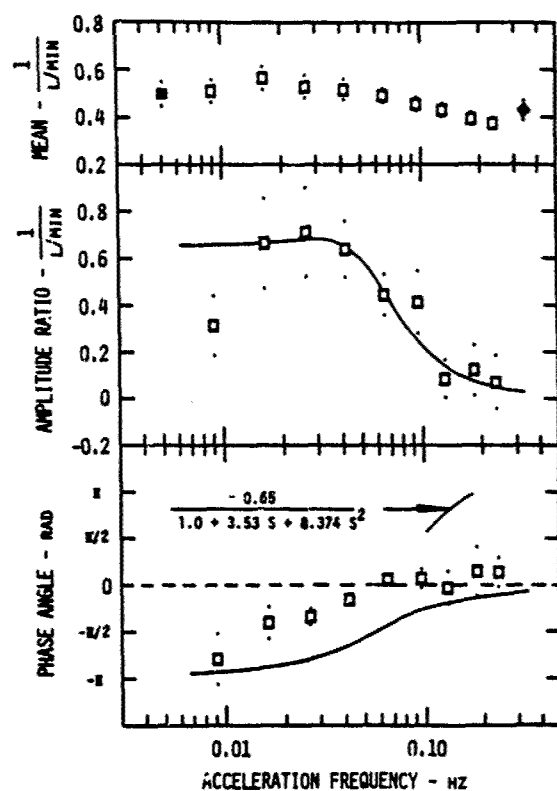


Fig. 14. RELATIVE RESISTANCE / AORTIC PRESSURE RESPONSE: the mean ratio, amplitude ratio and relative phase of the first Fourier components as a function of acceleration frequency, for a group of 5 unblocked animals (■ control and ♦ recovery values, \pm SEM).

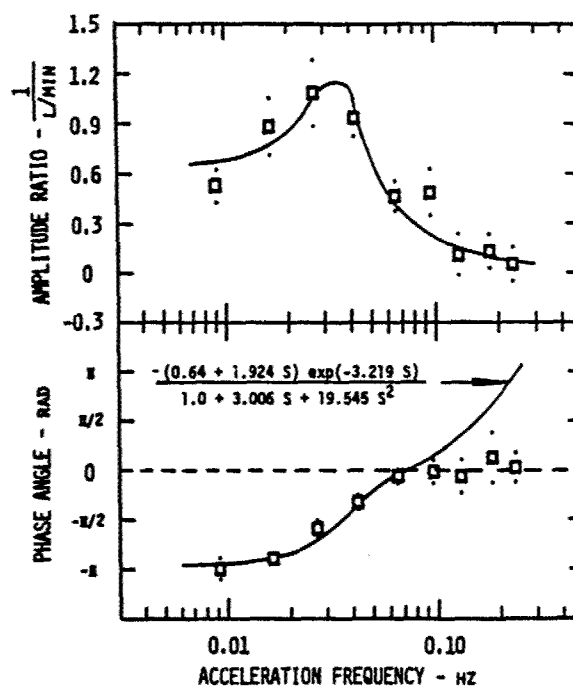


Fig. 15. RELATIVE RESISTANCE / DIASTOLIC RIGHT VENTRICULAR PRESSURE RESPONSE: amplitude ratio and relative phase of the first Fourier components as a function of acceleration frequency, for a group of 5 unblocked animals (■ control and ♦ recovery values, \pm SEM).

B. Systemic Vascular Mechanisms

The relative aortic pressure-to-effective systemic resistance response was calculated for individual animals. The group data were then compiled, and are presented in Figure 14. The top panel of Figure 14 shows the ratio of nonblocked ER mean to nonblocked AP mean, and is included to emphasize the high frequency decrease of ER mean reported earlier in the presentation of results. The relation ER amplitude was calculated as the difference between nonblocked and blocked ER amplitudes divided by the nonblocked AP amplitude. The difference between nonblocked and blocked ER amplitudes was used in this computation, because it was felt that this was a better index of the active baroreflex-mediated systemic vascular response than nonblocked ER amplitude alone. The relative ER phase, calculated as the difference between nonblocked ER phase and nonblocked AP phase, is also shown in Figure 14. With exception of the lowest frequency (0.009 Hz), it can be seen that the relative ER amplitude data is adequately represented as a critically-damped ($\xi = 1.22$) second-order response, with an undamped natural frequency of 0.055 Hz, of the form:

$$\frac{ER}{AP}(s) = \frac{-0.65}{1.0 + 3.53s + 8.374s^2}$$

[3]

On the other hand, this transfer function yields a predicted relative ER phase that does not match the experimental results. The addition of a time lag term to Equation 3 did not significantly enhance the overall fit of the predicted ER phase, and was therefore not included. It is important to note, however, that the damping coefficient and resonant frequency inherent in Equation 3 fall well within the range of values reported by previous investigators who studied the open loop carotid sinus/arterial pressure response. The present data suggest the arterial pressure-to-systemic resistance transfer relationship is higher than second-order, and that extra higher order terms need be added to Equation 3 in order to obtain an accurate predictive transfer function for the vascular component of the baroreflex control network.

Several investigators (42,43) have verified the existence of sympathetic afferent mechanoreceptors in the right atrium and pulmonary artery, and suggested that these may elicit efferent pressor responses in the peripheral vasculature, in response to changes in venous return or right heart pressure. Taking this suggestion and noting that whole body acceleration produces significant right atrial pressure changes (Figure 8), an attempt was made to derive a DRVP-to-ER transfer relationship. Using nonblocked DRVP instead of nonblocked AP as the input variable, a relative ER was computed, as described earlier. The experimental data based upon this computation are presented in Figure 15, along with a fitted transfer function of the form:

$$\frac{ER}{DRVP}(s) = \frac{-(0.64 + 1.924s)}{1.0 + 3.006s + 19.545s^2} \exp(-3.219s) \quad [4]$$

Equation 4 represents an underdamped ($\zeta = 0.68$) second-order response, with an undamped natural frequency of 0.036 Hz and an input/output time lag of 3.219 sec. Although this transfer function does not have a proven functional basis physiologically speaking, it could be used as a phenomenological predictor of effective systemic resistance (ER) responses for frequencies up to 0.1 Hz.

Two general observations may be made at this point regarding these efforts to model the experimental ER responses: 1) either baroreflex control of integrated, overall systemic resistance activity must be represented by a higher than second-order controller, or 2) aortic arch pressure alone is not a suitable input variable for modeling the systemic vascular mechanisms.

C. Cardiac Mechanisms

A relative HR response was computed using the nonblocked AP and HR responses as the input and output variables respectively. These group relative HR data are presented in Figure 16. The slight high frequency increase in relative HR mean probably indicates a reflex response to the high frequency decrease in ER mean (Figures 9 and 14). Relative HR amplitude exhibits a significant peaking response at about 0.06 Hz. A comparison of the phase data in Figure 11 and Figure 16 shows that while HR appears to be leading acceleration at the lowest frequencies, it is actually in "proper" phase with respect to AP, to which it responds. In other words, at the low acceleration frequencies HR increases as AP decreases. It was found that the relative HR amplitude/phase response (Figure 16) could be represented reasonably well as a second-order controller of the form:

$$\frac{HR}{AP}(s) = \frac{-(1.564 + 4.59s)}{1.0 + 2.6314s + 4.5032s^2} \exp(-0.626s) \quad [5]$$

which has an undamped natural frequency of 0.075 Hz, a damping coefficient $\zeta = 1.24$, and a time delay of 0.626 sec. The proportional-plus-derivative input term (numerator) in Equation 5 was suggested by the work of Katona (44) who demonstrated that the afferent baroreceptor firing rate could be modeled with both mean pressure (proportional term) and pulse pressure (derivative term) as input variables. Allison (6) reported a 0.4-1.0 sec time delay between step changes in pressure in the isolated aortic arch (i.e., arch baroreceptors) and reflex changes in heart rate. Similarly, Scher and Young (14) saw a 0.6-1.2 sec lag between step changes in carotid sinus pressure and heart rate response. Consequently, the 0.626 sec time lag term in Equation 5 would seem justified. Enhancement of the low frequency fit of Equation 5 to the relative HR amplitude (Figure 16) could probably be achieved by the addition of a second order term on the input side of the derived transfer function.

As noted in the presentation of results, the response of SF amplitude (Figure 12) appears to be largely frequency-invariant from 0.008-0.23 Hz. This, along with the fact that there was no significant difference between nonblocked and blocked SF phase indicate that the overall SF response to whole body acceleration is not effected neurally, but is rather the result of passive, nonneural factors. Comparing Figures 8 and 12, and noting that oscillations in DRVP and SF are in phase (0° phase difference) at the lower frequencies, one may conclude that the SF response is probably determined primarily by changes in venous pressure or venous return. The progressive lagging response of SF phase at higher frequencies can be explained (and modeled) as a right-to-left heart time lag phenomenon. The nonblocked and blocked SF phase data from Figure 12 were re-plotted on a linear frequency scale, Figure 17, and fitted with a least squares regression line. The results show that the response of SF phase can be modeled by sample time delay of about 2.0 sec, which is in good agreement with the right-to-left heart lag of at least three cardiac cycles reported by Franklin et al. (31) for the response to a rapid right atrial infusion of saline. Consequently, a passive noncontrolled model of the cardiovascular system should include a cardiopulmonary component which yields a passive DRVP-to-SF transfer relationship of the form:

$$\frac{SF}{DRVP}(s) = G_p \exp(-2.17/s) \quad [6]$$

where an approximate value of G_p is 0.12 (ml/b)/mmHg, based upon the blocked DRVP and SF amplitude/phase data from Figures 8 and 12.

The present efforts to model the response characteristics of the cardiac and vascular baroreflex mechanisms have shown that: 1) While there is significant frequency-dependent neural control of the systemic vascular mechanisms below 0.15 Hz, this control can not be satisfactorily modeled as a second-order response based upon aortic pressure as the input, 2) Neural control of heart rate is frequency-dependent below 0.23 Hz,

and can be adequately modeled by a second-order, time lag controller, and 3) Stroke flow response to whole body acceleration is predominantly influenced by passive venous pressure changes.

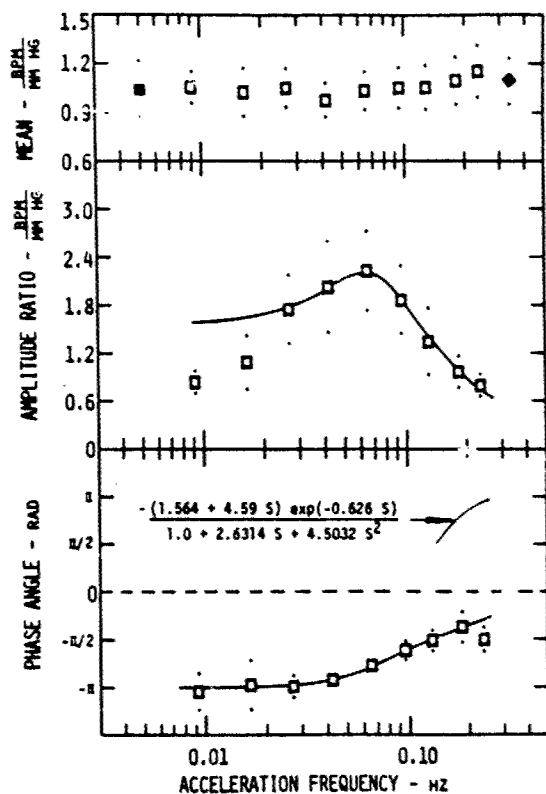


Fig. 16. RELATIVE HEART RATE / AORTIC PRESSURE RESPONSE: mean ratio, amplitude ratio and relative phase of the first Fourier components as a function of acceleration frequency, for a group of 5 unblocked animals (■ control and ● recovery values, \pm SEM).

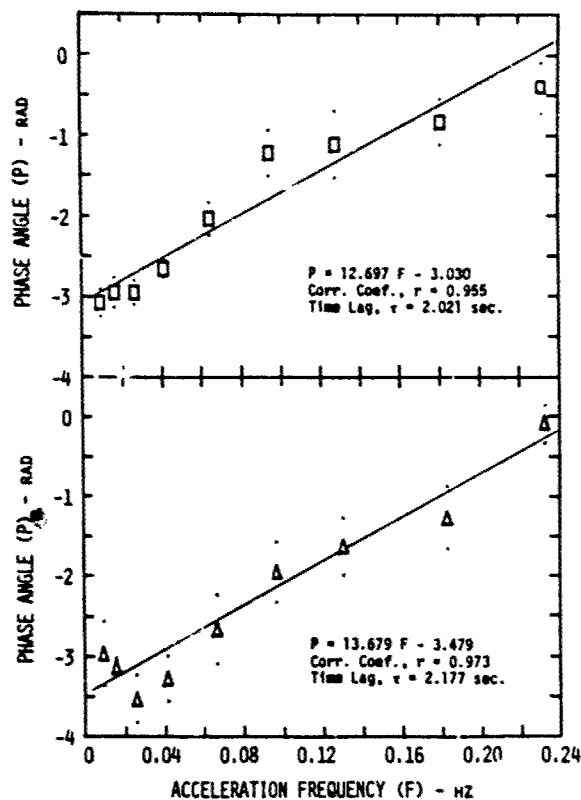


Fig. 17. STROKE FLOW: relative phase of the first Fourier component as a function of acceleration frequency (□ unblocked, Δ autonomic blockade, \pm SEM, and — least squares linear fit) for a group of 5 animals.

DISCUSSION

A. Arterial Pressure Regulation

With the reflex action of the neurally-mediated barostatic mechanisms pharmacologically blocked (Figure 6), the resultant AP oscillations represent the passive, acceleration-induced pressure changes which the cardiac and vascular control mechanisms should act to minimize in the nonblocked animal. A comparison of the amplitude of the nonblocked and blocked AP oscillations, Figure 7, indicates that the barostatic control network is able to achieve a 30-35% attenuation of the passive AP oscillations for frequencies up to 0.07 Hz. Above 0.10 Hz no effective regulation of AP was seen. These general features of the overall control of AP are in good agreement with the results of previous investigators (10,14,16) who have studied (specifically) carotid sinus control of arterial pressure, and reported a critically-damped (flat) second-order type of response, with a corner frequency of 0.04 - 0.06 Hz. Consequently, the results of these previous studies indicate that the carotid sinus reflex is unable to generate significant compensatory arterial pressure responses for input frequencies above around 0.1 Hz. Dynamic carotid sinus-to-systemic arterial pressure "open loop" gains of 2.0 - 6.0 were reported by Scher and Young (14) in dogs, while Grodins (7) reported a similar value of about 1.8. These gain values (G) would suggest that during normal "closed loop" operation, the carotid sinus reflex should be able to achieve a 64-86% attenuation of the "open loop" pressure disturbance [attenuation = $G/(1+G)$]. There is a significant difference between these predicted values and the 30-35% attenuation ($G = 0.43$ to 0.54) seen in the present study. Based upon evidence from the present study, this discrepancy can be explained by the response of acceleration-induced cardiac output fluctuations and the interaction between cardiac and vascular control mechanisms (which were not factors in these previous studies). This point will be addressed later in some detail.

The present results demonstrate a significant frequency-dependence of the passive acceleration-induced arterial pressure disturbance (Figure 13) which can be represented by a highly damped ($\zeta = 2.76$) single-zero double-pole transfer function (Equation 2) with an undamped natural frequency of 0.049 Hz. While similar data is not available for man in a "nonreflexive" state, Gillingham et al. (25) derived a single-zero double-pole acceleration to eye-level arterial blood pressure transfer relationship for awake humans exposed to simulated aerial combat maneuvers. Their transfer function was of the form:

$$\frac{AP}{ACC} (s) = -16.2 \frac{(1.0 + 12.0s)}{1.0 + 6.745s + 7.11s^2} \quad [7]$$

indicating a highly damped ($\zeta = 2.53$) response with an undamped natural frequency of 0.06 Hz. With a suitable adjustment of the leading gain term in order to match the low frequency asymptotes, Equation 7 is plotted in Figure 13 for comparison with Equation 2. This comparison is made simply to illustrate the potential importance of frequencies below 1.0 Hz in acceleration-induced cardiovascular changes in human as well as animal subjects, rather than to imply a functional or physiological basis for comparing responses in normal awake humans to those in autonomically-blockaded canines.

B. Systemic Vascular Control

Since past studies of the dynamic behavior of the carotid sinus/arterial pressure response (preceding discussion) involved the use of vagotomized animals, it was implied (although not reported) that cardiac output was relatively constant and did not influence measured arterial pressure changes. The "open loop" reflex responses were, therefore, attributed to systemic vascular activity and should constitute a basis for comparison with the present ER results (Figures 9 and 14). A comparison of nonblocked and blocked ER amplitude in Figure 14 illustrates that there is a significant neurally-mediated systemic vascular component in the dynamic baroreflex response for frequencies up to approximately 0.10 Hz. Using nonblocked AP as the input variable, a relative ER response was computed, as shown in Figure 14. For all except the lowest input frequencies (about 0.01 Hz), the relative ER amplitude response could be accounted for with a critically-damped ($\zeta = 1.22$) second-order model, Equation 3, with an undamped natural frequency of 0.055 Hz. While this transfer relationship is in good agreement with the results of previous studies of the open-loop carotid sinus/arterial pressure response, it predicts relative phase angles that are significantly lower than those measured experimentally in the present study. A number of factors could explain this discrepancy: 1) Reflex control of the overall systemic vascular response must be represented by a higher-order controller such as the proportional-plus-derivative sensitive, third-order model developed by Scher et al. (16) for composite data concerning the carotid sinus reflex system, 2) Aortic arch pressure alone is not a good index of the input to both the arch and carotid sinus baroreceptors, implying that carotid sinus pressure should have been measured separately in the present study, or 3) Other sensory inputs such as those from vestibular sensors or cardiopulmonary mechanoreceptors (Ref. Equation 4 and Figure 15) play a significant role in the response of vascular mechanisms to whole body acceleration stress.

An interesting feature was noted in the frequency-dependence of the mean systemic resistance level (Figures 9 and 14) during whole body acceleration. In both the nonblocked and blocked tests there was an overall mean system pressor response at frequencies below 0.04 Hz, with an apparent relaxation of this response at higher frequencies. For the nonblocked tests this trend in ER mean would probably be attributed to the "baroreceptor rectification" phenomenon reported by Scher and Young (14) and others (8,17,18,30). However, since this effect was also seen in the blocked tests, several possibilities arise: 1) the phenomenon is due to nonneural, passive or autoregulatory influences or 2) it is a "baroreceptor-rectification" effect which activates mechanisms that are not adrenergic or cholinergic in nature.

C. Cardiac Control

While the responses of the cardiac mechanisms (heart rate and stroke flow) were treated individually in the presentation of results and modeling, several important points are illustrated in the overall cardiac output response (Figure 10). Comparing nonblocked AP and AF phase (Figures 6 and 10), it can be seen that below 0.02 Hz, AF is decreasing at the same time AP is decreasing (i.e., they are roughly in phase), so that cardiac output does not augment or assist ER mechanisms in controlling aortic pressure for this frequency range. This indicates that for frequencies below 0.02 Hz, changes in systemic resistance are the major contributing factor to the minimization of acceleration-induced pressure changes (Figure 6). For frequencies between 0.04 and 0.10 Hz this situation is apparently reversed. Comparing Figures 6, 9, and 10 it can be seen that, within this range, AF and AP are approximately 180° out of phase while ER and AP are in phase, indicating that the AF response is acting to counter changes in AP while the ER response is augmenting AP. Consequently, for frequencies from 0.04 to 0.10 Hz, arterial pressure regulation is achieved principally by changes in cardiac output. Between 0.02 and 0.04 Hz, where some degree of reflexive barostatic regulation is also seen, both cardiac output and vascular resistance changes presumably are contributing factors. Because previous investigators have not looked at integrated baroreflex control, this type of interaction between cardiac and vascular mechanisms has not been reported in the past.

Another feature of the overall cardiac output response to note in Figure 10 is the tendency of AF mean to increase with frequency above 0.05 Hz, in both the nonblocked and blocked states, as compared to low frequency levels. This response could be caused by either, or both, of the following: 1) decreased left ventricular output impedance (decrease in FR mean, Figure 9) or 2) an increase in the relative level of venoconstriction (increased DRVP mean, Figure 8). The net effect of the response of ER mean and AF mean is a roughly constant level of AP mean (Figure 6) throughout the entire frequency range from 0.008 to 0.25 Hz.

Although baroreceptor control of heart rate is well recognized, only in the work of Scher et al. (15) has an attempt been made to quantify the dynamic frequency response of this control, in terms of gain and phase characteristics, with arterial pressure as the input variable. By periodic inflation of a cuff occluder on the ascending aortic arch, Scher et al. generated oscillatory intravascular arterial pressure changes (presumably at both the arch and carotid baroreceptors) in unanesthetized canines. Oscillatory reflex changes in heart interval were measured and the following gain and phase values reported: 0.027 sec/mmHg and 0° at 0.06 Hz, 0.026 sec/mmHg and 20° at 0.14 Hz, and 0.017 sec/mmHg and 40° at 0.25 Hz. Noting that heart rate rather than heart interval was measured in the present study, and allowing for an approximate 180° phase shift in the conversion from one to the other, it can be seen that the data of Scher et al. is qualitatively similar to the present results (Figure 16), i.e. there is a progressive decrease of gain and increase in phase lag from 0.06 to 0.25 Hz. For the range of frequencies examined in the present study (0.008-0.25 Hz), the relative HR response to AP as the input variable (Equation 6) could be accounted for with a proportional-plus-derivative sensitive, critically-damped second-order controller with time lag. This model yielded a good fit to both the amplitude and phase data, with some inaccuracy of the predicted amplitude below 0.02 Hz. The modeled input/output time lag of 0.626 sec, is well within the 0.4-1.2 sec delay range reported previously (6,14) for heart rate response to step changes in carotid sinus pressure.

Results of the present study also indicate that during whole body acceleration loadings, changes in stroke flow are influenced primarily by changes in heart rate (HR) and right heart filling pressure (DRVP). Comparing DRVP response in Figure 8 and blocked SF response in Figure 12, it can be seen that while DRVP amplitude and phase, and SF amplitude are roughly constant throughout the frequency range from 0.008 to 0.25 Hz, SF phase exhibits a progressive phase lag at higher frequencies. This was modeled as a simple proportional-gain plus time-lag response, in Equation 6. The derived time lag of 2.18 sec is in good agreement with the right-to-left heart lag of at least three cardiac cycles reported by Franklin et al. (31) for a rapid right atrial injection of saline. Assuming that there is a comparable quantitative relationship between DRVP changes and SF, and changes in left heart filling pressure and stroke volume, it can be noted that the derived gain of roughly 0.12 (ml/b)/mmHg from Equation 6 is in the low range of values 0.12-0.36 (ml/b)/mmHg reported by Scher et al. (45) for stroke volume changes caused by changes in left ventricular filling pressure. Looking next at the nonblocked SF response (Figure 12), it can be seen that the nonblocked SF amplitudes are considerably larger than for the blocked case, while there is little difference in the phase angle responses. A comparison of nonblocked SF phase with nonblocked HR phase (Figure 11) indicates an approximate 180° phase difference for most of the frequency range from 0.008 to 0.25 Hz. Considering this phase difference, and noting the reciprocal relationship between changes in heart rate and stroke volume, the difference between nonblocked and blocked SF amplitude can be attributed to the influence of HR oscillations in the nonblocked state.

CONCLUSIONS

A number of general conclusions may be drawn from the results of the present study:

1. Sinusoidal whole body spinal-axis acceleration is a suitable noninvasive stimulus for the study, evaluation and quantification of dynamic integrated barostatic cardiovascular regulation, using classical Systems Analysis techniques. This is primarily because oscillatory intravascular pressure disturbances, produced by sinusoidal whole body acceleration, elicit significant oscillatory responses from the major cardiac and vascular barostatic control mechanisms, thus enabling the use of "describing function" analysis to quantitatively represent the frequency response characteristics of these mechanisms.
2. The dynamic (oscillatory) frequency response of the major neurally-mediated baroreflex mechanisms is limited primarily to the frequency range below 0.25 Hz.
3. During whole body acceleration a significant degree of effective dynamic barostatic regulation is achieved only at frequencies below 0.1 Hz.
4. The ability of the "closed loop", integrated baroreflex system to minimize or counteract acceleration-induced arterial blood pressure changes is less than would be predicted from previous studies of the "open loop" baroreceptor/arterial pressure response.
5. Effective barostatic regulation below 0.02 Hz is achieved principally through reflex action of systemic vascular mechanisms, through combined action of cardiac and vascular mechanisms from 0.02 to 0.04 Hz, and principally via the cardiac mechanisms from 0.04 to 0.10 Hz.
6. The frequency response characteristics of the systemic vascular mechanisms cannot be accounted for with a simple first or second-order control model, with aortic arch pressure as the input.
7. The low frequency dynamics of heart rate control can be satisfactorily modeled as a proportional-plus-derivative sensitive, critically-damped second order time lag response, using aortic arch pressure as the input variable.
8. Stroke flow is passively controlled, primarily through changes in right heart filling pressure (venous return) and heart rate, rather than by direct neural factors or changes in arterial output impedance (aortic pressure).

REFERENCES

1. Frazer, T.M. Human response to sustained acceleration. NASA SP-103:10, 1966.
2. Gauer, O.H. and G.D. Zuidema. Gravitational Stress in Aerospace Medicine. Little Brown and Company, Boston: 16, 1961.
3. Knapp, C.F. Models of the Cardiovascular System under Whole Body Vibration Stress, Proceeding of the AGARD Aerospace Medical Panel Specialists Meeting, Oslo, Norway, April, 1974.
4. Marquis, J.A. Low Frequency Dynamics of Cardiovascular Regulation in Canines Exposed to Sinusoidal Whole Body Acceleration. Ph.D. Dissertation, University of Kentucky, 1978.
5. Peterson, D.F., V.S. Bishop and H.H. Erickson. Cardiovascular changes during and following 1-minute exposure to +G_z stress. Aviat. Space Environ. Med. 46(6):755, 1975.
6. Allison, J.L., K. Sagawa and M. Kumada. An open loop analysis of the aortic arch barostatic reflex. Am. J. Physiol. 217 (6):1576, 1969.
7. Grodins, F.S. Control Theory and Biological Systems. Columbia University Press, New York:188, 1963.
8. Herndon, C.W. Servoanalysis of the cardiovascular system. Ph.D. Dissertation, University of Mississippi, 1969.
9. Ito, C.S. Nonlinear effects of carotid sinus pressure changes on peripheral resistance. Annals New York Acad. Sci. 165:796, 1969.
10. Levison, W.H., G.O. Barnett and W.D. Jackson. Nonlinear analysis of the baroreceptor reflex system. Circ. Res. 18:673, 1966.
11. Penaz, J. and R. Burianek. Dynamic performance of vasomotor responses of resistance vessels of the carotid vascular bed in the rabbit. Arch. Int. Physiol. Biochem. 71:499, 1963.
12. Penaz, J., P. Burianek and B. Senard. Dynamic aspects of vasomotor and autoregulatory control of blood flow in Circulation in Skeletal Muscle (O. Hudicka, ed.), Pergamon Press, Oxford: 255, 1966.
13. Scher, A.M. and A.C. Young. Nonlinearity in the control of blood pressure and heart rate. Annals New York Acad. Sci. 16:772, 1969.
14. Scher, A.M. and A.C. Young. Servoanalysis of carotid sinus reflex effects on peripheral resistance. Circ. Res. 12:152, 1963.
15. Scher, A.M., et. al. Sympathetic and parasympathetic control of heart rate in the dog, baboon and man. Federation Proc. 31:1219, 1972.

16. Scher, A.M., et al. Studies on the carotid sinus reflex in Physical Basis of Circulatory Transport: Regulation and Exchange. (Reeve and Guyton, eds). Q.B. Saunders, Philadelphia: 113, 1967.
17. Schmidt, R.M., M. Kumada and K. Sagawa. Cardiovascular responses to various pulsatile pressures in the carotid sinus. Am. J. Physiol. 233(1):1, 1972.
18. Stegemann, J. and U. Tibes. Sinusoidal stimulation of carotid sinus baroreceptors and peripheral blood pressure in dogs. Annals New York Acad. Sci. 16:787, 1969.
19. Skolnick, A. Crew performance requirements in the vibration environments of surface effects ships in Vibration and Combined Stress in Advanced Systems, AGARD CPP-145, Oslo, Norway, 1974.
20. Speakman, J.D., et al. Crew exposure to vibration in the F-4C aircraft during low altitude, high speed flight. AMRL-TR-70-99, Aerospace Medical Research Laboratory, Wright-Patterson Air Force Base, Dayton, Ohio, 1971.
21. Bhattacharya, A. Modification of Cardiac function by Heart-synchronous whole body vibration applied to awake, chronically-instrumented canines. Ph.D. Dissertation, University of Kentucky, Lexington, Kentucky 1975.
22. Edwards, R.G., E.P. McCutcheon and C.F. Knapp. Cardiovascular changes produced by brief, whole-body vibration of animals. J. Appl. Physiol. 32(3):386, 1972.
23. Von Cierke, H.E. and N.P. Clarke. Effects of vibration and buffeting on man in Aerospace Medicine. 2nd edition. (H.W. Randel ed.) Williams and Wilkins Company, Baltimore:108, 1971.
24. Erickson, H.H. and J.R. Ritzman. Cardiovascular responses to repetitive and combat maneuvering acceleration. Proceedings for the 1975 Annual Scientific Meeting of the Aerospace Medical Association, San Francisco:24, 1975.
25. Gillingham, K.K., J.J. Freeman and R.C. McNee. Transfer functions for eye-level blood pressure during +G stress. Aviat. Space Environ. Med. 48(11): 1026, 1977.
26. Sagawa, K., M. Kumada and L.P. Schramm. Nervous control of the circulation in Cardiovascular Physiology (A.C. Guyton and C.E. Jones, eds). MPT International Review of Science, Physiology Series One, University Press Park, Baltimore: 197, 1974.
27. Guyton, A.C., T.C. Coleman and T.C. Granger. Circulation: Overall regulation. Ann. Rev. Physiol. 34:13, 1972.
28. Sagawa, K. The use of control theory and systems analysis in cardiovascular dynamics in Cardiovascular Fluid Dynamics, Vol. 1 (D.K. Bergel, ed.) Academic Press, New York: 115, 1972.
29. Doba, N., and D. Reis. Role of the cerebellum and the vestibular apparatus in regulation of orthostatic reflexes in the cat. Circulation Res. 34:9-18, 1974.
30. Angell James, J.E. and M.B. Daly. Comparison of the reflex vasomotor responses to separate and combined stimulation of the carotid sinus and aortic arch baroreceptors by pulsatile and nonpulsatile pressure in the dog. J. Physiol. 209:257, 1970.
31. Franklin, D.L., R. Van Citters and R.F. Rushmer. Balance between right and left ventricular output. Circ. Res. 10:17, 1962.
32. McCutcheon, E.P. and H.L. Stone. Introduction, the significance of chronically implanted instrumentation in Chronically Implanted Cardiovascular Instrumentation. (E.P. McCutcheon, ed.) Academic Press, New York:3, 1973.
33. McCutcheon, E.P., J.M. Evans and F.H. Wibel. A fabric pouch for maintenance of multiple chronically implanted lead terminations. Proceedings 4th Annual Meeting, BME Society, Los Angeles, 1973.
34. Evans, J.M., C.F. Knapp and T.R. Lowery. Pressor response buffering by beta adrenergic and cholinergic vasodilation in tranquilized dogs. Submitted for publication in Am. J. Physiol. Manuscript No. H30-8R1, May 1978.
35. Knapp, C.F. Response of the cardiovascular system to vibration and combined stress. Annual Progress Report, Air Force Office of Scientific Research Contract No. F44620-74-C-0012, 1976-77.
36. Frazier, F.E. Heart rate response of conscious canines to low frequency (14z) whole-body sinusoidal acceleration. MS Thesis, University of Kentucky, 1978.
37. Richards, P.I. Computing reliable power spectra. IEEE Spectrum: 83, Jan. 1967.
38. Bruning, J.L. and B.L. Kintz. Computational Handbook of Statistics, (2nd ed.) Scott, Foresman and Company, Glenview, Illinois: 18, 1977.
39. Harrison, H.L. and J.G. Bollinger. Introduction to Automatic Controls. International Textbook Company, Scranton, Pennsylvania:331, 1969.
40. Camill, P., C.F. Knapp and J. Collins. Computer modeling of whole body sinusoidal acceleration on the cardiovascular system. Proceedings of the 9th Annual IEEE Region III Convention:25, 1971.
41. Conley, S.W. Software design for simulation and instrumentation. Ph.D. Dissertation, University of Arizona, 1977.
42. Mancia, G., J.T. Shepherd and D.E. Donald. Interplay among carotid sinus, cardiopulmonary, and carotid body reflexes in dogs. Am. J. Physiol. 230(1):19, 1976.
43. Uchida, Y. Afferent sympathetic nerve fibers with mechanoreceptors in the right heart. Am. J. Physiol. 228(1):223, 1975.
44. Katona, P.G. Computer simulation of the blood pressure control of heart period. Sc.D. Thesis, Massachusetts Institute of Technology, 1965.
45. Scher A.M., A.C. Young and T.H. Kehl. The regulation of stroke volume in the resting, unanesthetized dog. Comp. Biomed. Res. 1:315, 1968.

ACKNOWLEDGMENTS

This research was supported by the Air Force Office of Scientific Research (AFSC) Contract #F44620-74-C-0012. The authors wish to acknowledge the assistance of the technical staff of the Wenner-Gren Research Laboratory and the Department of Surgery, in particular Surgical Technicians: C. Woolfolk, M. Gray and D. Cloyd; Computer System Analysts: T. Lowery, B.S., Beaver, B.S., C. Young, M.S., and M. Vannier, M.D.; Data Analysts: C. Fischer and G. Hirsch; Instrumentation Specialists: B. Stanifer; and Typist: J. Wu.

DISCUSSION

DR. H. VON GIERKE (USA)

What are the next steps you plan in your research?

AUTHOR'S REPLY

We try to put relevance to some of the terms we come up with in these transfer forms. We are, for example, trying to add instrumentation to our chronically instrumented animal preparation such that we can measure, say the difference between the carotid sinus pressure and the aortic heart pressure in order to look at those two sensors in the cardiovascular system and to further add terms in these transfer forms.

DR. H. VON GIERKE (USA)

How about applying it to the human? Or do you leave this to the next speaker?

AUTHOR'S REPLY

Well, yes and no. We would be very interested in obtaining any data from human experiments, especially heart rate response. Then, we could compare these data to the animal data and the whole idea of using a chronically instrumented animal could be validated. We could go from the heart rate information to some of the mechanisms that might be responsible for these responses. So we sure would like to be able to fly subjects through all kinds of maneuvers and get heart rate responses. But that's not necessary, we could use regular air combat type maneuvers as well.

DR. K. GILLINGHAM (USA)

I am very gratified to see the material that you have presented. I am also going to take you up on your offer to take bushel baskets full of heart rate data that we have collected over the past several years on human subjects on the centrifuge. I hope you come over with a large luggage allowance and take some of the material from us.

AUTHOR'S REPLY

Thank you Dr. Gillingham. I guess I can thank Dr. von Gierke for getting me into some more trouble.

MATHEMATICAL MODELING OF ARTERIAL OXYGEN SATURATION AND EYE-LEVEL BLOOD PRESSURE DURING $+G_z$ STRESS

Kent K. Gillingham, M.D., Ph.D., and Richard C. McNee
 Biodynamics Branch, Crew Technology Division, and Advanced Analysis Branch, Biometrics Division
 USAF School of Aerospace Medicine, Brooks AFB, TX 78235
 USA

Summary

Mathematical descriptions of the dynamics of human arterial oxygen saturation (SaO_2) and eye-level arterial blood pressure (ELBP) under conditions of varying $+G_z$ stress were obtained by Fourier analysis. Simulated aerial combat maneuvering (SACM) G-stress profiles and the resulting physiologic responses to the G stress provided input-output data from which transfer functions were derived. Ensemble averaging of single-run transfer functions generated enhanced empirical G-to- SaO_2 and G-to-ELBP transfer functions, which were approximated by various synthetic functions. Examination of predictive abilities of the empirical and synthetic transfer functions was accomplished by comparison of predicted and mean actual responses to SACM and non-SACM G-stress profiles.

Introduction

Physiologists are inclined to describe physiologic responses to stress by means of tables and graphs, whereas concise mathematical expressions are traditionally employed by engineers. This is because physiologists and engineers are educated in separate disciplines and function largely independently of one another, and the language barrier resulting from the lack of interaction prevents full appreciation by the one for the utility and limitations of the other's methods. To the engineer, the use of Fourier analysis to find a mathematical relation between a perturbation and the resulting response of a physiologic system seems a straightforward approach, compromised mainly by the notorious nonlinearities and nonstationarities of such systems. To the physiologist, however, the tried-but-true approach of tediously cataloguing each type of response to a variety of perturbations satisfies convention, and avoids the rigors of complex mathematical manipulation. The relative merit of the former approach becomes apparent when the obtained description of the behavior of the physiologic system must be used; i.e., when predictions of its responses to an infinitely variable set of perturbations must be made, and when the function of the system must be communicated efficiently and in a form compatible with other components of a larger model.

Our renewed interest in describing the physiologic response to G stress has come about as a result of the almost incredible maneuverability of the latest generation of fighter aircraft, which can readily challenge a pilot's ability to maintain vision and consciousness during aerial combat. A sound, quantitative understanding of the physiologic mechanisms of G stress and G tolerance is certainly a desirable foundation upon which to develop G-protective strategies. The post hoc analysis of the arterial oxygen-saturation (SaO_2) response to G stress in anti-G suited, straining subjects riding the USAFSAM Human Centrifuge was our initial attempt to apply Fourier analysis to G-stress data (3). The moderate success of this venture encouraged the undertaking of another study, specifically designed for Fourier analytic techniques, in which a description of the eye-level arterial blood-pressure (ELBP) response to G stress in relaxed humans was sought (4). The procedures employed and the results obtained in these two studies will be recounted briefly.

G-to- SaO_2 Transfer Function

Inspection of a typical time-domain display of the G-stress forcing function and ear-oximeter SaO_2 response in the data collected by Burton, et al (1) (Fig. 1) suggested that sufficient spectral richness might be present in the simulated aerial combat maneuvering (SACM) G-stress profile to obtain a useful transfer function. To test this idea, the Fourier transform of the output SaO_2 response was divided by the Fourier transform of the input G stress to obtain the G-to- SaO_2 transfer function, $H(f)$, which was inspected for signs of mathematical shapeliness underlying the random-noise irregularities. Observing what appeared to be a kernel of true form in the transfer function, we multiplied it by the Fourier transform of a different input G stress for which we had response data, and compared the inverse transform of the product--predicted SaO_2 response--with the actual SaO_2 response. Fig. 2 shows how the predicted response to a 60-sec, 6-G pulse was similar to, and at least as well behaved as, the actual SaO_2 response. We then obtained a G-to- SaO_2 transfer function with an improved signal-to-noise ratio by ensemble averaging the 12 individual transfer functions from the runs of four different subjects riding the same SACM G profile at three different seatback angles (23°, 28° and 40°) (Fig. 3 and Table I). By multiplying this average transfer function, $\bar{H}(f)$, by the transform of the 60-sec, 6-G pulse, and inverse transforming the product into the time domain, the predicted mean response to the G pulse was generated. The predicted mean response and the actual mean response again showed encouraging similarities (Fig. 4.). The early rise in saturation, the subsequent gradual fall, the bottoming out of the response, a short-lived dip in saturation at the offset of acceleration, and the less-than-instantaneous return to normal saturation were evident in both the predicted and actual responses, although the correlation during the recovery phase was admittedly imperfect.

The voluntary informed consent of the subjects used in this research was obtained in accordance with AFR 80-33. The research reported in this paper was conducted by personnel of the Crew Technology and Biometrics Divisions, USAF School of Aerospace Medicine, Aerospace Medical Division, AFSC, United States Air Force, Brooks AFB, TX.

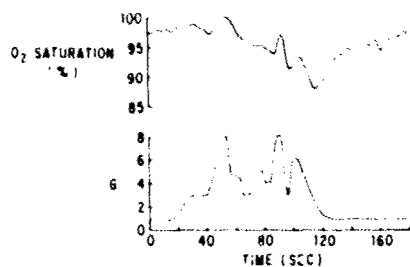


Fig. 1. Typical SaO_2 response (above) to SACM G stress (below). Data are from subject CK in 23° seat.

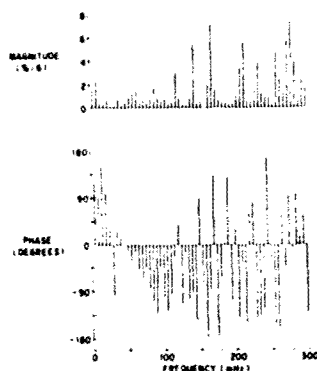


Fig. 3. Ensemble-averaged, 4-subject, 12-run transfer function for SaO_2 response to G stress.

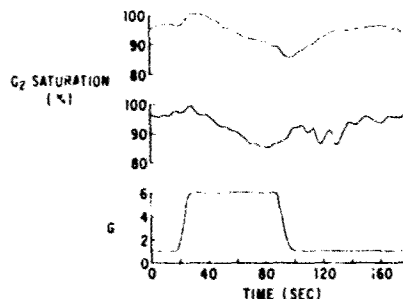


Fig. 2. Predicted (above) and actual (middle) SaO_2 responses to sustained 6-G pulse (below) for subject CK in 23° seat.

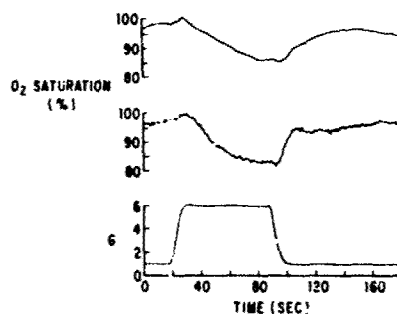


Fig. 4. Predicted mean SaO_2 response (above) and actual mean response (middle) to 6-G pulse (below) of 4 subjects run at 3 different seatback angles.

The next task was to determine the mathematical form of the average transfer function. Not having ready access at that time to a method for determining unknown frequency-domain parameters of a transfer function, we elected to shape an impulse response (the inverse Fourier transform of a transfer function) by trial-and-error manipulation until its frequency-domain equivalent seemed to match the average transfer function derived empirically. The average impulse response, $h(t)$ [the transform of $H(f)$], provided a starting point for the process of synthesizing the desired impulse response. By successively truncating $H(f)$ to eliminate high-frequency noise from $h(t)$, we were able to discern an early positive wave peaking at about 2 sec, followed by a negative-going, oscillating, negative-exponential recovery wave with a time constant of approximately half a minute. The synthetic impulse response finally derived, and its frequency-domain equivalent, are shown in Fig. 5. Mathematically, the synthetic impulse response is described thus:

$$\begin{aligned} \text{SaO}_2 &= 0, & t < 1.17 \\ &= 100, & 1.17 \leq t \leq 1.95 \\ &= 0, & 1.95 < t < 4.69 \\ &= -19.5 \exp[-(t-4.69)/37.5], & t \geq 4.69 \end{aligned}$$

where SaO_2 is arterial oxygen saturation in %, and t is time in seconds. The reasonable performance of the transfer function obtained by trial-and-error impulse-response shaping can be seen in Figs. 6 and 7. In Fig. 6, the actual mean SaO_2 response to the SACM G stress is compared with the response predicted by the synthetic transfer function. In Fig. 7, the predicted response to the 6-G pulse based on the empirically determined average transfer function is compared with the predicted response based on the synthetic transfer function.

It was not surprising that the synthetic impulse response took the form that it did. The negative-exponential recovery portion of the impulse response of the G-to- SaO_2 system indicates that the dynamics of lung tissue under G stress are those of a first-order system, wherein the rate of restoration of the anatomic relations in the lung--and, therefore, the rate of restoration of SaO_2 --is proportional to the remaining amount of G-induced distortion. The negative direction of the SaO_2 displacement during the negative-exponential recovery signifies that, in general, an increase in acceleratory stress results in a decrease in oxygen saturation. The 4.69-sec delay before the onset of the desaturation in the synthetic impulse response represents the circulation time between the lungs and the ear oximeter during G stress. The early positive spike in the impulse response describes the anticipatory rise in saturation that most subjects exhibited at the time the G-stress began to change to a higher level. This effect probably resulted from hyperventilation and/or hyperarterialization of the ear occurring in conjunction with the straining maneuver begun several seconds in advance of the increase in G load. The peak of the spike at 1.56 sec in the impulse response suggests that the straining actually began about 3 sec in advance of the increase in G stress, since a 4.69-sec delay in the overall response was evident as

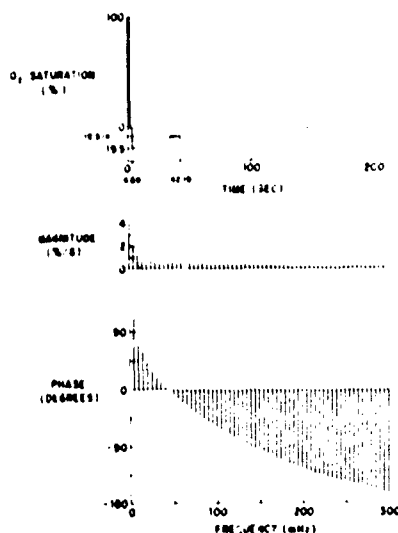


Fig. 5. Synthetic impulse response (above) and associated transfer function (below) used to predict SaO_2 in Figs. 6 and 7.

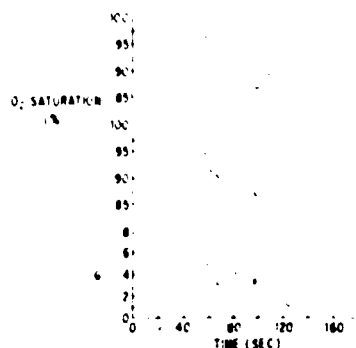


Fig. 6. Actual mean response (above) and mean response predicted by synthetic transfer function (middle) to SACM G stress.

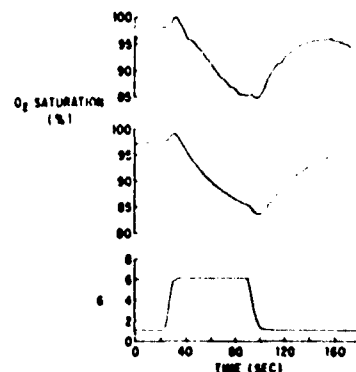


Fig. 7. Predicted response to 6-G pulse based on 4-subject, 12-run, average transfer function (above) and predicted response based on synthetic transfer function (middle).

Further manipulation of the synthetic impulse response would have further improved the quality of the predictions; but the goal of obtaining reasonable predictive performance from simple mathematical expressions, based on the data available, was accomplished to our satisfaction.* The successful use of Fourier analysis in obtaining a mathematical description of a dynamic physiologic function was demonstrated by the development of the G-to- SaO_2 transfer function. This method was, therefore, employed again--this time under experimental conditions designed specifically for Fourier analysis--in an attempt to describe in simple terms the dynamics of the human eye-level arterial blood-pressure response to G stress.

G-to-ELBP Transfer Function

Three healthy, male, 24, 25 and 26 year-old volunteer members of the USAFSAM Acceleration Stress Panel provided the data reported herein. The left radial artery of each was cannulated with a 5-cm, 18-gauge catheter; saline-filled, noncompliant tubing connected the arterial catheter to a Statham P37 pressure transducer mounted on a headband at eye level. The output voltage of the pressure transducer, corresponding to instantaneous eye-level blood pressure, was recorded on magnetic tape. Subjects were exposed in a seated (13° seatback angle), relaxed condition--without benefit of anti-G suit or straining maneuver--to three different categories of $+G_z$ stress on the centrifuge: 1) gradual-onset runs (GORs), in which the G load increased linearly with time at the rate of 0.067 G/sec; 2) rapid-onset runs (RORs), in which the G load rose at 1.0 G/sec to a predetermined level and remained at that level for either 15 sec or 1 min; and 3) simulated aerial combat maneuvers (SACMs), in which G loads were applied in a varying manner over a 100-sec period. The SACM G-stress profiles were of eight different shapes, each profile having been produced by a random function generator with bandwidth set to match the capabilities of the USAFSAM Human Centrifuge; some profiles were augmented or clipped, as necessary, to challenge the subjects' visual functioning without rendering them unconscious. Subjects were instructed to relax completely during all test runs, and to release a hand-held enabling switch--thus terminating the run--

*Once an efficient computer-based means of estimating transfer function parameters became available (6), several analytic forms were fitted to the first 23 frequencies of the 12-run average empirical G-to- SaO_2 transfer function. The four-parameter function,

$$H(s) = -3.87 \frac{1 + 7.20s}{1 + 48.2s} e^{-8.46s}$$

where $s = j2\pi f$, seemed to provide as good a fit as could be expected. Examination of the predictive

whenever they experienced the visual endpoint, which consisted of total loss of peripheral vision plus significant deterioration of central vision. Each subject was exposed to the following: one GOR to visual endpoint; three to five 15-sec RORs, the final one eliciting the visual endpoint; at least one 60-sec ROR; and four to 11 SACMs, several of which elicited the visual endpoint in two of the three subjects.

To convert the instantaneous blood-pressure signal to mean blood pressure, and to prevent spectral aliasing of the Fourier transformed data, both input and output signals were low-pass filtered (3 dB at 0.5 Hz). The paired input and output waveforms were sampled 256 times during the 200-sec analysis period, T ; the spectra obtained, therefore, had a maximum frequency of 0.64 Hz [$f_{\max} < (2 \Delta t)^{-1}$] and a frequency resolution of 5.0 mHz ($\Delta f = 1/T$). As the transient time-domain signals of interest began and ended well within the 200-sec analysis period, a rectangular time window was used. The transfer function between a G-stress input and blood-pressure output was obtained by dividing the Fourier transform of the output by that of the input. By ensemble averaging transfer functions obtained from single input-output pairs, a mean transfer function derived from all pertinent data in a data set (e.g., all responses to one type of G-stress profile) was readily obtained. Spectral inconsistencies (noise) were appreciably reduced by this process. The mean transfer function obtained by ensemble-averaging the transfer functions from the 23 completed or aborted SACMs was examined most thoroughly and with the greatest expectations (Fig. 8). In this mean, empirically determined, transfer function a resonance peak was seen at 60 mHz, a phase crossover occurred at between 40 and 45 mHz, and a local maximum in the phase characteristic was noticeable at 25 mHz. In addition, a 4-dB/octave decline in magnitude could be estimated for frequencies beyond the resonance. Above 200 mHz no useful information appeared in the frequency response curve, as input power associated with the SACM G-force profiles was virtually non-existent above this frequency. The first 40 terms of the 23-run mean transfer function are given in Table II.

Having obtained the empirical transfer function relating eye-level blood pressure to G stress from the ensemble average of the SACM-generated transfer functions, we looked for several mathematically well behaved substitutes for the empirical transfer function. The analytic transfer functions sought were of three forms: 1) single-zero, double-pole; 2) double-zero, double-pole; and 3) single-zero, double-pole with a delayor. Parameter estimates were obtained for each analytic form by minimizing the weighted sum of the squared error of the fit of real and imaginary terms of the analytic form to the first 40 frequencies of the empirical transfer function. The weight used at each frequency was inversely proportional to the variance of the data comprising the empirical function at that frequency.† Marquardt's algorithm, combining the Taylor series expansion and negative gradient methods, was used in the computations (6). The lowest standard error of estimate, and thus the best fit, was exhibited by the double-zero, double-pole transfer function,

$$H(s) = -18.3 \frac{1 + 7.18s + 4.39s^2}{1 + 3.99s + 7.93s^2}$$

where s is the conventional complex frequency variable, $j2\pi f$. This transfer function is graphed in 5-mHz increments in Fig. 9.

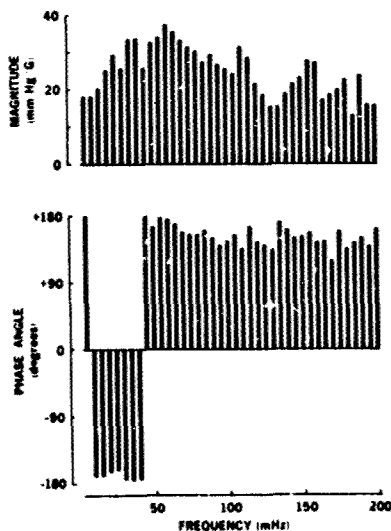


Fig. 8. Mean G-to-ELBP transfer function for 23 SACM G-stress runs on 3 subjects. Each run was given equal weight in the averaging.

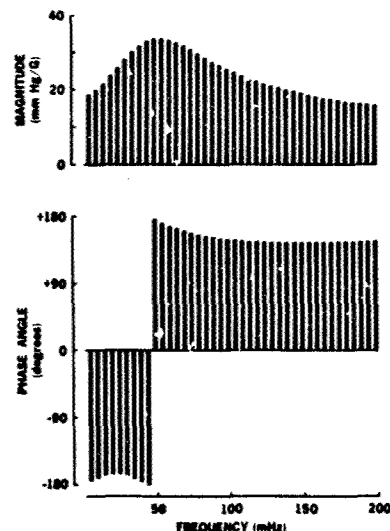


Fig. 9. Double-zero, double-pole transfer function fitted to empirical transfer function in Fig. 8.

† After reconsidering our assumptions of stochastic independence of the real and imaginary terms of empirical transfer-function data points, we decided that parameter estimates based on equal weights, rather than on weights inversely proportional to the variance of the data, would actually be more appropriate. When equal weights were used in fitting the analytic forms to the empirical G-to-ELBP data, the best fitting double-zero, double-pole transfer function was

$$H(s) = -19.0 \frac{1 + 6.89s + 4.84s^2}{1 + 3.89s + 8.07s^2}$$

The predictive performance of this transfer function should be similar to that of the other double-zero, double-pole function reported above, as the corresponding parameters are quite similar.

Predictions of eye-level blood-pressure responses to GOR, ROR, and SACM G stress, based on the empirical and various analytic transfer functions, were compared with the mean actual responses to the same G-stress inputs (Figs. 10-13). Such comparisons gave visual evidence of the relative merits of each of the transfer functions being studied. A particularly rigorous test of the predictive abilities of the various transfer functions was the 60-sec ROR G profile (Fig. 12), since subtle differences in the responses were accentuated by the long, straight lines of the forcing function. The mean actual response to ROR G stress showed a number of characteristics coinciding with expectations based on prior experience: 1) an anticipatory rise in blood pressure prior to onset of G stress; 2) a rapid fall in pressure at onset of G stress; 3) a partial recovery of pressure several seconds after the G load had stabilized; 4) a secondary gradual decline in pressure following the peak of the partial recovery; 5) a rapid rise in pressure at the offset of G stress; 6) an overshoot in pressure coincident with termination of the G load; and 7) a small undershoot immediately following the terminal overshoot. Whereas the empirical and analytic transfer functions all predicted the pressure drop at onset, pressure rise at offset, partial recovery at stabilization, and overshoot at termination of G stress, they met with varying degrees of success in predicting other components of the waveform. Not one recreated the anticipatory rise in eye-level blood pressure. Only the empirical transfer function predicted the gradual decline in pressure during the constant G stress, and only the empirical provided a noticeable undershoot following the terminal overshoot.

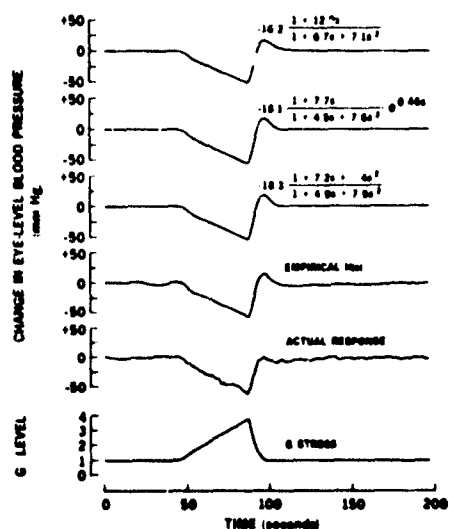


Fig. 10. Predicted and mean actual ELBP responses to GOR G stress. In this and Figs 11-13, top trace is prediction based on single-zero, double-pole transfer function; second, single-zero, double-pole, exponential; third, double-zero, double-pole; fourth, 23-run mean empirical. Fifth trace is mean actual response of 3 subjects to G stress indicated in bottom trace.

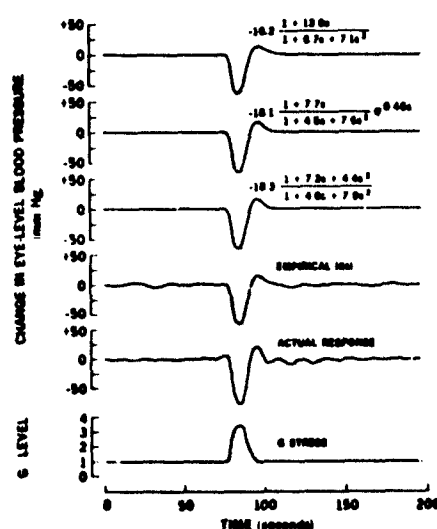


Fig. 11. Predicted and mean actual ELBP responses to aborted ROR G stress.

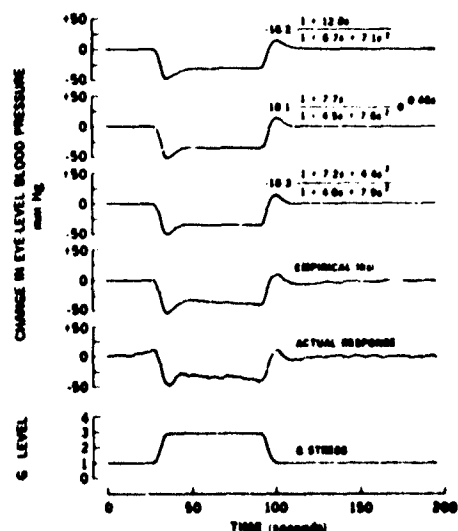


Fig. 12. Predicted and mean actual ELBP responses to 60-sec ROR G stress.

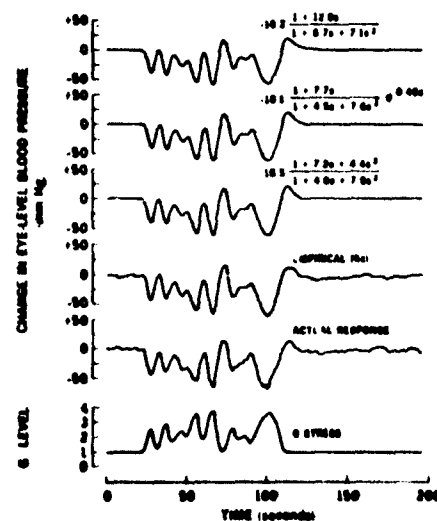


Fig. 13. Predicted and mean actual responses to #8 SACM G stress. To avoid contaminating prediction with actual response data, data from each subject's #8 SACM run were subtracted from empirical transfer function prior to making prediction.

The inverse Fourier transform of the complete empirical transfer function was too corrupted by high-frequency noise for a meaningful impulse response to be recognized, and inverse transforms of truncated versions of the empirical transfer function were somewhat distorted by Gibbs' phenomenon. The inverse transforms of the analytic transfer functions, however, appeared as reasonable impulse responses. Fig. 14 is the impulse response corresponding to the double-zero, double-pole transfer function. The initial negative-going blood-pressure response is readily apparent, as is the zero-line crossing at 4 sec and the subsequent rebound peak at 7 sec. One may infer from the characteristics of the impulse response that the ELBP requires on the order of five seconds to recover from $+G_z$ stress of rapid onset; this is, in fact, the actual behavior of the system.

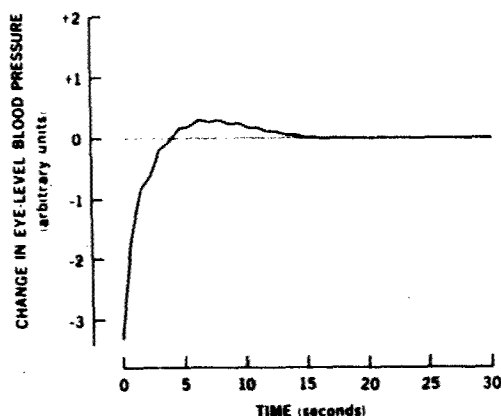


Fig. 14. Inverse Fourier transform (impulse response) of double-zero, double-pole transfer function.

Despite the aforementioned limitations of using linear systems analysis techniques on a physiologic system, the blood-pressure control system was tractable to Fourier analysis: well behaved frequency-response functions could be recognized and substantial predictive ability of derived transfer functions could be demonstrated. With regard to selection of the most appropriate transfer function, the first 40 terms of the empirical transfer function would be the logical choice if one requires greatest predictive accuracy and closest ties to experimental data. If concise mathematical expression is of greater importance, the double-zero, double-pole transfer function should be sufficient. A discussion of the contributions of the various components of the blood-pressure control system to the form of the G-to-ELBP transfer function is presented elsewhere (4); but the experimental evidence cited suggests that the combined transfer function, incorporating the elastic and inertial elements, the vestibulocerebellar pathway, and the baroreceptor feedback loop, contains at least one zero and two or more poles at frequencies below 1.0 Hz. Of particular significance is the evidence of Knapp, et al. (5), who obtained G-to-blood-pressure transfer characteristics for dogs exposed to $\pm 2 G_z$ sinusoidal stress at frequencies below 1.5 Hz, and essentially corroborated our findings in humans.

Conclusion

Data relating SaO_2 response to G stress in anti-G-suited, straining subjects, and data relating ELBP response to G stress in unprotected, relaxed subjects, have been presented in mathematical form as transfer functions developed by means of Fourier analysis. The primary purpose for obtaining these mathematical descriptions was to aid in the development of a model of an aircrewmember's physiologic processes during high-G aerial combat maneuvering, in the hope that inferences could be made about his safety and performance in the high-G environment. Further development of such a model is currently being undertaken by Collins, et al. (2).

References

1. Burton, R., P. Iampietro, and S. Leverett, Jr. 1975. The physiologic effects of seatback angles $< 45^\circ$ (from the vertical) relative to G. *Aviat. Space Environ. Med.* 46:887-897.
2. Collins, R., R. Calvert, H. Hardy, and D. Jenkins. Mathematical simulation of the human cardiopulmonary system during G stress. Physics Department, University of Houston (AFOSR Grant 75-2905). To be published.
3. Gillingham, K., and R. Burton. 1975. Transfer functions for arterial oxygen saturation during $+G_z$ stress. *Aviat. Space Environ. Med.* 46:1329-1335.
4. Gillingham, K., J. Freeman, and R. McNee. 1977. Transfer functions for eye-level blood pressure during $+G_z$ stress. *Aviat. Space Environ. Med.* 48:1026-1034.
5. Knapp, C., D. Randall, J. Evans, and J. Marquis. 1976. Frequency response of cardiovascular regulation in canines to sinusoidal acceleration at frequencies below 1.5 Hz. Presented at Review of Air Force Sponsored Basic Research in Environmental and Acceleration Physiology. Wright-Patterson AFB, OH, 13-15 October.
6. McNee, R., and W. Jackson. 1978. A Fortran program to fit a complex-valued transfer function. SAM-TR-78-7. USAF School of Aerospace Medicine, Brooks AFB, TX.

TABLE I. EMPIRICAL G-TO-SaO₂ TRANSFER FUNCTION--
MEAN OF 12 SACM RUNS ON 4 SUBJECTS

Frequency (mHz)	Magnitude (%/G)	Phase (degrees)
5	1.65	118.95
10	2.60	92.13
15	0.56	150.72
20	0.47	98.50
25	0.76	30.32
30	0.37	-95.63
35	0.57	27.96
40	0.88	15.83
45	0.73	0.99
50	1.01	-18.28
55	1.08	-31.09
60	1.50	-19.97
65	1.46	-47.25
70	0.81	-64.25
75	0.89	-49.67
80	0.73	-84.05
85	0.89	-107.84
90	1.79	-133.80
95	0.96	-41.67
100	0.67	-99.74
105	0.84	-128.21
110	0.42	-97.78
115	0.56	-23.30
120	3.34	37.59

TABLE II. EMPIRICAL G-TO-BLOOD-PRESSURE TRANSFER
FUNCTION--MEAN OF 23 SACM RUNS ON 3 SUBJECTS

Frequency (mHz)	Magnitude (mm Hg/G)	Phase (degrees)
5	18.2	178.7
10	18.2	-169.3
15	20.3	-168.6
20	25.1	-163.0
25	29.4	-161.1
30	25.8	-174.2
35	33.6	-174.9
40	33.8	-174.4
45	25.8	178.0
50	32.8	163.9
55	34.1	176.0
60	37.4	174.1
65	35.6	167.8
70	33.1	156.4
75	31.3	154.2
80	30.1	154.1
85	27.4	159.3
90	29.3	149.0
95	26.7	139.2
100	25.6	145.1
105	24.2	152.0
110	31.3	135.0
115	28.5	163.7
120	21.5	143.4
125	18.7	138.9
130	15.4	133.1
135	15.3	170.3
140	18.9	159.9
145	21.4	149.3
150	23.1	151.3
155	27.6	155.3
160	27.1	143.2
165	17.2	144.5
170	18.7	118.9
175	20.0	156.8
180	22.6	134.9
185	12.9	142.3
190	23.8	149.3
195	16.0	138.1
200	15.6	160.7

UNSTEADY-STATE RESPONSE OF THE VASCULAR SYSTEM TO TRANSIENT AND SUSTAINED AEROSPACE ACCELERATION PROFILES

Xavier J.R. Avula
Professor of Engineering Mechanics
University of Missouri-Rolla
Rolla, Missouri 65401 U.S.A.

and

Hans L. Oestreicher
Chief, Mathematics and Analysis Branch
Biodynamics and Bioengineering Division
Aerospace Medical Research Laboratory
Wright-Patterson Air Force Base, Ohio 45433 U.S.A.

SUMMARY

In this study a mathematical method to determine the response of the blood vessels to transient and sustained acceleration forces is presented. The method is based on coupling of the Navier-Stokes equations for blood flow and the large elastic deformation theory for the deformation of the blood vessels, and solving them numerically under the appropriate initial and boundary conditions. A mathematical reasoning to neglect the effect of acceleration on microcirculation *per se* is given. However, microcirculation is indirectly affected by acceleration forces which tend to pool blood and bring about pressure changes in large vessels. Aortic pressures are calculated for examples of monotonically increasing and transient $-G_z$ acceleration profiles, and one of the solutions is compared with an available, experimentally measured pressure from an animal experiment. In the absence of proper physiological scaling laws, the qualitative agreement between the theory and experiment is satisfactory.

INTRODUCTION

Recent developments in spacecraft and high performance aircraft have resulted in the exposure of the human body to the hazards of high accelerations beyond tolerance levels. In addition to injury to various parts of the body, cardiac insufficiency and the consequent physiological malfunctions such as headache, abdominal pain, change in heart rate, chest pain, loss of vision and hemorrhage are some of the manifestations of acceleration trauma. The knowledge of the response of the cardiovascular system to acceleration stress is essential to the development of protective devices which are designed to increase acceleration tolerance by the human body during aircraft and spacecraft maneuvers. The objective of the present investigation is to understand the response of the blood vessels to transient and sustained aerospace acceleration profiles.

Since it is impossible to actually subject the human body to abnormal high accelerations without inflicting an injury, the response of the vascular system to transient and sustained accelerations is investigated mathematically. Theoretical analyses are extremely helpful for evaluating the relative injury potential for various acceleration functions, in guiding experimental investigations, and in developing and understanding protective measures. Mathematical procedures also provide the basis for establishing precise dynamic and physiological scaling laws needed to translate experimental data obtained with various species into meaningful results for humans.

In recent years, numerous mathematical investigations of arterial dynamics have appeared in the scientific literature. Womersley [1] and Moordergaaf [2] have presented a mathematical analysis of blood flow through arteries by using a lumped parameter model. Taylor [3], Kenner [4], Attinger et. al. [5] used distributed parameter models to analyze pressure-flow relationships in arteries and veins. Several articles related to blood flow in arteries have appeared in the book by McDonald [6]. An elastic tube theory of blood flow has been treated by Lambert [7] and Skalak and Stathis [8]. Kivity and Collins [9] presented a viscoelastic tube model for aortic rupture under decelerative forces. Rudinger [10] studied the effect of shock waves on mathematical models of aorta for better understanding of the behavior of the actual aorta.

To understand the blood flow characteristics in the arterial system, the knowledge of the material properties of the arterial wall is essential. Bergel [11], Fung [12], Demiray and Vito [13] have utilized mathematical models of the constitutive properties of the arterial tissue to determine the stresses in the arterial walls. In the present study, the strain energy function given by Demiray and Vito [13] for an arterial wall specimen has been used in determining the aortic pressure that is compatible with large deformation of the aorta and the associated flow under acceleration stress.

The present study also considers the effect of acceleration on the microcirculation. Microcirculation under normal conditions was investigated by Prothero and Burton [14], Whitmore [15], Gross and Arosely [16], Gross and Intaglietta [17], Skalak [18] and Fung [19] who presented various theories of flow in the capillary bed connecting the arteries and veins.

Several experimental investigations on the effects of acceleration stress on the human body have been performed at the USAF School of Aerospace Medicine at Brooks Air Force Base, Texas. Burton [20] subjected miniature swine to G_z acceleration to study its effects on the organism and extrapolated the results to human beings. Parkhurst, et. al. [21] conducted experiments on human tolerance to high $+G_z$ forces. Leverett, et. al. [22] investigated the physiologic response to high sustained acceleration stress. Peterson, et. al. [23] studied the cardiovascular responses during and following exposure to $+G_z$ forces in chronically instrumented anesthetized dogs. Burton and MacKenzie [24] determined the extent of heart pathology as a function of acceleration stress.

MATHEMATICAL FORMULATION

A. Equations of Fluid Motion

The geometry of the elastic tube containing blood in motion is shown in Fig. 1. Let r, θ, z be the cylindrical polar coordinates and let u, v , and w be the velocity components in the corresponding directions. Assuming axial symmetry in flow and tube deformation, the Navier-Stokes equations for the flow of blood can be written as:

$$\frac{\partial u}{\partial t} + u \frac{\partial u}{\partial r} + w \frac{\partial u}{\partial z} = -\frac{1}{\rho_0} \frac{\partial p}{\partial r} + \nu \left[\frac{\partial^2 u}{\partial r^2} + \frac{1}{r} \frac{\partial u}{\partial r} + \frac{\partial^2 u}{\partial z^2} - \frac{u}{r^2} \right] \quad (1)$$

$$\frac{\partial w}{\partial t} + u \frac{\partial w}{\partial r} + w \frac{\partial w}{\partial z} = -\frac{1}{\rho_0} \frac{\partial p}{\partial z} + \nu \left[\frac{\partial^2 w}{\partial r^2} + \frac{1}{r} \frac{\partial w}{\partial r} + \frac{\partial^2 w}{\partial z^2} \right] + g(t) \quad (2)$$

where p is the pressure, ν is the kinematic viscosity, ρ_0 is density of blood and $g(t)$ is the body force per unit mass caused by the acceleration. The continuity equation is

$$\frac{\partial u}{\partial r} + \frac{u}{r} + \frac{\partial w}{\partial z} = 0 \quad (3)$$

The above equations are nondimensionalized using a typical length, R_0 , which is the initial (undeformed) radius of the aorta, and U , the average velocity of blood in the aorta. Introducing the new quantities

$$\begin{aligned} t^* &= \frac{tU}{R_0} & r^* &= \frac{r}{R_0} & z^* &= \frac{z}{R_0} & w^* &= \frac{w}{U} \\ u^* &= \frac{u}{U} & p^* &= \frac{p}{\rho_0 U^2} & g^* &= \frac{R_0 g}{U^2} & Re &= \frac{UR_0}{\nu} \end{aligned} \quad (4)$$

the equations of motion and the continuity equation in terms of the newly defined variables become

$$\frac{\partial u^*}{\partial t^*} + u^* \frac{\partial u^*}{\partial r^*} + w^* \frac{\partial u^*}{\partial z^*} = -\frac{\partial p^*}{\partial r^*} + \frac{1}{Re} \left[\frac{\partial^2 u^*}{\partial r^{*2}} + \frac{1}{r^*} \frac{\partial u^*}{\partial r^*} + \frac{\partial^2 u^*}{\partial z^{*2}} - \frac{u^*}{r^{*2}} \right] \quad (5)$$

$$\frac{\partial w^*}{\partial t^*} + u^* \frac{\partial w^*}{\partial r^*} + w^* \frac{\partial w^*}{\partial z^*} = -\frac{\partial p^*}{\partial z^*} + \frac{1}{Re} \left[\frac{\partial^2 w^*}{\partial r^{*2}} + \frac{1}{r^*} \frac{\partial w^*}{\partial r^*} + \frac{\partial^2 w^*}{\partial z^{*2}} \right] + g^*(t^*) \quad (6)$$

$$\frac{\partial u^*}{\partial r^*} + \frac{u^*}{r^*} + \frac{\partial w^*}{\partial z^*} = 0 \quad (7)$$

Deleting the "stars" for simplicity, the governing equations in the dimensionless form will become

$$\frac{\partial u}{\partial t} + u \frac{\partial u}{\partial r} + w \frac{\partial u}{\partial z} = -\frac{\partial p}{\partial r} + \frac{1}{Re} \left(\frac{\partial^2 u}{\partial r^2} + \frac{1}{r} \frac{\partial u}{\partial r} + \frac{\partial^2 u}{\partial z^2} - \frac{u}{r^2} \right) \quad (8)$$

$$\frac{\partial w}{\partial t} + u \frac{\partial w}{\partial r} + w \frac{\partial w}{\partial z} = -\frac{\partial p}{\partial z} + \frac{1}{Re} \left(\frac{\partial^2 w}{\partial r^2} + \frac{1}{r} \frac{\partial w}{\partial r} + \frac{\partial^2 w}{\partial z^2} \right) + g(t) \quad (9)$$

$$\frac{\partial u}{\partial r} + \frac{u}{r} + \frac{\partial w}{\partial z} = 0 \quad (10)$$

The boundary and initial conditions are

$$\begin{aligned} u &= \frac{dR_1}{dt} \quad \text{at } r = R_1 & t &\geq 0 \\ w &= 0 \quad \text{at } r = R_1 & t &\geq 0 \\ w &= 1 \quad \text{at } z = 0 & t &\geq 0 \end{aligned} \quad (11)$$

where R_1 is the inside radius of the blood vessel in the deformed state.

B. Equations of Motion for Thin-walled Elastic Tube:

The theory of large elastic deformations is utilized to describe the time-dependent deformation of the blood vessels. In view of the published results on blood pooling and the consequent cardiac insufficiency, the application of large deformation theory appears necessary. Demiray and Vito [13] have previously used this theory to calculate the deformation of arteries.

The undeformed and deformed cylindrical tubes are shown in Fig. 2. Let r, θ, z represent a point in the wall of the undeformed tube, and R, θ, z in the deformed tube. r_1, r_2 are inside and outside radii, respectively, of the undeformed tube, and R_1, R_2 those of the deformed tube. Axial stretch of the tube is neglected because of tethering caused by the surrounding tissue. Assuming the material of the blood vessels to be homogeneous, incompressible, and isotropic, the stress at any point can be written as:

$$\tau^{ij} = \phi g^{ij} + \psi \delta^{ij} + p g^{ij} \quad (12)$$

where $\phi = 2(\partial W / \partial I_1)$, $\psi = 2(\partial W / \partial I_2)$, $B^{ij} = I_1 g^{ij} - g^{ir} g^{js} G_{rs}$, P is a scalar function which represents a hydrostatic pressure, W is the strain energy function, I_1 and I_2 are the strain invariants, and g^{ij} , g_{ij} , G^{ij} , and G_{ij} are the contravariant and covariant metric tensors [25, 26]. The indices i and j take the values 1, 2, and 3. The equations of motion are given by:

$$\tau^{ij} || i + \rho_w F^j = \rho_w f^j \quad (13)$$

where $||$ denotes covariant differentiation, ρ_w is the density of the vessel wall, F is the body force, and f is the acceleration. Let us neglect the body force on the vessel wall in comparison to its effect on the fluid flowing in the cylindrical tube. Performing the covariant differentiation on the remaining part of the equation of motion we get

$$\tau^{ij} || i + \Gamma^i_{ir} \tau^{rj} + \Gamma^j_{ir} \tau^{ir} = \rho_w f^j \quad (14)$$

where Γ^i_{jk} represent the Christoffel symbols of the second kind [25, 26].

It has been shown that for a biomaterial, a reasonable strain energy function as shown in [13] is

$$W = \frac{\beta}{2\alpha} \left[e^{\frac{\alpha(I_2 - 3)}{2}} - 1 \right] \quad (15)$$

in which α and β are material constants. Defining the circumferential stretch ratio $\lambda = R/r$, the stresses in the r , θ , z directions can be expressed as

$$\tau^{11} = P + \beta \left(1 + \frac{1}{\lambda^2} \right) e^{\frac{\alpha(I_2 - 3)}{2}} \quad (16)$$

$$R^2 \tau^{22} = P + \beta \left(1 + \lambda^2 \right) e^{\frac{\alpha(I_2 - 3)}{2}} \quad (17)$$

$$\tau^{33} = P + \beta \left(\frac{1}{\lambda^2} + \lambda^2 \right) e^{\frac{\alpha(I_2 - 3)}{2}} \quad (18)$$

Substitution of the above equations and the appropriate Christoffel symbols in Eq. (14) gives the equation of motion in the form

$$\frac{\partial}{\partial R} \left[P + \beta \left(1 + \frac{1}{\lambda^2} \right) e^{\frac{\alpha(I_2 - 3)}{2}} \right] + \frac{\beta}{R} \left(\frac{1}{\lambda^2} - \lambda^2 \right) e^{\frac{\alpha(I_2 - 3)}{2}} = \rho_w \frac{\partial^2 R}{\partial t^2} \quad (19)$$

The incompressibility condition leads to:

$$R^2 - R_1^2 = r^2 - r_1^2 \quad (20)$$

and

$$\frac{\partial^2 R}{\partial t^2} = - \frac{R}{R^3} \left(\frac{dR_1}{dt} \right)^2 + \frac{1}{R} \left(\frac{dR_1}{dt} \right)^2 + \frac{R_1}{R} \frac{d^2 R_1}{dt^2} \quad (21)$$

With p_1 , p_2 denoting the pressure on the inside and outside wall, respectively, of the blood vessel, the use of the boundary conditions, $\tau^{11} = -p_1(t)$ at $R = R_1$ and $\tau^{11} = -p_2(t)$ at $R = R_2$, substituting Eq. (21) into Eq. (19) and integrating yields

$$\begin{aligned} p_1(t) - p_2(t) &= \rho_w R_1 \frac{d^2 R_1}{dt^2} \ln \frac{R_2}{R_1} + \left(\frac{dR_1}{dt} \right)^2 \rho_w \left[\ln \frac{R_2}{R_1} + \frac{1}{2} \left(\frac{R_2^2}{R_1^2} - 1 \right) \right] \\ &\quad - \beta \int_{\lambda_1}^{\lambda_2} \frac{1+\lambda^2}{\lambda^3} e^{\frac{\alpha(\lambda^2 + 1/\lambda^2 - 2)}{2}} d\lambda \end{aligned} \quad (22)$$

It must be recognized that the relationship $I_2 = 1 + \lambda^2 + 1/\lambda^2$ has been used to obtain Eq. (22).

The following dimensionless quantities are introduced into Eq. (22):

$$P^* = \frac{P}{\rho_w U^2}, \quad R_1^* = \frac{R_1}{R_0}, \quad R_2^* = \frac{R_2}{R_0}, \quad t^* = \frac{tU}{R_0}, \quad \beta^* = \frac{\beta}{\rho_w U^2}, \quad \rho_w^* = \frac{\rho_w}{\rho_0} \quad (23)$$

Then the equation of motion in the radial direction becomes

$$\begin{aligned} (P_1^* - P_2^*) &= \rho_w^* R_1^* \frac{d^2 R_1^*}{dt^{*2}} \ln \left(\frac{R_2^*}{R_1^*} \right) + \rho_w^* \left(\frac{dR_1^*}{dt^*} \right)^2 \left[\ln \frac{R_2^*}{R_1^*} + \frac{1}{2} \left(\frac{R_2^{*2}}{R_1^{*2}} - 1 \right) \right] \\ &\quad - \beta^* \int_{\lambda_1}^{\lambda_2} \frac{1+\lambda^2}{\lambda^3} e^{\frac{\alpha(\lambda^2 + 1/\lambda^2 - 2)}{2}} d\lambda \end{aligned} \quad (24)$$

If the "stars" are dropped for convenience, Eq. (24) can be written as:

$$p_1(t) - p_2(t) = \rho_w R_1 \frac{d^2 R_1}{dt^2} \ln \frac{R_2}{R_1} - \rho_w \left(\frac{dR_1}{dt} \right)^2 \left[\ln \frac{R_2}{R_1} + \frac{1}{2} \left(\frac{R_2^2}{R_1^2} - 1 \right) \right] \\ - \beta \int_{\lambda_1}^{\lambda_2} \frac{1+\lambda^2}{\lambda^3} e^{-\alpha(\lambda^2 + 1/\lambda^2 - 2)} d\lambda \quad (25)$$

The initial conditions are:

At time $t = t_0$, $R_1 = R_0$, $dR_1/dt = u$, radial velocity of fluid.

C. Effect of Acceleration on Microcirculation

The blood vessels of microcirculation are extraordinarily small, and their typical dimensions are of the order of microns. Under normal circumstances, the velocity of the blood in the microcirculation is 1 mm/sec and the Reynolds number is of the order $O(10^{-3})$, which is sufficiently small so that the Stokes flow approximations are applicable. Neglecting the inertial effects and assuming that the stream lines are nearly parallel, the dimensionless equation of fluid motion in the axial (z) direction become:

$$\frac{\partial w}{\partial t} = -\frac{\partial p}{\partial z} + \frac{1}{Re} \left(\frac{\partial^2 w}{\partial r^2} + \frac{1}{r} \frac{\partial w}{\partial r} + \frac{\partial^2 w}{\partial z^2} \right) + g(t) \quad (26)$$

which can be rearranged to read

$$Re \frac{\partial w}{\partial t} = -Re \left(\frac{\partial p}{\partial z} \right) + \left(\frac{\partial^2 w}{\partial r^2} + \frac{1}{r} \frac{\partial w}{\partial r} + \frac{\partial^2 w}{\partial z^2} \right) + Re g(t) \quad (27)$$

In the earth's natural gravitational field, the dimensionless g , as given in Eq. (4), is of the order $O(10^{-2})$, and with the effect of $Re \sim O(10^{-3})$ in the last term $Re g(t)$ in Eq. (27) becomes physiologically insignificant, being of the order $O(10^{-5})$. We estimate that the effect of acceleration on microcirculation *per se* can be safely neglected up to 100 g. However, the pressure of the blood pooled in the arteries and veins can affect the flow rate in the small vessels. For this reason it is necessary to determine a relationship between the pressure gradient and the flow rate in the small blood vessels.

For the flow of a Newtonian fluid in a uniform tube Szymanski [27] showed that the flow would be fully developed if $vt/D^2 \gg 1$, where t = time, v = kinematic viscosity, and D = tube diameter. An extension of this criterion to microcirculation yields $v\Delta t/D^2 \gg 1$ for flow to be quasi-steady, where Δt is the smallest characteristic time of the unsteadiness in flow. According to Burton [28], $\Delta t \approx 0.1$ sec; using $v = 0.04$ Stokes, one finds that the diameter D must be greater than 600μ (microns) for any significant effect of unsteadiness. Since, in microcirculation the diameters of blood vessels are much less than 600μ , changes in flow due to unsteadiness become entirely negligible. On this basis Benis [29] argued that the effect of unsteadiness on non-Newtonian flow could also be neglected. Thus, the use of steady-flow equations can be justified for microcirculation.

For steady capillary flow, the flow rate through a circular tube can be expressed by

$$Q = 2\pi \int_0^R r w \, dr \quad (28)$$

where Q = flowrate, R = tube radius, and w = blood velocity. Integration by parts of the right hand side yields

$$Q = \pi \int_0^R d(r^2 w) - \pi \int_0^R r^2 \left(\frac{dw}{dr} \right) dr \quad (29)$$

The first integral on the right hand side of Eq. (29) is zero. In the second integral the domain of integration can be divided into two regions: a cone of unshered fluid extending to radius R_y , and the annular region bounded by the unshered fluid and the tube wall. Then,

$$Q = -\pi \int_0^{R_y} r^2 \left(\frac{dw}{dr} \right) dr - \pi \int_{R_y}^R r^2 \left(\frac{dw}{dr} \right) dr \quad (30)$$

The first term on the right hand side in Eq. (30) which represents the core integral is zero. By changing the variables from r to τ in the second term as suggested by Merrill et. al. [30], Eq. (30) can be written as

$$Q = \frac{8\pi}{(\Delta P/L)^3} \int_{\tau_y}^{\tau_w} \tau^2 \dot{\gamma} \, d\tau \quad (31)$$

where L = length of the capillary

ΔP = pressure drop

τ = shear stress

$\dot{\gamma}$ = shear rate.

The shear stress and the shear rate are related by an empirical equation

$$\tau^{1/2} = \tau_y^{1/2} + \mu^{1/2} \dot{\gamma}^{1/2} \quad (32)$$

in which τ_y is the yield shear stress, and $\mu^{1/2}$ is a constant which represents the slope of the Casson plot relating the viscometric parameters of blood. In Poiseuille's flow μ becomes the blood viscosity. Substitution of Eq. (32) into Eq. (31) and integration yields

$$Q = \frac{\pi R^4 (\Delta P/L)}{8\mu} - \frac{4\pi \tau_y^{1/2} R^{7/2} (\Delta P/L)^{1/2}}{7\sqrt{2} \mu} - \frac{2\pi \tau_y^2}{21(\Delta P/L)^{3/2} \mu} + \frac{\pi \tau_y R^3}{3\mu} \quad (33)$$

which is valid under the assumption that the flow is steady, laminar and incompressible, and blood is homogeneous. In the above equation, τ_y and μ are known constants; then plots of Q vs. $\Delta P/L$ for capillaries of various radii can be easily constructed. An example of this relationship is shown in Fig. 6.

RESULTS AND DISCUSSION

To determine the response of the blood vessels one must solve Eqs. (8), (9), (10) and (25) under the appropriate boundary conditions. Since these equations were coupled a numerical solution using a digital computer was sought as described in an earlier paper [11].

The following constants were used in the solution: $R_0 = 1.47$ cm, $U = 11.9$ cm/s, $\rho_w = 1.05$ gr/cm³, $\rho_0 = 1.05$ gr/cm³, $\nu = 0.038$ Stoke, $\alpha = 0.8$ and $\beta = 11.35 \times 10^4$ dynes/cm². The constants α and β are elastic constants which appear in the strain energy function W , Eq. (15). These values are reported in literature for a specimen of human aorta. The elastic constants for specimens of veins are not available, primarily because the research of determining the strain energy function in the form of Eq. (15) is relatively new.

As examples, two deceleration profiles were used in the solution: one, a linear, monotonically increasing function of time represented by $g(t) = 7840t$ cm/s², and a transient type (Fig. 3) which increased and decreased rapidly [32]. For both these cases, aortic pressures were calculated by utilizing a finite difference technique which involved Runge-Kutta integration procedure and Adams-Bashforth predictor-corrector method. The dimensions of the human aorta were chosen from the physiological data presented in Westerhof et al. [33]. The aortic pressures calculated for the sustaining linear deceleration profile is shown in Fig. 4. The aortic pressure in response to the transient profile of Fig. 3 is presented in Fig. 5 along with an experimentally determined pressure in the thoracic aorta of a beagle dog which was subjected to the same transient deceleration profile for comparison. The shapes of the pressure vs. time curves are nearly the same indicating satisfactory qualitative agreement. An exact quantitative agreement cannot be expected because of the anatomical and physical differences between the subjects.

The method of calculation described above for an artery can be easily extended to a vein, and the pressure difference across the capillary bed can be determined. Equation (33) represents a relationship between the flow rate and the pressure gradient in a small tube. For selected values of $\tau_y = 0.042$ dyne/cm², $\mu = 0.05$ dyne-sec/cm², $D = 100$ microns, $L = 2.5$ cm, the flow rate Q is computed for various pressure drops in the range $\Delta P/L = 10 \sim 10000$ dyne/cm³ and shown in Fig. 6. If the pressure of the blood pooled on the venous side is known, the effect of acceleration on the flow in microcirculation can be determined from Fig. 6. It must be noted that the flow rate indicated in Fig. 6 is for a narrow blood vessel of specific dimensions. To obtain the total blood flow one must formulate the solution on a statistical basis which includes the arterioles, venules and capillaries of various dimensions and changing rheological properties of blood.

The results presented in this paper are part of an effort to describe the cardiovascular system in terms of its physical and mechanical properties. Most investigations hitherto reported have dealt with electrical analogs of the cardiovascular system in which various parameters were introduced in terms of resistances, impedances and capacitances. These electrical quantities may not truly represent the cardiovascular parameters under high g conditions, and an analysis of the cardiovascular system which is based on its original properties is therefore desirable.

REFERENCES

- [1] Womersley, J.R., "Mathematical Analysis of the Arterial Circulation in a State of Oscillatory Motion," Wright Air Development Center, Technical Report WADC-TR-56-164, 1958.
- [2] Moordergraaf, A., "Hemodynamics," in *Biological Engineering*, Schwan, H., ed., McGraw-Hill, New York, 1969.
- [3] Taylor, M.D., "The Input Impedance of an Assembly of Randomly Branching Elastic Tubes", *Biophys. J.*, Vol. 6, 1966, pp. 25-51.
- [4] Kenner, T., "Flow and Pressure in Arteries" in *Biomechanics: It's Foundations and Objectives*, Fung, Y.C. et al. eds., Prentice-Hall, Englewood Cliffs, New Jersey, 1972.
- [5] Attinger, E.O., Anne, T., Mikami, T., and Sugawara, H., "Modeling of Pressure Flow Relationships in Veins", *Hemorheology*, Copley, A., ed., McGraw-Hill, New York, 1964.
- [6] McDonald, D.A., *Blood Flow in Arteries*. E. Arnold (Publishers) Ltd., London, 1960.

- [7] Lambert, J.W., "On the Nonlinearities of Fluid Flow in Nonrigid Tubes", J. Franklin Inst., Vol. 26, 1958, pp. 83-102.
- [8] Skalak, R. and Statius, T., "A Porous Tapered Elastic Tube Model of a Vascular Bed", in Biomechanics, Fung, Y.C., ed., ASME Symposium, New York, New York, 1966.
- [9] Kivity, Y. and Collins, R., "Nonlinear Wave Propagation in Viscoelastic Tubes: Application to Aortic Rupture", J. Biomechanics, Vol. 7, 1974, pp. 67-76.
- [10] Rudinger, G., "Shock Waves in Mathematical Model of the Aorta", J. Appl. Mech. ASME Vol. 37, 1970, pp. 34-37.
- [11] Bergel, D.H., "The Dynamic Elastic Properties of the Arterial Wall", J. Physiol. Vol. 156, 1961, pp. 458-469.
- [12] Fung, Y.C., "Elasticity of Soft Tissues in Simple Elongation", Am. J. Physiol. Vol. 213, 1967, pp. 1532-1544.
- [13] Demiray, H., and Vito, R.P., "Large Deformation Analysis of Soft Biomaterials", Developments in Theoretical and Applied Mechanics, 8, Proc. 8th Southeast. Conf. on Theor. and Appl. Mech., 1976, pp. 515-522.
- [14] Prothero, J. and Burton, A.C., "The Physics of Blood Flow in Capillaries. I. The Nature of the Motion", Biophys. J. Vol. 1, 1961, pp. 565-579.
- [15] Whitmore, R.L. "A Theory of Blood Flow in Small Vessels", J. Appl. Physiol. Vol. 22, No. 4, 1967, pp. 767-771.
- [16] Gross, J.F. and Aroesty, J., "Mathematical Models of Capillary Flow: A Critical Review" Biorheology, Vol. 9, 1972, pp. 225-264.
- [17] Gross, J.F. and Intaglietta, M., "Effects of Morphology and Structural Properties on Microvascular Hemodynamics" Report No. P-5000, The Rand Corporation, Santa Monica, California, 1973.
- [18] Skalak, R., "Mechanics of the Microcirculation", in Biomechanics: It's Foundations and Objectives, Fung, Y.C. et. al. eds., Prentice Hall, Englewood Cliffs, New Jersey, 1972.
- [19] Fung, Y.C., "Microscopic Blood Vessels in the Mesentery", Biomechanics, Fung, Y.C., ed., ASME Symposium, New York, New York, 1966.
- [20] Burton, R.R., "Positive (+G_z) Acceleration Tolerances of the Miniature Swine: Application as a Human Analog", Aerosp. Med., Vol. 44, 1973, pp. 294-298.
- [21] Parkhurst, M.J., Leverett, S.D., Jr., and Shurbrooks, S.J., Jr., "Human Tolerance to High, Sustained +G_z Acceleration", Aerosp. Med., Vol. 43, 1972, pp. 708-712.
- [22] Leverett, S.D., Jr., Burton, R.R., Crossley, R.J., Michaelson, E.D., and Shurbrooks, S.J., Jr., "Physiologic Responses to High Sustained +G_z Acceleration", USAF School of Aerospace Medicine, Tech. Rep. No. 73-21, 1973.
- [23] Peterson, D.F., Bishop, V.S., and Erickson, H.H., "Cardiovascular Changes During and Following 1-min Exposure to +G_z Stress", Aviat. Space Environ. Med., Vol. 46, No. 6, 1975, pp. 775-779.
- [24] Burton, R.R., and MacKenzie, W.F., "Heart Pathology Associated with Exposure to High Sustained G_z", Aviat. Space Environ. Med., Vol. 46, No. 10, 1975, pp. 1251-1253.
- [25] Green, A.E. and Zerna, W., Theoretical Elasticity, Oxford University Press, New York, London, 1968.
- [26] Klip, W., The Foundations of Medical Physics, University of Alabama Press, Birmingham, Alabama, 1969.
- [27] Ronse, H. (ed.) Advanced Mechanics of Fluids, Wiley, New York, 1959.
- [28] Burton, A.C., Physiology and Biophysics of the Circulation, Year Book Medical Publishers, Chicago, 1965.
- [29] Benis, A.M., "Laminar Flow of Power-law Fluids Through Narrow Three-dimensional Channels of Varying Gap. Chem. Engr. Sci., Vol. 22, 1967, pp. 805-822.
- [30] Merrill, E.W., Benis, A.M., Gilliland, E.R., Sherwood, T.K., and Salzman, E.W., "Pressure-Flow Relations of Human Blood in Hollow Fibres at Low Flow Rates", J. Appl. Physiol. Vol. 20, No. 5, 1965, pp. 954-967.
- [31] Avula, X.J.R. and Oestreicher, H.L., "Mathematical Model of the Cardiovascular System Under Acceleration Stress", Aviat. Space Environ. Med., Vol. 49, No. 1, 1978, pp. 279-286.
- [32] Hanson, P.G., "Pressure Dynamics in Thoracic Aorta During Linear Deceleration", J. Appl. Physiol. Vol. 28, No. 1, 1970, pp. 23-27.
- [33] Westerhof, N., Bosman, F., DeVries, C.J., and Noordergraaf, A., "Analog Studies of the Human Systemic Arterial Tree", J. Biomech. Vol. 2, 1969, pp. 121-143.

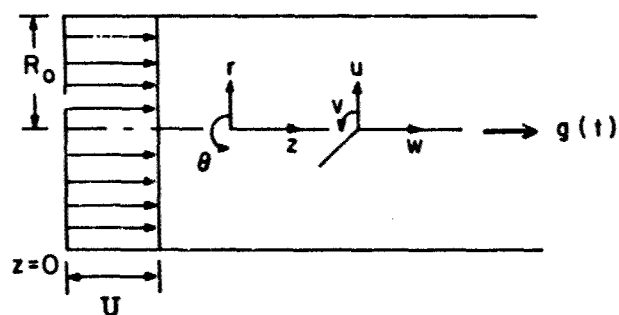


Figure 1. Definition sketch for fluid flow variables.

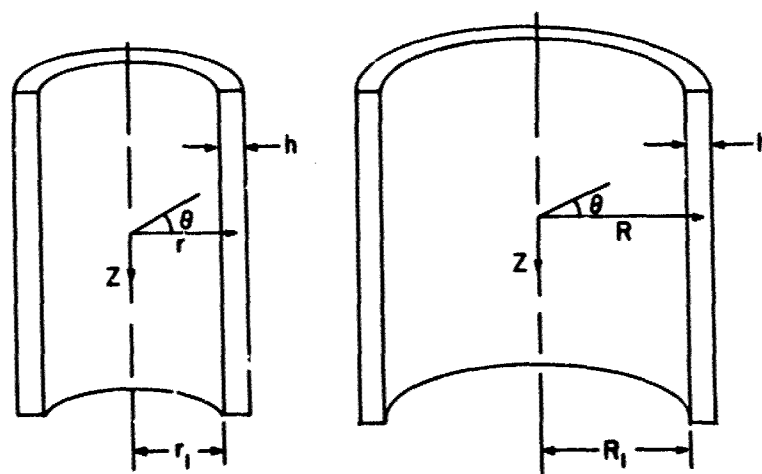


Figure 2. Geometry of the undeformed and deformed elastic tube.

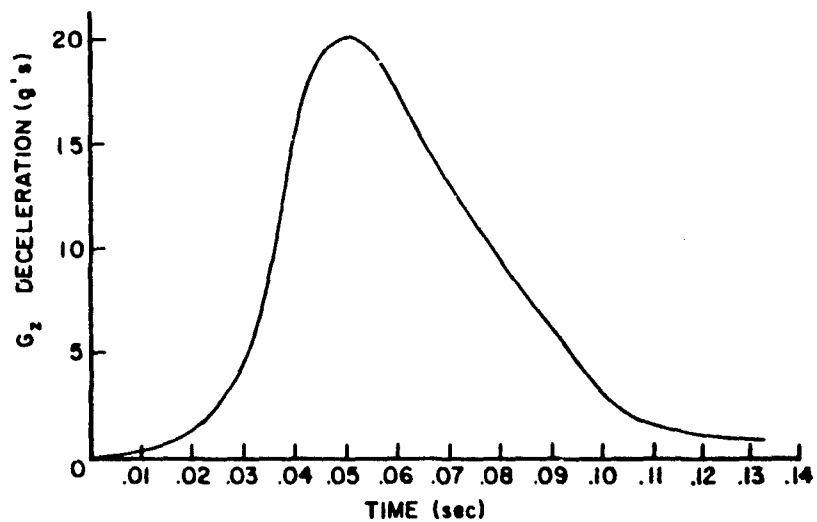


Figure 3. Deceleration function measured in the experiment by Hanson [32].

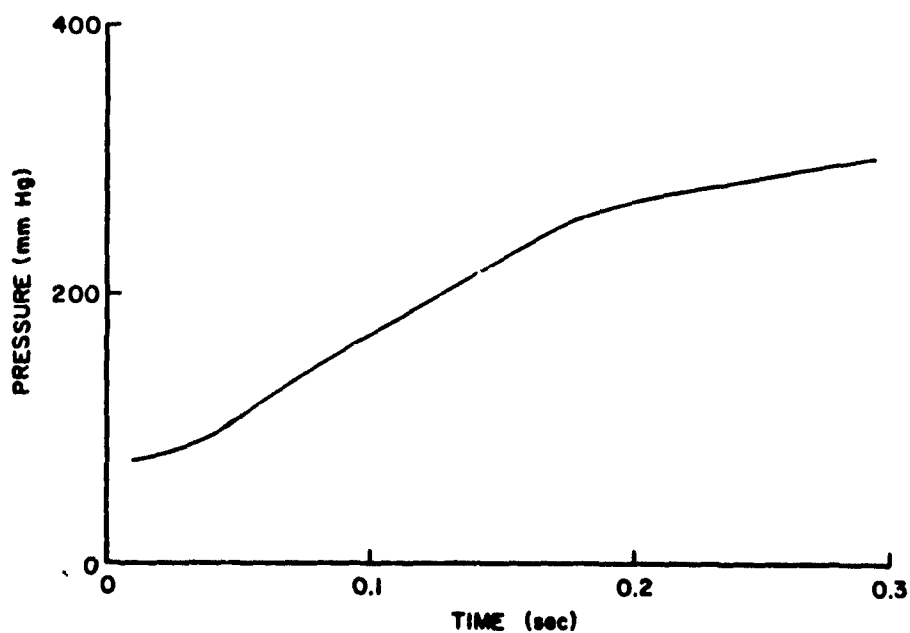


Figure 4. Calculated pressure in the aorta for the linear deceleration $g(t) = 7840 t \text{ cm/s}^2$.

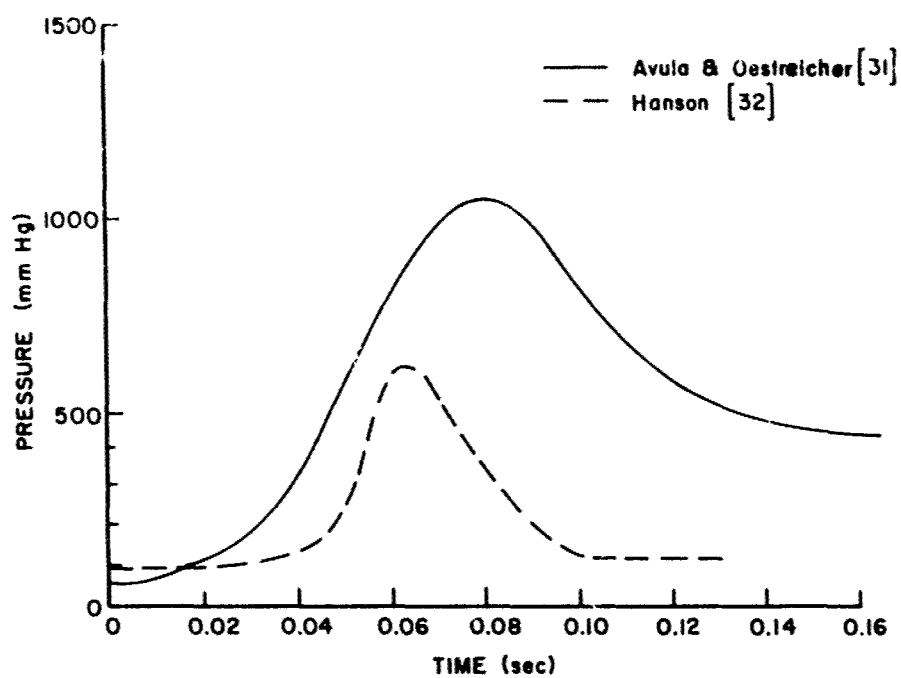


Figure 5. Comparison of theoretical and experimental pressures for the deceleration in Hanson's [32] experiment.

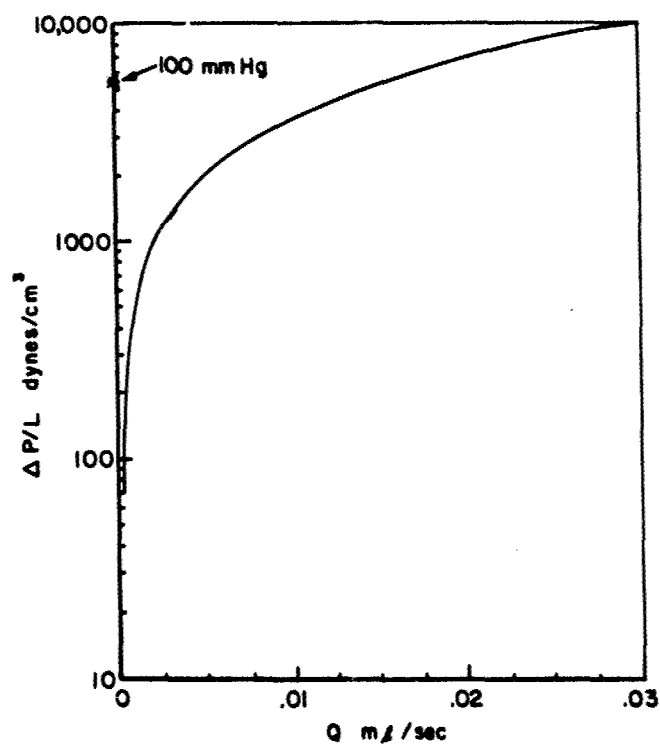


Figure 6. Pressure - Flow relationship for a narrow blood vessel (Eq. 33).

A HEAD INJURY MODEL

Carley Ward, Ph D
 Research Structural Engineer
 Civil Engineering Laboratory
 Naval Construction Battalion Center
 Port Hueneme, California 93043

SUMMARY

The history of analytical head injury modeling is briefly reviewed, and the design restrictions that limit their usefulness are discussed. One of the most recent models, a linear finite element idealization of the human brain, is presented. Intracranial pressures computed by this model are compared to pressures measured in human cadaver head impact tests. The computed pressures and observed injuries are correlated for a series of ten tests. Injury prediction based on maximum intracranial pressure is compared to prediction based on the Gadd Severity Index and the Head Injury Criterion Index.

INTRODUCTION

In the past, the dynamic response of the human brain to head impact could only be described in general, nonspecific terms. It was known that a pressure gradient develops in the brain, but, with few exceptions,* pressure magnitudes, their time durations, and their effects on injury were unknown. The mechanics of closed skull brain injury had been theorized but never proven, and the validity of head injury indices computed from head accelerations had been questioned. Quantitative cause and effect relationships do not exist, although head trauma is a serious and common injury.

The brain with its surrounding tissue and fluids form a complex dynamic system. The dynamic response characteristics of the integral system are just beginning to be understood. Approximately thirty analytical continuum models of the head have been suggested and studied since 1964. (Detailed reviews of these models are presented in Ref 3 and 4.) It was hoped that the models would reveal new information about the mechanical responses associated with brain injury. But aside from the satisfaction obtained from solving a classical mechanics problem, the research was disappointing. Many problems are encountered in modeling the head. Large displacements and rotation of the head, the need for a nonlinear neck (the response of which is as yet undefined), cumbersome mathematics, inadequately defined material properties, and a scarcity of experimental data for model validation are some of the problems facing the modeler.

In attempts to minimize or circumvent these difficulties, simplifications have been made in the models that critically limit their usefulness and accuracy. A common simplification is to idealize the head as a closed shell, which adversely affects the results. In many continuum models, those which do not utilize finite elements, the skull is modeled as a closed axisymmetric or spherical shell. The shell is considered filled with an incompressible or nearly incompressible brain-like substance (fluid or soft viscoelastic material). A small deformation produced by a moderate impact would initiate high pressures in the simulated brain. A change in volume of only one one-thousandth ($dv/v = 1/1000$) would produce internal pressures of several hundred psi.

Obviously, high brain pressures accompanying low skull stresses is not what nature intended, and it is not the invivo result. Measured intracranial pressures are seldom above 40 psi at impact. The brain and skull do not form a closed system; blood flows through the arteries and veins, the cervical cord is easily deformed, and the cerebrospinal fluid (CSF) can move in or out through the foramen magnum (opening in the base of the skull). Experimental research (reviewed in Ref 5) shows that as the skull is deformed at impact the intracranial pressure is modulated by the CSF space and vascular bed. This effect is referred to as the volume elastance (dP/dV) or volume distensibility (dV/dP) of the central nervous system (CNS) and contained fluids. Although now believed to be a primary factor in brain injury modeling, its importance has just recently been established. Only a few specialized pressure-volume relationships from tests on animals have been published (Ref 6, 7, and 8). The appropriate volume elastance to use when modeling human head impact has not been established.

With finite elements, some of the simplifications required for solution in earlier models are unnecessary. Finite elements provide the badly needed capability to model irregular shapes. This is especially important for a skull fracture model. The human skull thickness varies significantly from point to point and from skull to skull. Yet thickness is the most important dimension in simulating the skull. The deformation is inversely proportional to thickness cubed (t^3). As a result it is difficult to obtain agreement between measured skull stresses and model compacted stresses. Even in a finite element skull model the thickness must be varied from node to node. Any model that uses a constant skull thickness will surely fail in a validation test comparison with the response of a real skull.

* Some pressure gradients have been measured in cadavers (Ref 1) and fluid-filled skulls (Ref 2).

DISCUSSION

Simplifying assumptions were also made in the finite element brain model described in this paper. Because the invivo properties of the brain have not been defined for high strain rates, the brain is idealized as being linear elastic and homogeneous. Elastic brick elements represent the soft tissue, and membrane elements represent the partitioning internal folds of dura, the falx, and tentorium (Fig 1). To avoid the problems associated with modeling the skull and neck, the equations were rewritten in such a way that these structures need not be modeled.* This simplification greatly reduces the number of equations and facilitates solution. Local skull deformation under the load is also neglected in this approach. But the head itself can experience large rotational and translational accelerations. The effect in accuracy of these simplifications is believed to be minimal, since the model responses have been checked against measured data from four laboratories (Ref 9, 10, and 11).

Solution Procedure

The equations of motion are solved on the digital computer using a linear finite element analysis program that is a modified version of the SAPV computer program for structural analysis. Displacements of the brain relative to the skull are computed. The transformation to relative coordinates is unique to this study and can be described as follows.

The finite element matrix equation of motion is written first in inertial coordinates,

$$\ddot{M}\ddot{U} + K\ddot{U} = R \quad (1)$$

where M is the diagonal lumped mass matrix, K is the structural stiffness matrix, and U , \ddot{U} , and R are the column matrices of inertial displacements, inertial accelerations, and generalized loads, respectively. The inertial displacements are rewritten in terms of rigid body and relative elastic displacements

$$U = X + Q \quad (2)$$

where X is the displacement relative to the skull fixed axis (elastic displacement) and Q is the rigid head displacement. The inertial accelerations are also separated into rigid body and relative accelerations

$$\ddot{U} = \ddot{X} + \ddot{Q} \quad (3)$$

However, \ddot{Q} is not a simple relationship; it is a combination of translational acceleration, rotational velocity and acceleration, and centripetal acceleration. The terms in \ddot{X} are the node translational acceleration measured relative to the skull fixed anatomical axis. Substituting Eq (2) and (3) into Eq (1) provides

$$\ddot{M}\ddot{X} + \ddot{M}\ddot{Q} + KX + KQ = R \quad (4)$$

Since there is no strain energy associated with rigid body motion

$$KQ = 0 \quad (5)$$

and Eq (4) can be written as

$$\ddot{M}\ddot{X} + KX = R - \ddot{M}\ddot{Q} \quad (6)$$

The $\ddot{M}\ddot{Q}$ matrix is computed using measured or specified head accelerations and rotations. In this particular simulation, because no forces are applied directly to the brain, $R = 0$. Forces applied to the skull are accounted for in the inertial loads matrix $\ddot{M}\ddot{Q}$. The program applies the appropriate inertial load to each node in the system, just as forces would be applied. The resulting equations are solved using standard structural analysis procedures and direct time integration.

Experimental Validation Tests

In this research program, head impact tests are simulated with the model and then the computed results are compared to measured brain responses (Fig 2). In the past two years the models have been changed and upgraded to improve the correlation. Although live animal brain responses have been used, the best data for substantiating the models were obtained from unembalmed, pressurized cadaver tests at University of California at San Diego (UCSD) (Ref 10 and 12). In those experiments, the cadaver was seated in front of a sliding impact device. Suture attachments to an overhead frame positioned the head but did not interfere with its movement. To minimize head rotation, the anatomical axis

* Comparison of intracranial pressures from a brain model with and without an attached skull showed the effect of the skull deformation on intracranial pressures to be minimal. Pressure gradients developing in the brain are caused primarily by the acceleration of the head.

of the skull, the Frankfort Plane, was inclined 45 degrees relative to the horizontal. Simulated normal *in vivo* pressures were obtained in the vascular and cerebrospinal fluid systems prior to impact. The vascular fluid contained India ink so that contused areas could be marked by turning black, just as bleeding would turn them red in a living brain. In one series of tests, pressures were measured subdurally at five or six locations on the brain surface. These tests were also simulated with the brain models, and the measured and computed pressures were compared. The responses of the earlier (1976) models were slow and lagged the measured pressures as shown in Fig 3. Although this delay was corrected by changing the material properties, computational inaccuracies due to the brain's near incompressibility had to be eliminated. The regular element in the 1977 model was replaced with a new split energy element. This element, described in Ref 13, is accurate for all values of compressibility.

Material Properties

The *in-situ* material properties of the brain and its contained fluids have not been adequately defined for the high strain rate injury-producing event (Ref 5). Experimental research on brain specimens indicate that the response is viscoelastic, loading-rate sensitive, and nonlinear (Ref 14). However, because the event is of short duration, the nonlinear properties in this study were approximated with effective linear material constants. These constants were determined in a parametric study (Fig 2). Thirteen impact tests were simulated using a range of possible material constants, and then the computed and measured pressures were compared. This study revealed that for the composite material (brain, vascular system, and fluid), a Young's Modulus (E) of 6,670,000 dynes/sq cm gave good results. The stress-strain modulus for brain material is very strain-rate dependent (Ref 14), and, for the high strain rates at impact, a value in this range could be expected.

The parametric study revealed that a single value for Poisson's ratio (ν) was not adequate; hard surface impacts require higher values. The padded impact has a long acceleration pulse (Fig 4a), while the unpadded and ineffectually padded impacts have a sharp spike-shaped acceleration pulse (Fig 4b and c). A higher Poisson's ratio that represents a more nearly incompressible material is required to simulate these spike-shaped acceleration traces. The underlying reason for this requirement is still being researched. It may be that the material constants should be varied throughout the model to more accurately represent the brain, or it may be a natural consequence of the system mechanics. The pressure-release mechanisms associated with the volume elastance are a function of the event time duration. During the spike-shaped acceleration, these mechanisms would have less time to act or affect the pressure response. Then, as the pulse duration decreases, the nearly incompressible character of the brain tissue would begin to predominate.

To simulate this nonlinear loading-rate effect, three values for ν (0.48, 0.49, and 0.499) were selected, defining Models I, II, and III. Model selection is based on the shape of the acceleration trace. The value of the acceleration peak magnitude, A , divided by the average pulse width, T , is the model selection parameter. Refer to Fig 4 and Table 1. When the three models are employed as specified in Table 1, the correlation between the measured and computed intracranial pressures is good (Table 2). Sample correlations for the three models are shown in Fig 5, 6, and 7. When the selection procedure in Table 1 is not followed, a variation between measured and computed peak pressures results. This is demonstrated in Fig 6: the lower Poisson's ratio model, Model I, was used to compute peak pressure in an unpadded impact.

Correlation Between Frontal Pressure and Injury

Although the model can predict pressures, the research objective is to predict injury. Using the three models, ten additional pressurized cadaver head impact tests were simulated. In these experiments the brain injuries were graded, but pressures were not measured (Ref 12). Injury codes of 1, 2, and 3 were established to indicate minor, moderate, and severe injury, respectively. Because the injuries were primarily in the frontal region of the brain, the computed frontal pressures, shown in Table 2, were compared to injury severity. A plot of the pressures and corresponding injury severity numbers, Fig 6, shows the following relationship:

<u>Injury</u>	<u>Pressure</u>
Severe	$> 2.30 \times 10^6$ dynes/sq cm
Moderate	$1.80 \text{ to } 2.30 \times 10^6$ dynes/sq cm
Minor	$< 1.80 \times 10^6$ dynes/sq cm

The same relationship exists between the magnitude of occipital computed pressures and occipital brain injury in four live animal tests (Ref 15).

Pressure as an Injury Predictor

Currently, the Head Injury Criterion (HIC) and Gadd Severity Index (GSI) are used to predict injury; a HIC or GSI index above 1000 would correspond to a serious injury. The index value of 1000 is considered to be the human tolerance level. No serious injury should occur if the HIC and/or GSI index is below 1000. The indices are defined as

$$GSI = \int_{t_0}^{t_n} a^n dt \quad n \text{ is usually } 2.5 \quad (7)$$

$$HIC = \left[(t_2 - t_1)^{-1} \int_{t_1}^{t_2} a dt \right]^{2.5} (t_2 - t_1) \quad (8)$$

where a is the resultant head acceleration. In the GSI calculations, Eq (7), the integration is over the complete acceleration pulse, but in the HIC calculations, Eq (8), the time interval $t_2 - t_1$ is selected to maximize the value. (The integration is performed using various time periods; then the period that results in the highest HIC value is selected.) Because these indices include the effect of acceleration duration, they are a significant improvement over the earlier practice of using only peak head acceleration in establishing tolerance levels. But a measure of the effect of the acceleration on the brain may be an even better indication of injury. Injury correlation with frontal pressure (a brain response measure) can be correlated with the HIC and GSI indices. Graphs similar to the one used for frontal pressure were prepared for the HIC and GSI (Fig 7 and 8). These indices do not predict the serious injury that occurred in Test 29. However, the frontal pressure correctly predicts a grade 3 injury. In this particular test series the frontal pressure magnitude is a better predictor of injury than the HIC or GSI. The frequency and shape of the forcing function (head acceleration) and the system response characteristics of the brain predominate in the calculation of the intracranial pressures. The HIC and GSI are computed by using only the integration of the head acceleration raised to the 2.5 power (Eq 7 and 8). In this integration the contribution of the spike-shaped accelerator pulse is small. But the effect of the acceleration spike on intracranial pressure is significant as shown in Test 29.

Padding to Eliminate High Intracranial Pressure Pulses

These results demonstrate the importance of adequate padding. Appropriate padding would have eliminated the spike-shaped acceleration pulse and ensuing high intracranial pressures in Test 29. No injury would have occurred in Test 29 if the impactor had been adequately padded. Extrapolating to head impacts in vehicle accidents, lives could be saved by covering potential hard-surface head impact sites with compressible material. Also, padding in helmets may be more important than originally believed. High-magnitude, short-duration intracranial pressures occur when the padding is too hard, or when it compresses completely (bottoms out) under the load. Helmet padding should be designed to minimize the pressure pulses developing in the brain by providing optimum crush rates for a range of impacts.

FUTURE RESEARCH

This combined analytical and experimental research effort has revealed important facts about the response of the brain to impact. A better understanding of frontal impact injury has resulted. But there is much more to learn. A great amount of additional experimental research is needed. The results used in this study reported in References 10 and 12 constitute only a small injury sample. Additional impacts, such as side and occipital, need to be performed and simulated to test the models. The effects of high head rotational accelerations and velocities need to be studied. Response measures other than pressure may be important when rotation is significant. Experimentally, in-situ brain material properties need to be defined for these short-duration, high-loading-rate events.* Also, the compressibility provided by fluids flowing out of the cranial cavity needs to be investigated.

CONCLUSIONS

1. Models now exist that can predict intracranial pressures for frontal head impact.
2. A relationship between frontal pressure magnitude and frontal lobe injury severity is demonstrated.
3. In this particular test series, the frontal pressure magnitude is a better indicator of injury than the HIC or GSI indices.
4. Adequate padding of possible head impact surfaces and helmets could be very effective in preventing the type of injury observed in these tests. Such padding would eliminate the high-magnitude, impulsive-type head accelerations that produce high-magnitude pressure pulses in the brain.

* The properties probably vary throughout the brain, but with the limited information available, uniform material properties had to be assumed.

REFERENCES

1. S. O. Lindgren, "Experimental Studies of Mechanical Effects in Head Injury," *Acta Chirurgica Scandinavica, Supplementum* 360, Stockholm, 1966.
2. V. L. Roberts, V. Hodgson, L. M. Thomas, "Fluid Pressure Gradients Caused by Impact to the Human Skull," ASME paper (66-HUP-1), Biomechanics Monograph, 1967.
3. N. Akkas, "Continuum Modeling of Head Injury," Proceeding NATO Institute Progress in Biomechanics Conference, Ankara, Turkey, July 1978.
4. A. I. King and C. C. Chou, "Mathematical Modelling, Simulation and Experimental Testing of Biomechanical System Crash Response," *Journal of Biomechanics*, Vol 9, No. 5, 1976, pp 301-317.
5. Y. K. Liu, "Biomechanics of Closed Head Impact," ASCE Journal, Engineering Mechanics Division, Feb 1978.
6. Rinder, L., "Concussive Response and Intracranial Pressure Changes at Sudden Extradural Fluid Volume Input in Rabbits," *ACTA Physiologica Scandinavica*, Vol 76, 1969, pp 352-366.
7. Ryder, H. W., et al., "The Mechanism of the Change in Cerebrospinal Fluid Pressure Following an Induced Change in the Volume of the Fluid Space," *Journal of Laboratory and Clinical Medicine*, Vol 41, 1953, pp 428-435.
8. Lindgren, S. and Rinder, L., "Production and Distribution of Intracranial and Intraspinal Pressure Changes at Sudden Extradural Fluid Volume Input in Rabbits," *Acta Physiologica Scandinavica*, Vol 76, 1969, pp 340-351.
9. C. C. Ward and R. B. Thompson, "The Development of a Detailed Finite Element Brain Model," Proceedings 19th Stapp Car Crash Conference, 1975.
10. A. M. Nahum, R. Smith, and C. C. Ward, "Intracranial Pressure Dynamics During Head Impact," Proceedings 21st Stapp Car Crash Conference, 1977. (SAE 770922)
11. C. C. Ward, "An Analytical Brain Model for Head Impact," Proceedings IRCOBI International Conference on Biomechanics of Impact Trauma, Berlin, Germany, 1977.
12. A. M. Nahum and R. W. Smith, "An Experimental Model for Closed Head Impact Injury," Proceedings 20th Stapp Car Crash Conference, 1976. (SAE 760825)
13. D. S. Malkus and T. J. R. Hughes, "Mixed Finite Element Methods Reduced and Selective Integration Techniques: A Unification of Concepts," submitted to *Computer Methods in Applied Mechanics and Engineering*.
14. "Determination of the Physical Properties of Tissues of the Human Head - Final Report," Biomechanics Laboratories of Department of Theoretical and Applied Mechanics College of Engineering, West Virginia University. Contract no. PH-43-6-1137, May 1970.
15. C. C. Ward, P. E. Nikravesch, and R. B. Thompson, "Biodynamic Finite Element Models Used in Brain Injury Research," presented at Symposium on Biodynamic Models and Their Applications, Dayton, Ohio, Feb 1977. Published in the *Journal of Aviation, Space and Environmental Medicine*, Vol 49, No. 1, 1978.

ACKNOWLEDGMENTS

The author wishes to acknowledge the help of Dr. Parviz Nikravesch and Dr. A. Nahum in this research and the National Highway Traffic Safety Administration of the Department of Transportation for their financial support under Contract No. DOT-HS-5-01132.

Table 1. Model Properties

Model No.	A/T* x 10 ⁸ (cm/sec ³)	Type of Element	Young's Modulus (dynes/sq cm x 10 ⁶)	Poisson's Ratio
I	0 - 1.5	Split Energy	6.67	0.48
II	1.5 - 2.5	Split Energy	6.67	0.49
III	>2.5	Split Energy	6.67	0.499

*A/T = peak head acceleration/average pulse width

Table 2. Simulated Frontal Pressures

UCSD Test No.	A/T* x 10 ⁸ (cm/sec ³)	Model Used	Pressure (dynes/sq cm x 10 ⁶)
15	0.8	I	1.53
17	2.7	III	4.17
18	2.2	II	1.41
19	1.1	I	1.76
26	0.45	I	1.09
27	0.15	I	0.40
28	1.37	I	1.98
29	4.16	III	3.10
31	0.63	I	1.32
32	1.65	II	2.43

*A/T = peak head acceleration/average pulse width

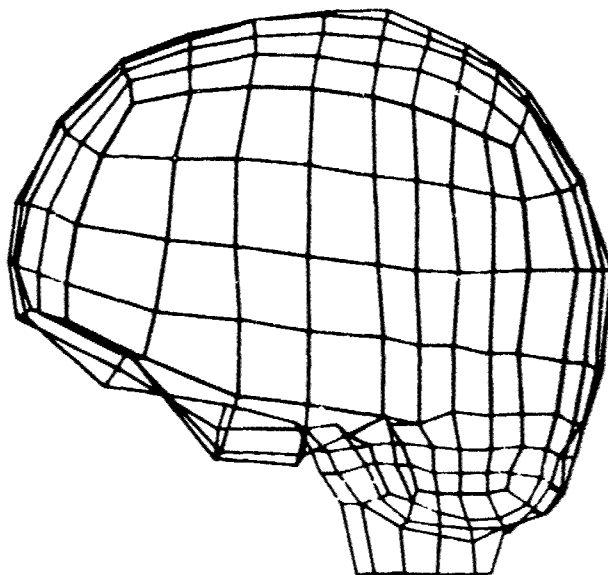


Figure 1. Finite element human brain model.

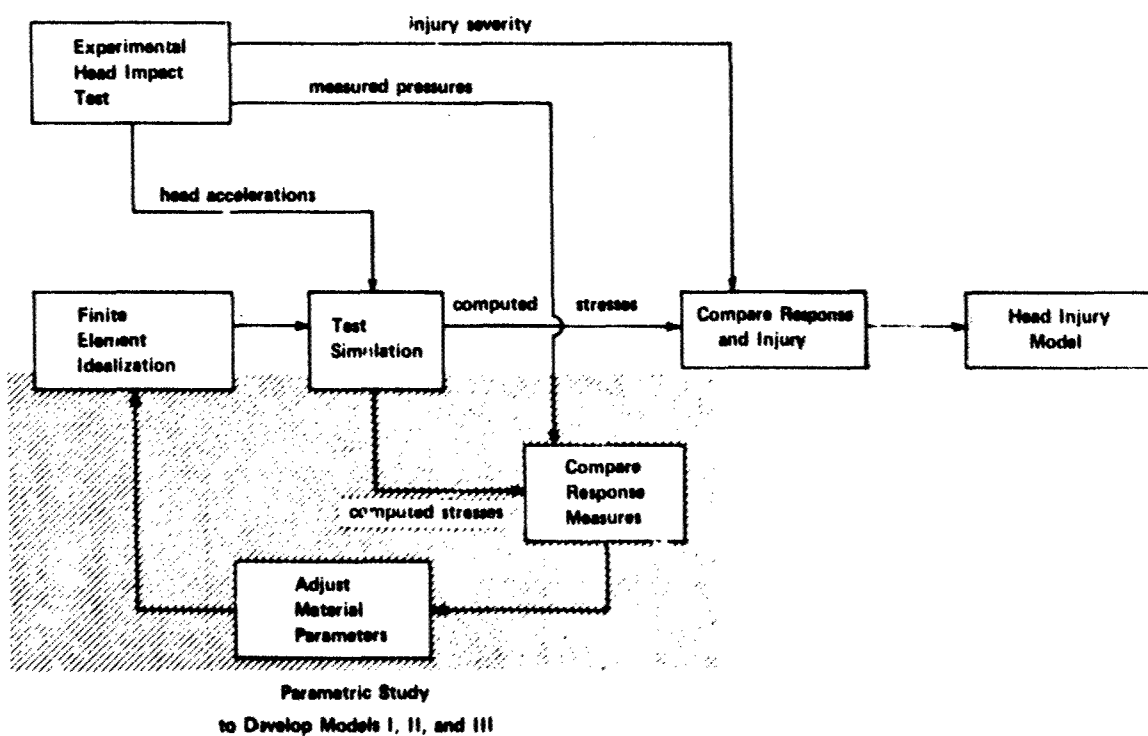


Figure 2. Research program.

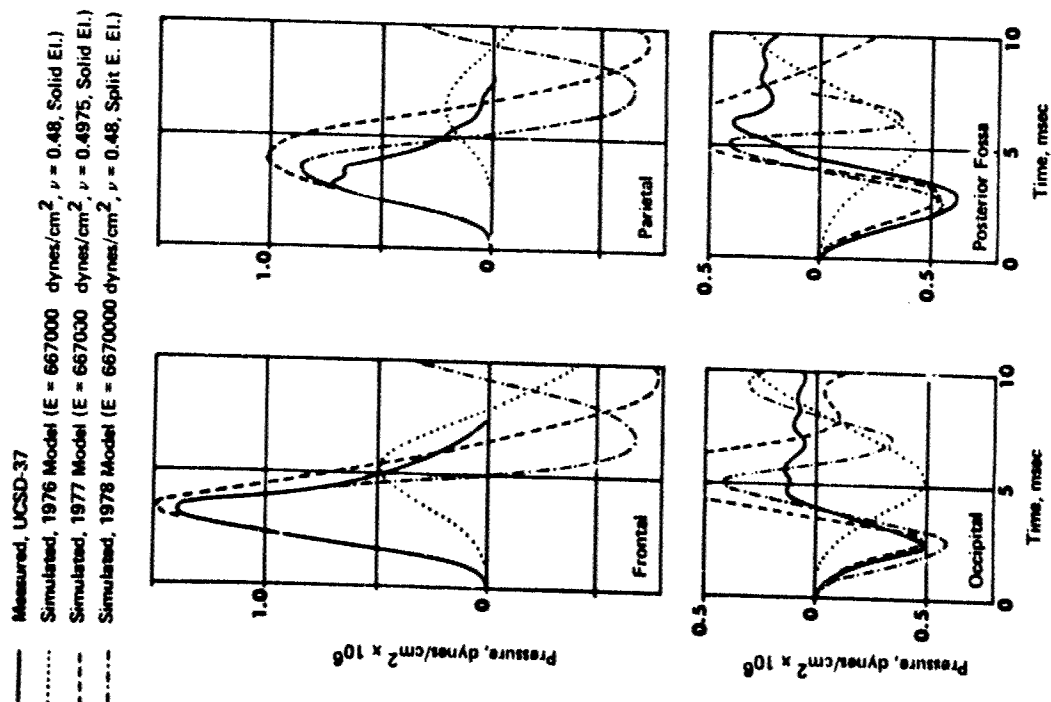


Figure 3. Measured and computed intracranial pressures for UCSD Test 37.

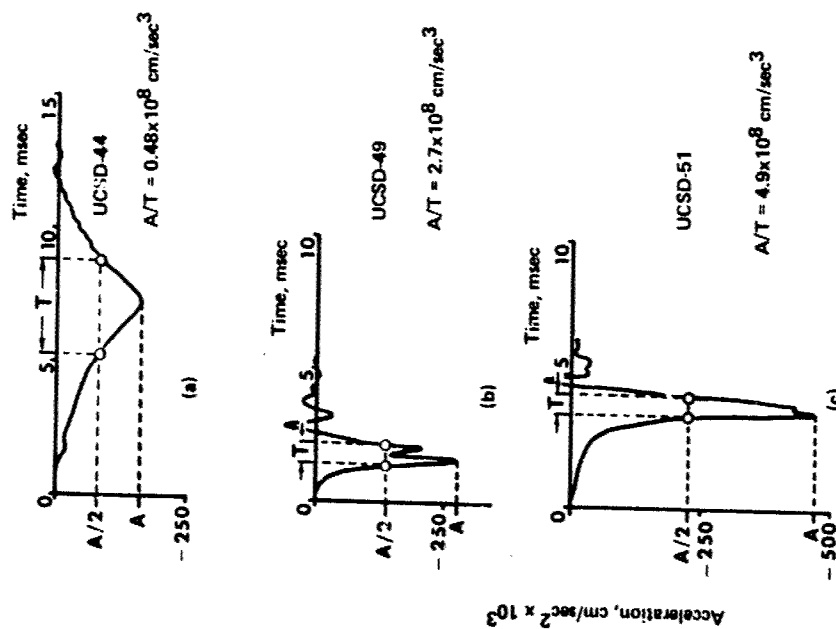


Figure 4. Measured head accelerations for UCSD Tests 44, 49, and 51

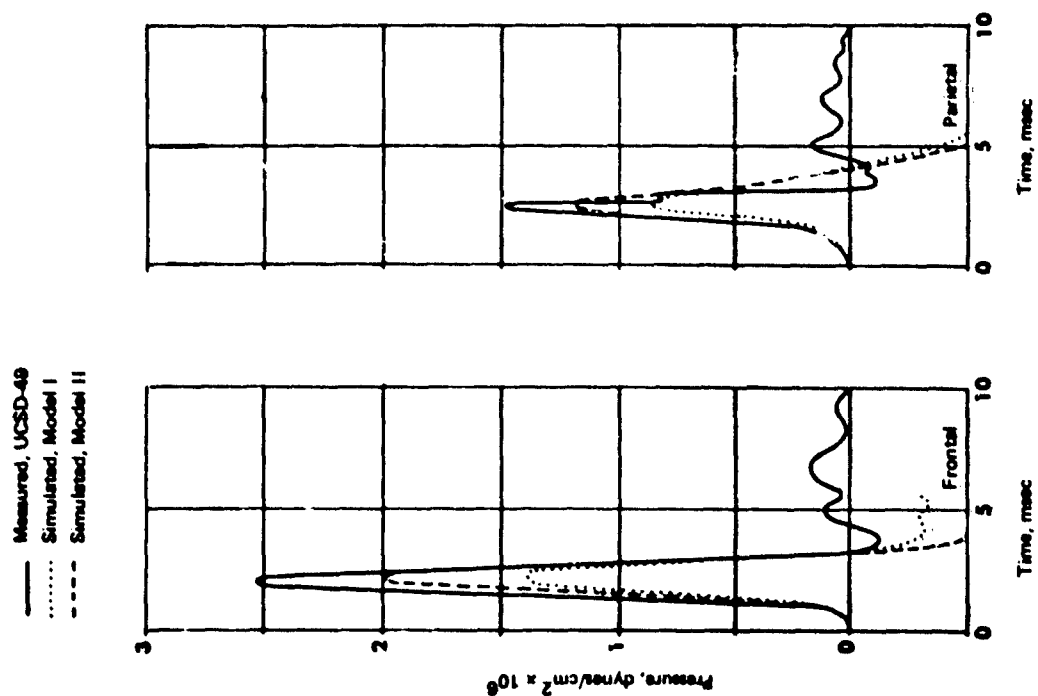


Figure 6. Measured and Model I and II intracranial pressures for UCSF Test 49 (unpadded head impact).

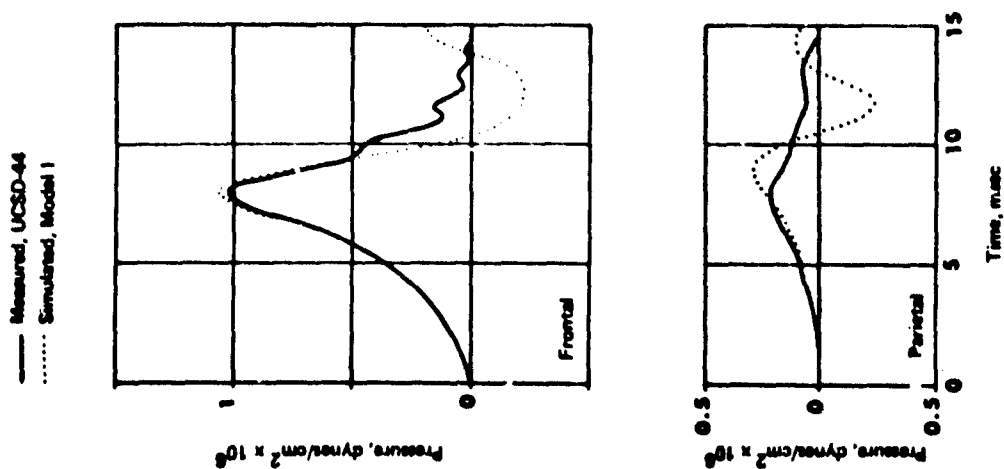


Figure 5. Measured and Model I computed intracranial pressures for Test 44 (padded frontal impact).

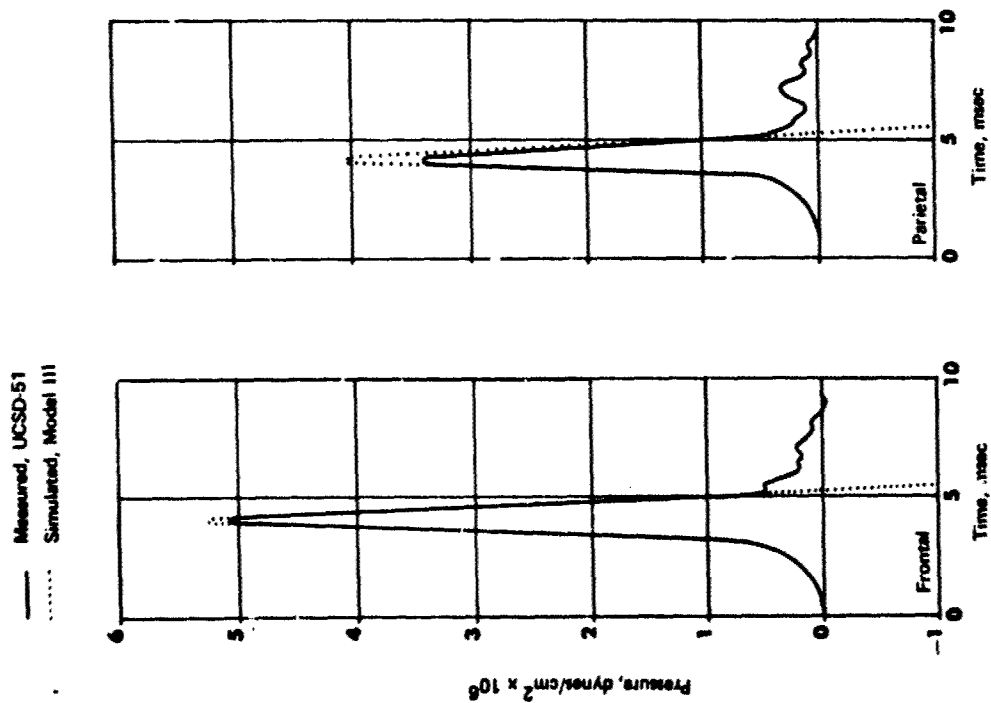


Figure 7. Measured and Model III intracranial pressures for UCSD Test 51 (ineffectually padded head impact).

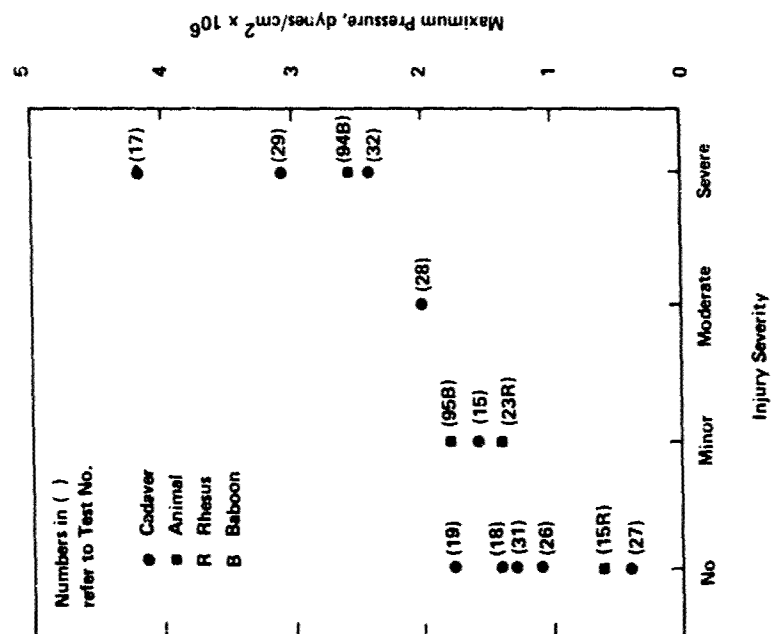


Figure 8. Comparison of injury severity and computed maximum pressures for ten UCSD human cadaver head impact tests and four HSR1 live rhesus and baboon head impact tests.

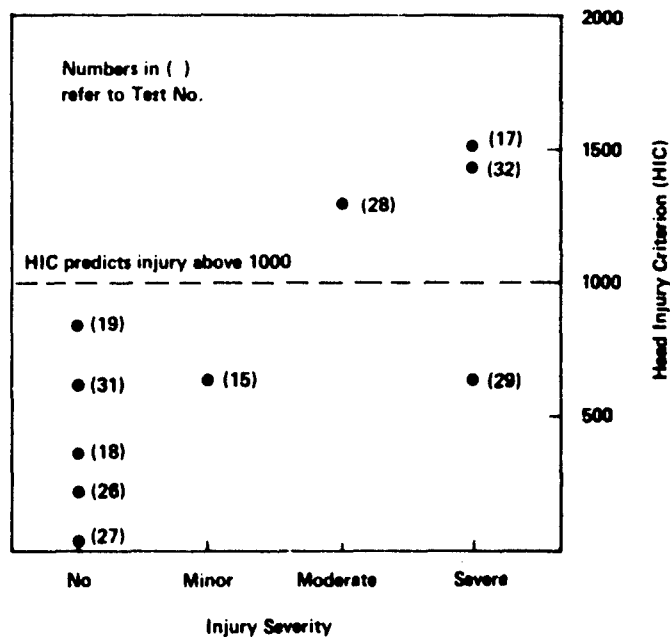


Figure 9. Comparison of Injury Severity and Head Injury Criterion Index for ten UCSD head impact tests.

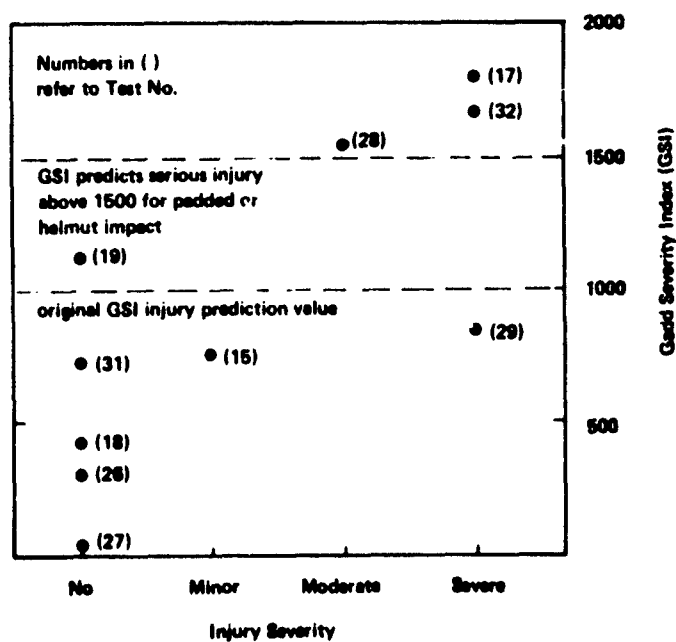


Figure 10. Comparison of Injury Severity and Gadd Severity Index for ten UCSD head impact tests.

DISCUSSION

COL C. KNAPP (USA)

Are you or have you attempted any correlation between survivable closed head injury and the pressure values and the cadaveric anatomic findings?

AUTHOR'S REPLY

We have no data from humans on survivable injuries at the present time. However to obtain more information from the real world a study to record injuries from live patients has been started. We have currently agreed what the coding should be, how we should describe the severity of the injury and now I expect that in the near future we will have such information to correlate with.

COL C. KNAPP (USA)

I guess it will be very difficult to take the clinically survived head injury and place on that injury description a specific pressure value?

AUTHOR'S REPLY

That is true. It will be hard to reconstruct what happened to that person.

COL C. KNAPP (USA)

Are you satisfied with the correlation of the HIC (Head Injury Criterion) with your pressures? Have you done some regression correlation work on that or are you satisfied with the HIC value of 1,000 for concussive injury?

AUTHOR'S REPLY

There will always be a deviation between the HIC and the intercranial pressures, because the HIC integrates the acceleration pulse and tends to smooth it out; the pressure responds to the acceleration pulse and in a certain frequency range the brain response is amplified so that it also has a sharp spike. Therefore the sharper the spike the greater the deviation between what's indicated as injury by pressure and what would be indicated as injury by the HIC. As far as looking at the HIC itself, I haven't evaluated it.

COL C. KNAPP (USA)

If we are going to accept head protective gear based on HIC or SI (Severity Index) criteria, it would seem that we need to work toward correlation of these parameters to biologic injury as an end goal and I would hope that your modeling work would eventually try to come to some correlation, because there seems to be a great deal of difference of opinions in the community right now whether that HIC = 1,000 value represents a real limit.

AUTHOR'S REPLY

I agree.

DR. VON GIERKE (USA)

Taking the intercranial pressure as indicator for injury can only be a very rough approximation. It will never give you the distribution of the injury. The pressure distribution will be an important factor which produces local tissue stress. I wonder where are the limits for the application of your model? What are your plans for really going further down to the prediction of localized injury we must expect from the different types of blows?

AUTHOR'S REPLY

Right now we compute pressures throughout the head and we intend to look at the merit of other measures. There are a number of other things that we would like to look at. So far this is only for frontal impact. We plan to proceed this year to side impact. And then, of course, we're going to do occipital impact. We have already started some helmeted impacts, but in each case we are only measuring pressure. Probably a year from now, if the study goes on, we will start to measure strain. Strain could be a very important quantity in injury. As yet there's no experimental data on strain. The tests we proposed and had conducted did not produce measurable strains; so as yet strain has evaded us. We will have to deal with that problem after we have completed the pressure study.

POTENTIAL RELATIONSHIP BETWEEN HUMAN CENTRAL NERVOUS SYSTEM INJURY AND IMPACT FORCES BASED ON PRIMATE STUDIES

Unterharnscheidt, F., M.D.
Medical Director
Rehabilitationsklinik Loipl
D-8242 Bischofswiesen/Berchtesgaden, FRG

and

Ewing, C.L., M.D.
Scientific Director
Naval Aerospace Medical Research Laboratory Detachment
New Orleans, LA 70189, USA

SUMMARY

Different species of monkeys underwent impact acceleration forces delivered to the head and neck by three different mechanisms. The first applied linear impact forces directly to the calvarium of the animal approximately through the center of gravity of the head resulting primarily in translational motion and deformation of the calvarium. The second mechanism applied angular impact forces directly to the calvarium by a device molded to the calvarium which forces the head through 45° of forward flexion. The third mechanism applied impact forces indirectly to the head and neck by acceleration of the entire animal using a pelvic-torso restraint in which the head and neck were unrestrained. Low level - no injury experiments to high level - fatal injury experiments were accomplished by each mechanism.

The characteristic cylindrically symmetrical central nervous system lesion results from direct linear acceleration. A radial distribution results from direct angular acceleration. The most extensive lesions for indirect impact acceleration experiments occur at the atlanto-occipital junction. The quality and severity of these lesions are dependent upon the level of acceleration applied. The possible relation of these injury patterns to the mechanism of injury in humans will be developed. The neuropathological procedures necessary to conduct these evaluations will be described.

BACKGROUND

In a continuing medical research program designed to define the means for objective evaluation of crash protective and escape systems, there are three major projects:

A. Measurement of the living human kinematic response envelope to impact accelerations in up to 27 different vector directions; up to the limit of voluntary tolerance for peak acceleration, rate of onset of acceleration, and duration at peak acceleration; and with three different sizes of human volunteer subject covering the range of 3rd through 98th percentile of sitting height relative to the U.S. Navy anthropomorphic survey of 1965.

B. Derivation of performance specifications for human analogues from these data, and development of those analogues, including mathematical models and a family of dummies, and

C. Definition of that portion of the human kinematic response envelope which is injurious, using primate models, so that a human injury model can be developed.

The research reported here is a portion of project C. As part of this project, primates are fitted with both inertial and physiological instrumentation; first to measure the kinematic response and then to measure the physiological response to the kinematic response. The determination of the neuropathological cause of the neuro-physiological response completes the evidentiary chain from inertial input to the tissue injury.

PREVIOUS WORK

The pathomorphological findings of a large series of animals which were subjected to acceleration levels in the +Gz and the +Gx vectors by direct impact to the head with intensities which extended from subconcussive to lethal intensities were described previously (1,2,3).

Unterharnscheidt and Higgins carried out carefully controlled studies of non-deforming head angular acceleration using squirrel monkeys undergoing flexion of the head and neck through 45° (4,5,6).

Acceleration of the head may be translational (linear) or angular in nature. Translational acceleration is produced in a body if the resultant of the applied forces passes through the center of gravity of the body. If the applied force system does not go through the center of gravity, acceleration is produced. For the head, attached as it is to the neck, any prolonged translational acceleration would lead eventually also to angular acceleration.

In addition to these accelerations which may be thought of as steady-state whole-body effects the blow also produces waves of compression which propagate through the skull and eventually develop a highly transient but very complicated stress pattern. This process is further complicated by differences in the propagation characteristics of the skull and the brain. In any local stresses in the developed stress pattern exceed the level of tolerance of the tissue. At that point presumably lesions will be produced, or

some form of tissue damage will occur.

Translational acceleration was administered from above (impact direction V according to SPATZ 1950) using the concussion gun described by FOLTZ et al. (7). A single impact of subcommotio strength, at a speed of 7.1 m/sec, resulting in a peak of 205 g, imparted to the freely movable head of a cat, caused neither behavioral nor histologic changes in the CNS; whereas repeated impacts of the same intensity, without causing primary traumatic lesions, did produce secondary traumatic alterations due to circulatory disturbances. Lesions in the cerebellum included scattered loss of Purkinje cells (especially at the summits of the lobuli of the vermis), proliferation of Bergmann's glia, thinning of the granular cell layer with glial reaction, and glial proliferation in the striae medullares and white substance. Alterations in the cerebrum were less severe; they consisted of disseminated ischemic nerve cells and a moderate glial proliferation in the white substance.

Impacts of concussive (commotio) strength, i.e., producing the clinical symptoms of cerebral concussion in cats, namely unresponsiveness, have a velocity of 8.3-9.4 M/sec, resulting in peak accelerations of 280-400 g. After one such impact, the histologic alterations prove to be traceless with the methods of investigation used to that time. We found, in particular, no evidence for glial cell proliferation. However, after repeated impacts of equal intensity and intervals of one to two days, the cerebral cortex showed, in addition to scattered ischemic nerve cells, extensive focal and pseudolaminary necroses of the parenchyma and loss of nerve cells in various parts of the Ammon's horn formation. Tissue alterations in the cerebellum, although less intense, corresponded in quality to those caused by successive impacts of subcommotio strength.

It follows that blunt impacts of intensities that do not cause noticeable tissue alterations when applied singly may elicit secondary alterations due to circulatory disturbances when applied successively in repeated experiments. A sustained permanent brain injury can therefore result from secondary lesions alone, with no primary traumatic alterations present at all. The time interval between impacts has a distinctive influence on the nature of the morphologic alterations.

Considerable primary traumatic lesions are produced by impacts with a velocity of 10.5 m/sec or more, which produce peak accelerations of 400 g or more. In all instances there were subarachnoid and subdural hemorrhages, so-called cortical contusions at the pole and the counterpole, single intracerebral hemorrhages, and traumatic necroses. Speeds of the impacting instruments of 17.2 and 18.3 m/sec are fatal to a cat. Accelerations produced by these impacts were not measured because fractures occurred (1,2,3,8,9). See Table in reference (10).

Rotational Acceleration. Unterharnscheidt and Higgins carried out carefully controlled studies using 24 squirrel monkeys (*Saimiri sciureus*) undergoing flexion of the head and neck through 45° (4,5,6). The equipment used in these studies was designed by Higgins and Schmall (11). The monkeys were subjected to rotational accelerations ranging from 101000 to 386000 rad/sec². The result was a continuum of clinical effects from no observable signs through concussion to death. See Table in reference (5).

The lowest rotational accelerations employed (101 000 - 150 000 rad/sec²) caused apparently no primary or secondary alterations in the cerebrum. However, the next higher accelerations, up to 197 000 rad/sec², produced in 10 of 13 animals subarachnoid hemorrhages, combined in one instance with primary traumatic hemorrhages in the oculomotor nerve, and tears and avulsions, mainly of veins and capillaries, in superficial cortical layers in 8 animals. Accelerations of more than 200 000 rad/sec² caused severe primary traumatic hemorrhages in the cortex and white substance. Rotational acceleration of more than 300 000 rad/sec² were not survived. The monkeys subjected to these extremely high accelerations were the only animals to show additional hemorrhages in more central regions of the brain, i.e., very close to the central pivot.

Nearly all the animals tested showed small rhectic hemorrhages in various segments of the spinal cord. Capillary and venous hemorrhages were more frequently found disseminated in the gray substance and were caused by longitudinal and transverse stretching of ascending and descending vessel branches. They were seen in all segments of the cord. These lesions were not fatal and produced no clinical signs in the animals. In two instances a subdural hemorrhage was found in the cauda equina.

It must be pointed out that the primary traumatic lesions found in the cortex are venorhectic, and occasionally arterio- or capillary rhectic hemorrhages of the more superficial cortical layers, as evidenced by torn vessel walls. Also, these hemorrhages are always associated with vessel systems running at right angles to the cortical surface. See Table in reference (10).

In summary, not only does a qualitative difference exist between the primary traumatic cortical hemorrhages produced by rotational acceleration and the so-called cortical contusions found in translational injuries, but there are also different patterns of distribution for the primary traumatic lesions encountered in both types of acceleration, inasmuch as these lesions are arranged in a cylindrically symmetric pattern after translational acceleration, as compared to a radially symmetric pattern located close to the midline after rotational acceleration.

Except for the question of location, these considerations seem to be valid also for the interpretation of findings in the spinal cord, although correlations are not as patently manifest here as they are in the brain. Nevertheless, the relation between severity of primary traumatic lesions and magnitude of acceleration is evident throughout the entire CNS.

The present study reports on a carefully ^{/controlled} series of experiments with whole body -Gx impact acceleration exposures of Rhesus monkeys with completely restrained torso but unrestrained head and neck. That is, the animal is accelerated backwards with the unrestrained head and neck undergoing flexion. Thus, impact acceleration is transmitted from the sled to the torso, and then indirectly via the vertebral column to the head.

EXPERIMENTAL EQUIPMENT

A 225,000 Pound Thrust Horizontal Accelerator with sled, control console and enclosed environmentally controlled 700-foot track at NAMRLD in New Orleans was used. This can impart 200 G to the lightweight primate sled.

The Inertial Data Acquisition System samples 24 channels of inertial data at 2000 samples/sec/channel, digitizes it, and stores the digitized data in magnetic discs in real time.

The Physiological Data Acquisition System is designed to acquire EEG, ECG, somatosensory evoked potential and respiration, for 16 channels via FM/FM telemetry with a maximum band width of DC - 100 Hz.

The Photographic Data Acquisition System includes sled and laboratory mounted cameras, lights and control console, as well as phototarget design, necessary to obtain precise 3-dimensional photographic data of primate kinematic response, especially displacement. A complete description is published elsewhere (12).

The Transducer Monitoring System was developed for primates which permits precise determination of acceleration, velocity and displacement at the mounting site. Transformation of the data to coordinate systems fixed in the anatomy is accomplished using the results of x-ray anthropometry which measures the precise three dimensional spatial position of the instrumentation coordinate system relative to the head anatomical coordinate system. A complete description is published elsewhere (13). The head acceleration was measured by a rigidly mounted array of six linear accelerometers locked to an implanted pedestal bolted to the calvarium capable of measuring angular and linear acceleration and velocity in three dimensions. A complete description is published elsewhere (14,15,16).

Sled acceleration was also measured.

Two different types of restraint systems were used, namely a rigid moulded one and a harness vest. There seems to be no difference in the lesions produced, since the head and neck kinematic response is not markedly altered.

EXPERIMENTAL PROCEDURES

Eleven Rhesus monkeys were subjected to sled accelerations ranging from 10.3 to 158.2G in the -X vector. Animals No. 3912, 4099, 3146 and 3935 were run repeatedly until severe fatal or injury occurred. Subsequently the other animals were run only once in order to avoid possible cumulative effects of multiple runs. The results of the injurious run or the solitary run for the animals run once are listed in table 1.

The 5 surviving animals were sacrificed after different survival times. One of these animals was so severely injured (the sled acceleration was 122.9G) that it had to be sacrificed in an moribund state 90 hours after the run. It was determined that this was a threshold case of medullo-cervical injury without subluxation.

Before, during and after the acceleration, epidural EEG, somatosensory evoked potential, and ECG were recorded pre, during, and post run. Non-fatal runs were followed periodically with these neurophysiological recordings. These data will be reported separately.

Pre and post run x-rays of the entire spine were performed.

Maintenance and utilization of the primates was under the direct control of a specialist in laboratory animal medicine, who will report the clinical findings separately.

PATHOLOGICAL TECHNIQUE

The autopsy report has to show not only the cause of death, but also a concise description of the distribution and quality of the tissue alterations in brain and spinal cord which can be considered the morphological end states of the applied mechanical inputs. This requires comprehensive and detailed neuropathological procedures which are not ordinarily undertaken.

Techniques for removal of brain and spinal cord in necropsies vary to some degree. But in order to describe, evaluate, qualify and compare the morphological end states a standardization of the techniques used is a necessity, as outlined earlier (17).

This should include, but not be limited to, a detailed gross and microscopic examination of all injured organs, exclusive of the central nervous system, which will be handled separately as described below. It should also include a description of the status of both common and internal carotid arteries and both vertebral arteries. In case of an evident injury to these vessels, the entire specimen should be taken out and examined.

In these experiments, the area between lower medulla and upper cervical spinal cord, that is, the atlanto-occipital junction, is the zone of the most extensive stress. The brain and spinal cord down to the cauda equina must be removed in toto, leaving the unopened spinal dura mater on the specimen, using a posterior incision and laminectomy. This is quite important because the level of the cranio-cervical junction is destroyed by using ordinary autopsy procedures.

After photography in black and white and color, and describing the brain and spinal cord, a Spielmeyer assortment of tissue blocks for histological examination using different staining techniques was taken and processed under standardized conditions.

Serial sections of brain and spinal cord were processed using different staining techniques. The histological examinations are intended to determine the threshold at which partial transections occur and the levels which will be tolerated without any structural damage. The results will be demonstrated later. The entire cervical spine is thoroughly examined, especially the alterations in the bony structures, muscles, ligaments, and the discs, and will be reported in detail.

RESULTS

Gross Pathology

A preliminary report of these findings was reported elsewhere (18).

The results of these experiments can be expressed in terms of damage to:

A. Central nervous system, B. Vascular structures, C. Skeletal system.

A. Central nervous system. At 120 - Gx (sld), complete traumatic transections occurred between lower medulla and upper cervical spinal cord.

B. Vascular system. At 120 - Gx (sld), the vertebral arteries were ruptured and subsequent subdural and subarachnoid hemorrhage occurred at the base of the brain and around the spinal cord, extending into different levels, in some cases into the cauda equina.

There were two subtypes of rupture of the vertebral arteries:

(1) The more frequent injury, in which both vertebral arteries, and in a few instances the basilar artery also, were completely avulsed.

(2) The less frequent injury in which a separation of the vertebral arteries occurred immediately above the foramen magnum, so that their proximal parts remained intact in the specimen in situ. In this second type there was a C₁ - C₂ subluxation instead of an atlanto-occipital separation. Since the cardiac actions in these traumatically transected animals continued for about 20 minutes, relatively large hemorrhages developed which in some instances became space-occupying lesions, and were, therefore, termed hematomas.

In no case did a rupture of the carotid arteries occur.

Another remarkable finding is the occurrence of subdural hemorrhages over both cerebral hemispheres due to ruptured bridging veins. Since EEG and ECG were recorded in the cases with these developing and expanding hemorrhages, interesting insights into the neurophysiological aspects can be expected.

C. Skeletal system. Two types of lesions of the cervical spine occurred:

(1) atlanto-occipital subluxations with massive dislocation of the segments, and (2) in one case only a C₁ - C₂ subluxation. Comparisons of the pre- and post run skeletal x-rays showed no fracture. This is of considerable interest because the lethal injuries were all soft tissue injuries. This indicates that the use of x-rays, in the absence of autopsies to determine injuries in cadaveric research of this type, should be interpreted with great caution.

A summary of force inputs and gross results is presented as Table 1.

CONCLUSIONS

As we have shown before, each vector direction of the input acceleration directly to the head produces a different and predictable type of injury in regard to quality and distribution. This was demonstrated in the experiments where the linear and rotational acceleration was translated directly to the head.

The specific injury pattern in -Gx acceleration transmitted indirectly to the head via the vertebral column consists of tissue damage at the zone of maximal stress at the atlanto-occipital junction, and of subdural hemorrhages over both cerebral hemispheres due to ruptured bridging veins most likely as the result of rotational acceleration.

As we have demonstrated before a neurophysiological and neuropathological continuum from no lesions to severe and lethal ones can be demonstrated, described and quantified. The system we are dealing with can be described by input-output relationships. Each effective mechanical input to the head and neck corresponds to a predictable and typical morphological end state.

REFERENCES

1. Unterharnscheidt, F.: Experimentelle Untersuchungen über die Schädigungen des ZNS durch gehäufte stumpfe Schädeltraumen. Zentralbl. Ges. Neurol. Psychiatr. 147:14, 1958
2. Unterharnscheidt, F.: Die gedeckten Schäden des Gehirns. Experimentelle Untersuchungen mit einmaliger, wiederholter und gehäufte stumpfer Gewalteinwirkung auf den Schädel. Monographien a.d. Gesamtgebiet d. Neurologie und Psychiatrie, Heft 103. Berlin-Göttingen-Heidelberg, Springer 1963.
3. Unterharnscheidt, F., and K. Sellier: Mechanics and pathomorphology of closed brain injuries. Conference: Head Injury Planning Committee, Chicago, Febr. 7-9, 1966, Chapt. 26, pp. 321-341. Philadelphia, Lippincott, 1966
4. Unterharnscheidt, F., and L.S. Higgins: Pathomorphology of experimental head injury due to rotational acceleration. Acta Neuropath. 12, 200-204 (1969).
5. Unterharnscheidt, F., and L.S. Higgins: Traumatic lesions of brain and spinal cord due to non-deforming angular acceleration of the head. Tex.Rep.Biol.Med. 27, 127-166 (1969).
6. Unterharnscheidt, F., and L.S. Higgins: Neuropathological effects of translational acceleration of the head in animal experiments. In: Late Effects of Head Injury. Edit. by Walker, A.E., Caveness, W.F., and McD. Critchley. Springfield, Ill., Thomas 1969.
7. Foltz, E.L., Jenkner F.L. and A.A. Ward: Experimental cerebral concussion. J. Neurosurg. 10, 332-352 (1953).
8. Unterharnscheidt, F.: Mechanics and pathomorphology of closed head injuries. Proceed.: Impact Injury and Crash Protection, May 9-10, 1968, Wayne State University, Detroit. Edit. by Gurdjian, E.S., Lange, W.L., Patrick, L.M., and L.M. Thomas. Springfield, Ill., Thomas 1970, pp 43-62.
9. Unterharnscheidt, F., and E.A. Ripberger: Mechanics and pathomorphology of impact-related closed brain injuries. In: Dynamic Response of Biomedical Systems. Edit. by N. Perrone. New York, A.S.M.E., 1970.

10. Unterharnscheidt, F.: Injuries due to boxing and other sports. In: Handbook of Clinical Neurology. Edit. By Vinken, P.J. and G.W. Bruyn. Vol. 23 Amsterdam, North-Holland Publ. Co., 1975, pp 527-593.

11. Higgins, L.S., Schmall, R.A., Cain C.P., Kielpulski, P.E., Primiano, E.O., Barber, T.W., and J.A. Brockway: The investigation of parameters of head injury related to acceleration and deceleration. Technology Inc., Life Science Division, San Antonio, Report No. T1-11A-67-1, 1967.

12. Becker, E.B., A Photographic Data System for Determination of 3-Dimensional Effects of Multiaxis Impact Acceleration on Living Humans. Proceedings Society of Photo-Optical Instrumentation Engineers, V.57. Box 1146, Palos Verdes Estates, CA 90274. 1975.

13. Becker, E.B. Stereoradiographic Measurements for Anatomically Mounted Instruments. Proceedings of the 21st Stapp Car Crash Conference, SAE, 400 Commonwealth Drive, Warrendale, PA 15096. October 1977.

14. Ewing, C.L. and Thomas, D.J., Human Head and Neck Response to Impact Acceleration. Naval Aerospace Medical Research Laboratory, Monograph 21. August 1972, 377 pp.

15. Becker, E. and Willems, G., A Validated Method for Instrumental Measurement of Human Head and Neck Response to Impact Acceleration. Proceedings 19th Stapp Car Crash Conference, SAE 400 Commonwealth Drive, Warrendale, PA. 15096, 1975.

16. Willems, G., A Detailed Performance Evaluation of Subminiature Piezoresistive Accelerometers, Presented to the 23rd International Instrumentation Symposium in Las Vegas, 1-5 May 1977. Proceedings of Instrumentation in the Aerospace Industry-Vol 23 Instrument Society of America, 400 Stanwix St. Pittsburgh, PA 15222, pp 531 - 540.

17. Ewing, C.L. and F. Unterharnscheidt: Neuropathology and cause of death in U.S. Naval aircraft accidents. Paper presented at the Aerospace Medical Panel Specialists' Meeting held in Copenhagen, Denmark, 5-9 April, 1976. AGARD Conference Proceedings No. 190, B 16-1-6, Recent Experience/Advances in Aviation Pathology, Dec. 1976.

18. Unterharnscheidt, F., Ewing, C.L., Thomas, D.J., Jessop, M.E., Rogers, R.E., and G. Willems: Preliminary Report on the neuropathological findings in rhesus monkeys undergoing short duration -Gx acceleration. Paper presented at the Sixth International Congress of Neurological Surgery, San Paulo, Brazil, 19-25 June 1977. Preprint only.

ACKNOWLEDGEMENTS

Major funding and support for this work was provided by the Naval Medical Research and Development Command and research contracts and other valuable assistance by the Biophysics Division, Office of Naval Research. Invaluable assistance was also furnished by QEI, Inc.

Opinions or conclusions contained in this report are those of the authors and do not necessarily reflect the views or the endorsement of the Navy Department.

Trade names of materials or products of commercial or nongovernment organizations are cited only where essential to precision in describing research procedures or evaluation of results. Their use does not constitute official endorsement or approval of the use of such commercial hardware or software.

Sled Parameters				Peak Head Parameters				Death	Restraint Type	Autopsy Findings
Animal Run No.	Accel. G	Dur. sec.	Rate of Onset G/sec.	Ang. Accel. Rad/sec.	Linear Accel. M/sec.	Ang. Vel. Result. Rad/sec.				
3948	LX1892	83.6	.0171	7,333.1	22,000	1,640	137	Sacrificed	Rigid	Normal
3943	LX1891	83.8	.0158	6,325.8	29,800	1,955	150	Sacrificed	Rigid	Normal
3933	LX1894	108.5	.0146	9,291.1	31,700	2,540	138	Sacrificed	Rigid	Normal
3921	LX1365	108.6	.0096	13,398.2	58,100	9,250	350	Immediate	Rigid	Atlanto-occipital subluxation
3924	LX1893	110.4	.0142	9,292.4	31,000	2,400	142	Sacrificed	Rigid	Normal
3935	LX1363	122.9	.0166	20,761.9	22,800	1,945	106	Moribund, sacrificed after 90 hrs	Rigid	Normal
4101	LX1905	126.3	.0136	13,796.9	16,700	2,820	52	Immediate	Harness-Vest	Atlanto-occipital subluxation
4099	LX1360	128.1	.0136	21,421.4	56,400	5,210	248	Immediate	Rigid	C1-C2 subluxation
3951	LX1895	130.6	.0129	12,682.0	49,200	2,850	220	Immediate	Rigid	
3946	LX1896	131.4	.0135	14,961.5	26,500	2,485	105	Immediate	Rigid	Atlanto-occipital subluxation
3146	LX0661	158.2	.0087	14,991.2	*	*	*	Immediate	Rigid	Atlanto-occipital subluxation

* Instrumentation Failure

Table 1. Summary of the Injury Effects

DISCUSSION

DR. C. WARD (USA)

Since involvement and rupture of the vertebral artery is common in motorcycle accidents, would you comment on the injury mechanism?

AUTHOR'S REPLY (DR. C. EWING, USA)

The mechanisms of injury in motorcycle accidents are difficult to separate out sometimes; for example, helmets sometimes cause injuries in motorcycle accidents; sometimes the injuries are due to direct impact, sometimes due to indirect impact. It is very difficult to separate out the specific causes of a set of injuries in a motorcycle victim. We are interested in aviators, and there are several instances where individuals exposed to this type of acceleration have suffered transections of the spinal cord, and exhibit intracranial and intrathecal hemorrhages. We feel that we are on the tail of something and that continuation of our research will provide interesting new answers.

AUTHOR'S REPLY (DR. UNTERHARNSCHEIDT, FRG)

May I continue with the pathological aspect. First, what we are trying to do for about 25 years is to deal with sudden subtypes of injuries with definable impact vectors. In the case of a motorcycle rider we cannot exactly say whether there was a direct or indirect impact. In our case we have a model and these ruptures and transections are the direct result of overstretching or kind of sliding motion. I have seen similar cases in human accidents. I remember two race drivers who drove at very high speed into a barrier at the Indianapolis race track. We haven't had a complete transection similar to this one here between lower medulla and upper cervical spinal cord. A racing driver has a 4 point belt comparable to the one we used in our animal experiments. In both cases the over stretching and gliding motion leads to this total transection of the spinal cord and of the vertebral arteries; partly the basilar arteries are involved too. I repeat again that in no case the carotid arteries were involved, at least not with the acceleration we used. Whether the carotid arteries get involved at higher G loads I don't know.

DR. GILLINGHAM (USA)

Regarding the practical application of the research presented, are you actively pursuing development of protective equipment that would prevent such injuries as those shown?

AUTHOR'S REPLY

Protective systems were designed back in the 50's, against this type of injury, but the aviators, absolutely refused to fly using those systems. The systems were over-designed. The question is what is a good design, when do you provide enough protection but not too much. For that you simply have to have first the information about human kinematic response, the response magnitudes which will be injurious and finally a complete mathematical model of the human body. This combined information will then permit you to evaluate protective systems against almost anything.

DR. VON GIERKE (USA)

If I may add a comment here: unfortunately, a protective system for one type of impact might increase the injury probability for another type. For example, a restraint harness to prevent impact of the torso with cockpit walls at relatively low accelerations might make the neck injuries described in your paper at high acceleration levels more severe.

DR. E. HENDLER (USA)

Work is being done in the US Navy Air Development Center on effective restraint systems for the head and neck and many of the people here are probably aware of the work on an inflatable restraint system that will encase the neck. Prototypes of this system are being tested to reduce head-neck motion during ejection. This principle could be extended to prevent the violent motions discussed here.

AUTHOR'S REPLY

In regard to your comment, I think a restraint system connected with the head of the pilot could avoid a great part of these injuries here.

DR. VON GIERKE (USA)

On the other hand, there are different approaches to protection one can take depending on the situation. In our air bag tests with monkeys we were not able to do any such severe injury to them and at least theoretically the air bag is still one of the best protection principles I am aware of.

AUTHOR'S COMMENT (DR. C. EWING, USA)

I would like to comment on the situation which was the starting point for our experiments: the ditching of aircraft. When an aviator crashes into the water at slow to medium speeds, stretching of the neck is believed to occur and the helmet on the man's head makes the stretching worse; so even though his head is protected by the helmet against direct impact, he is not protected against the additional weight that is put on his head by the helmet, that may cause his neck to stretch more. We believe that stretching of the neck is associated with the production of concussion or stated differently changes in neurophysiological function. Our next paper is to report our researches on this subject.

AUTHOR'S REPLY (DR. UNTERHARNSCHEIDT, FRG)

I would say some type of concussion. There are different types. It is not a cerebral concussion, but a special type of concussion caused by stretching of the spinal cord.

CORRELATION OF HEAD INJURY WITH MECHANICAL FORCES BASED ON HELMET DAMAGE DUPLICATION

Bruce Slobodnik, LT, Naval Aerospace Physiologist
Bioengineering and Life Support Equipment Division
US Army Aeromedical Research Laboratory
P. O. Box 577
Fort Rucker, Alabama 36362

SUMMARY

Human tolerance to head impact was assessed by correlating the force levels required to duplicate damage seen in 14 SPH-4 aviator helmets retrieved from US Army helicopter crashes with resulting head injury. The data obtained were used to validate the following:

- (a) the Wayne State University Concussive Tolerance Curve;
- (b) the Severity Index value of 1500 currently used in the US by the National Operating Committee on Standards for Athletic Equipment as the concussive threshold for helmeted head impacts;
- (c) the Head Injury Criterion value of 1000 currently used in the US by the Department of Transportation in occupant crash protection tests as the concussive threshold for impacts to the unprotected head;
- (d) the peak acceleration value of 400 G currently used by the US Army in evaluating aircrew protective headgear as the survivable limit; and
- (e) the peak transmitted force value of 5000 lb currently specified in British Standard 2495 as the survivable limit for helmeted head impacts.

The data did not validate the values stated for items a, b, c or e above. The peak acceleration value of 400 G appears to approximate the human survival limit for head accelerations, but the prudence of using the survivable limit rather than the head injury threshold limit as a pass-fail criterion in evaluating aircrew helmet performance can be questioned. Peak transmitted force may be a more effective criterion in evaluating the impact attenuation performance of protective headgear than is peak G, SI, or HIC.

INTRODUCTION

One of the limiting factors in the development of effective protective headgear has been an inadequate definition of human tolerance limits to head impact. Most research efforts to establish these limits have been confined, necessarily, to animal or human cadaver studies. Many indices of head injury have been proposed, based on such studies, and some are widely used by a variety of organizations. The Wayne State University (WSU) Cerebral Concussion Tolerance Curve published in 1962¹ served as the basis for several of these indices, in particular, the Severity Index (SI) and the Head Injury Criterion (HIC). The WSU Tolerance Curve is plotted with the ordinate representing the average acceleration of the skull measured at the occipital bone for impacts of the forehead against plane, unyielding surfaces while the abscissa represents pulse duration. The SI, Eq.(1), originally described by Gadd², is currently used in the United States by the National Operating Committee on Standards for Athletic Equipment (NOCSAE) in the evaluation of the impact attenuation performance of football helmets.³ An SI value of 1500 is used as a helmet pass-fail criterion because it is assumed that this value represents the threshold of concussion for helmeted head impacts. The HIC, Eq.(2), as defined by Chou⁴, is currently used in the United States by the Department of Transportation (DOT) in Federal Motor Vehicle Safety Standard No. 208⁵ for occupant crash protection tests. A HIC value of 1000 is used as a pass-fail criterion for automotive designs because it is assumed that this value represents the threshold of concussion for impacts to the unprotected head.

$$SI = \int A^{2.5} dt$$

A = resultant acceleration (G) (1)

t = time (sec)

$$HIC = \left[\frac{\int_{t_1}^{t_2} A^2 dt}{(t_2 - t_1)} \right]^{2.5} (t_2 - t_1) \quad (2)$$

t_1 = an arbitrary time in the pulse

t_2 = for a given t_1 , a time in the pulse which maximizes the HIC

a = resultant acceleration

In addition to the mathematically derived values of SI and HIC, two other indices of head injury in current use are directly measurable parameters of head impact. One index is peak acceleration and the other is peak transmitted force. The modified ANSI Z90.1-1971⁶ method currently used by the US Army (Military Specification MIL-H-43925⁷) for evaluating the impact attenuation performance of prospective aircrew helmets relies primarily on peak acceleration as a helmet pass-fail criterion. A candidate helmet is attached to an instrumented metal headform and dropped from a height yielding 70 ft lb of input energy onto a 1.9 inch radius steel hemisphere. Helmets which prevent the peak acceleration experienced by the headform in such impacts from exceeding 400 G meet the US Army standard for impact performance. It is assumed that peak accelerations of 400 G are survivable for helmeted head impacts. Studies reported by Snively⁸ and Searingen⁹ support this assumption. British Standard 2495:1960¹⁰ relies on peak transmitted force in evaluating the impact attenuation performance of protective helmets. A value of 5000 lb is specified as a helmet pass-fail criterion because that value is assumed to represent the limit for survivability for head impacts.

In 1972 the US Army's establishment of the Life Support Equipment Retrieval Program provided a unique opportunity to directly research human tolerance to head impact and to validate head injury indices such as those previously discussed. Since 1972, helmets involved in Army aircraft accidents worldwide have been retrieved for laboratory analysis. If it is assumed that the damage seen in a retrieved helmet accurately reflects the forces and accelerations experienced by the wearer's head in the crash situation, then, by duplicating that degree of damage on a similar helmet under controlled conditions, those acceleration and force levels can be identified. By comparing acceleration and force levels to resulting head injury, human tolerance limits to head impact can be defined.

Out of 170 SPH-4 helmets received through the retrieval program, 14 were selected for impact damage simulation. The criteria used to select these 14 helmets were: (a) helmet damage resulted from only one impact and (b) the impact was not a glancing blow. Therefore, in these 14 cases all head injury is assumed to have resulted primarily from translational acceleration and to have resulted from a single blow. The centers of the impact locations on both the helmet and the head for the 14 cases selected for impact damage duplication is summarized in Fig. 1. The impact locations shown on the helmet shell are precise; those on the head are approximate since some relative movement is possible between the helmet and head during the impact.



Fig. 1. Of the 14 cases studied, six were frontal impacts, 4 were crown, 2 were side, and 2 were located at the back of the head. The center of each impact shown on the helmet is precise; those on the head are only approximate since some movement between helmet and head is possible during impact.

METHOD

Spare helmet components were assembled to produce several duplicates for each of the 14 retrieved helmets. Each duplicate helmet was prepared so that its shell thickness, liner thickness, and adjustment of suspension straps matched that of the retrieved helmet as closely as possible. To reproduce the damage of a given retrieved helmet, duplicates for that helmet were attached to a modified version of the humanoid headform specified by the NOCSAE for evaluating football helmets. As shown in Fig. 2, the head-neck connection of this headform was modified to increase its adjustability and permit mounting on the standard carriage assembly specified by the ANSI Z90.1971 method. A tri-axial accelerometer (Endevco Model 2267C-750) was positioned at the headform's center of mass. Its signal was amplified by a signal conditioner (Endevco Series 4470) and fed to a Microtronics three-channel vector analyzer. The vector resultant of the three accelerometer signals was then transmitted to a hybrid computer which computed the values of peak G, SI, and HIC. Total weight of the headform and carriage was 11 lb. The helmeted headform was then dropped onto an impacting surface whose shape had been selected to reproduce the type of damage seen on the retrieved helmet. Some helmets required a concave impact surface to duplicate the area of compression seen in the foam helmet liner. These concave impact surfaces were prepared by taking an impression of the helmet shell at the impact site using dental cement. These cement impressions were then used as impact surfaces. Three piezoelectric load washers (Kisler type 9021) were positioned beneath the impact surface as shown in Fig. 2.

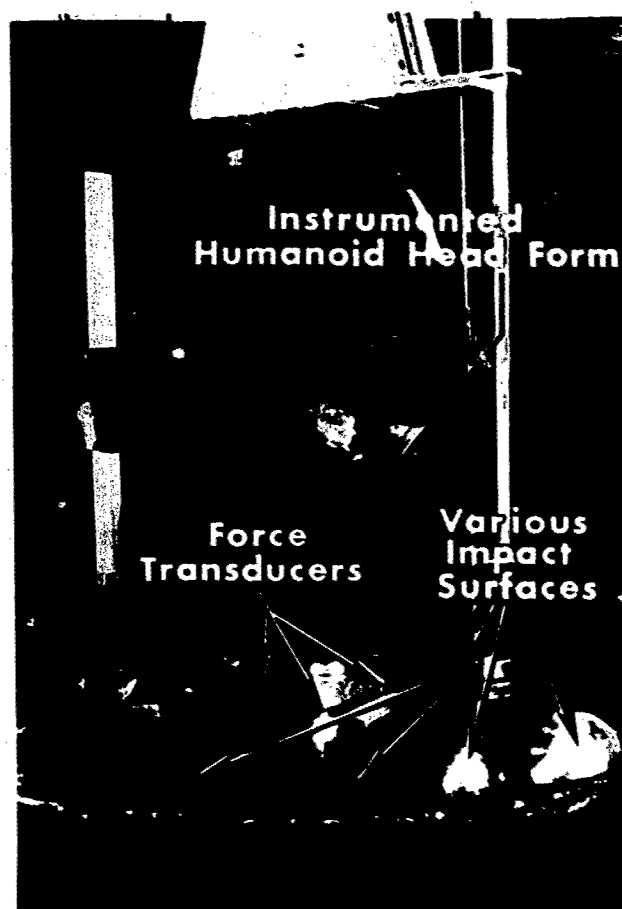


Fig. 2. Damage seen in retrieved helmets was duplicated by attaching a test helmet to this instrumented humanoid headform and impacting it onto a surface of appropriate shape. Peak transmitted force was measured using the resultant of three force transducers located beneath the impact surface. Drop height was varied until the best damage duplication was achieved. Peak acceleration was measured using a tri-axial accelerometer mounted at the headform's center of mass.

The drop height was varied until the damage produced in the duplicate helmet matched that of the retrieved helmet. Damage was assumed to have been duplicated when (a) the amount of bending in the 6 suspension strap anchor clips was duplicated, as shown in Fig. 3, (b) the area and maximum compression of the foam helmet liner was duplicated, as shown in Fig. 4, and (c) the degree of fracture in the fiberglass helmet shell, as shown in Fig. 5, matched that of the retrieved helmet. Acceleration vs time and force vs time traces were recorded for each impact as shown in Fig. 6. A description of head injuries associated with any of the 14 helmets was obtained by reviewing the original accident reports supplied by the US Army Agency for Aviation Safety. All head injuries were assigned a severity value using the Abbreviated Injury Scale (AIS).

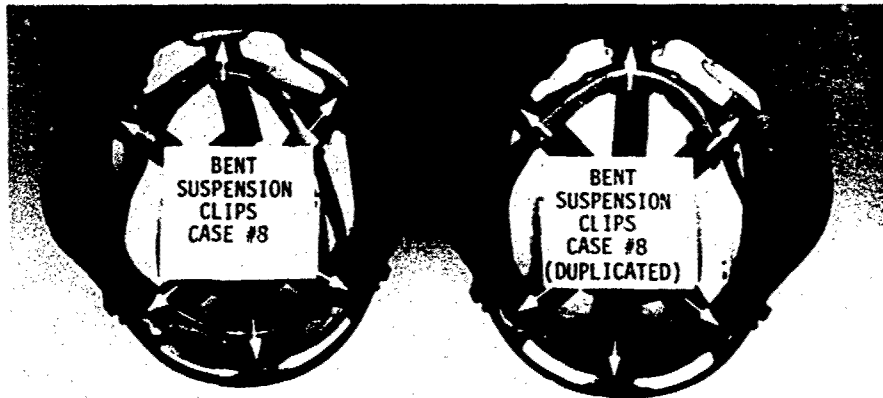


Fig. 3. The amount of bending in the six suspension strap anchor clips was duplicated for each of the 14 cases.

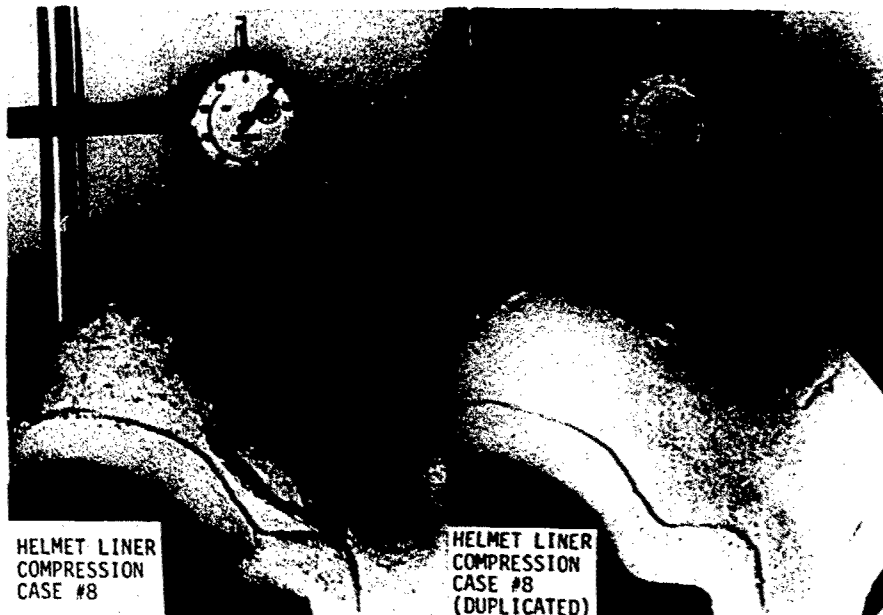


Fig. 4. Helmet liner damage was duplicated by matching the area and maximum compression produced in the test helmet liner with that of the retrieved helmet liner. Maximum compression was duplicated to within a few thousandths of an inch.

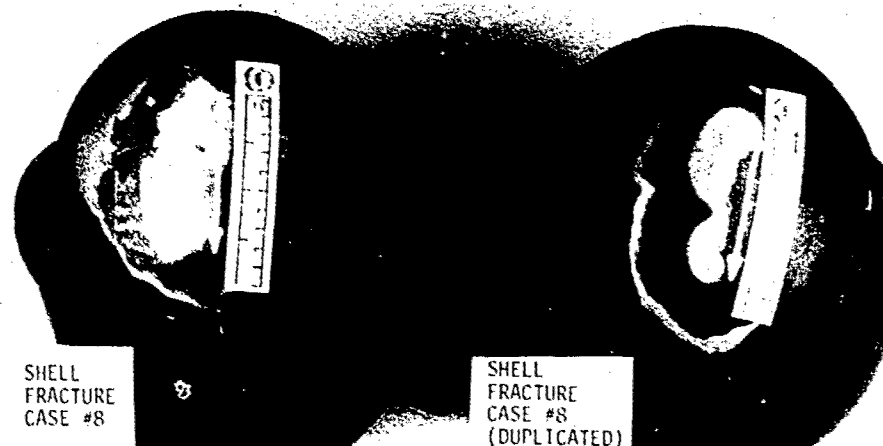


Fig. 5. The degree of fracture in the fiberglass helmet shell was duplicated for those cases in which shell fracture occurred.

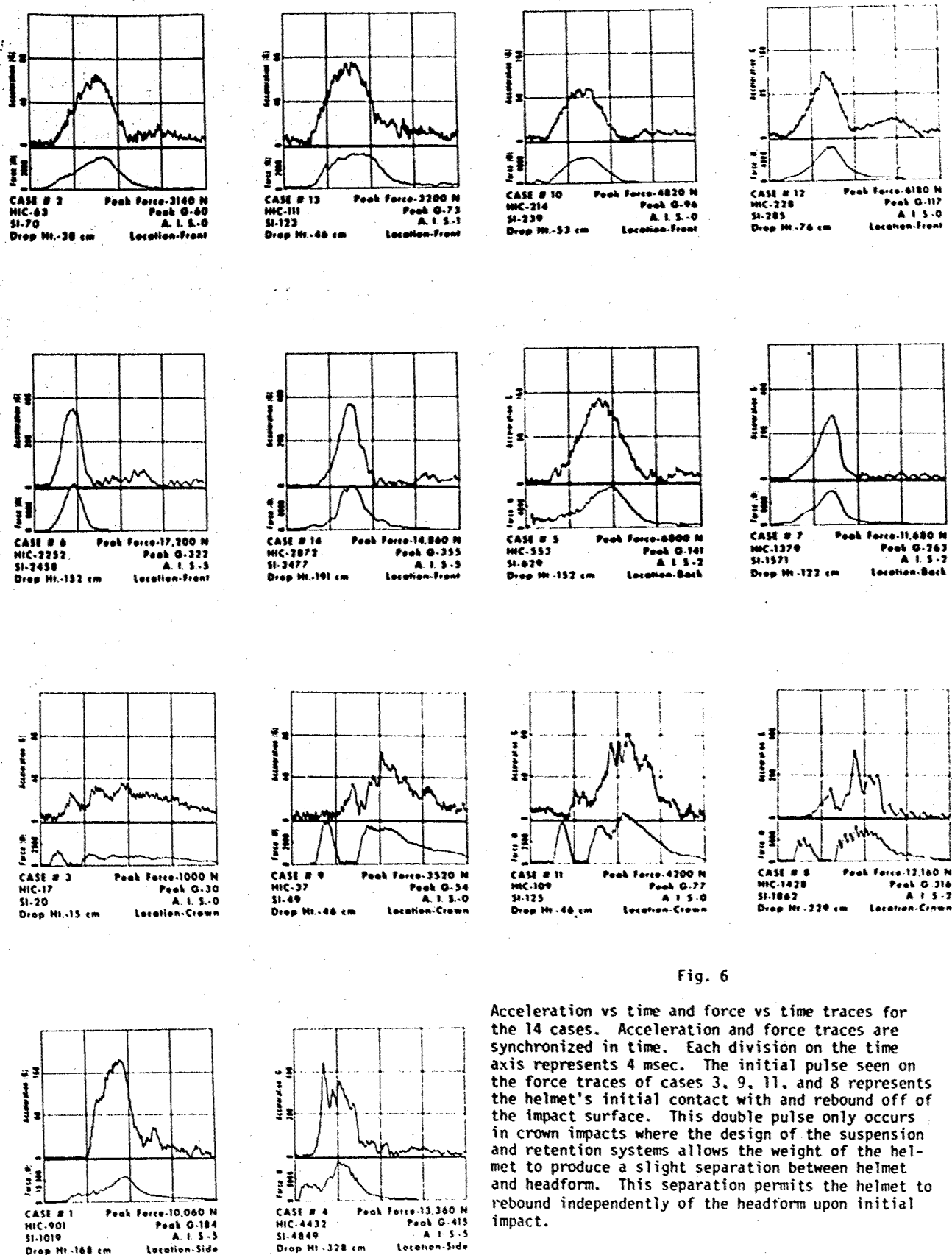


Fig. 6

Acceleration vs time and force vs time traces for the 14 cases. Acceleration and force traces are synchronized in time. Each division on the time axis represents 4 msec. The initial pulse seen on the force traces of cases 3, 9, 11, and 8 represents the helmet's initial contact with and rebound off of the impact surface. This double pulse only occurs in crown impacts where the design of the suspension and retention systems allows the weight of the helmet to produce a slight separation between helmet and headform. This separation permits the helmet to rebound independently of the headform upon initial impact.

RESULTS AND DISCUSSION

A description of head injuries, of conditions required to duplicate helmet damage, and of the data recorded for each of the 14 cases is shown in Table I. The low incidence of penetrating types of head injuries among US Army helicopter crash victims appears to be due primarily to (a) an absence of sharp rigid cockpit surfaces and (b) the effectiveness of the SPH-4 aviator helmet as a load spreading device. Only three of the 14 cases required an impact surface to duplicate helmet damage whose shape was more severe than that of a flat surface. In only one case (case #5) in which head injury occurred did the injury result from the impact surface penetrating through the helmet shell. However, the energy absorbing capacity of the helmet appears inadequate based upon the high incidence of concussive types of head injuries observed. In all eight cases involving head injury, the foam helmet liner was not compressed to the maximum extent possible. This deficiency can have disastrous effects as seen in cases 4 and 6 where basilar skull fracture occurred as a result of the helmet transmitting rather than absorbing the impact force. Recent in-house studies (unpublished) have shown that the energy absorbing ability of the helmet can be more than doubled by simply increasing the thickness and decreasing the density of the foam helmet liner.

An attempt to validate the WSU Concussive Tolerance Curve was made by comparing the plots of average acceleration and corresponding pulse duration for each of the 14 cases with the WSU curve. As shown in Fig. 7, the WSU curve failed to predict three of the eight cases where at least concussive head injury occurred. The WSU curve was derived from acceleration levels required to produce linear fracture in the frontal bone of unprotected cadaver heads. Even though concussion often accompanies linear skull fracture, it was not surprising to find concussion occurring at subfracture acceleration levels among individuals wearing protective headgear. While the WSU curve may reflect human tolerance to linear skull fracture, it can be questioned whether or not it accurately reflects human tolerance to concussion.

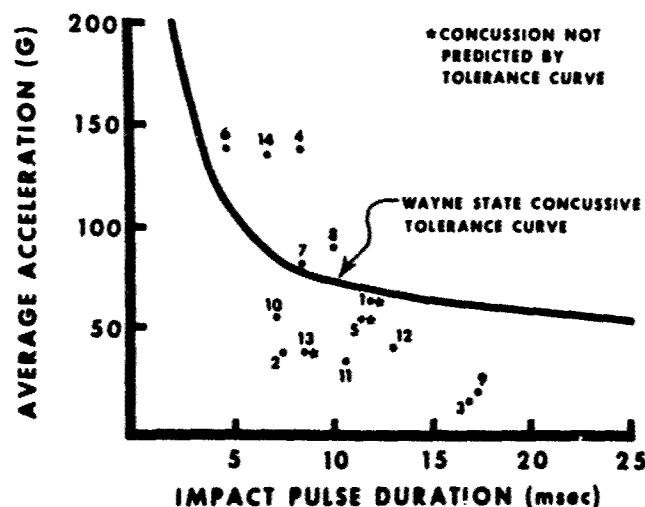


Fig. 7. Average acceleration vs pulse duration for the 14 cases plotted with the WSU Concussive Tolerance Curve. The WSU curve failed to predict three of the eight cases where at least concussive head injury occurred. See Table I for a description of head injuries.

SI values were calculated for the acceleration pulses of the 14 duplicated cases in an attempt to validate the concussive threshold value of 1500 used in the US by the NOCSAE. As shown in Fig. 8, cases 13, 5, and 1 had at least concussive head injuries occurring at SI values of 123, 629, and 1019 respectively. Case 13 probably represents the lower extreme in human tolerance to concussion (a "glass jaw" type). However, it can be questioned whether or not an SI value of 1500 accurately reflects the concussive threshold for individuals with average concussive tolerance.

HIC values were calculated for the acceleration pulses of the 14 duplicated cases in an attempt to validate the concussive threshold value of 1000 used in the US by the DOT. As shown in Fig. 9, cases 13, 5, and 1 had at least concussive head injuries occurring at HIC values of 111, 553, and 901 respectively. Again, with case 13 representing the lower extreme in human tolerance to concussion, it can be questioned whether or not a HIC value of 1000 accurately reflects the concussive threshold for an individual of average tolerance.

TABLE 1. SUMMARY OF IMPACT DAMAGE DUPLICATION DATA FOR 14 HELMETS
RETRIEVED FROM US ARMY HELICOPTER ACCIDENTS

Case No.	Impact Loca- tion	Shape of Impact Surface (m)	Drop Ht. (m)	Peak Accel- eration (G)	Average Accel- eration (G)	Pulse Dura- tion (ms)	SI	HIC	Peak Force (N)	Helmets Liner Thickness Before Impact (cm)	Maximum:		Impact Energy (J)	Head Injury Description	AIS
											Liner Con- pression After Impact (%)	Total Liner Area Com- pressed (cm ²)			
2	front	flat	0.38	60	38	7.2	70	63	3140	--	none	none	24	none	0
13	front	concave	0.46	73	38	8.4	123	111	3200	0.983	38	17.0	29	dazed several minutes	1
10	front	flat	0.53	96	55	7.0	239	214	4820	1.054	13	20.6	34	none	0
12	front	flat	0.76	117	40	13.0	285	228	6180	1.021	39	14.6	48	none	0
6	front	flat	1.52	322	139	4.5	2458	2252	17200	1.029	43	21.3	97	basilar skull fracture, uncon- scious 30 hours	5
14	front	concave	1.91	355	136	6.5	3477	2872	14860	0.983	52	45.6	121	subdural hema- toma	5
3	crown	flat	0.15	30	14	16.8	20	17	1000	--	none	none	10	none	0
9	crown	flat	0.46	54	18	17.4	49	37	3520	--	none	none	29	none	0
11	crown	flat	0.46	77	34	10.6	125	109	4200	--	none	none	29	none	0
8	crown	rod 1.27 cm radius	2.29	316	90	9.8	1862	1428	12160	1.118	34	30.5	145	unconscious 2 min, semi- conscious 6 hours, fracture of C ₁	2
5	back	bolt head 1.27 cm diameter	1.52	141	54	11.3	629	553	6800	1.029	78	14.7	97	deep scalp laceration, dazed several minutes	2
7	back	flat	1.22	263	81	8.3	1571	1379	11680	0.909	63	26.8	77	unconscious several minutes	2
1	side	hemi- sphere 4.83 cm radius	1.68	184	67	10.9	1019	901	10060	1.080	51	25.0	107	unconscious 100 hours	5
4	side	concave	3.28	415	138	8.1	4849	4432	13360	0.991	14	13.2	208	basilar skull fracture with subarachnoid hemorrhage, fatal	5

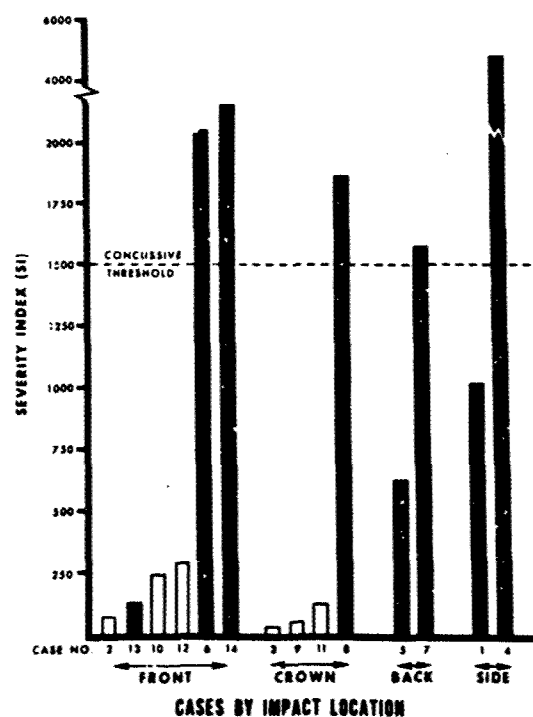


Fig. 8. Severity Index values for the impact best duplicating helmet damage for each of the 14 cases. Solid bars represent cases in which head injury resulted from the impact. Concussion occurred below the SI value of 1500 used by NOCSAE as the concussive threshold. See Table I for a description of head injuries.

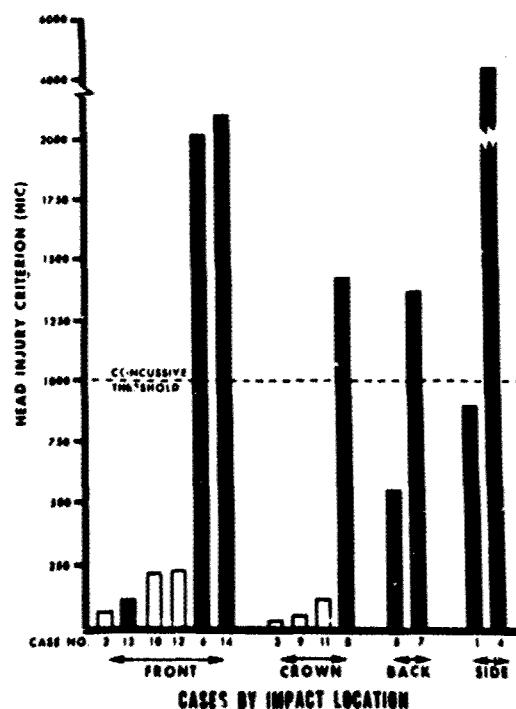


Fig. 9. Head Injury Criterion values for the impact best duplicating helmet damage for each of the 14 cases. Solid bars represent cases in which head injury resulted from the impact. Concussion occurred below the HIC value of 1000 used by DOT. See Table I for a description of head injuries.

Peak acceleration values for the 14 cases were recorded in an attempt to validate the 400 G survivable limit currently used by the US Army as a pass-fail criterion in evaluating the impact performance of prospective aircrew helmets. As shown in Fig. 10, the one case of fatal head injury (case 4) occurred at a peak acceleration value of 415 G. It would appear that the pass-fail criterion currently used by the US Army accurately reflects the limit of survivability for head accelerations. However, its use permits helmets to be selected for use by aircrewmembers which for the most part prevent death in crash situations, but certainly do not prevent concussive head injury. Considering the potentially hostile elements which may be experienced by an aircrewman in the post crash environment such as fire, drowning, and capture, the injury level permitted by the current US Army pass-fail criterion is unacceptable. Concussion occurred at a peak acceleration value as low as 73 G (case 13). With this individual representing the lower extreme for human tolerance to concussion, it is estimated that an average individual's concussive tolerance for helmeted head accelerations would approximate 150 G. This tolerance level is significantly lower than that reported by Swearingen³ who duplicated the impact conditions involving the crash of a military helicopter. He reported that the pilot involved received a frontal head impact and experienced a peak acceleration of 435 G without sustaining any head injury. Even though differences exist between individuals in their tolerance to head impact, it seems highly unlikely that very many individuals exist who could withstand head accelerations of this magnitude without experiencing at least concussion. As shown in Fig. 7, the peak acceleration associated with all eight cases involving head injury in this study fell below 435 G. In particular, cases 6 and 14 were frontal impacts in which very severe head injuries resulted (AIS value 5) from peak accelerations of 322 G and 355 G respectively.

The values of peak transmitted force were recorded for each of the 14 cases in an attempt to validate the value of 5000 lb currently specified in British Standard 2495 as the limit of survivability for helmeted head impacts. As shown in Fig. 11, the one case of fatal head injury occurred at a peak transmitted force of 2982 lb. In addition, severe head injury occurred (AIS value 5) in cases 6, 14, and 1 at peak transmitted force values of 3839 lb, 3317 lb, and 2246 lb respectively. It would appear that a peak transmitted force value of 5000 lb exceeds the limit of survivability. Depending upon the location of the head impact, a peak transmitted force value of between 3000 lb and 4000 lb would seem to reflect the survivable limit for helmeted head impacts.

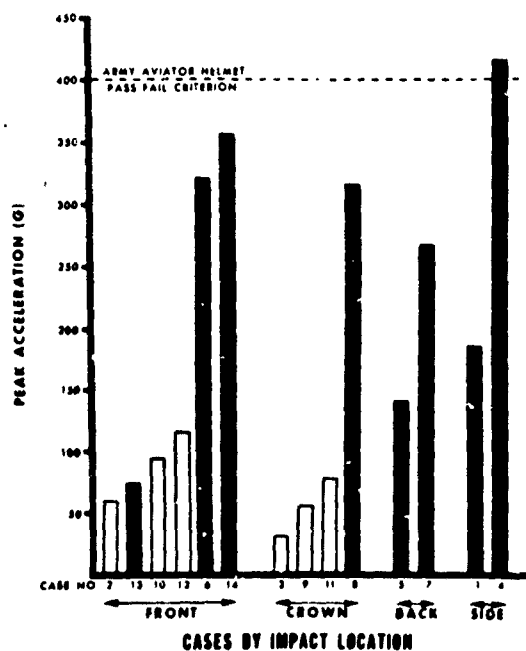


Fig. 10. Peak acceleration values for the impact best duplicating helmet damage for each of the 14 cases. Solid bars represent cases in which head injury resulted from the impact. Head injury occurred at peak acceleration levels well below 400 G. See Table 1 for a description of head injuries.

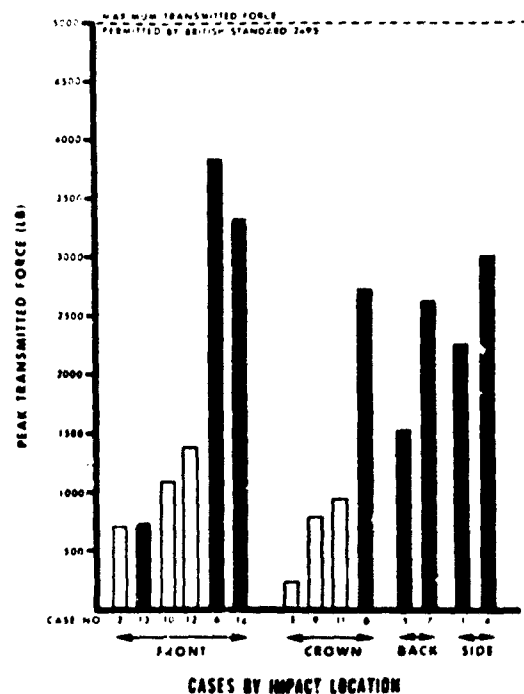


Fig. 11. Peak transmitted force values for the impact best duplicating helmet damage for each of the 14 cases. Solid bars represent cases in which head injury resulted from the impact. Cases 6, 14, 1, and 4 had an AIS value of 5 with case 4 being fatal. The survivable limit appears to be between 3000-4000 lb, depending upon impact location, rather than 5000 lb permitted by British Standard 2495.

A stepwise regression analysis of the impact data was performed to determine the ability of each of the head injury indices shown in Table II to estimate the AIS values assigned to the 14 cases. Each head injury index was first analyzed separately as an estimator of AIS values. The standard error of estimating the AIS values for each head injury index was used as an indicator to rank the indices in their ability to estimate AIS values. The lower the standard error for a given index the more accurately it estimated the 14 AIS values. Table II shows the four head injury indices ranked in decreasing ability to estimate AIS values. Peak transmitted force was the best estimator of the severity of head injury. The four indices were then analyzed jointly to determine to what extent each index contributed to the variance seen in the AIS values. These results are also shown in Table II. Peak transmitted force accounted for a dramatic 76% of the variance. No other injury index contributed significantly to the variance. These results suggest that peak transmitted force might be more effective as a criterion for evaluating helmet impact performance than peak G, SI, or HIC. Glaister¹² attributed the poor correlation between peak transmitted force and severity of head injury that he reported to a headform whose response to impact did not accurately reflect human head response. This underlines the important role headform design plays when research into human tolerance limits to head impact is conducted. Metal Headforms are of little value in this area.

TABLE II. FOUR HEAD INJURY INDICES AS ESTIMATORS OF AIS VALUES

Variable (head injury index)	Contribution to Variance in AIS values		Standard Error of Estimate when a given head injury index was used separately to estimate AIS values*
	R ² (%)	Increase in R ² (%)	
Peak transmitted force	76.0	76.0	± 1.105
Peak acceleration	80.0	4.0	± 1.224
Severity Index	83.5	3.5	± 1.259
Head Injury Criterion	84.2	<1	± 1.262

*Using the linear regression model: $y_j = b_0 + b_1 x_{ij} + e_j$

where $y_j = \text{AIS value}$

$x_{ij} = \text{a given head injury index}$

$j = 1, 2, \dots, 14$

$i = 1, 2, 3, 4$

CONCLUSIONS

The data obtained from duplicating the damage seen in 14 SPH-4 helmets retrieved from US Army helicopter crashes did not validate concussive threshold levels or survivable limits currently used in conjunction with the five head injury indices discussed. Concussion can occur below the limits specified by the WSU Concussive Tolerance Curve. Concussion can also occur below SI values of 1500 and below HIC values of 1000 which are the concussive threshold values currently used in the US by the NOCSAE and the DOT respectively. Fatal head injury can occur below a peak transmitted force value of 5000 lb which is currently used as the survivable limit for helmeted head impacts as specified in British Standard 2495. To be effective in selecting aircrew helmets which will prevent concussive head injuries from occurring in survivable helicopter crashes, the pass-fail criterion of 400 G currently used by the US Army should be reduced to at least 150 G. While the SPH-4 aviator helmet adequately protects against penetrating types of head injury, its energy absorbing qualities do not adequately protect against concussive head injuries. The severity of impact surfaces encountered by US Army aircrewmembers in survivable helicopter crash situations seldom exceeds that of a flat surface. Peak transmitted force may be a more effective criterion in evaluating the impact attenuation performance of protective headgear than is peak G, SI, or HIC.

REFERENCES

1. Gurdjian, E. S., H. R. Lissner, and L. M. Patrick. Protection of the Head and Neck in Sports. JAMA. Vol. 82, pp. 509-512. November, 1962.
2. Gadd, C. Use of a Weighted Impulse Criterion for Estimating Injury Hazard. Proceedings of 10th Stapp Car Crash Conference. Society of Automotive Engineers, pp. 164-174. New York. 1966.
3. Hodgson, V. R. National Operating Committee on Standards for Athletic Equipment Football Helmet Certification Program. Medicine and Science in Sports. Vol. 7, No. 3, pp. 225-232. 1975.
4. Chou, C. C. and G. W. Nyquist. Analytical Studies of the Head Injury Criterion (HIC). Presented at the SAE Automotive Engineering Congress. Detroit, Michigan. SAE Paper No. 740082. February, 1974.
5. Department of Transportation, National Highway Traffic Safety Administration. Occupant Crash Protection Head Injury Criterion. S6.2 of MVSS 571.208, Docket No. 69-7, Notice 17.
6. American National Standards Institute. Specifications for Protective Headgear for Vehicular Users. ANSI Z90.1. New York. 1971.
7. Military Specification MIL-H-43925. Helmet, Flyer's Protective. SPH-4. March 1975.
8. Snively, G. G. and C. O. Chichester. Impact Survival Levels of Head Acceleration in Man. Aerospace Medicine. Vol. 32, p. 316. April, 1961.
9. Swearingen, J. J. Tolerances of the Human Brain to Concussion. Department of Transportation Federal Aviation Administration Report No. FAA-AM-71-13. 1971.
10. British Standard 2495: 1960. Protective Helmets and Peaks for Racing Car Drivers. April, 1960.
11. Joint Committee on Injury Scaling of Society of Automotive Engineers, American Medical Association and American Association for Automotive Medicine. The Abbreviated Injury Scale. Proceedings of 19th Conference of the American Association for Automotive Medicine, p. 438. 1975.
12. Glaister, D. H. Evaluation of Aircrew Protective Helmets Worn During Crashes and Ejections. Presented at the Royal Air Force Institute of Aviation Medicine. Farnborough Hampshire, England. October, 1973.

DISCUSSION

DR. E. HENDLER (USA)

When the helmets are dropped are they dropped from higher and higher heights until you duplicate the damage?

AUTHOR'S REPLY

Yes, that is correct, except the same helmet is not dropped more than one time. There are several duplicates made for each test. New helmets are dropped each time from different heights until by trial and error the exact damage is reproduced.

WING COMMANDER D. G. GLAISTER (UK)

The 5,000 pound transmitted force limit used in the former BS 2495 is a pass/fail load for routine batch testing of helmets. Any manufacturer who wishes to avoid the loss of large fractions of his production must design to a much lower figure, probably of the order of 3,500 lbs. This appears to correspond better with your findings.

AUTHOR'S REPLY

Yes. I agree.

THE EFFECT OF IMPACT ACCELERATION ON THE ELECTRICAL ACTIVITY OF THE BRAIN

Marc S. Weiss, Ph.D., Neurophysiologist
 Michael D. Berger, Ph.D., Assistant Neurophysiologist

Naval Aerospace Medical Research Laboratory Detachment (NAMRLD)
 P.O. Box 29407
 New Orleans, Louisiana 70189

SUMMARY

In a series of pilot experiments, eight Macaca Mulatta with chronically implanted cortical recording electrodes were tested using a range of $-X$ impact accelerations. Both EEG and somatosensory evoked potential (SEP) data were collected and analyzed. The results suggest that for the peak acceleration levels used (281 m/s^2 to 1550 m/s^2) the SEP is a more sensitive index of the inertial load on the brain than is the EEG. In particular, the duration of changes in shape of the early part (less than 100 ms latency) of the SEP is monotonically related to the peak sled acceleration. This has important implications for the physiological monitoring of human subjects in impact acceleration experiments.

INTRODUCTION

One of the major aspects of the impact acceleration research at the Naval Aerospace Medical Research Laboratory Detachment in New Orleans is an attempt to discover the neurophysiological mechanisms underlying concussion resulting from an indirect inertial input to the head. Concussion, for the purposes of this discussion, will be defined as a condition of impaired brain function due to a transient inertial input to the head and neck structure. By relating neurophysiological events to the measured head-neck dynamic response, the important mechanical parameters can be determined and used in developing appropriate mathematical and mechanical models. In particular, a goal of this research effort is the development of an impact-injury model for restrained humans in a simulated crash environment. The steps in the development of such a model can be briefly summarized as follows:

1. Select animal model.
2. Identify appropriate injury criteria.
3. Obtain reliable data over wide range of impact force.
4. Develop animal impact-injury model.
5. Extend data to include human results.
6. Develop animal to human scaling criteria.
7. Extend impact-injury model to humans.

The results reported here are from the first of a series of experiments designed to complete steps 1 - 4.

For our animal model we have selected male adult rhesus (Macaca Mulatta) weighing approximately 10 kilograms. The injury criteria we use fall into two categories: long-term or permanent brain injury and short term or transient brain dysfunction. Long-term injury is characterized by persistent (over several days) changes in brain electrophysiology, clinical symptomatology or identifiable neuropathology resulting from the impact event. Transient dysfunction is identified by brief (less than 24 hours) changes in brain electrophysiology or clinical symptomatology.

Data were obtained from animals subjected to impact forces in the $-X$ direction ranging from 281 m/s^2 to 1550 m/s^2 . Electrophysiological and inertial data were collected. To assess brain function, we have chosen to examine parameters derived from the measurement of the electroencephalogram (EEG) and the somatosensory evoked potential (SEP). It is important that similar measurements can be obtained from our human subjects, so that the remaining steps as outlined above can be completed.

METHODS

Eight adult male Macaca Mulatta ranging in weight from nine kilograms to twelve kilograms were used as subjects in a total of 15 experiments. Each had six epidural stainless steel recording screws (4 millimeters in diameter) implanted in the skull located approximately as indicated in Figure 1. Wires attached to these screws were brought to an external connector, anchored into the skull using dental acrylic. Fixation hardware for head accelerometers and photographic targets were also implanted in each of the subjects. Several months elapsed between the surgery and the impact acceleration experiments in order to allow bone to regrow so that the head implant would remain secure under extreme inertial loads. In each experiment the subject was restrained in custom fitted fiberglass couch which permitted freedom of motion for the head and neck. Physiological data, consisting of four channels of EEG and SEP information and three channels of vector cardiographic information were recorded for approximately 30 minutes prior to the impact event and for 30 minutes following. For four of the subjects, follow-up recordings of physiological data were made 24 and 48 hours post-impact.

The recorded neurophysiological data were telemetered through an amplifying system with a nominal gain and bandpass of 40,000 and $1 - 100 \text{ Hz} \pm 1 \text{ dB}$, respectively, and recorded on analog tape. During the recording of the data in all but four of the experiments, the subject's median nerve was stimulated by brief electrical pulses (.1 millisecond duration) delivered to the skin near the right wrist. Stimulus intensity was adjusted to determine the threshold for a thumb twitch and then

set to a level which produced good SEP's as monitored on a storage oscilloscope. The actual intensity used ranged from 4 to 8 milliamperes and was presented at an interval of one every two seconds except for experiments LX 1364 and LX 1365 in which a rate of one every three seconds was used. In most of the experiments in which median nerve stimulation was used, the stimulus was presented for periods of five to ten minutes separated by three to five minute intervals of no stimulation. This permitted collection of periods of continuous EEG data free of evoked potentials.

The physiological data were played back after the completion of a series of experiments and digitized using an EAI Pacer 600 computer. The data were sampled at rates from 400 to 850 samples per second, depending on the experiment. The digitized data were output on tape and then processed at the NASA Slidell Computer Center on a Univac 1108 system. In addition to the physiological data, the stimulus event marker was also digitized and provided a time reference for the EEG and SEP analysis. This analysis was done using software developed by the authors.

DATA ANALYSIS

The data analysis was carried out independently for the EEG and SEP data. In order to analyze EEG data collected during median nerve stimulation, approximately one second of data immediately following each stimulus was discarded. In the absence of median nerve stimulation all the EEG data were used. A general purpose time series analysis program computed averaged power spectral density estimates from these data. Raw spectral estimates were made using one to two second intervals of data and five of these were averaged. Each spectral estimate thus represented five to ten seconds of data and this was the basic time resolution of the EEG analysis. From these spectra ten parameters were computed. These parameters were 1) Total EEG power and 2) Percentage EEG power in each of the five spectral bands: 0 - 4 Hz (Delta); 4 - 8 Hz (Theta); 8 - 12 Hz (Alpha); 12 - 16 Hz (Sigma); 16 - 32 Hz (Beta). Figure 2 illustrates for one experiment a plot of the EEG power in each of the spectral bands as a function of time.

In addition to the ten spectral parameters, spectral moments were estimated using zero-crossing techniques. This measure reflects the relative distribution of EEG spectral energy as a function of frequency. Increase in the 2nd and 4th moments indicates a shift in energy from low frequency to higher frequencies. Also, a variety of statistical parameters based on the EEG amplitude distribution were also measured. These parameters yielded no additional useful information.

Analysis of the SEP data was based on the computation of averaged SEP's (ASEP). Data immediately preceding and following each of ten sequential median nerve stimuli were averaged, using standard computational procedures.

This resulted in a series of ASEP's each representing approximately 20 seconds of data. Figure 3 illustrates selected ASEP's computed for one experiment immediately preceding and following the impact event.

A variety of computerized measurements were made of the ASEP's and these derived measures were used to assess the effects of impact on the SEP. Two measures in particular appeared to be of value. One is an amplitude measure, the root mean square (RMS) value of the ASEP computed for the post-stimulus interval of five to 100 milliseconds. In the data discussed here, this is considered the "early" component of the ASEP. The second measure is a shape measure and complements the first. This is the "pre-impact correlation" and uses the ASEP computed from all the pre-impact data as a reference waveform. A Pearson product-moment correlation coefficient is then computed point for point between the early component of the reference waveform and the early component of each (ten stimulus) ASEP. Both measures can be plotted as a function of time relative to the impact event and Figure 4 illustrates this for the same data shown in Figure 3.

RESULTS

TABLE 1 SUMMARY OF SEP & EEG RESULTS (Channel 1 - Figure 1)

Run No.	Subject	Peak Sled Acceleration (m/s ²)	Duration of EEG Ratio Changes (sec)	Duration of SEP Changes RMS (sec)	Shape (sec)	Clinical Symptoms
LX 656	A03146	281	29	118	99	NONE
LX 1364	A03921	361	71	199	28	NONE
LX 654	A03146	502	20	353	137	NONE
LX 659	A03146	553	59	490	98	NONE
LX 1892	A03948	818	38	NO DATA		NONE
LX 1891	A03943	820	13	NO DATA		NONE
LX 1359	A04099	1047	99	238	139	NONE
LX 660	A03146	1052	137	196	233	NONE
LX 1894	A03921	1062	26	NO DATA		NONE
LX 657	A03146	1065	10	177	197	NONE
LX 1365	A03921	1065	--	--	--	FATAL
LX 1893	A03924	1080	16	NO DATA		NONE
LX 1363	A03935	1205	218	> 1200	297	SEVERE*
LX 1360	A0499	1256	--	--	--	FATAL
LX 661	A03146	1550	--	--	--	FATAL

*Marked neurological and cardiac dysfunction, progressive deterioration, sacrificed 90 hours post-impact.

Table 1 summarizes the most important findings from this set of pilot experiments. For the EEG data, values of all parameters measured immediately post-impact were compared to the pre-impact values using both a t-test and a graphical median measure. The t-test results were statistically insignificant. Based on the graphical procedures, the most useful parameter was the ratio of the power in the Delta band to the total power in the non-Delta bands. The results listed in Table 1 were obtained by measuring the time the post-impact Delta/non-Delta ratio exceeded the pre-impact median level of the ratio. The median was computed using three minutes of data immediately preceding the impact event. As Table 1 indicates, these results are mixed and inconsistent. In general, the EEG changes seemed to reflect an overall transient decrease in total power, possibly indicating an increased level of behavioral arousal due to the impact.

Similar procedures were used for the SEP data. The early component RMS and correlation parameter measured immediately post-impact was compared to the median value of all the pre-impact measurements. The time which the post-impact results took to return to their pre-impact median level was determined and related to the measured peak sled acceleration. The RMS amplitude measure shows an effect, but as is the case for the EEG results these are inconsistently related to sled acceleration. The correlation shape measure, on the other hand, showed a strong monotonic relationship to sled acceleration. The correlation between the duration of the shape change and the sled acceleration is significant at the .02 level ($r=0.85$). This is illustrated in Figure 5, where the best linear fit to the data is shown.

CONCLUSION

It appears that in the unanesthetized adult rhesus, the shape of the early (latency less than 100 ms) portion of the SEP is the most sensitive correlate of the sled acceleration, among all the measures of brain electrical activity that we have investigated. The EEG and SEP amplitude are far more variable and inconsistent measures. In terms of concussive type injury at the acceleration levels reported here except for the one clear long-term result (LX 1363) one may tentatively infer the possibility of short-term brain dysfunction increasing in severity with increasing levels of impact acceleration. Experimental work currently underway is directed at elucidating the details of the physiological mechanical mechanisms responsible for this change in brain function. Future plans include the extension of our SEP methodology to monitoring the human subjects in our impact acceleration studies. The validation and extension of these results with human data is an important step in the development of a human impact-injury model.

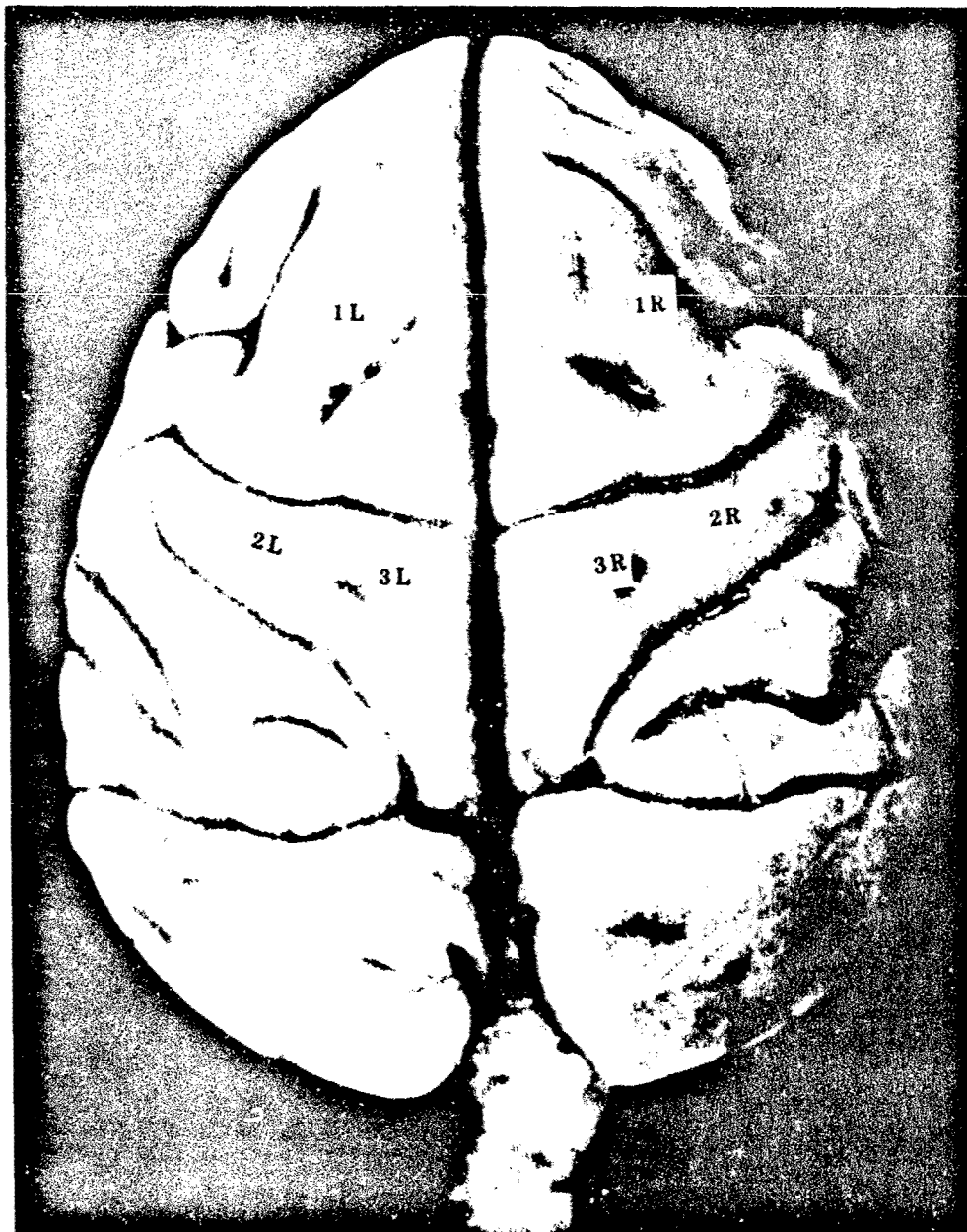


Figure 1: Approximate location of epidural recording electrodes. Channel 1 transmitted data recorded from electrodes 1L and 3L. Results from these data were not significantly different from those using data recorded from the three other electrode pairs (2L - 3L; 1R - 3R; 2R - 3R).

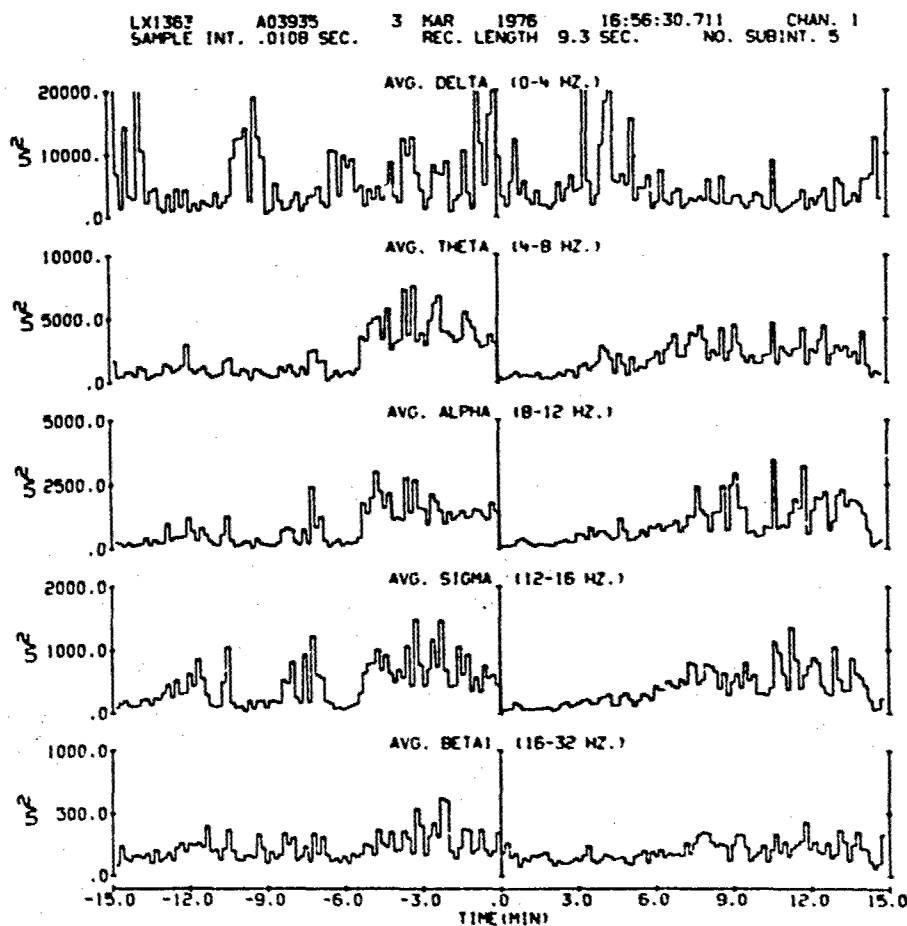


Figure 2: EEG spectral power for run LX 1363 (1205 m/s^2 peak sled acceleration). Impact occurs at time = 0.0 and 15 minutes of pre-impact and post impact data are shown. The vertical scale is in microvolts squared.

RUN LX1363 AVERAGED SEP CHANNEL 1
N: 10 A03935 $-G_x: 1206 \text{ M/S}^2$

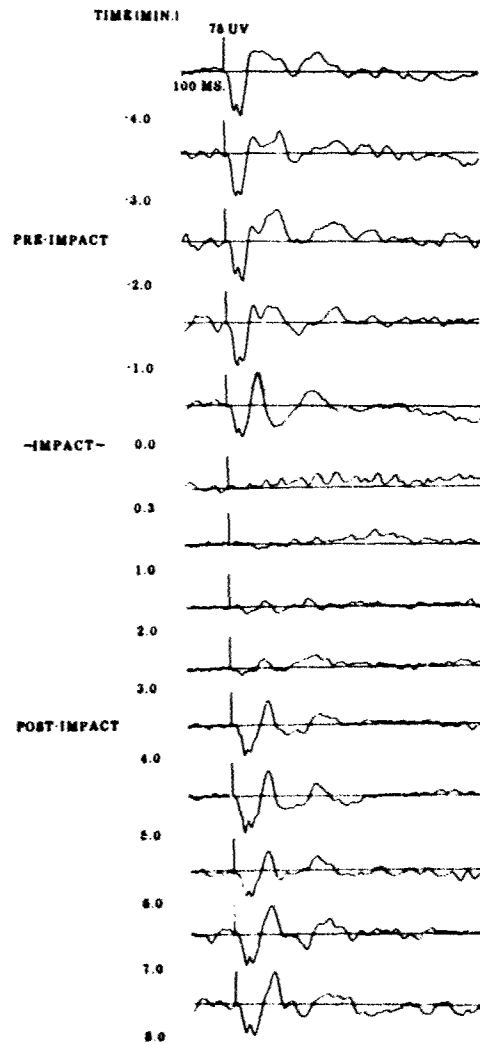


Figure 3: Sequence of ASEP's computed at times relative to the impact event for run LX 1363. Ten individual SEP's were averaged for each ASEP. Note the disappearance and gradual recovery of the ASEP post-impact.

RUN LX1363

SEP MEASUREMENTS

CHANNEL 1

A03935

$-G_z: 1206 \text{ M/S}^2$

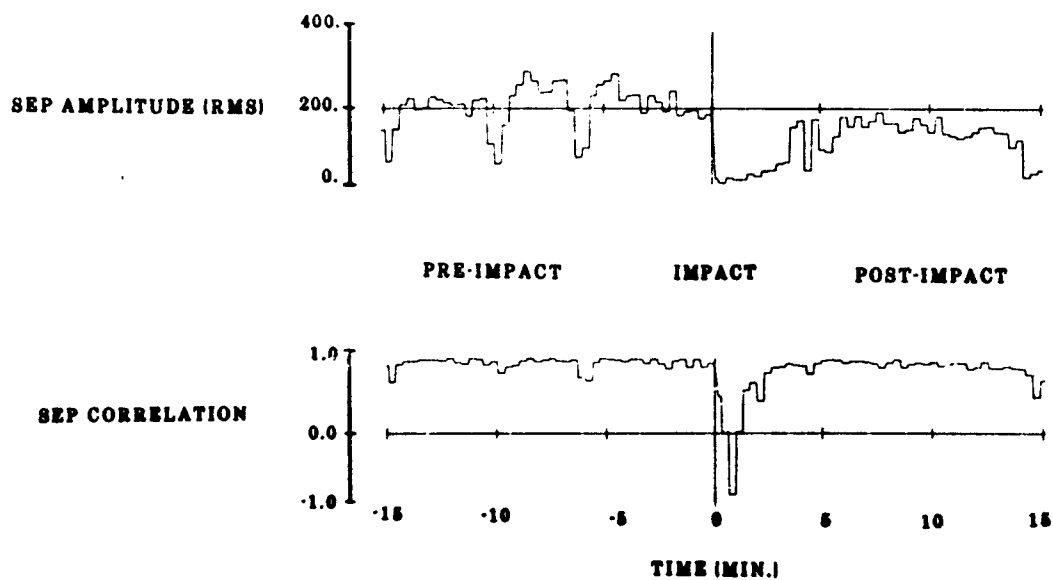


Figure 4: Plot of two parameters derived from ASEP's similar to those illustrated in Figure 3, plotted for 15 minutes pre- and post-impact. The EEG results for this run are illustrated in Figure 2. These plots are based on that portion of the ASEP appearing between 5 and 100 milliseconds after median nerve stimulation. See text for details.

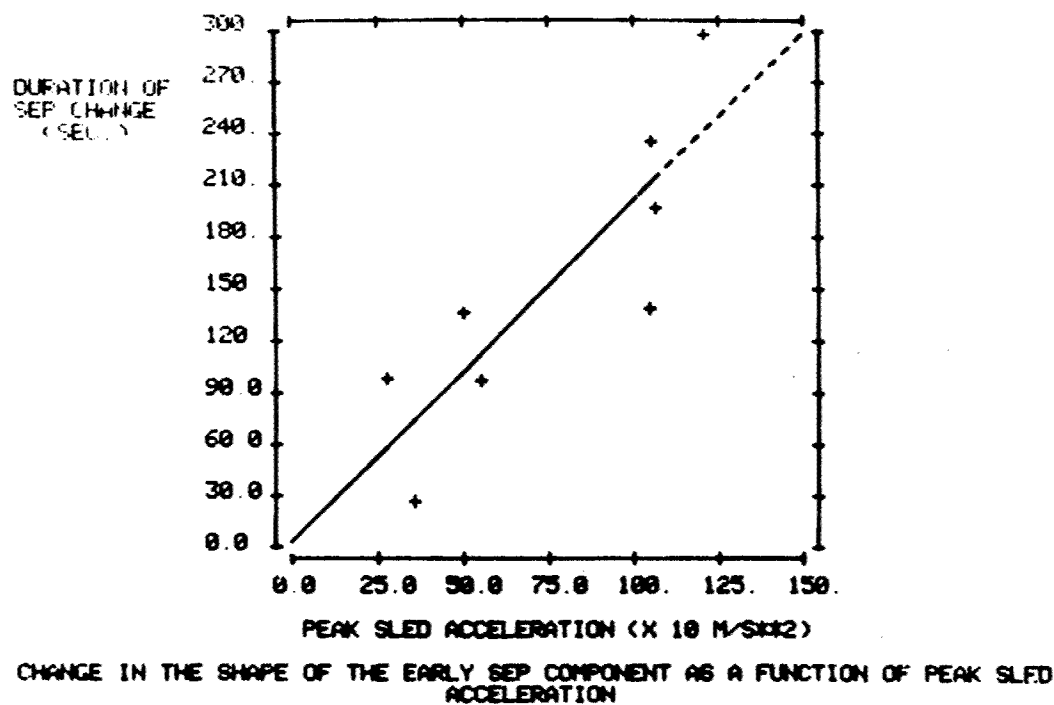


Figure 5: Plot of SEP shape data from Table 1, with the linear regression best-fit also shown. The correlation is .85 (.02 significance level). The dashed portion of the line indicates the approximate LD_{50} region for $-X$ peak acceleration this series of experiments.

DISCUSSION

DR. H. JEX (USA)

I am interested in the criterion that you used to detect the changes in shape of the evoked potential following the impact.

AUTHOR'S REPLY

We computed an average of all the pre-impact responses then we take the discrete post-impact and pre-impact averages - arranged over 10 events - and compute for the interval of interest, which in this case is 5 to 100 milliseconds post stimulus, a Pearson product moment correlation coefficient. This gives us an amplitude independent shape match index, and that's what you saw plotted as SEP correlation.

A HUMAN BODY and CREW STATION MODELLING SYSTEM for MOTION STUDIES

Georg D. Frisch
 Naval Aerospace Medical Research Laboratory, Detachment 1
 Michoud Station, New Orleans, LA. 70189

attached to
 Aircraft and Crew Systems Technology Directorate
 Naval Air Development Center, Warminster, PA. 18974

ABSTRACT

The need to visualize and interpret human body movement data from experiments and simulations has led to the development of a computerized, three-dimensional representation of the human body and crew station. Particular emphasis has been placed on head and neck motion within the confines of the A7E, LAMPS H2, and F18 crew stations, although the program is general enough to accommodate any geometrical configuration. There are numerous computer programs for the analysis or simulation of human movement in various environments, but perhaps the only common feature of all these systems is that they produce motion data to manipulate some skeletal model of the human body. While conventional charts and graphs can be used to follow movements of individual body parts, it has been our experience that only by observing the entire movement of the various body segments can experimental results be integrated with simulation studies. Such a process requires that program output be used to animate a realistically formed and jointed human body model incorporated within an existing or projected crew station. Animations are essential whenever the volume of data collected or generated is too great to assimilate piecemeal, or when the complexity of the motion under study leads to visualization difficulties in a two-dimensional graph. Dissatisfaction with existing body models and stick figure displays led to the development of a new human and crew station model for the computer with distinct advantages in display realism, movement definition, collision or interaction detection and cost-effectiveness in a real-time animation play-back environment. Development of this program was meant to provide an improved method for evaluating the physical compatibility of crew members with crew stations under all types of G environments. With proper human input data used as validation, computer generated results should serve as a design tool as well as for purposes of evaluation.

INTRODUCTION

Evaluation of the physical compatibility of crew members with crew stations has traditionally been based on anthropological, environmental and task sequence data. With today's sophisticated aircraft the ability of crew members to perform under adverse conditions is becoming increasingly crucial, making the man-machine interface an extremely important design consideration. Unfortunately, evaluation techniques of man's performance have not kept pace with the evolution of aircraft design. Physical compatibility of man and machine must be evaluated not only in terms of physical and visual interface, but also in terms of reach and clearance envelopes. Techniques such as drawing reviews, mockups, flight simulators, prototype flight, and track tests are important and produce useful data but suffer from the limitation of not being able to take into account the full variability in crew anthropometry and environmental factors. Mathematical models have produced some additional significant insight into the problems but their usage has been limited due to their complexity, lack of evaluation criteria, and the inability to get an adequate data base which can be used to validate evaluation results.

When analyzing crew station geometry two apparently distinct types of mathematical models have emerged. The first deals with the human factors aspect of the problem as opposed to those whose primary concern is the biodynamic response of crew members to acceleration forces generated by aircraft maneuvers or catastrophic events such as ditching, crashes, and ejections (1,2,3,4,5,6,7). Although logically compatible, results from these two sources have not been adequately correlated or used interactively due to the lack of standardization of input data, methodologies employed, format, and output descriptors.

A complete evaluation of a given crew station must consider not only the ability of a crew member to perform his tasks but also assure that the crew station geometry does not pose a problem during emergency egress. Information gained from gross body motion simulation (i.e. movement of body segments in response to applied forces) should be used to revise clearance and reach envelopes, which in turn could significantly alter the placement of crucial controls or cockpit geometry in general.

Motion of a crew member within his seating and restraint system will change the location of joints which can significantly alter the areas within his reach. Only when both static and dynamic factors are used in conjunction can a representative evaluation of a given crew station be effectively undertaken. Accident statistics amply demonstrate this point.

SCOPE

In formulating the graphics model presented here, the primary consideration was ease of use and generality in application. The intent was not to reformulate capabilities of existing models but rather to develop a tool which would use data generated by these programs as input for further analysis. The bulk of the data analyzed by this laboratory consists of human dynamic response data, simulation results

(primarily based on the Calspan Program discussed later), dummy and hardware testing programs conducted at the Naval Air Development Center, Naval Air Engineering Center, and Naval Weapons Center. The complexity of instrumentation employed and consequently both quantity and caliber of the data obtained from these various sources differs sharply but must be considered as state of the art and used in conjunction with other test results. The computer program was structured in such a fashion that human response data, simulation results, and test track and ejection tower test data could be used as inputs, and be compared on a common basis in terms of man-machine interface.

Injuries to aircraft crews must be viewed in terms of limitations of the escape system as distinguished from inadequate crew station geometry. Injuries due to the first classification are usually a result of high G forces and inadequate restraint, whereas injuries due to the latter can be related to direct impact between body segments and the crew station interior. Of the two, direct impact injuries are the easier to prevent and all available data should be used to define clearance envelopes required.

The three major areas of simulation to be incorporated consist of crew station geometry, occupant dynamics, and trajectory analysis. Computer programs which were considered as sources of input to this model are briefly discussed below under the classification to which they pertain.

CREW STATION GEOMETRY

The Cockpit Geometry Evaluation Computer Program System (CGECPS) was used to check and transform digitized crew station data (1). In our application of the program, two reference systems were used. The first is the design coordinate system (using buttock, water, and station lines), where the cockpit plane vertices and control locations are expressed in this reference system using crew station drawings. The data is then transformed to a Euclidean coordinate system (x,y,z) with the origin at the design eye reference point (figure 1). Before each evaluation run the occupant's eye midpoint (defined in the head coordinate system) was made coincident with the design eye reference point origin. The crew member's anthropometry and seating position was used to define seat pan location, which was then checked against the allowable seat adjustment range. If within range, an ideal initial seating position was defined (i.e. crew member seated at the design eye reference point) and the simulation was ready to proceed. Exceeding the seat adjustment range defines a problem of accommodation. Permissible seat adjustment values were then used (together with the seating position data) to redefine a new eye reference point (as distinguished from the design eye reference point) and all cockpit information was transformed to this new origin.

It is important to remember that several types of inputs can be used to drive the occupant segments and consequently determine initial positions. If dynamic test data is used (sled and tower tests using dummies), then link lengths, joint ranges, weights of segments and other initial position data is determined from the test conditions. The primary aim of such a simulation is to detect possible strikes between occupant segments and crew station interior. This type of analysis is used primarily for validation purposes where one is looking for replication of motion monitored and analyzes this motion within the constraints of the crew station configuration. Once this validation phase has been completed, then a more general and informative analysis can be performed. Since control locations have been defined in terms of the eye reference point, the CGECPS program can be used to determine initial angular orientation of occupant segments, given that certain controls are being contacted. This can be accomplished in terms of general anthropometric categories or for specific dimensional data under investigation.

Human test data is treated in a similar fashion. Experiments conducted at the Naval Aerospace Medical Research Laboratory Detachment monitored head and neck motion in response to acceleration, using both inertial instrumentation and high speed photography (8). Locations of the head and T1 (first thoracic vertebral body) coordinate system origins are determined throughout the entire course of the run (figure 2). The graphics representation of the head and neck system can now be driven using human data and analyzed in terms of the crew station geometry. The midpoint of the infraorbital notches, defined in the head anatomical coordinate system, is placed at the design eye reference point, and the monitored head and neck motion can be analyzed in terms of the crew station dimensions. There are two significant factors that must be kept in mind. The first is that only head and neck positions are known and consequently only head interference can be detected. Secondly, initial position is predetermined by the test configuration. Seat back angles in human tests are somewhat different, as is the restraint system employed. Human test subjects are much better restrained than would be the case of a pilot flying a particular aircraft. Both of these factors could significantly affect clearance envelopes. Results, however, could be interpreted as representative of a best case situation (i.e. perfectly restrained, sitting at the design eye reference point). One can vary the initial position of the occupant and restraint system parameters using the simulation program discussed below.

It should not be forgotten that the CGECPS program is employed in human factors analysis, using the anthropological, environmental, and task sequence data. Used to its full capacity, the system provides information concerning data consistency, reach capability, crew station compliance to selected military standards, and localization of visual and/or physical interference of the occupant with the crew station. This effort extends application to a high G environment where segment motion is beyond the occupant's voluntary control.

TRAJECTORY ANALYSIS

In order to be able to estimate occupant response to a given acceleration profile,

the seat time history has to be well defined over the time of interest. The forces at the seat are modified by restraint-torso and seat-torso interactions, so that when investigating head and neck response, the forces at the dummy's neck pivot (T1 in the case of humans) must be considered as the driving function to the head and neck system. It is easy to see that errors in defining the seat time history will be compounded when propagated to the head and neck or other extremities. Seat and restraint system properties (such as force deflection, strap elongation, etc.) are difficult to estimate and their effects on occupant response can be significant. It becomes crucial, therefore, that both the seat and the dummy be properly instrumented so that modifications to the driving function can be determined. Seat and dummy instrumentation locations must be surveyed to readily identifiable landmarks so that the effects of the seating and restraint system can be estimated (figure 3). Additionally, if one knows the time history of a precise point on the dummy, and dummy dimensions are related to that point, then the model of the dummy can be driven (using that point for input) independent of the seating and restraint system. This approach is routinely adopted in simulations based on human data, where the monitored T1 data is used as the driving function to the head and neck system.

From a standpoint of occupant dynamic response, the most difficult emergency egress condition to analyze and simulate is that of ejection. In this particular case, one is dealing with a closed loop system where occupant motion within his seating and restraint system can significantly alter the trajectory achieved, which in turn is the driving function of the seat-man system. This differs from crash simulation where the mass of the vehicle is such that the response of the occupant to the crash pulse leaves the driving function (time history of the seat) unaltered. This problem becomes particularly vexing in the latter stages of trajectory simulation (such as parachute opening shock). Test results are extremely variable and confidence in simulation results is marginal due to errors propagated and compounded by inaccuracies in stipulating catapult, sustainer rocket, and stabilization forces. Additionally, calculation of the effects of windblast and the aerodynamics of the seat-man system are oversimplifications at best. However, during the initial phases of an ejection, when man-machine interface is of major concern, the trajectory and seat forces are well defined since the seat is still on the rails and propelled by the catapult.

When data from the tower tests is employed, the seat time history is well defined since the seat motion is constrained to a two dimensional trajectory. Track tests, on the other hand, are conducted to replicate the real world and the data is of a three dimensional nature. To replicate these tests and draw inferences to other test conditions, the ICARUS program is used to estimate trajectories to be expected (9). The program considers the seat-man trajectory starting from initial catapult initiation to parachute opening shock and beyond. Seats presently available for analysis include Martin Baker, Stencel, and Escapac. Aircraft initial conditions, catapult and sustainer rocket forces, stabilization system forces, the aerodynamics of the seat man system, and parachute deployment forces are all considered in various degrees of complexity. Aspects beyond the present capability of the program include modelling of complex stabilization systems such as MPES (Maximum Performance Ejection Seat) and modification of the trajectory due to occupant motion within his restraint system. Although the whole occupant center of gravity is allowed to move within the seat coordinate system (simulating torso compression and restraint system elongation) perfect restraint is assumed, precluding possible effects of flailing due to windblast forces. However, when used with a reasonable amount of caution, adequate time histories (especially in the early stages of ejection) can be achieved.

OCCUPANT MOTION SIMULATION

Having the crew station data and seat time history (either monitored or simulated), the man-machine interface under G can now be analyzed. If human data is used and initial conditions of the aircraft can be related to those of the human test (no angular velocity on the seat), then the human data can be used directly in evaluating the crew station design. However, as mentioned previously, only head and neck data is presently available and one must resort to simulation if information on other segments or other test situations is desired. Dummy test data can also be used directly for the specific test conditions available. To expand the data base to include other conditions, simulation must again be considered.

The program routinely used to simulate occupant response is the Calspan Simulator (4), which has been the subject of several validation papers by the author (10,11,12). The model is quite flexible and modular in design so that the complete range of anthropometric variation, weight distribution, moment of inertia of segments, and joint limiting angles can be handled effectively. The occupant can be modelled by up to 20 segments, connected by 19 joints. The inclusion of tension elements and spring dampers facilitates the representation of muscles and ligaments, and flexible elements such as the neck can be handled with relative ease. The complete flexibility in anthropometric dimensioning, together with the ability of specifying omnidirectional input and dynamic initial conditions, make this program an ideal tool for evaluating the occupant-crew station compatibility under acceleration. Segment-segment and segment-crew station contacts are also monitored and evaluated in terms of forces generated. Modifications to the original version include evaluation of the effects of belt interactions and windblast forces.

One can in fact drive any segment and make the simulation as simple or as complex as desired. For example, if one is only concerned with head clearance, and the time history of T1 is known, then only the head and neck system need be driven using the T1 anatomical coordinate system origin as the locus where the acceleration is applied. In most dummy tests the head is hinged to the upper torso via a rigid neck and consequently constrained to move in the midsagittal plane. However, the forces applied

are such that yawing and rolling of the head would result if the constraints were removed. In such a case, if the location of the neck pivot in relation to the dummy's 3-D instrumentation is known, then an acceleration profile for this pivot point is easily calculated and can be used to drive a revised head-neck system. One can also model all segments according to the restrictions of the test and allow the head the freedom of motion warranted. Incremental changes to input parameters can also be investigated in terms of their contribution to simulation precision.

ANTHROPOMETRY

Options for several different graphical representations of the human body are provided, their usage depending on the complexity desired and likelihood of strikes occurring. The Calspan program provides optional output of segment time histories and contact ellipsoid information. Each segment is modelled via an ellipsoid, whose origin (in relation to the segment C.G. location) and force deformation properties are specified (figure 4). Use of this package greatly facilitates interpretation of data and can be used as a preprocessor to isolate specific crew station surfaces with which contact might occur. As an example, previous ejection simulation results can be used to define segment motion in the inertial reference frame. Analyzing this motion within the confines of a specific crew station will isolate the areas of concern. A full simulation, employing the exact seat time history and initial conditions of the aircraft, together with the pilot's initial position within the crew station, can then be undertaken. Only those crew station surfaces previously isolated need be included in the interference checks conducted during simulation, greatly reducing the computer costs involved. The entire crew station can still be plotted and visual checks undertaken to assure that in fact only those surfaces stipulated needed to be monitored.

To increase the resolution by attaining a better representation of the human form, a revised graphics package was formulated which can be driven by either Calspan Program output or test data (figure 5). As in the case of the elliptical representation, the flexibility of specifying the range of anthropometric variation was maintained through application of scaling parameters. Joint and segment C.G. locations are defined on input, determining the skeletal configuration of the occupant. Each segment has a series of spheres associated with it, the origins of which are located on the local segment coordinate system. The locations of these origins, as well as the radii of the spheres, depend on the anthropometry of the modelled occupant. Segment representation by a series of spheres was chosen because most body contours could be adequately represented. Additionally, when viewed from any angle, each sphere, projected onto a viewing plane, reduces to a circle. This minimizes computer execution time significantly.

A further refinement of anthropometric representation was recently undertaken, employing the methodology of the Biostereometrics Laboratory, Baylor College of Medicine, from whom a data set was gratefully obtained (13), (figure 6). Using a three dimensional photographic technique, the topography of the subject is established in the inertial reference frame, as are the locations of up to 80 bony skeletal landmarks. The resulting data base consists of successive slices, each one having a common z level and a defined center of gravity. This center of gravity constitutes the average of coordinates of all points of the cross section. The number of slices required for simulation input is a function of resolution sought. As an example, figure 6A contains twice as many data points as 6B. From the bony landmarks, the anthropometric dimensions of the subject can be established and the location of the joints estimated. These joint locations determine the skeletal structure and segment lengths. Segment orientations are calculated from the data and the various slices, or partial slices, assigned to the segments modelled (figure 7). Figures 7A through 7M demonstrate this assignment. 7A constitutes the head; 7B head and neck; 7C head, neck, and shoulder, etc. In articulating this body, each slice and the defined joints must be transformed into the segment local coordinate system (i.e. in terms of the segment C.G. locations). Initially, these C.G. locations are estimated from anthropometric dimensions, but as better estimates become available the slice transformations can be easily recalculated. As before, the entire skeletal structure, or portions thereof, can be driven either under computer control or using monitored human data.

The advantage of this topographic method is that a permanent record is attained which can be redigitized if more data points are needed. Additionally, locations of non bony skeletal landmarks can also be defined. X ray anthropometry of all human subjects tested at NAMRL det. is used to localize photographic targets and inertial instrumentation relative to the head and neck anatomical coordinate systems (figure 8). If three-dimensional photography is taken with the mounts in place, the location of these coordinate systems, in the inertial reference frame, can then be established. As was the case in the spherical representation, it is a relatively simple task to dimension the data to accommodate various anthropometric categories. Changes in link lengths, keeping the number of slices the same, will result in the spacing between each successive slice being increased, and vice versa. Increasing or decreasing the size of the slices themselves is accomplished by defining a vector extending from the center of gravity of a slice to each point constituting the outline. Upward or downward scaling of the vector lengths is used to redefine the location of these outline points.

No matter how precise the definition of the human body, clearance envelopes and possibility of contact are directly related to equipment worn by crew members. Serious injuries to the head, resulting from direct contact, must be viewed in terms of head-helmet displacement within the crew station. Even under the assumption that the helmet does not move relative to the head, which itself can cause serious injuries, the increase of the volume represented by the helmet must be accounted for. Although digitized information on various helmets is readily available, relating this data to

the head coordinate system must be repeatable and consistent. A preliminary experiment was conducted, using a medium HGU-35P helmet and phantom head (human skull covered with rubber material to simulate features), in which the head anatomical coordinate system was defined. Lead pellets were attached to the left and right center of rotation points of the helmet, as well as to the middle of the front trim line. The helmet was then placed on the marked phantom head and X rays were taken. The XY plane of the helmet coordinate system was defined by the three lead markers and the Z axis was taken as normal to this plane, with its origin midway between the two center of rotation pellets. The original helmet data, expressed in terms of water, buttock and station lines, was transformed to the above defined helmet coordinate system. The location of the helmet coordinate system origin was defined on the head anatomical coordinate system from the X ray data. The helmet shell contour data was then retransformed to the head coordinate system. Figure(9) illustrates the increase in volume attributable to the helmet. It should be pointed out, that although a definition of a helmet coordinate system is necessary for proper localization of helmet contour data on the head anatomical coordinate system, the one chosen need not be considered as the ideal, and another can be substituted as long as it can be repeatedly defined (using the same landmarks) across helmet types. Further experiments are planned to determine the repeatability with which a subject can place the helmet on his head and the variability, across subjects, of helmet contour locations on the head coordinate system. Since mouth mount locations are defined relative to the head coordinate system, subjects wearing these mounts and helmets can be analyzed using photographic techniques. This eliminates the necessity for non-medical use of X rays.

Since many applications of head dynamic response data do not consider a protected head, it was deemed necessary to provide a program option in which precise head data could be displayed independent of other body segments. Clearly, if a helmeted head strikes an object, the precision necessary to describe the skull outline need not be that high; as long as the helmet contours are localized on the head coordinate system. It is, after all, the helmet that will make contact. With the unhelmeted head, however, precision is required to establish the existence and location of contact and the dynamic conditions existing at the time. The digitized skull information, employing the same coordinate system previously described, was obtained from T.A. Shugar's Finite Element Head Injury Model (14). Although at present not representative of any particular anthropometric categorization, the computer input library can be expanded as additional information becomes available. Head contour data obtained from stereo photography (figure 7A) can also be used since it was redefined in terms of the head anatomical coordinate system. This system was estimated from the location of the auditory meatus and infraorbital notches. The head-helmet data can again be driven by either computer simulation results or by human head trajectory data.

Care must be taken when analyzing helmeted head trajectories using human data as input. The trajectories monitored are those of human, unhelmeted subjects, suitably restrained, with a seatback angle of 90 degrees. Displaying this motion within the cockpit (figure 10 left), with the initial position determined via the methodology previously described, provides significant insight into the crew station-pilot compatibility. Range of motion under less restrictive restraint will, in all probability, be increased and therefore results from human data tend to be on the optimistic side. Inclusion of a helmet (figure 10 right) expands the displacement volume and increases the likelihood of contact. The additional weight of the helmet, and its effect on the head trajectory, has as of yet not been properly defined. The effect, however, is expected to be detrimental in terms of increasing head range of motion. Viewed from this perspective, results obtained must be considered as the best case situation and that in actual situations the hazard would be increased.

APPLICATIONS

The graphics package described was designed not only to handle various sources of input but to be flexible enough to provide the best possible insight into results. As such, the object observed can be viewed from any position (as if a camera were placed there) using any perspective desired. Enlargement or reduction can also be specified as required. Presently conducted work will expand the capability to include stereo views (to be viewed with special glasses) to attain a better depth perspective and to vary display intensity of data sets for contrast purposes. As an example, the crew station can be displayed dimmer than the crew member so that confusion as to contour intersections can be minimized. A hidden line option has been completed but its usage has been limited. Although the aesthetic quality of the graphics is enhanced using this option, information obtainable is limited since segments hidden behind crew station surfaces can not be observed. The various data sets can be displayed separately or together, depending on the simulation. Occupant response to acceleration can be displayed together with the crew station or analyzed independently, using any of the three configurations provided.

Since occupant response to an omnidirectional input can be simulated, applications to specific test or accident situations become self evident. The case of ejection has already been discussed in some detail. Additionally, carrier arrested landings and ditching can be investigated. Typical deceleration profiles of carrier landings are available and data, when transformed to the crew station from its original locus, can be used to drive the crew station model. The same holds true if accelerations seen during ditching are ever quantified. If the resulting data from these two sources can be correlated to that monitored during human tests, then human data can be used directly to drive the head within the crew station. In such situations, all possibility of contact must be eliminated. There is no sense in providing elaborate underwater escape systems if the crew member is unable to activate them as a result of unconsciousness sustained from direct impact.

Since the viewing location can be specified to be at the eye reference point, the pilot's perspective of the crew station interior can be used as a design tool. Control locations can be manipulated, using graphics, so that ease of pilot viewing and activation, when necessary, can be maximized. This should be done before crew station prototypes are ever constructed. Additionally, aircraft carrier flight decks can be digitized and for given aircraft time histories, the pilot's view during landing can be displayed.

Crew station geometry can be expanded to include any enclosure, such as automobile interiors. Usually, in such cases, greater clearance is provided and the effects of various seating and restraint arrangements can be investigated. If direct contact is detected (using the skull representation provided) results can also be used directly as inputs to a finite element head injury model.

REFERENCES:

1. R. Katz, "Cockpit Geometry Evaluation." Report No. D162-10127-3, JANAIR Report 720402, The Boeing Aerospace Group, Seattle Washington, 1972.
2. K. H. E. Kroemer, "Combiman - Computerized Biomechanical Man-Model." Report No. AMRL-TR-72-16, Aerospace Medical Research Laboratory, Wright Patterson Air Force Base, Ohio 45433, 1973.
3. R. Edwards, A. Osgood, K. Renshaw, H. Chen, "CAR - Crew Station Assessment of Reach." Report No. N62269-75-C-0419, The Boeing Aerospace Co., Seattle, Washington, 1975.
4. J. T. Fleck, F. E. Butler, S. L. Volgel, "An Improved Three Dimensional Computer Simulation of Crash Victims." Volume 1 - Volume 4. Final Report for Contract No. DOT-HS-053-2-485, DOT Report Nos. DOT-HS-801-507 through 510, NHTSA, 1975.
5. B. M. Bowman, R. O. Bennett, D. H. Robbins, "MVMA - Two Dimensional Crash Victim Simulation." Report No. PB-235-753, Highway Safety Research Institute, University of Michigan, Michigan 48105, 1974.
6. C. Passerello, R. L. Huston "UCIN Vehicle-Occupant Crash-Study Model." Office of Naval Research Contr. No. N00014-72A-0027-0002, Report No. ONR-UC-EA-050174-2, University of Cincinnati, Ohio 45221, 1974.
7. D. H. Laananen, "Development of a Scientific Basis for Analysis of Aircraft Seating Systems." Report No. 1510-74-36, Ultrasystems, Inc., Dynamic Science Division, Phoenix, AZ., 1974.
8. C. L. Ewing, D. J. Thomas, "Human Head and Neck Response to Impact Acceleration." Naval Aerospace Medical Research Laboratory Detachment, New Orleans, Monograph 21, 1972.
9. C. Gracey, "Aircrew Automated Escape System Simulation Model." NWL Technical Report TR-3098, Naval Weapons Laboratory, Dahlgren, Virginia 22448, 1974.
10. G. Frisch, L. D'Aulerio, J. O'Rourke, "The Mechanism of Head and Neck Response to -Gx Impact Acceleration. A Math Modelling Approach." Aviation Space and Environmental Medicine, 48(3);223-230, 1977
11. G. Frisch, J. O'Rourke, L. D'Aulerio "The Effectiveness of Mathematical Models as a Human Analog." Paper No. 760774, Mathematical Modeling of Biodynamic Response to Impact, Warrendale, PA.: Society of Automotive Engineers, Inc. 1976.
12. G. Frisch, C. Cooper, "Mathematical Modelling of the Head and Neck Response to -Gx Impact Acceleration- Minimum Articulation Requirements." Aviation Space and Environmental Medicine, 49(1);196-204, Jan. 1978.
13. R. E. Herron, J. R. Cuzzi, J. R. Hugg, "Mass Distribution of the Human Body Using Biostereometrics." Report No. AMRL-TR-75-18, Texas Institute for Rehabilitation and Research, Biostereometrics Laboratory, Houston, Texas 77030, 1976.
14. T. A. Shugar, "A Finite Element Head Injury Model." Report No. TR-854-I, Civil Engineering Laboratory, Naval Construction Battalion Center, Port Hueneme, CA. 93043, 1977.

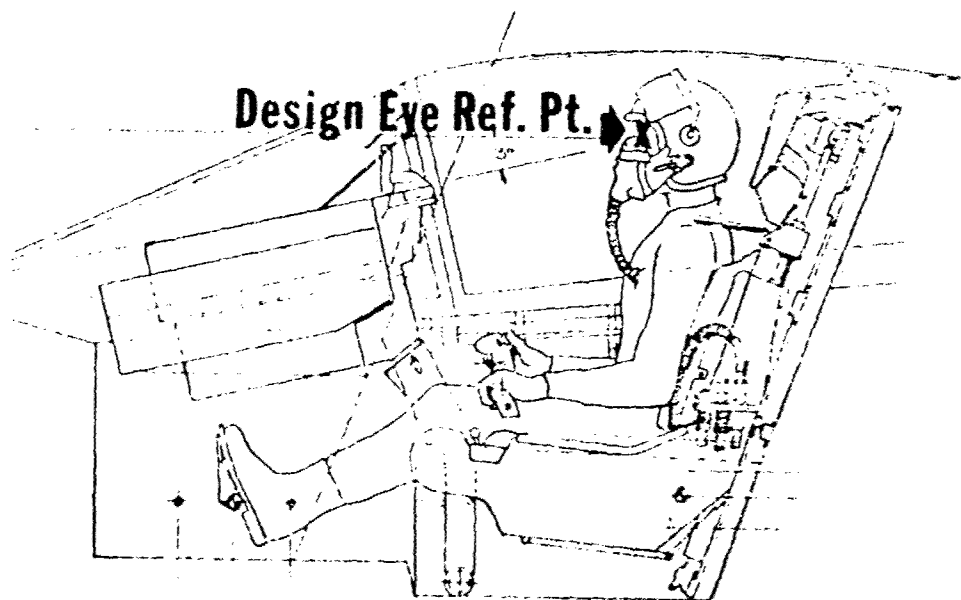


Fig.1 Location of design eye reference point in crew station

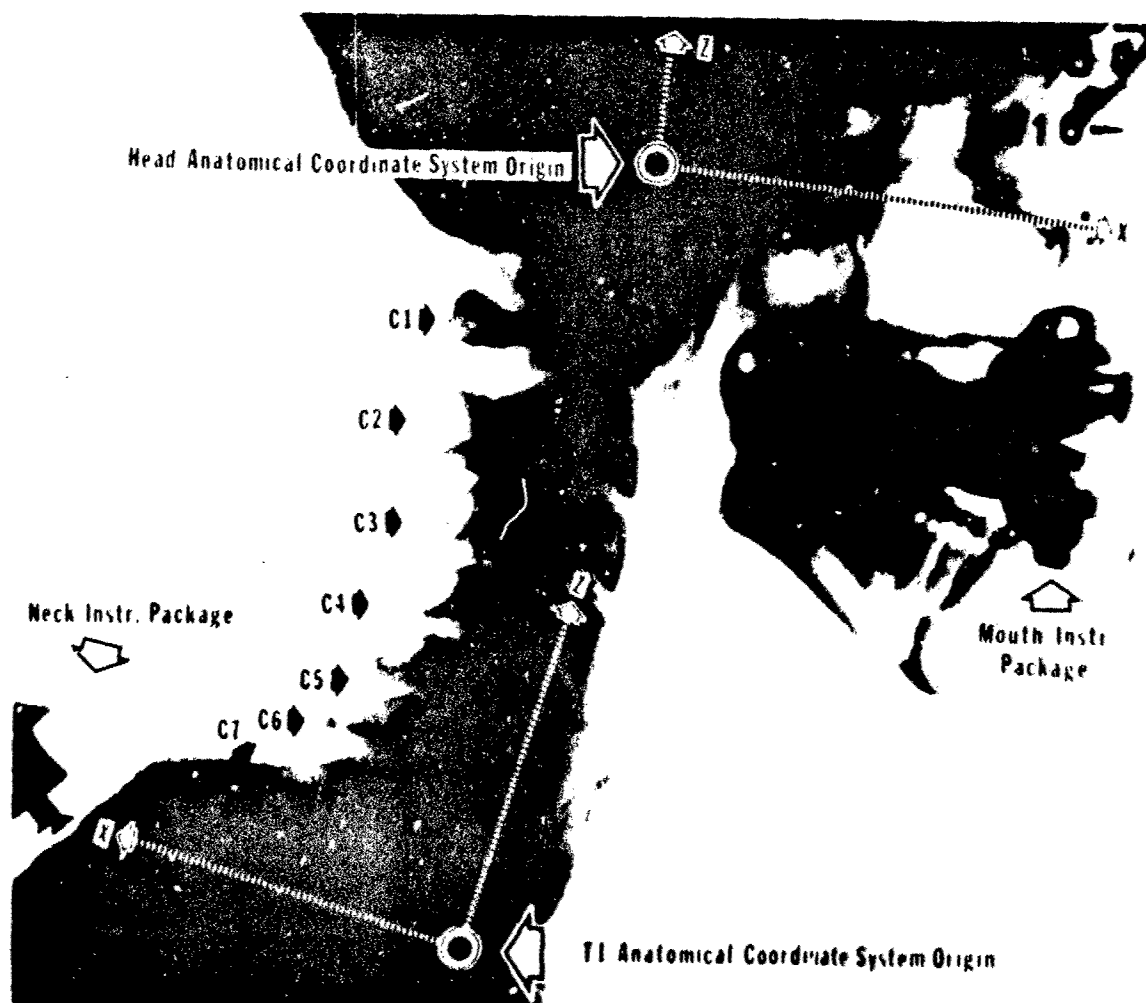


Fig.2 Definition of head and neck anatomical coordinate systems
Note the location of mouth and neck instrumentation packages

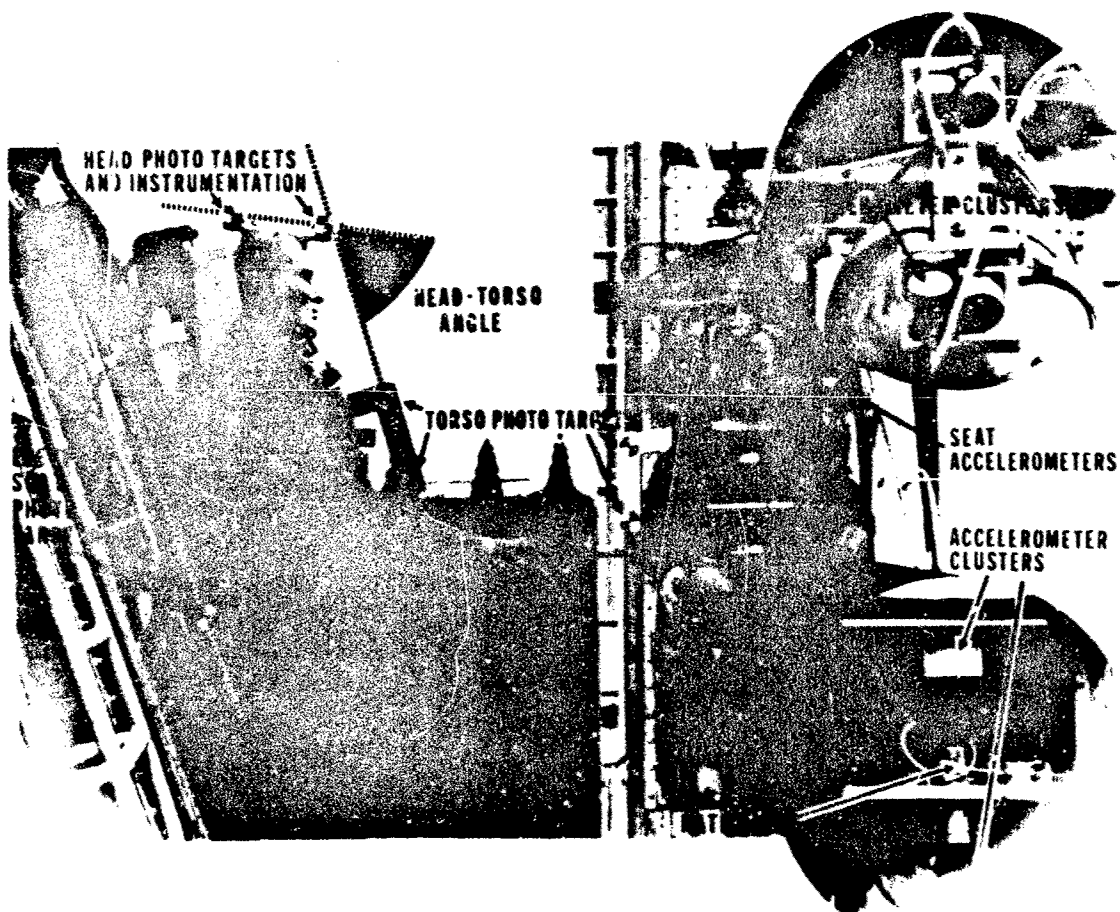


Fig.3 Ejection tower test using instrumented dummy. From photo targets, initial positions of monitored segments can be determined. Inertial instrumentation locations should be defined relative to specific landmarks

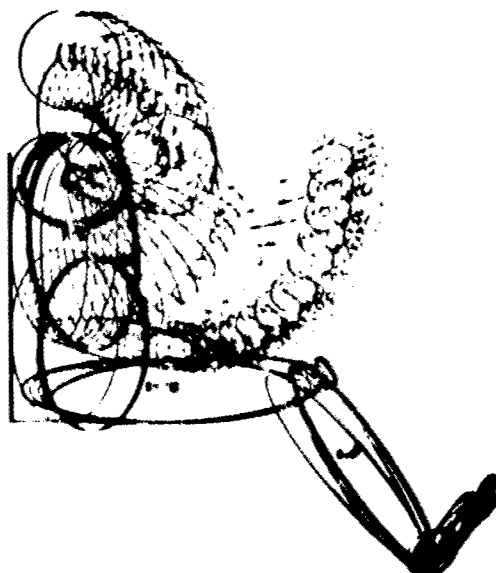


Fig.4 Ellipsoidal representation of crew member using program output as driving function

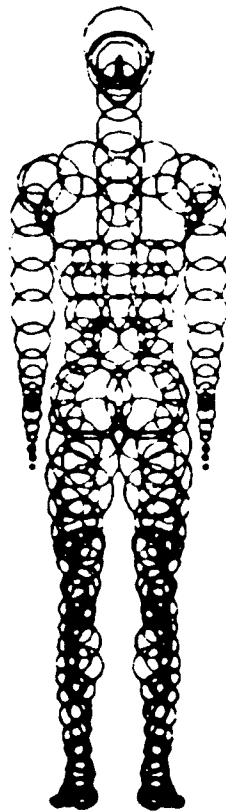


Fig.5 Spherical representation of crew member. Location and dimension of spheres determined by anthropometry

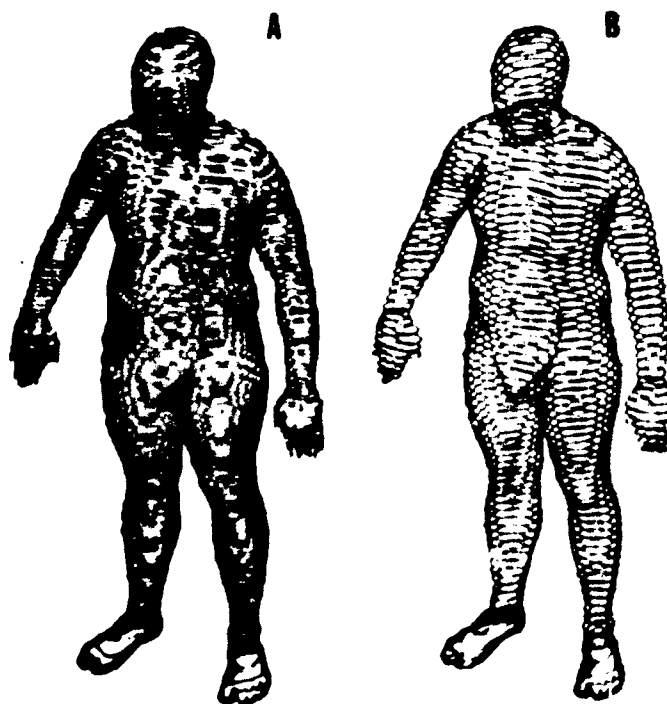


Fig 6 Contour data representation of crew member. From location of bony landmarks, joint locations and segment lengths are estimated. Increase in resolution is a function of number of data points used. Figure A consists of twice as many points as Figure B

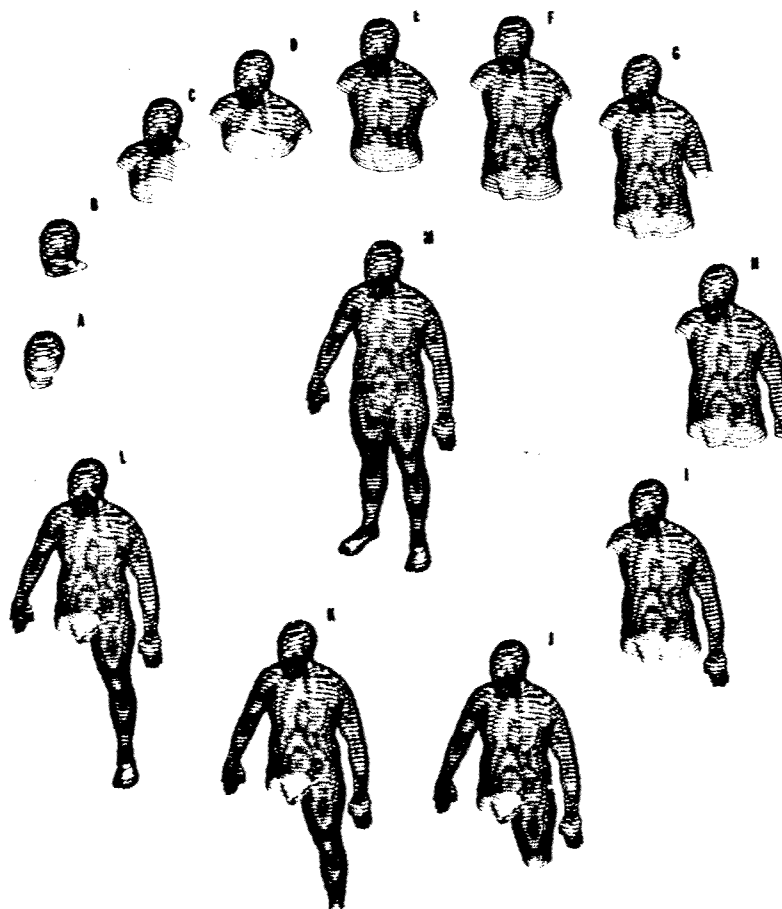


Fig.7 Segmentation of contour data. Figure A -- head only; Figure B -- head and neck; Figure C -- head, neck and right shoulder; Figure D -- head, neck and thorax; Figure E -- inclusion of abdominal region; Figure F -- inclusion of lumbar region; Figure G -- inclusion of upper arm; etc.

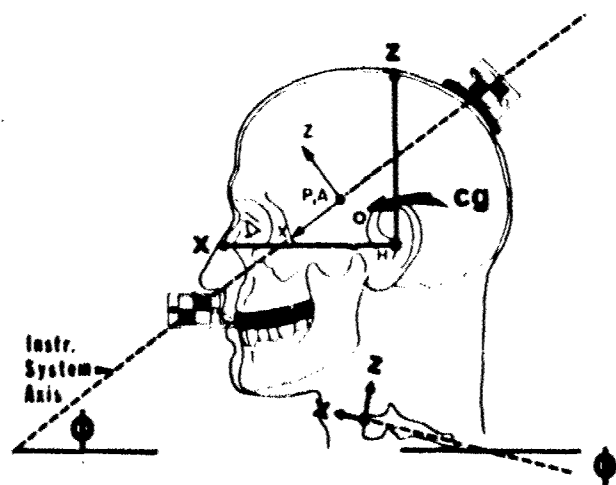
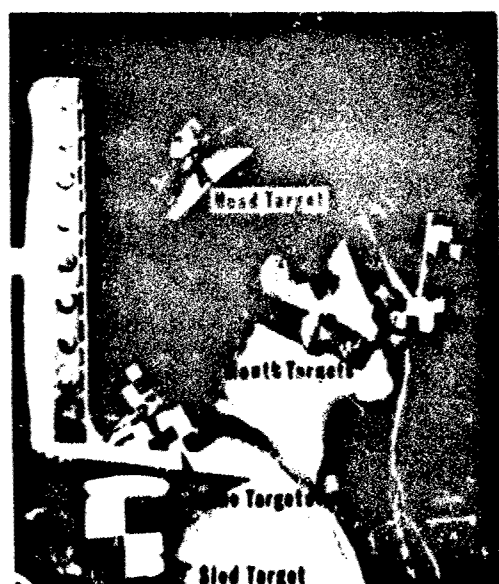


Fig.8 Localization of photographic targets to head and neck anatomical coordinate systems

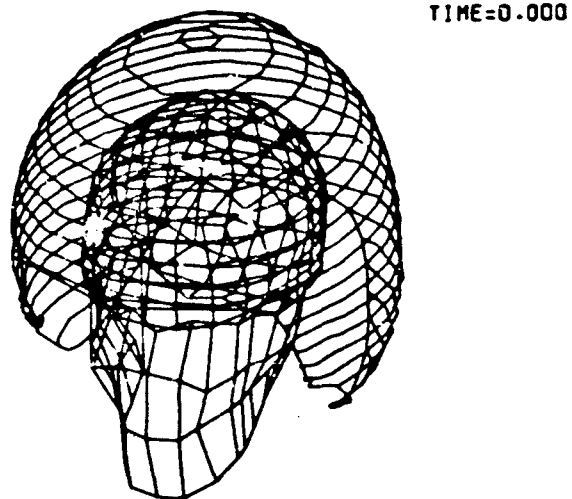


Fig.9 Helmet contour data defined on digitized skull

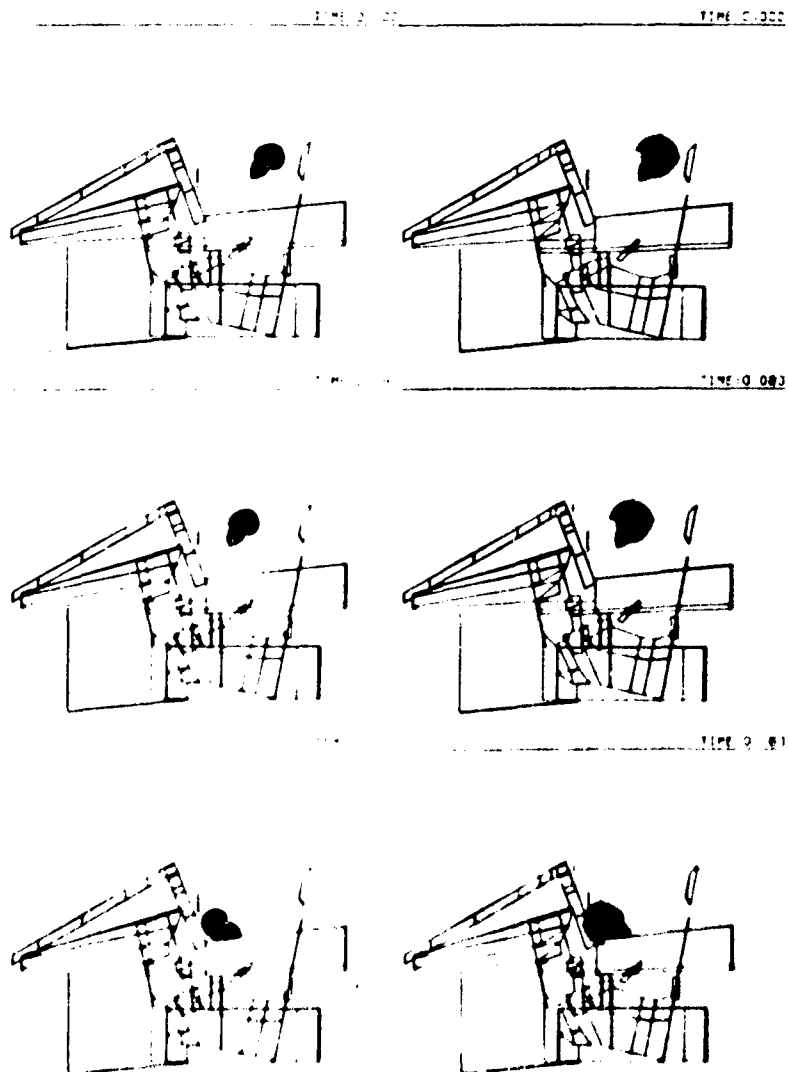


Fig.10 Head displacement within the A7E crew station (Human data 12 G, 535 G/sec.)
Onset. Note increase of clearance required with the addition of helmet

DISCUSSION

DR. H. JEX (USA)

What is the form in which the prepositioning of limbs is determined for the model? Do you use a table of numbers or computer graphics techniques?

AUTHOR'S REPLY

Positioning of the occupants within our crew station is obviously a function of anthropometry. There are two distinct types of simulation one can consider. In the first case, one might want to replicate a test that has been conducted and compare model results with those monitored in the test. In such a situation, link lengths and initial position data is predetermined from the test conditions. In the second case, one is interested in either extrapolating test data to other situations or using a model in a predictive fashion to estimate response before having conducted the test. In such cases, anthropometry can be determined from a statistical model, resulting in an appropriate scaling of link lengths. Given these link lengths and the crew station geometry, an idealized initial position can be determined. In the past we have assumed the pilot to be sitting at the eye reference point and define specific controls to be contacted. For example, the feet are to be on the rudder pedals; one hand on the throttle and the other hand on the control stick. Since the location of these controls is defined relative to the eye reference point, a preprocessing program calculates, using the link lengths and angular limitations of the joints, the angular orientation of all the various segments relative to the crew station.

DR. G. ALLEN (UK)

It was not quite clear to me what experimental validation you've done on your simulation. Could you address the extent of your validation?

AUTHOR'S REPLY

Validation efforts have been twofold in nature. Model performance has been compared to live subject tests conducted at New Orleans. Simulated head and neck response have proven to be quite reproducible, especially at high G levels. Additional dummy tower tests conducted at Warminster, PA have been used extensively to validate the program performance. More complex trajectories, such as the vertical seeking maneuver employed by the Maximum Performance Ejection Seat (presently being developed by the Navy) have also been employed as input, with equally adequate results. These tests, conducted at China Lake, were fully instrumented so that we feel that an adequate data base exists, and further refinements to the existing program can be effectively undertaken.

THE USE OF MATHEMATICAL MODELING IN CRASHWORTHY HELICOPTER SEATING SYSTEMS

George T. Singley III
US Army Aviation Research and Development Command
Research and Technology Laboratories
Applied Technology Laboratory, Fort Eustis, Virginia 23604

and

Joseph L. Haley
US Army Aeromedical Research Laboratory
Bioengineering and Life Support Equipment Division
Fort Rucker, Alabama 36362

INTRODUCTION

A new generation of US Army helicopters has been designed for unprecedented crashworthiness. These new aircraft are expected to prevent fatalities and minimize injury during accidents with impact velocities as severe as 42 feet per second down, 50 feet per second forward, 30 feet per second sideward, and a combined (resultant) velocity change not to exceed 50 feet per second. The severity of the vertical impact necessitates that crash force attenuation be provided to limit seat occupant spinal loading to human tolerance levels. Even when high sink rate (load-limiting) alighting gear are used, decelerative force attenuation is still necessary in the aircraft seats. Seats have been developed to meet the crashworthiness criteria of MIL-S-58095(AV)⁽¹⁾ and the Army's "Crash Survival Design Guide."⁽²⁾ However, the state of the art is such that there is no validated probability of injury model for the seat designer or evaluator to determine if a particular seat design minimizes injury.

This paper discusses crashworthy helicopter accident data revealing injury types related to seat design, seat occupant injury criteria, recent crashworthy seat test data, and crashworthy seat/occupant modeling technology. The designer's dilemma in finding the minimum injury solution by designing to the many conflicting variables is presented. Finally, the relationship between the spinal vertebra stress-strain characteristics and irreversible injury is discussed.

ACCIDENT DATA

Accident experience shows that helicopter seats should be designed to:

- a. Possess sufficient strength and load-deflection characteristics to maintain structural integrity and occupant retention.
- b. Provide the most full body, low elongation restraint system that operational considerations permit in order to properly position the body for minimum risk of decelerative injury and to minimize occupant motion.
- c. Attenuate crash impact decelerative forces imparted to the occupant to humanly tolerable values.

Recent accident data analyses (see Table I) have shown that approximately one-half of all injuries in Army helicopter accidents are due to decelerative impact forces.⁽³⁾ A recent analysis of US Army attack helicopter accident data by the US Army Agency for Aviation Safety (USAAVS) revealed the influence of vertical impact velocity on the incidence of spinal injury. Figure 1 shows a back injury rate of 50 percent for a sink speed of 25 ft/sec, i.e., the equivalent of a 9.7-ft free fall. The seat and restraint system play a major role in preventing these injuries, as well as those injuries due to lack of occupant restraint, ejection from the aircraft on impact, the occupant striking surrounding structure/components, and even the postcrash hazards of drowning and fire.

CRITERIA

MIL-STD-1290⁽⁴⁾ requires that the seats and occupant restraint systems of future US Army aircraft be crashworthy. Seats are required to be aft-facing whenever operational considerations permit and not to be side-facing unless absolutely necessary to meet operational requirements. Seats are also required to restrain the occupant during crash impacts as severe as the 95th percentile potentially survivable accident defined in Table II and to attenuate impact decelerations to accepted human tolerance levels for the 5th through 95th percentile occupant population. Seats and restraint systems must pass a series of six static and two dynamic crash tests. The dynamic tests are summarized in Table III. The crashworthy seat ultimate static load factors required by MIL-S-58095(AV) and MIL-STD-1290 are compared in Table IV with the older, superseded seat criteria.

Because vertical accelerations that are input to the seat from the floor in severe but potentially survivable helicopter accidents (48G for the 95th percentile survivable accident) exceed human tolerance, vertical crash force attenuation is required in all seats. MIL-S-58095(AV) and the Army's "Crash Survival Design Guide" require a minimum of 17 inches of vertical seat stroking distance. Seat vertical energy absorption mechanisms must stroke at a limit load of $(14.5 \pm 1.0) \times$ (effective weight of the 50th percentile occupant and stroking portion of seat).

These energy attenuation requirements are necessary to limit headward decelerations to within the human tolerance criteria of Figure 2. This curve is based on the findings of Eiband.⁽²⁾ MIL-S-58095(AV) requires that headward decelerations measured on the seat can be limited to the acceptable levels of Figure 2. Because the 95th percentile survivable accident deceleration along the aircraft's longitudinal axis is 24G, it exceeds the human tolerance of sideward facing cabin seat occupants and crash force attenuation must be

provided by the seat for that direction as well as in the vertical direction. Human tolerance limits to decelerative loads in all three axes are presented in the "Crash Survival Design Guide."

The Army's UH-60A BLACK HAWK and YAH-64A Advanced Attack Helicopter (AAH) are equipped with crash-worthy seats. The armored pilot/copilot seats and restraint systems are designed to comply with MIL-S-58095(AV). The UH-60A cabin seats are designed in accordance with the Army's "Crash Survival Design Guide." The UH-60A crashworthy armored crew seat is shown in Figure 3. The UH-60A cabin seats are based on the prototype design shown in Figure 4.

CRASHWORTHY SEAT ANALYSIS AND TEST EXPERIENCE

In recent years there has been considerable interest and research activity by both the automotive and aviation community in the development of mathematical models for seat and occupant crash impact analysis. References 6, 7, and 8 discuss several of the mathematical models developed to date. Unfortunately for the crashworthy helicopter seat designer, many of these models were developed for simulation of forward and/or sideward impact, not for vertical impact. The crashworthy seat designer has a need for validated, economical seat and occupant crash impact mathematical models for use as:

a. Structural Analysis Tools - Several structural analysis computer programs employing the finite element method are available to help the seat designer achieve a lightweight seat structure capable of withstanding the design criteria crash loads.

b. Seat and Occupant Motion Simulator - The seat and occupant motion during a crash should be analyzed to determine if the occupant might strike surrounding structure or potentially injurious objects such as cyclic sticks or sights during the crash sequence. Seat motion must be analyzed, particularly during the seat stroking phase, to insure that stroking is not impaired by the seat striking surrounding structure. This is particularly important for pilot and copilot seats designed to stroke into a well in the floor (see Figure 5) in order to achieve the full 12 inches of vertical stroking distance required by MIL-S-58095(AV).

c. Occupant Injury Models - Although injury models for head/neck injury and body contact type injuries are useful in assessing the injury potential for seated occupants, the need is greatest for a validated injury model capable of predicting seat occupant injury due to headward (+G_z) decelerative forces during crash impacts involving longitudinal, lateral, and vertical forces. Emphasis is placed on +G_z forces because the 95th percentile survivable helicopter accident vertical floor accelerations (48G peak) greatly exceed specified human tolerance (approximately 23G). The attenuation of injurious crash impact accelerations is illustrated in Figure 4, which shows how peak vertical accelerations as high as 62.95G were attenuated to less than 24G during the full-scale crash testing of a CH-47C helicopter. Aircraft impact conditions were a 95th percentile survivable accident; i.e., 50 ft/sec flight path velocity, 30 ft/sec forward velocity, 40 ft/sec vertical velocity, 10° nose-up pitch, and 10° roll at impact.⁽⁹⁾ A spinal injury model, extensively correlated with experimental and operational data, would enable the seat designer to "tune" the seat's vertical crash force attenuation characteristics for minimum probability of injury for a given set of input pulse and occupant population criteria. Seat and restraint system characteristics affecting the probability of injury due to +G_z forces include: body position, seat cushion dynamic overshoot, amount of vertical stroking distance available, and energy absorber load-deflection profile.

Application of mathematical modeling techniques to the crashworthy seat design process has lagged considerably. In large part this is due to the resources required to productively apply the computer program (e.g., computer, personnel qualifications, time, and funds) to the design problem and/or concerns about the extent of model correlation with test data. The companies that manufacture helicopter seats are often small businesses that find it more practical to develop a crashworthy seat by design, hand analysis, and test, without the use of mathematical models. Some examples of where mathematical models have been used are discussed in the following paragraphs.

The crashworthy helicopter crew seat design criteria of MIL-S-58095(AV) were verified with the aid of the lumped-parameter model shown in Figure 6.⁽¹⁰⁾ This 5-degree-of-freedom lumped-parameter system predicts the vertical dynamic response of the seat and occupant to the crash impact vertical acceleration time history input to the model at the floor. The occupant is modeled with three masses, three linear springs, and three viscous dampers. Masses M₃, M₄, and M₅ represent the occupant's pelvis, chest, and head respectively. Springs K₃, K₄, and K₅ represent the buttocks, spinal column, and neck. Masses M₁ and M₂ represent the mass of the seat and seat cushion. K₁ and K₂ represent the vertical load-deflection characteristics of the seat and seat cushion. The nonlinear energy absorber and cushion load-deflection characteristics are modeled with springs K₁ and K₂ in a piecewise linear fashion. This model was used to investigate the effect of the following variables on decelerative loading during a vertical impact: crash pulse, seat movable mass, cushion properties, energy absorber limit load, and stroking distance. Reference 10 contains a complete description of this model and the parametric analysis performed. Based on the parametric analysis and a series of seven vertical and one triaxial seat drop test, it was concluded that crashworthy seat energy absorbers should be set at a limit load factor of 14.5 ± 1.0 for the 50th percentile occupant, and at least 12 inches of vertical stroking distance is required for the 95th percentile occupant in the 95th percentile survivable accident. This model was used in Reference 11 to further investigate seat system sensitivity to: floor acceleration, energy absorber load-deflection profile, cushion load-deflection characteristics, and occupant size.

The effect of helicopter occupant restraint system webbing elongation, width, and slack on injury potential was investigated during the effort described in Reference 12. The two-dimensional computer program SIMULA⁽¹³⁾ was used to perform an analysis of the following variables: crash pulse shape and magnitude, occupant size, restraint system slack, webbing stiffness, energy-absorbing webbing, and different combinations of shoulder harness and lap belt straps. The Gadd Severity Index was used to indicate the relative injury potential of the various restraint systems analyzed. High elongation webbing was shown to not only increase the occupant strike envelope but also to significantly amplify occupant loading as shown in Figure 7.

Another example of the use of mathematical modeling to study seat and occupant motion during a crash is presented in Reference 14. During development of a crash-force-attenuating armored crew seat under Navy contract, ARA Incorporated used a single rigid-body, 3-degree-of-freedom (vertical translation, longitudinal translation, and pitching) mathematical model to predict the seat bucket and occupant motion during crash impact energy absorber stroking. A single rigid body representing the seat bucket and occupant was cantilevered from the vertical axis by three stroking energy absorbers. This model provided the following information: rigid-body acceleration, velocity, and displacement; energy absorber forces, and amount of energy absorbed.

Although MIL-STD-1290, MIL-S-58095(AV), and the "Crash Survival Design Guide" define human tolerance to headward accelerations in terms of the findings of Eiband, the Dynamic Response Index (DRI) has been employed in a number of efforts in an attempt to determine the cumulative probability of spinal injury from ejection seat operational experience, for want of a correlated probability of spinal injury model for crash impact. The cumulative probability of spinal injury during vertical crash impact for various "notched" or "square" energy absorber load-deflection characteristics (see Figure 8) was investigated using the DRI in the Reference 15 and 16 efforts. Basic assumptions of these efforts included: (1) the DRI is valid for the crash impact problem, and (2) because the crash environment and occupant weight can be described statistically, the cumulative probability of injury can then be calculated using the DRI for a given energy absorber. The analytical model of Figure 9 was used to calculate the seat stroke and dynamic response of the seat and man for a given triangular vertical input pulse. It was concluded from these efforts that: (1) for a survivable helicopter vertical crash impact, there is a 12.4-percent probability of spinal injury without a crash force attenuating seat; (2) the "square wave" energy absorber with 12 inches of stroke offers a 17-percent reduction in spinal injury probability in comparison to no attenuation; and (3) an optimized "notched" energy absorber offers a 50-percent improvement in comparison to no attenuation. The potential of the "notched" energy absorber was investigated further during the crashworthy troop seat development effort of Reference 17 in comparison to the curvilinear load-deflection curve characteristic of tensile yielding of annealed tube and the trapezoidal curve of invertube and wire-through-roller type attenuators. Because of the extreme sensitivity of the DRI to minor changes in the "notched" attenuator load-deflection profile and doubt concerning the feasibility of manufacturing a "notched" energy absorber of sufficient accuracy, the "notched" energy absorber was not deemed suitable for crashworthy troop seats.

The three-dimensional computer program Seat-Occupant Model: Light Aircraft (SOMLA) has been developed by Dr. D. H. Laananen under Federal Aviation Administration (FAA) sponsorship for the purpose of providing the seat designer a tool for analyzing seat, occupant, and restraint system dynamic response to crash impact. The 29-degree-of-freedom occupant model consists of 12 rigid mass segments with rotational springs and dampers at the joints. A finite element seat model is provided that consists of a seat pan and back which retains the same position for any seat being modeled. Energy absorbing seats may also be modeled. Five types of seat support structure are possible which approximate all known light aircraft seat types. SOMLA also predicts impact between the aircraft interior and occupant as well as calculates the relative velocity of impact. In addition to occupant segment positions, velocities, and accelerations, SOMLA outputs: restraint system loads; cushion loads; aircraft displacement, velocity, and acceleration; seat deflections; floor reactions; and injury criteria (DRI, Gadd Severity Index, and the Head Injury Criterion of Federal Motor Vehicle Safety Standard 208). The emphasis by the developer on program efficiency is reflected by the relatively low CPU times reported in Reference 18, e.g., 60 seconds of CDC 6600 CPU time for .150 second of solution time for simulation of a 44-ft/sec longitudinal impact using a rigid seat model. The FAA Civil Aeromedical Institute has been performing a test program since 1977 to provide a broad data base for validation of SOMLA and in particular to evaluate model accuracy for cases involving plastic deformation of the seat. Data from the first series of 40 tests is provided in Reference 19. Forward impact and combined forward and downward loading impact tests were performed using a rigid seat pan and back with deformable seat legs. SOMLA has been used to simulate the crash impact behavior of an energy absorbing seat for the Bell Helicopter Textron Model 222 commercial helicopter. The FAA CAMI dynamically crash tested two of these seats. Correlation between the SOMLA predictions and the CAMI test data is presented in Reference 18. This model appears promising for use as a design tool, considering its efficiency, the validation effort underway, its versatility, and ongoing FAA efforts to improve the seat structure model.

The crashworthy armored crew seat for the UH-60A BLACK HAWK, shown in Figure 3, was structurally optimized with the aid of the finite element structural analysis computer program STARDYNE. Analysis of this seat with a finite element computer program enabled the designer to provide the strength required by MIL-S-58095(AV) with a seat frame weighing only 52 pounds.

Crashworthiness technology has advanced to the point that a crashworthy seat design can be achieved with little or no weight increase in comparison to the noncrashworthy seats of earlier aircraft. Although crashworthy helicopter seats have been designed and tested that offer vastly improved retention strength and vertical crash-force attenuation characteristics certain to reduce the probability of a seat occupant injury, the validated analytical and testing tools are not available to permit the determination of the probability of seat occupant injury to crash impact loading. Because seat stroking distance is limited (usually from 7 to 17 inches), the seat designer and evaluator need an analog to predict the statistical probability of injury. If the seat crash force attenuation behavior is to truly be designed to minimize injury, then an analytical tool is needed which the designer can use to determine the sensitivity of the cumulative probability of injury of the potential occupant population as a function of seat variables. The cumulative probability of injury analyses documented in References 15 and 16 are examples of the type of analysis needed; however, only vertical forces were considered and the DRI was used in these studies. The DRI was developed and validated for ejection seat injury analysis. Because of the combined loading, the varying pulse shapes with onset rates an order of magnitude greater than ejection seats, the multiple impact pulses during a crash, and the difference in helicopter and fixed-wing occupant body restraint, the probability of crash injury predicted by the DRI must be considered suspect.

There is also a need for the aviation R&D community to develop and validate an anthropomorphic dummy capable of simulating human response to three-dimensional impact, and in particular, impulsive loading of the crash impact type parallel to the spine. Although extensive effort has been expended by the automotive R&D community on anthropomorphic dummies, these simulators have been designed and tested for accurate

response to loading normal to the spine, not parallel. Furthermore, the anthropometry of the military population varies from that of the civilian population. The need for such a validated, repeatable, standard dummy is illustrated by the proposed crashworthy troop seat test criteria of Reference 5. The injury criteria of Figure 2 are based on acceleration history measured at the seat pan of a crew seat; however, the typical troop seat is fabric over a tubular frame, thereby preventing meaningful seat pan acceleration measurements. This necessitates the use of dummy accelerometer data to show compliance with Figure 2. A high-fidelity dummy is required for such compliance testing, but such a dummy is yet to be designed.

Prior to the design of the most simple anthropomorphic dummy, the anthropometry and mass distribution of the live human being duplicated must be known. This data is not available for US Army personnel, and to our knowledge, it is not available for other populations either.

MASS DISTRIBUTION AND MECHANICAL PROPERTIES OF THE 50TH PERCENTILE US ARMY AIRCREW

Several authors have reported the distribution of mass in cadavers and in living subjects (References 20 through 24). The correlation of these individual studies to the entire population or to selected groups has not been attempted to the best of our knowledge. The relation of the anatomical dimensions of Reference 20 to the mass distribution of cadavers as reported in References 21, 22, and 23 is reported herein. In addition, the isolated vertebral compressive strength and deformation properties of the lumbar, thoracic, and cervical segments as reported by Kazarian in Reference 24 are extracted and expanded on the basis of more recent tests conducted at the same laboratory. The deformation of the pelvis and skull due to G_z (headward) load is also estimated on the basis of related tests on the skull at Wayne State University. (25)

The anthropometric survey of 1482 Army aircrewmembers of Reference 20 was studied to determine which dimensions could be related to the dimensions found from the dissection of cadavers. The anthropometric dimensions of value for this purpose are shown in Table V. The lengths of the arm and leg bones were taken from the Reference 21 study. The average value of the stature of the six cadavers used in the Reference 21 study was only 1.4 percent less than that of the 50th percentile male found in the Reference 20 study. Since the stature difference is small, it appears to be feasible to use a simple ratio of stature to translate the cadaver dimension to the desired 50th percentile size. Based on this rationale, skeletal joints and landmarks are illustrated in Figure 10.

It should be noted that the upper leg (femur) bone was lengthened by 1.0 cm and that the lower leg (fibula and tibia) bones were shortened by 1.0 cm from the values found for the Reference 21 cadaver study. This change was required to properly match the buttock-knee, buttock-popliteal, and floor-knee dimensions found on the 1482 live subjects of Reference 20. Considering the small number of cadavers, the change appears to be reasonable. Other than this change, all other dimensions are compatible between the two studies. The lengths of cervical, thoracic, and lumbar vertebrae are determined by an average of anatomy drawings and by the cervical height given in the anthropometric data. (20) The pelvic depth was determined by subtraction of head depth and spinal column length from sitting height.

In the interest of simplification and economy, the spinal column is divided into 8 segments instead of 24. This reduction is believed to be justifiable because of the small number of cadavers studied to date.

The thoracic vertebrae are separated into groups of three and the lumbar vertebrae into groups of two. The distribution of mass, shown in Figure 11 for a seated 50th percentile torso, is based on segmentation of the body in accordance with References 21, 22, and 23. The average body weight of the 1482 live subjects was 77.35 kg, while average total body weight of the six cadavers in Reference 21 was 65.17, i.e., 15.7 percent less for the segmented cadaver weight. Thus, it is assumed that the weight of segments in a 50th percentile male can be determined by using the ratio of live subject weight to the segmented cadaver weight, especially since their statures were so nearly identical. The mass distribution of body segments is also presented in Table VI.

It should be noted that good agreement is found between the knee height and popliteal height relative to the calf and foot bone length found in Reference 21. The same can be said for the relation between the femur (thigh) bone and the buttock-to-knee and buttock-to-popliteal lengths.

The arms of the seated body are illustrated in Figure 12 in a relaxed position with hands resting on the knee. The center-of-gravity locations of the arm and hand segments shown in Table VI are compatible with Figure 12. This arm position is considered to be typical location, and it is suggested that it be used as a standard in all crashworthy seat testing. It may be assumed that the arm is attached to the first two segments of vertebrae, T1-T6, for determination of load in the spinal column. The legs of the seated body in Figure 12 are shown with the center of the femur head horizontal with the center of the assumed knee hinge. The location of the knee hinge point is 1 to 2 centimeters into the femur (hip) bone from the femur-tibia (calf) interface point. Separation of thigh-to-calf segments at this location, in accordance with Reference 21, is desirable because the moving segments for the ZX plane do move about this hinge. The thigh is segmented from the pelvis by a cut through the femur (socket) head as outlined in Reference 21. Again, this segmentation appears to be reasonable because the mass of the thigh does move about the pelvis along a diagonal plane to the femur bone rather than a perpendicular plane. Note that the mass of the pelvis is relatively low, just slightly more than the mass of one thigh, i.e., 8.89 kg versus 7.91 kg.

Accurate strength and deflection properties of the seated human torso when exposed to inertial loads are urgently needed. The authors have attempted to collect the available data from Kazarian and Hodgson (References 24 and 25) for the head, and spinal column exposed to a Z-axis load. Kazarian's data for this isolated spinal vertebra minus any disk effect is shown in Figure 13. Reference 24 contains thoracic vertebra data only; the cervical, lumbar, and pelvis data were extrapolated based on personal communications with Dr. Kazarian in September 1978. The strength and stiffness properties in Figure 13 are based on the highest loading rate used by Dr. Kazarian (89 cm/sec) in his tests. This loading rate revealed strength and stiffness values more than twice those found in the quasi-static tests; therefore, only the

highest load rate properties (which are applicable to crashworthiness) are shown in Figure 13. A study of the actual load and deformation raw data showed that the stiffness of the vertebra contained three different slopes as illustrated by a typical curve in Figure 14. These three slopes were interpolated for the thoracic data in Figure 13 and the cervical, lumbar, and pelvis were extrapolated, but consideration was given to the data obtained by King in Reference 26. It was assumed that the vertebra would "bottom out" at approximately 50 percent deformation; thus, a "bottoming" slope was assumed to be 90,000 lb/in. for all vertebrae.

It is interesting to observe the load versus deformation properties of a typical isolated human vertebra in Figure 14, particularly the fact it contains a "yield" point similar to common structural steel. If further research shows this curve to be truly "typical" of live skeletal vertebrae, it is possible to use the spinal deformation shown in a test dummy or math model as a parametric criterion for load in the spine, because peak load has a fixed relation to the deflection. Prior to such use, the irreversible injury point must be established on the curve; i.e., how far can the vertebra be deformed and still recover without permanent damage?

The data in Figure 13 are extrapolated further in Figure 15. This figure shows the total load and deformation for the head, the vertebra-disk combination, and the pelvis. This data is presented as "food-for-thought" only; it is realized that further research is necessary before such data can be used with confidence. Nonetheless, Figure 15 illustrates the point that the load-deformation characteristics of the spinal column are definitely not simulated by a single stiffness linear spring. It is proposed that the format illustrated in Figure 15 be used by future modelers and bone researchers, i.e., the segmentation of the spinal column into 8 groupings rather than 24. Note in Figure 15 that the stiffness values of the middle slope are reduced in some areas because a greater length with more vertebrae are involved.

CONCLUSION

Helicopter seat and restraint systems have been developed that will restrain the occupant throughout the 95th percentile survivable Army helicopter accident and possess crash energy absorption features to reduce the incidence of back injury. Notwithstanding these major hardware improvements, there is a pressing need for validated anthropomorphic dummies for crash testing. Of no less importance is the need for better criteria for human tolerance to crash impact decelerative loading. Specifically, the seat designer and evaluator need an analog that will predict the statistical probability of injury. A "standard" set of anthropometric and mass distribution data describing several sizes of aircrewmembers is needed. A validated crashworthy seat occupant mathematical model is needed with the capability to predict: (1) seat and occupant dynamic response to three-dimensional crash impact, and (2) the probability of occupant injury to multi-axis, crash impact.

REFERENCES

1. Military Specification, MIL-S-58095(AV), "Seat System: Crashworthy, Nonejection, Aircrew, General Specification for," Aug 71.
2. Turnbow, J.W., et al, "Crash Survival Design Guide," USAAMRDL Technical Report 71-22, Eustis Directorate, US Army Air Mobility Research and Development Laboratory, Fort Eustis, VA, Oct 73.
3. Singley, G.T. III, and Sand, L.D., "US Army Helicopter Accident Experience," AGARD Proceedings No. 212 on Aircraft Operational Experience and Its Impact on Safety and Survivability, AGARD, P. 1-1, Jun 76.
4. Military Standard MIL-STD-1290(AV), "Light Fixed- and Rotary-Wing Aircraft Crashworthiness," 25 Jan 74.
5. Reilly, M.J., "Crashworthy Troop Seat Testing Program," USAAMRDL Technical Report 77-13, Applied Technology Laboratory, US Army Research and Technology Laboratories (AVRADCOM), Fort Eustis, VA, Nov 77.
6. Saczalski, et al, "Aircraft Crashworthiness," University Press, University of Virginia, Charlottesville, VA, pp. 197-365, Oct 75.
7. King, A.I., and Choy, C.C., "Mathematical Modeling, Simulation and Experimental Testing of Biomechanical System Crash Response" AIAA Paper 75-272, American Institute of Aeronautics and Astronautics, NY, NY, Feb 75.
8. Frisch, G.D., et al, "The Effectiveness of Mathematical Models as a Human Analog," SAE Paper No. 760774, Society of Automotive Engineers, Warrendale, PA, Oct 76.
9. Singley, G.T. III, "Full Scale Crash Testing of a CH-47C Helicopter," AHS Paper 1082, American Helicopter Society, Washington, DC, May 76.
10. Desjardins, S.P., and Harrison, H.D., "The Design, Fabrication, and Testing of an Integrally Armored Crashworthy Crew Seat," USAAMRDL Technical Report 71-54, Eustis Directorate, US Army Air Mobility Research and Development Laboratory, Fort Eustis, VA, Jan 72.
11. Singley, G.T. III, and Desjardins, S.P., "Crashworthy Helicopter Seats and Occupant Restraint Systems," Paper 6.7, NATO AGARD Aerospace Medical Panel Aerospace Specialists' Meeting on Operational Helicopter Aviation Medicine, Fort Rucker, AL, 1-5 May 78.
12. Kourouklis, G., et al, "The Design, Development, and Testing of an Aircrew Restraint System for Army Aircraft," USAAMRDL Technical Report 72-26, Eustis Directorate, US Army Air Mobility Research and Development Laboratory, Fort Eustis, VA, Jun 72.
13. Turnbow, J.W., et al, "Aircraft Passenger-Seat-System Response to Impulsive Loads," USAAVLABS Technical Report 67-17, US Army Aviation Materiel Laboratories, Fort Eustis, VA, Aug 67.

14. "An Armored Energy Attenuating Crewman's Seat for Rotary- and Light Fixed-Wing Aircraft," Report No. NADC-72186-CS, US Naval Air Development Center, Warminster, PA, Sep 72.
15. Carr, R.W., and Phillips, N.S., "Definition of Design Criteria for Energy Absorption Systems," NADC Report AC-7010, US Naval Air Development Center, Johnsville, Warminster, PA, Jun 70.
16. Phillips, N.S., et al, "A Statistical Evaluation of the Injury Potential of a 'Square Wave' Energy Absorber," USAAMRDL Technical Report 72-9, Eustis Directorate, US Army Air Mobility Research and Development Laboratory, Fort Eustis, VA, Jun 72.
17. Reilly, M.J., "Crashworthy Troop Seat Investigation," USAAMRDL Technical Report 74-93, Eustis Directorate, US Army Air Mobility Research and Development Laboratory, Fort Eustis, VA, Dec 74.
18. Laananen, D.H., "Mathematical Simulation for Crashworthy Aircraft Seat Design," AIAA Paper No. 77-1250, AIAA Aircraft Systems and Technology Meeting, Seattle, WA, Aug 77.
19. Chandler, R.F., and Trout, E.M., "Evaluation of Seating and Restraint Systems and Anthropomorphic Dummies Conducted During Fiscal Year 77," FAA-AM-78-24, Federal Aviation Administration Civil Aeromedical Institute, Oklahoma City, OK, Jun 78.
20. Churchill, E., McConville, J.T., and Laubach, L.L., "Anthropometry of US Army Aviators - 1970," US Army Natick Laboratories, Natick, MA, Dec 71.
21. Chandler, R.F., Clauser, C.D., McConville, J.T., Reynolds, H.M., Young, J.W., "Investigation of Inertial Properties of the Human Body," HS-801-430 Report, Department of Transportation, Washington, DC, Mar 75.
22. Walker, L.B., E.H. Harris, U.R. Pontiac, "Mass, Volume, Center of Mass, and Mass Moment of Inertia, of Head and Neck of Human Body," Report 730985, Tulane University, New Orleans, LA, 1972.
23. Kenedi, R.M., Perspectives in Biomedical Engineering, "Inertial Property Distribution of the Human Torso," Y. King Liu, Jack K. Wickstrom, pp. 203-212, University Park Press, Baltimore, MD, Jun 72.
24. Kazarian, Leon, Dr. Ing and G.A. Graves, M.S., "Compressive Strength Characteristics of the Human Vertebral Centrum," AMRL-TR-77-14, Aerospace Medical Research Laboratory, Aeromedical Division, A.F.S.C., Wright-Patterson Air Force Base, OH, 1977.
25. Hodgson, V.R., and Thomas, L.M., "Head Impact Response - Proposal Number VRI 7.2," Society of Automotive Engineers, Inc., 1975.
26. King, A.I., and Prasad, P., "An Experimentally Validated Model of the Spine," Journal of Applied Mechanics of the American Society of Mechanical Engineers, NY, Sep 74.

TABLE I. FATAL AND NONFATAL INJURY FACTORS (ALL
FY70 THROUGH FY75) HELICOPTER ACCIDENTS (3)

CAUSE	PERCENTAGE OF TOTAL INJURIES
Deceleration	49.9
Aircraft Structure	12.1
Thermal (0 in FY74 and 75)	11.2
Restraint	5.9
Ejection	5.6
Main Rotor	3.3
Flight Controls	2.7
Intrusions (except rotor)	2.5
Personal Equipment	2.1
Aircraft Parts	1.2
Drowning	1.1
Other	2.4

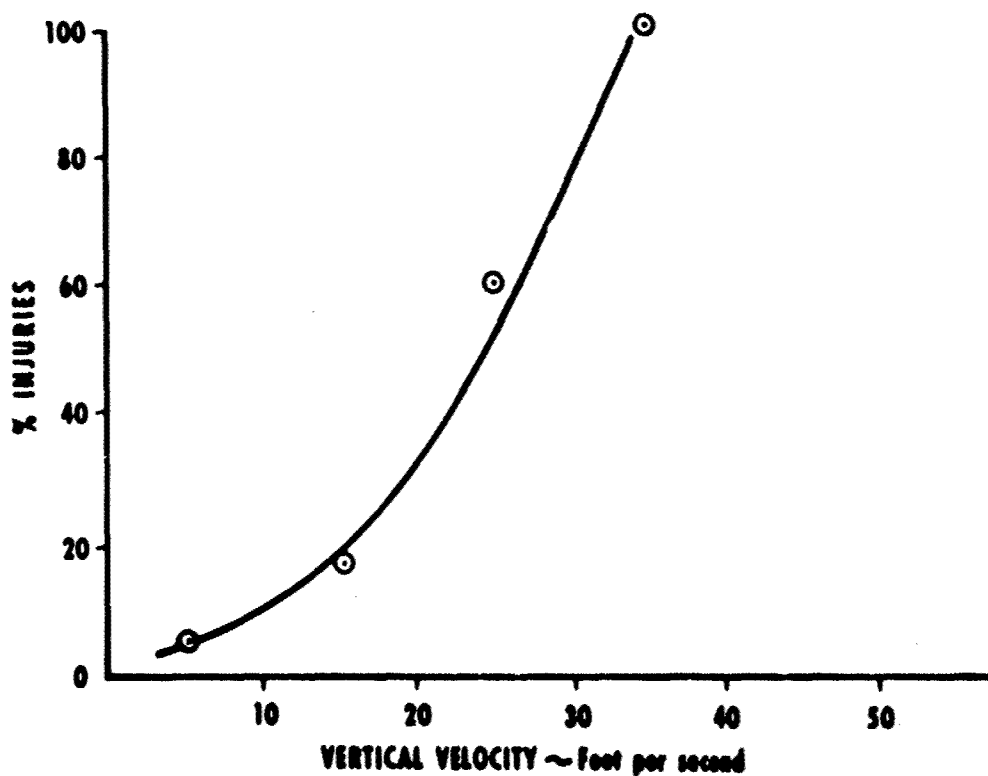


Figure 1. Relative Frequency of Attack Helicopter Occupant
Spinal Injury vs Vertical Velocity of Impact.

TABLE II. DESIGN ENVIRONMENT (4)

SUMMARY OF DESIGN PULSES FOR ROTARY-WING AIRCRAFT*			
IMPACT DIRECTION	VELOCITY CHANGE (ft/sec)	PEAK G	PULSE DURATION 'T' (sec)
Longitudinal (Cockpit)	50	30	0.104
Longitudinal (Passenger Compartment)	50	24	0.130
Vertical	42	48	0.054
Lateral (Rotary-Wing)	30	18	0.104


* Pulse Shape: 

TABLE III. DYNAMIC TEST CONDITIONS FOR AIRCRAFT SEATS

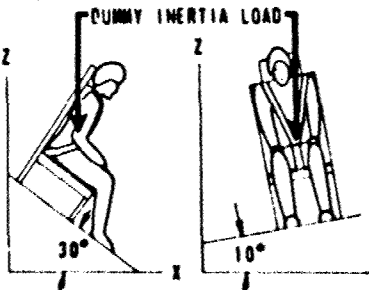
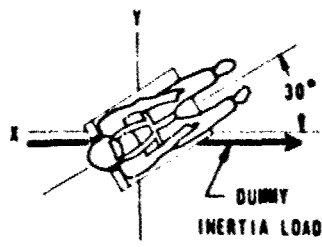
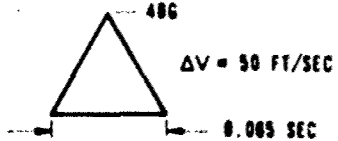
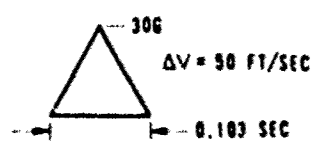
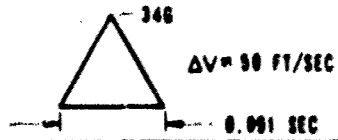
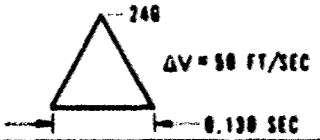

SEAT ORIENTATION	
TEST 1 DOWNWARD, FORWARD, AND LATERAL LOADS	TEST 2 FORWARD AND LATERAL LOADS
	
TEST PULSE FOR COCKPIT SEATS (1)*	
	
TEST PULSE FOR CABIN SEATS (5)*	
	
<p>* THE RISE TIME FOR THE TRIANGULAR PULSES MAY VARY BETWEEN THE TWO VALUES ILLUSTRATED.</p> 	

TABLE IV. CRASHWORTHY SEAT ULTIMATE STATIC LOAD FACTORS

LOAD DIRECTION WITH RESPECT TO AIRCRAFT	CREW SEAT LOADS (G)		TROOP SEAT LOADS (G)	
	MIL-S-5822*	MIL-S-58095	MIL-S-27174*	MIL-STD-1290
	(1957)	(1971)	Type 1 (1960)	(1974)
Forward	8.0	35.0	1.1	30.0
Aft	5.0	12.0	-	12.0
Down	15.0	48.0	10.0	48.0
Up	7.5	8.0	-	8.0
Side	10.0	20.0	3.0	20.0

* For comparison purposes, the ultimate static loads presented in MIL-S-5822 and MIL-S-2714 have been converted to load factors in terms of G, based on a 199.7 lb occupant.

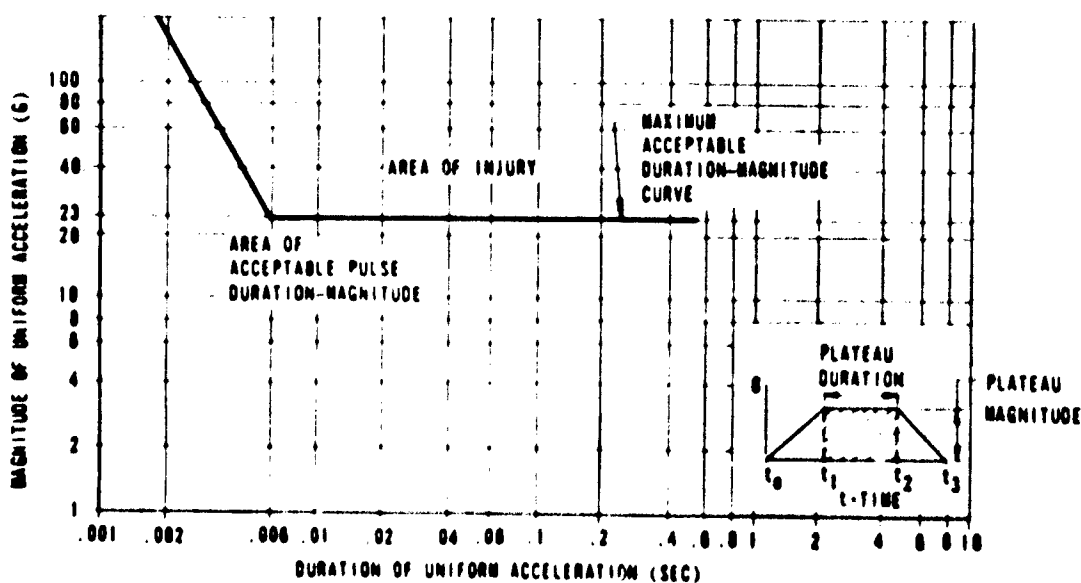


Figure 2. Maximum Acceptable Vertical Pulse Acceleration and Duration Values. (2)

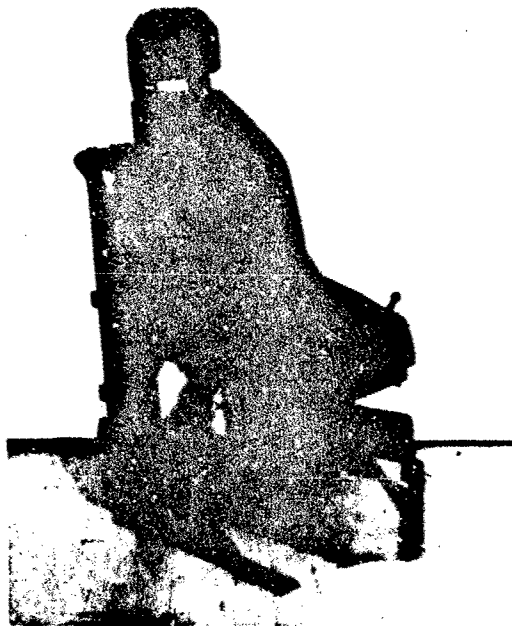


Figure 3. UH-60A Crashworthy Armored Crew Seat

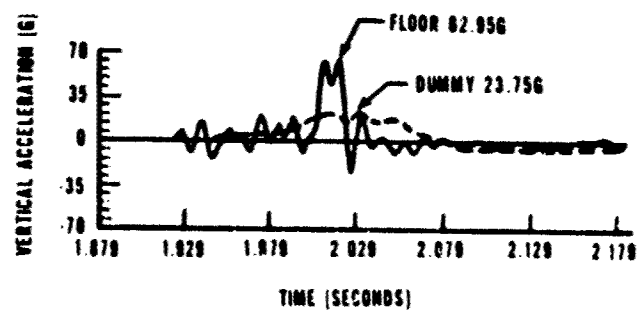


Figure 4. Vertical Response of Crashworthy Troop Seat to Full-Scale 50 ft/sec CH-47C Crash Test. (9)



Figure 5. Prototype Armored Pilot/Copilot Seat Stroked Into Floor Well After Drop Test.

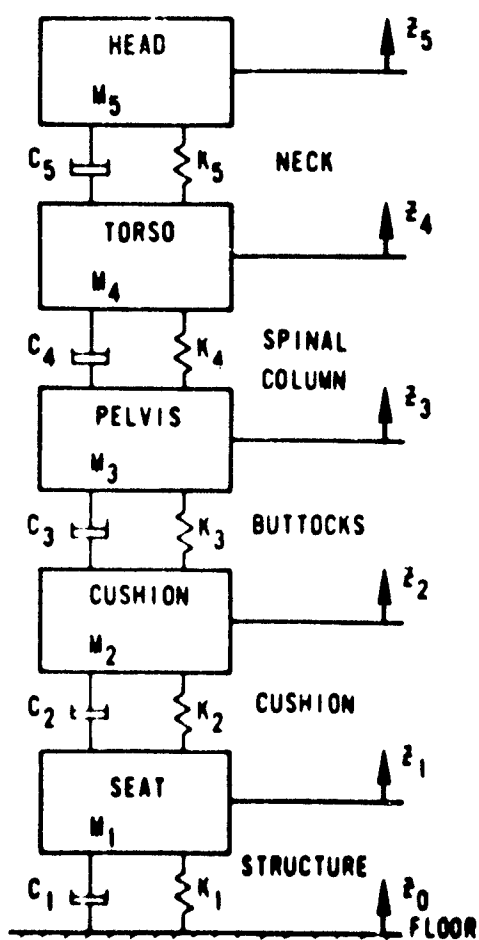


Figure 6. Seat Model.

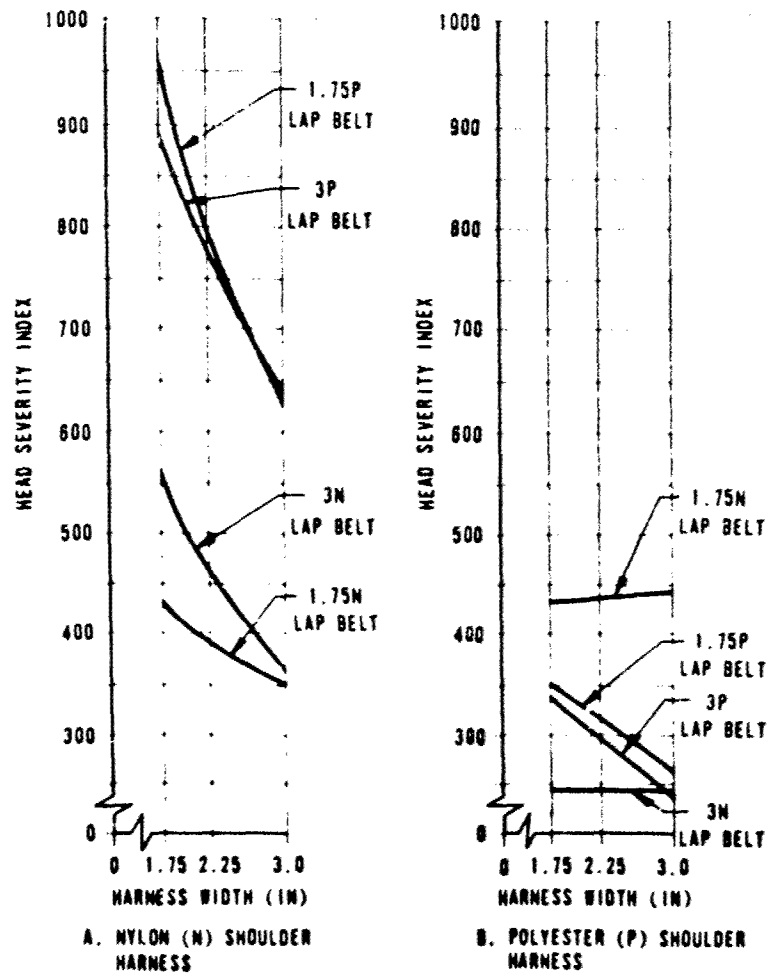


Figure 7. Head Severity Index Versus Material Stiffness (Calculated for a Longitudinal Crash Pulse, $\Delta V = 50$ ft/sec, Peak Deceleration of 30G, and a 95th Percentile Occupant. (12))

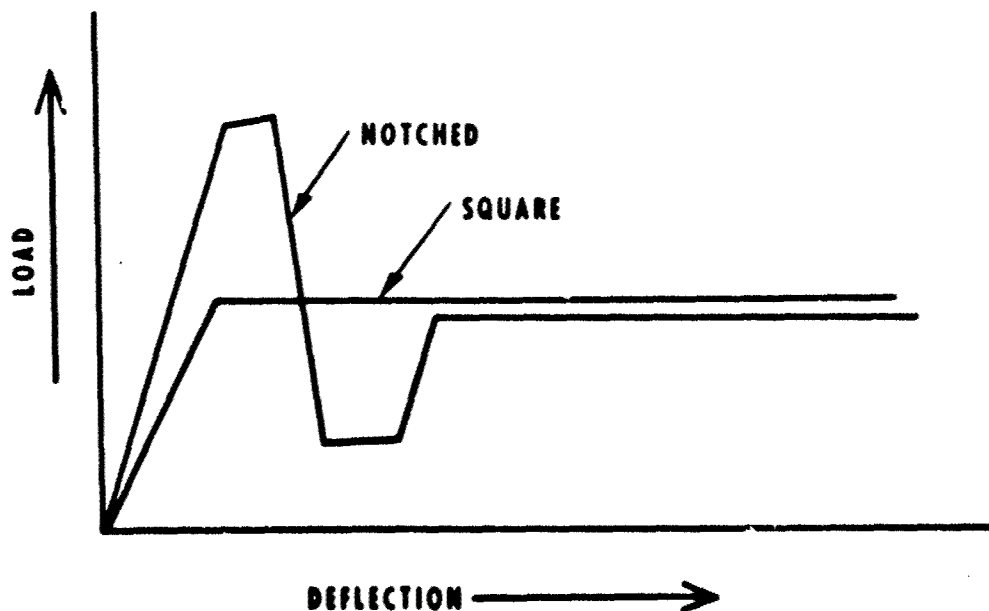


Figure 8. "Notched" and "Square Wave" Energy Absorber Profiles.

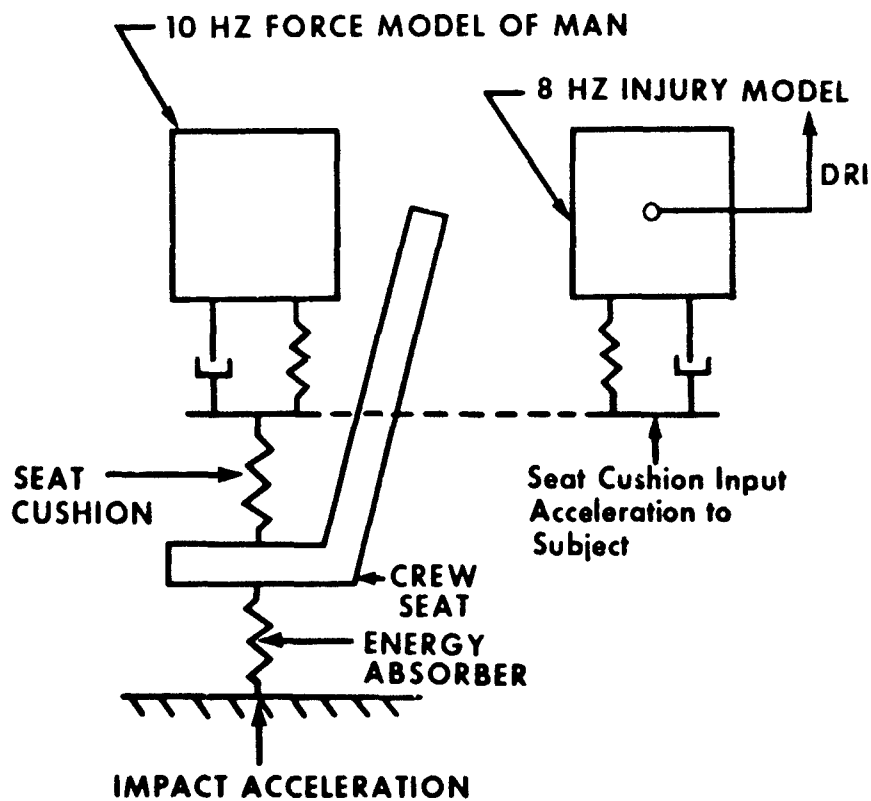


Figure 9. Analytical Representation of Seated Subject.(16)

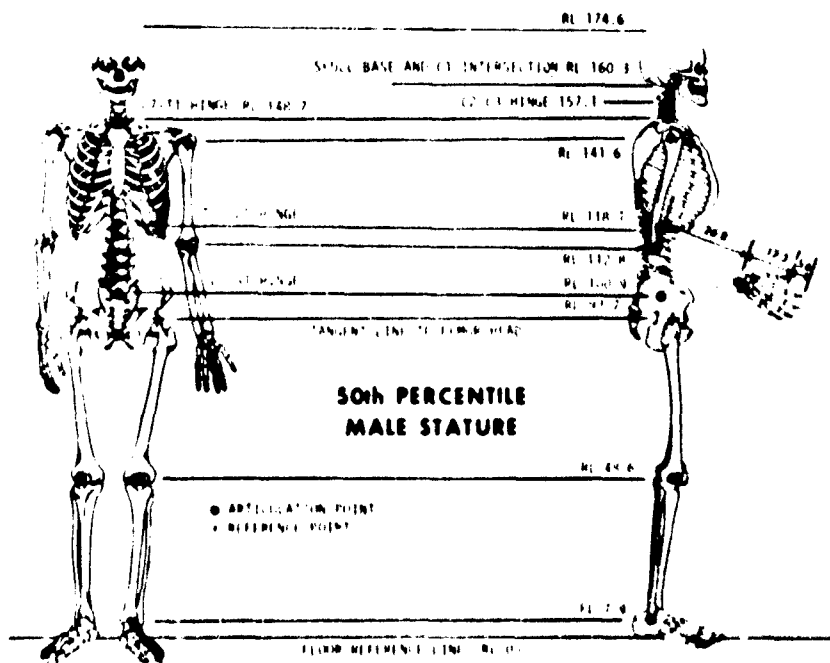


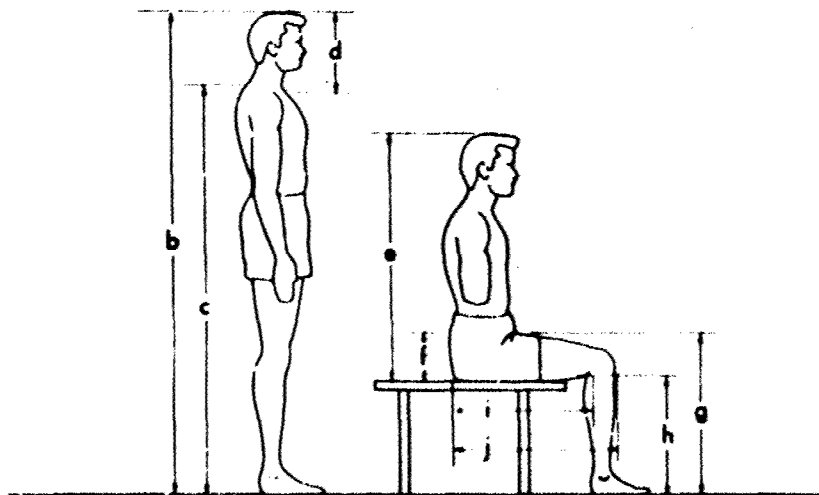
Figure 10. Standing Skeletal Joint and Landmark Locations Based on Anthropometric and Cadaver Measurement From References 20 Through 21.

TABLE V. ANTHROPOMETRIC DATA FOR US ARMY AIRCREW PERSONNEL*

	PERCENTILE		
	5TH	50TH	95TH
a. Weight - Kilograms	60.37	77.35	96.00
b. Height - Centimeters (cm)	164.18	174.58	185.02
c. Cervical Height (cm)	139.77	149.68	159.51
d. Head & Neck Height (cm)**	25.41	25.90	26.51
e. Sitting Height (cm) (Seat Cushion to Top of Head)	85.66	90.90	96.30
f. Thigh Clearance Height (cm)	12.41	14.71	17.04
g. Knee Height (cm)	48.91	52.93	57.40
h. Popliteal Height (cm)	38.38	42.23	46.56
i. Buttock-Popliteal Length (cm)	44.86	49.07	53.41
j. Buttock-Knee Length (cm)	55.91	60.15	64.58

* Data taken from Reference 20.

** This dimension obtained by subtraction of cervical height from stature and adding 1 cm for a portion of C7 vertebra thickness.



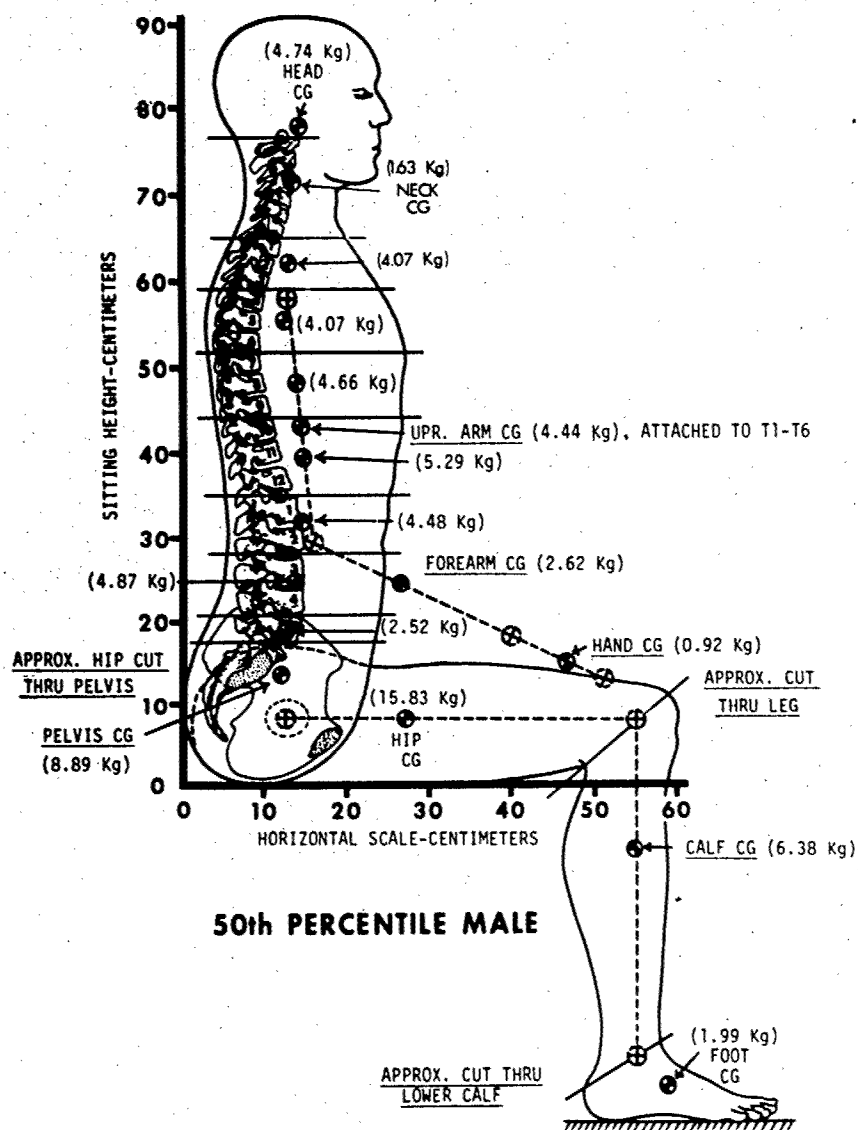


Figure 11. Mass Distribution of Seated Torso Referenced to the Skeletal Structure.

**TABLE VI. CENTER OF MASS DISTRIBUTION OF SEATED
TORSO — 50TH PERCENTILE MALE**

BODY SEGMENT IDENTITY	SEGMENT WEIGHT (KILOGRAMS)	Z AXIS LOCATION (CM)*	X AXIS LOCATION (CM)**
Head	4.74	77.6	10.1
Neck (C1-C7)	1.63	71.3	9.7
Upper Thoracic (T1-T3)	4.07	62.4	10.0
Upper Mid Thoracic (T4-T6)	4.07	55.6	9.7
Lower Mid Thoracic (T7-T9)	4.66	48.1	11.2
Upper Arm	4.44	43.5	12.2
Lower Thoracic (T10-T12)	5.29	40.2	13.0
Lumbar (L1 and L2)	4.48	31.8	13.2
Lumbar (L3 and L4)	4.87	24.5	13.1
Forearm	2.62	24.6	23.7
Lumbar (L5)	2.52	19.0	12.2
Hand	0.92	15.3	45.1
Pelvis	8.89	13.0	11.2
Thigh (Hip)	15.83	7.6	27.2
Calf	6.38	-8.6	55.0
Foot	1.99	-37.1	50.0
TOTAL	77.40		

* Location is based on floor level of zero with 50th percent male head crown equal to reference line of 174.8 cm.

** Location is based on seat back with reference line equal to zero. Seat back is perpendicular to seat bottom, and torso touches seat back at head, shoulders, and buttocks.

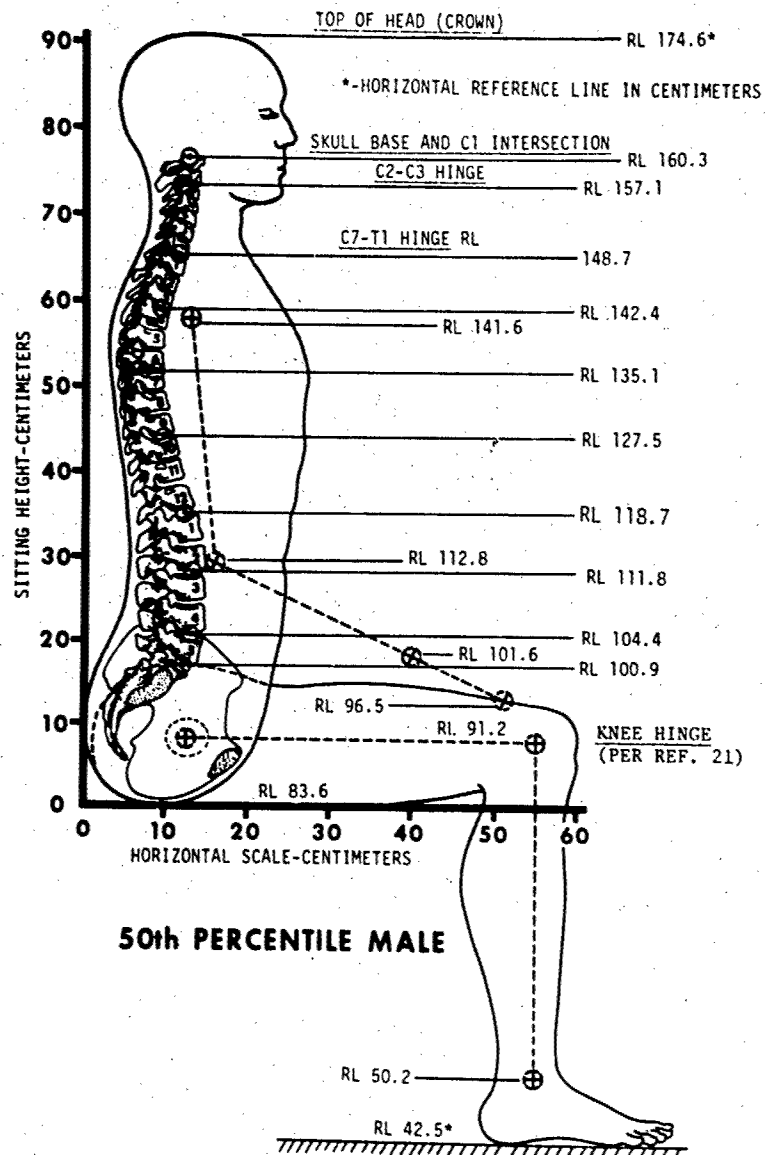


Figure 12. Sitting Skeletal Joint Locations Based on Anthropometric and Cadaver Measurement and Interpolations From References 20 Through 24.

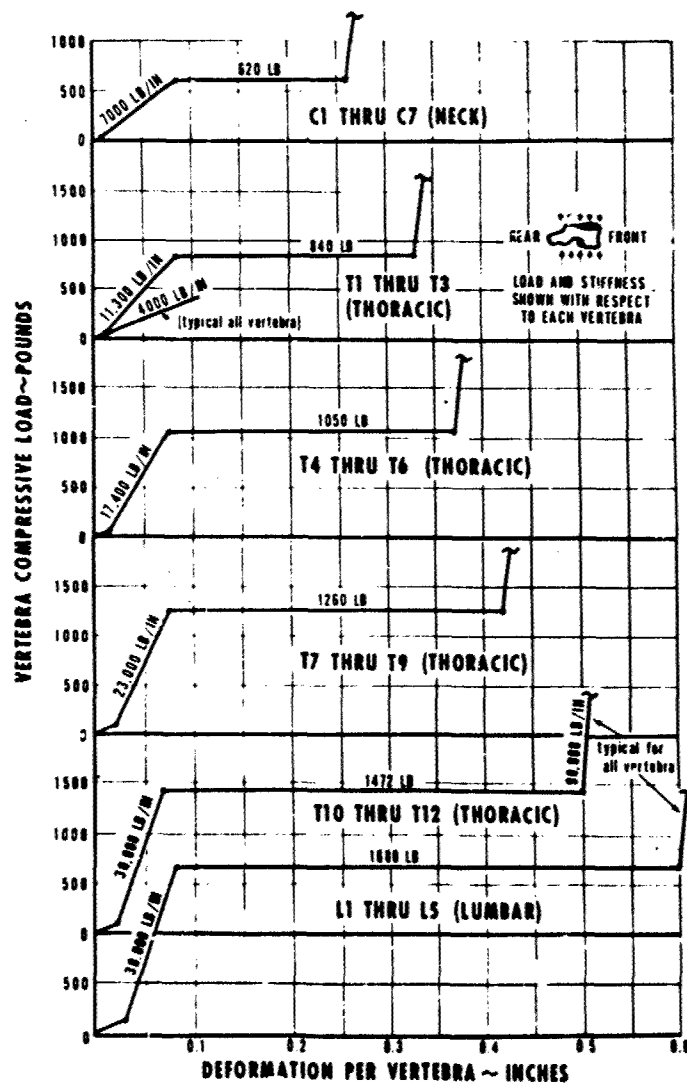


Figure 13. Proposed Average Load Versus Deformation Properties of the Isolated Vertebral Centrum

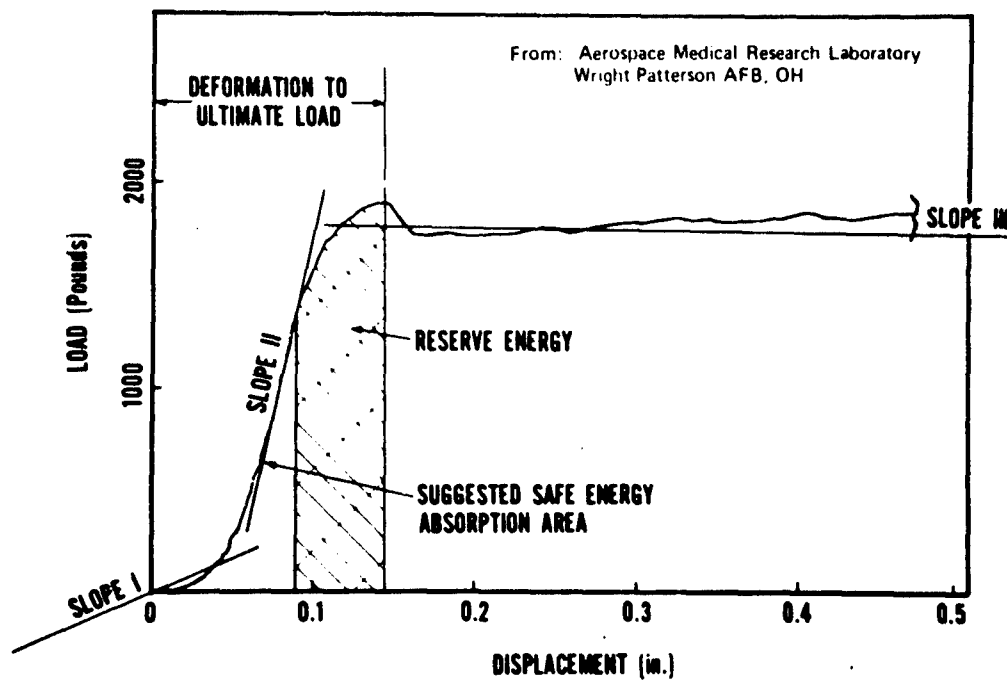


Figure 14. Typical Load Versus Displacement Test Curve Obtained During Compression Testing of Individual Vertebral Bodies.

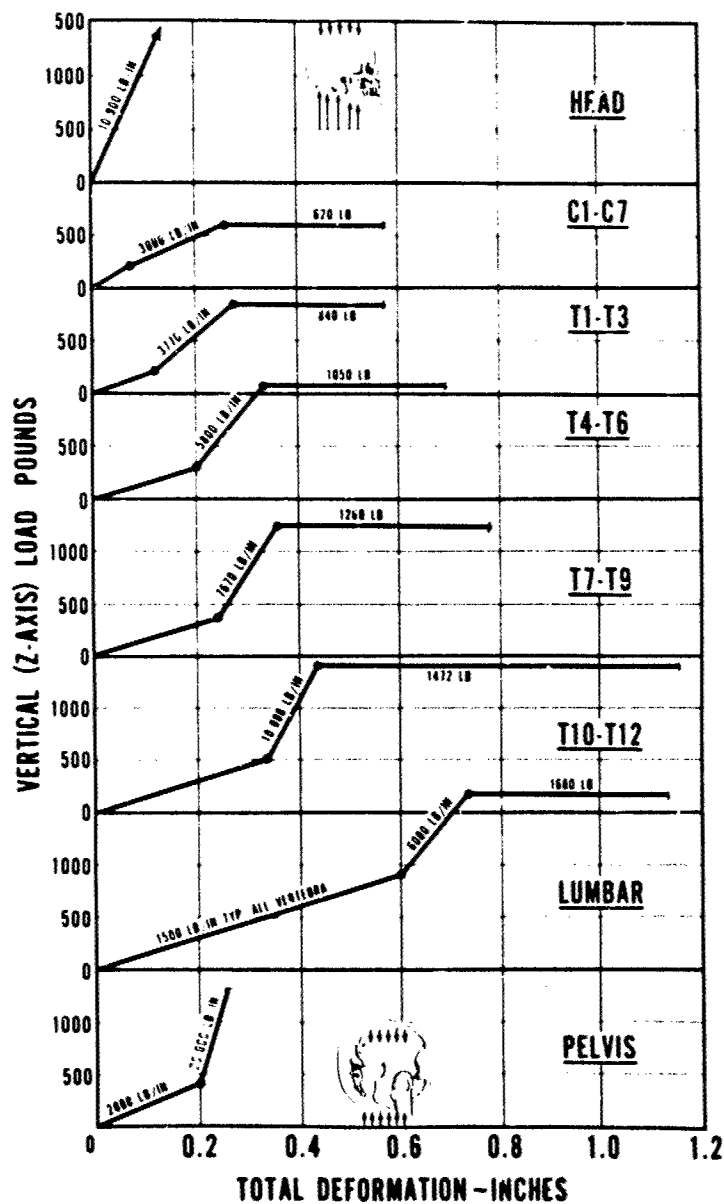


Figure 15. Proposed Z Axis Load-Deformation Properties of the Human Skull, Cervical Vertebra, Thoracic Vertebra, Lumbar Vertebra, and Pelvis.

DISCUSSION

DR. H. VON GIERKE (USA)

In what respect would the model you envision differ from the one Dr. Belytschko presented yesterday? It includes the same data from Kazarian, it includes the same anthropometric data to the extent that they are being needed for the model, so I think what is primarily needed is to exercise it for your particular condition.

AUTHOR'S REPLY (MR. J. L. HALEY, USA)

The key thing that we're trying to get across is that right now there is no standardization of anthropomorphic dummies, there is no standardization of the mass distribution and the anatomical distribution for man. Consequently, every time that we see a model illustrated it is stated to be based on some cadaver study somewhere. We are proposing that we get together and decide what is a "standard man."

AUTHOR'S REPLY (MR. G. T. SINGLEY, USA)

We found Dr. Belytschko's model and the work he has published so far to be very attractive for this type of application. But as we heard yesterday we're still quite far from having a validated model. Unfortunately, we're in the process right now of qualifying hardware and have to determine whether we are in fact minimizing injury. We are just putting out a plea for an accelerated development of that type of model and other models.

MAN, DUMMY, TEST VEHICLE

A comparison of test results for escape systems with the
3 different test methods

by

H.-D. Melzig

E. A. Bockemüller

U. Schmidt

Deutsche Forschungs- und Versuchsanstalt
für Luft- und Raumfahrt e. V. (DFVLR)
33 Braunschweig-Flughafen
Germany

SUMMARY

To prove the validity of experimental results gained with dummies or test vehicles for the qualification of man carrying parachutes series of tests were conducted with parachute jumpers and their 2 analogues: rubber torso dummies and bomb shaped test vehicles (Fig. 1).

The results for the maximum filling force (opening shock) show significant differences, with highest values for the test vehicle, 75 % less for the rubber dummy and an additional 75 % less for the man.

LIST OF SYMBOLS

n opening shock factor, $= F_f / W_T$
 F_f maximum filling force
 W_T total weight of load and parachute
 v_a launch velocity
 v, a parameters

INTRODUCTION

Rubber dummies and test vehicles are analogues for the testing of escape systems and personnel parachutes. The most important criteria for a parachute: the filling behaviour and the filling force history with its maxima are dependent upon the attitude at the time of opening, the connection of the parachute with the load and the rigidity and shape of the load.

For the breaking strength of the material and for the human tolerance the maximum filling force (opening shock) is the limiting factor.

Since all tests of a new development are made with a human analogue like a dummy or a test vehicle the question of validity of the test results for the human jumper always arises, especially for the meeting of requirements and specifications.

A number of comparison tests have been conducted with these 3 methods and the same parachute system to detect the deviation in test results.

TEST METHOD

All tests were drops or jumps from an aircraft. The Do 27, Pembroke or Transall were used as carriers for the different speed ranges.

The test vehicles were fixed at a bomb rack under the wing, released, and 1.8 sec after drop the rear lid was pyrotechnically blown backwards. It pulled out a pilot chute, which itself pulled the parachute to line stretch first, with the canopy still stowed in an inner bag. After tearing a break cord the inner bag was opened and the canopy pulled to stretch by the pilot chute fixed to the canopy vent lines.

The jumpers parachute was released by a timer 1.8 sec after jump. It opened the outer pack and released a pilot chute which then operated the same way as explained under the test vehicle case.

With the rubber dummy the parachute was released by a static line which remains fixed to the aircraft with one end and to the inner bag with the other end, thus opening the outer bag, pulling the inner bag to line stretch, tearing a break cord and pulling the canopy to stretch by another break cord fixed to the vent lines while the dummy is falling away from the aircraft. The inner bag remains fixed to the static line and therewith to the aircraft to which they are pulled back. This is the normal method of releasing parachutes (called automatic release in the contrary to manual release) for military paratroopers some emergency rescue parachutes (e. g. for gliders) and all beginners in sport parachuting. There is a difference to the other methods in the stretch position (Fig. 2), which is the initial condition for the filling period. This may be of influence to the filling process but could rather cause a delay than an acceleration of the filling time and so not be responsible for the higher maximum filling force.

At all 3 configurations the outer parachute bag is opened 1.8 sec after drop or jump. The speed of the aircraft at drop or jump was kept the same for all 3 methods. The speed of vehicle, dummy or jumper at the beginning of canopy filling however may be slightly different due to the different drag coefficient and drag area of the 3 different bodies. With lowest drag coefficient and area the bomb shaped test vehicle will have lost only little of its speed, the jumper who performs a high drag frog position will loose more. The dummy which falls unstable after it slides out of the door of the aircraft probably lies between the other two.

The drop altitude was 300 m above ground in all the cases. Parachute was a standard circular flat with a nominal diameter $D_0 = 8.6$ m and 28 gores (CF-8.6-28). It was connected with the dummy and the man by a harness and with the test vehicle at a central point of the structure.

TEST RESULTS

The experimental results were evaluated with emphasis to the problem how the maximum filling forces (opening shocks) of parachutes with different load configurations could be presented in a mathematical formula.

At first the opening shock factor

$$(1) \quad n = \frac{F_f}{W_T}$$

was calculated from the results and plotted as a function of the launch velocity v_a . Figures 3, 4, 5 show that n is only dependant upon the launch velocity, and not upon the suspended load. This is valid as well for the man as for the dummy and for the test vehicle.

Using the method of least square fit a number of formulas were tried, the best result was gained with the following:

$$(2) \quad n = v [1 + a v_a^2]$$

It contains the parameters v and a which had to be determined. The values received for the parameter a by the method of least square fit were in good agreement for all 3 configurations: man, dummy and test vehicle. Its value is 0.0003 if v_a is used in m/sec. Then formula 2 can be written as:

$$(3) \quad n = v \left[1 + 3 \left(\frac{v_a}{100} \right)^2 \right]$$

n remains dimensionless in this equation.

Using formula (3) again for the determination of parameter v with the method of least square fit the following values were received:

For the man $v_M = 3.4$
 For the dummy $v_D = 4.6$
 For the test vehicle $v_V = 6.0$

These values were received by a stronger consideration of the variance to higher values. This gives regard to the safety of the parachute, the strength of which is affected more by the high forces.

It follows from formula (3) that the ratio of the opening shock factors for the 3 configurations is independent upon the launch velocity v_a . This makes a simple evaluation and transversion of results possible using the relationship:

$$(4) \quad v_M : v_D : v_V = 3.4 : 4.6 : 6.0$$

It can be seen from this ratio and from figure 6 that the opening shock factor n for the dummy is approximately 75 % of the one for the test vehicle. The n for a man is again approximately 75 % of the one for the dummy.

CONCLUSION

For the testing of parachutes rubber dummies as well as test vehicles can be used as human analogues. Using the method of least square fit a relatively simple mathematical formula was found which describes the opening shock factor versus launch velocity curve. The 3 curves for man dummy and test vehicle differ only by a factor. Therefore values for the man can be easily calculated from experimental results gained with dummies or test vehicles.

REFERENCES

- Melzig, H.-D. Fallschirmtechnik und Bergungssysteme
 DLR-Mitt. 69-11, 1969

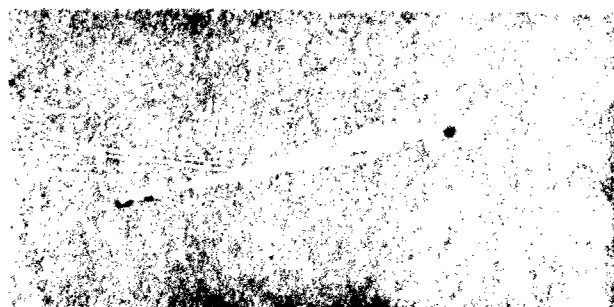
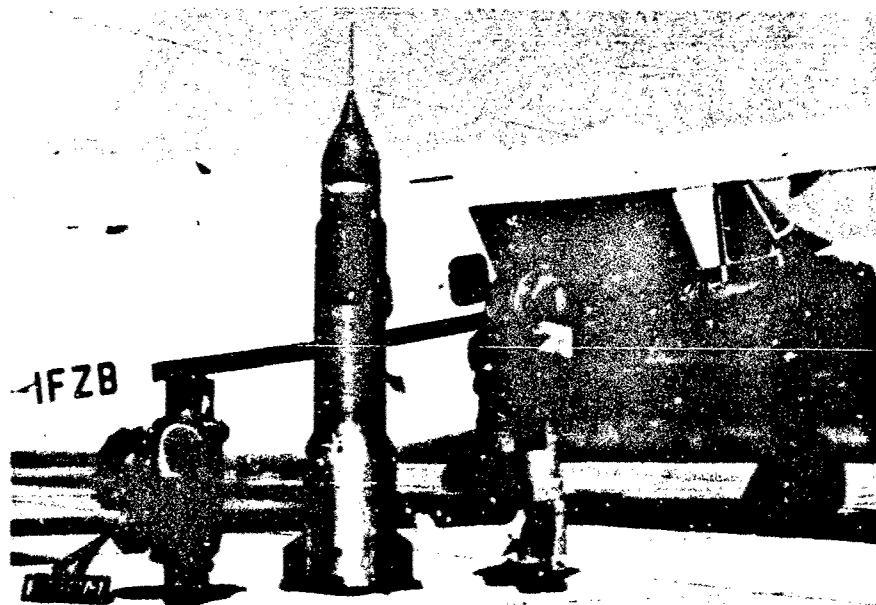


Fig. 2
Parachutes in stretch position for dummy,
test vehicle, man test configurations

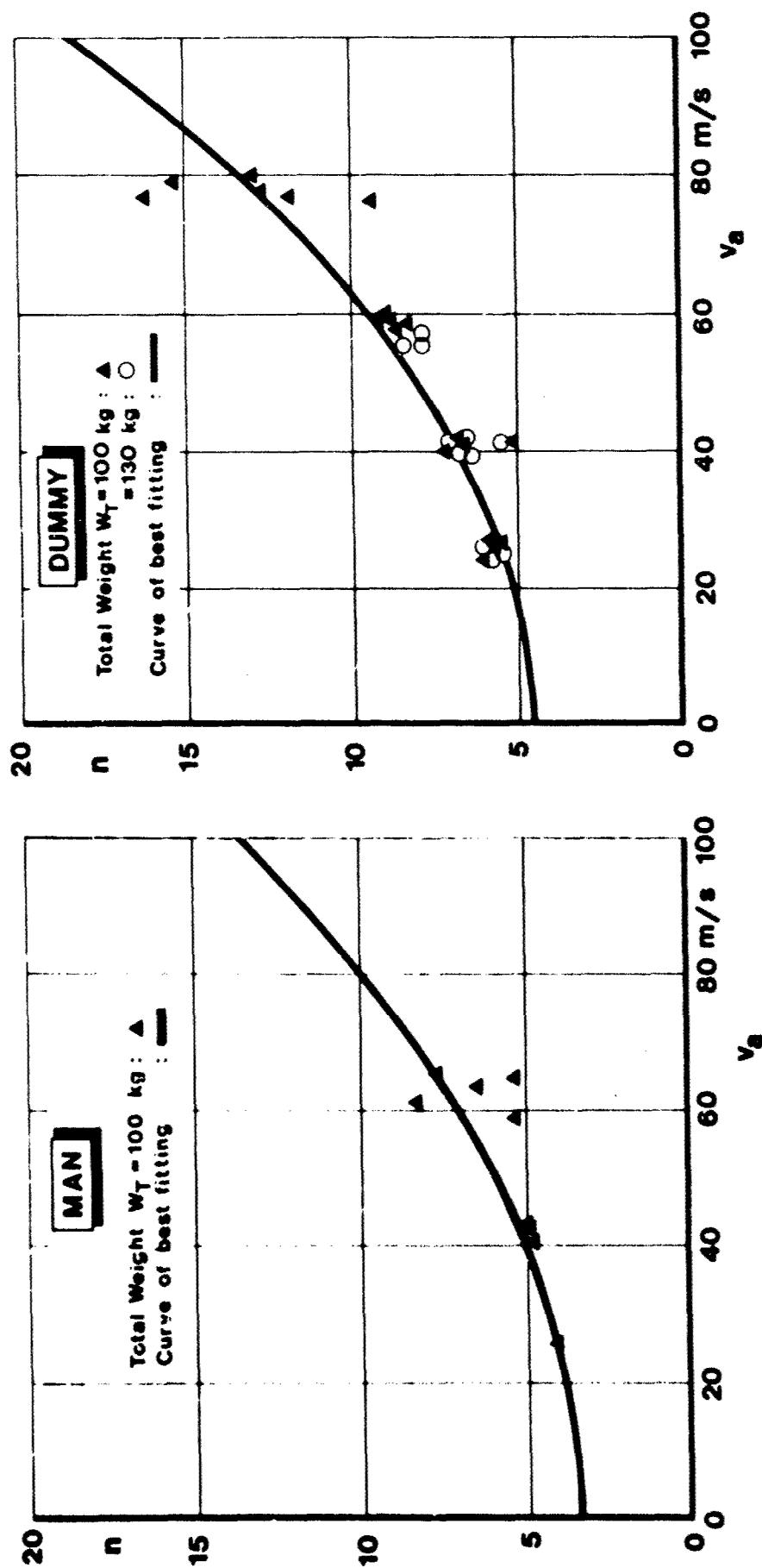


Fig. 3:

Filling factor n versus launch velocity v_a

Fig. 4:

Filling factor n versus launch velocity v_a

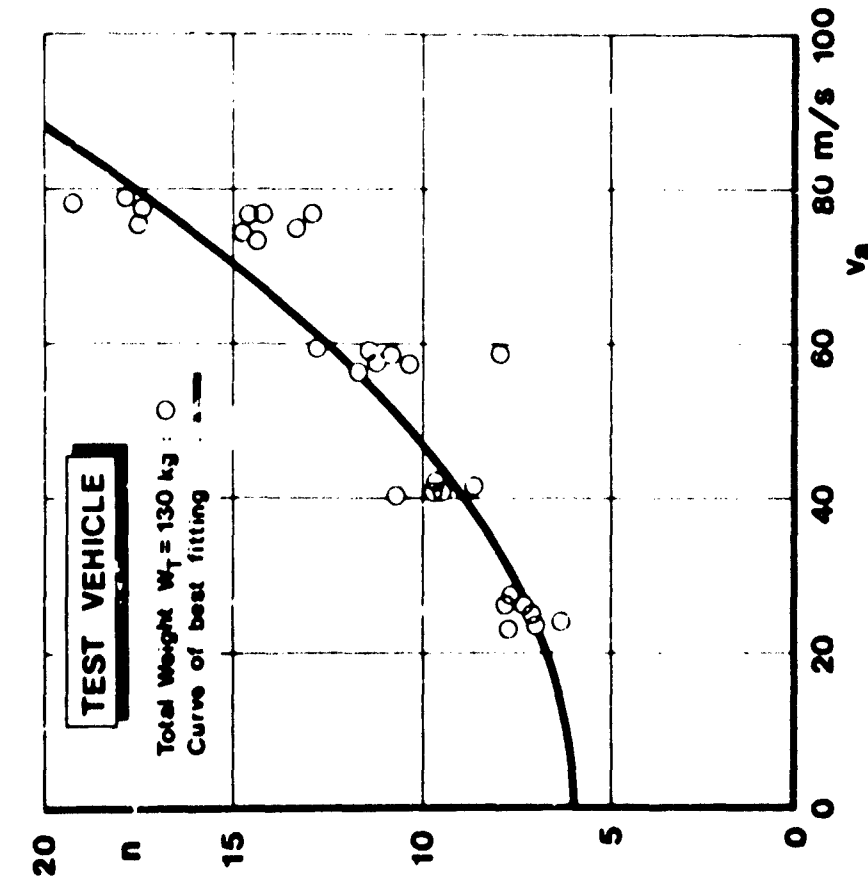


Fig. 5:

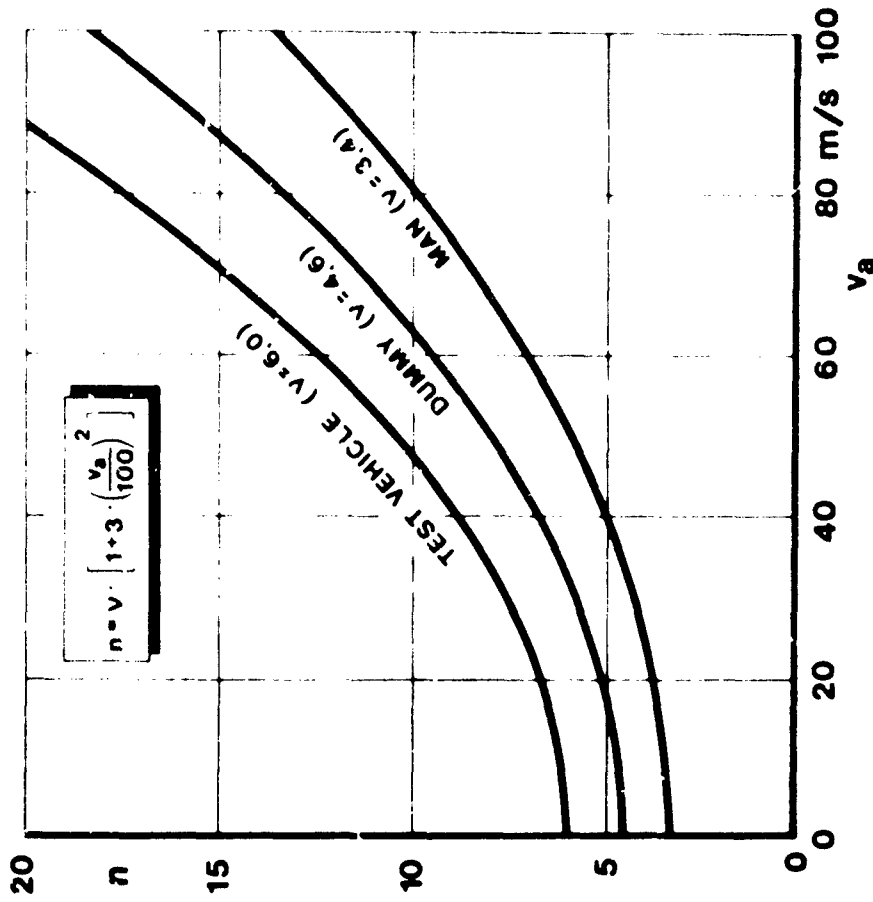
Filling factor n versus launch velocity v_a 

Fig. 6:

Filling factor n versus launch velocity v_a

DISCUSSION

DR. MEIER-DORNBERG (FRG)

Have you tried to explain this factor v by some kind of resiliency of the whole system? It may be an easy plain relation between resilience of the whole system, for instance, man or resilience in the parachute and, your correction number v I think.

AUTHOR'S REPLY

As I said, my explanation is that the main difference lies in the rigidity and elasticity differences between these three bodies. I think that this is the most important factor.

DR. MEIER-DORNBERG (FRG)

It should be possible to calculate the resiliency of the systems and get curves for n without measuring them.

DR. VON GIERKE (USA)

I think before you look to the resiliency of the bodies, the data should be adjusted for constant drag. We know and you have said yourself that the jumper adjusts to minimum drag.

AUTHOR'S REPLY

We tried to eliminate this by opening the parachute very early, 1.8 seconds after launch velocity. The launch velocity was the same for all three bodies. Then one has only the difference between the 3 bodies which develop during the 1.8 seconds and this difference can be neglected because it is small. We looked into these things, the different attitudes, and the difference in velocity. The important velocity would be the velocity at time of snatch when the lines are stretched and the parachute begins to inflate. This velocity is within a very narrow range if you open the parachute very early. It would be different if you would let them fall 10 seconds and you would have to take this into consideration. We made lots of measurements so we are really sure that we can neglect the velocity differences.

DR. VON GIERKE (USA)

Do you have windtunnel measurements of the drag of the three bodies?

AUTHOR'S REPLY

We have windtunnel measurements. But the problem is that if you drop the dummy it is hard to predict which attitude it takes and if the man jumps he normally does not do what you tell him to do. So you have some scattering due to these factors and windtunnel data don't bring you much farther. I really believe that the main difference we see - a 25% reduction for the dummy and another 25% reduction for the man - is caused by the rigidity differences and the moving masses of the man.

DR. VON GIERKE (USA)

I think this particular situation could be relatively easily simulated with the articulated total body model discussed by Mr. Kaleps where the friction of the restraint system over the body is incorporated into the model.

HENRY JEX (USA)

In work done some years ago with Dr. Theo Knacke at El Centro, California, similar results (with regard to maximum snatch-loads) were obtained; therefore, I agree with many of Mr. Melzig's conclusions. Analyses of snatch load dynamics have been made, and it turns out that the opening geometry versus time is dominated by the "apparent mass" terms of the air which accelerates the canopy, and which exceeds the canopy mass. Therefore, canopy weight and design details are not as important as the initial canopy geometry, which determines the subsequent filling dynamics. The filling process tends to be invariant with respect to spatial distance traveled, therefore, explaining the shorter duration of snatch-forces at higher speeds. However, the aerodynamic wake of the leading body, dummy or flailing human are often different and increase the filling times (and thereby reduce the peak loads). Could this be the reason for your different v factors?

AUTHOR'S REPLY

You are completely right. This difference in the wake is included in the parameter v . It is hard to tell how much this contributes, but I don't think it is much in the speed range we are in. If you go to higher speeds and if you go to higher masses, then this becomes more important.

TENTATIVE D'ESTIMATION DES LESIONS POUVANT SURVENIR AU COURS
D'UN CRASH D'HELICOPTERE GAZELLE SA 341 A PARTIR
D'UNE ETUDE SUR MANNEQUINS.

par

Le Médecin en Chef B. VETTES
Chef de la Section Accélération
et Poste de Travail du Personnel Navigant
du Laboratoire de Médecine Aéronautique
CENTRE D'ESSAIS EN VOL
91220 - BRETIGNY-AIR (FRANCE)

L'Ingénieur R. ECKERT
Chef de la Section Moyens d'Essais
du Laboratoire de Médecine Aéronautique
CENTRE D'ESSAIS EN VOL
91220 - BRETIGNY-AIR (FRANCE)

RESUME

Dans le cadre des études de crash d'hélicoptères, un essai avec impact réel est effectué avec pour but d'estimer les chances de survie des occupants, d'améliorer la résistance de la structure et de réaliser un modèle mathématique de structure anticrash.

L'hélicoptère Gazelle SA 341 est largué sur le sol avec des vitesses horizontales et verticales de même grandeur.

Outre les différents capteurs fixés sur la structure, trois mannequins anthropomorphiques installés dans l'appareil représentant le pilote, le copilote et un passager sont équipés d'accéléromètres placés dans la tête, le thorax, le bassin et une jauge de contrainte est disposée dans la région dorso-lombaire du pilote.

A l'issue du crash l'expertise des dommages structuraux est réalisée. Les accélérations subies par les occupants sont données sur des courbes intensité en fonction du temps.

D'une façon générale, les accélérations les plus importantes sont sur l'axe Z et se situent entre 25 et 30 g pour des durées de l'ordre de 20 ms avec un jolt moyen de 1000 g/s et une compression vertébrale de près de 400 daN.

Suivant l'axe X les accélérations sont moindres, elles ne dépassent pas 15 g.

Selon toute vraisemblance, les dommages corporels des occupants seraient localisés sur la colonne dorso-lombaire (fracture-tassement). Par manque de données, les lésions éventuellement infligées à la colonne cervicale basse ($C_5 - C_7$) par le "coup du lapin" ne sont pas parfaitement connues.

INTRODUCTION

Dans le cadre des études entreprises sur la vulnérabilité des hélicoptères, à la demande du Service Technique de l'Aéronautique, un crash d'hélicoptère Gazelle SA 341 est effectué par l'Aéronautique et le Centre d'Essais Aéronautique de TOULOUSE (C.E.A.T.) en collaboration avec le Centre d'Essais des LANDES (C.E.L.) et le Centre Aéroporté de TOULOUSE (C.A.P.). Cet essai a pour but d'estimer les possibilités de survie pour les occupants, d'étudier la résistance de la structure et de réaliser à plus ou moins longue échéance un modèle mathématique d'une structure d'hélicoptère résistante au crash. Le Laboratoire de Médecine Aéronautique du Centre d'Essais en Vol est chargé d'apprécier les chances de survie de l'équipage.

1. - Conditions de l'essai.

Les conditions retenues sont celles qui consistent à réaliser le crash rencontré le plus fréquemment, à savoir un impact symétrique sur un terrain plat et dégagé : sol en terre compactée avec un coefficient de frottement suffisant pour développer une accélération vers l'avant sans avoir de vitesses trop élevées et une distance d'arrêt trop grande. La vitesse d'impact choisie est de 8,49 m/s sous un angle de 45°, ce qui nécessite un vecteur vitesse horizontal V_x de 6 m/s et un vecteur vitesse vertical V_z de 6 m/s impliquant une hauteur de chute de 3,67 m. L'impact doit être symétrique, les patins orientés parallèlement au sol avec successivement une chute guidée, puis une chute libre représentant une autorotation manquée ou une perte soudaine de puissance. La cellule d'essai dont la masse est de 1 730 kg avec centrage neutre est retenue par trois câbles fixés au mât rotor et sur la traverse avant de l'atterrisseur, ce qui assure une chute à assiette constante. Un quatrième câble, fixé également sur la tête rotor permet de soulever l'appareil à la hauteur choisie (3,67 m). Au largage ce câble est détaché de l'appareil par un délateur pyrotechnique. Afin d'obtenir un impact en chute libre, les trois câbles de guidage sont également séparés de la cellule au moyen d'un dispositif pyrotechnique, à 10 cm du sol, sur l'ordre d'un capteur placé sous le patin droit.

2. - Moyens de mesure

Les chaînes de mesure comprenant différents types de capteurs (accéléromètres, jauges de contrainte, capteurs de déplacement et de pression) sont placés sur la structure et dans trois mannequins anthropomorphiques représentant l'équipage et un passager. Parmi les 36 accéléromètres dont la plupart sont du type piezo résistif, 9 sont situés sur le plancher, au niveau des ferrures avant et arrière des sièges pilote et copilote, 18 jauges métalliques classiques collées sur la structure permettent de mesurer les contraintes et les efforts exercés. 3 capteurs de déplacement de course ± 50 mm sont également placés sur l'appareil. Un capteur de pression à jauge est immergé dans le réservoir par une fixation sur le bouchon de fermeture. Sa gamme de mesure est comprise entre 0 et 100 bars.

Le mannequin pilote type Sierra 50 pourcentile est équipé d'accéléromètres triaxes XYZ fixés respectivement dans la tête, le thorax et le bassin (fig. 1-2-3). La mesure de la compression vertébrale est effectuée au niveau dorso-lombaire par 4 rondelles de force piezo électriques avec amplificateur de charge.

Le mannequin co-pilote type Alderson 50 pourcentile ne dispose que de deux tri-axes, l'un dans la tête, l'autre dans le thorax.

Le mannequin passager type Alderson 50 pourcentile est équipé seulement de 2 blocs d'accéléromètres biaxiaux XZ, l'un dans la tête, l'autre dans le bassin.

Dans la zone du crash sont implantées 7 caméras 16 mm, 4 latéralement sur le côté droit, 1 trois quart avant et 2 face avant. Leur vitesse varie entre 24 et 800 images par seconde. Il s'y ajoute une caméra supplémentaire de 35 mm, tournant à 40 images par seconde, placée latéralement. Une autre caméra 16 mm à grand angle, tournant à la vitesse de 40 images/seconde est fixée à l'intérieur du cockpit sur le tableau de bord. Elle est dirigée face aux mannequins pour visualiser leurs déplacements éventuels lors du crash (figure 4).

Les tensions d'alimentation des capteurs et des amplificateurs embarqués sont transmises par fil avec un double cheminement depuis les deux baies de mesure ; les mesures cheminent également par fil. L'enregistrement est fait en modulation de fréquence sur 7 enregistreurs magnétiques synchronisés par enregistrement d'un même créneau avant et après l'impact. Les prises de vue sont également synchronisées. La bande passante est de 0 à 2000 Hz pour tous les paramètres. Les mesures sont numérisées après essai, à une cadence de 8.800 échantillons par seconde. Elles sont ensuite filtrées grâce à un filtre de Fourier de bande passante 0-100 Hz. Pour les accéléromètres placés en Z, la vitesse est obtenue par intégration de l'accélération.

3. - Déroulement de l'essai

Cet essai a lieu à TOULOUSE le 24 février 1977 dans le grand hangar "Concorde" du C.E.A.T. Les mannequins revêtus d'une combinaison de vol type cabine étroite mais sans casque sont installés à bord sur leur siège respectif : le pilote en place avant droite sur un siège type UK, le copilote en place avant gauche sur un siège type ALAT, le passager en place arrière droite sur la banquette dont le dossier est constitué par la cloison de l'appareil. Ils sont alors saignés par un harnais à 4 points pour le pilote et le copilote et seulement à 3 points pour le passager (harnais type UK : ceinture et baudrier). Sur les bretelles d'épaule gauche et droite du pilote sont collées des jauges de contrainte. La porte droite de l'hélicoptère est enlevée de façon à pouvoir filmer correctement les déplacements des occupants (fig. 5).

L'impact s'effectue dans un nuage de poussière sur la terre compactée selon le plan indiqué. En effet, les mesures montrent que les vitesses obtenues à l'impact sont pour la vitesse horizontale V_x de $5,7 \pm 0,1$ m/s et pour la vitesse verticale V_z de $5,7 \pm 0,1$ m/s, soit une vitesse résultante de 8,1 m/s.

Sous le choc, la portière gauche s'ouvre et vient battre violemment contre la structure. A la simple impression visuelle, on distingue nettement une cassure du patin droit et un affaissement du plancher ainsi qu'un plissement de la partie moyenne de l'appareil. Le pilote et le copilote semblent s'enfoncer dans leur siège et leurs têtes être projetées vers l'avant, tandis que le crâne du passager paraît heurter le plafond.

4. - Résultats

L'expertise des dégâts montre une pénétration de la fixation turbine dans la "niche à chien" sur une hauteur de 90 mm, un plissement de la peute de queue, un flambage de la cloison - dossier derrière la banquette passagers et des cadres sous les sièges, un écrasement du fond de la structure de 80 mm et un affaissement des poutres de barque. La verrière est brisée dans son cadran inférieur droit. Les mannequins (pilote et copilote) sont restés assis sur leur siège et aucune partie de leurs corps n'est venue heurter le tableau de bord ou la verrière (fig. 6).

A partir du dépouillement des films des caméras rapides et des mesures d'accélération la chronologie de l'essai peut être établie :

t = 0 : largage
 t = 1,040 s : premier contact de l'atterrisseur avec le sol
 t = 1,060 s : rapture de l'atterrisseur
 t = 1,120 s : écrasement de la structure inférieure
 t = 1,144 s : flambage de la cloison arrière de la cabine
 t = 1,170 à 1,230 s : fin des accélérations
 t = 1,310 s : la vitesse verticale s'annule après rebond.

Les résultats des mesures effectuées sur la cellule sont donnés pour les accélérations, pour les mesures de contrainte et d'effort et pour les mesures de déplacement et de pression sur des courbes intensité en fonction du temps.

De même les accélérations subies par l'équipage et le passager sont représentées sur des courbes intensité en fonction du temps axe par axe (seules les plus significatives sont reproduites ici - planches - 7-8).

Pour l'accéléromètre Y placé dans la tête du pilote, les résultats sont inexploitable.

Chaque courbe est découpée de 2,5 en 2,5 g. Chaque tronçon représente un plateau élémentaire d'accélération en fonction du temps ; ce qui permet de tracer une courbe des plateaux d'accélération en fonction du temps. A partir de cette courbe nous relevons les valeurs pendant le temps 0 - 5 - 10 - 20 - 30 et 40 ms. Les points sont alors placés sur le diagramme de tolérance aux accélérations de brève durée : Gz et Gx établi par WEEB en 1964. Cette opération est répétée pour chaque mannequin. (planches 9-10-11 et 12)

Pour le pilote sur l'axe Z la pointe d'accélération maxima se situe au niveau du thorax (+ 32 g). Elle est encore de 25 g pour une durée de 20 ms. Les points relevés se trouvent dans la zone dite de blessures légères bien au-delà de la limite caractéristique du siège éjectable (planche 9). La tête subit également des accélérations importantes 24,5 g pendant 10 ms et 20 g pendant 20 ms.

La compression vertébrale mesurée au niveau de la colonne dorso-lombaire est de l'ordre de 400 daN.

50 ms après, cette pointe d'accélération est suivie d'une pointe inverse d'une intensité 3 fois moindre. Dans ce cas les niveaux d'accélération, aussi bien pour le thorax que pour la tête, correspondent sur le diagramme à une zone bien en deça de celle de l'exposition volontaire étudiée par STAPP.

Si l'on considère que l'accélération relevée au niveau du siège ne dépasse pas en moyenne 25 g, on constate qu'il y a simple transmission au niveau du bassin, amplification au niveau du thorax et amortissement au niveau de la tête où l'accélération est cependant supérieure à l'excitation initiale.

Sur l'axe X les accélérations rencontrées sont de faible intensité, elles sont toujours inférieures à 10 g ; de même les mesures d'effort effectuées sur les bretelles du harnais sont faibles 70 et 45 daN. Sur le diagramme ces valeurs prennent place dans une zone bien au-dessous de celle de l'exposition volontaire n'entraînant aucun trouble.

Sur l'axe Y au niveau du bassin l'accélération atteint 12 g.

Pour le copilote sur l'axe Z au thorax, la pointe atteint 26 g, les différents plateaux sont de 24 g pendant 5 ms, de 19 g pendant 10 ms, de 15,5 g pendant 20 ms, ce qui correspond au domaine du siège éjectable. (planche 10)

Au niveau de la tête cette accélération est très amplifiée, pointe à 37,5 g et reste encore à 27,5 g pendant 10 ms. Dans ce cas on se trouve en plein dans la zone des blessures légères près de la frontière toute théorique de la zone des blessures graves.

Comme pour le pilote elle s'inverse mais de façon plus précoce. Elle atteint 12,5 g pendant 20 ms : zone d'exposition volontaire.

Ici également sur l'axe X, les accélérations sont de faible intensité, 12,5 g pendant 5 ms au niveau du thorax avec succession extrêmement rapide d'oscillations de l'ordre de 10 g. Au niveau de la tête, elles sont du même ordre et apparaissent plus tard. (planche 11)

Sur l'axe Y seules les accélérations sont ressenties au niveau de la tête, 9,5 g pendant 5 ms.

Pour le passager sur l'axe Z au niveau du bassin l'accélération est de 24,5 g pendant 10 ms, ce plateau est amorti au niveau de la tête, 18,5 g pendant 10 ms. Ces valeurs ne font guère soupçonner ce qu'indiquent les séquences filmées : choc du crâne contre le plafond. (planche 12)

Sur l'axe X les valeurs sont les plus importantes, pointe de 16 g, puis 12,5 g pendant 10 ms et retour au 0, inversion avec une pointe à 16 g et un plateau de 5 ms à 12,5 g. Ce phénomène n'apparaissant que 110 ms après.

Lorsque l'on mesure les pentes de montée de ces différentes accélérations (jolt) on constate qu'elles sont toutes très importantes, supérieures très souvent à 1000 g/s et peuvent atteindre 1300 g/s. De telles valeurs ne sont pas tolérables suivant le diagramme rapporté par ELBAND en 1959.

DISCUSSION

Si nous considérons les résultats ainsi obtenus nous pouvons dire que les mannequins ont subi des taux d'accélérations Gz, certes élevés, mais de durées très brèves qui ne devraient pas entraîner des lésions graves, puisque par rapport au diagramme de WEEB, ils se situeraient au pire dans la zone des blessures légères et relèveraient le plus souvent du domaine du siège éjectable. (planches 9 et 10)

Cependant il ne s'agit là que d'approximation théorique et il est bien difficile de tracer une frontière nette entre zone de blessures légères et zones de blessures graves. En outre, l'expérience que nous avons des éjections, tant en France qu'à l'Etranger, montre que même pour des accélérations moins importantes, il n'est pas rare d'obtenir des fractures plus ou moins graves et plus ou moins complexes du rachis dorso-lombaire (AUFFRET et DELAHAYE - 1975).

Ce type de dépouillement ne tient pas compte du jolt, or le dernier est un facteur déterminant pour apprécier la tolérance humaine lors d'un impact.

De plus le découpage adopté permet une schématisation pour chaque élément corporel : tête, thorax, bassin, mais n'est pas représentatif du corps humain entier. Ce dernier ne peut être considéré comme une masse rigide mais comme un ensemble de masses élémentaires réunies entre elles par des ressorts et des amortisseurs (DIECKMANN 1957, COERMANN 1962) donnant lieu soit à des phénomènes de résonance, soit à des phénomènes d'amortissement.

C'est pour cette raison que pour analyser la réponse élastique du corps du mannequin (tête, thorax, bassin) nous avons représenté pour un axe toutes les accélérations sur un même graphique en les superposant (planches 13- 14 et 15)

En premier lieu, on constate que les phénomènes ont la même allure mais apparaissent avec un déphasage plus ou moins important. Afin de faciliter l'interprétation de ces courbes, les impulsions sont découpées en tronçons élémentaires de manière à constituer des impulsions trapézoïdales, caractérisées par une montée en accélération, suivie d'un plateau d'accélération constante, puis d'une descente (partie basse du graphique).

La planche n° 13 prise comme exemple, et concernant le pilote et l'axe Z, nous amène à faire un certain nombre de remarques.

Les accélérations antérieures au temps 1,100 qui sont dues à l'écrasement de l'atterrisseur, ne seront pas étudiées.

Le phénomène se présente alors comme une sinusoïde amortie d'une période de 130 ms, soit une fréquence d'excitation voisine de 8 Hz. Le mouvement infligé au bassin est amplifié au niveau du thorax, ce qui tendrait à démontrer que l'excitation se produit à une fréquence voisine de la fréquence propre de la masse suspendue, constituée par le thorax, qui provoque une amplification de 1,5 environ (le terme thorax doit être envisagé dans son sens le plus large : partie supérieure du corps). Comme l'a montré LATHAM, (1957) à 8 Hz on observe une amplitude maximale de la région thoracique supérieure par rapport aux hanches. Il semble que l'élasticité vertébrale soit intervenue de façon notable dans la transmission du mouvement. En effet, les mesures d'efforts pratiquées sur la colonne dorso-lombaire basse (400 daN) confirment la dure épreuve subie par cette dernière. On peut craindre des lésions vertébrales basses : fracture par compression (JONES et coll. 1964).

L'analyse de l'impulsion élémentaire fait également apparaître une mise en accélération très courte, soit un jolt de 1000 g/s au niveau du bassin, retransmis au thorax où il est amplifié 1200 g/s et ramené à 900 g/s au niveau de la tête.

Le plateau de stabilisation de l'accélération d'une durée initiale de 30 ms (bassin) diminue de moitié au thorax et à la tête.

Nous avons sollicité les prédispositions vibratoires de la partie supérieure du corps et la résonance des organes de ces régions a pu être atteinte. Comme le signale WEISS et coll. (1963) au cours d'un tel impact, le foie se déplace vers le bas, ce déplacement peut aller jusqu'à 4,5 cm. Le mouvement se fait de façon synchrone avec le cœur et les poumons. Même dans un tel cas, il convient de tenir compte du rôle bénéfique apporté par l'action du tonus et de la contraction des muscles avoisinants. Cette tension musculaire augmente la tolérance comme l'ont souligné COERMANN et coll. 1962 ; EDWARDS et LANGE 1964 ; VON GIERKE 1960.

Dans notre cas, un calcul approximatif montrerait que les déplacements relatifs bassin-thorax sont de l'ordre de 4 cm : compression verticale et flexion en avant. Ainsi se trouvent réunies les conditions idéales de fracture du rachis dorso-lombaire : compression et hyperflexion (AUFFRET et DELAHAYE 1975, KING et coll. 1975). Cette capacité de fracture peut être réduite de façon importante par l'hyperextension modérée de la colonne vertébrale (EWING et coll. 1972). Cette condition est réalisée par le sangleage correct du pilote sur son siège éjectable.

Cependant, comme le montre le graphique, il existe un coefficient d'amortissement non négligeable puisque la demi-sinusoïde suivante atteint des accélérations d'une intensité 4 fois moindre (7,5 g pour 30 g).

Les mêmes constatations peuvent être faites pour le copilote, avec une constance aggravante : une accélération d'intensité plus grande au niveau de la tête. Il est vraisemblable que l'énergie absorbée par la rupture du patin droit soit plus importante que celle absorbée par le patin gauche non rompu, ceci explique que le copilote installé en place gauche reçoive une énergie plus grande qui se transmet au niveau de la tête (35 g). Toutefois, la conception du modèle anthropomorphique est différente et les comparaisons sont donc difficiles. (plans 14)

Une analyse comparable des accélérations sur l'axe X montre que les intensités sont faibles, elles ne dépassent pas au thorax 10 g. C'est bien ce que confirme les mesures d'effort réalisées sur les bretelles de contention du harnais du torse du pilote. Ces valeurs (70 daN au maximum) sont parfaitement tolérables et ne risquent pas de provoquer de traumatismes même légers ou de contusions au niveau du thorax et des épaules. Elles sont très loin des normes normalement admises. (RUFF 1950, STAPP 1951-1955..).

Par contre, au niveau de la tête, si les accélérations sont du même ordre (parfois très légèrement supérieures), le changement rapide de sens entraînant dans un premier temps une hyperflexion de la colonne cervicale basse, suivie d'une extension brutale "coup du lapin" risque de provoquer des lésions hautes graves, sinon mortelles (PATRICK et coll. 1965). Les mouvements se trouvent facilités par le fait que le dossier du siège ne monte pas assez haut et ne comprend pas un appui-tête. (planche 15).

Bien qu'aucun mouvement latéral ne caractérise la trajectoire de la cellule de l'hélicoptère, une accélération d'environ 12 g sur le bassin du pilote est répercutée au thorax avec un léger amortissement (10 g). Elle semble due à l'écrasement dissymétrique des patins lors de l'impact. Une observation faite a posteriori sur les films et les photographies montre en effet que le patin gauche s'est moins affaissé que le patin droit qui est complètement détruit. D'ailleurs, les accélérations subies par le copilote sur l'axe Z sont plus élevées. De même les efforts mesurés sur les bretelles de contention du harnais du pilote accusent cette dissymétrie (70 et 45 daN).

Il est fort regrettable que le mannequin passager ne dispose pas d'accéléromètre dans le sens Y alors que les séquences filmées révèlent un mouvement latéral important, conséquence d'une contention peu efficace et des dégâts de la cloison arrière. Ces accélérations sont dans l'ensemble assez mal supportées et entraînent des troubles cardiaques (ZABOROWSKI 1966).

Comme on peut s'y attendre, ce type de crash, étant donné le faible déplacement qui amorti le mouvement, est plus sévère sur l'axe Z que sur l'axe X.

Cependant, si dans cette direction les accélérations sont toujours peu intenses, elles provoquent des mouvements forcés alternés de la tête, préjudiciables à la colonne cervicale basse. Une étude plus complète mettant en jeu la mesure des accélérations angulaires aurait peut être permis une meilleure objectivation du phénomène.

Les résultats ainsi mentionnés et analysés permettent de tirer des conclusions concernant la survie des occupants. Cependant, des réserves importantes doivent être apportées. Les mannequins anthropomorphiques, modèles conventionnels ne sont qu'une grossière approximation du corps humain où le facteur musculaire est totalement absent.

Quoi qu'il en soit, s'il n'est pas possible d'affirmer que le pilote et le copilote n'auraient pas survécus à ce type d'accident, on peut penser qu'ils auraient été vraisemblablement victimes de fractures plus ou moins graves du rachis dorso-lombaire aggravées par des mouvements intempestifs au niveau de la colonne cervicale basse "coup du lapin". Les accélérations d'intensité élevée obtenues avec un jolt très important au niveau de la tête du copilote nous paraissent un facteur de gravité supplémentaire (choc, hypertension intracrânienne).

Compte-tenu des enregistrements incomplets effectués sur le mannequin passager, il est bien difficile de se prononcer sur son sort, cependant le pronostic doit à notre avis, être très réservé.

CONCLUSION

Dans le cadre du programme anticrash élaboré par la France, un essai de crash de l'hélicoptère Gazelle SA 341 est réalisé à TOULOUSE le 24 février 1977 par la Société AéroSpatiale et le Centre d'Essai Aéronautique de TOULOUSE. Les conditions de l'essai impliquent une hauteur de chute de 3,67 m avec une vitesse verticale de 6 m/s et une vitesse horizontale de 6 m/s, soit une vitesse résultante de 8,49 m/s.

Le Laboratoire de Médecine Aérospatiale du Centre d'Essais en Vol de BRETAGNE sur Orge est plus spécialement chargé d'apprécier les chances de survie de l'équipage et d'un passager.

A cet effet, 3 mannequins sont installés dans la cabine de l'hélicoptère, munis d'accéléromètres dans les sens X Y Z pour l'équipage et X Z pour le passager.

Le crash s'effectue selon le plan indiqué.

Les accélérations les plus importantes se situent sur l'axe Z et sollicitent la résonance de la partie supérieure du corps. La compression vertébrale avec la flexion en avant qui en découle provoque vraisemblablement des fractures de la région dorso-lombaire basse des occupants. Ces lésions sont aggravées par les mouvements forcés de la tête dus aux accélérations Gx.

L'exploitation de cette première expérimentation, malgré des résultats encore insuffisants permet déjà l'élaboration d'un programme de calcul anti-crash, tenant compte uniquement pour l'instant de facteurs physiques, mais dans lequel pourront être ajoutés dans l'avenir les facteurs humains. A cet effet, vient d'être réalisé cette année le crash d'un hélicoptère plus gros (PUMA SA 340), comprenant un équipage de trois hommes et huit passagers (hommes de troupe) placés dans la carlingue, soit face à l'avant, soit latéralement et assis sur des sièges dits "anti-crash". Les résultats ne sont pas encore connus à ce jour.

BIBLIOGRAPHIE

Les passages techniques de cet exposé sont extraits de la note technique n° 29/N/77 de la Société Aéronautique et du rapport du Centre d'Essai Aéronautique de TOULOUSE du 17 avril 1978.

AUFFRET, R. et DELAHAYE R.P.
Lésions vertébrales après éjection.
Rapport consultatif AGARD N° 12 (1975).

COERMANN, R.R. et al.
The mechanical impedance of the human body in sitting and standing position at low frequencies.
Human Factors - 1962 - 4 - 227-253.

DIECKMANN, D.
Einfluss vertikaler mechanischer Schwingungen auf den Menschen International Z angew Physiol. einschl.
Arbeitsphysiol. 1957, 16 - 519-564.

EDWARDS, R.G. and LANGE, K.O.
A Mechanical Impedance Investigation of Human Response to Vibration.
AFSC TR AMRL-TR 64-91 WPAFB Ohio oct. 1964.

EIBAND, A.M.
Human tolerance to rapidly applied accelerations ; a summary of the literature NASA Memorandum 5-19-59E (National Aeronautics and Space Administration Washington D.C. June 1959.

EWING, C.L., KING, A.I. and PRASAD, P.
Structural consideration of the human vertebral column under + Gz impact acceleration.
J. Aircraft, 1972, 9 (1) 84-90.

JONES, W.L., MADDEN, W.F. and EUEDEMAN, G.W.
Ejection seat accelerations and injuries.
Aerospace Med. 1964, 41 (3), 294-300.

KING, A.I., PRASAD, D., and EWING, C.L.
Mechanism of Spinal Injury due to caudocephalad acceleration.
Orthopedic clinics of North America, 1975, 6 (1), 19-31.

LATHAM, F.
A study in body ballistics seat ejection.
Proc. Roy. Soc. 1957, (B), 147, 121-139.
(*)

RUFF, S.
Brief acceleration less than one second.
German Aviation Medicine - World War II 1950, 1, 122 and 139, Department of the Air Force, Washington D.C.

SNYDER, R.G.
State-of-the-Art-Human Impact Tolerance.
Society of Automotive Engineers, New-York.
SAE Paper n° 700398, revised August 1970, reprinted May 1970 from 1970 International Automobile Safety Conference Compendium.
Publication SAE p. 30, reprinted octobre 1972.

STAPP, J.P.
Human exposures to linear deceleration - Part; II, The forward-facing position and the development of a crash harness. December (1951) (a).

STAPP, J.P.
Human exposure to linear decelerative force in the backward facing seated positions
Military Surgeon 1951, (b) 109, 106-108.

STAPP, J.P.

Tolerance to "abrupt deceleration."

Collected Papers on Aviation Medicine, AGARD

Butterworths Scientific Publications London 1955, 122-139.

VON GIERKE, H.E.

Response of the body to mechanical forces.

Tech. Rpt ARML WPAFB oct. 1966, 66-251.

WEBB, P.

Impact and vibration in WEBB, P. (Ed.).

Bioastronautics data book NASA, SP 3006, 1964, et NASA SP 3006, 1973.

WEISS, E.B., Jr. CLARKE, N.P., and BRINKLEY, J.W.

Human response to several impact acceleration orientations and patterns.

Aerospace Med; 1963, 24, 1122.

ZABOROWSKI, A.V.

Human Tolerance to lateral impact with Lap Belt only Eight Stapp car crash and Field Demonstration Conference.

Wayne State University, Detroit Michigan 1966.

(*)PATRICK, L.M. ; LISSNER, H.R; and GURDJIAN, E.S.

Survival by Design - Head Protection, 7th STAPP car crash Conference.

Springfield, III. Charles C. THOMAS, 1965.

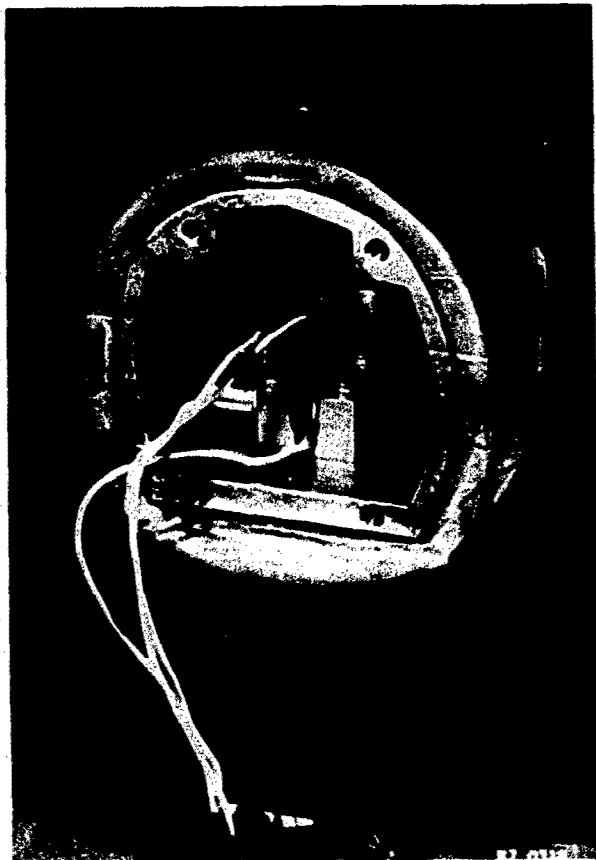


Fig. 1 - Placement des accéléromètres dans la tête.

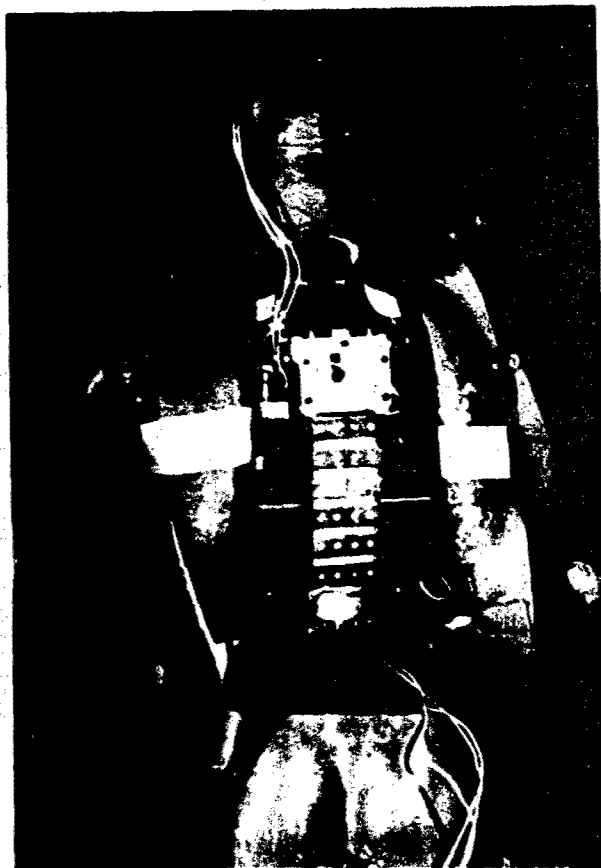


Fig. 2 - Placement des accéléromètres dans le tronc supérieur.
- le capteur de forces est situé au niveau dorso-lombaire bas.

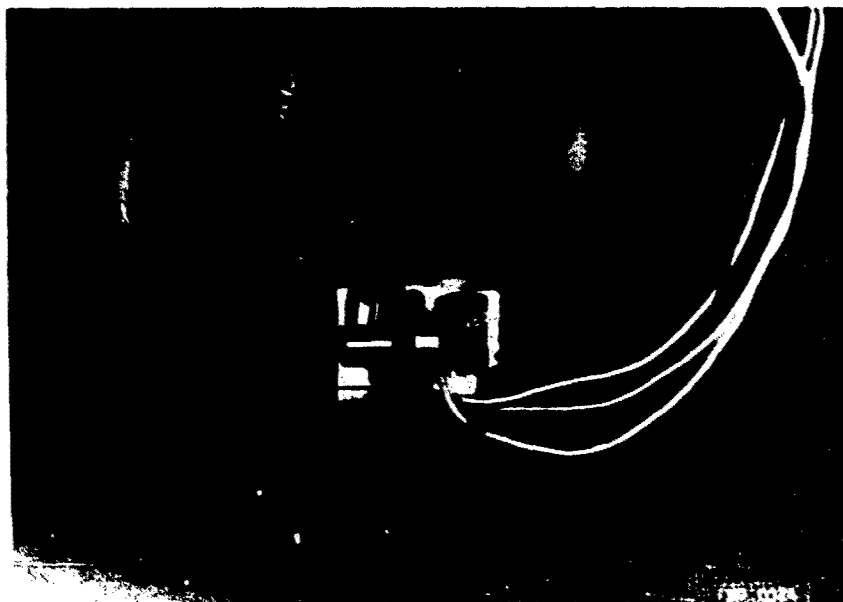


Fig. 3 - Placement des accéléromètres dans le bassin.



Fig. 4 - Place du co-pilote , et devant on voit la caméra embarquée.

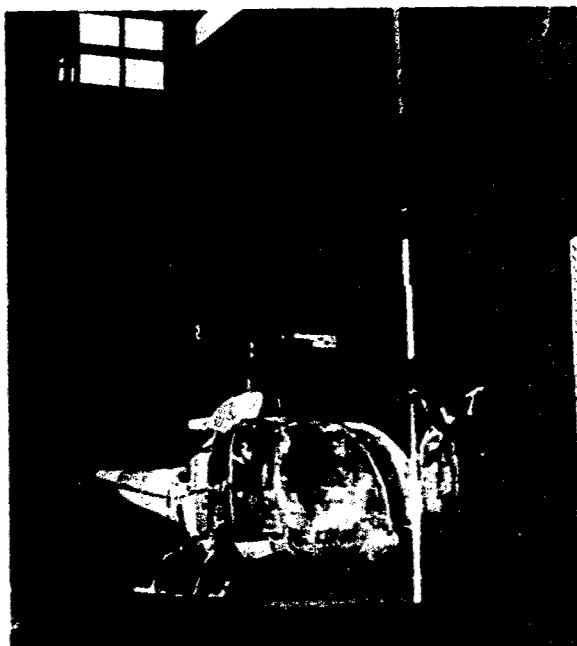


Fig. 5. Vue générale de l'installation avant le crash. Par la porte entr'ouverte on distingue nettement le passager.

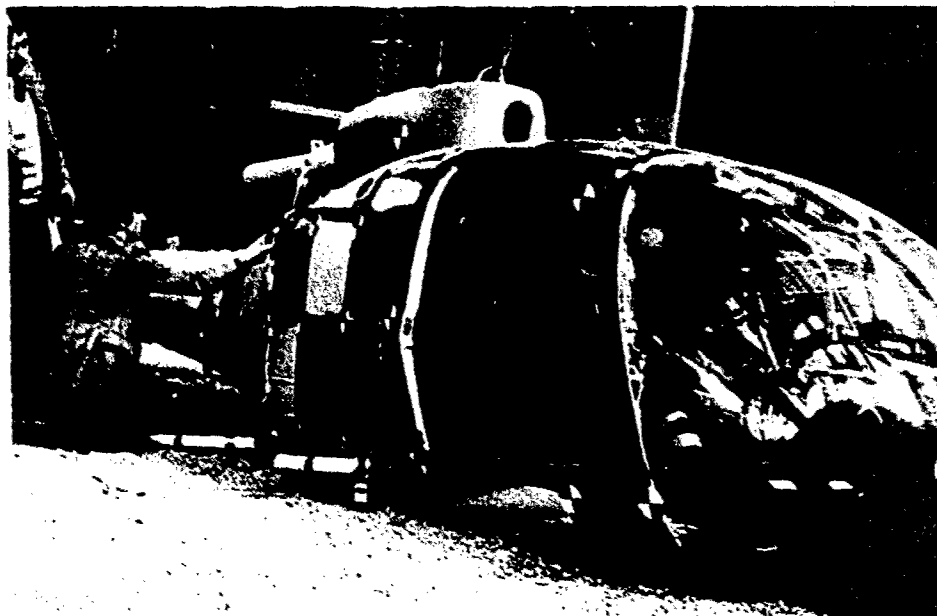


Fig. 6 - Vue générale de l'hélicoptère après l'impact.

PLANCHE 7

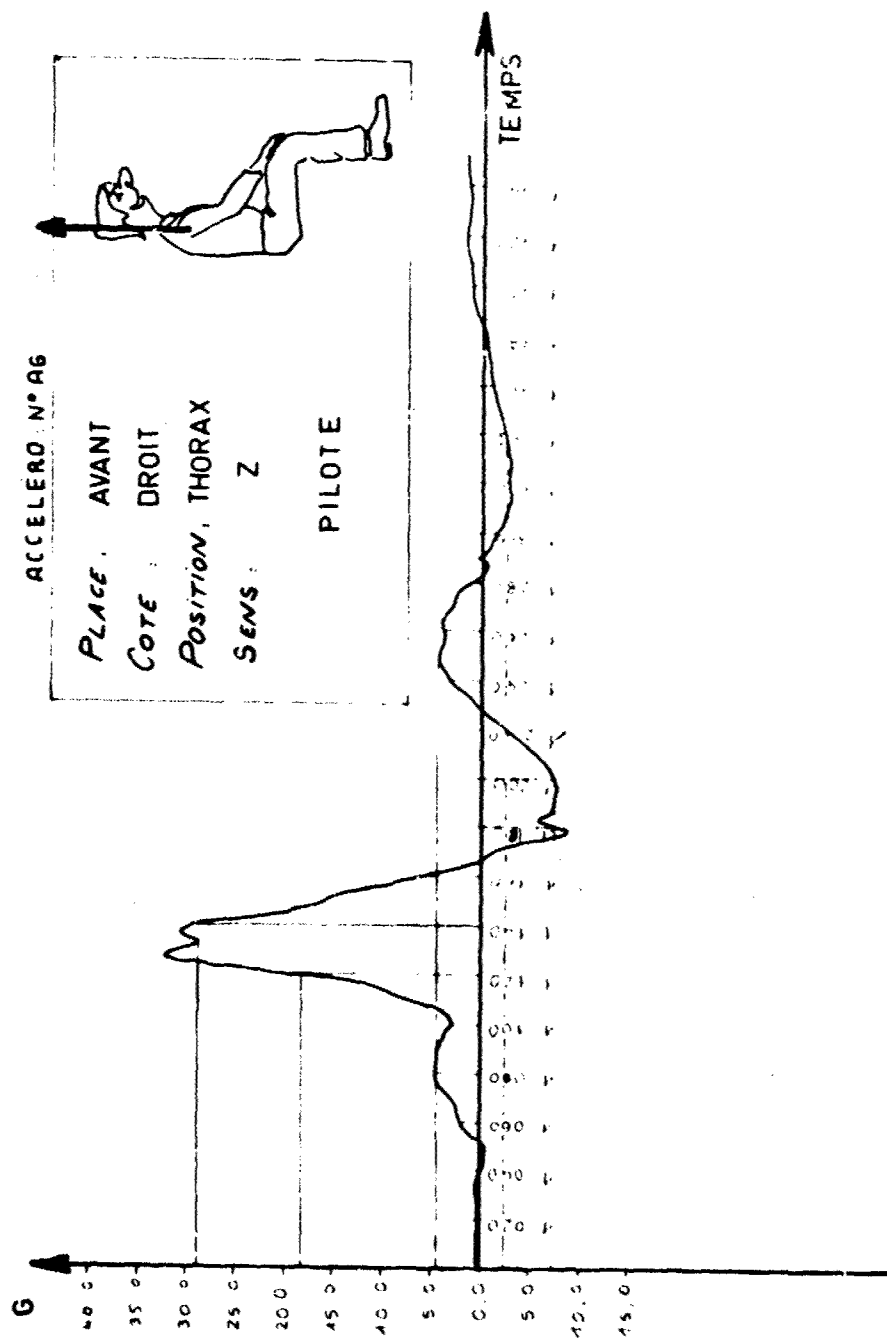
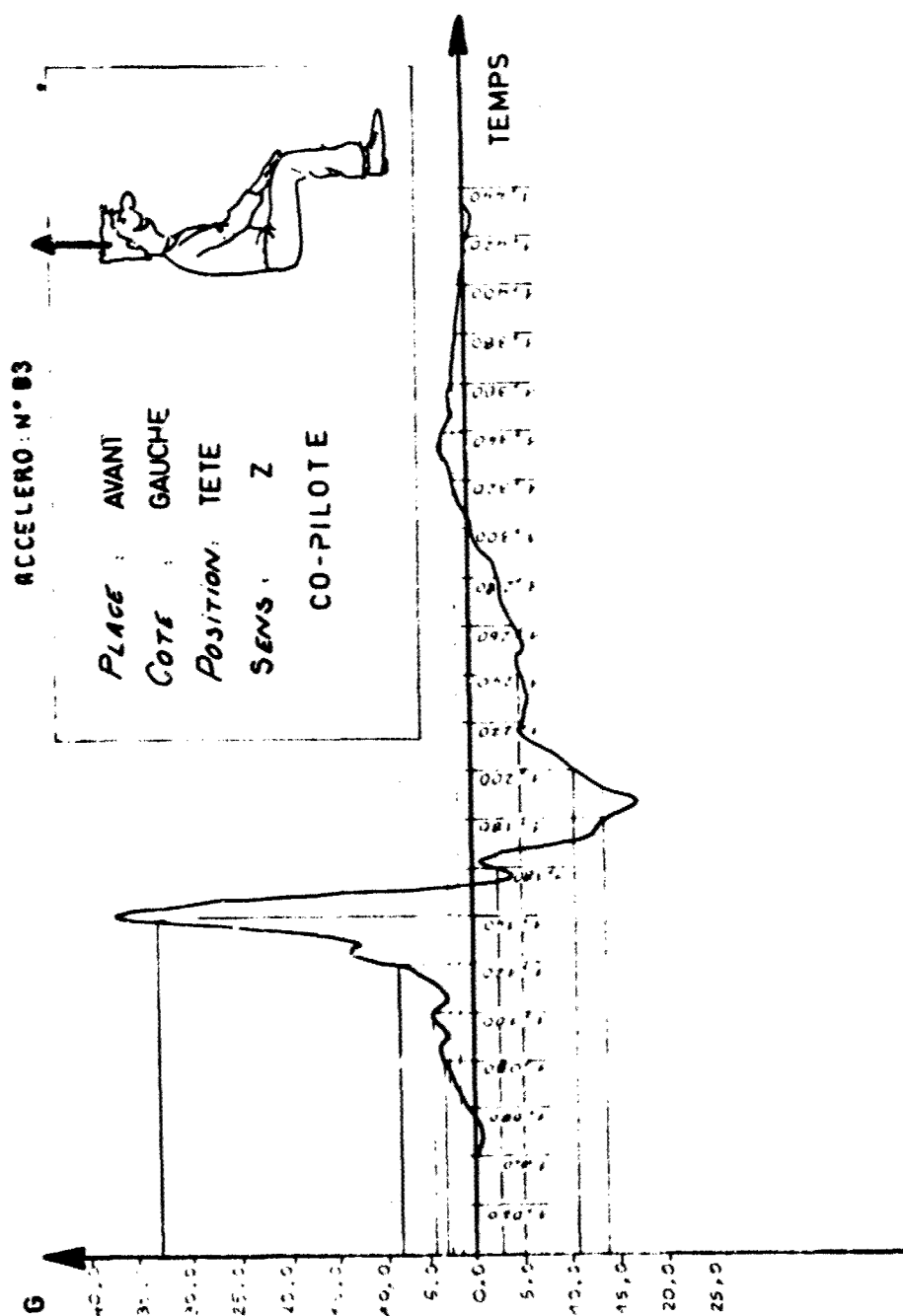


PLANCHE 8



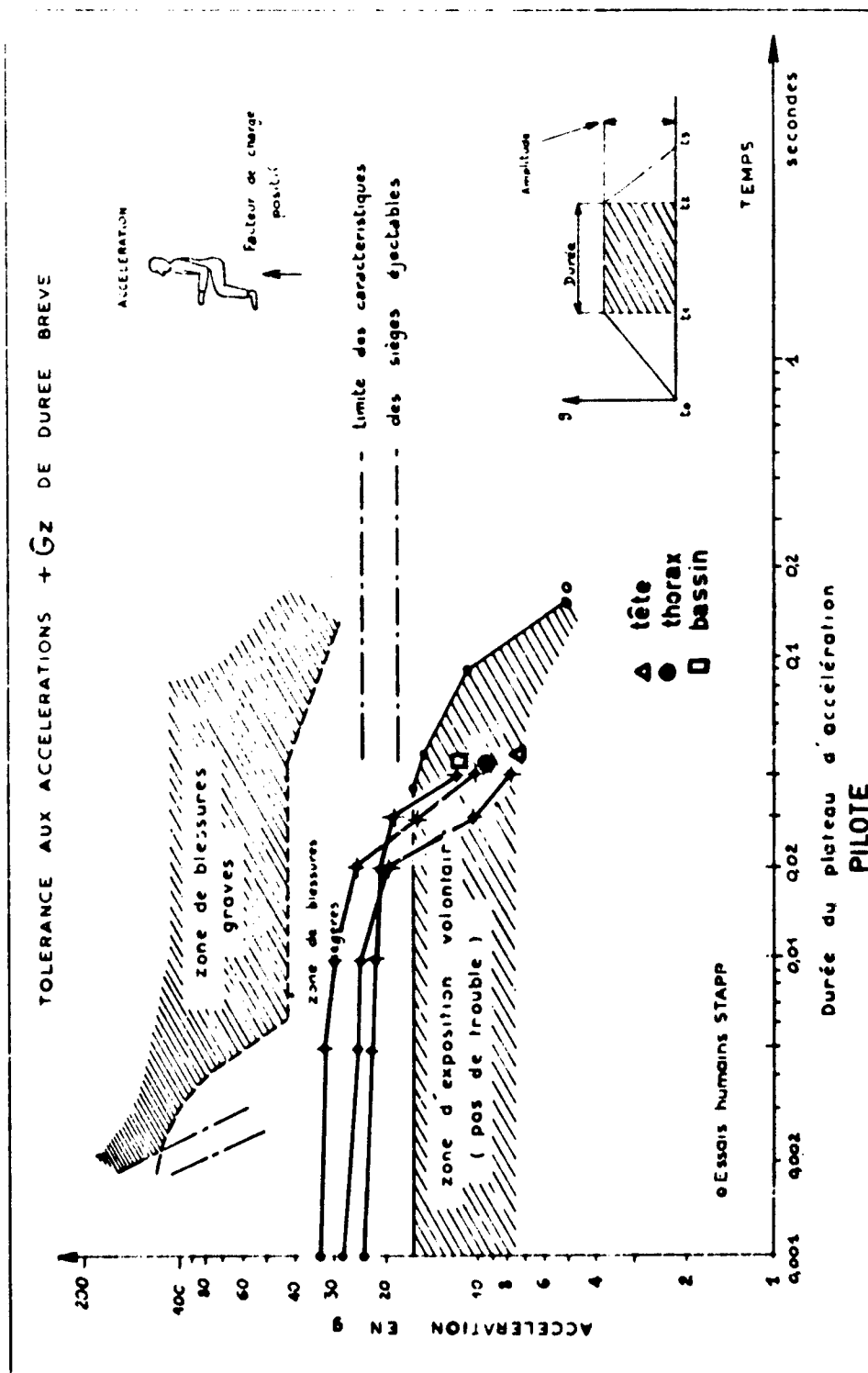
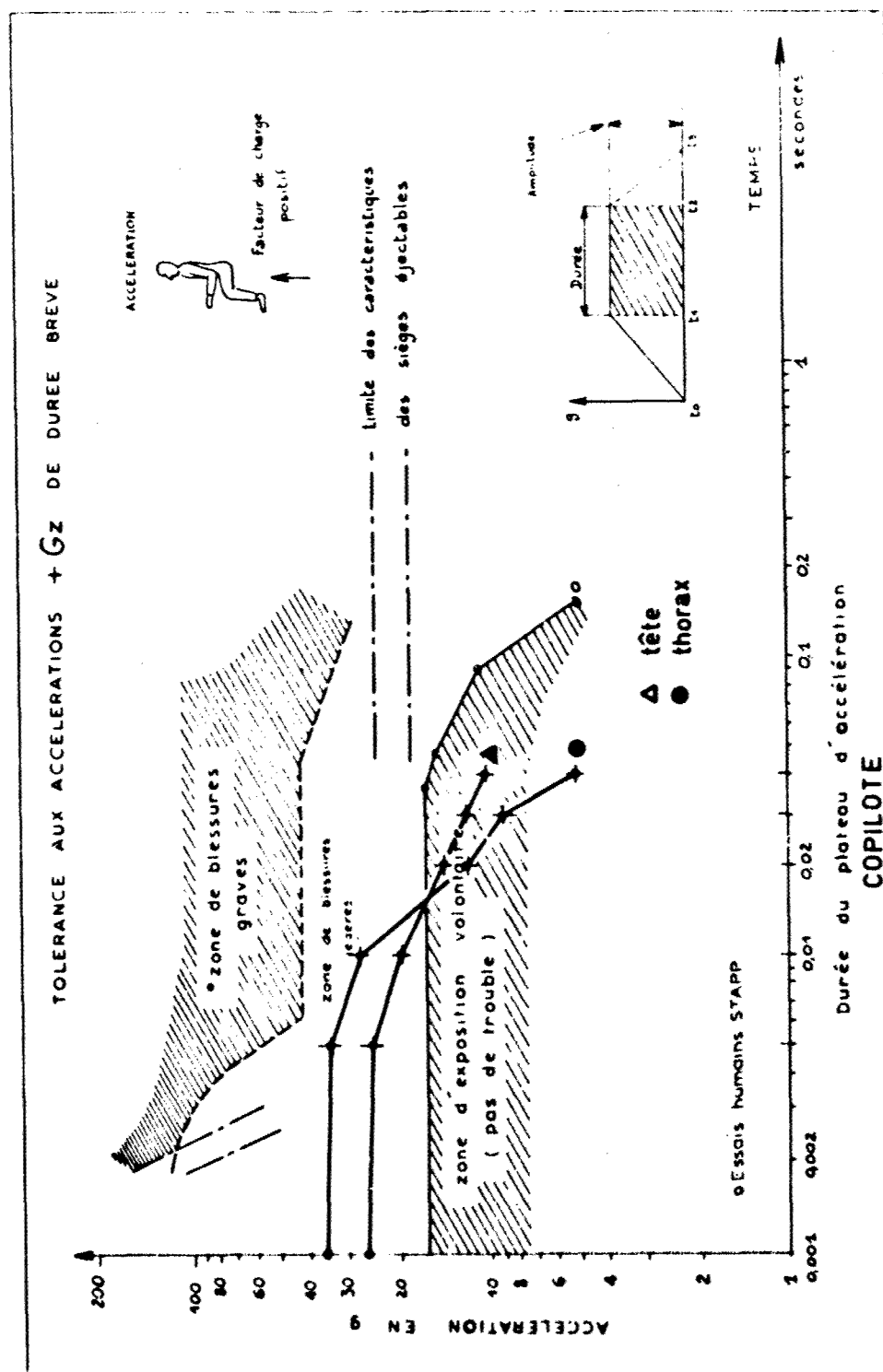
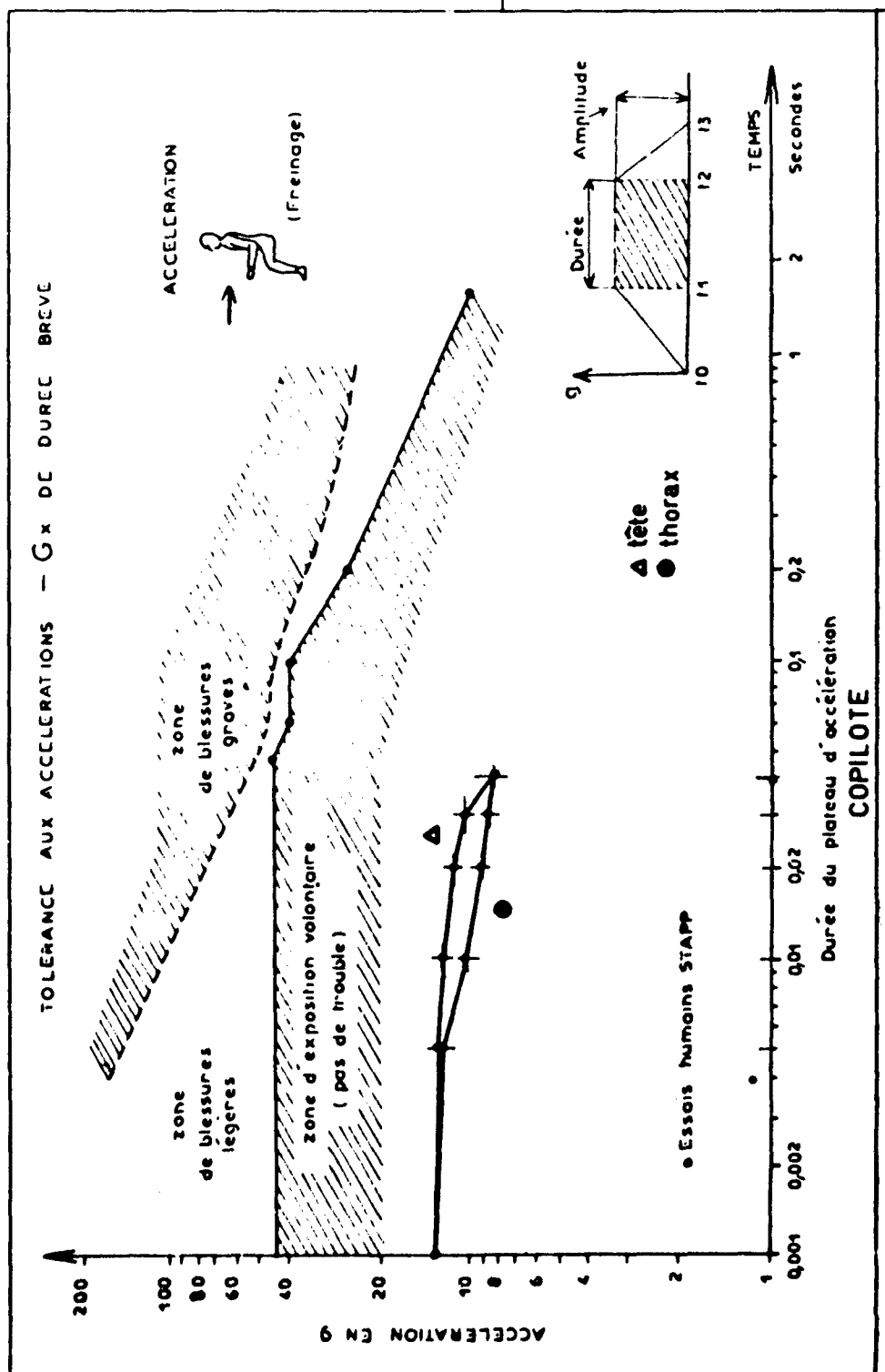
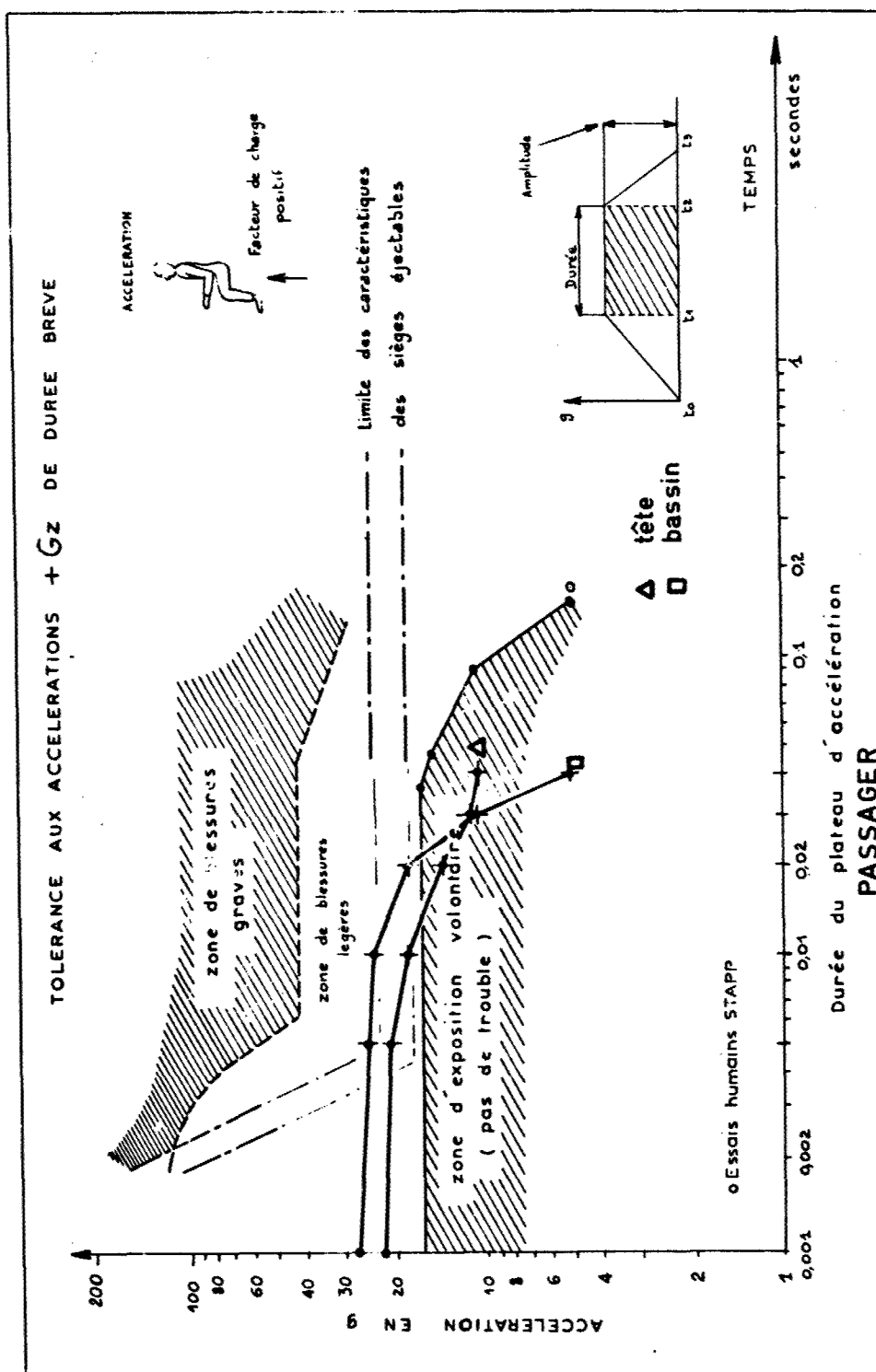
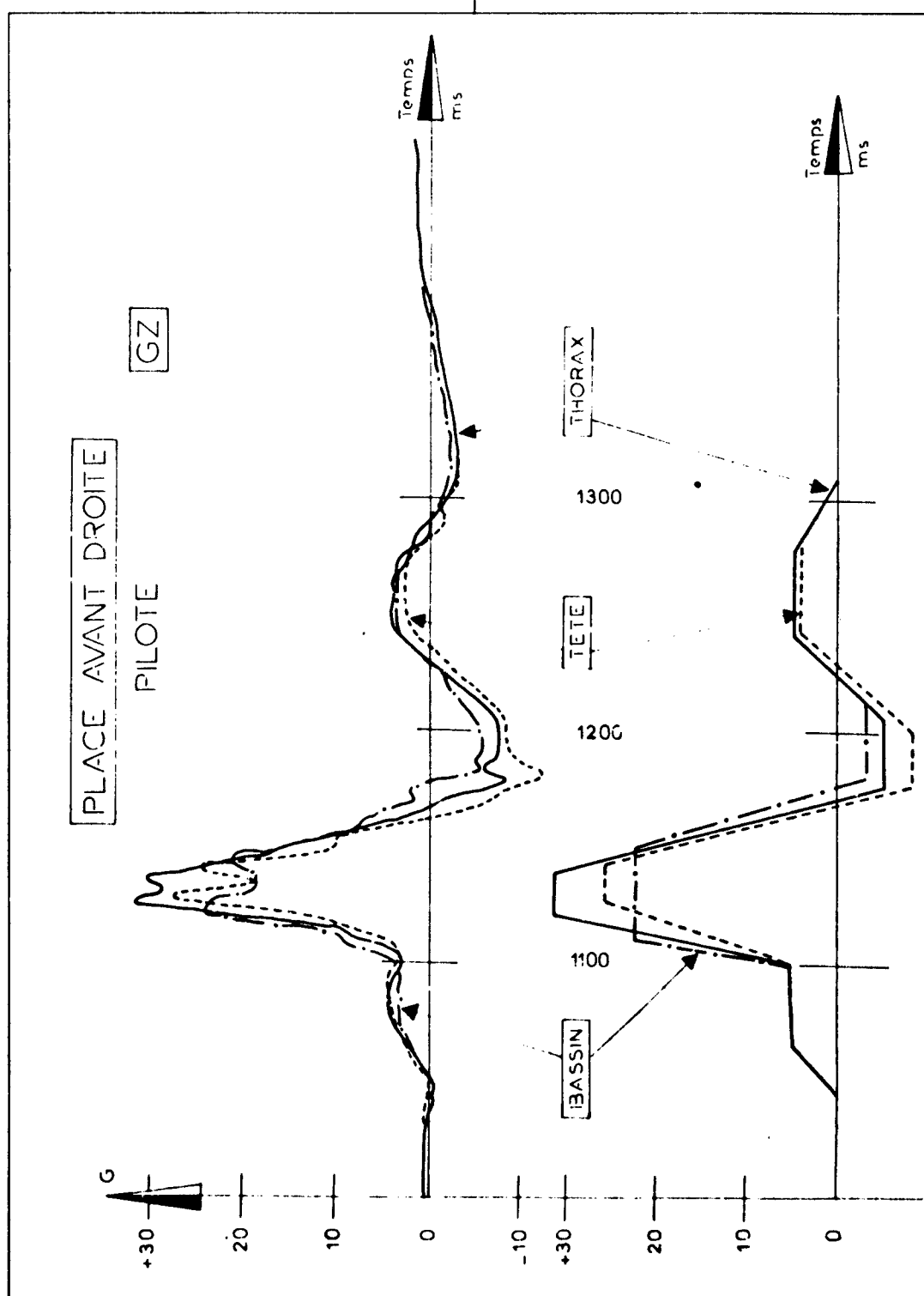


PLANCHE 10

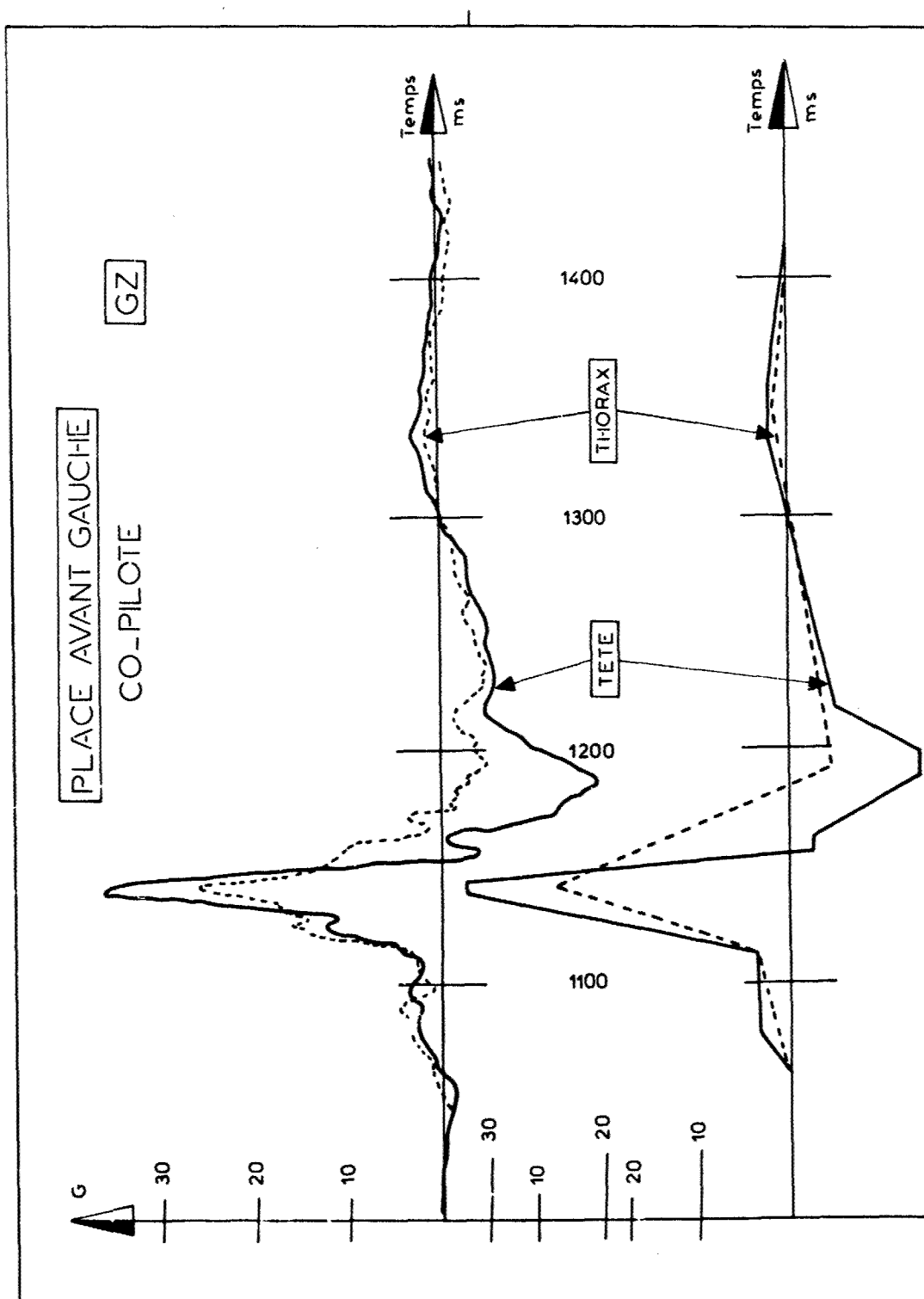


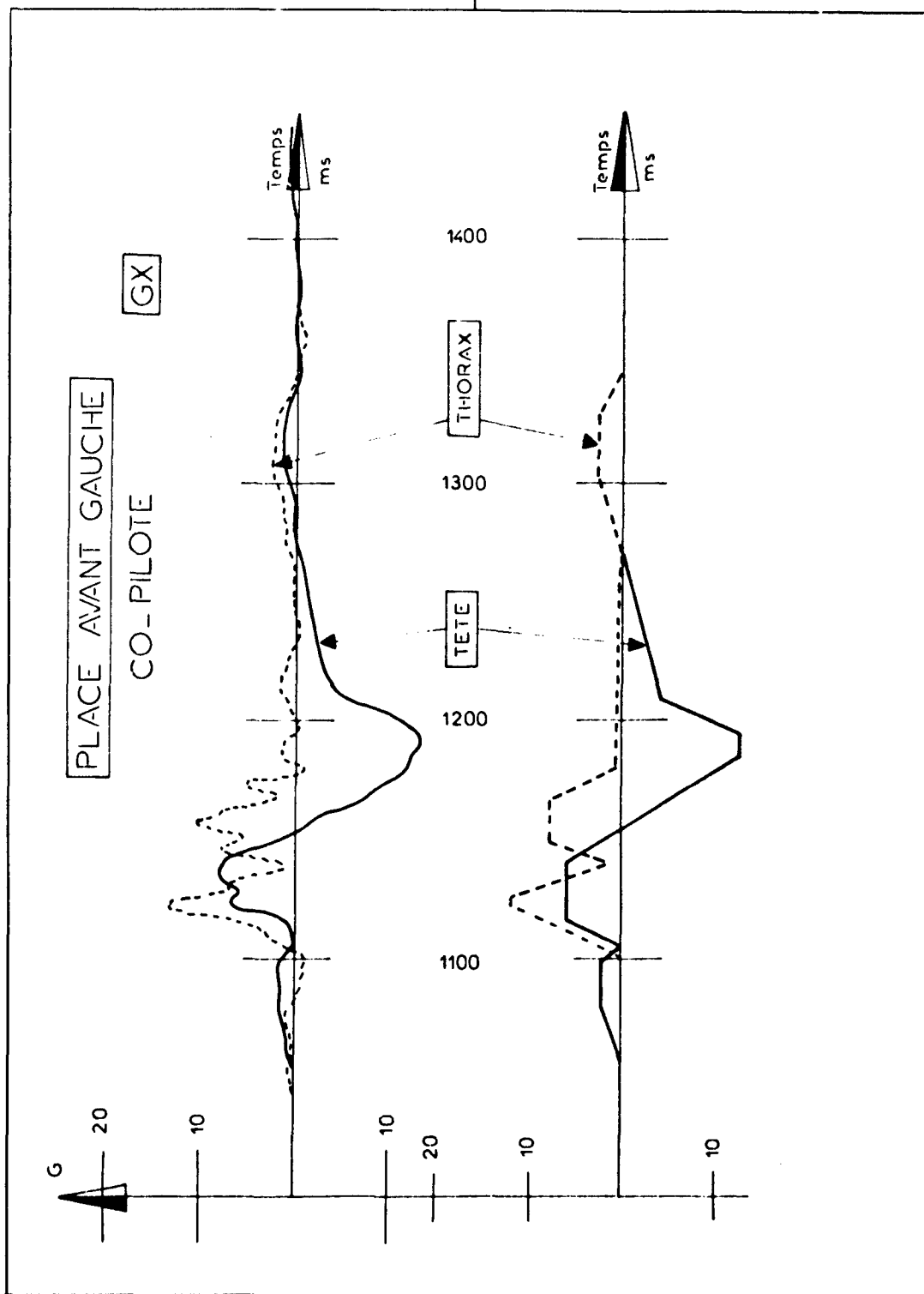






PLANCIE 14





DISCUSSION

DR. VON GIERKE (USA)

Do you have the dynamic characteristics of the dummy used, particularly of the vertebral column of the dummy?

AUTHOR'S REPLY

Unfortunately, we are not absolutely certain of the rigidity of the neck in the case of pilot. We don't know how the neck was made.

WING CDR D. C. READER (UK)

In contrast to UK experience with actual impacts involving Gazelle helicopters, you choose a low impact velocity for your tests which produced little structural damage. In our real world experience the damage to the aircraft was always complete. Why did you choose such trivial impact forces for your experiments?

AUTHOR'S REPLY

We decided on these values because we wanted to show a final crash in auto rotation or after a sudden loss of power.

PART I: THE USE OF A SPINAL ANALOGUE TO COMPARE HUMAN TOLERANCE OF REPEATED SHOCKS WITH TOLERANCE OF VIBRATION

by

Geoff Allen
Human Engineering Division, Flight Systems Department,
Royal Aircraft Establishment, Farnborough, Hampshire, England

SUMMARY

A method is evolved for comparing theoretically the compatibility between ISO 2631 'limits' for human tolerance of vertical vibration and recent proposals for limits of tolerance of repeated shocks based on a spinal analogue.

The method is applied to both limits over a wide range of conditions including a proposal for the maximum acceptable vibration crest factor to be increased from the present value of 3, to 6. The results suggest that '4' is about the maximum value, if vibration and repeated shock limits are to be compatible, but it is emphasized that the comparison is based on tentative proposals for repeated shocks and the ISO 2631 controversial vibration/time dependency relationship. The main thrust of the paper is to illustrate a *method* of comparison rather than to reach definite conclusions from its application.

A plea is made for comments on the method, for the provision of more laboratory and field data and for more consideration of the use of biomechanical analogues in the evolution of standards.

1 INTRODUCTION

The compatibility between tolerance of vibration as defined in ISO 2631¹ and tolerance of repeated shocks, as tentatively proposed by the author², has been queried several times. Recently it has been raised in relation to that part of Griffin's proposed short term amendments³ to ISO 2631¹, which cover high crest factors (peak/rms acceleration).

The purpose of this note is to compare theoretically the two approaches, particularly in relation to exposure boundaries and to vibrations with high crest factors, which may be considered as a type of shock. A simplified comparison is made by considering only nominally-sinusoidal vibrations of varying amplitude at various discrete frequencies and only repeated shocks composed of one or more isolated sinusoidal-type inputs, again at various discrete frequencies.

The analysis is intended primarily to demonstrate a *method* of comparing repeated shock tolerance with vibration tolerance. It should not be regarded as producing definite conclusions either way, particularly in view of the tentative nature of the proposals for tolerance of repeated shocks.

2 METHOD AND RESULTS

First we will assume that the ISO 2631¹ (safe) 'Exposure Limit' should be reasonably compatible with the proposed 'Severe Discomfort' boundary for repeated shocks.

The ISO 2631¹ 'Exposure Limit', as for the similarly-shaped 'Fatigue-decreased Proficiency' and 'Reduced Comfort' boundaries is frequency dependent. The shape of the tolerable input acceleration v frequency curve, shown dotted in Fig 1, is based on suggestions by von Gierke and Coermann⁴ that overall tolerance is the envelope of tolerance of three body sub-systems termed 'spine-abdomen', 'lumbro-sacral' and 'head'. 'Tolerance' is assumed to equate to the input acceleration required to maintain constant (relative) displacement of each sub-system, that is, constant load.

Using data from ISO 2631, exposure limits for vertical vibration of seated persons for daily durations of 1-4 min, $\frac{1}{2}$ hr, 1 hr and 8 hr, and for sinusoidal input frequencies from 1-80 Hz, are given in Table 1. As well as the usual rms acceleration levels, the table includes peak values for crest factors of 1.414 (normal sinewave), 3 (the maximum recommended in the Standard), and 6 (the maximum proposed by Griffin³). For the last two, it is assumed that the number of vibration peaks with high crest factors is small enough (say not more than a few per cent) not significantly to increase the rms value compared with that of a steady sinusoidal input.

We have therefore, obtained values of the maximum permissible 'Exposure Limit' peak input

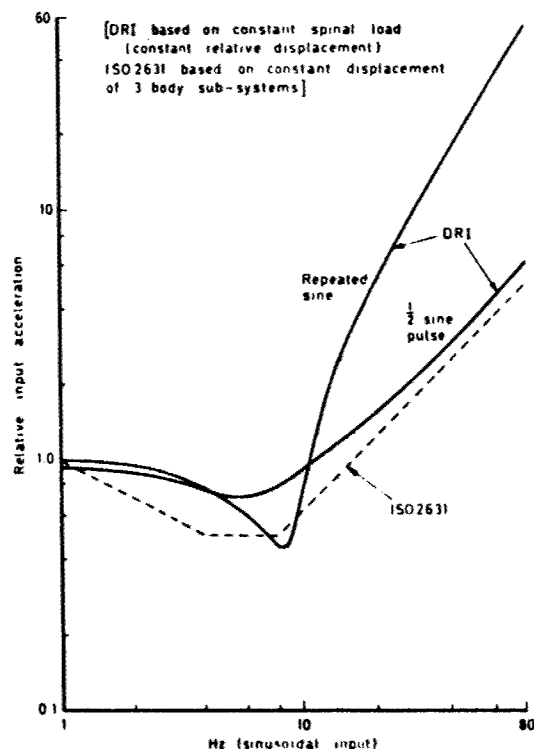


Fig 1 DRI v ISO frequency weighting - tolerance curves

Table 1

Freqy Hz	ISO 2631 a _z (Safe) 'Exposure Limits'															
	rms m/s ²				Peak input g											
	1- min	1/4 hr	1 hr	8 hr	1-4 min			1/4 hr			1 hr			8 hr		
					CF* 1.41	CF 3	CF 6	CF 1.41	CF 3	CF 6	CF 1.41	CF 3	CF 6	CF 1.41	CF 3	CF 6
1	11.2	6.7	4.7	1.26	1.6	3.4	6.8	0.96	2.0	4.1	0.68	1.44	2.88	0.18	0.39	0.78
4 & 5 ⁺	5.6	3.4	2.4	0.63	0.8	1.7	3.4	0.48	1.02	2.04	0.34	0.72	1.44	0.09	0.19	0.38
8.4 ⁺	6.0	3.6	2.5	0.68	0.9	1.8	3.6	0.54	1.08	2.16	0.36	0.77	1.54	0.10	0.21	0.42
11	8.0	4.8	3.4	0.91	1.2	2.4	4.8	0.72	1.44	2.88	0.49	1.03	2.06	0.13	0.28	0.56
30	21.6	12.9	9.1	2.43	3.1	6.6	13.2	1.85	3.95	7.9	1.31	2.78	5.56	0.35	0.74	1.49
80	56.0	33.5	23.6	6.30	8.0	17.1	34.2	4.8	10.2	20.5	3.40	7.22	14.4	0.91	1.92	3.85

* Crest factor

+ Frequency for minimum tolerance of 1/4 sine input (DRI shock criterion)

† Frequency for minimum tolerance of transient sinewaves (DRI shock criterion)

NB The crest factor of '6' is a proposed amendment³ to ISO 2631, in which the present recommended maximum value is 3.

accelerations over the frequency range 1-80 Hz for steady sinusoidal inputs and for a limited number of large amplitude sinusoids (high crest factors) superimposed on a lower background level. To compare these with the tentative proposals² for human tolerance of repeated shocks, it is necessary to convert the shock limits, which are expressed as maximum equivalent output accelerations (Dynamic Response Index ('DRI')) (that is, a direct function of the peak load in the spine) into the equivalent input accelerations. To provide a reasonably-simple basis of comparison, it is assumed that each shock is limited in frequency content to 80 Hz (the maximum covered by ISO 2631) and is applied in one of two forms, either as a limited number of high crest factor sinusoids ('transient') or as a single half sinewave pulse.

Following suggestions by Maslen⁵, and using work by Payne⁶ on the Dynamic Response Index and Barrett and Payne⁷ on the response of a single order mass-spring-damper system to a 'steady' and transient input, the relative values of the input acceleration which will produce a constant peak spinal load ('DRI') over a range of applied frequencies of 1-80 Hz, are shown in Fig 1. Two curves are given, one for a half sinewave input pulse, the other for a limited number of full sinewaves (transient), the latter assuming that effectively, the steady-state response has been reached.

We can now explore how the ISO 2631 'Exposure Limit' for vertical sinusoidal vibration compares with the proposed boundary to prevent severe discomfort from daily exposure to repeated shocks. The latter extracted from Ref 2, is given in Fig 2, expressed as DRI (a function of spinal 'output' load) against N, the number of shocks per day. We have to convert these DRI values into equivalent peak input g's over the ISO 2631 frequency range of 1-80 Hz. The conversion factors, peak input g/DRI¹, for various shock input frequencies, and extracted from Fig 1 are given in Table 2, for a half sine pulse and for a transient sinusoidal input. These factors are then applied to the DRI values to obtain 'peak input g versus N shocks per day' for various pulse frequencies. (Table 3 and Figs 3 and 4).

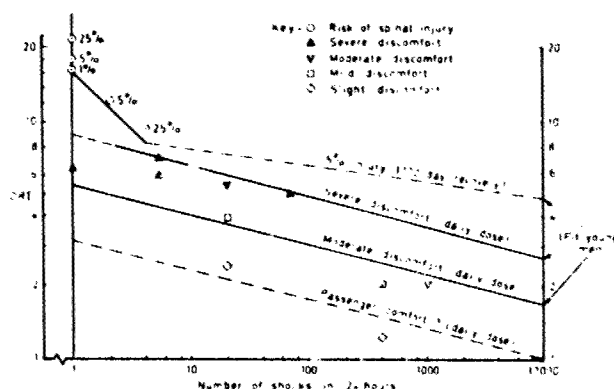


Fig 2 Shock data and proposed limits

Table 2

Pulse freq Hz	peak input 'g'/DRI	
	1/4 sine	Repeated sine
1	0.93	1.0
4	0.75	0.8
5	0.7	0.67
8.4	0.84	0.46
30	2.1	10.0
80	6.0	56.0

The ISO 2631 exposure limit peak input g's in Table 1 (for steady sinewave, and crest factors of 3 and 6) are then applied to the curves in Figs 3 and 4 to obtain the corresponding maximum permissible number of shocks per day ('A'). A few examples are marked on the curves to show the method, the rest are omitted for clarity. The results are given in Table 4, and in the associated text. This table includes the maximum permissible number, 'B', of sinusoidal cycles per day obtained from the ISO 2631 criterion. There is a potential hazard if A/B is less than unity and a likely hazard if A/B is much less than 1. The latter cases, which, it will be seen, only occur for vibrations with a crest factor of 6, are marked with an asterisk in Table 4.

At the time of writing, it was not possible to carry out a more detailed analysis of all the cases marked * in Table 4 (where the DRI criterion is potentially in conflict with ISO 2631 if crest factors

Table 3

N (shocks/day)	'DRI' (Severe discomfort boundary)	Peak input g											
		1 (&11) Hz		4 Hz		5 Hz		8.4 Hz		30 Hz		80 Hz†	
		‡s*	ts*	‡s	ts	‡s	ts	‡s	ts	‡s	ts	‡s	ts
1	9	8.4	9.0	6.7	7.2	6.3	6.0	7.6	4.1	18.9	90	54	504
10	6.5	6.0	6.5	4.9	5.2	4.6	4.4	5.5	3.0	13.6	65	39	364
100	5	4.6	5.0	3.8	4.0	3.5	3.4	4.2	2.3	10.5	50	30	280
1000	3.6	3.3	3.6	2.7	2.9	2.5	2.4	3.0	1.7	7.6	36	22	202
10000	2.6	2.4	2.6	2.0	2.1	1.8	1.7	2.2	1.2	5.5	26	16	146
100000	1.9	1.8	1.9	1.4	1.5	1.3	1.3	1.6	0.9	4.0	19	11	106

† basic pulse frequency

* ‡ sine wave input (repeated)

+ transient sine wave (repeated) input

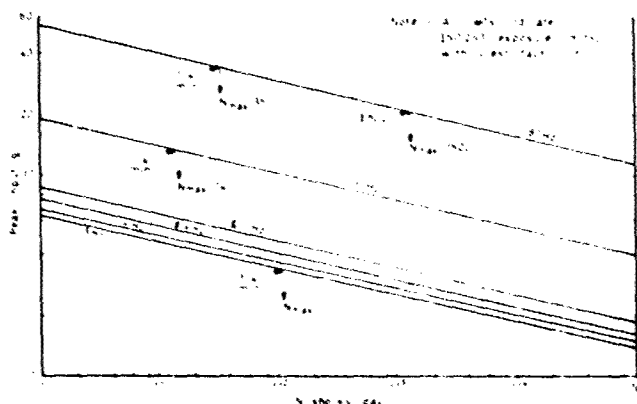


Fig 3 Shocks/day v peak input g - transient sine input ('severe discomfort')

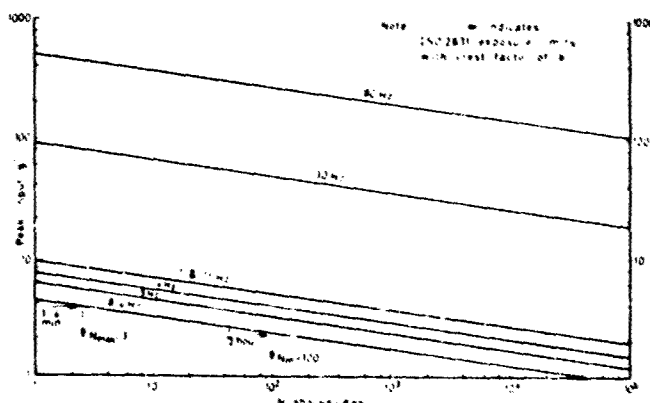


Fig 4 Shocks/day v peak input g - 1/2 sine pulse ('severe discomfort')

significant change in the DRI/N slope for repeated shocks (Fig 2) or in the ISO 2631 time dependency curve would considerably affect the comparison.

To conclude, comments on the paper are welcomed, and the author's usual plea is made for the provision of more laboratory and field data, in this instance on human tolerance of repeated shocks and on vibration/time dependency. Also, this investigation has re-emphasized the fundamental importance of biomechanical analogues in the evolution of Standards for human tolerance of vibration and shock. It is considered that this topic, including which 'output' parameter (absolute displacement, relative displacement, load, 'energy', etc) is appropriate to a particular situation, warrants far more attention than it is getting at present.

Acknowledgments

I am indebted to those who laid the foundations of this paper by their pioneering work on biodynamical modelling, particularly Henning von Gierke, Peter Payne and the late Ralph Giermann. Kate Maslen provided her usual unstinted help in translating my thoughts into something approaching a scientific framework, but does not necessarily agree with all the contents of the paper.

of 6 are assumed). Three cases marked '+' were explored however, and it was found that the maximum permissible crest factors to make the shock criterion compatible with ISO 2631 ranged from 3.7 to 5.

3 CONCLUSIONS AND COMMENTS

A method has been developed whereby specifications for human tolerance of repeated shocks can be compared theoretically with tolerance of vibration, particularly vibration with high crest factors.

The method has been used to compare the current ISO 2631 'Exposure Limit' for vertical vibration with that in the draft proposal for the 'Severe Discomfort Boundary' for tolerance of repeated shocks. It was found that the two limits are compatible for the wide range of conditions explored, for vibration crest factors up to 3 (the maximum value permitted in the current ISO 2631 standard¹). A crest factor of 6, as proposed in a draft amendment³ to ISO 2631, would however give values of vibration peak acceleration, for certain frequencies and duration of exposure, which would not be acceptable against the present repeated shock criteria. A limited check indicates that crest factors up to 4 would be acceptable, in all but perhaps one isolated case.

The results of this comparison should be regarded as very tentative, firstly because of the preliminary nature of the repeated shock proposals, and secondly because of the considerable uncertainty regarding the present time dependency relationship in ISO 2631. For example, any

Table 4

Freqy Hz	Max No. shocks/day, ('A') (ISO peak g applied to PR1)			Max No. sine waves ('B') (ISO)	A/B			Remarks
	CF 1.41	CF 3	CF 6		CF 1.41	CF 3	CF 6	
1	$>10^5$	1100	6	240	>1	>1	*0.025*	4 min ISO Exposure Limit and 1/2 sine shock pulse
4	"	40000	180	960	"	"	0.19	
5	"	20000	110	1200	"	"	0.09*	
8.4	"	45000	230	2000	"	"	0.12	
11	"	12000	90	2640	"	"	0.034	
30	"	2200	14	7200	"	0.41	0.002*	
80	"	5000	35	19200	"	0.26	0.02*	
1	$>10^5$	1000	7	240	>1	>1	0.029*	4 min ISO Exposure Limit and repeated (transient) sine input
4	"	15000	150	960	"	"	0.16*	
5	"	4000	40	1200	"	"	0.033*	
8.4	"	400	3	2000	"	0.2	*0.002*	
11	"	14000	100	2640	"	>1	0.038*	
30	"	$>10^5$	$>10^5$	7200	"	"	>1	
80	"	"	"	19200	"	"	"	
1	$>10^5$	50000	320	1800	>1	>1	0.18*	1/2 hour ISO Exposure Limit and 1/2 sine shock pulse
4	"	$>10^5$	10000	7200	"	"	>1	
5	"	"	5200	9000	"	"	0.58	
8.4	"	"	7400	15000	"	"	0.49	
11	"	"	3000	19800	"	"	0.15	
30	"	"	700	54000	"	"	0.013*	
80	"	"	1500	144000	"	"	0.010*	
1	$>10^5$	60000	260	1800	>1	>1	0.145*	1/2 hour ISO Exposure Limit and repeated (transient) sine input
4	"	$>10^5$	7500	7200	"	"	>1	
5	"	"	1700	9000	"	"	0.19	
8.4	"	40000	100	15000	"	"	*0.007*	
11	"	$>10^5$	7000	19800	"	"	0.35	
30	"	"	$>10^5$	54000	"	"	>1	
80	"	"	"	144000	"	"	"	
1	$>10^5$	$>10^5$	4000	3600	>1	>1	>1	1 hour ISO Exposure Limit 1/2 sine shock pulse
4	"	"	$>10^5$	14400	"	"	"	
5	"	"	70000	18000	"	"	"	
8.4	"	"	$>10^5$	30200	"	"	"	
11	"	"	45000	39600	"	"	"	
30	"	"	9000	108000	"	"	0.08	
80	"	"	20000	288000	"	"	0.07	
1	$>10^5$	$>10^5$	7000	3600	>1	>1	>1	1 hour ISO Exposure Limit repeated (transient) sine input
4	"	"	$>10^5$	14400	"	"	"	
5	"	"	20000	18000	"	"	0.11	
8.4	"	"	2000	30200	"	"	0.07*	
11	"	"	50000	39600	"	"	>1	
30	"	"	$>10^5$	108000	"	"	"	
80	"	"	"	288000	"	"	"	

* Repeated shock criteria may not be satisfied

+ See text

(The 8 hour ISO exposure limit was checked in the same way and yielded values of A/B greater than 1 in all cases, that is, there is no danger of the proposed N shocks/day limits being exceeded.)

REFERENCES

- 1 ISO/TC108 Guide for the evaluation of human exposure to whole-body vibration. International Organisation for Standardization. 1974. ISO 2631-1974(E)
- 2 Allen, G.R. Progress on a specification for human tolerance of repeated shocks. 1976. International Organisation for Standardization ISO TC108/SC4/2/N47
- 3 Griffin, M.G. Proposed amendment to ISO 2631-1974. 1977. Draft proposal to Secretariat ISO/TC108/SC4
- 4 von Gierke, H.E. Coermann, R.R. The biodynamics of human response to vibration and impact. Industrial Medicine and Surgery, Volume 32 Part 1, 1963
- 5 Maslen, K. Personal communication. 1977. F/S Dept RAE
- 6 Payne, P.R. On quantifying ride comfort and allowable accelerations. 1976. AIAA Paper 76-173
- 7 Barrett, S. Payne, P.R. Response of a linear damped dynamic system to selected acceleration inputs. 1965. AMRL-TR-65-40 Wright-Patterson Air Force Base, Ohio

PART II A CRITICAL LOOK AT BIODYNAMIC MODELLING IN RELATION TO SPECIFICATIONS FOR HUMAN TOLERANCE OF VIBRATION AND SHOCK

by

Geoff Allen
Human Engineering Division, Flight Systems Department,
Royal Aircraft Establishment, Farnborough, Hampshire, GU14 6TD, England

SUMMARY

Previous work on biodynamic modelling is briefly reviewed in relation to its application to Standards for human tolerance of vibration and shock. It is shown that there are considerable deficiencies in our knowledge and approach on this important relationship. Particularly, insufficient attention has been paid to the differences among the several types of response of the body/analogue to applied vibration and their relevance to real life. To underline this, the paper analyses the various response characteristics of two simple mass-spring-damper systems analogous to the human body. It then considers the relevance of these responses to practical situations and hence to the derivation of Standards. The usefulness of analogues in predicting response to complex vibration inputs is also shown. Some other neglected topics, including the effects of the active and adaptive powers of the human body, of seating and of duration of exposure, are briefly considered. Suggestions are offered for further work, some of which would be relevant to the forthcoming major revision of ISO 2631.

1 INTRODUCTION

In the search for an understanding of the many effects of mechanical vibration and shock on man, it has long been recognised that the biodynamic response of this remarkable, complex human machine¹ is a fundamental link in the chain between the applied motion and the resultant human reaction. Biodynamic analogues, that is mathematical, structural models of the body, have therefore been the basis of several specifications for human tolerance to vibration^{2,3} and shock^{4,5}. During recent years there have been at least three International Conferences⁶⁻⁸, concerned with biodynamic, or as some prefer to call them, bio-mechanical models, particularly, with their practical applications. At one⁸ of these a plea was made for the translation of recent knowledge on modelling into vibration and shock limits. It has been recognised that biodynamic models will play an important role in the major revision now proceeding of ISO Standard IS 2631³.

However, in the practical application of analogues to human tolerance of vibration and shocks, insufficient attention seems to have been given to certain important, fundamental questions. For example, what analogues are appropriate and what responses ('outputs') of these analogues apply to particular situations? Is absolute displacement, relative displacement, load or 'energy' likely to dominate tolerance? How do complex inputs affect the response of the analogue; how do we model the effect of duration of exposure and recovery from it? The need to answer such questions became increasingly apparent in the preparation of papers on tolerance of repeated shocks⁵ and on comparing vibration with shock tolerance⁹.

Against this background, this paper has four main objectives:-

- (i) to review briefly some previous work, particularly on the use of analogues in specifications concerning limits for human tolerance of vibration and shock;
- (ii) using two simplified body analogues as examples, to underline the importance of different responses in relation to practical applications and to the derivation of limits;
- (iii) to point out some of the gaps in knowledge;
- (iv) to suggest directions for further laboratory and field work related to the derivation of improved specifications.

The paper mainly covers modelling of response to whole-body vertical vibration and to a lesser extent, to repeated shocks. It does not explore response to single violent, accident-type shocks, which has already been the subject of extensive mathematical and physical modelling and the derivation of tolerance limits.

2 BRIEF HISTORICAL REVIEW

In view of the importance of the topic it is surprising that, as far as is known, there has been no comprehensive, critical review of the considerable amount of literature related to biodynamic modelling. For this paper it was only possible to examine a small portion of this literature and to select for comment, a few references, particularly those relevant to specifications for human tolerance of vibration and shock.

Following measurement of whole-body impedance by von Békésy¹⁰ as long ago as 1939, one of the earliest classical works on modelling was by Dieckmann¹¹ in 1957. Based on measurements of the driving point impedance of the human body under applied vertical vibration, he proposed a single mass-spring-damper analogue of the body. He considered that total input force to the body, that is, the total force on the body mass, was the main factor governing human tolerance, and from this derived the well-known K value curves which were used in a German VDI specification⁴ for vibration.

More-sophisticated models, based mainly on impedance, transmissibility and stress/strain measurements, were developed in the USA in the early 60s by Coermann, von Gierke and others. These include a familiar model originally covering response to mechanical vibration only¹² and later extended¹³ to include response to impact and to external pressure loads.

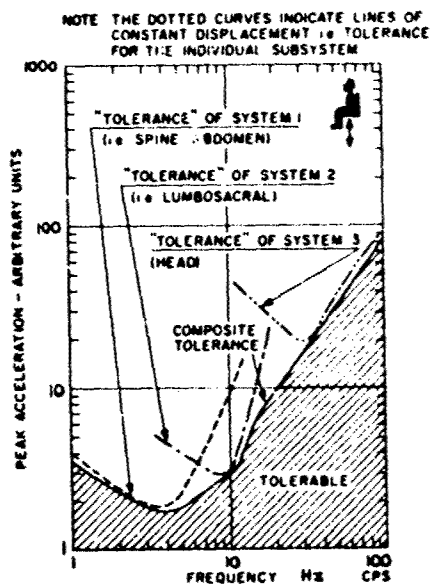


Fig 1 Overall tolerance curve
(from von Gierke and Coermann, Ref 14)

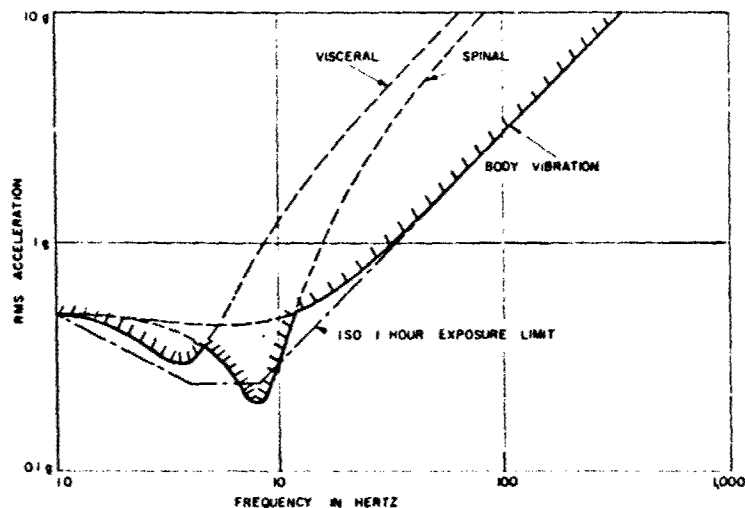


Fig 2 Payne's ride quality model response (from Ref 21)

In 1963 von Gierke and Coermann¹⁴ put forward the ingenious concept that the body's overall tolerance curve (input acceleration v frequency) is the envelope of tolerance of three body sub-systems termed 'spine-abdomen', 'lumbro-sacral' and 'head'. They assumed that the criterion for the tolerance curve was the maintenance of a constant amplitude of relative displacement, that is, a constant amplitude of spring force in each sub-system (Fig 1). The shape of the vertical vibration tolerance curves in ISO 2631 (Fig 2) is based on this concept. Also in the 60s, Pradko and his colleagues¹⁵ suggested that human tolerance is closely related to the absorbed power (or heat) produced in the body by vibration. From a model derived from impedance measurements they showed how, theoretically, absorbed power could be calculated and input acceleration v frequency response curves for constant power, obtained.

The scope of work on modelling has since expanded considerably. Some investigators, such as Muxsian and Nash¹⁶, have developed sophisticated, anatomically-based segmented models of the body. Others, including Jex and Magdeleno¹⁷, have derived analogues in which man is modelled as part of a control loop, the model including his bio-mechanical, perceptual and neuro-muscular responses. Rowlands¹⁸ and Griffin *et al*¹⁹ have explored some of the many variables which affect transmission of vibration through the body, such as posture, limb position, muscle tension, seat harness and intra- and inter-subject variability. Garg and Ross²⁰ have investigated vibration transmission to the head of standing, in contrast to the more usual research on seated persons, and successfully matched their experimentally-derived curves with those from a sophisticated mathematical analogue of the body.

All the investigations briefly reviewed above have provided valuable information on the biodynamics of human reaction to vibration, but generally, only some of the earlier papers attempted to relate biodynamic data to curves or limits for human tolerance. Payne, however, with his considerable experience of modelling and defining human tolerance of violent shocks, has recently proposed²¹, (Fig 2) for ride quality assessment, a model comprising three parallel mass-spring-damper sub-systems termed 'visceral', 'spinal' and 'body vibration', and the associated tolerance criteria. For sinusoidal vibration he assumes that the tolerance curve of input acceleration v frequency is the envelope of the curves for constant amplitude of total force on the mass in each sub-system. For repeated shocks he assumes that the response of the spinal sub-system, which is based on work on Dynamic Response Index (URI)⁴ is critical (and presumably therefore, that the 'spring', not the total load is the criterion). He then develops Allen's suggestion⁵ that tolerance can be expressed as the DRI (that is maximum spinal load) v maximum number of shocks per day, to derive limiting curves.

In considering the overall significance of the past work in relation to limits for human tolerance, two important facts emerge. Firstly there has been a considerable measure of agreement concerning the composition of the mass-spring-damper systems which simulate the body or its component parts. Thus there is general agreement that resonances, such as the 'whole body' one around 5 Hz, play an important part in determining the shape of, or at least the troughs in tolerance curves.

But, secondly, few investigators seem to have considered in any depth the significance of the various types of response of the body (or its analogues) to applied vibration, that is, what is the critical 'output' criterion for a particular situation? Does total load, 'spring' load, absolute displacement, relative displacement or absorbed power dominate tolerance? Those who have considered this important aspect of modelling by no means always agree. As previously indicated Dieckmann¹¹, and for some applications, Payne²¹, considered that total force dominates, whereas von Gierke and Coermann¹⁴ regarded 'spring' force (relative displacement) as more important. Pradko *et al*¹⁵ postulated that absorbed power was the important criterion.

In fact, admittedly without having been able to search diligently, the writer has only found two recent papers which briefly explored this topic. Lange²² presented the different frequency weighting

curves obtained from various body analogues and various response criteria, particularly in relation to complex inputs. Payne, in an Appendix to his paper¹ on quantifying ride comfort, showed the difference between 'total' load and 'spring' load tolerance curves. Neither of these investigators however explored in any depth the need to relate response (output) criteria to particular vibration situations, a topic which is covered in more detail in the next section.

3 BODY/ANALOGUE RESPONSE CRITERIA

3.1 How can we in this short paper demonstrate convincingly the important part played by body and hence analogue response criteria in the derivation of vibration tolerance curves?

There are four main links in the biodynamic chain coupling vibration input with human tolerance, namely:

- (i) the nature of the vibration input (sinusoidal, random, etc);
- (ii) the physical characteristics of the body analogue;
- (iii) the various output responses from the body analogue;
- (iv) the criteria of tolerance (health, performance, comfort, etc) and hence the appropriate body/analogue response from which tolerance curves are derived.

Generally, the importance of (i) and (ii) has been fully appreciated and their characteristics have been adequately defined and understood. (iii) however, and its coupling with (iv) has received much less attention and we will therefore concentrate mainly on this aspect. For simplicity we shall demonstrate the approach needed, but will not attempt to present an accurate detailed mathematical analysis of any particular vibration situation.

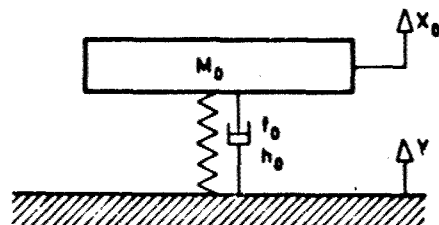


Fig 3 Single system body analogue

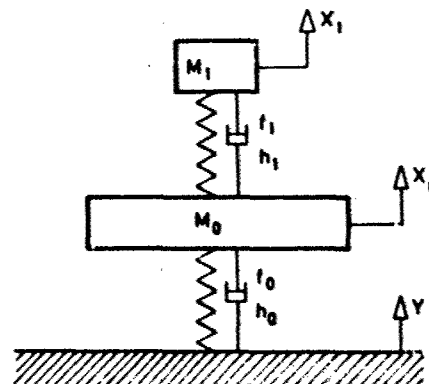


Fig 4 Double system body analogue

We will concentrate mainly on the simplest type of passive whole-body analogue, the single order linear spring-mass system with velocity damping, shown in Fig 3, and will consider only briefly the effects of adding in series a second similar system notionally representing the head (Fig 4). The component characteristics of these analogues have been chosen to correspond very approximately to those of a human body, namely

- | | |
|---------------------------------------|---|
| Primary system - natural frequency, | $f_0 = 5 \text{ Hz}$ |
| damping coefficient, | $h_0 = 0.3$ |
| mass, | $M_0 = 50 \text{ kg}$ |
| Secondary system - natural frequency, | $f_1 = 17 \text{ Hz}$ |
| damping coefficient, | $h_1 = 0.05$ (somewhat lower than the true value to emphasize effect of the secondary system) |
| mass, | $M_1 = M_0/10 = 5 \text{ kg}$ |

We shall first consider the simplest case, namely a sinusoidal acceleration input to the base of the analogue; the effects and implications of complex inputs will be touched on later. Our main objective is to explore the several different outputs or responses of the analogue which are obtained from the same input.

Consider the response of the single system analogue to a sinusoidal input acceleration

$$\ddot{Y} = A \sin \omega t = A \sin 2\pi f t,$$

giving an absolute displacement of the mass, at the same frequency, of amplitude X_0 .

The amplitudes of most responses ('peak' for 'peak' input, or 'rms' for 'rms' input) can be defined in terms of the mass-spring-damper parameters of the analogue, and the following two functions of the

frequency ratio, $\alpha = \omega/\omega_0 = f/f_0$.

$$(P(\alpha))^2 = (1 - \alpha^2)^2 + (2h_0\alpha)^2 \quad \text{and} \quad (Q(\alpha))^2 = 1 + (2h_0\alpha)^2.$$

Any one of several types of response may dominate tolerance. The amplitudes of five possible dominant responses, for input accelerations of amplitudes A_1, A_2 etc, are:

- (i) total force on the mass M_0 = total input force = $M_0\ddot{X}_0 = A_1 M_0 Q(\alpha)/P(\alpha)$;
- (ii) spring force = $(X_0 - Y)M_0\omega_0^2 = K(X_0 - Y) = A_2 M_0/P(\alpha)$;
- (iii) spring deflection (movement of mass relative to input) = $(X_0 - Y) = A_3/\omega_0^2 P(\alpha)$;
- (iv) absolute deflection of mass, relative to an external fixed datum = $X_0 = (A/\omega^2)Q(\alpha)/P$
 $= (A_4/\omega_0^2 \alpha^2)Q(\alpha)/P(\alpha)$
- (v) absorbed power, i.e. the heating effect produced by the damping in the body
 $= E_1$, say = $A_5^2 h_0 M_0 \alpha^2 / \omega_0 (P(\alpha))^2$.

We follow the usual assumption that tolerance curves of input acceleration v frequency are those which will give constant amplitude responses, hence

$$A_1 = \ddot{X}_0 P(\alpha)/Q(\alpha)$$

$$A_2 = A_3 = (X_0 - Y)P(\alpha)\omega_0^2 \quad (\text{for the constants of this analogue and the values of relative deflection and spring force below})$$

$$A_4 = X_0 \omega_0^2 \alpha^2 P(\alpha)/Q(\alpha)$$

$$A_5 = (E_1 \omega_0 / h_0 M_0)^{1/2} (P(\alpha)/\alpha)$$

We shall take some arbitrary but reasonable values for the response amplitudes, selected partly so that the curves are close together in the region of 5 Hz. The simplifying approximation $(10\pi)^2 \approx 1000$ has been used.

- (i) $\ddot{X}_0 = 1 \text{ m/s}^2$ ($M_0 \ddot{X}_0 = 50 \text{ newtons}$)
- (ii) $K(X_0 - Y) = 50 \text{ newtons}$
- (iii) $(X_0 - Y) = 1 \text{ mm}$
- (iv) $X_0 = 1 \text{ mm}$
- (v) $E_1 = 0.25 \text{ watt}$.

From these equations, we can derive a set of input acceleration against frequency curves (Fig 5) which show clearly the different shapes, and arbitrarily the different levels of the input accelerations required to produce the various constant amplitude responses. Similarly, tolerance curves for a constant amplitude of acceleration of each of the primary and secondary masses in the double system, that is, a constant total force in each system, are given in Fig 6.

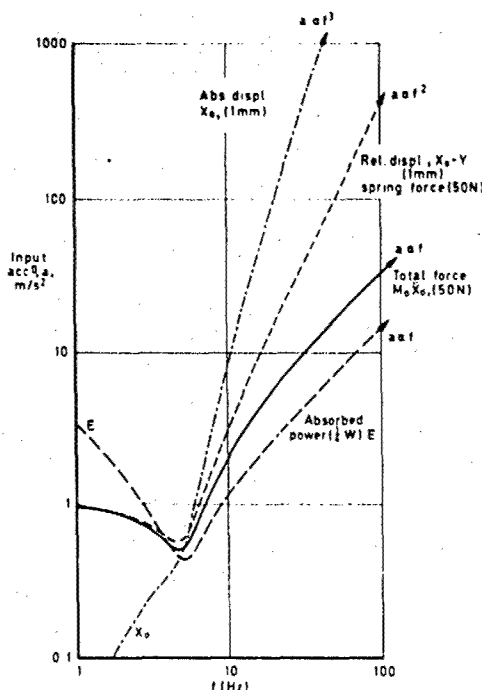


Fig 5 Response curves for single analogue

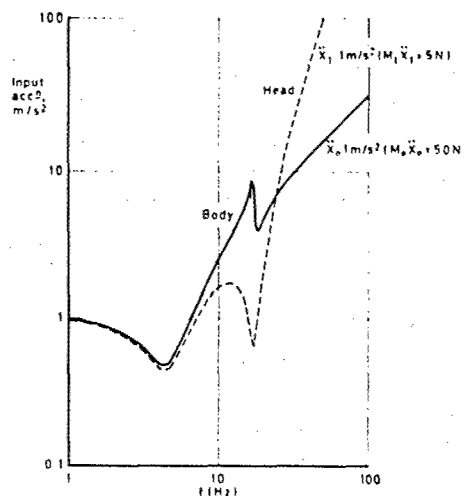


Fig 6 Response curves for double analogue

What does analysis using the eyeballs computer tell us about these curves? For the single system (Fig 5):

- (i) all responses, except that for constant absolute displacement, show a minimum at, and are of similar shape around the natural frequency (5 Hz);
- (ii) the response curve for constant absolute displacement is the only one to decrease with decreasing frequency below the natural frequency;
- (iii) the responses for constant total force and the constant spring force (or constant spring deflection) are almost identical in shape below the natural frequency. Both become asymptotic to the horizontal (a line of constant input acceleration) at low frequencies;
- (iv) the curves have three distinctly different asymptotic slopes at frequencies well above the natural frequency, namely
 - (a) for constant energy and total force, A_{af} , which is analogous to a line of constant velocity. (This does not necessarily mean that the body senses and bases tolerance on velocity, at higher frequencies),
 - (b) for constant spring force (and hence, constant spring deflection, and constant mass deflection relative to the input), A_{af}^2 ,
 - (c) for constant absolute displacement of the mass, A_{af}^3 .

For the double system, only the response for constant amplitude of acceleration of the primary and secondary masses has been derived (Fig 6). Here the secondary system dominates tolerance over a band of frequencies above and below secondary resonance. This dominance is of course, critically dependent on the relative 'tolerance' of the primary and secondary masses; in this example it was assumed that both tolerate the same acceleration.

3.2 Complex inputs

The above analysis is for a simple single frequency input only. However, assuming that the body behaves as a passive, linear bio-mechanical system, we may use the analogue output characteristics to explore, theoretically at least, the response of the body to complex inputs. Hence theoretically, we can determine tolerance of any type of dynamic input against any of the five output criteria in section 3.1 above, or, for that matter against any other output criteria. This can be done either using 'long hand' mathematics or an analogue computer.

It is beyond the scope of this paper to explore this aspect in detail; response of a body analogue to a repeated shock-type input has already been covered elsewhere⁵. The response of the single system analogue to a multi-frequency input will, however, be considered briefly, since this will provide useful evidence on the controversial question of whether the 'worse $\frac{1}{3}$ octave band acceleration' or the 'summed weighted acceleration' dominates tolerance. The crucial point here is not so much which response characteristic is important, but what feature of that response dominates tolerance - is it rms, or peak output, or a mixture of both?

If the rms value of the response, be it load, displacement or any other parameter, is the critical factor, then it can easily be shown that tolerance is dependent on A_e

$$\text{where } A_e = \sqrt{A_a^2 + (w_b A_b)^2 + (w_c A_c)^2 + \dots}$$

and A_e = effective rms input acceleration, summed and weighted to input frequency f_a

A_a = rms input acceleration at f_a

A_b = rms input acceleration at f_b

w_b = weighting factor: $\frac{\text{acceleration tolerance at } f_a}{\text{acceleration tolerance at } f_b}$

etc.

Thus if we assume, as does ISO 2631³, that tolerance is dependent on rms acceleration, then the summed weighted input acceleration method is appropriate. If, of course weighted acceleration at one frequency (or in one $\frac{1}{3}$ octave band) dominates, then the single rms value at this frequency will be a good approximation.

If however tolerance depends on *peak* rather than *rms* output acceleration and if the input frequencies are not harmonically related, then it can be shown that, using the same symbology as before,

$$A_e \approx A_a + w_b A_b + w_c A_c$$

so that arithmetical rather than rms weighted summing is more appropriate (and in fact, more 'severe').

If the input frequencies are harmonically related and/or if their acceleration levels fluctuate, then phase relationships are important, the mathematics becomes complex and such situations can probably best be explored with an analogue computer.

3.3 Relevance to real life

The practical relevance of the previous philosophizing, to real life vibration situations will next be briefly explored.

First, in line with ISO 2631 it will be assumed that human tolerance of vibration can be classified against three dominant criteria:

- (i) *Safety* - direct protection of health, prevention of pain, injury etc (ISO 2631 term, 'exposure limit');
- (ii) *Performance* - maintenance of efficiency during a particular, usually working, activity (ISO 2631 term, 'fatigue-decreased proficiency boundary');
- (iii) *Comfort* - prevention of significant discomfort, which may in some cases be synonymous with maintenance of performance on ordinary activities such as eating and reading, (ISO 2631 term, 'reduced comfort boundary').

What body/analogous outputs or responses are likely to be appropriate to these criteria? ISO 2631 assumes that the same response (relative displacement or spring force, see section 2) applies equally to all three. Thus, 2631 specifies three identically shaped tolerance curves, with a fixed hierarchical relationship, 'exposure limit' being the highest and 'reduced comfort boundary' the lowest.

This seems patently unlikely, certainly as a generalization. Intuitively, 'safety' is likely to be dependent on the forces in the body or body parts, whereas 'performance' will be linked with absolute or relative displacements, often involving body parts different from those appropriate to safety. The particular biodynamic response related to 'comfort' could be almost any one or more of those previously listed in section 3.1, again involving one or more body parts. In many practical situations however, acceptability will be greatly affected by psychological influences such as experience, expectancy and motivation, and by the effect of vibration on activities such as eating, drinking and reading.

To underline this last point, which has been discussed in depth elsewhere^{1,23}, biodynamic reaction is only one of several major factors controlling human reaction to vibration. On the reasoning above, biodynamic reaction is likely to dominate 'safety', to be less dominant for 'performance', and even less regarding 'comfort'.

Therefore, assuming that the shape, if not the level of acceleration/frequency tolerance curves is to be dictated largely by biodynamic reaction, ideally many different shapes will be needed if we wish to cover anything but a very few specific situations. These will need to cover the different criteria of acceptability (safety, performance or comfort) and different applications (passenger v driver, car v aeroplane for example).

Some idea of the large number of different shapes ideally required to cover comprehensively just one particular situation is given in Table 1, using vibration of a helicopter pilot as an example. S_1, S_2 etc denote the different shapes required, but their actual forms are not derived here.

Table 1
ESTIMATED NUMBER OF SHAPES OF TOLERANCE CURVES (A/f) TO COVER VIBRATION OF HELICOPTER PILOT

Criteria	Appropriate body analogue	Appropriate analogue response	Curve shape
1 <i>Safety</i>			
(a) Short term emergency conditions	Spine	Load, $K(X - Y)$	S_1
(b) Long term, cumulative effects	Spine or other critical body part	Load Absorbed power (possibly)	S_1 , possibly S_X S_2
2 <i>Performance</i>			
(a) Inside vision	Body/head/eye	Relative displacement ($X - Y$) or absolute displacement (X)	S_3 S_4
(b) Outside vision	Body/head/eye	Absolute displacement	S_4
(c) Manual control	Body/arm/hand	Relative displacement	S_5
(d) Foot control	Body/leg/foot	Relative displacement	S_6
etc			
3 <i>Comfort</i>			
(a) Psychological (fear of helicopter malfunction)	(Any change in normal vibration causing a noticeable decrement in performance)		S_3-S_6
(b) Fatigue	(Perhaps related to absorbed power or repeated spinal or other organ loading)		S_2 S_1 S_X

The previous analysis has given some idea of the complexities of deriving realistic tolerance curves based on biodynamic modelling, and the large number of curve shapes needed to cover even a reasonable breadth of application. Also, in the analysis, two questionable, major simplifying assumptions were made. These oversimplifications, other shortcomings in our knowledge of body analogues in relation to tolerance curves, and the relevance of other important factors influencing human reaction to vibration, will be discussed in the next section.

4 SHORTCOMINGS IN ANALOGUE MODELLING, RELATED TO THE DERIVATION OF VIBRATION TOLERANCE CURVES

4.1 In section 3.1, the analogues explored were assumed to be passive and linear, whereas in many actual vibration situations, the body behaves as an adaptive and active, not as a passive system. This important topic merits a detailed study in its own right - few investigators seem to have explored it - and here only a few largely intuitive, qualitative comments can be made. Shortage of time precludes considerations of non-linearity effects, which are probably less important.

Several workers including Rowlands¹⁸ and Griffin¹⁹ have conclusively demonstrated that under certain conditions, the body can adapt to minimize the effects of vibration. Muscle relaxation or tension can be used to reduce or increase the natural frequency of the body or body part, and thus minimize the transmission of the applied vibration, for example to the head. Change in position of the head, torso or limbs can also be employed to the same end. Such adaption changes the composition of the body analogues, presumably by adjusting the geometry, the effective spring rate and perhaps, the damping, and should where possible be allowed for in modelling tolerance curves.

The active properties of this remarkable body system in minimizing response to vibration seem to have been explored even less, except perhaps in relation to the ocular pursuit reflex. Here it has been well established that rapid self-induced movements of the eyes can counteract the effects of vibration on vision, up to 3 or 4 Hz at least. In the absence of specific objective measurements, consideration of the tactile dexterity of pianists, and the body, leg and arm dexterity of, for example, runners and conductors suggests that fingers and hands can track (oscillate) up to perhaps 8 Hz and limbs up to about 5 Hz.

In practice, this means that the body, certainly as far as performance of certain tasks is concerned, is probably much more tolerant of low frequency vibration than passive or even adaptive modelling would suggest. Also, the body is likely to be particularly tolerant of vibration around walking frequency (1-2 Hz). Compared with curves derived only from passive modelling, actual tolerance curves at frequencies below the main body trough around 5 Hz, are therefore likely to climb more steeply with decreasing frequency, reaching a plateau around 1 Hz and falling again as inertial and motion sickness reactions dominate²⁴. At higher frequencies, say above 10 Hz, the body is much less likely to be able actively to neutralize applied vibration, and in this region tolerance curve shapes are more likely to follow those derived from passive analogue modelling. The above remarks of course apply mainly to repetitive sinusoidal type vibration. The body is likely to be less adaptive to random or unexpected changes in vibration.

At low frequencies, therefore, the body is likely to behave as a position-controlled servo system, where motion of the body or body parts induced by external vibration is counteracted by internally induced movements.

Based on the reasoning above and in section 3, and backed by some experimental work, in Fig 7 some conceptual tolerance curve shapes are shown and compared with that in ISO 2631.

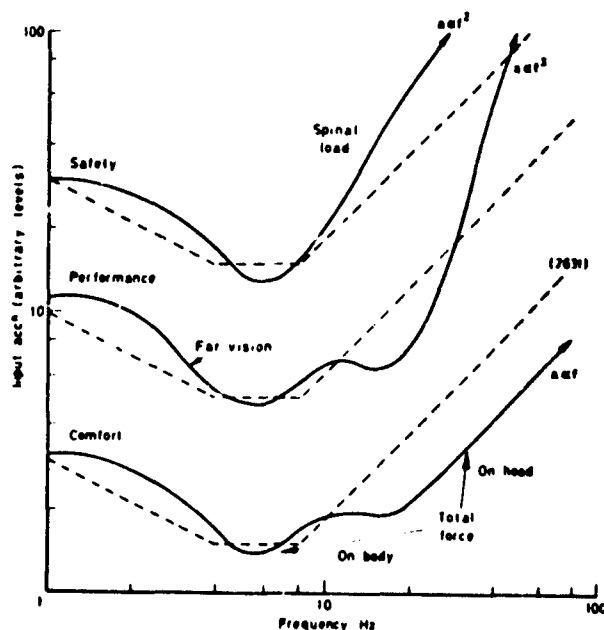


Fig 7 Some conceptual changes to ISO 2631 shape

4.2 There are many other gaps in modelling, in providing a scientific, quantifiable basis for human tolerance of vibration. Some of these gaps are listed in Table 2; here it is only intended to comment on one or two of the more important of them.

Table 2

GAPS IN MODELLING HUMAN RESPONSE TO VIBRATION

BIO-MECHANICAL

Seating, harness
 Lateral, fore and aft, rotational
 Limbs
 Body orientation
 Geo-centric, basi-centric, bio-centric
 Females

OTHERS

Active and adaptive systems
 Duration effects
 Chemical, hydraulic, electrical systems

Seating and harness Several investigators^{19,20} & others have confirmed that these can play an important, sometimes a dominant part in transmission of, and hence in human response to, vibration. They affect vibration inputs to the arms, back and head, and couple an external mechanical system to the body. Sometimes the net effect is to suppress whole body response (increase tolerance around 5 Hz), and increase head vibration (reduce tolerance around 15 Hz).

Body orientation Recent work by Dupuis and others has confirmed that different analogues and different shaped response (tolerance) curves are needed to cover recumbent as compared with seated and standing persons.

Duration of exposure Apart perhaps from the absorbed power theory, generally, biodynamic modelling has not been used to calculate any effects of duration of exposure and recovery from it (in contrast for example, to modelling the cumulative effects of, and recovery from thermal stress). In his proposals²³ on tolerance of repeated shocks, this author introduced a cumulative dose characteristic into the body analogue employed, analogous to metal fatigue, and used Miner's rule for assessing the effects of a complex dose. Surely, for some applications, we do need to introduce duration-dependent characteristics into body analogues, but how? Perhaps at low frequencies at least, the active (muscular) control of body vibration referred to in section 4.1, and achieved at the expense of body energy, could be modelled. If so it would probably need to be related to total power input rather than absorbed power.

Chemical, hydraulic, electrical and other body systems If we are ever to achieve a deeper understanding of the effects of vibration on this complex human machine, then we must be able to explain, that is model, the known effects on other body systems such as the hydraulic (cardio-vascular), the pneumatic (respiratory), and the electrical (neuro-muscular), to cite just three. (This is the real all-embracing 'biodynamics' - surely 'bio-mechanics' is the more-specific description for the structural-type response covered in the other parts of this paper!)

4.3 Having demonstrated the magnitude and complexity of the task, we will in the next section list some suggestions concerning the further work which is needed. Perhaps this will at least incite some investigators to react, if only to prove that many of the assumptions, suppositions and assertions in this paper are incorrect!

5 SUGGESTIONS FOR FUTURE WORK

5.1 A general plea is made for all investigators of human reaction to vibration to consider how, in any future work, they can best provide data which will help to increase our understanding and knowledge of the application of biodynamic modelling to the derivation of specifications for human tolerance. In particular, work along the following lines would appear to be profitable:

- (i) A more detailed, critical review of the literature, particularly to see if the problems discussed in this paper have been investigated, and to help in the planning of future work;
- (ii) laboratory based work -
 - (a) to establish which body/analogue responses are appropriate to particular vibration applications covering safety, performance and comfort criteria,
 - (b) first, biodynamic measurements and then, biodynamic modelling of the responses established in (a),
 - (c) derivation of tolerance curves from (a) and (b),
 - (d) subject to the findings of (i) above, work is particularly needed to fill in the major gaps in knowledge discussed in section 4;
- (iii) field work to explore the relevance of laboratory based findings to real life.

More specific lines for further work are implicit in sections 3 and 4.

6 IN CONCLUSION

It is apparent that there are considerable shortcomings in our knowledge of, and our approach to biodynamic modelling as related to human tolerance of vibration and shock.

Particularly, insufficient thought has been given to the important differences between the several types of responses of the body/analogue to applied vibration, and their relevance to real-life. A technique for exploring these differences has been demonstrated theoretically using simple body analogues and relating their responses to a typical vibration situation involving human safety, performance and comfort. The usefulness of analogues in predicting response to complex vibration inputs has also been shown.

Some other gaps in knowledge, particularly of the effects of the adaptive and active properties of the body, of seating and of duration of exposure, have been briefly discussed, and finally, suggestions have been offered for further work.

It is hoped that this controversial paper will further stimulate thought and action on a subject which is particularly important for the pending revision of ISO 2631.

Acknowledgments

I am indebted to all those investigators whose work on biodynamic modelling and on vibration standards stimulated the production of this paper. Kate Maslen gave her usual invaluable help with the mathematics and sorted out some of the English.

REFERENCES

- 1 Allen, G.R. Human reaction to vibration. J. Envir. Sci. 14(5), 1971
- 2 Verein Deutscher Ingenieure Beurteilung der Einwirkung mechanischer Schwingungen auf der Menschen. VDI 2057, 1963
- 3 ISO/TC108 Guide for the evaluation of human exposure to whole-body vibration. International Standard ISO 2631-1978 (E)
- 4 USAF Seat System: Upward Ejection, Aircraft, General Specification for. MIL-S-9479A, USAF, 1967
- 5 Allen, G.R. Human tolerance of repeated shocks. Proceedings of the European Symposium on Life Sciences Research in Space, Cologne. ESASP-130 pp 343-349, 1977
- 6 WPAFB (USA) (1st) Symposium on Biodynamic Models and their Applications. 1970. AMRL-TR-71-29 (1971)
- 7 SAE (USA) SAE Meeting on Mathematical Modelling Biodynamics Response to Impact. SAE SP-412, 1976
- 8 WPAFB (USA) (2nd) Symposium on Biodynamic Models and their Applications. Bergamo Center, Dayton, 1977
- 9 Allen, G.R. The use of a spinal analogue to compare human tolerance of repeated shocks with tolerance of vibration. Paper at AGARD AMP Conference 1978 (to be published in AGARD-CP series)
- 10 von Békésy, G. Über die Empfindlichkeit des stehenden und sitzenden Menschen gegen sinusförmige Erschütterungen. Akust Ztschr. 4, 360, 1939
- 11 Dieckmann, D. Einfluss vertikaler mechanischer Schwingungen auf der Menschen. Int z angew Physiol einschl Arbeits physiol 16, pp 519-564, 1957
- 12 Coermann, R.R. *et al* The passive dynamic mechanical properties of the human thorax-abdomen system and of the whole body system. Aerospace Med 31, 443, 1960
- 13 von Gierke, H.E. Biodynamics response of the human body. Appl. Mechanics Rev. 17, pp 951-958, 1964
- 14 von Gierke, H.E. Coermann, R.R. The biodynamics of human response to vibration and impact. Industr. Med. Surg. 32(1), 30, 1963
- 15 Pradko, F. *et al* Theory of human vibration response. ASME publication 66-WA/BHP-15, 1966
- 16 Muksian, R. Nash Jr., C.D. On frequency-dependent damping coefficients in lumped parameter models of human beings. J. Biomechanics, Vol 9, pp 33-342, 1976
- 17 Jex, H.R. Magdaleno, R.E. Biomechanical models for vibration feedthrough to hands and head for a semi-supine pilot. Aviation, Space Environ. Med. January 1978
- 18 Rowlands, G.F. Transmission of vertical vibration to the heads and shoulders of seated men. RAE Technical Report 77068, 1977
- 19 Griffin, M.G. *et al* The biodynamic response of the human body and its application to standards. Paper at AGARD AMP Conference 1978 (to be published in AGARD-CP series)

- 20 Garg, D.P.
Ross, M.A. Vertical mode human body vibration transmissibility. IEEE Trans. Systems, Man & Cybernetics, Vol. SMC-6 No.2, 1976
- 21 Payne, P. On quantizing ride comfort and allowable accelerations. Paper at SNAME Meeting on Advanced Marine Vehicles, 76-873, 1976
- 22 Lange, W. A review of biomechanical models for the evaluation of vibration stress. AGARD-CP-145 (B21), 1975
- 23 Allen, G.R. Ride quality and International Standard ISO 2631. NASA TM X-3295/DOT-TSC-OST-75-40, 1975
- 24 Allen, G.R. Proposed limits for exposure to whole-body vertical vibration, 0.1 to 1.0 Hz. AGARD-CP-145(B26), 1975

DISCUSSION

COL JOHNSON (USA)

You mentioned a need for more study of man's ability to tolerate vibration over time. I can understand the problem in helicopter aircraft, but have you had identified to you as a researcher by someone from the operational community any problems in vibration in turbine aircraft, jet fighter or jet transportation? Do the operators really feel that there's a problem, or do you, the researchers, feel that there's a problem for more research in vibration?

AUTHOR'S REPLY

In many of the routine flying environments in strike aircraft the vibration environment is not severe. However, there is a problem if one runs into turbulent flight. Then the body is being subjected to considerable motions at low frequency, large amplitude, and the crew has to do a lot of physical work to correct for that. There I think we have to consider vibration fatigue as an important factor. The vibration problem is also severe in helicopters.

DR. VON GIERKE (USA)

If Dr. Ewing would be here, I am sure he would remind us that the vibration environment is a major problem on surface effects ships.

DR. GRATZL (FRG)

Would you comment on the applicability of the ISO Standard 2631 on human vibration exposure to the military situation?

AUTHOR'S REPLY

I prefer that Dr. von Gierke answers this question.

DR. VON GIERKE (USA)

The international standard on vibration exposure applies to the whole general population including female and children. The US Department of Defense has a military specification which allows the exposure limits to be twice as high with respect to the acceleration levels as in the international standard. This recommendation is strictly for the US Department of Defense and relevant precautions are well justified. In many situations even this limit can be exceeded but it should not be exceeded without specifically assessing the need and the risk involved.

DR. JEX (USA)

Many of the things which you advocate such as the use of more elegant biodynamic models to look at the stresses and strains as bases for comfort, fatigue or performance changes are being examined and I will talk about them later in my paper.

THE RESPONSE OF A REALISTIC COMPUTER MODEL FOR SITTING HUMANS TO DIFFERENT TYPES OF SHOCKS.

by
H. Mertens, and
L. Vogt

DFVLR - Institute of Aviation Medicine
Godesberger Allee 70, D - 5300 Bonn 2 / F.R.G.

SUMMARY

A mechanical model of the human body in the sitting posture is described. The model parameters were derived from the results of steady state vibration experiments conducted under various levels of static acceleration up to +4 Gz. The resulting nonlinear behaviour of the human body was modeled by calculating the characteristics of the model elements. To investigate the model's response under impact loads, the characteristics of the elements were extrapolated beyond 4 G. The model was exercised with different input pulse shapes and the resulting forces and mass displacements were calculated. The results show that the model is able to predict the forces in the vertebral column for arbitrary input pulse shapes. The fact that a rectangular acceleration pulse of 20 Gz causes spinal injuries could be demonstrated by the response of the model. These findings are compared with the Dynamic Response Index (DRI) concept. The characteristic of the nonlinear elements under high load was estimated, and the results indicate that the present model emphasizes the high frequency contents of the input pulses more than the Dynamic Response Index model.

INTRODUCTION

Mechanical models of the human body have been used to assess its behaviour under dynamic loading. Forces and displacements within the body can be calculated from such a model if it represents the human body in a realistic way. If the forces of the input functions exceed those which are encountered in our nonhazardous everyday-life, the nonlinear properties of tissues have to be taken into account. [1]

THE MODEL

In the past, we have developed such a model which is still rather simple; however it represents the main body parts. The design is shown in Fig. 1. The properties of most of the elements contained in the model are known from test results. For example the values for the masses were taken from tables of human body anthropometric measurements [2]. The static and dynamic properties of the vertebral column were investigated, among others, by KAZARIAN [3]. The natural frequency of the abdominal viscera was derived from internal pressure measurements conducted by WHITE et al. [4]. As the mass of this system is known, the spring-constant can be deduced.

The body parameters which are not known were estimated and inserted into the model. By variation of the free parameters on a digital computer, mechanical impedance and transmissibility from seat to head could be simulated simultaneously for magnitude and phase for small vibration amplitudes (≈ 0.3 G) (see Fig. 2).

The values for stiffness and damping determined by this procedure are only valid for the normal static preload of 1 G in the upright sitting posture and for small vibration amplitudes encountered in everyday life. However, if the forces of gravity acting on the body increase, the values for stiffness and damping are shifted to different regions of their characteristic curve. To determine these nonlinear characteristics quantitatively, the model parameters were varied until the theoretical behaviour of the model was in accordance with vibration test results derived from human subjects under increased static gravity up to +4 Gz [5] (see Fig. 3).

During the process of varying the model parameters, all the masses were kept constant and only the values for spring stiffness and damping were varied. The resulting characteristics for the springs and dampers are shown in Fig. 4 - 10. Their numerical values are given in Tab. I. The model containing these parameters has already been used in a previous study [5] dealing with vibration isolation problems. By minimizing the model output, seat cushions could be designed which would give optimal vibration protection under normal and under increased gravity.

THE MODEL UNDER IMPACT

The purpose of this paper is, to describe our efforts to investigate the behaviour of the model under impact conditions and to calculate the resulting forces within the model. Certain limitations, however, have to be considered when the model output is applied to situations in the real world. The first and most important limitation is that the characteristics of the elements are only known in the region between 1 G and 4 G. Most impacts, however, contain considerably higher accelerations. Therefore, the trends of the characteristics had to be extrapolated beyond 4 G. This extrapolation is based on the fact that most characteristics that have a sharp curvature between 1 G and 2 G tend towards linearity under increasing loads. As a first approximation we have assumed that the springs and dampers, when compressed under high G-loads, double their value in comparison with the +4 G condition. We are aware that this assumption may need to be changed to incorporate the results of future tests. The second limitation, when transferring results from theoretical studies to humans, is that the breaking strength of biological tissue is not constant as in technical systems, but rather depends on the velocity with which the load is applied. For the vertebral column, this was shown by KAZARIAN [6]. The spine is especially sensitive to impacts acting in the headward direction, and is the site of the majority of injuries. According to KAZARIAN [6] and GEERTZ [7], the breaking strength of the vertebral column is between 9000 N and 11000 N for the lumbar part and between 6000 N and 9000 N for the thoracic part. Another limitation of our model is that it has only one dimension in the Z-axis: this means that it does not simulate any torque forces.

RECTANGULAR PULSE

In order to improve our model, we made a computer simulation with different input pulses. The force was applied through spring K 2 and damper D 2 which form the buttocks portion of the model. In Fig. 11, we employed a rectangular acceleration pulse as the force input. The acceleration rises to 20 G and returns to 0 G after 0.15 seconds. In the center of the figure, the seat acceleration is shown as a rectangular curve together with the corresponding acceleration of mass 7 of the model plotted against time. M 7 represents the head. While the seat acceleration stays constant at 20 G, the head shows a short overshoot to 30 G. This is the result of the energy initially stored in the springs of the spine. Also noteworthy is the negative acceleration of the head after the abrupt decay of the seat acceleration. This, however, has no practical meaning since in a real world situation the subject is not rigidly connected to the seat.

In the upper part of the figure, the forces in the model spine are plotted against time. F 3 is related to the lumbar portion of the vertebral column while F 5 represents the forces in the thoracic section. The resulting forces are 15440 N in the lower part of the vertebral column and 10900 N in the upper. These values significantly exceed the breaking strength of the spine. We also calculated the "Dynamic Response Index" (DRI) [8] for the tested impact pulses. The resulting index for the rectangular impact pulse is 30.2 which would represent a spinal injury rate of theoretically more than 100 %. In the lower part of the figure, the total displacement of the model along its Z-axis is plotted against time and has a maximum of 34 mm. The displacement does not return exactly to its initial value after one second. This is caused by inaccuracies in the digital computer which arise when the reactions of the model are calculated in small discrete steps of time.

TRAPEZOIDAL PULSE

According to EIBAND [9], a headward impact of 20 G is tolerable if the rate of onset does not exceed 200 G/sec. An impact of this type is shown in Fig. 12. The area under the curve is equal to the rectangular pulse shown previously in Fig. 11, thus giving an equal velocity change of 20 m/s. After a constant rise with 200 G/sec., an acceleration plateau of 20 G is reached after 0.1 seconds. It remains at this level for 0.1 seconds and returns with a step function to 0 G. The calculated model response is plotted in the same manner used for the rectangular input function. As expected, there is a reduction of the maximum force in the spine to 9800 N for the lumbar region and to 6380 N for the thoracic portion. These values are very close to the breaking strength of the spine. The calculated DRI equals 22.9. This value is still related to a spinal injury rate of approximately 100 %.

HALF-SINE PULSE

In another series of computer simulations, we used a half sinewave as a forcing function (see Fig. 13). The area under the curve, again, is also equal to the rectangular pulse used in Fig. 11. Compared with this rectangular pulse, there is a reduction of forces to 9300 N in the lumbar region and to 6100 N in the thoracic region, respectively.

These values are lower than the breaking strength. There is almost no overshoot of body masses as a result of the slow onset and decay of the input pulse. The maximum forces are only 5 % above those minimum forces which can theoretically be produced by a 20 G acceleration. The calculated DRI for this half sinewave is 20.3 which gives a spinal injury rate of 32 %.

F 111 EJECTION PULSE

Finally we exercised the model with a realistic input pulse for an escape system. As an example we used the acceleration time-course of the F 111 escape system. It is shown in Fig. 14 together with the model's response. The escape system has a very steep onset of acceleration during the first 50 milliseconds, which is produced by the build-up of rocket gas pressure between the crew escape module and the aircraft fuselage [15]. The calculations for this pulse shape show maximum forces for the lumbar spine of 12310 N and 8980 N for the thoracic portion of the vertebral column, respectively. These values are slightly above the breaking strength of the spine. However, the calculated DRI is 18.8 for this input pulse, producing a spinal injury rate of 16 %. These findings are opposed to our results concerning the maximum forces in the vertebral column; but it must be taken into account that in our model there are no coupling elements between the accelerated floor and the body as in the real escape module.

CONCLUSIONS

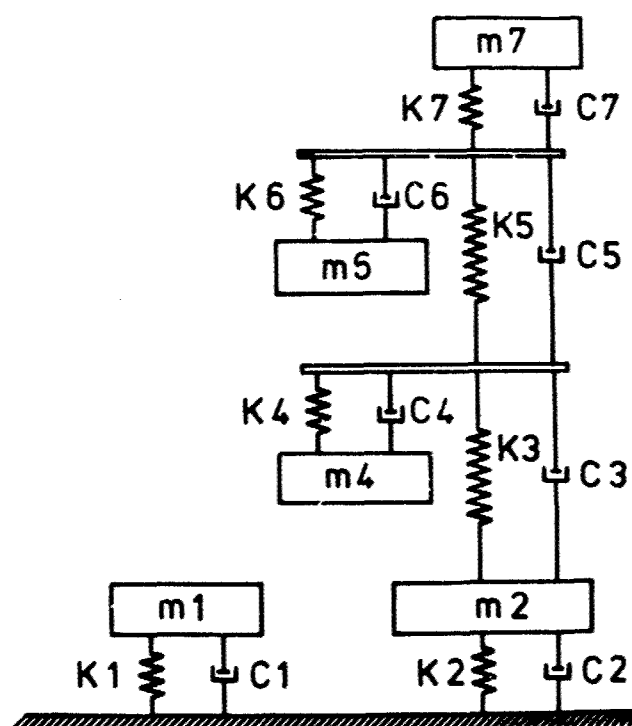
The described model is based on the results of steady state vibration experiments, which were carried out under different levels of static acceleration. If the nonlinear behaviour of the human body which is thus revealed is taken into account such a model can be used to assess the impact tolerance of the human body. It has been shown that the presented system is able to predict the forces in the human spine for arbitrary pulse inputs. The effect that a rectangular acceleration shock of 20 Gz results in injuries, other than a trapezoidal or sinusoidal shock of the same maximum acceleration and the same velocity change could be demonstrated quantitatively. If these findings are compared with the Dynamic Response Index concept which uses only linear model elements it becomes obvious that the high-frequency components of the input pulse have a more pronounced effect on the forces produced in the vertebral column than predicted by the DRI. This fact may explain discrepancies which sometimes arise between predicted and actual tolerance levels when using the DRI concept. Another advantage of the approach described in this paper is that the impact tolerance of the human body may be predicted by a system which may be designed without actual impact tests with human subjects. Thus avoiding most of problems which are usually comprised in such test situations.

REFERENCES

- [1] Vogt, H L.
Coermann, R.
Fust, H.D. Mechanical Impedance of the Sitting Human under Sustained Acceleration.
Aerospace Medicine 39 (1968) S. 675 - 679
- [2] Clauser, C.
McConville, J.
Young, J. Weight, Volume, and Center of Mass of Segments of the Human Body
AMRL - TR - 69 - 70 (1969)
- [3] Kazarian, L. Dynamic Response Characteristics of the Human Vertebral Column.
Stockholm: Trycheri Balder, 1972
- [4] White, G.
Lange, K.
Coermann, R. The Effects of Simulated Buffeting on the Internal Pressure of Man
in: S. Lippers, Human Vibration Research Oxford - London - New York
- Paris: Pergamon Press, 1963
- [5] Mertens, H. Nonlinear Behaviour of Sitting Humans under Increased Gravity
Aviat. Space Environ. Med. 49 (1): 287 - 298
- [6] Kazarian, L.
George, A.
Graves, Jr. Compressive Strength Characteristics of the Human Vertebral Centrum
AMRL - TR - 77 - 14
- [7] Geertz, A. Grenzen und Sonderprobleme bei der Anwendung von Sitzkatapulten
Dissertation Technische Hochschule Stuttgart, 1944
- [8] Stech, E.
Payne, P. Dynamic Models of the Human Body
AMRL - TR - 66 - 157 (1969)

- [9] Eiband, A. Human Tolerance to Rapidly Applied Acceleration: A Summary of the Literature
NASA Memo - 5 - 19 - 59 E, 1959

- [10] Brinkley, J. Dynamic Simulation Techniques for the Design of Escape Systems:
Shaffer, J. Current Applications and Future Air Force Requirements
AMRL - TR - 71 - 29 (1971)



Model Parts

M 1	Mass)	
K 1	Spring)	of the legs, resting on the seat
C 1	Damper)	
M 2	Mass)	
K 2	Spring)	of the buttocks
C 2	Damper)	
K 3	Spring)	of the spine from L 1 to S 1
C 3	Damper)	
K 5	Spring)	of the spine from T 1 to T 12
C 5	Damper)	
K 7	Spring)	of the spine from C 1 to C 7
C 7	Damper)	
M 4	Mass)	
K 4	Spring)	of the abdominal system
C 4	Damper)	
M 6	Mass)	
K 6	Spring)	of the chest system
C 6	Damper)	
M 7	Mass of the head	

Fig. 1. Model of the sitting human body

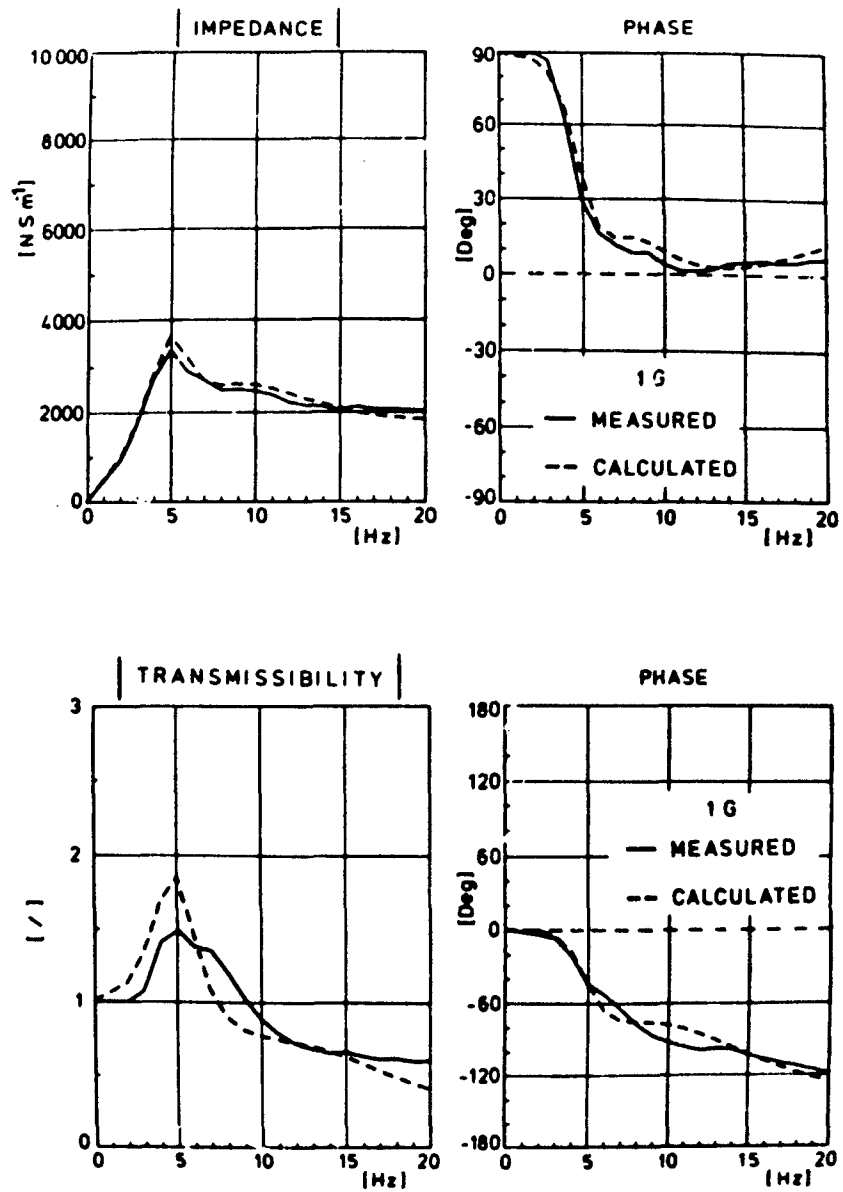


Fig. 2 . Impedance and transmissibility curves as measured and calculated for the model under +1 G_z sustained acceleration.

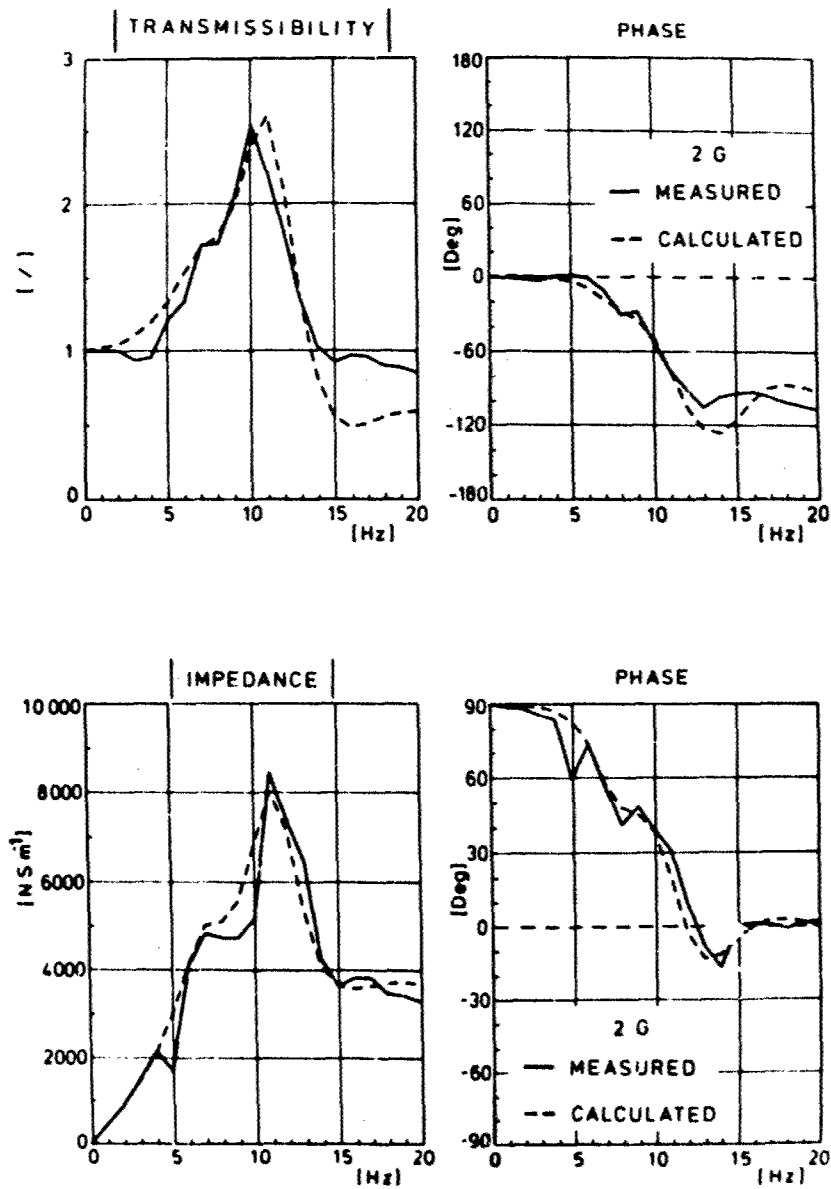


Fig. 3. Impedance and transmissibility curves as measured and calculated for the model under +2 G_z sustained acceleration.

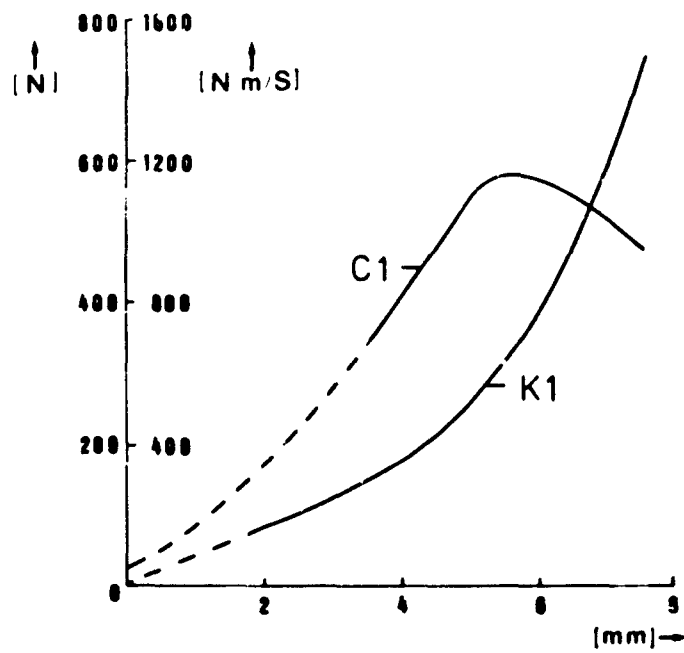


Fig. 4 . Spring- and damper characteristic of the legs.

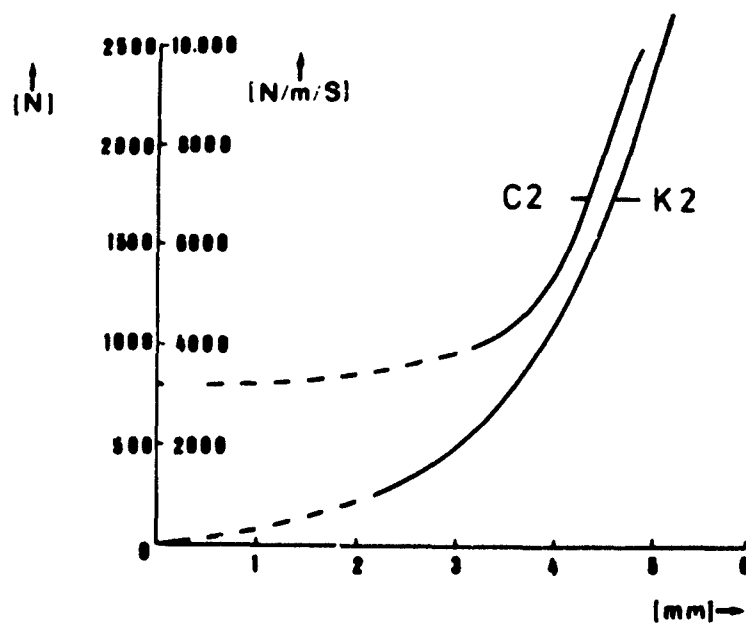


Fig. 5 . Spring- and damper characteristic of the buttocks.

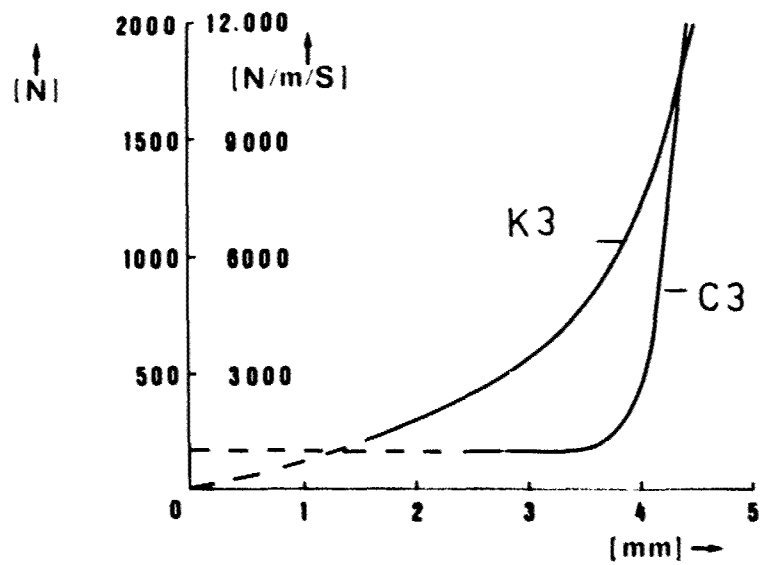


Fig. 6 . Spring- and damper characteristic of the spine between L 1 - S 1.

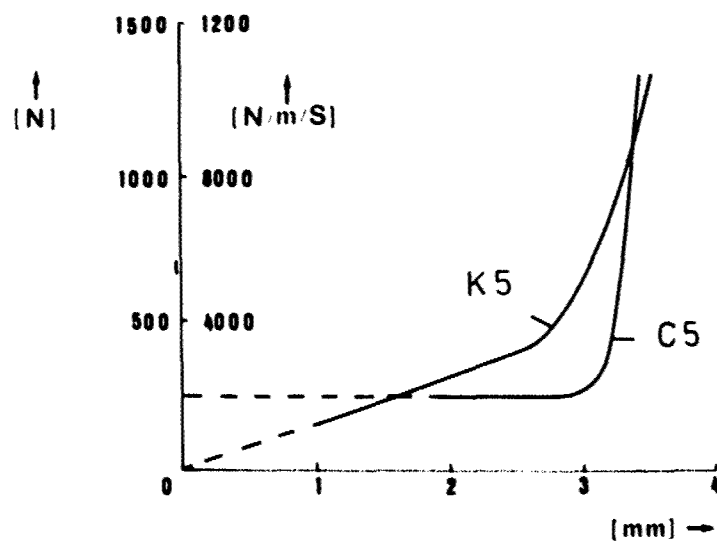


Fig. 7 . Spring- and damper characteristic of the spine between T 1 - T 12.

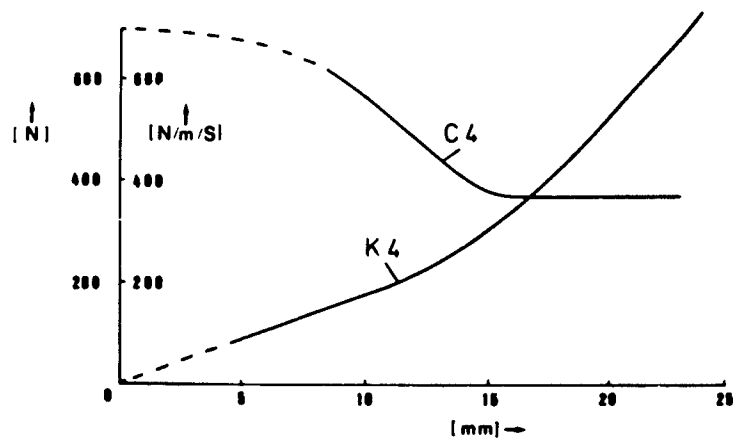


Fig. 8 . Spring- and damper characteristic of the abdomen.

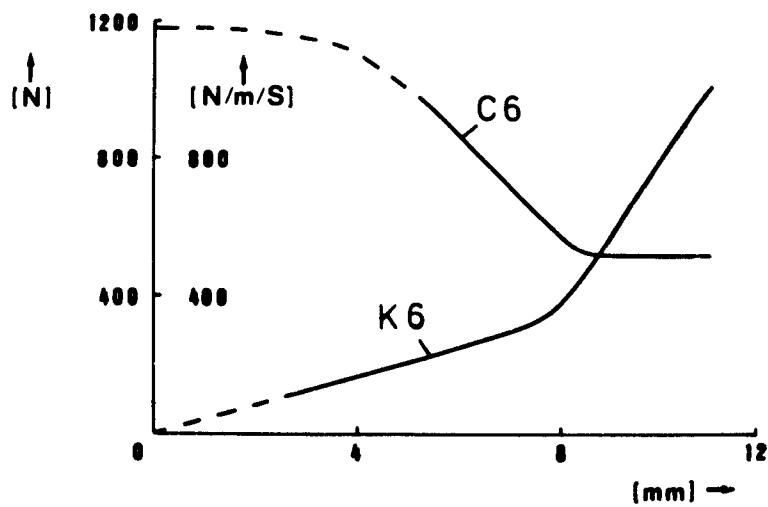


Fig. 9 Spring- and damper characteristic of the chest.

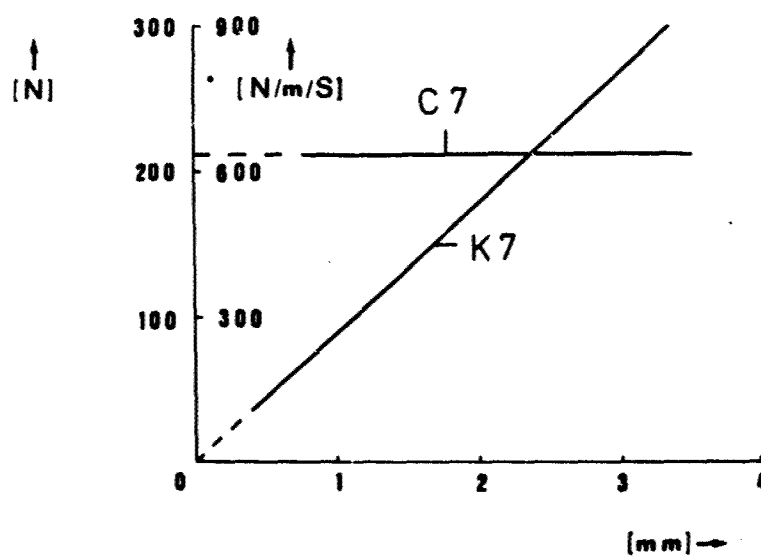


Fig. 10 . Spring- and damper characteristic of the head.

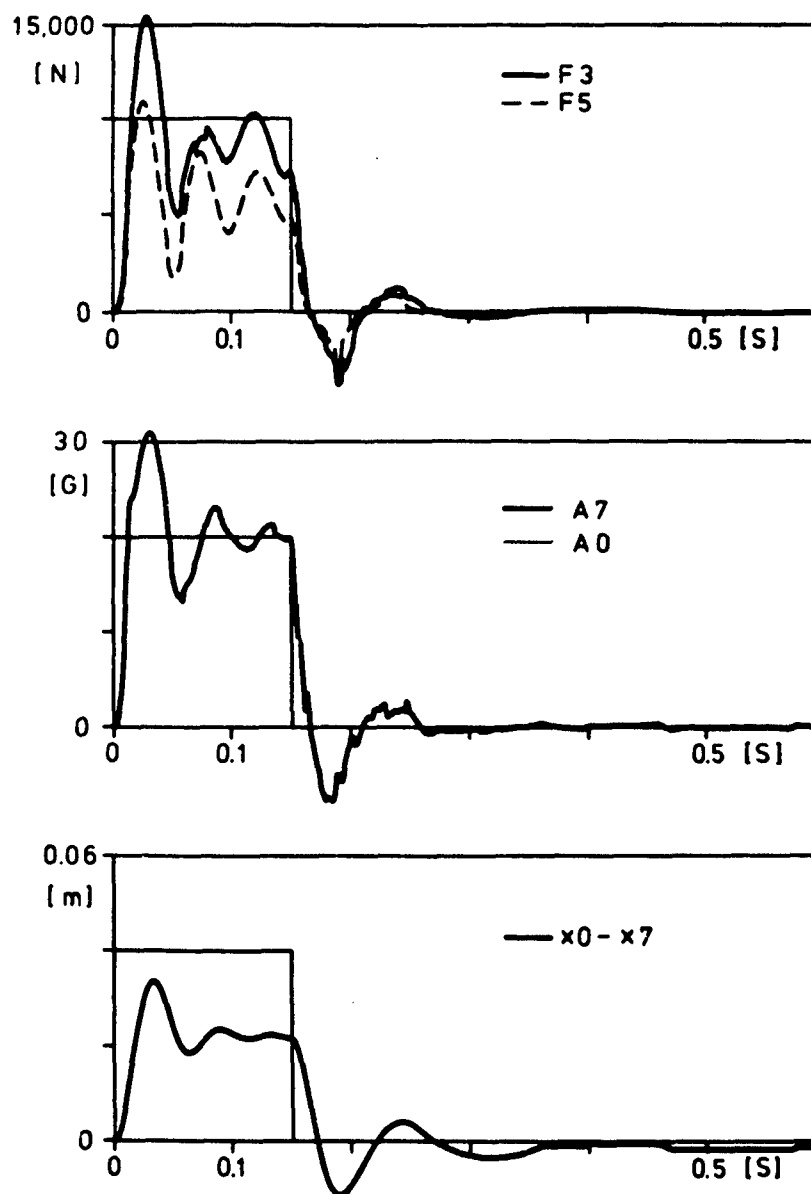


Fig. 11 . Rectangular pulse and model reaction.

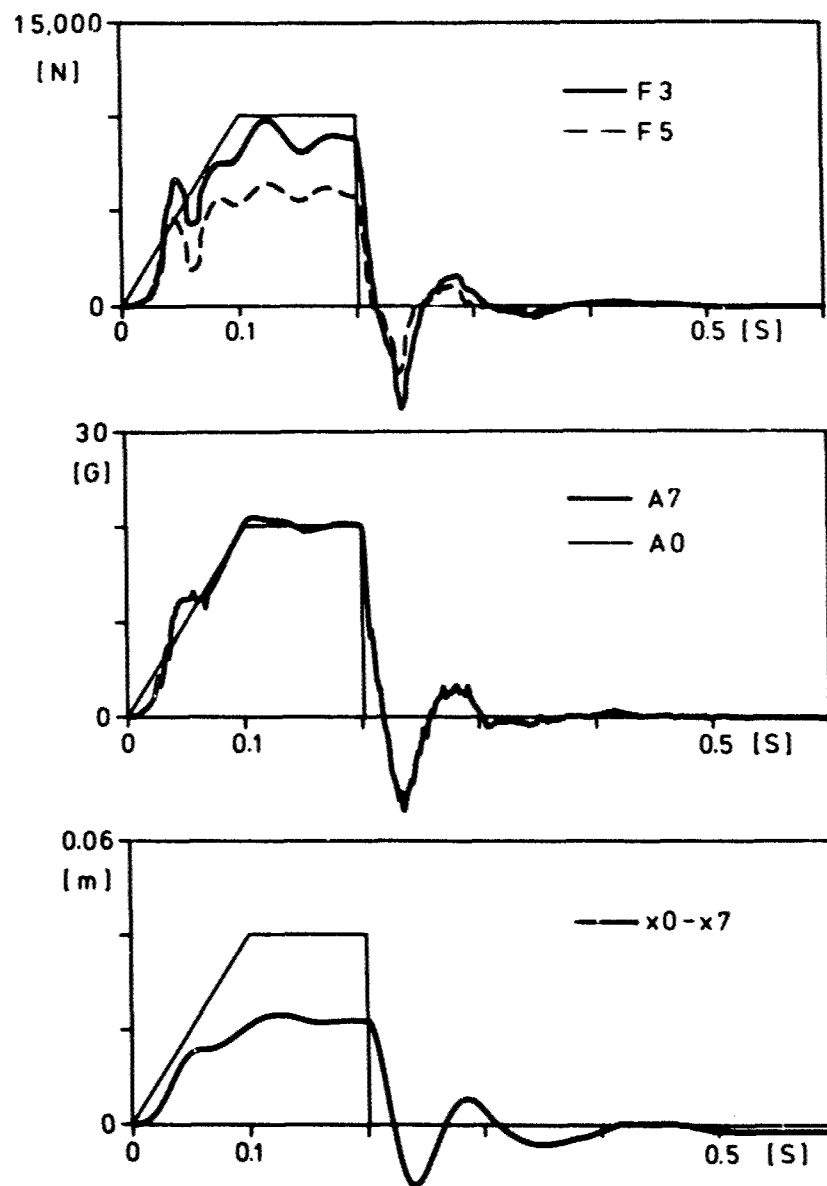


Fig. 12 . Trapezoidal pulse and model reaction.

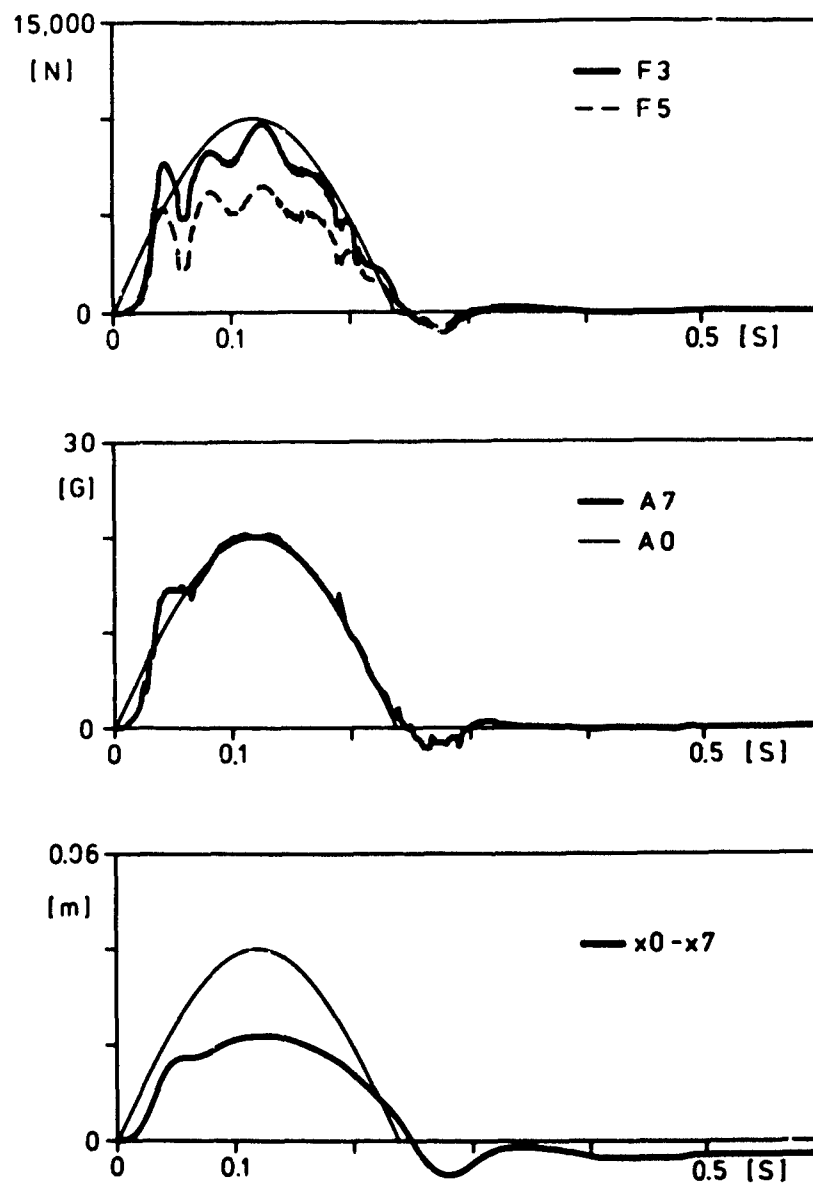


Fig. 13 . Half-sine pulse and model reaction.

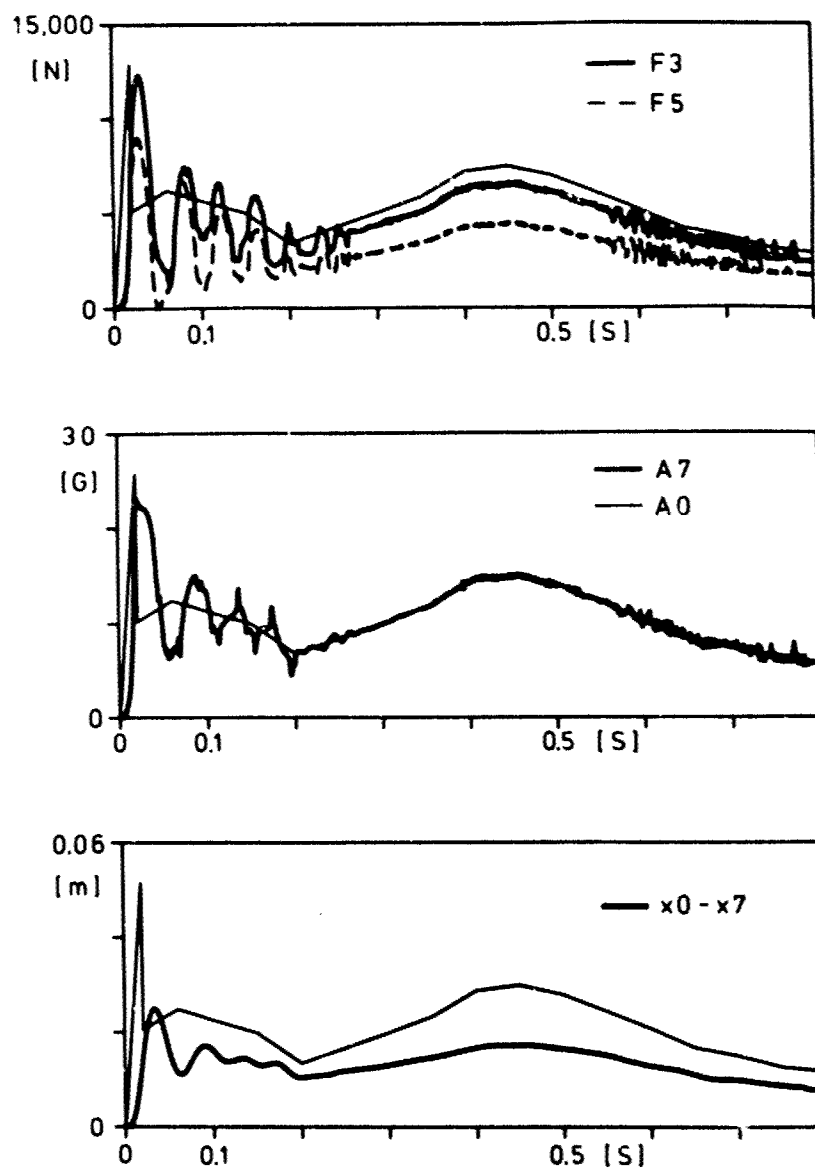


Fig. 14 . F 111 ejection seat pulse and model reaction.

G	M 1	K 1	C 1	f _d 1	ζ 1	M 2	K 2	C 2	K 3	C 3
/	kg	N/m	N/m/s	Hz	/	kg	N/m	N/m/s	N/m	N/m/s
1	15	47,966	678	8.25	0.40	10	250,000	4,000	200,000	1,000
2	15	171,139	1,154	15.86	0.36	10	600,000	5,000	1,000,000	1,000
3	15	191,865	1,119	17.00	0.33	10	1,000,000	8,000	1,500,000	3,000
4	15	225,175	1,029	18.72	0.28	10	2,000,000	10,000	1,800,000	10,000

G	M 4	K 4	C 4	f _d 4	ζ 4	K 5	C 5
/	kg	N/m	N/m/s	Hz	/	N/m	N/m/s
1	15	17,913	622	4.40	0.60	160,000	2,000
2	15	33,310	372	7.24	0.26	900,000	2,000
3	15	52,325	372	9.19	0.21	1,200,000	3,000
4	15	52,325	372	9.19	0.21	1,600,000	10,000

G	M 6	K 6	C 6	f _d 6	ζ 6	M 7	K 7	C 7	f _d 7	ζ 7
/	kg	N/m	N/m/s	Hz	/	kg	N/m	N/m/s	Hz	/
1	22	42,558	968	6.06	0.50	7	89,537	633	16.50	0.40
2	22	208,663	514	15.40	0.12	7	89,537	633	16.50	0.40
3	22	208,663	514	15.40	0.12	7	89,537	633	16.50	0.40
4	22	208,633	514	15.40	0.12	7	89,537	633	16.50	0.40

Table I

DISCUSSION

DR. VON GIERKE (USA)

Did you make a comparison of your model predictions with actual accidents?

AUTHOR'S REPLY

No, we compared the model's response to some drop test results. We found again that our model overemphasizes this very short duration pulse. So we have to change our model parameters to get the model response closer to reality.

DR. VON GIERKE (USA)

Are the drop test results data on subjective judgment of severity or are they on cadaver specimen?

AUTHOR'S REPLY

No, they were on living subjects. But these drop tests were not our own experiments; we got the data from the literature. As indicators they used the accelerations at the head.

DR. JEX (USA)

Your model as shown in the seated figure shows a separate mass for the leg as compared to the rest of the body; we would say, you have your thigh bone disconnected from your leg bone. That may be a satisfactory model for matching the impedance at the seat, but it cannot affect transmissibility to the head. Is that correct? The mass of the legs will vibrate in your model independently of the rest of the body?

AUTHOR'S REPLY

That is correct.

DR. VON GIERKE (USA)

But your combined mass adds up to the total mass of the body. That is the reason for your configuration?

AUTHORS REPLY

Yes.

SOME HUMAN RESPONSES TO REPEATED $+G_z$ PULSES

Edwin Hendler, Ph.D. and David C. Johanson, LTJG MSC USNR
 Life Sciences Division
 Aircraft and Crew Systems Technology Directorate
 Naval Air Development Center
 Warminster, PA 18974

SUMMARY

Six unprotected and relaxed subjects were exposed to haversine-shaped acceleration pulses while seated upright in a centrifuge and simultaneously performing a continuous tracking task and a discrete visual-motor response-time task. Twenty-five different acceleration pulses were used, resulting from all combinations of 1.5, 2.0, 2.5, 3.0, and 3.5 G_z levels and "0," 10, 20, 40, and 80 s plateau G_z durations ("0" s represents a pulse which momentarily peaked at one of the desired levels). Each subject made 5 successive runs a day, with each run containing a different acceleration pulse; each week of 5 test days therefore included all 25 pulses. The order of runs for weeks 1 and 3 were identical for each subject individually, and in weeks 2 and 4, the run order was reversed. The time of day when each subject was exposed was varied systematically. A run consisted of a 1 minute pre phase, an acceleration phase, three 1 minute recovery phases, and a 1 minute rest period. From the data collected, relationships were explored between the dependent variables (mean heart rate (MHR), mean respiration rate (MRR), mean tracking error (MTE), and mean response time (MRT)) with pulse level (G_z) and plateau duration (t) for the entire runs and for the individual phases of runs. Multiple regression equations were derived relating MHR and MTE to both G_z and t . Correlations between dependent variables were calculated, as were measures of relative variability. Changes induced in the dependent variables by the acceleration pulses declined to insignificant levels by the second minute of recovery. Pre phase values for each run across the 20 day test period showed changes in MRT and MTE which could be related to interruptions in the test program. Consistent within-day changes in pre-phase MTE were found, as well as indications of task trade offs. Only MHR showed a significant relationship to the impulse ($G_z \times t$) represented by the acceleration pulses. Finally, analyses of blood and urine were found to yield largely negative results, confirming the impression that the subjects recovered rapidly from any stress effects.

Introduction

Two years before his brother's first powered flight, Wilbur Wright pointed out that the inability of the pilot to "balance and steer" his aircraft constituted one of the chief obstacles to ushering in the age of flying machines (1). From the early days of World War II to the present, numerous studies have been conducted to establish human pilot dynamics and develop predictive models from which improved manual control elements can be specified. As pointed out recently (2), the influence of a multitude of potentially relevant variables must be established to permit accurate modeling. One category of key variables is pilot-centered, and is concerned with such factors as motivation and fatigue. The latter is of particular interest, since it is the term frequently employed by pilots in describing their reactions after engaging in air combat maneuvers in modern fighter aircraft.

It is the purpose of the present study, a part of which is described here, to quantify some of the physiological and performance responses of human subjects to repeated accelerations, so that the cumulative effects of such exposures may be determined, as well as the recovery times required to reverse any decrement that occurs. The first phase of this study represents an attempt to obtain baseline response measurements with relaxed and unprotected subjects exposed to single pulses of acceleration having various durations. In the second phase, emphasis will be directed to the effects of interval duration between successive acceleration pulses. Later phases will explore these relationships when higher G levels are employed, in conjunction with the use of protective measures, such as anti- G suits, performance of the M-1 maneuver, and supination of the supporting seat.

General

All tests were made using the Naval Air Development Center Dynamic Flight Simulator (DFS) facility. This facility consists essentially of a man-rated centrifuge having an arm 15.2 m long and a spherical gondola, about 3 m in diameter. The gondola is mounted within a two-gimbal system, so that controlled motions in pitch and roll can be applied to the test load. Disorientation and nausea, commonly experienced by persons riding centrifuges, but which are less common in actual flight maneuvers, are minimized in the DFS by proper gimbal movements relative to the resultant acceleration. Acceleration was measured by accelerometers mounted on the seat within the gondola to an accuracy of $\pm .05G$. A more complete description of this facility has been previously given (3, 4).

Subjects

Five young men who volunteered to participate in this study were selected from a group of volunteers on the basis of their ability to withstand an exposure to 3.5 G_z , while relaxed, without suffering loss of peripheral vision (greyout). The subjects were fully informed regarding the purpose of the study, the procedures to be followed, and the possible hazards involved. Despite the screening, it was necessary to replace one of the subjects (Subject 3) early in the series of runs with an alternate (Subject 6). Physical characteristics of the subjects are presented in Table 1. All subjects were trained under both static and dynamic conditions to perform the tasks described below until they approached stable levels of performance.

Subject Preparation

Each subject wore ECG electrodes on his chest and one or two doppler flowmeter transceivers over the temporal artery on one or both sides of his head. The flowmeters used were L&M Electronics, Inc. Directional Ultrasonic Flowmeters Model 1012; the transceiver was carefully positioned to obtain maximum signal strength, based upon an audible rendition of pulsatile blood flow. Clothing consisted of underwear, shoes, socks, and a light-weight coverall.

Work Space

A special articulating seat located within the gondola was adjusted so that the subject, when restrained with a standard Navy torso harness, could view a 13 cm black and white TV screen positioned about 86 cm directly in front of, and level with, the seat headrest. The seatback was fixed at an angle of 15 degrees back from the vertical. A two-axis, force-displacement sidearm controller mounted horizontally on the right arm rest, was used by the subject to perform the tracking task described below. A switch on the controller provided the subject with the option of stopping the centrifuge. Activation of a spring-loaded button on a hand grip located on the left arm rest extinguished a red light located at eye-level, 38 cm to the subject's left of the center of the TV screen. Continuous surveillance of the subject by the medical monitor and other observers was assured by the use of a TV camera, sensitive to both visible and infrared radiation, which was mounted in the gondola so that it provided a close-up image of the subject's face on externally located TV monitors. Two-way voice communication was maintained through a microphone positioned in front of the subject's lips, and a speaker mounted in the gondola close to the subject's head.

Ambient light levels within the gondola were subdued, and varied from a high of 3.2 ft-c at the subject's eye location to 0.8 ft-c behind the seat. The subjects were adapted to general light levels of about 9.6 log uul, for which an instantaneous threshold is estimated to have been about 8 log uul. The targets viewed by the subjects were at least 1.5 to 2 orders of magnitude above visual threshold levels, even with the changes in threshold calculated to have been induced during exposure to the maximum G level (5).

Performance Tasks

Two visual-motor tasks were simultaneously employed to assess performance capability. The first was a continuous tracking task, in which the subject manipulated the hand controller mentioned above to adjust the positions of two mutually perpendicular lines (needles) of an aircraft Attitude-Direction Indicator (ADI). An image of the ADI was displayed on the TV screen in front of the subject; the subject's task was to keep the needles crossed in the center of the display (null position). Both needles were continuously driven by the mixed input from three oscillators, set at 0.33, 0.14, and 0.09 Hz, respectively, so that the horizontal (x) needle moved vertically on the screen while the vertical (y) needle swept horizontally across the screen. The proportions of each of the frequencies applied to each of the needles were not the same. To the subject, the direction and magnitude of needle movements therefore appeared to be erratic and unpredictable. When either or both of the needles moved more than one-fourth of their full scale displacement from the null position (out of an unmarked area designated as the "target circle"), an electronic buzzer sounded. The intensity of sound was adjusted to be proportional to the distance of the needle cross point outside the boundary of the target circle, thereby alerting the subject to deteriorating performance. Manipulation of the hand controller not only determined the direction in which the needles moved, but also their rate of movement. Thus, when force was exerted on the controller to move it both back toward the subject and to his left, the x needle was displaced upward on the viewing screen and the y needle moved toward the subject's left. The rate of these needle movements was directly dependent upon the amount of force exerted by the subject when manipulating the hand controller. When the hand controller was not activated, the needle cross point remained outside the target circle about 82 per cent of the time; activation of the hand controller could result in the needle cross point remaining outside the target circle between 0 and 100 per cent of the time, depending upon the skill of the subject. During training, the amplitude of imposed needle displacements to be nulled by the subject was gradually increased over a period of days, from about 50 per cent of maximum to maximum, as the subjects learned to perform this task.

The second task consisted of extinguishing the red light already described, by depressing the button on the left hand grip as soon as possible after the light was seen. The light source was a light emitting diode covered with a transparent red filter. By pushing the button, the subject deactivated the light, set a random timer to one of eight possible positions which determined the duration of the "off" period, stopped an elapsed time counter and caused a printer to print out the elapsed time in milliseconds. The eight "off" periods ranged in 2 s intervals from a minimum of 100 ms to a maximum of 14.1 s.

Clinical

Each subject had received a complete physical examination prior to exposure to assure that he was qualified to participate in this study; in addition, he received extra pay for hazardous duty. Subjects were examined by the medical monitor (flight surgeon) before and after each exposure to acceleration runs. Blood and urine samples obtained before and after each day's runs for the first five days, and before the first and after the last run for each subsequent five day period, were quantitatively analyzed.

Experimental Design

Five acceleration levels (1.5, 2.0, 2.5, 3.0, and 3.5 G_x) were combined with five durations of plateau G_x level ("0," 10, 20, 40, and 80 s) to produce 25 different pulses. The plateau duration shown as "0" indicates the condition where the pulse peaked at one of the desired G_x levels, remaining at this level for a very brief period. Each of 5 subjects was exposed on a daily basis to 5 different pulses, so that all 25 pulses were experienced by all 5 subjects each day, and by any given subject, every 5 days. The sequence of pulse exposures for each subject was reversed every 5 days, so that each

subject experienced the same daily sequence of pulses during his first and third 5 day periods, and the reverse sequence on the second and fourth 5 day periods (Figure 2). For convenience, each 5 day period is referred to as a "week," although the test weeks and calendar weeks did not always coincide (see below). The total test period encompassed 20 days, or 4 weeks.

The components of a single run are diagrammed in Figure 1. In addition to the acceleration phases, a run included a one minute pre phase and three successive post minute phases. A rest period of 1 min separated one run from the next; five successive runs, each containing a different acceleration pulse, constituted each subject's daily exposure. The daily exposure order of the subjects was arranged so that a given subject was exposed at a different time of the day on successive days of the weeks. The acceleration phase included a 4 s onset and 4 s offset, applied to produce a haversine shape to the acceleration pulse. Between pulses, the centrifuge was rotated slowly (applying a load of 1.03 G_z to the subject) to eliminate any slight motion artifacts incidental to its being completely stopped and started.

Some deviations from the above design were necessary to accommodate unanticipated events. For example, run sequences planned for test days 1 and 2 of the first week were actually conducted on test days 14 and 15, following an 18 day interruption in the program. As previously indicated, subject 3 was removed early in the program and replaced with subject 6. Because of the unavailability of two subjects at planned times, subject S2 was exposed twice on the last test day and subject S5 was exposed twice on the 19th test day. At least five hours intervened between the first and second exposures for both these subjects. Of 500 runs planned, 472 were successfully completed (over 94 per cent).

Biopotential and Performance Data Collection and Analysis

Biopotential and performance data were recorded on a group of Brush, Mark 200, 8-channel strip chart recorders. Amplified ECG signals were not only recorded directly, but were also fed into a Hewlett-Packard Model 78201B Cardiometer or a Narco Bio-Systems Inc. Model BT-1200 Biotachometer to obtain measures of heart rate, in beats per minute. Average heart rate was recorded as pen deflections over selected intervals ranging from 4 s to 12 s. Signals from a thermistor attached to the lip microphone were recorded as indications of respiratory rate. Relative movements between the subject's mouth and the thermistor, especially during G, caused occasional degradation of this record. Both pulsatile and mean blood flow were recorded on separate channels.

On and off status of the response time light was recorded on the strip chart, and, in addition, response times to the nearest millisecond were printed out on paper tape using a Hewlett-Packard Model 5245L Electronic Counter and a Model 562A Digital Recorder. Six channels of recordings were dedicated to the tracking task: movements of the x and y needles from their null positions, per cent of time outside the target circle, and the integration of each of these over selected time intervals to indicate average values. Acceleration load in -G_z units was recorded on all strip charts.

In addition to acceleration load, ECG, average x and y tracking needle displacements, and pulsatile blood flow, a complete recording of all voice communications was made on FM magnetic tape.

Results

Tables 2, 3, 4, and 5 summarize the principal data collected and analyzed from Phase I of this study. The statistics of the samples shown for acceleration level and duration were derived from the complete runs containing acceleration pulses having the dimensions specified. The only statistics based upon samples drawn from the separate phases of the runs are labelled "phases." As expected, variation among subjects in all responses was rather marked. A comparison among subjects of the performance responses indicates that a reciprocal sort of relationship exists between scores on the two tasks. Those subjects showing higher scores on tracking error show relatively low response times, and vice versa.

The method of least squares was used to obtain the best fitting equations for the data in the tables cited (6). Both heart rate and tracking error showed regular increases with increasing plateau G_z level, while the relationship for response time appeared more complex. Equation (1) describes the relationship of mean heart rate (MHR) for the runs containing the various plateau G levels; equation (2) does the same for the corresponding standard error of the mean (SEM).

$$\text{MHR} = 78.90 + 1.32 G_z \quad (1)$$

$$\text{SEM}_{\text{MHR}} = 0.23 e^{0.30 G_z} \quad (2)$$

When values for MHR and SEM_{MHR} are extrapolated to the 1.03 G_z conditions existing during the pre phase, MHR differs by about 1.2 per cent from the value for MHR derived from measurements made during the pre phase. The SEM_{MHR} calculated by equation (2) differs from the SEM_{MHR} at 1.03 G_z by about 29 per cent. Corresponding equations for mean tracking error (MTE) are:

$$\text{MTE} = 20.21 e^{0.07 G_z} \quad (3)$$

$$\text{SEM}_{\text{MTE}} = 0.31 e^{0.24 G_z} \quad (4)$$

The value of MTE calculated from (4) for 1.03 G_z differs by 13.1 per cent from the measured value during the pre phase, while the calculated SEM_{MTE} value differs by 0.93 per cent from that measured.

The value for mean response time (MRT) at 3.5 G_z differs significantly from the values at all other G_z levels. In addition, the minimum value of MRT at 2.5 G_z also differs significantly from the values at all other G_z levels, except for that at 2 G_z. Values for mean respiration rate (MRR) at the various plateau G_z levels do not form any regular pattern, nor are the differences between these values statistically significant, when averaged across all phases of the runs. However, as shown later, values of MRR during the acceleration phase assume a definite pattern and are statistically different.

The relationships of the dependent variables to the durations of the plateau G_z levels, where duration in seconds is designated as t , may be expressed as follows:

$$\text{MHR} = 80.43 + 0.657 \ln t \quad (5)$$

$$\text{SEM}_{\text{HR}} = 0.44 + 0.025 \ln t \quad (6)$$

$$\text{MTE} = 25.42 - 0.57 \ln t \quad (7)$$

$$\text{SEM}_{\text{TE}} = 0.70 - 0.049 \ln t \quad (8)$$

A value of 1, for the shortest duration pulse, was used in deriving the last four equations. Differences between MRT values as functions of pulse duration were found to be non-significant. However, values of MRR with relation to the duration of plateau G_z do show a regular trend, which can be described by the following equation:

$$\text{MRR} = 16.88 - 0.22 \ln t \quad (9)$$

where t , as above, designates duration in seconds.

A significant positive correlation coefficient of 0.96 was calculated for MHR with MTE, when both dependent variables were viewed as functions of plateau G_z level; the sign of the coefficient changed, in accordance with the almost mirror image relationship between MHR and MTE as functions of plateau G_z duration. Although not statistically significant, the correlation coefficients for MHR and MRT showed the same sign reversal, while those for MRT and MTE did not. No significant correlation coefficients were found for MRR and the other dependent variables as functions of G_z level, but significant correlation coefficients were determined for MRR and MHR ($r = -0.95$) and for MRR and MTE ($r = 0.94$), as functions of plateau G_z duration.

As can readily be seen in tables 2, 3, 4, and 5, the values of all dependent variables increased quite markedly during the acceleration phase of the runs, as compared to the preceding and following phases. For MHR, values in the pre phase and the first post acceleration phase (+1) are significantly lower than the values in the second and third post acceleration phases (+2 and +3), while the latter do not differ significantly from each other. Two-way analyses of variance were made for each of the dependent variables on the effects of G_z level and plateau duration over the acceleration and post-acceleration phases. To normalize the data for the effects of differing initial values in the dependent variables, pre values were subtracted from those in the succeeding phases. Quite clear effects were evident during the acceleration phase for both G_z level and plateau duration for MHR and MTE. A significant difference in MRT was shown for G_z level, but not for plateau duration. In the first post acceleration minute, MHR continued to show significant differences for both G_z level and plateau duration of the preceding acceleration pulse, while MTE showed a significant difference for plateau duration only. None of the differences were significant by the post acceleration second and third minutes.

In order to compare the relative variability of the dependent variables, coefficients of variation, expressed as percentages (ratio of standard deviation to the mean, multiplied by 100) were calculated for each phase and are shown in table 5. Two facts are particularly evident from the figures in this table: first, the relatively great variability of the performance measures and respiration rate with respect to that of heart rate, and second, the marked increase of response time variability to acceleration. There is also a tendency for the variability during the first post acceleration minute to be somewhat greater than that in the succeeding periods.

Examination of changes in the dependent variables across all subjects, but limited to each phase of the run, shows more pronounced relationships with G_z plateau level and duration. These are shown in figures 3-6. Except for the obvious increase in the values of the coefficients given in the previous equations for the acceleration phase, the basic relationships remain the same. Of particular interest are the clear fall in MHR during the first minute of recovery above the 2.5 G_z level and in the 10 to 40 s duration interval, the increase in MTE from pre to post acceleration phases with G_z plateau level and duration, and the relatively erratic behavior of MRT over the G_z plateau level and duration ranges. Above 2.5 G_z , during the acceleration phase, both MRT and MRR show a very abrupt and rapid rise with increasing plateau G_z level. While MRT values for levels at and below 2.5 G_z are only slightly greater than corresponding pre and recovery phase values, MRR values at and below 2.5 G_z are appreciably greater during the acceleration phase than during all of the other phases.

Multiple regression equations were derived for MHR, MTE, and MRR during the acceleration phase:

$$\text{MHR} = 59.99 + 9.03 G_z + 3.44 \ln t, R^2 = 0.87 \quad (10)$$

$$\text{MTE} = 36.18 + 0.63 e^{G_z} - 3.31 \ln t, R^2 = 0.91 \quad (11)$$

$$\text{MRR} = 22.23 + 0.108 e^{G_z} - 1.516 \ln t, R^2 = 0.73 \quad (12)$$

The relatively high values of R^2 , especially for MHR and MTE, show that almost all the variation in the dependent variables is determined by the combined effect of G_z level and plateau duration. For MHR, MTE, and MRR, the percentages of explained variation accounted for by variations in G_z level are about 55, 57, and 32, respectively, while the percentages of explained variation accounted for by variations in plateau duration are about 45, 43, and 73, respectively.

Mean pre-phase values of the dependent variables were studied for each run over the twenty day test period. The values for MHR shown in Figure 7 reveal no consistent pattern either within runs or across days. A comparison was made of MHR for each subject's daily exposure of five runs with his second exposure to the same run sequence, generally about ten test days later. The mean differences (first run minus second run) between run pairs were calculated for each daily exposure and are plotted in Figure 8. MHRs during the second exposures were generally somewhat lower than those of the first;

however, as is evident in the figure, the line of no difference (0) is included within the 95 per cent confidence interval. A non-significant regression coefficient ($b = 0.37$) was calculated when an attempt was made to fit a straight line to the data, and r^2 was only 0.017. For MRT, however, although no consistent within-days patterns are evident, certain changes across the days of testing are worthy of note (Figure 9). MRT increases from day 4 to day 8 and then shows a general decreasing trend over the next 6 days. In addition, the daily range of pre-phase values (which is far greater than that for MHR and MTE) is reduced from day 14 to day 19. Pre-phase values for MRR seem to lie, for the most part, either at a lower or a higher level, with relatively few values between (Figure 10). No consistent daily trend in respiration rate is evident among runs. Pre-phase MRR decreases somewhat progressively over the first four days and from days 14 to 16; in both instances, a shift from the low level reached to the higher level occurs abruptly. The most consistent within-day patterns are seen in Figure 11 for MTE. In 19 out of 20 days, the score for tracking error before the first acceleration pulse is higher than that preceding the second pulse. The distribution of tracking error scores among the daily runs is also noteworthy: the highest error scores occur most often in the first and fourth runs ($p < .001$, when evaluated by the chi-square test), while the lowest error scores occur most often in the third and second runs ($p < .05$). The trend across days for MTE shows some oscillations, and interestingly, these appear to be in the opposite direction to those for MRT.

An attempt was made to relate dependent variable changes occurring across entire runs, and during the acceleration phase only, to the amount of impulse (G multiplied by duration, or I) contained in the acceleration pulses. Only for MHR could a linear relationship be established; for the entire run,

$$\text{MHR} = 81.16 + 0.013 I \quad (13)$$

where the t test of the regression coefficient is significant at the $.02 < p < .05$ level, and r^2 is equal to 0.17; for the acceleration phase alone,

$$\text{MHR} = 82.534 + 0.089 I \quad (14)$$

Here the t test of the regression coefficient is very highly significant at the $p < .001$ level, and r^2 equals 0.55.

Measures made on blood and urine (Figure 12) were essentially negative, except for an occasional value which exceeded the normal limits. The serum of subject 6 showed values of alkaline phosphatase which were appreciably above normal, but further tests failed to show any liver or bone disease and the subject appeared otherwise asymptomatic.

In addition to these measures, 24 hour urine samples collected at the end of the study were examined for indicators of anoxic and anxiety stress (7). Subject 6 excreted relatively large amounts of one of these indicators (phenolic acids) which exceeded previously established normal limits. Subject 5 just exceeded the normal limit for urinary phenolic acids. Values of the other two indicators, free radicals and lipid peroxides, were normal for both subjects. The overall results were interpreted as indicating no residual stress in the subjects who participated in the test program.

Discussion

An attempt to construct a useful model of a dynamic system should begin with some knowledge of how that system responds when disturbed by an external force under reasonably controlled conditions. The system response of interest, in the present case, consists of the human operator's ability to perform two simultaneous psychomotor tasks while being subjected to a transient change in the force field of the environment. It was of interest here to determine the nature and duration of the effect on the system produced by an external force. The disturbance of the external force on the system was assumed to be related to both its magnitude and its duration. There is ample evidence (8) to show that the rate of force application also plays a critical role in determining the cardiovascular response of the human operator, which, in turn, may be expected to influence his ability to perform both simple and complex tasks. Although the rate of force application is controllable over a very wide range (up to 10 G/s with the NADC Dynamic Flight Simulator), a haversine-shaped acceleration pulse was chosen in which the onset and offset times remained constant at 4 s. Past experience had demonstrated that most subjects were able to tolerate acceleration pulses of this shape with less disorientation and kinesthetic illusions than was the case for pulses of other shapes, particularly those in which the rate of acceleration changed abruptly. Many experienced fighter pilots attribute their adverse reactions to "rides" on centrifuges as being partly due to their lack of control over the rate and magnitude of the applied G loads.

The most widely known effects of $+G_z$ on human operators consist of a decrease in blood flow to the head and eye and impairment of bodily movements. For example, Keighley, Clark, and Drury (9) showed that for levels between 3.4 and 4.8 G_z , there was a small but significant reduction in the threshold for visual flicker fusion frequency; no changes in this threshold were measured at up to 3.2 G_z . At very low luminance levels, White (5) found that the visual threshold for signal light intensity increased with increasing G load at levels up to 4 G_z . For higher light intensities, on the other hand, Rogge (10) found the blackout G level to be essentially independent of the luminance of the central light. Brightness discrimination thresholds were shown to increase with increasing G_z levels by Braunstein and White (11) and Chambers (12). White and Jorve (13) described a decrease in visual acuity with increasing G_z levels, and White later (14) showed this effect to be enhanced at low luminance levels. Error in reading dials was shown to increase with increasing levels of $+G_z$, particularly at lower luminance levels (15). Simple and complex reaction times to visual stimuli also increased under $+G_z$ conditions (16), as did tracking error (17).

As already pointed out, the intensity of the stimulus light used in this study to measure response time and the intensity of the tracking display were adjusted to sufficiently high levels to preclude conditions where visual impairment would be expected to play a significant role at the applied G_z levels. At the same time, only relatively small movements of the finger of the left hand and of the right hand

and wrist were required to perform the assigned tasks. Both arms were fully supported by the seat arm rests and constrained to prevent any significant lateral displacements.

The similarities of the relationship of both MTE and MRR with duration of plateau G_z are obvious from the highly significant positive correlations they show with each other, and the highly significant negative correlations they both show with MRR. The positive correlation between MRR and MTE as functions of G_z level has also been reported by Bowman and von Bockh (18) for much higher levels of complex acceleration patterns simulating those encountered in air combat maneuvers.

In centrifuge runs reaching 3, 3.5, and 4 G_z levels, for durations of 15 s, and at onset rates slower than those described in this paper, Browne and Fitzsimons compared the heart rates of experienced centrifuge riders and novices (19). Using equation (10), predicted values of MRR were calculated for comparison with the consistently higher average heart rates reported by Browne and Fitzsimons. For the experienced riders, percentage differences between reported and predicted values are, 3 G_z : 0.63%, 3.5 G_z : 20%, 4 G_z : 8.1%; corresponding percentage differences for the novices are: 3 G_z : 25%, 3.5 G_z : 26%, and 4 G_z : 23%. In spite of the many differences in experimental conditions described by Browne and Fitzsimons and those reported here, it is interesting that for their experienced subjects, a good fit was obtained at 3 G_z and a fair fit at 4 G_z . The large discrepancy at 3.5 G_z represents a deviation from the linear relationship between MRR and G_z level which our data support. Of course, any appreciable efforts exerted by the subjects, especially experienced ones, to counteract the effects of higher G_z loads, would be expected to result in higher heart rates.

Although no systematic measures were made in our study of heart rate outside of the test environment, it has been shown that subjects seated in a centrifuge have increased heart rates before being exposed to G loading. This increase has been attributed by Webb (20) to psychic stimulation resulting from anticipation of impending G loads; it occurs even in experienced centrifuge riders and is greater when higher G loads are expected. Webb's subjects had control heart rates which averaged 94 ± 14 beats per minute and rose to an average of 101 ± 21 beats per minute immediately prior to 3.8 G_x runs. Assuming that the same proportional change in MRR occurred during the pre period for our subjects, control heart rates would have averaged about 73 beats per minute, a not unreasonable mean resting level for healthy young men.

All of the evidence seems to indicate that even though the relaxed and unprotected subjects participating in this study were exposed to substantial levels and durations of acceleration, both physiological and performance recovery occurred primarily within the first minute following G exposure. The ability to detect differences depends not only on the mean values of the dependent variables, of course, but also on their relative variability. The most erratic response by the subjects occurred during the acceleration phase on the task of extinguishing the lateral light. Apparently, the tracking task required so much additional effort during this phase of the runs, that the subjects devoted more of their available resources to tracking and less to responding to the light. However, within the first minute following the end of the acceleration period, the subjects were performing at a level of stability about equal to that in the pre phase. Small but non-significant changes in variation in all the dependent variables continued into the succeeding phases.

The decrease in MRR after exposure to 3 and 3.5 G_z pulses in the first minute of recovery may be evidence of a bradycardia reflex effect which is too weak and transient to be apparent at the lower acceleration levels. Almost the opposite effect, but more attenuated, occurred with increasing acceleration plateau durations. Recovery of MTE seems to have occurred across most plateau G_z levels and durations during the first two post acceleration minutes. Increased levels of MTE during the third minute may have resulted from fatigue. The tracking task required considerable effort, and since it was continuous throughout the run, no relief was provided until the rest period intervened. Some of the subjects were observed to slump forward during rest periods, with head bowed and eyes closed.

The level of 2.5 G_z seemed to act as a threshold load for MRT and MRR during the acceleration phase. At and below 2.5 G_z there were no marked changes in response with G_z level, while above 2.5 G_z there were dramatic increases. Perhaps this response was similar to that for the flicker fusion response cited earlier. Values of MRT during the acceleration phase, at and below the 2.5 G_z level, were only slightly greater than MRT values for the other phases; however, over the same range of G_z levels, values of MRR during the acceleration phase were about 20 per cent greater than those of the other phases. MRT responses to the duration of applied pulses also appears to have been dichotomous, with the shorter duration pulses associated with longer response times and the longer duration pulses (40 and 80 s) associated with shorter response times. This kind of relationship suggests an adaptation response; for the longer duration pulses, the subject has more time to adapt to the imposed conditions. Performance on the tracking task clearly shows this effect and so does respiration rate. Heart rate, over which the subjects had no direct voluntary control, did not show this compensatory behavior with time. Perhaps the relative stability of heart rate, when compared to that of the other dependent variables, is also linked to its isolation from direct voluntary control.

A comparison of pre phase MRT and MTE values for each run and test day (Figures 9 and 11) reveals the type of trade off behavior in performance described by Norman (21). Peaks of MRT accompany valleys in MTE, indicating the reciprocal sort of relationship mentioned earlier with respect to the performance of the individual subjects. The rise in MRT from the 4th test day to the 8th test day, with the concurrent decrease in MTE, may represent a continued learning period on the tracking task, at the expense of performance on the response time task. Similar patterns of lesser magnitude occur in both dependent variables at later times. Of particular interest is the increase in MTE on day 14, after an 18 day interruption in the test program. Following the pattern just described, while MTE increases, MRT falls. MTE would be expected to increase, since some retraining occurred as proficiency was being regained. The fact that tracking error scores were somewhat higher on the first run of each day indicates the adverse effects of even relatively short lapses in performing this complex task. By the fourth run of the day, it is likely that the subjects were experiencing fatigue or boredom, which then was somewhat dissipated on the last run in their anticipation of being released from the experimental situation.

It should prove challenging in future phases of this study to test the applicability of the multiple regression equations which have been presented. For example, it will be interesting to see if G_z level and plateau duration continue to exert about equal effects on MHR and MTE, when more than a single acceleration pulse is applied. It will also be of considerable interest to find if the relationships between the variables established during this first phase will continue to hold at higher G_z levels.

References

1. McFarland, M. W.: The Papers of Wilbur and Orville Wright, Vol. 1, McGraw-Hill Company, New York, 1953, pp 90-100.
2. McRuer, D. T. and E. S. Krendel: Mathematical Models of Human Pilot Behavior, AGARDograph 188, Advisory Group for Aerospace Research & Development, NATO. Technical Editing and Reproduction Ltd. London, 1974.
3. Crosbie, R. J.: Directional control of accelerative forces in centrifuge by system of gimbals. J. Aviation Med. 27:505-511, 1956.
4. Gell, C. F.: Descriptive catalog of aerospace medical biodynamics facilities in the United States and Canada. In: Principles of Biodynamics Applicable to Manned Aerospace Flight - Prolonged Linear and Radial Acceleration. AGARDograph No. 150. North Atlantic Treaty Organization, Advisory Group for Aerospace Research & Development, Chap. 5, 1971.
5. White, W. J.: Variations in absolute visual thresholds during acceleration stress. WADD Tech. Report 60-34, April 1960, Wright Air Development Division, Air Research & Development Command, USAF, Wright-Patterson Air Force Base, Ohio.
6. Steel, R. G. D. and J. H. Torrie: Principles and Procedures of Statistics, McGraw-Hill Book Company, Inc., New York, 1960.
7. Polis, B. D.: Molecular determinants for the prediction and survival of ischemic anoxic stress pathology. AGARD Conference Preprint No. 231, October, 1977.
8. Stoll, A. M.: Human tolerance to positive G as determined by the physiological endpoints. J. Aviation Med. 27:356-367, 1956.
9. Keighley, G., W. G. Clark and D. R. Drury: Flicker fusion frequency measurements on man subjected to positive acceleration on a human centrifuge.
10. Rogge, J. D.: Relation of signal light intensity to physiologic end points during +G_z acceleration. SAM TR 68-38, School of Aviation Medicine, Brooks AFB, Texas, 1968.
11. Braunstein, M. L. and W. J. White: Effects of acceleration on brightness discrimination. J. Opt. Soc. of Amer. 52:931-933, 1962.
12. Chambers, R. M.: Operator performance in acceleration environments. In: Unusual Environments and Human Behavior, N.M. Burns, R.M. Chambers, and E. Hendler (Eds.). Collier-Macmillan Limited, London, Chap. 7, 1963.
13. White, W. J. and W. R. Jorve: The effects of gravitational stress on visual acuity. WADC TR 56-247 (AD 110 444), Wright Air Development Center, Wright-Patterson AFB, Ohio, 1956.
14. White, W. J.: Acceleration and vision. WADC TR 58-333, Wright Air Development Center, Wright-Patterson AFB, Ohio, 1960.
15. White, W. J.: Quantitative instrument reading as a function of illumination and gravitational stress. J. Engineer. Psychol. 3:127-133, 1962.
16. Canfield, A., A. L. Comrey, and R. C. Wilson: Study of reaction time to light and sound as related to increased positive radial acceleration. J. Aviation Med. 20:350-355, 1949.
17. Fletcher, D. E., C. C. Collins, and J. C. Brown: Effects of positive acceleration upon performance of an air-to-air tracking task. J. Aviation Med. 29:891-897, 1958.
18. Bowman, J. S. and H. J. von Beckh: An integrated dynamic approach in physiologic and performance measurements in simulated airborne combined stress environments. Preprints of Scientific Program. Aerospace Med. Association, 1977, pp 69-70.
19. Browne, M. K. and J. T. Fitzsimons: Electrocardiographic changes during positive acceleration. Institute of Aviation Med. RAF Flying Personnel Research Committee. FPRC 1009, June 1957.
20. Webb, M. G.: Some effects of acceleration on human subjects. J. Aviation Med. 29:879-884, 1958.
21. Norman, D. A.: On data-limited and resource limited processing. Cognitive Psychology 7:44-64, 1975.

Table 1. Characteristics of Volunteer Subjects

<u>Subject Designation</u>	<u>Age (Yrs.)</u>	<u>Wt. (Lbs.)</u>	<u>Ht. (Ins.)</u>	<u>Prior G Experience</u>
1	19	144	67	No
2	25	114	71	Yes
3	23	165	68	Yes
4	23	140	70	Yes
5	27	200	68.5	Yes
6	27	133	67.5	Yes

Table 2. Heart rate in beats per minute

		MEAN	S.D.	N	95% C.I.	
					UPPER	LOWER
SUBJECT	S1	89.8	9.3	500	90.6	89.0
	S2	79.9	11.1	500	80.8	78.9
	S3	83.6	8.5	87	85.4	81.8
	S4	80.5	12.4	487	81.6	79.4
	S5	76.6	7.5	450	77.3	75.9
	S6	84.1	8.4	300	85.1	83.2
ACCELERATION LEVEL (G)	1.5	80.8	8.1	465	81.5	80.1
	2.0	81.6	8.8	460	82.4	80.8
	2.5	82.2	10.0	465	83.1	81.3
	3.0	82.7	12.1	470	83.8	81.6
	3.5	83.5	14.5	464	84.8	82.2
PHASE	PRE	79.3	9.5	466	80.1	78.4
	ACC	91.8	13.1	466	93.0	90.7
	+1	79.0	8.9	464	79.8	78.2
	+2	80.3	8.2	464	81.0	79.6
	+3	80.5	8.5	464	81.3	79.7
DURATION (S)	0	80.5	9.6	465	81.3	79.6
	10	81.9	10.6	462	82.9	80.9
	20	82.3	11.1	465	83.4	81.3
	40	82.8	11.1	465	83.8	81.8
	80	83.4	12.2	467	84.5	82.3
WEEK	1	83.4	10.7	552	84.3	82.6
	2	82.2	11.9	525	83.2	81.2
	3	81.7	11.2	625	82.6	80.9
	4	81.5	10.1	622	82.3	80.7

Legend:

S.D. = Standard Deviation
 N = Number
 C.I. = Confidence Interval

Table 3. Percentage of time outside of target circle while tracking

SUBJECT		MEAN	S.D.	N	95% C.I.	
					UPPER	LOWER
	S1	21.1	10.4	498	22.0	20.2
	S2	30.8	11.9	500	31.8	29.7
	S3	30.0	13.9	111	32.6	27.4
	S4	21.1	9.9	485	22.0	20.3
	S5	15.4	9.2	447	16.3	14.6
	S6	32.6	11.4	250	34.0	31.2
ACCELERATION LEVEL (G)	1.5	22.5	9.8	458	23.4	21.6
	2.0	23.0	10.3	453	23.9	22.0
	2.5	23.6	11.7	459	24.7	22.5
	3.0	24.1	13.0	462	25.2	22.9
	3.5	25.8	15.8	459	27.3	24.4
PHASE	PRE	19.1	8.4	461	19.9	18.3
	ACC	37.1	16.1	453	38.6	35.6
	+1	20.8	8.9	459	21.6	20.0
	+2	20.4	8.1	459	21.1	19.7
	+3	21.7	8.3	459	22.5	20.9
DURATION (S)	0	25.3	14.6	457	26.7	24.0
	10	24.3	13.3	456	25.7	23.3
	20	23.3	12.3	458	24.6	22.3
	40	22.9	10.6	458	24.0	22.1
	80	23.1	10.3	462	24.0	22.2
WEEK	1	26.8	13.1	544	27.9	25.7
	2	23.9	11.8	500	24.9	22.9
	3	23.0	12.8	625	24.0	22.0
	4	21.8	11.1	622	22.7	20.9

Legend:

S.D. = Standard Deviation
 N = Number
 C.I. = Confidence Interval

Table 4. Response time in seconds

SUBJECT		MEAN	S.D.	N	95% C.I.	
					UPPER	LOWER
	S1	0.721	0.158	498	0.735	0.707
	S2	0.760	0.430	498	0.798	0.722
	S3	0.799	0.872	87	0.982	0.616
	S4	1.045	0.708	475	1.109	0.981
	S5	0.984	0.444	443	1.025	0.943
	S6	0.701	0.191	300	0.723	0.679
ACCELERATION LEVEL (G)	1.5	0.843	0.397	461	0.879	0.807
	2.0	0.816	0.509	456	0.863	0.769
	2.5	0.796	0.299	463	0.823	0.769
	3.0	0.848	0.429	460	0.887	0.809
	3.5	0.932	0.706	461	0.996	0.868
PHASE	PRE	0.804	0.336	461	0.835	0.773
	ACC	1.002	0.848	453	1.080	0.924
	+1	0.814	0.340	463	0.845	0.783
	+2	0.806	0.323	463	0.835	0.777
	+3	0.814	0.355	461	0.846	0.782
DURATION (S)	0	0.842	0.519	449	0.889	0.801
	10	0.863	0.496	460	0.911	0.821
	20	0.864	0.567	465	0.916	0.822
	40	0.835	0.422	464	0.878	0.808
	80	0.831	0.428	463	0.873	0.797
WEEK	1	0.805	0.403	539	0.839	0.771
	2	0.991	0.615	521	1.043	0.937
	3	0.834	0.442	621	0.869	0.799
	4	0.777	0.459	620	0.813	0.741

Legend:

S.D. = Standard Deviation
 N = Number
 C.I. = Confidence Interval

Table 5. Respiration rate in breaths per minute

SUBJECT		MEAN	S.D.	N	95% C.I.	
					UPPER	LOWER
SUBJECT	S1	14.9	11.3	500	15.9	13.9
	S2	14.5	6.0	475	15.1	14.0
	S3	15.1	6.3	85	16.5	13.8
	S4	20.0	7.8	487	20.7	19.3
	S5	17.7	5.7	450	18.2	17.2
	S6	14.2	6.5	298	15.0	13.5
ACCELERATION LEVEL (G)	1.5	16.7	11.8	460	17.8	15.6
	2.0	15.9	6.6	455	16.5	15.3
	2.5	16.0	6.5	458	16.6	15.4
	3.0	16.6	7.2	465	17.2	15.9
	3.5	16.7	7.4	457	17.4	16.0
PHASE	PRE	16.0	11.1	460	17.0	15.0
	ACC	19.8	9.3	459	20.7	19.0
	+1	15.1	6.1	458	15.7	14.6
	+2	15.5	5.9	459	16.0	14.9
	+3	15.4	6.0	459	16.0	14.9
DURATION (S)	0	16.9	7.9	460	17.6	16.2
	10	16.8	11.9	453	17.9	15.7
	20	16.3	6.8	460	16.9	15.7
	40	15.9	6.5	460	16.5	15.3
	80	16.0	6.4	462	16.6	15.4
WEEK	1	16.6	6.3	600	17.1	16.1
	2	18.1	6.4	500	18.7	17.6
	3	14.9	7.4	623	15.4	14.3
	4	16.3	11.1	572	17.2	15.4

Legend:

S.D. = Standard Deviation

N = Number

C.I. = Confidence Interval

Table 6. Coefficients of Variation for
Dependent Variables (in per cent)

PHASE	MHR*	MRT**	MTE***	MRR****
Pre	11.93	41.67	43.96	35.75
Accel.	14.30	84.63	43.29	46.69
Post 1	11.33	41.77	42.83	40.24
Post 2	10.25	40.07	39.87	38.29
Post 3	10.61	43.61	38.44	38.89

* Mean Heart Rate

** Mean Response Time

*** Mean Tracking Error

**** Mean Respiration Rate

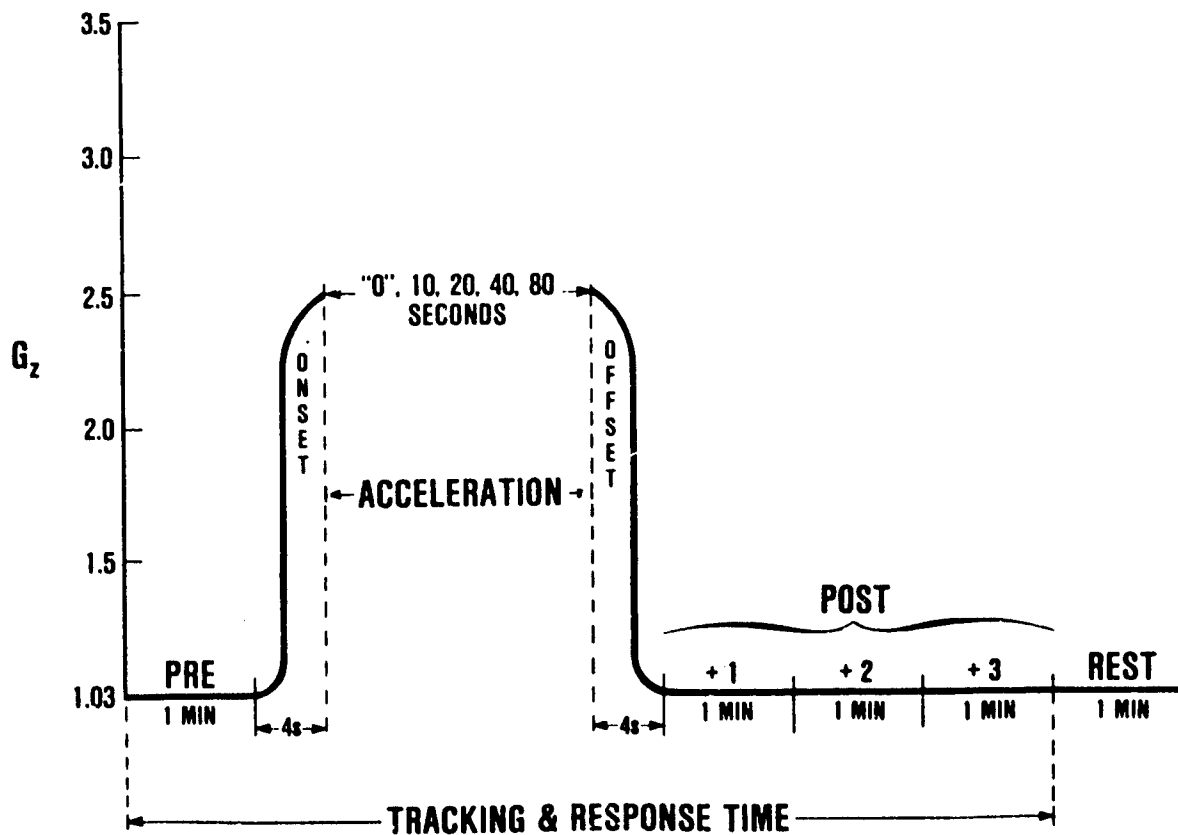


Figure 1. Diagram of a run.

WEEKS 1 AND 3					
WEEKS 2 AND 4					
G _z	1.5	2.0	2.5	3.0	3.5
DAY 1	"0"	10	20	40	80
DAY 2	10	20	40	80	"0"
DAY 3	20	40	80	"0"	10
DAY 4	40	80	"0"	10	20
DAY 5	80	"0"	10	20	40

SEQUENCE OF RUNS FOR SUBJECT 1
(MATRIX SHOWS PLATEAU G_z DURATION IN SEC)

Figure 2. Scheme for daily and weekly run sequences for one subject.

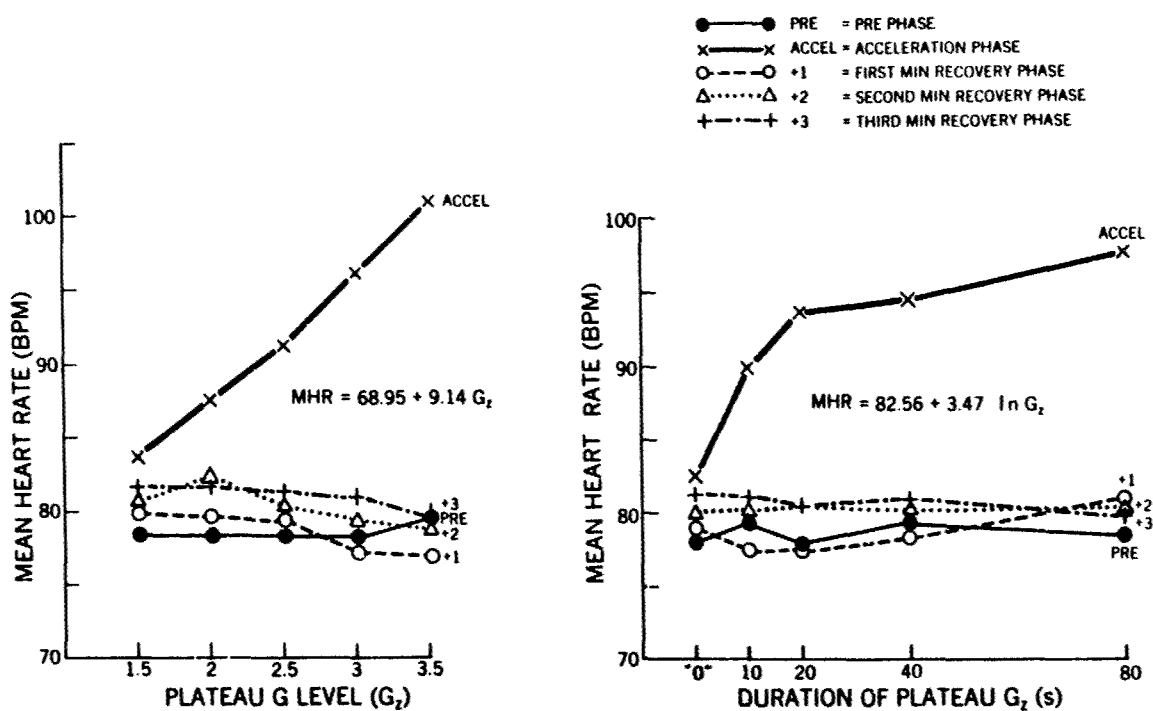


Figure 3. Mean heart rate during each phase of the runs.

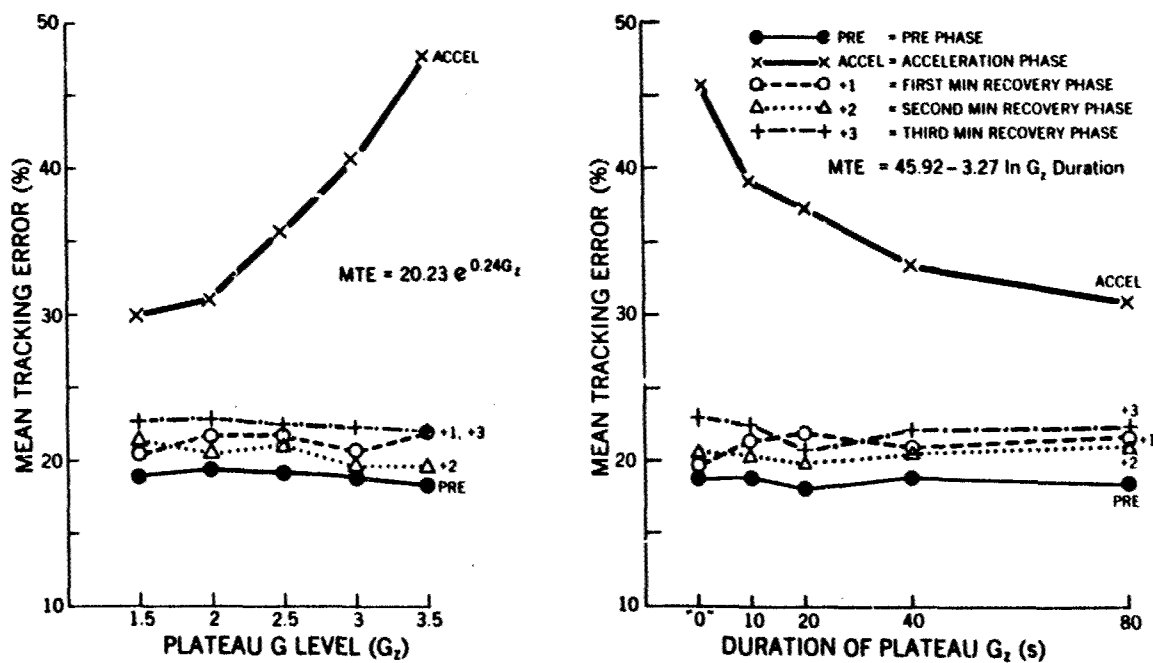


Figure 4. Mean tracking error during each phase of the runs.

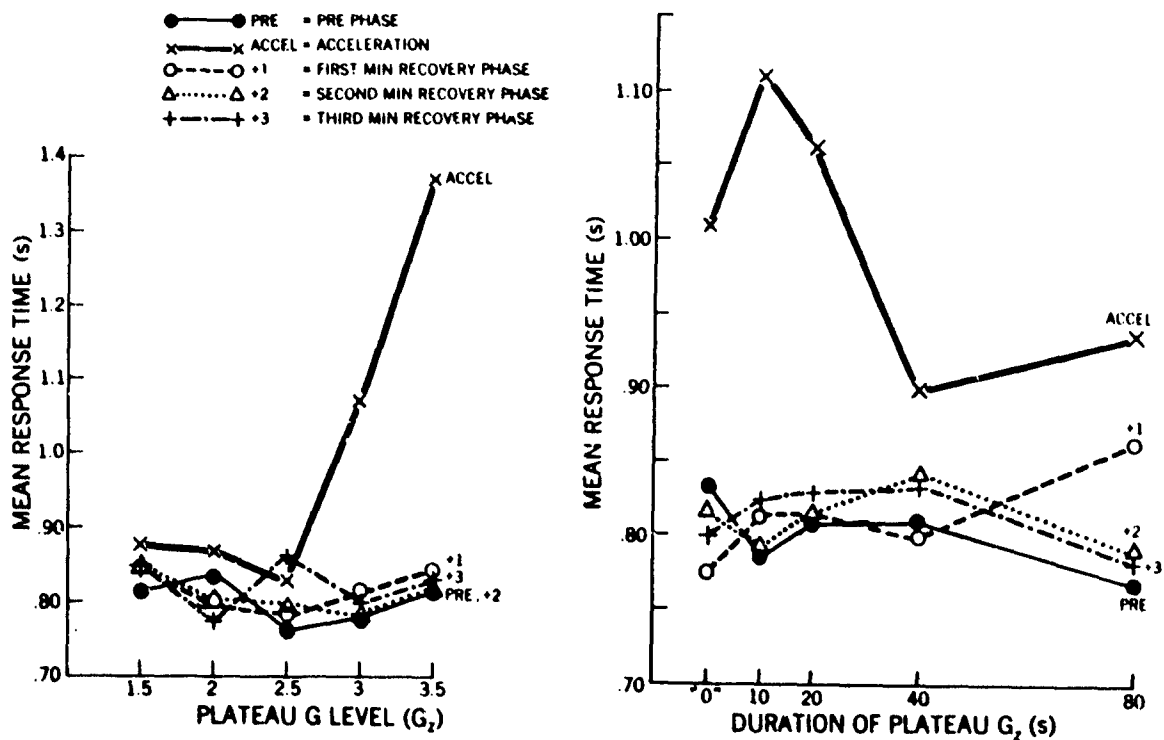


Figure 5. Mean response time during each phase of the runs.

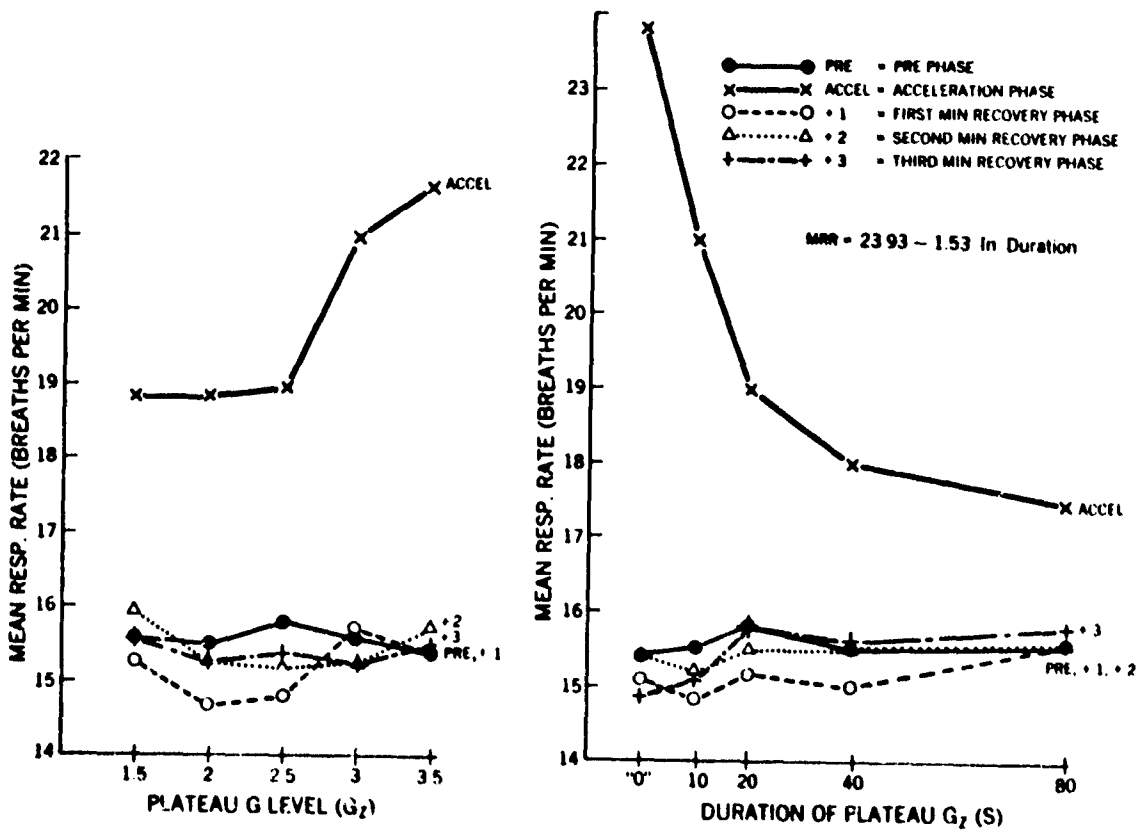


Figure 6. Mean respiration rate during each phase of the runs.

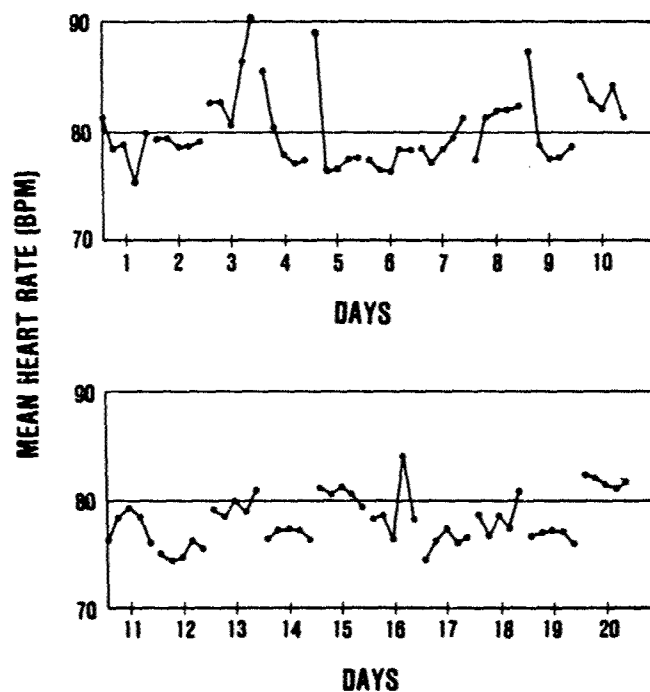


Figure 7. Pre-phase mean heart rates for each run and each day.

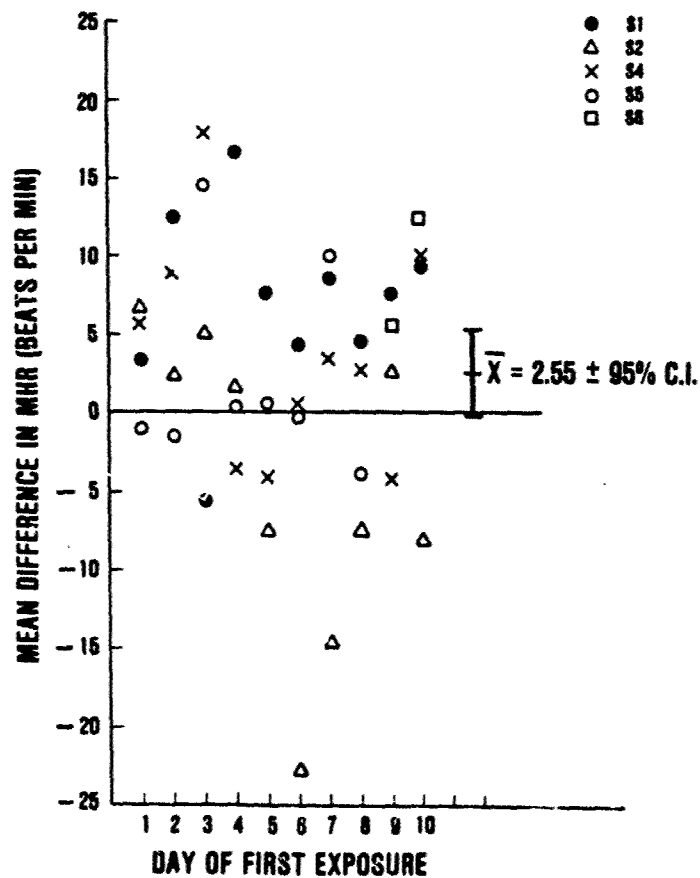


Figure 8. Mean differences in mean heart rate between first and second exposures to the same daily run sequences.

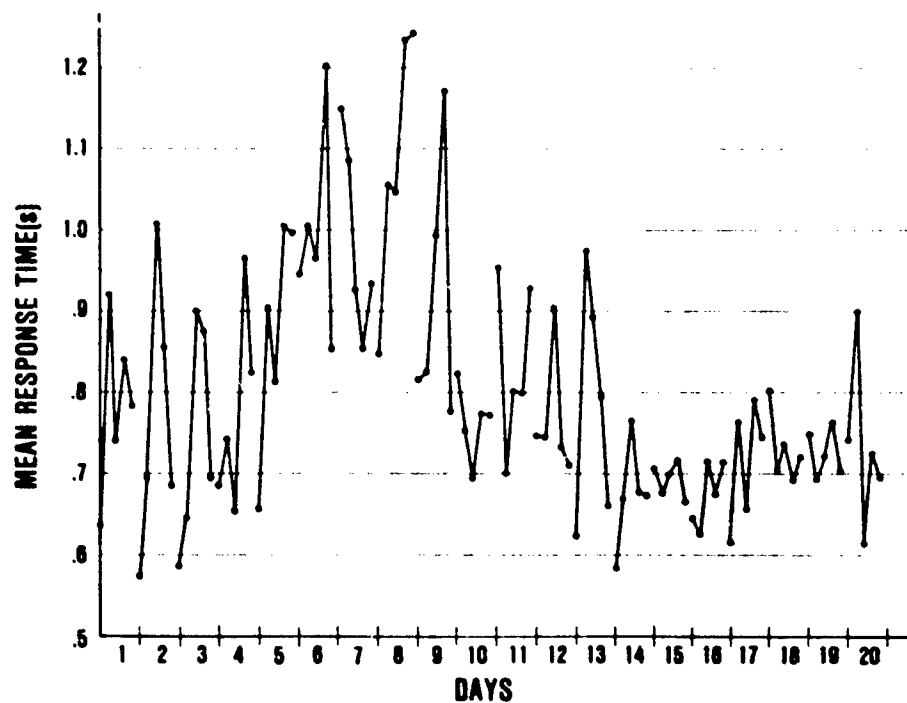


Figure 9. Pre-phase mean response times for each run and each day.

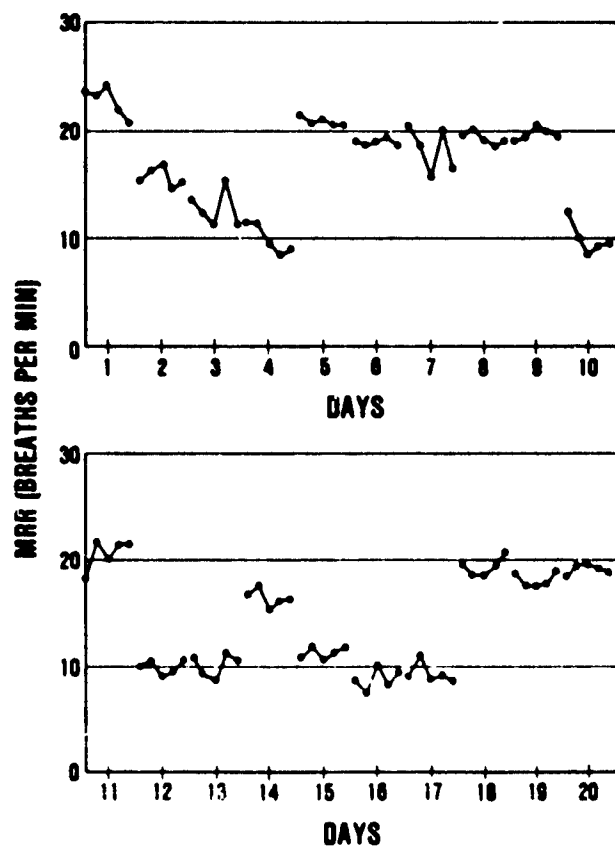


Figure 10. Pre-phase mean respiration rates for each run and each day.

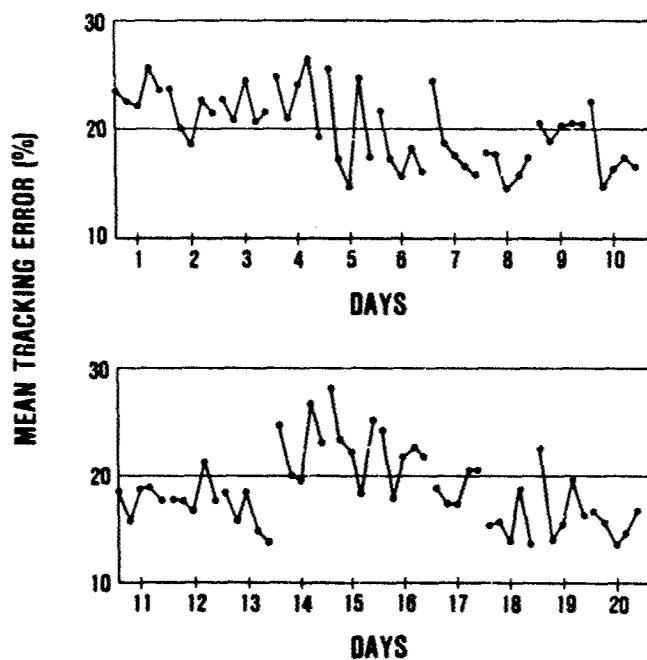


Figure 11. Pre-phase mean tracking error for each run and each day.

- **WHOLE BLOOD:** WBC, RBC, Hct, Hgb
- **URINE:** OCCULT BLOOD, KETONES, GLUCOSE, PROTEIN, pH, sp. gr.
- **BLOOD SERUM:** ALK. PHOS., LDH, TOTAL BILIRUBIN, SGOT, CPK, BUN, URIC ACID, TOTAL PROTEIN, ALBUMIN, GLUCOSE, CHOLESTEROL, CALCIUM, CHLORIDE, SODIUM, POTASSIUM

Figure 12. Clinical laboratory determinations.

DISCUSSION

DR. GILLINGHAM (USA)

You are to be complimented for beginning to obtain much needed performance data during G stress. Rather than studying simple eye-hand coordination, however, you could, with your facility, incorporate the subject into the motion-control loop, and be one step closer to providing G-induced pilot performance-decrement data to the operational community. Do you plan to do this?

AUTHOR'S REPLY

I certainly agree that it would be much more realistic to have the man in the loop and we hope to work up to this condition.

DR. H. JEX (USA)

To what do you attribute the negative correlation between the reaction times and the tracking error, assuming that a low score in tracking is good and a low reaction time is good. Do you have any ideas as to why, contrary to normal expectations, where the tracking error was low the reaction time was high?

AUTHOR'S REPLY

It seems as though the subjects share their time between the two tests and although we very carefully instructed them to perform both tasks equally well, invariably they were concentrating on one task. As a result the other task suffers.

THE BIODYNAMIC RESPONSE OF THE HUMAN BODY AND ITS APPLICATION TO STANDARDS

by

Michael J. Griffin, Christopher H. Lewis, Kenneth C. Parsons and Eleri M. Whitham
Human Factors Research Unit
Institute of Sound and Vibration Research
University of Southampton
Southampton SO9 5NH
England

SUMMARY

Biodynamic data may be used to predict the effects of vibration and impact on the human body. However, the biodynamic response of the body is dependent on how it is determined, it varies greatly between individuals and can change within an individual by large amounts.

This paper presents the results of five experiments with groups of up to one hundred-and-twelve subjects and ten experiments with a single subject. The experiments were designed to investigate factors that affect the transmission of vertical (z-axis) vibration to the head over the frequency range 1 to 100 Hz. The distributions of response within subject groups were determined as a function of vibration frequency and it was found that subject weight affected seat-to-head transmissibility. There were differences in transmissibility between men and women and between men and boys. Changes in subject posture had a large effect on transmissibility and it is suggested that a subjects' control over posture may partly explain the changes in transmissibility that occur with changes in vibration level and spectrum. The effects of changes in muscle tension, head and foot position were also studied and methods of determining transmissibility with discrete sine, swept sine and random vibration inputs were compared. It was found that seat configuration greatly affected the transmission of vibration to the head.

The experimental results are considered in the context of the possible development of Standards on the biodynamic response of the body. It is concluded that the variability in subject seat-to-head transmissibility is so large that a single average transmissibility curve could be misleading. The effects of inter- and intra-subject variability and seating configurations should be considered in the preparation of any Standard.

1. INTRODUCTION

The extent to which vibration is transmitted through the body determines the degree to which the vibration is uncomfortable, impairs performance and causes injury. The human body is an immensely complex active dynamic system whose properties can vary from moment to moment and from one individual to another. The definition of the mechanical response of the human body is, therefore, complex and requires a large amount of experimental data.

Earlier researchers have shown that the body has several resonances and the data obtained from studies of the mechanical impedance and transmissibility of the body have been used to evolve simple biodynamic models. For example, Payne and Band (1) tested one-, two-, three- and four-degree of freedom models of the body. Other more complex models have been devised to estimate the movement and internal body forces during aircraft ejection or body impact. For example, Belytschko et al (2) have described a general three-dimensional model of the body which includes the vertebrae, pelvis, head and ribs as rigid bodies connected by ligaments, cartilaginous joints, viscera and connective tissue. The model allows for variations in seat geometry and harness and for nonlinearities. Between the complexity of some of the models now evolved and the relative simplicity of the one- and two-degree-of freedom lumped parameter models there are many other possible representations of the dynamic response of the human body. (See, for example, Aviation, Space and Environmental Medicine, 49 (1), Section II (3).)

It is unlikely that simple models will be sufficient to predict the site of injury caused by impact or vibration or how injury is affected by body position and posture. However, the complexity required for this prediction currently restricts the scale of application of sophisticated models and prohibits their inclusion in Standards. Further, the complex models require detailed knowledge of the characteristics of body elements and this is not yet fully known. The one-degree-of-freedom model employed in the Dynamic Response Index (D.R.I.) simplifies the body to a single mass representing the head and upper torso and a parallel spring and damper for the spine. The only data required to evolve this model was mechanical impedance data showing the principal natural frequency of the body. The mathematical simplicity of the system aids the use of the D.R.I. and, despite its simple form, it has usually been considered useful since the D.R.I. values recorded from different aircraft ejection seats correlated well with their injury rates. However, the response of many other simple and complex biodynamic models may also be expected to achieve a good correlation and it would be unwise to assume that the D.R.I. model will predict injury for motions other than those for which it has been evaluated.

Whether a model is simple or complex it will not be better than the data upon which it is based. The complex models require data on the shape, size, weight, stiffness, non-linearities etc. of their elements. This information is partially available as average values in a variety of sources but many values often require estimation. The simple models are less constrained by the realities of the system being modelled. After selecting a realistic mass, the stiffness and damping are adjusted to fit average impedance or transmissibility curves obtained experimentally. Although the parameters in both types of model may be adjusted to predict the response of individuals, they are almost always based on average data from a group of subjects not data from individuals.

The experiments reported in this paper provide fundamental data on the biodynamic response of the human body to vibration. The particular response reported is vertical (z-axis) seat-to-head transmissibility. The experiments were conducted to determine the magnitude and cause of both inter- and intra-subject variability in dynamic response. From the data it is possible to assess the potential merits of both simple and complex models for seat-to-head transmissibility.

2. APPARATUS

The experiments were conducted with Derritron electrodynamic vibrators and, except where stated, the subjects sat on a flat horizontal wooden seat 360 mm by 360 mm firmly attached to an aluminium plate 12 mm thick secured to the vibrator table. The feet and upper legs of each subject were positioned horizontally and the lower legs vertically by means of a non-vibrating adjustable footrest. Subjects were not restrained but normally required to sit in a comfortable upright posture. Vertical vibration of the seat was measured by means of an Endevco 2265/20 piezoresistive accelerometer mounted within the aluminium plate beneath the wooden seat surface. The vertical (z-axis) head vibration was indicated by an Endevco 2265/20 accelerometer mounted within a magnesium block secured to one end of a 150 mm long stainless steel bar covered with a nylon sleeve. This bite-bar was placed in the mouth parallel to the lateral (y-axis) of the head such that the accelerometer was 75 mm from the midsagittal plane. The nature of the motion reproduced on the vibrators and the methods used to measure the vibration levels are outlined in the report of each experiment.

3. INTER-SUBJECT VARIABILITY IN SEAT-TO-HEAD TRANSMISSIBILITY

3.1 Introduction

The weight, height, age, sex, attitude etc. of a person might be expected to affect the transmission of vibration through the body. Griffin (4) presented the transmissibility data of twelve subjects and commented on the large differences between the response of individuals without being able to provide an explanation of the differences. The experiments reported below seek to quantify the nature and extent of the differences between individuals and determine the degree to which they are associated with the age, sex and physical characteristics of the subjects.

Much of the data is presented as the mean response of a group of subjects or the distribution of responses across a subject group since it is not practicable to present the data on all of the individuals who have been tested. An example of the differences to be found between individuals may be seen in Figure 1 which shows the transmissibilities of four of the male subjects tested in the experiment described under Section 3.4 below. All four subjects exhibit amplification at some frequencies and attenuation at frequencies above about 20 Hz. However, the transmissibility at any particular frequency differs greatly between the subjects. For example, at 16 Hz subject 4 has a transmissibility of about 0.4 while subject 5 has a transmissibility of about 1.2.

3.2 Population Distributions of Transmissibility

In an experiment previously reported by two of the present authors the seat-to-head transmissibility of 56 men, 28 women and 28 children was determined at 4 and 16 Hz at a level of 1 m/s² r.m.s. (see Griffin and Whitham (5)). The sinusoidal motions were each presented for 20 seconds and the vertical seat and head acceleration levels were measured by a digital true r.m.s. meter. The age, height, weight, hip size and the relative discomfort produced by the two vibration frequencies were also determined for each of the 112 subjects.

It was found that for both frequencies and the three populations the distributions of transmissibilities were near normal. Cumulative distributions of the measured data points and fitted normal distributions are shown in Figures 2 and 3.

There was no significant difference (at the 5% level) between the distributions of transmissibilities provided by the men, women and children. (At 16 Hz the mean transmissibility of the women was 0.74 compared to 0.58 for the men and this difference was significant at the 10% level.) In all three populations there were negative correlations between subject size (height, weight and hip circumference) and 16 Hz transmissibility. By determining partial correlation coefficients it was concluded that for both the men and the women the principal correlation was between 16 Hz transmissibility and weight ($p < 0.05$). Transmissibility at 4 Hz was not significantly correlated with subject size although all three groups showed negative correlations between transmissibility at 4 Hz and transmissibility at 16 Hz. The data obtained from the 56 men show a significant positive correlation ($p < 0.05$) between transmissibility at 16 Hz and the discomfort produced by 16 Hz vibration relative to the discomfort produced by 4 Hz vibration.

Knowledge of the nature of the distribution of transmissibilities is of assistance in interpreting experiments with smaller groups of subjects. The data presented in Figure 2 and 3 show that there is a large variability between individuals. For example at 4 Hz the mean transmissibility of the men was 1.35 but 10% had transmissibilities less than about 0.9 and 10% greater than about 1.8.

3.3 Differences Between Male and Female Transmissibility

An experiment was conducted in which 18 men and 18 women were required to judge the discomfort of a wide range of vibration stimuli. Following the experiment their seat-to-head transmissibilities were determined at each of the third-octave centre frequencies from 1 to 100 Hz. The vibration stimuli were short (4 sec) periods of sinusoidal motion and transmissibility was measured by a digital computer as the ratio of r.m.s. seat and head acceleration at each frequency.

Figure 4 compares the mean transmissibilities determined from the men and the women. From 1.25 Hz to 4 Hz the mean transmissibilities of the men are greater than those of the women. From 5 Hz to 100 Hz the women have the highest average transmissibility. These differences are significant at the 5% level for 2.4 Hz, 12.5 Hz, 32 Hz, 40 Hz, 50 Hz and 64 Hz and were significant at the 10% level at most frequencies above 8 Hz. At some of the higher frequencies the average female transmissibility is almost double that

of the males. The mean transmissibilities of the two groups at 4 Hz and 16 Hz are within about 10% of those reported for a different group of subjects in the previous experiment (see Section 3.2 above).

3.4 Effect of Body Size

The experiment reported under Section 3.2 above resulted in the conclusion that body weight had a significant effect on seat-to-head transmissibility. It was further determined that for all three groups (i.e. men, women and children) there was a negative correlation between transmissibility at 4 Hz and transmissibility at 16 Hz. This finding would be expected if, for example, their response is approximated by a single degree of freedom system with a resonance in the region of 4 to 16 Hz. Subjects with a resonance near 4 Hz would tend to have greater transmissibilities at 4 Hz and lower transmissibilities at 16 Hz than subjects having a resonance near 16 Hz. If the stiffness and damping remain constant the heavier subjects would have a resonance at lower frequencies than the lighter subjects and, as observed, the transmissibility at 16 Hz would decrease with increasing body weight. Although the body is more complex than a single degree of freedom system and the stiffness and damping are not likely to be constant this model may still be correct in principle.

The experiment outlined under Section 3.3 above also provided data on the correlation of transmissibility (from 1 to 100 Hz) with the height, weight, age, hip size, thigh size and leg size of subjects. At 1.25, 1.6 and 3.15 Hz there was a significant correlation between the transmissibilities of the men and their weights ($p < 0.05$). (The correlation between their transmissibilities and weights was negative at all except 2 of the 21 frequencies). For the women a negative correlation between weight and transmissibility was only significant at 2.5 Hz.

3.5 Effect of Age

Although in the experiment described in Section 3.2 the age of the adults ranged from 17 to 70 years and that of the children from 8 to 16 years there were no significant correlations within groups between age and transmissibility. There were no significant differences in transmissibility at 4 Hz or 16 Hz between the children and those of either the men or women. There were, however, signs of lower transmissibilities in the children at 16 Hz.

In Figure 5 are shown the mean seat-to-head transmissibilities of 18 men and 12 boys (aged 9 to 16 years). (This experiment is outlined under Section 4.3 below.) It may be seen that from 10 to 100 Hz the transmissibility of the boys is lower than that of the men. From 40 to 70 Hz the average transmissibility of the men is about twice that of the boys.

4. INTRA-SUBJECT VARIABILITY IN SEAT-TO-HEAD TRANSMISSIBILITY

4.1 Introduction

In the previous sections it has been shown that seat-to-head transmissibility varies greatly between individuals. It is also the case that the seat-to-head transmissibility of an individual is highly variable. The presence of significant correlations between subject characteristics and transmissibility, for example, implies that under conditions investigated intra-subject variability was not as great as inter-subject variability. However, this may not always be the case. In the next sections a series of experiments to quantify the extent and causes of intra-subject variability are described.

4.2 Repeatability of Seat-to-head Transmissibility Measurements

The 1 to 100 Hz transmissibility of a single subject was determined on 20 occasions over a period of two weeks with no more than two measurements on any one day. The subject (a male, weighing 68 kg) was exposed to 21 short periods of sinusoidal vibration at each of the third-octave centre frequencies from 1 to 100 Hz. Transmissibility was determined as the ratio of head to seat r.m.s. acceleration level at each frequency. It was found that normal distributions could be fitted to the subjects' transmissibilities at each frequency. Figure 6 shows the median and the 10th and 90th percentiles of the subjects' transmissibilities as determined from the 21 fitted normal distributions.

When transmissibility measures are averaged over a group of subjects the average response is sometimes a fairly smooth curve - even though the responses of many of the subjects are far from smooth. When a number of measures on a single individual are averaged the peaks and troughs associated with the individual's response are not lost. The present subject, for example shows clear resonance peaks at about 2, 5 and 12.5 Hz. Generally, approximately 80% of the transmissibility measurements on this subject were within about $\pm 20\%$ of his median transmissibility. Slight differences in sitting posture may be the principle cause of this variability.

4.3 Effect of Sitting Posture

It may be easily observed that variations in sitting posture can often greatly alter the transmission of vibration through the body. In Figure 7 the mean data obtained by Griffin (5) over the frequency range 7 to 75 Hz with twelve subjects seated in two extreme postures are shown. The postures are 'extreme' in that the upper curve in Figure 7 was determined with subjects adjusting their sitting posture to produce the maximum sensation at the head. The lower curve corresponds to the minimum sensation of head vibration at each frequency. The subjects, who sat on a hard flat seat, did not sit in unreasonable sitting positions and the difference between the two extreme sitting postures was often not apparent to an observer. Even so, the difference in transmissibility is considerable.

In the above experiment the extreme transmissibilities for the seat configuration was determined but the transmissibility for a normal sitting posture was not measured. An experiment was therefore conducted with a group of 18 men and a group of 12 boys in which their transmissibility was determined in three postures. First they were required to sit in a 'normal upright posture' next they sat in a 'relaxed posture' and finally they were asked to sit in a 'stiff posture'. (In this experiment it was the intention that the

subjects should maintain the same posture for all vibration frequencies. In the experiment mentioned above the subjects were required to adopt the extreme postures appropriate for each frequency in turn.) Transmissibilities were determined as the ratio of head to seat r.m.s. acceleration at each of the 21 third-octave frequencies from 1 to 100 Hz.

Figure 8 shows the mean transmissibilities determined in the three sitting positions for both groups of subjects. Above about 6 Hz the stiff posture resulted in increased transmission of vibration to the head, but below 6 Hz this posture reduced transmissibility. The relaxed postures resulted in slightly lower transmissibilities than the normal postures above about 10 Hz but, although these two postures often look different to an observer, they otherwise give similar mean transmissibilities.

The transmissibility of one subject (subject z weighing 80 kg) was determined with a swept sine vibration input with the subject sitting in seven postures from slouched to erect. The sweep covered the frequency range 100 Hz to 1 Hz in 100 seconds at a level of 1 m/s^2 r.m.s. Transmissibility was determined by computing the power spectra and cross spectrum of the seat and head acceleration measurements as described in Section 5.7 below. Figure 9 shows, in a three-dimensional form, the effect of posture on the modulus of this subject's transmissibility. The data is shown for a 1 Hz frequency resolution and from 1 to 50 Hz only. Figure 10 compares the modulus and phase of this subject's transmissibility in the two extreme postures. Apart from the large increase in transmissibility at higher frequencies it can be seen that the change to an erect posture has accentuated the resonance peak in the 15 to 25 Hz region.

4.4 Effect of Muscle Tension

While maintaining the same normal sitting posture the transmissibility of subject z was determined with both normal and increased muscle tension. For the latter condition the subject tensed the muscles of his arms, neck, shoulders, abdomen and legs as much as possible during the 100 second period of the sine sweep.

It may be seen in Figure 11 that the effect of an extreme increase in muscle tension is not as great as the effect of posture reported in Section 4.3. Increased tension slightly increased the seat-to-head transmissibility over most of the frequency range. The greater effect is present from 5 to 10 Hz and from 35 to 60 Hz. From about 15 to 55 Hz decreased tension also resulted in increased phase lag.

4.5 Effect of Head Position

The orientation of the head normally varies according to the desired line of sight of the eyes although it will also change during a substantial body impact. Subject z was exposed to 100 second 1 m/s^2 r.m.s. vibration sweeps with his head at five angles: normal (looking horizontally ahead), approximately 25 degrees and 50 degrees above horizontal, and 25 degrees and 50 degrees below horizontal. Apart from altering his head position the subject sat in the normal relaxed posture. The head accelerometer was always orientated in the vertical axis irrespective of the angle of the head.

It may be seen in Figure 12 that raising the head above the normal position increased transmissibility at low frequencies. Lowering the head reduced transmissibility. The greatest effect occurred at about 16 Hz where, for example the level of head vibration increased by 800% between 50 degree down and 50 degree up positions.

4.6 Effect of Foot Position

The position of the feet affects body posture and muscle tension as well as altering the area of contact between the vibration input and the body. Subject z was exposed to the standard 100 second 1 m/s^2 r.m.s. sine sweep with various positions of the stationary footrest. It was found that the orientation of the lower leg from the normal vertical through to the horizontal (i.e. ahead of the subject at the same level as the seat) had little influence on seat to head transmissibility. However, altering the footrest height while keeping the lower leg vertical did affect transmissibility (see Figure 13). There was not a great difference between no footrest (feet hanging) and the normal footrest height. However, increasing the height of the footrest so as to raise the thighs well above the level of the seat reduced transmissibility in the frequency range from 6 to 9 Hz.

5. EFFECT OF METHOD OF DETERMINING SEAT-TO-HEAD TRANSMISSIBILITY

5.1 Introduction

Apart from the effect of the variation between and within people on seat-to-head transmissibility, the experimenter is also faced with the problem of how to measure transmissibility. There are three principal problems (a) location of transducers on the head (b) choosing the input motion and (c) selecting a method of analysis. Some studies of the influence of the choice of motion and analysis method are presented in the following sections.

The location of the transducers on the head has been the same throughout the experiments described in this paper. This position can be important and, indeed, the difference in level recorded by two accelerometers as close as 100 mm apart has been used to measure the pitch motion of the head (e.g. Griffin (4)). The measurement of high frequency head motion leads to the use of some form of bite-bar and, often, a location for the transducers near to the mouth. It is not possible to predict the level at other parts of the head without knowing the rotational head motions and the centres of rotation. Such data as exist imply that the transmissibility will possibly not usually vary by more than about 25% for head measurement positions within 100 mm of that used in this study. (In many cases, particularly where visual performance is concerned, rotational motion of the head is important because not only does it affect the measurement of translational motion but it also causes eye movements via the vestibulo-ocular reflex. Predicting the vertical translational motions of the head will sometimes be of less importance than predicting motions in other directions.)

5.2 Effect of Vibration Level

There have been various attempts to determine the degree to which the mechanical response of the body is non-linear, and varies either with the level of vibration or with constant vibration level at various steady state acceleration levels such as may be produced in a centrifuge. There are data which show increased stiffness and an increase in the frequency of principle resonance under increased sustained acceleration (e.g. Vogt et al (6)) and Mertens (7)). Under normal gravity Griffin (4), for example, found reductions in transmissibility with increases in vibration level at frequencies below 20 Hz. In both cases it should not be forgotten that the subjects were fully conscious and undoubtedly consciously modified their responses with the changing conditions. Under increased sustained acceleration subjects will deliberately try to keep their heads up and at higher levels of vibration subjects will tend to adopt postural changes to reduce the discomfort, or fear, they experience from the vibration. Common interpretations of the available data imply that the non-linearities in biological material may give rise to the observed non-linearities in whole-body mechanical impedance and transmissibility data. However, considering the data from Sections 3 and 4 above it would seem likely that such non-linearities would often have less effect than the deliberate actions of subjects.

Subject z was exposed to seven 100 second sine sweeps at 0.4, 0.8, 1.2, 1.6, 2.0, 2.4 and 2.8 m/s² r.m.s. The subject maintained the same normal posture for all motions - even though this proved most uncomfortable in some conditions. The results are shown in Figure 14 where it can be seen that even with a seven-fold change in vibration level the subject's transmissibility barely changed. The phase was also unchanged by vibration level. It appears that any effect of vibration level may be insignificant compared with the variability caused by inter- and intra-subject differences. (Note: greatest change in Fig.14 is 30%.)

5.3 Effect of Spectrum of Vibration Input

It appears that conscious adaptation to the more uncomfortable high vibration levels is the principle cause of non-linearities. If transmissibility is determined with different input vibration spectra this would be expected to result in different transfer functions as subjects adjust their posture to that which is least uncomfortable for each spectrum. It is not clear, however, whether different transfer functions will be obtained if subjects are asked to maintain the same posture for each spectrum.

Subject z was exposed to 100 second periods of three random vibration spectra - all with an acceleration level of 1 m/s² r.m.s. The spectra were (a) a nearly flat acceleration spectrum, (b) a predominantly high frequency acceleration spectrum and (c) a predominantly low frequency acceleration spectrum. The subject attempted to sit in the same normal posture for all three spectra. His transmissibility was determined by computing both power spectra and cross spectra of the seat and head acceleration as described in Section 5.7.

In Figure 15 the three seat-to-head transmissibilities for the three input spectra are shown. Above about 9 Hz the differences due to the spectra are fairly small. Between 4 and 8 Hz the transmissibility is inversely proportional to the amount of low frequency energy in the spectra. It appears that although he attempted to keep the same posture for all three motions the subject unconsciously modified his posture slightly to reduce the transmissibility for those motions which contributed most to his discomfort.

5.4 Effect of Sweep Rate for Swept Sine Inputs

The swept-sine method of determining transfer functions can be quick and convenient. For the measurements reported earlier in this paper the sweep duration has been 100 seconds and the sweep rate 1 Hz/sec. If subjects adapt to the motion it may be expected that the transfer functions will depend on the sweep rate.

Subject z was exposed to six 100 second periods of vibration consisting of sweeps of different durations: 100, 20, 10, 4, 2 and 1 second. The sweeps were repeated (after a 1 second pause) as often as necessary throughout the 100 second test period. The number of degrees of freedom was therefore the same for the analysis of all motions (412 degrees of freedom with 1 Hz resolution). The seat-to-head transmissibility is shown as a function of sweep rate in Figure 16. In general the effects are small. A decrease in input energy at low frequencies with the shortest sweeps leads to values below 1 Hz being unreliable. Between about 4 and 8 Hz there is a lower transmissibility with the longer sweeps. As in the case of different random motion inputs (see Section 5.3) this may be due to the subject unconsciously modifying his posture to reduce his transmissibility for these more uncomfortable motions. With high sweep rates it is not possible to modify posture with sufficient speed.

5.5 Effect of Sweep Duration for Swept Sine Inputs

Experimenters using the swept sine technique usually select a sweep rate and analyse the data from a single sweep. The consequence of increasing sweep rate is usually therefore a reduction in the duration of the signals to be analysed. If the analysis resolution is held constant, reductions in duration will result in fewer degrees of freedom in the analysis and less reliability in the transfer function which is determined.

Subject z was exposed to six sine sweeps of duration 100, 20, 10, 4, 2 and 1 second. His seat-to-head transmissibility was determined with a 1 Hz resolution for each sweep duration giving, for decreasing sweep durations: 412, 86, 42, 18, 10 and 4 degrees of freedom. These transfer functions are shown in Figure 17.

Although the variability increases slightly with reduced sweep duration it can be seen that the transfer function is broadly similar for all sweep rates. In Figure 18 the transfer functions for the 100 second sweep and the 2 second sweep are compared. Also shown are the 5th and the 95th percent confidence limits. The mean values show differences similar to those reported in the previous section where there was a constant period of analysis. The most important difference is the increase in the confidence interval with reduced analysis period. On the basis of the present results a 1 Hz resolution may be obtained for a 1 to 100 second sweep with a sweep rate of 10 Hz per second. Shorter sweeps may be possible where, as in

the present case head motion is solely determined by the swept sine inputs. Short analysis periods will not be acceptable with random or pseudo-random inputs.

5.6 Effect of Varying the Frequency Resolution

A frequency resolution of 1 Hz has been employed in most of the studies with subject z reported in this paper. Other data are reported in which transmissibility has only been measured at third-octave centre frequencies (see Sections 3 and 4). For some purposes (e.g. investigating seating response) a finer frequency resolution would certainly be required. Increasing the resolution requires more data to obtain the same reliability in the measured values. Decreasing the resolution increases the reliability but a coarse resolution will not accurately describe the response where it is changing rapidly near a resonance frequency.

Subject z was exposed to a single 100 second 1 m/s^2 r.m.s. sine sweep while sitting in the normal posture. His response to this sweep was analysed with six different frequency resolutions 0.125, 0.25, 0.5, 1.0, 2.0 and 4.0 Hz corresponding to 100, 100, 204, 214, 826 and 1654 degrees of freedom respectively.

Above 12 Hz there was no consistent difference in the seat-to-head transmissibility determined with any of the six frequency resolutions. Above 6 Hz there was no difference in response with the five resolutions from 0.125 to 2 Hz. At about 4 Hz the subject exhibited a resonance. The amplification at resonance was less for the coarser resolutions. The amplifications were approximately 1.05 at 4 Hz resolution, 1.2 at 2 Hz, 1.35 at 1 Hz, 1.45 at 0.5 Hz, 1.5 at 0.25 Hz and also at 0.125 Hz. Figure 19 shows a comparison of the transfer functions determined with 0.25 to 2.0 Hz resolutions and it can be seen that a peak at 2 Hz is also more clearly defined with the finer resolution.

One-third octave analysis corresponds approximately, to the resolution of 4 Hz at 16 Hz, 2 Hz at 8 Hz, 1 Hz at 4 Hz and 0.5 Hz at 2 Hz. The results suggest that this will be as good as the 1 Hz resolution above 4 Hz and somewhat better below 4 Hz. The precise determination of response at the principle resonance requires a finer resolution.

5.7 Effect of Analysis Method

Response to a swept-sine input may be determined by three methods. The method used in most of the studies reported here involves the computation of $G_{ss}(f)$ (the power spectrum of the seat acceleration time history), $G_{hh}(f)$ (the power spectrum of the head acceleration time history) and $G_{sh}(f)$ (the cross spectrum of the seat and head acceleration time history). The transfer function $H(f)$ is determined from: $H(f) = G_{sh}(f)/G_{ss}(f)$. $H(f)$ is a complex quantity giving both the modulus and phase of the seat to head transmissibility. (In general phase measurements have not been illustrated but an example will be found in Figure 10.)

Transmissibility may be determined from the square root of the division of $G_{hh}(f)$ by $G_{ss}(f)$. This does not require the computation of the cross spectrum, it does not yield phase data and it assumes that all the energy at the head is due to energy of the same frequency on the seat. The values determined may be the same or greater than those determined using the cross-spectrum method.

A third method is to use the property of the sine sweep that predetermines the moment at which each frequency is presented. From the start and end frequencies of the sweep and the sweep duration it is known what frequency is present at any time during the sweep. For example, suppose a 100 second 1 Hz per second sweep is used from D.C. to 100 Hz. If the r.m.s. seat and r.m.s. head acceleration are determined over each of the one hundred 1 second periods of the sweep the seat-to-head transmissibility may be determined with a resolution of 1 Hz. This method does not yield phase data, it assumes that the motion at the head is due to that currently presented at the seat and that both motions are undistorted sinusoids.

Subject z was exposed to a 100 second 1 m/s^2 r.m.s. and 1 Hz per second sine sweep from 100 Hz to D.C. His transmissibility as determined by the above three methods using a digital computer are shown in Figure 20. It may be seen that above about 7 Hz the three methods give very similar values. The third (RMS) method (the division of 1 second intervals on the head by corresponding intervals on the seat) appears to produce the greatest difference. The first value with this method is at 2 Hz since it comes from the average levels between 1 Hz and 2 Hz. The peak occurs at 3 Hz rather than 4 Hz with the other two methods probably because of a slight timing error between the sweep duration and computer acquire time. The increased level of this peak may be caused by head motions occurring at the time of 3 Hz and 4 Hz vibration but not at these frequencies. The good agreement between the cross spectrum method (CSD) and power spectrum (PSD) suggests that this subject responded as a near-linear system. These results, although with only one subject, suggest that any of the three methods may be used. However the RMS method is susceptible to timing errors and assumes the vibration levels on the seat and head are free from distortion. The comparison of the PSD and CSD methods may be used as indicators of body behaviour.

5.8 Comparison of Discrete Sine, Sweep Sine and Random Input Methods

The discrete sine method, as used in some of the experiments reported in Section 3 and 4 of this paper, assumes that the seat and head motions are undistorted and of the same frequency. In Figure 21 the transmissibility of subject z obtained using this method at each one-third octave from 1 to 100 Hz is compared with that obtained with 100 second 1 m/s^2 r.m.s. random (flat spectrum) and sweep sine inputs. The random and sweep sine transmissibilities were determined on a different day using the cross spectrum method.

It may be seen that there is general agreement between the results obtained by the three methods. At the 4 Hz resonance the sweep gave the highest transmissibility and the discrete sinusoidal motions gave the lowest transmissibility. The discrete frequency motions produced a peak at 2.5 Hz which might, in part, be due to the harmonic distortion on the vibrator at this frequency. The difference between the random and sweep motions are greatest in the range 16 to 40 Hz where transmissibility is greatest with the swept sine motion. At 20 Hz the discrete sine transmissibility is almost double that determined from the random motion. It is possible that these differences are solely due to postural changes. The results suggest that any of the three methods is acceptable but further investigation to optimise their use may be desirable.

5.9 Effect of Seating Conditions and Seat Harness

All results previously reported in this paper have been determined with subjects seated on a hard flat seat with no backrest or seat harness and a stationary footrest. The only area of contact between the body and the source of vibration was around the ischial tuberosities and along the thighs. In practice the body is often in contact with vibration at many other points (e.g. feet, hands, back, neck, head) and this may alter the level of vibration at the head.

An experiment was conducted with 12 male subjects exposed to vertical (z-axis) sinusoidal vibration at 2, 4, 8, 16, 32 and 50 Hz. They were required to sit in several positions in a hard replica of a Sea-King helicopter seat. For each position their seat-to-head transmissibility was determined as the ratio of seat and head r.m.s. acceleration at each of the above frequencies. In Figure 22 the mean transmissibilities for the normal posture (as defined earlier: feet stationary; thighs horizontal; no back support or harness) are compared with those for the subjects secured by a harness and leaning against the backrest but with no foot vibration. It may be seen that the backrest and harness greatly change head vibration causing an increase in transmissibility at 16, 32 and 50 Hz but a decrease at 2 Hz.

6. BIODYNAMIC MODELS

6.1 Introduction

This section considers the degree to which the transmissibility simple dynamic systems can approximate to the transmissibility of individual subjects and groups of subjects. It is clear that the dynamic response of the human body is determined by the complex interaction of many elements. The body is not a single mass, single spring and single damper system and simple models of this type have very limited application. One possible application is the provision of a simple summary of the seat-to-head transmissibility of human subjects. Transmissibility varies so greatly between and within subjects that for some purposes a more complex model may not be necessary.

6.2 A One-degree-of-freedom Model of the Seat-to-head Transmissibility of Subject Groups

In Figure 4 the mean transmissibilities of 18 men were compared with those of 18 women. At each of the third-octave centre frequencies from 1 to 100 Hz the distributions of male transmissibility were fitted with normal distributions. Figure 23 shows the median, 5th and 95th percentiles of these transmissibilities. Also shown is the transmissibility curve for a system comprising a single mass supported by a parallel spring and damper. For the parameters of the single degree of freedom illustrated in the figure (i.e. a natural frequency of 14 Hz and damping of 0.6 of critical) agreement with the shape of the median transmissibilities of the males may not appear very good. At 9 Hz, for example, the median transmissibility is about 0.75 compared to a 1.05 transmissibility for the model. It is possible to obtain a better fit to the data than that illustrated here. However, it may be seen that even with this model the transmissibility falls within the 5th and 95th percentiles of measured subject transmissibilities throughout the 1 to 100 Hz frequency range. So, for every vibration frequency, at least 5% of subjects (and usually more) have transmissibilities greater than that of the model and at least 5% have transmissibilities less than that of the model. In many situations the inter- and intra-subject variability will be such that the difference between transmissibility in the real environment and the laboratory environment will be greater than the difference between the median transmissibility in the laboratory and that of a simple biodynamic model.

Obtaining an adequate fit between a model and the average response of a group of subjects does not mean that the subjects have the same natural frequencies or damping as the model. This is certainly not true for the model shown here (see Figures 1 and 23) and is often not true for more complex models.

6.3 One-degree-of-freedom Models of the Seat-to-head Transmissibility of Individual Subjects

While the average transmissibility of a group is sometimes given by a relatively smooth curve the response of individuals reflects their own resonance frequencies. When modelling the response of individuals there is likely to be a greater need to employ models more complex than the one-degree-of-freedom model used for group response.

The response of the single subject shown in Figure 6 and discussed in Section 4.2 suggests that a three-degree-of-freedom model should be used. However, the subject's response varied by some degree during the test and would have changed far more if posture, foot position, seating etc. had been altered. In Figure 24 the 5th and 95th percentiles of the subjects' response are compared with the response of the same single-degree-of-freedom model used in Section 6.2 (i.e. natural frequency 14 Hz, damping 0.6 of critical). It is not possible to fit such a curve between the 5th and 95th percentiles at all frequencies but for the curve shown the difference between the median response of the subject and the model is only about 25% below 30 Hz. Larger differences occur due to posture, head position, seating conditions etc. Referring to Figure 1 it is clear that another model would be required for other subjects.

7. CONCLUSIONS

It is often convenient to summarise the complex response of the human body by suggesting that resonances of the head, shoulder-girdle, abdomen, etc. occur at specific frequencies. Improved knowledge of such resonances and other aspects of biodynamic response could have practical benefits. However, the results reported in this paper suggest that the transmissibility of the human body is highly variable and simple statements of its response could be misleading. The table in Appendix 1 summarises some of the principal factors that have been found to affect the seat-to-head transmissibility of the body.

The data provided from the present and previous studies might be used in the evolution of a Standard on the biodynamic response of the body. Such a Standard could consist of the definition of the damping and natural frequency of a single-degree-of-freedom system as considered in Section 6.2 above. However the mass, stiffness and damping of this model would not be representative of any definable part of the human body. These parameters would merely be convenient numbers chosen to approximate by means of the appropriate

equation the average response of subjects. The equations would, however, appear to be a model of the body with a certain mass, damping, stiffness and resonance frequency. The possible misinterpretation of such a model may make it less attractive than an idealised response chosen to be either easy to describe (as in ISO 2631 (8) for example) or convenient for the construction of a satisfactory electronic weighting with the correct response.

An alternative approach to a biodynamic standard is to identify three or four degrees of freedom and define the values of the masses, springs and dampers. The values of these parameters could each be defined as a distribution making it possible to explore the response of selected extremes of the population. However this requires more data than is currently available, multiple degree of freedom models become complex to solve conveniently and simple models may not be any more accurate than an idealised response based on empirical data as described above. As mentioned in Section 1, very complex models are required to predict the site of injury due to impact or vibration and since, at present, their sophistication restricts their use to a few research laboratories there is little current need to standardise their characteristics.

Whatever approach to the standardisation of biodynamic response is adopted it is important that the restrictions and assumptions implicit in any such Standard are clearly identified. If the effects of posture, seat configuration, inter-subject variability etc. are not defined, the applicability of the Standard will be greatly restricted. Conversely, if their effects are defined it may be necessary to restrict the application of the Standard to particular seating conditions, subject groups etc. Whether this is desirable depends on the definition of the purpose of the Standard and a consideration of whether publication of an agreed approximation to existing data will be beneficial.

8. REFERENCES

- 1) Payne, P.R.
Band, E.G.U. A four degree-of-freedom lumped parameter model of the seated human body.
AMRL-TR-70-35 (1971).
- 2) Belyteschko, T.,
Schwer, L.
Schultz, A. A model for analytical investigation of three-dimensional head-spine
dynamics.
AMRL-TR-76-10 (1976).
- 3) Anon Symposium on biodynamic models and their applications.
Aviat. Space Environ. Med. 49 (1) Section II (1978).
- 4) Griffin, M.J. Vertical vibration of seated subjects: effects of posture, vibration
level and frequency.
Aviat. Space Environ. Med. 46 (3) 269-276 (1975).
- 5) Griffin, M.J.
Whitham, E.M. Individual variability and its effect on subjective and biodynamic
response to whole-body vibration.
J. Sound Vib. 58 (2) 239-250 (1978).
- 6) Vogt, H.L., Krause, H.E.,
Holweck, H., May, E. Mechanical impedance of supine humans under sustained acceleration.
Aerospace Med. 44 (2) 123-128 (1973).
- 7) Mertens, H. Nonlinear behavior of sitting humans under increasing gravity.
Aviat. Space Environ. Med. 49 (1) 287-298 (1978).
- 8) International
Organization for
Standardization. Guide for the evaluation of human exposure to whole-body vibration.
ISO 2631-1974(E) (1974).

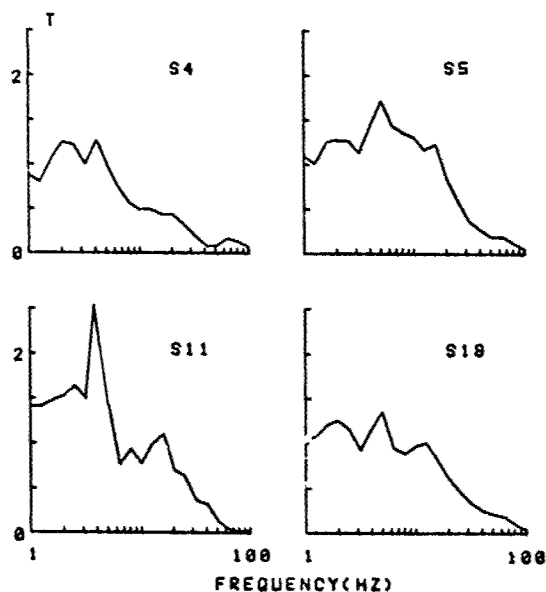


Figure 1. Examples of the differences in seat-to-head transmissibility that may be found between individuals. (See Sections 3.1 and 3.4).

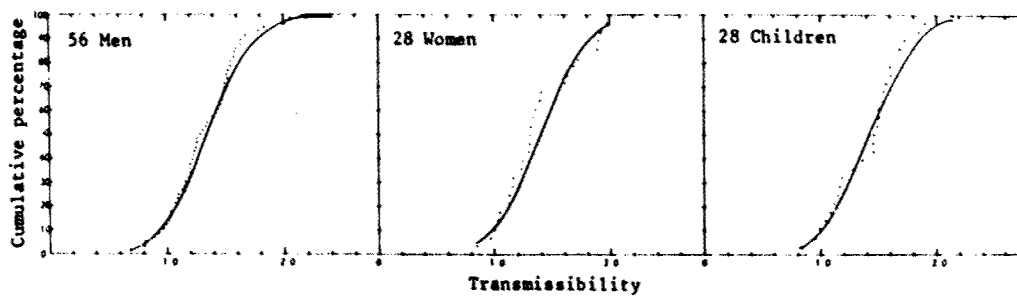


Figure 2. Cumulative distributions of seat-to-head transmissibility for 4 Hz vertical, z-axis vibration. (Points indicate measured data, lines represent fitted normal distribution.) (See Section 3.2).

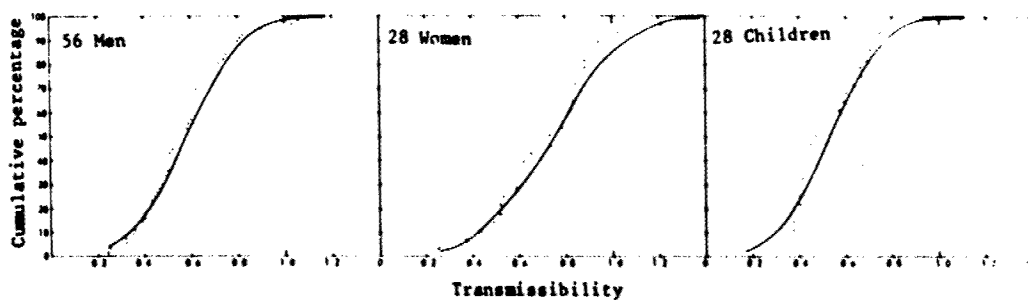


Figure 3. Cumulative distributions of seat-to-head transmissibility for 16 Hz vertical, z-axis vibration. (Points indicate measured data, lines represent fitted normal distribution.) (See Section 3.2).

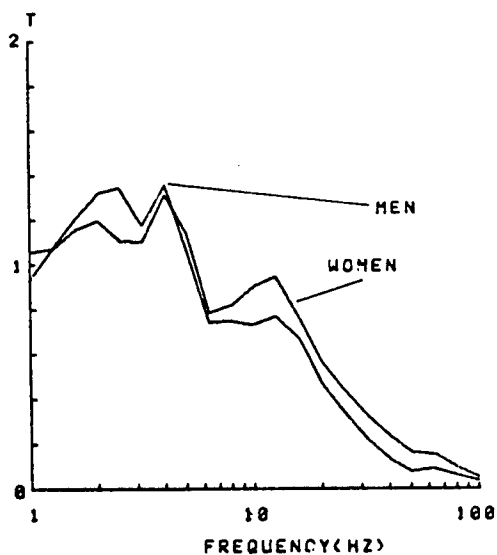


Figure 4. Mean seat-to-head transmissibilities of 18 men and 18 women (See Section 3.3).

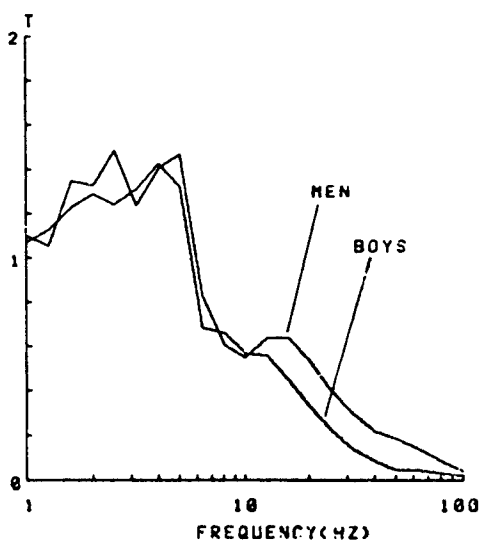


Figure 5. Mean seat-to-head transmissibilities of 18 men and 12 boys (See Section 3.5).

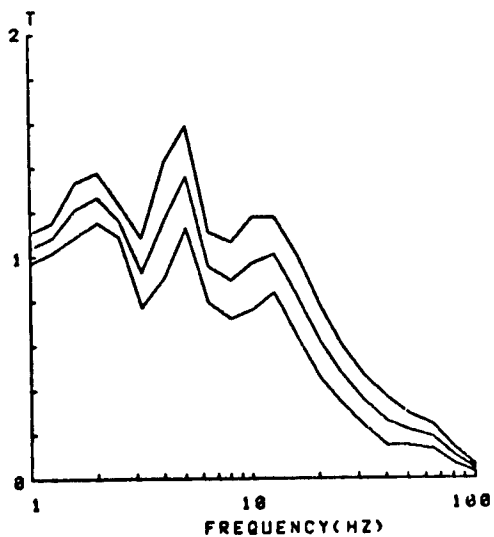


Figure 6. Median, 10th and 90th percentiles of the seat-to-head transmissibility of a single subject (See Section 4.2).

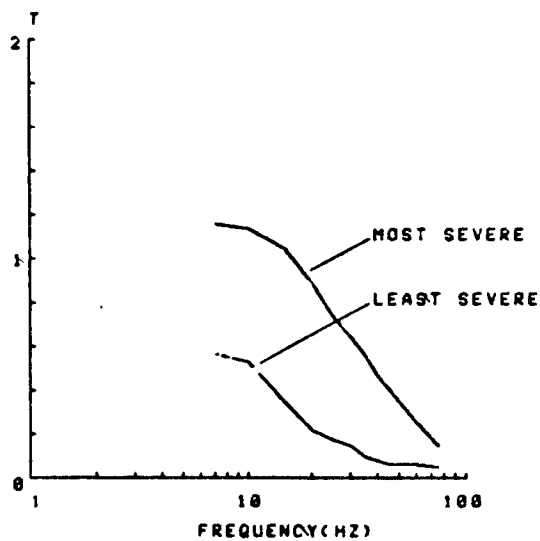


Figure 7. Effect of posture on the mean seat-to-head transmissibility of 12 subjects. (Data from Griffin, 1975) (See Section 4.3).

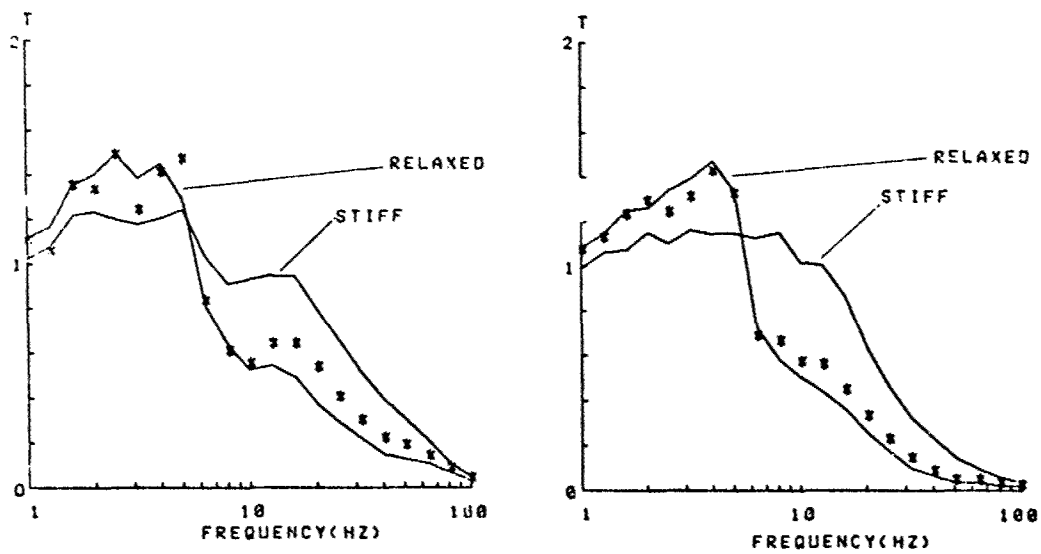


Figure 8. Effect of posture on the mean seat-to-head transmissibility of 18 men (above left) and 12 boys (above right). "Normal upright posture" shown as asterisks; "stiff" and "relaxed" postures as continuous lines. (See Section 4.3).

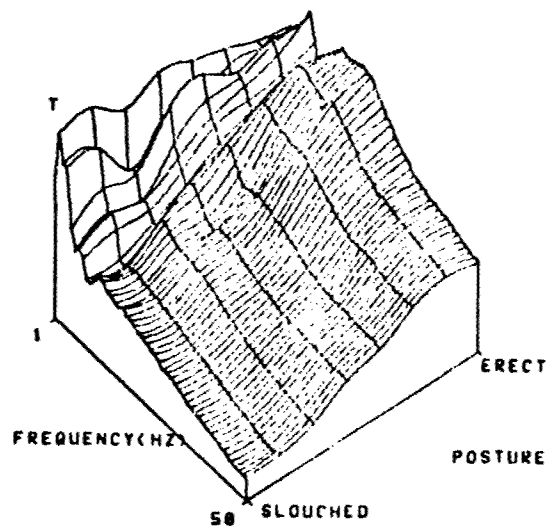


Figure 9. The seat-to-head transmissibility from 1 to 50 Hz of a single subject sitting in 8 postures from slouched to erect. (See Section 4.3).

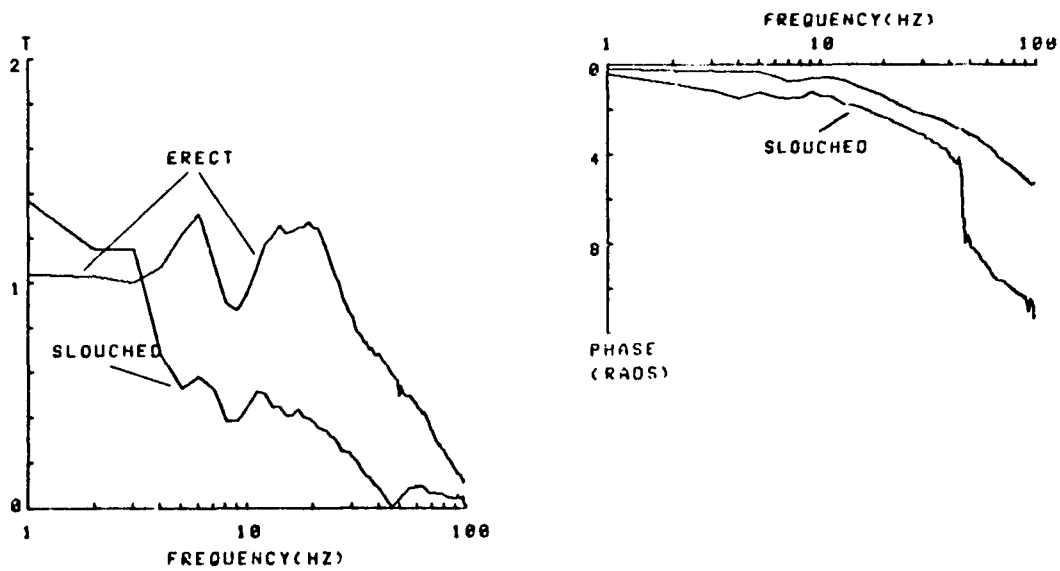


Figure 10. Comparison of the modulus and phase of the seat-to-head transfer function of a single subject sitting in slouched and erect postures. (See Section 4.3).

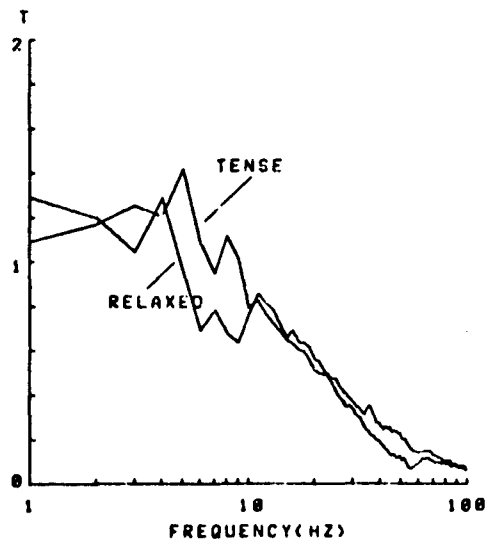


Figure 11. Comparison of the seat-to-head transmissibility of a single subject sitting in tense and relaxed postures. (See Section 4.4).

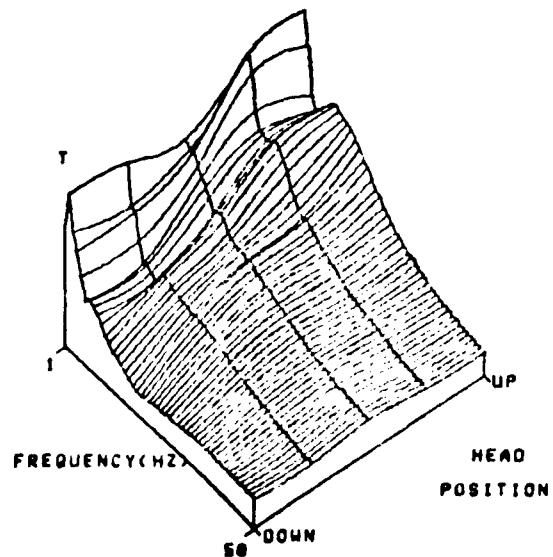


Figure 12. The seat to head transmissibility from 1 to 50 Hz of a single subject sitting with 5 head positions (25 and 50 degrees down, horizontal, and 25 and 50 degrees above horizontal). (See Section 4.5).

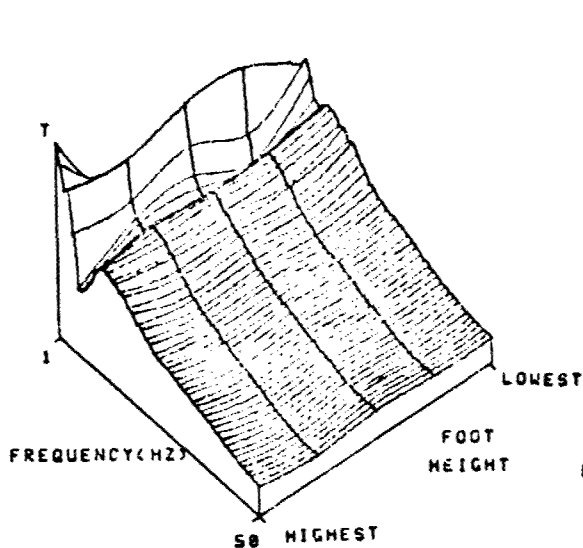


Figure 13. The seat-to-head transmissibility from 1 to 50 Hz of a single subject sitting with 5 foot heights. (Highest position with feet on the same level as the seat, central position with horizontal thighs, lowest position with unsupported feet). (See Section 4.6).

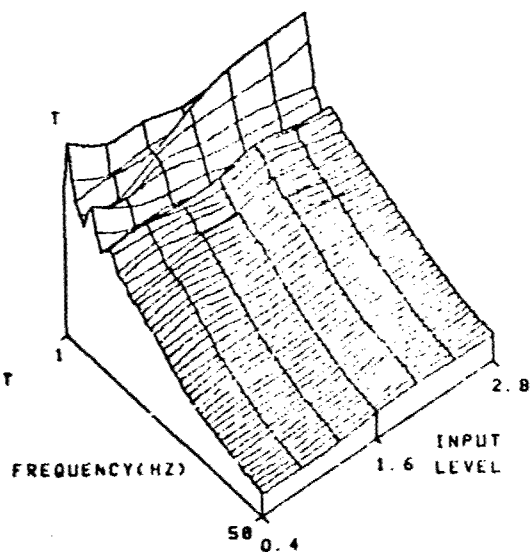


Figure 14. The seat-to-head transmissibility from 1 to 50 Hz of a single subject exposed to 7 vibration levels (0.4, 0.8, 1.2, 1.6, 2.0, 2.4 and 2.8 m/s^2 r.m.s.). (See Section 5.2).

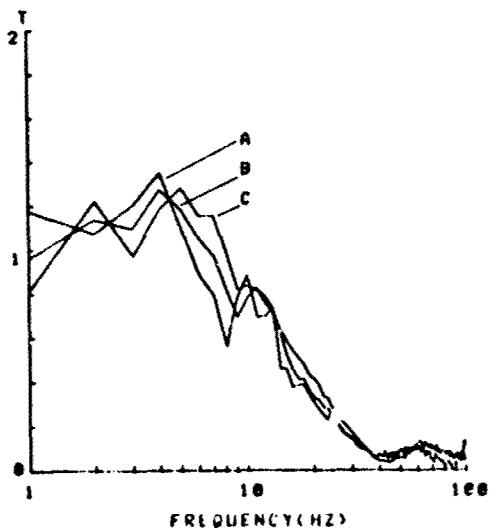


Figure 15. Comparison of the seat-to-head transmissibility from 1 to 50 Hz of a single subject exposed to three different spectra of random vibration. (A: low frequency; B: flat spectrum; C: high frequency spectrum). (See Section 5.3).

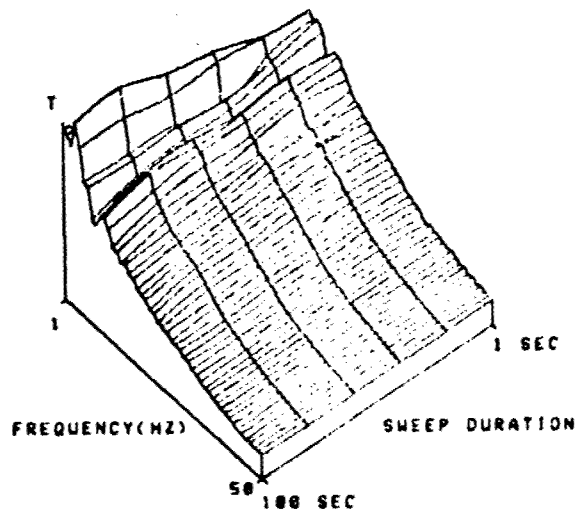


Figure 16. The seat-to-head transmissibility from 1 to 50 Hz of a single subject exposed to 100 seconds of swept sine vibration at 6 sweep rates (1, 5, 10, 25, 50 and 100 Hz/sec). (See Section 5.4).

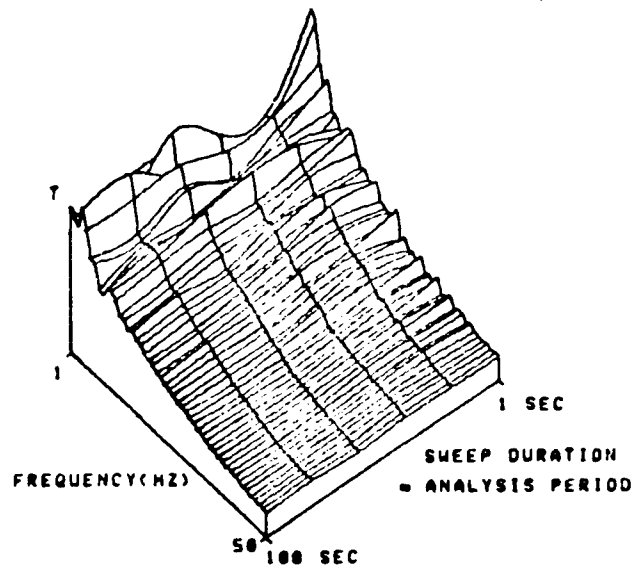


Figure 17. The seat-to-head transmissibility from 1 to 50 Hz of a single subject exposed to single sine sweeps of 6 durations (100, 20, 10, 4, 2 and 1 second). (See Section 5.5).

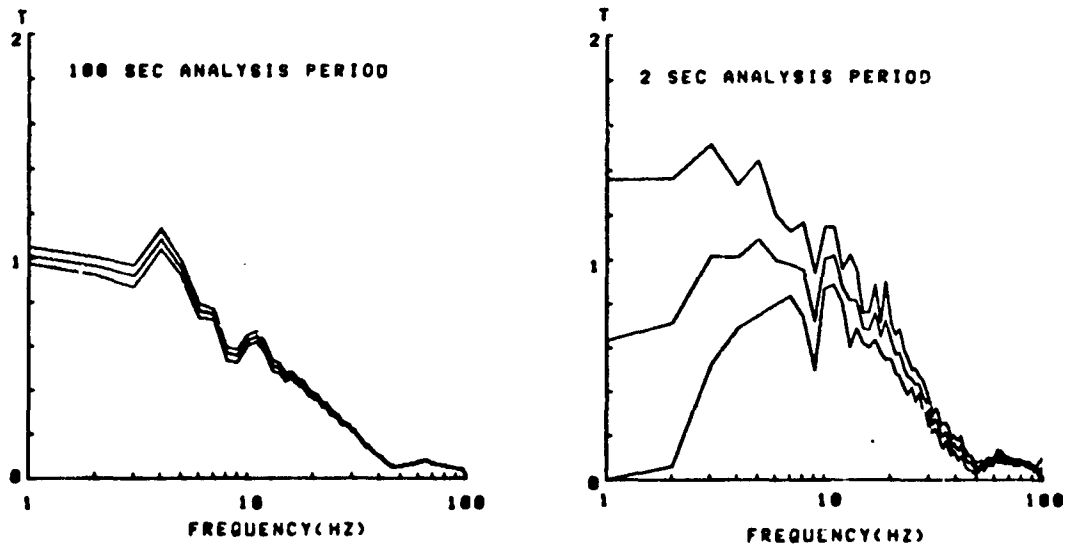


Figure 18. Comparison of the mean seat-to-head transmissibility and 5th and 95th percent confidence intervals for sweeps with durations (and computer acquisitions) of 100 seconds and 2 seconds. (See Section 5.5).

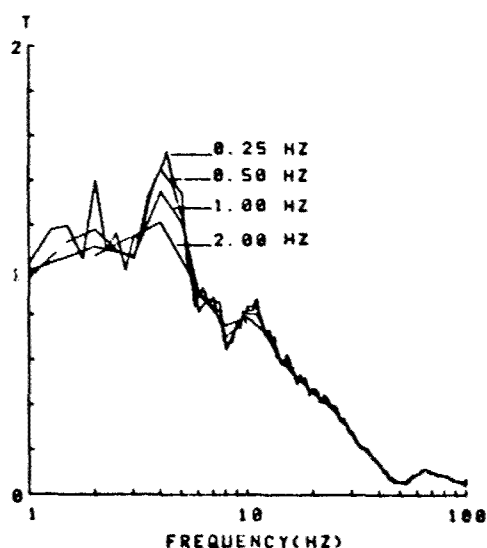


Figure 19. Comparison of the seat-to-head transmissibility of a single subject determined with 4 frequency resolutions (0.25, 0.5, 1.0 and 2.0 Hz). (See Section 5.6)

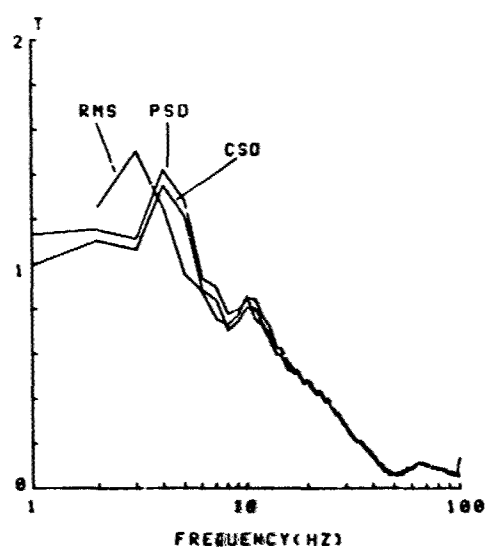


Figure 20. Comparison of the seat-to-head transmissibility of a single subject determined by three analysis procedures (from the cross spectra (CSD), division of power spectra (PSD) and divisions of r.m.s. values (RMS). (See Section 5.7).

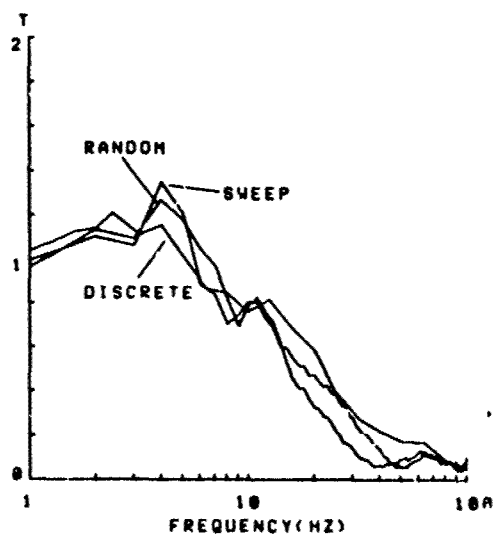


Figure 21. Comparison of the seat-to-head transmissibility of a single subject determined with three types of input motion: random vibration spectrum, swept sine and discrete sinusoidal vibration. (See Section 5.8).

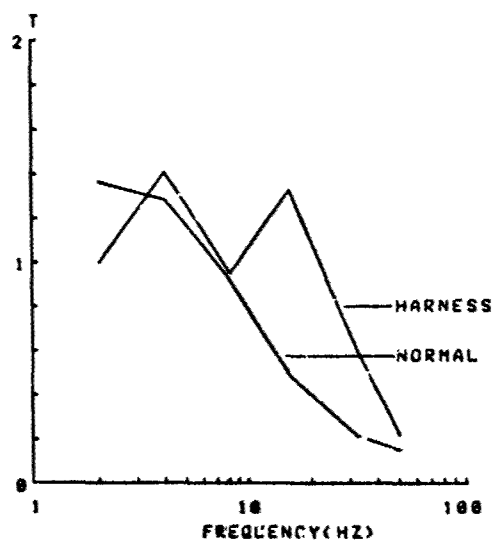


Figure 22. Comparison of the mean seat-to-head transmissibility of 12 subjects sitting in a normal posture (no harness or backrest) and sitting with a harness and backrest. (See Section 5.9).

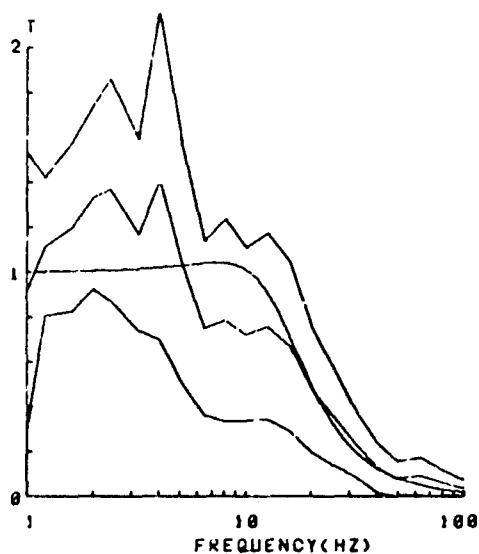


Figure 23. Median, 5th and 95th percentiles of the seat-to-head transmissibilities of 18 men compared with the response of a single degree-of-freedom system with 14 Hz natural frequency and damping 0.6 of critical. (See Section 6.2).

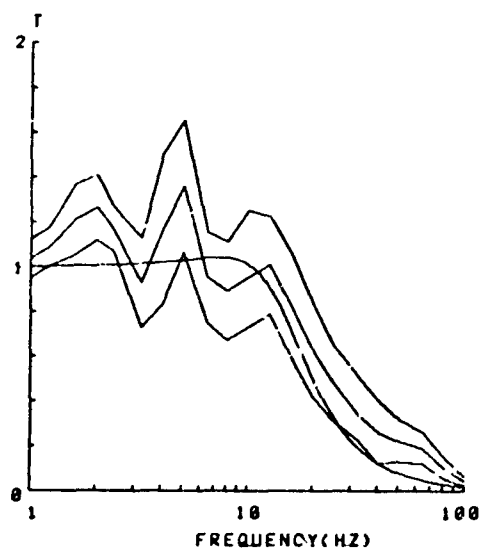


Figure 24. Median, 5th and 95th percentiles of the seat-to-head transmissibility of one subject compared with response of a single degree-of-freedom system with 14 Hz natural frequency and damping 0.6 of critical. (See Section 6.3).

APPENDIX ONESOURCES OF VARIABILITY IN THE SEAT-TO-HEAD
TRANSMISSIBILITY OF THE HUMAN BODYINTRINSIC VARIABLESINTER-SUBJECT VARIABILITY

- effects are large and frequency dependent (e.g. at 4 Hz about 20% of transmissibility measurements fall outside 0.9 - 1.8 range). Subjects differ in the dominance and frequency of their principal resonances.
- Weight - tendency towards lower seat-to-head transmissibilities in heavier subjects.
- Sex - men tend to have higher transmissibilities than women from 1.25 - 5 Hz and lower transmissibilities than women from 5 - 100 Hz.
- Age - from 10 - 100 Hz the transmissibility of boys tends to be lower than that of men.

INTRA-SUBJECT VARIABILITY

- large effects of small changes in position and posture. Repeatability in one posture may be 80% of measurements within $\pm 20\%$ of median.
- Posture - potentially a very large source of variability. Posture may change voluntarily or involuntarily and may often be modified to reduce subjects' discomfort.
- Muscle tension - increasing muscle tension tends to slightly increase transmissibility.
- Head position - affects transmissibility at low frequencies by large amounts.
- Foot position - footrest height can affect transmissibility with high footrests.

EXTRINSIC VARIABLES

- Vibration frequency - subjects exhibit 1, 2, 3 or more resonance peaks. Without back support transmissibility is often in excess of 1 below about 10 Hz and decreases above 20 Hz.
- Vibration level - transmissibility may change with changes in vibration level but this may be due to modifications in posture.
- Vibration axis - vertical seat vibration causes motion in other axes at the head; horizontal and rotational seat motions are transmitted differently to the head - although not studied here.
- Vibration spectra etc. - the spectrum of a random motion or the sweep rate of a swept-sine input might have small effects on transmissibility - possibly due to postural changes in subjects.
- Frequency resolution - if the frequency resolution is more than 1 Hz or one-third octave the amplification at resonance will be underestimated; finer resolution is desirable.
- Seat configuration - seating conditions can greatly alter seat-to-head transmissibility by altering posture etc. and by providing a vibration input near to the head.
- Analysis method - transmissibility may be determined by several alternative methods (e.g. via computation of cross spectra and power spectra, power spectra alone or only r.m.s. levels of seat and head acceleration at each frequency). The method depends on the type and quality of the input motion. The differences that exist between the results of the alternative methods may often be relatively small but sometimes useful and important.

DISCUSSION

MR. A. JUNKER (USA)

You indicated that even if you photographed the position of the subject, you are not sure of the posture he is assuming. How did you control the various postures the subjects were taking, to guarantee you had what you thought you had?

AUTHOR'S REPLY

In the data I showed the cooperation of the subject was heavily involved in the experimentation. They had to understand what was required to produce this sort of data. The group data obtained from naive subjects could not result in such systematic data. One can instruct the subject either by saying: "sit very upright" or "sit very slush" and there is data of that type in the paper. Alternatively, you can say: "change your posture until you feel the most vibration in some part of the body," that again will give you the extremes and in the paper you will see those extremes compared with what you will get if you just ask the subject to sit on a vibrator in a normal relaxed position.

DR. G. ALLEN (UK)

As the next part of your work do you intend to make mathematical models for your work?

AUTHOR'S REPLY

I think the model has to be related to the application. The application of much of this work is concerned with visual performance and subjective response and the answer in those areas is yes.

PROGRESS IN MEASURING AND MODELING THE EFFECTS OF LOW FREQUENCY VIBRATION ON PERFORMANCE

by
Henry R. Jex and Raymond E. Magdaleno
Systems Technology, Inc.
13766 S. Hawthorne Boulevard
Hawthorne, California 90250
U.S.A.

SUMMARY

Several facets of the comprehensive biodynamic modeling program presented at the AGARD Aerospace Medical Panel Meeting at Oslo, 1974, have been successfully completed and are reported here. The objectives and approach (an ensemble of physical models of just-adequate complexity, with adjustable or adaptive parameters) are first reviewed.

The development of a variety of lumped parameter models to explain and codify the known data on low-frequency vibration effects and to predict likely effects in new situations has been brought to a useful level. These are described with presentations of typical validation data:

- a) BIODYN-78, a user-interactive computer program which is capable of modeling the biomechanical properties of a variety of pilot/crewman posture and control situations in which active neuromuscular systems are involved.
- b) PIVIB, a user-instructed batch program (developed by others) for modeling effects of vibration on tracking performance, and which requires information supplied by BIODYN-78 in its use.

The relationship and applications of these and other related new models are discussed with respect to their development status and potential applications.

Specific recommendations are made for more refined experimental data (e.g., simultaneous accelerations on various body locations and better postural and dynamic mode shapes via cinematography, etc.) and interface compatibility among various models.

OBJECTIVES

This is a progress report on recent work and achievements in measuring and modeling the effects of low-frequency vibration (0.2-20 Hz) on the performance (visual, tracking, etc.) of vehicular crewman. Although the main research relates to pilots and operators of equipment in aircraft, there are examples from high-speed ships, and the resulting technology certainly applies to land vehicles.

Typical problems for which these models are being developed are shown in Fig. 1. Vibration effects on performance usually occur at the operator interfaces with his environment, such as: the seating/restraint system (and any isolation features such as cushions or springs); displays (whether or not they

EYE/HEAD/HELMET DYNAMICS:

- Analyze vibration interference with vision
- Biodynamic design of helmet-mounted displays under high G_z and buffet

DISPLAYS:

- Analyze display mounting, isolation, stabilization concepts
- Analyze effects of size, viewing distance, orientation, etc.

CONTROLS/MOTOR COORDINATION:

- Analyze competing control configurations (e.g., fly-by-wire vs. center stick) for (a) effects of rough air excited bending modes for large aircraft, or (b) high g buffet for fighters
- Design vibration resistant controls

RESTRAINT/SEATING AND ISOLATION SYSTEMS:

- Analyze performance consequences of competing restraints and cushions
- Design new restraint and isolation systems
- Analyze performance effects of various postural situations (i.e., supine seating)
- Ride quality implications on various tasks and locations in aircraft

OVERALL

- Optimize among various tradeoffs prior to testing, also simulations to operational situations
- Predict pilot control/vehicle motion interactions (e.g., pilot induced oscillations)

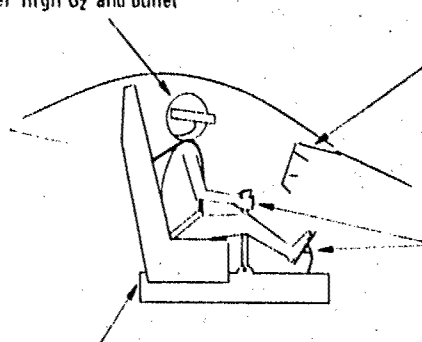


Figure 1. Problem Areas of Interest.

130.3

move with the seat or cockpit); controls (especially tracking control sticks or devices held and aimed by the operator); eye/head motions as they affect the perceived image motions (and effect of helmets and helmet-mounted sights). Finally, there are the overall tradeoffs between better seating and restraints versus better controls versus better displays (e.g., vibration-compensated displays, head-mounted displays, etc.). For such problems as these, one needs "uniformly valid first approximation" models, which can capture the essential features of a variety of vibration interface problems in a computationally efficient manner. That is the overall goal of this research.

APPROACH

Overall

A more detailed discussion of these problems and possible approaches toward solving them was presented at the Aerospace Medical Panel Specialist's on "Vibration and Combined Stresses in Advanced Systems," at Oslo, Norway, in April 1974 (Ref. 1). After reviewing the relevant definitions and measures of task performance, behavior, stresses, and strains, that paper considered three approaches:

- A purely experimental investigation of all possible situations (which would never be even partially completed).
- An ad hoc simulation of each problem as it arose (which gives relevant data for the case at hand but cannot be extrapolated to new situations).
- A comprehensive, empirically based theory (which requires carefully coordinated cycles of modeling, validation/refinement experiments, and the development of a user-oriented "catalog" of models and data that can be extrapolated to new situations even before a proper ad hoc simulation can be developed).

The comprehensive theory approach was recommended in Ref. 1 for a number of reasons, given therein, and the USAF Office of Scientific Research and Aerospace Medical Research Laboratory have sponsored the majority of the program. This paper reports progress as of mid 1978, at which time the first really usable, albeit embryonic, models are available.

Scope and Status

As noted above and discussed in Refs. 1-3, the basic approach is to use simplified physical models with dynamic elements analogous to those of the body/limb/head/eye system and their interfaces with the seat, display, and controls. The complete three-dimensional assemblage of bones, muscles, and organs, plus the complex neuromuscular control system, is far too complex to model efficiently enough for practical solutions of the problems described, and such complexity is not really needed. Instead, only those elements required for a likely class of problems, such as those of Fig. 1, are employed.

Most of this work to date has emphasized vertical and fore/aft vibration (e.g., Refs. 4-6), with some work on lateral vibration (e.g., Refs. 2 and 7) and very limited work on combined vibrations (e.g., Ref. 8).

Figure 2 shows the fundamental model structure used for evaluating biodynamic interference with visual and control tasks, adapted from Ref. 1. The main blocks delineate the "human operator," "controlled element" (which is also the source of vibrations via the disturbance inputs), and "manipulated object" (such as a book, aimed device, or simply a visually fixated external object). The main interfaces at the display, seat, and controls are also shown. Within each major block are the main elements we have modeled, e.g., seat-interface, body, head, eyes, limb, etc. We will expand on these later.

The checks (✓) or question marks (?) beside each element denote the status of its math model. The earlier (1974) status is shown dashed to reveal where progress has been made. There are few "?" left, implying that the models are approaching a new level of maturity in which they are ready for more widespread validation, refinement, and application.

The selection of specific models from the available ensemble starts with Fig. 2, using its blocks to define the task and its measures of performance; the controlled element with its dynamic elements including structural modes, seat-response properties, and control excitation of vehicle motions; the forcing functions (commands to be followed and disturbances to be suppressed or which produce vibration); the interface properties such as display distances and sizes; control stick "feel" properties; etc. The specification of all the dynamic elements of Fig. 2 is essential to any application and requires a fairly complex model structure and an input-descriptor file containing several dozen parameters.

The next step is the calculation of the biodynamic "feedthrough" or transmissibility to the seat, head, eyes, and image motions (for visual performance effects) and/or to limb and control stick (for manual control performance). All of the models used here have special features to allow the redundant and active neuromuscular forces due to body/limb coupling with the control sticks or arm rests to be efficiently modeled. The manual control situation precludes the use of the passive "open chain" anthropomorphic models now highly developed for crash research (e.g., Ref. 9).

The model and user's program we have been developing to compute these biomechanical transmissibilities is called "BIODYN-78" (BIODYNamics, and the number denotes the model year), and its scope and role are depicted on Fig. 3, which is an expansion of the center region of Fig. 2 (Ref. 10). Even for relatively simple situations involving tracking a CRT display with a spring-restrained control stick, there are numerous biodynamic elements in the causal chain, and dozens more parameters must be specified to define the operator's size, posture, tenseness (neuromuscular gains), eye-to-display locations, etc. As noted by the numbers in parentheses in Fig. 3, there are 5 seat/pelvis/interface parameters (such as seat force gradient, damping, lower body effective mass, compliance and damping), 10 torso parameters,

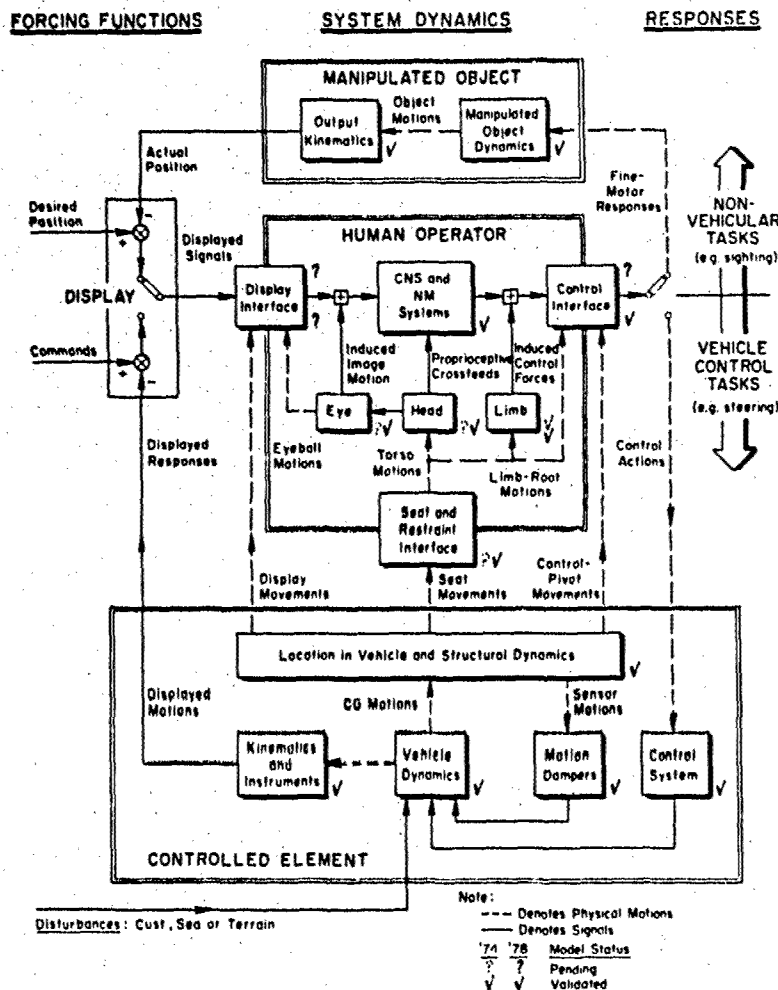


Figure 2. Overall Model Structure for Evaluating Biodynamic Interference

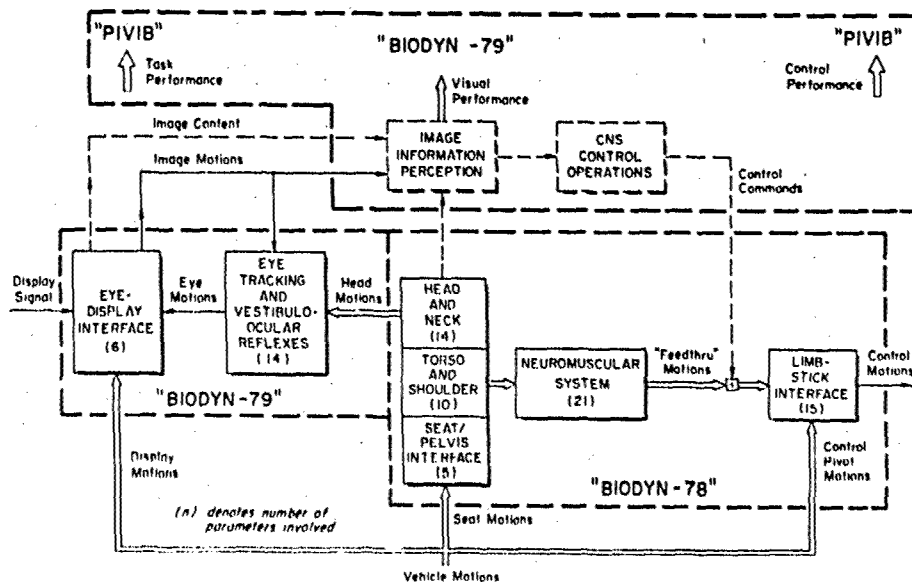


Figure 3. Modeling of Operator Elements and Interfaces

21 neuromuscular (NM) items, 15 limb/stick interface or arm rest parameters, and 14 head/neck/shoulder parameters. These are in the 1978 version, which computes limb/stick transmissibility or force impedance as well as head-point-of-regard and translation, shoulder motions, etc., as illustrated in Fig. 4. Only the main body links are shown in Fig. 4a. The basic equations of motion are nonlinear in the postural and neuromuscular variables, but the equations are automatically trimmed about the average operating point and linearized equations are used to compute the vibration effects.

A first cut at a model for vibration-induced image motions has been made (Ref. 11) which takes as inputs the head rotations and translations and accounts for the vestibulo-ocular reflex (which roughly stabilizes the eye inertially up to about 6-8 Hz) and the fixation reflex (which can follow display image motions up to about 1-2 Hz). It is denoted on Fig. 3 as "BIODYN-79" in anticipation of its inclusion in the current BIODYN-78 computer program, and is illustrated in Fig. 5. About 14 eye/head quantities are specified along with five or six display interface parameters. (For details see Ref. 11.) We also plan to include the additional effects of a helmet and helmet-mounted displays or sights in the 1979 version.

As the third step the computed vibration-induced motions of the head, stick, shoulder, and points of regard (at the display) of the head and eye are used to determine the visual task performance decrements via empirical relationships between these motions and perceptual or motor performance (e.g., detection errors, tracking "indifference threshold," etc.). The connection between the net performance of various tasks and the computed (or actual limb or head) motions remains the weakest link in the chain from vibration input to measured task performance.

Further systematic experiments of the type originally performed by Drazin (Ref. 12) and lately by Benson and Barnes (Refs. 13 and 14) need to be performed to provide a data base for this final link in the visual performance chain.

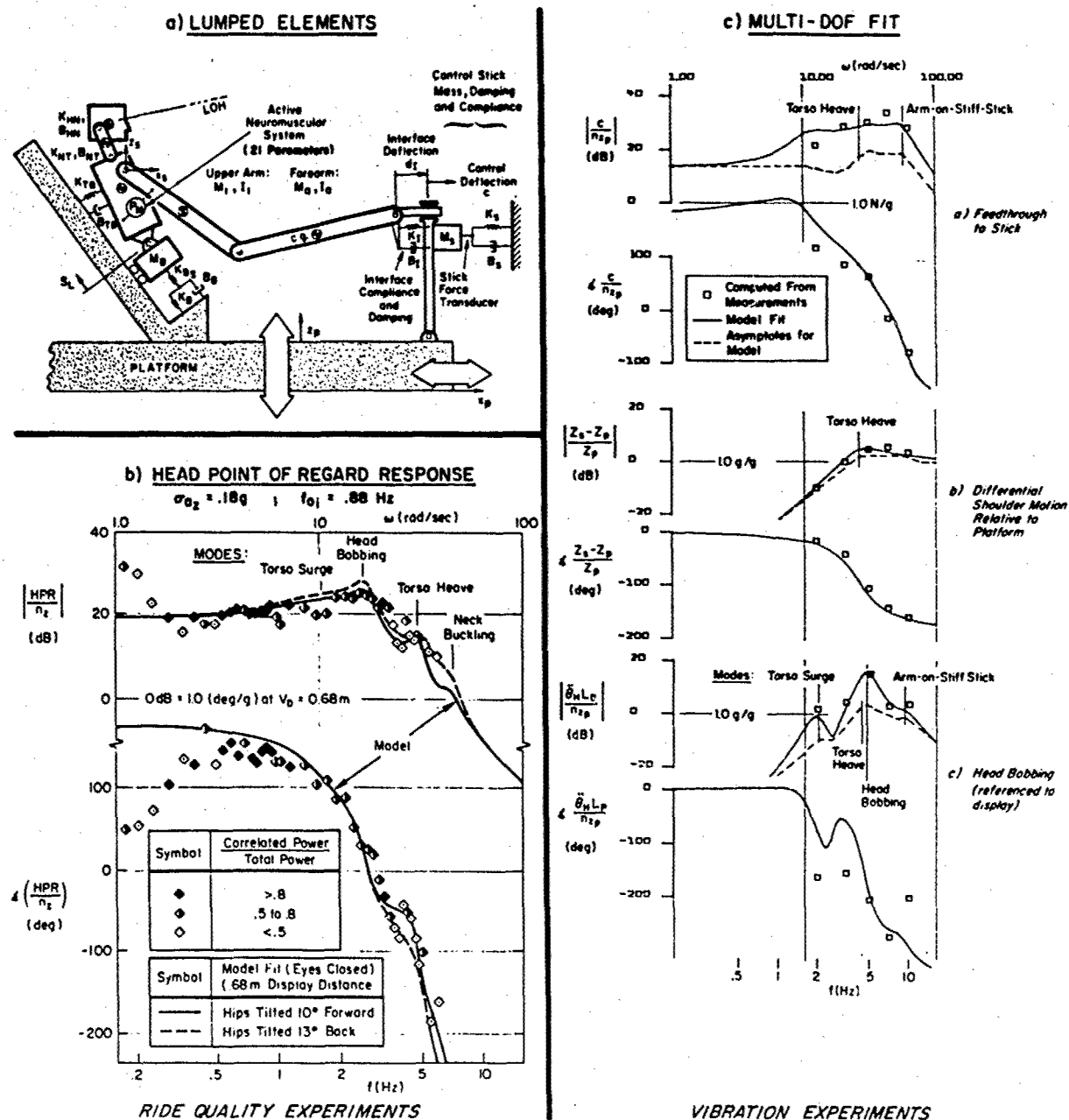


Figure 4. Control Feedthrough Model and Validation

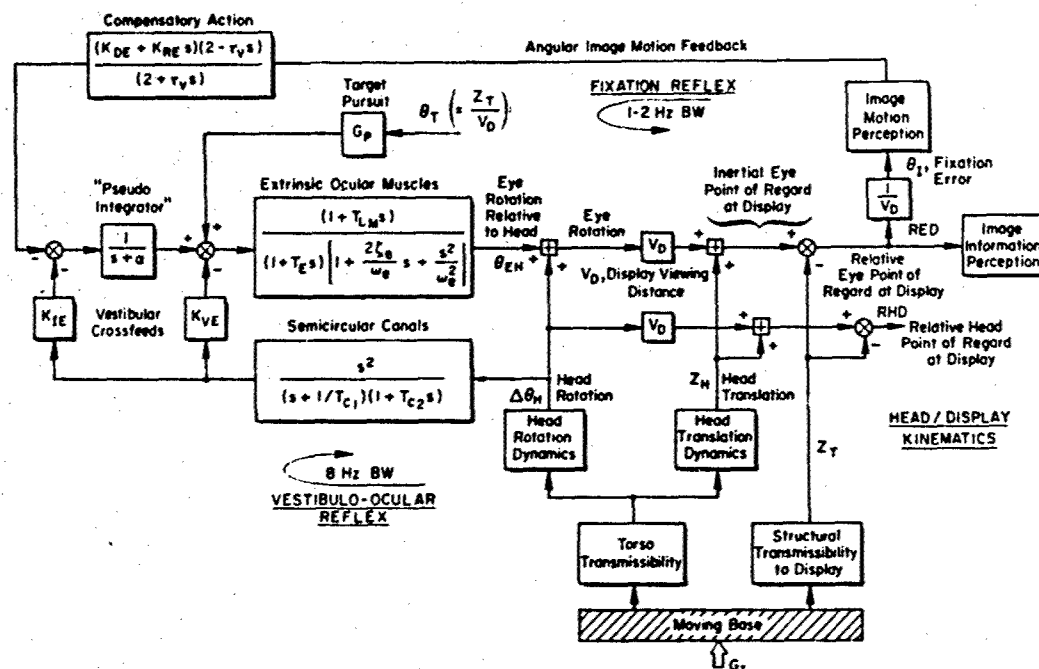
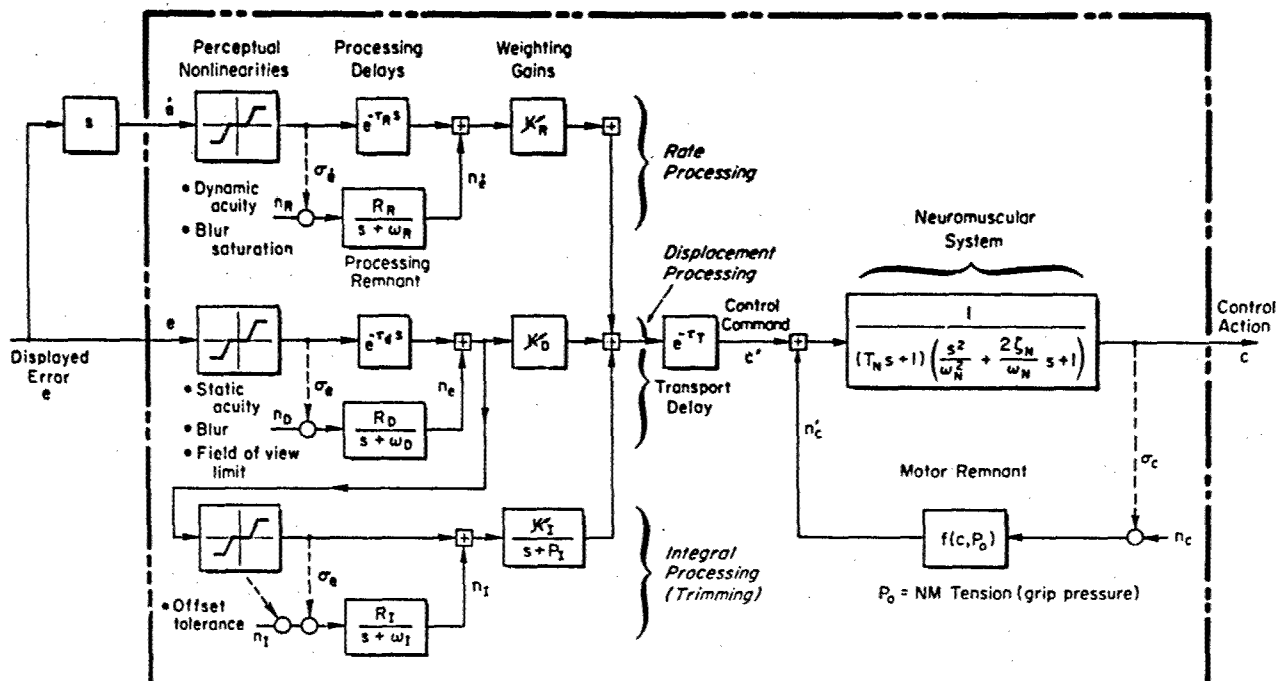


Figure 5. Model for Image Motions Due to Head Vibration

When tracking performance (or performance on a manipulated object task) is desired, the fourth, and most difficult, step is necessary. All of the vehicle dynamics and biomechanical transmittances must be included in a complex model of the human operator's adaptive tracking strategies. The "classical" models for doing this are typified by those of McRuer and his associates (e.g., Refs. 15 and 16). They use lumped-parameter submodels for the perceptual, equalization, and neuromuscular processes, with adjustable parameters which covary with various task variables, including vibration (e.g., see Ref. 2). A current version of this, the so-called "Compleat" Human Tracker model is summarized in Fig. 6.

The modern equivalent to this is the optimal control theory model of Kleinman, et al. (e.g., Ref. 17), in which the catalog and adaptation "rules" of the classical human operator model are replaced by an



Systems:	PERCEPTUAL	PROCESSING AND COMPENSATION (Central)	NEUROMUSCULAR
Effects:	<ul style="list-style-type: none"> • Sensitivity • Thresholds • Saturations 	<ul style="list-style-type: none"> • Adjustable gains L^{-1} • Processing delays • Remnant (noise) due to time variations and nonlinearities 	<ul style="list-style-type: none"> • $T_N, \omega_N, \zeta_N = f(\text{NM tension})$ • Motor remnant, tremor

Figure 6. Typical Human Operator Performance Model

optimal control law algorithm whose cost functional is adjusted (based on fitting empirical data) to provide the covarying parameter trends observed in experiments.

The optimal control model for tracking has been highly refined and applied to modeling performance under various axes and types of vibration by Levison (e.g., Refs. 6-8) and has been put in a user-oriented computer program as "PIVIB" (Pilot VIBration, Ref. 18), which in accordance with our dating scheme will be designated herein as "PIVIB-77." As implied on Fig. 3, PIVIB-77 can use BIODYN-78 (or experimental data, if available) to provide the various biomechanical transmissibilities required. The current PIVIB has some oversimplified assumptions regarding the performance decrements due to head-point-of-regard motion (e.g., it does not yet properly account for vestibular or image tracking effects of the eye's control system). Nevertheless, it does give a good first approximation to performance changes for a wide range of task variables (such as input spectra, stick scaling, vibration-induced blur threshold). As should be expected from the discussion of Figs. 2 and 3, hundreds of parameters are required in the PIVIB input files, because it has to cover all of the elements in Fig. 2.

We have shown that each of the four steps in assessing vibration effects on performance now has math models of varying degrees of confidence and ease of use. The selection of individual models depends on the axes of vibration and of manual control, the type of vibration, and the availability of purely empirical data (e.g., experimental frequency responses) or the need for prediction before the experiment or design is frozen.

VALIDATIONS

The biomechanical model, BIODYN-78, and its antecedents have been progressively refined and validated as experimental data of suitable format and quality became available. Typical fits of the body, limb, and head-point-of-regard data are shown in Fig. 4c from one of a series of experiments with quasi-random vibration (i.e., the sum of five sinusoids of non-simple-harmonic ratios). Further details are given in Ref. 3. The main point to note from Fig. 4c is that one model (albeit complex) simultaneously fits all of the several degrees of freedom measured. More experiments are needed with simultaneous measurements at several well-defined body points, e.g., shoulder, sternum, head (2 places), and arm bones or joints, along with the main seat input (e.g., via a 10 cm "ISO" disk with accelerometers between the buttocks and seat). Since small differences between large accelerations are important, very high grade instrumentation and inputs are required.

Figure 4b shows another example, also described in Ref. 3, where wideband vehicle vertical motions in the 0.5 to 5 Hz range (from the high-speed ship simulation program described at Oslo in Ref. 1) were imposed on crewmen sitting in various degrees of postural relaxation (here relaxed, eyes closed). The main point is that the multimodal character of the data is well matched by the model. One subject noted that he "tilted his hips forward" (dashed line in Fig. 4b) to relieve some of the head bobbing; the model correctly captures this effect.

The head/eye/control image motion model of Fig. 5 is much less well validated, but it shows promise. It relies on the fact that under most low-frequency vibrations the eye only moves a degree or two (not enough to trigger visual saccades) and thereby permits a quasi-linear modeling.

At the bottom of Fig. 7 are some image motion predictions made for three types of display/head interface: target alone moved (head fixed); target fixed (head and eye moved); and a head-mounted display (image moving with the head). Notice the different bandwidths of image (error) motion, as mentioned earlier — poor for target moved and good for head moved. More interestingly, the head-mounted display gives rise to large image motion errors because the counterpitching tendency of the eyes works against a head-mounted display. Vibration-induced decrements in digit reading accuracy as measured recently by Benson and Barnes' experiments, are shown at the top of Fig. 7. The similarity of trends in computed image

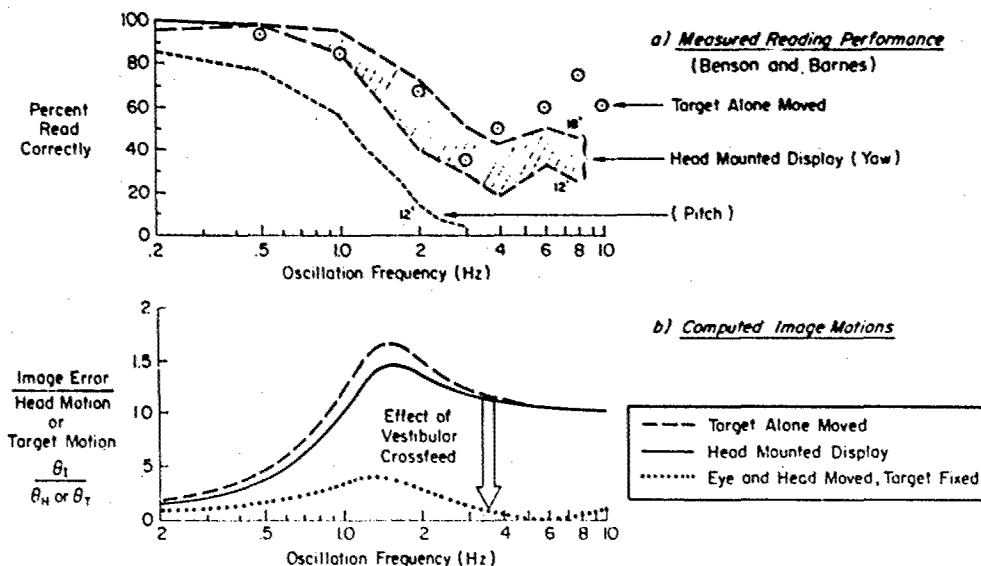


Figure 7. Computed Image Motions and Digit Reading Performance

motion and measured accuracy suggests some validation for assuming that visual performance can be related to image motion. Again, much more experimentation is needed, and we recommend that eye motion be measured in as many cases as feasible.

The overall ability of the complex PIVIB-77 model structure and algorithms to model manual control performance is demonstrated in Fig. 8, which includes overall error scores (top) and control actions (bottom) from three different experiments performed at the USAF Aerospace Medical Research Laboratory. A couple of general points are illustrated by Fig. 8:

- The PIVIB model (after adjustment of its algorithms) was able to fit all three experiments fairly well without further changes, both for error and control action.
- The effects of vibration versus static on task error are generally not very large and are often within the range of individual subjects. Adversely sensitive control stick gains or postures can greatly increase the vibration effects, especially on the rms control activity, as shown.
- Big effects occur due to input scaling, stick and display scaling, etc. These effects are currently modeled by PIVIB.

PIVIB is not computationally very efficient, because it incorporates optimum Kalman filter subroutines which require the solution of Riccati equations. However, it has been put in usable form with a user's guide, and it is ready to be tested and further refined.

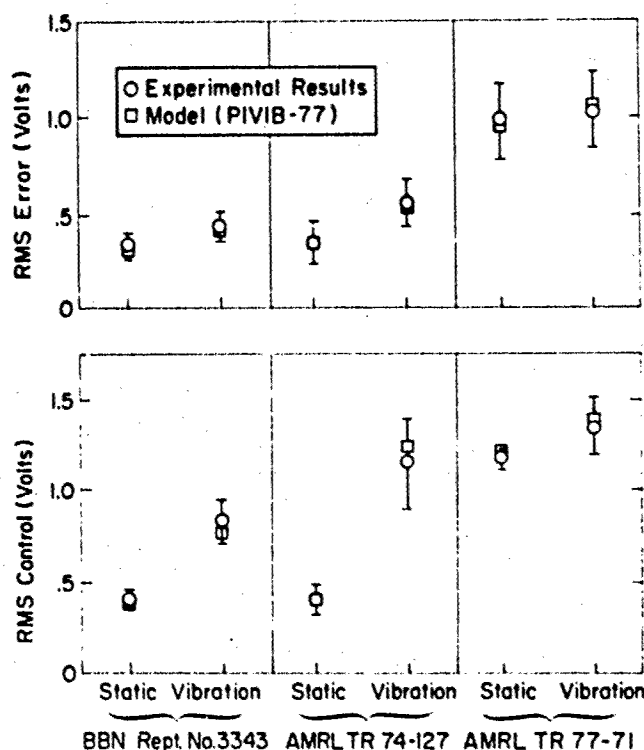


Figure 8. Vibration Effects on Tracking Performance Measures vs. PIVIB Model (From Ref. 8)

PREDICTIONS

An objective of these models is to permit prediction of problem areas or solutions before actual simulation data are available. One such prediction of BIODYN-78 is shown in Fig. 9, which compares the head-line-of-sight transmissibility (which the eyes have to compensate for) for a standard 13 deg tilt-back fighter aircraft seat with an advanced 65 deg tilt-back seat designed for High Acceleration Cockpits (HAC) (for details see Ref. 3). An order of magnitude increased sensitivity to vibration-induced head bobbing is predicted if the head or neck is not supported (as assumed here). Vibration experiments on such configurations seem warranted, with comprehensive measurements of seat and torso motion, head and limb motions, and tracking and visual identification task performance.

Other predictions have been made as to the influence of an arm rest on vibration feedthrough (depends on the percentage of arm weight carried by the rest and on the limb angles involved) and on the effects of various postures.

The usefulness of such models for this sort of prediction, parameter-tradeoff study depends on how convenient is its access and how easy it is to modify the parameters. BIODYN-78 has been designed for user-interactive operations on the Tymshare, Inc., timeshared computer network, and it could eventually be accessed by anyone with a simple teletype terminal with telephone coupler to Tymshare (not yet available, however). Among the advantages are the very convenient, well documented, and powerful Editor and Executive modes for Tymshare, which make it easy to change the variables, select new inputs or outputs,

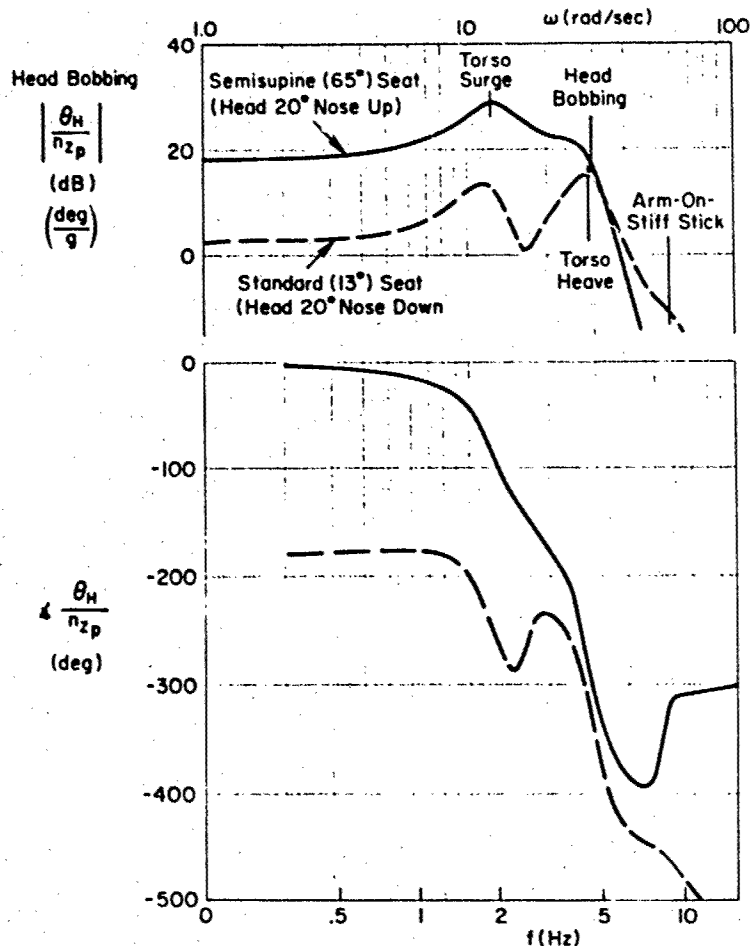


Figure 9. Use of Model for Problem Prediction
(Increased Head Motions in High-G Seats)

and store and plot the results on a simple terminal. We hope that this scheme can be made more available for general use and we encourage others to do the same. PIVIB is a batch-oriented program presently available on the WPAFB CDC-6600 computer for USAF projects only.

PROBLEMS

Neither BIODYN-78 nor PIVIB-77 are complete programs, and numerous gaps and weak areas exist which need attention. Some of these are as follows:

- 1) BIODYN-78 needs to be extended to incorporate the lateral model previously derived in Ref. 2, the head-eye model of Ref. 11, and helmets and helmet-mounted displays and active neuromuscular control of the head/neck system.
- 2) PIVIB-77 needs better interface models with respect to image motion effects, free stick effects, as well as a more convenient interactive mode of operation (in addition to the efficient batch mode).
- 3) The links between head, hand, and eye motions and visual perception effects need to be forged on a sound scientific basis. The theory should be used to guide the experimental plans and measurements.
- 4) The validity of the neck-head-vestibular-eye system needs to be extended to very low frequencies (below 0.5 Hz) where some anomalies have consistently shown up (e.g., see Fig. 4b). Eye movement data are essential here, and postural controls must be imposed.
- 5) More users have to try to apply these models to their data. One ideal candidate is Rowlands' extensive compilation of seat to head and shoulder transmissibilities under a wide variety of postures (Ref. 19). The main obstacle here is the lack of documented postural information (e.g., two-view photos) or of vibrational "mode shapes" at the salient peaks and dips of each frequency response (e.g., via high-speed cinematography). Please document your postures and dimensions for each subject!
- 6) The movement of the eyes under vibration is very difficult to measure, because nothing of any mass can be attached to the face (electro-oculograms are no good when facial tissues jiggle around) and the motions are very small. The TV scanning oculometer such as Honeywell's would seem ideal, but its effective sampling lag is excessive for vibration work.

To illustrate one of the more challenging problems, consider Fig. 10, which compares tracking scores (actually "critical instability" levels, λ_c , to which tracking performance is strongly correlated, see Ref. 20) for a number of naval crewmen for the static case versus wideband ship motion conditions generating severe kinetosis (motion sickness) in each subject (all shown are those which aborted the motion condition sooner or later and the degree of kinetosis is shown by the numbers by each symbol). The results show that:

- When reasonably motivated (as here), typical crews will retain about 80 percent of their static performance even when feeling quite queasy.
- As kinetosis proceeds to frank nausea, the tracking performance suddenly deteriorates.
- The performance decrements from kinetosis lie within the range of performance of different individuals.

Modeling the highly nonlinear progress of kinetosis (enhanced by low-frequency vibration in the 0.2-0.5 Hz region) and performance thereunder stands as a key challenge for the next AGARD AMP Specialist's Meeting on Vibration Effects.

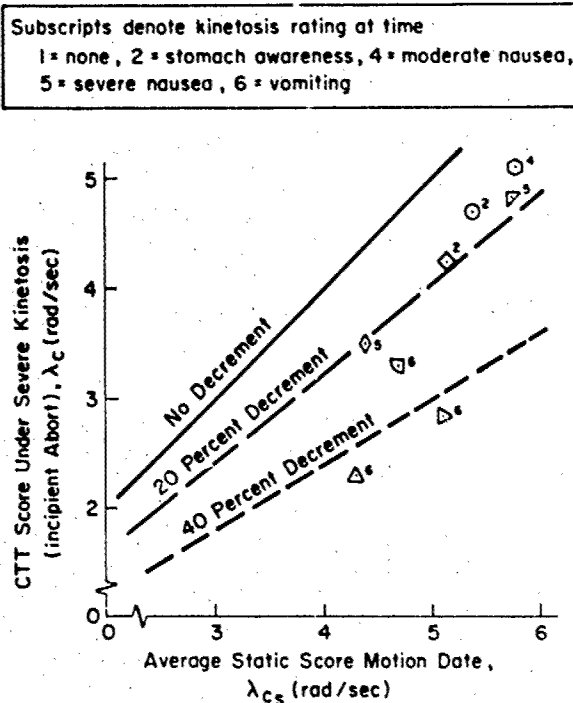


Figure 10. Tracking Performance Decrement During Severe Kinetosis

REFERENCES

1. Jex, H. R., and R. W. Allen, "Evaluating Biodynamic Interference with Operational Crews," Vibration and Combined Stresses in Advanced Systems, AGARD CP-145, Mar. 1975, pp. B24-1 to B24-18.
2. Magdaleno, R. E., and R. W. Allen, Modeling Biodynamic Effects of Vibration, July 1975, AFOSR 75-1236TR.
3. Jex, H. R., and R. E. Magdaleno, "Biomechanical Models for Vibration Feedthrough to Hands and Head for a Semisupine Pilot," Aviation, Space, and Environ. Med., Vol. 49, No. 1, Jan. 1978, pp. 304-316.
4. Allen, R. W., R. E. Magdaleno, and H. R. Jex, Systems Technology, Inc., Effects of Vertical Sinusoidal and Random Vibration on Manual Control Performance, June 1974, TR-1027-1.
5. Jex, H. R., and R. E. Magdaleno, Systems Technology, Inc., Modeling Biodynamic Effects of Vibration: Third Year Interim Scientific Report, Oct. 1976, ISR-1037-3.
6. Levison, W. H., and P. D. Houck, Guide for the Design of Control Sticks in Vibration Environments, Feb. 1975, AMRL-TR-74-127.
7. Allen, R. W., H. R. Jex, and R. E. Magdaleno, Manual Control Performance and Dynamic Response During Sinusoidal Vibration, Oct. 1973, AMRL-TR-73-78.
8. Levison, W. H., and C. B. Harrah, Biomechanical and Performance Response of Men in Six Different Directional Axis Vibration Environments, Sept. 1977, AMRL-TR-77-71.

9. Huston, R. L., J. C. Huston, and M. W. Harlow, "Comprehensive, Three-Dimensional Head-Neck Model for Impact and High-Acceleration Studies," Aviation, Space, and Environ. Med., Vol. 49, No. 1, Sec. II, Jan. 1978, pp. 205-210.
10. Jex, H. R., R. E. Magdaleno, and G. L. Teper, Systems Technology, Inc., BIODYN'78 — A User-Interactive Program for Modeling Biodynamic Motion Feedthrough to Limbs and Head. Vol. 1: User's Guide, forthcoming, TR-1037-2.
11. Magdaleno, R. E., and H. R. Jex, Systems Technology, Inc., A Linearized Model for Vibration Effects on the Eye Control System, 30 Aug. 1978, WP-1037-5.
12. Drazin, D. H., RAF, Farnborough, Inst. of Aviation Med., Factors Affecting Vision During Vehicular Vibration, May 1962.
13. Benson, A. J., and G. R. Barnes, "Vision During Angular Oscillation: The Dynamic Interaction of Visual and Vestibular Mechanisms," Aviation, Space, and Environ. Med., Vol. 49, No. 1, Sec. II, Jan. 1978, pp. 340-345.
14. Barnes, G. R., A. J. Benson, and A. R. J. Prior, "Visual-Vestibular Interaction in the Control of Eye Movement," Aviation, Space, and Environ. Med., Vol. 49, No. 4, Apr. 1978, pp. 557-564.
15. McRuer, D. T., and E. S. Krendel, Mathematical Models of Human Pilot Behavior, AGARD-AG-188, Jan. 1974.
16. McRuer, D. T., and H. R. Jex, "A Review of Quasi-Linear Pilot Models," IEEE Trans., Vol. HFE-8, No. 3, Sept. 1967, pp. 231-249.
17. Baron, S., and W. H. Levison, "An Optimal Control Methodology for Analyzing the Effects of Display Parameters on Performance and Workload in Manual Flight Control," IEEE Trans., Vol. SMC-5, No. 4, July 1977.
18. Berliner, J. E., and W. H. Levison, PIVIB: A Computer Program for Analysis of Pilot Biodynamic and Tracking Response to Vibration, Sept. 1977, AMRL-TR-77-72.
19. Rowlands, G. F., The Transmission of Vertical Vibration to the Heads and Shoulders of Seated Men, May 1977, RAE TR 77068.
20. Allen, R. W., and H. R. Jex, Visual Motor Response of Crewmen During a Simulated 90-Day Space Mission as Measured by the Critical Task Battery, May 1973, NASA CR-2240.

ACKNOWLEDGMENT

Various portions of the work reported herein were sponsored by USAF Office of Scientific Research (Life Sciences Branch), USAF Aerospace Medical Research Laboratory (Biodynamics Branch), USN Office of Naval Research and PMS-304.

DISCUSSION

DR. G. ALLEN (USA)

As I understand it you included a vestibular-ocular reflex as a sort of active correction for eye motion. Did you also include any active components for your body motion; e.g., limbs, below 2 Hertz?

AUTHOR'S REPLY

Yes, the limb control is an active loop, which can be used to correct. We do not have - and should have - an active system for the head and neck and that is something that should be added.

THE APPLICATION OF CONTROL THEORY TO THE INVESTIGATION
OF ROLL MOTION EFFECTS ON HUMAN OPERATOR PERFORMANCE

A. M. Junker, W. H. Levison*

Aerospace Medical Research Laboratory
Wright-Patterson Air Force Base, Ohio 45433

and

*Bolt, Beranek and Newman, Inc
50 Marlton Street
Cambridge, Mass. 02138

Abstract

The application of manual control theory to the investigation of the effects of motion cues on pilot control behavior is presented. Experiments and modeling approaches which have led to the development of a predictive motion sensitive optimal-control pilot-vehicle model for roll axis motion cues are described. The way in which human operators make use of disturbance and commanded motion cues are also delineated.

1. Introduction

Emphasis on expanding the use of ground based simulators has caused the Air Force to take a more critical look at the usefulness of moving base simulators. This has resulted in the realization that the technology necessary to specify adequately motion cue requirements is not available and that the effects of motion cues on pilot control behavior, as presently available on moving base simulators, are not clearly understood at this time.

At the Aerospace Medical Research Laboratory (AMRL) we believe that some of these deficiencies can best be minimized through the application of Manual Control technology. By making use of a predictive pilot model which is sensitive to motion environments, the effects of simulator motion on the pilot can be mathematically described. Having a quantitative measure of the motion cue effects, better design schemes can be implemented.

Considerable research has been performed in the area of manual control and a broad foundation has been built upon which we can now develop the needed technology. As stated in reference (18) there are two basic types of pilot models available; describing function models and state space models. The first type, which is formulated in the frequency domain, originated with classical control theory (19). The second type of pilot model, which is formulated in the time domain, was developed from modern control and estimation theory (9).

When we began our research program to include the effects of motion environments in a predictive pilot model neither modeling approach could account for motion cues adequately. Although a number of experimental studies have been conducted to determine the effects of motion cues on pilot response behavior (1-5), a generalized model has not been developed and tested. Rather, the conclusions reached in these studies have been restricted to the context of the experiments yielding the data.

Perhaps the most comprehensive study of the effects of motion cues on tracking performance was conducted by Shirley (3). He explored overall system performance and pilot response behavior in a series of tasks that include a wide range of vehicle dynamics. Most of his results conformed to the following set of rules; the human operator uses motion to generate additional lead at high frequencies, greatest percentage reduction in RMS error scores with motion is achieved for systems that respond to inputs above 3 rad/sec, and motion is used to greatest advantage in marginally stable systems. Stapleford et al. (2) also found that high-frequency phase lag decreased and gain crossover frequency increased when motion cues were present; furthermore, these effects generally decreased as the vehicle dynamics increased in difficulty. In contradiction to Shirley, however, they found that, on the average, the effects of motion cues on error score increased for increasing vehicle difficulty. In addition, other than the pitch axis motion experiment performed by van Gool and Mooij (5), the work done in this area has principally been for compensatory systems with the motion cues resulting from vehicle disturbance inputs. At AMRL we were also interested in quantifying the effects of motion cues on pilot control behavior for situation in which the motion cues resulted from pilot control inputs due to target following as encountered in air-to-air combat situations.

To investigate the effects of motion cues on pilot control behavior we built a simple closed loop moving base simulator. We chose motion about the roll axis because roll control as an inner loop is essential in flying an airplane and pilots normally experience the largest velocities and accelerations about this axis. The Roll Axis Tracking Simulator (RATS) was developed initially so that target following motion experiments could be performed. A series of experiments were run to determine if the presence of motion cues would affect tracking performance, and if so how would the motion cues modify pilot control behavior (6,7). From these experiments we found that motion cues could have both a positive and negative effect on tracking performance depending on the vehicle dynamics being controlled and the type of motion cues provided. At this time we also realized that because the effect of motion simulation on tracking performance is highly dependent on the details of the tracking task, generalization of the type reviewed above (1-5) and our experiments could not be reliably extended beyond situations similar to those studied experimentally. An alternative philosophy has been suggested and partially explored: Namely, to account for the pilot's use of motion cues by including additional sensory feedback paths in a pilot model (1). Given a model structure that allows one to predict the influence of these feedbacks on pilot response as a function of task parameters, one may then extend experimental results to a variety of control situations. At the time, the optimal-control pilot-vehicle model as developed by Bolt Beranek and Newman (BBN) (8-11) seemed to possess this structure. Therefore we provided data to BBN to explore the model's capability of accounting for the effects of motion cues on pilot control behavior by including additional sensory feedback paths in the model. The results of this effort (12) were highly successful.

At this same time we wanted to investigate the possibility of providing the equivalent of motion cue information to the pilot through means of a peripheral display system. We had subjects track statically on the RATS with vehicle roll rate driving the peripheral display. Analysis of the tracking data indicated that it was possible to achieve similar performance improvements with the peripheral display as with motion cues (?).

From our modeling efforts we had a pilot-model which could account for the effects of motion cues resulting from commanded inputs due to target following on the RATS. Since this was a predictive pilot model which had accounted for motion effects by additional sensory feedback loops, it was hoped that the model could also be used to account for motion cues resulting from vehicle disturbances and for different vehicle dynamics. To test this and to extend our data base of motion related human tracking, we developed a multi-axis tracking simulator (MATS) and performed disturbance tracking as well as target tracking experiments on this simulator. Prior to performing the experiment we used the pilot-vehicle model as an aid in the experimental design and to predict the experimental results (13). Experimental data was then collected and further adjustments were made to the pilot model (14). The results of this effort were highly successful yielding a predictive pilot-vehicle model sensitive to the presence of motion cues.

The above is a brief sketch of our research program which has led to a better understanding of the way in which man uses motion cues to aid his performance and to the development of a predictive motion sensitive pilot-vehicle model. In the remainder of this paper we will describe in some detail the experiments and modeling efforts which have enabled us to reach this point.

2. Experiment No. 1

This experiment was designed and performed for two reasons: first, to provide a data base of human operator tracking, with the presence of motion cues, for the situation in which motion had a positive affect on tracking performance and second, to understand the effects of linear and angular acceleration motion cues on tracking behavior.

While tracking in a moving base simulator that has roll motion, the human controller is exposed to both angular acceleration or velocity information and linear acceleration information of the simulator he is controlling. For modeling purposes it is desirable to understand the effects of the two types of motion separately. Due to changing alignment of the gravity vector while tracking in the RATS a human controller is provided with continuous information about his orientation relative to the vertical through proprioceptor cues and vestibular otolith stimulation. This alters the visual compensatory tracking task to one of a pursuit type task resulting in a possible improvement in performance. But a multiloop modeling approach to previous RATS data (15) suggested that the angular acceleration component was the principal source of information used for tracking performance improvement. Stapleford et al. (2) also concluded that the improvement in performance is primarily due to angular rate feedback via the semicircular canals. The desire to better clarify this situation by measuring the effects of each type of motion separately led us to devise an experiment in which the equivalent of angular velocity cues was provided to the human controller without the presence of linear acceleration information. This was accomplished through the use of a peripheral visual display. The impetus for using this technique came from the work of Ener (16).

For this experiment we used the RATS which consists of a roll axis drive system, seat, visual display and side mounted force stick for motion control. The rotating system dynamics were identified and simulated on a hybrid computer. A generalized block diagram of the resulting system is shown in Fig. 1. For this experiment DISTURBANCE was set to zero. The simulator could be operated in two modes: motion and static. In the motion mode the force stick output went to the plant dynamics as a velocity command. In this mode, the inputs to the human operator were motion cues and visual display.

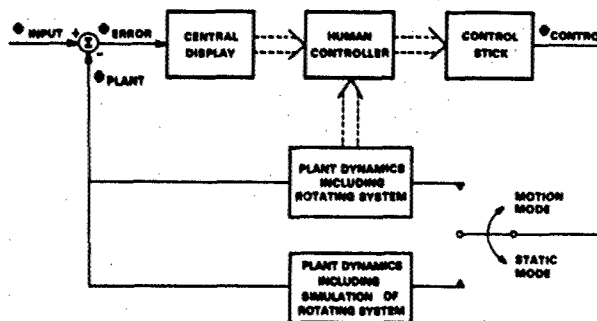


Fig. 1. Block Diagram of Target and Disturbance Tracking Tasks.

For the static mode, the stick output drove only the simulated plant dynamics. The plant dynamics given in Eq. (1) were used because we knew from previous work (6) that motion cues would have a beneficial effect on performance for these dynamics.

$$\text{PLANT DYNAMICS} = \frac{42}{s^2(s+0.5)(5+6)} \quad (1)$$

The task was to follow another aircraft in the roll axis. The target aircraft was driven by a second order noise process, consisting of 12 sine waves, with break point at 0.5 rad/sec and an RMS roll angle of 40° . The method used to select the 12 frequencies and amplitudes and generate the target signal was taken from Levison (17).

The RATS was run in the static mode for that portion of the study in which the peripheral display was used. The peripheral display was presented to the human controller on two 21-inch television monitors placed on opposite sides of the RATS (Fig. 2).

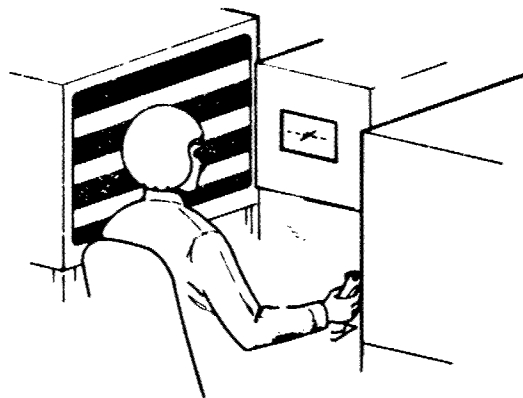


Fig. 2. Placement of Peripheral and Central Displays.

The central display used for all three conditions (static, with motion or with peripheral display) is shown in Fig. 3. The target aircraft, represented by the solid lines, rotated about the x-axis. Thus the visual tracking task was to null out the difference between the target and the controlled vehicle represented by the dashed line.

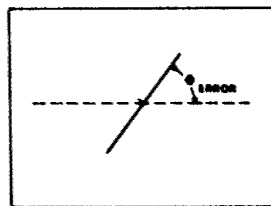


Fig. 3. Central (Foveal) Display.

The peripheral display presented plant roll rate information in the form of vertical movement of alternating black and white horizontal lines. The voltage representing plant roll rate was scaled and connected to the peripheral display circuitry. The circuitry was connected such that the displays of the two sets moved in opposite directions. Therefore a static plant roll rate signal resulted in horizontal line movement equal in magnitude and direction of the linear velocity stationary objects located in the position of the peripheral displays would appear to have if the RATS were to actually rotate.

Four subjects were used in the experiment. Each subject performed four tracking runs per day. The duration of each run was 165 sec and the order of runs (one for each experimental condition) was randomized. RMS error scores were computed after each run. Once the error scores indicated that the subject had "learned" the tracking task for a given experimental condition, time histories were recorded for subsequent use in analyzing subject control strategy. The sampled data recorded was converted to desired performance measures using a frequency analysis digital computer program modeled after one written by Levison (17).

RESULTS

The results of this experiment which are highlighted below are presented in greater detail in ref. (7). The daily tracking scores for each subject for each experimental condition were combined to yield group means and standard deviations. The results of the last four days of tracking (after asymptotic levels were reached) are plotted in Fig. 4. As was expected a significant improvement in performance with motion cues was measured. In addition the scores signify that nearly identical improvements were achieved with the peripheral display.

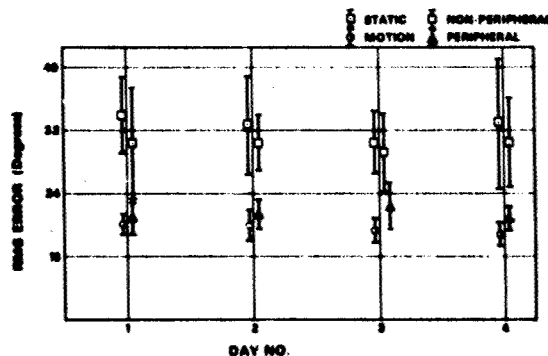


Fig. 4. Combined Error Scores, Last Four Days.

To see how subject performance was improved, describing functions were computed and evaluated. Group averaged subject describing function means for the motion, peripheral and static conditions have been plotted in Fig. 5. The significant effects are improvements in low frequency phase lead with motion. This same trend was measured for the peripheral display condition as well.

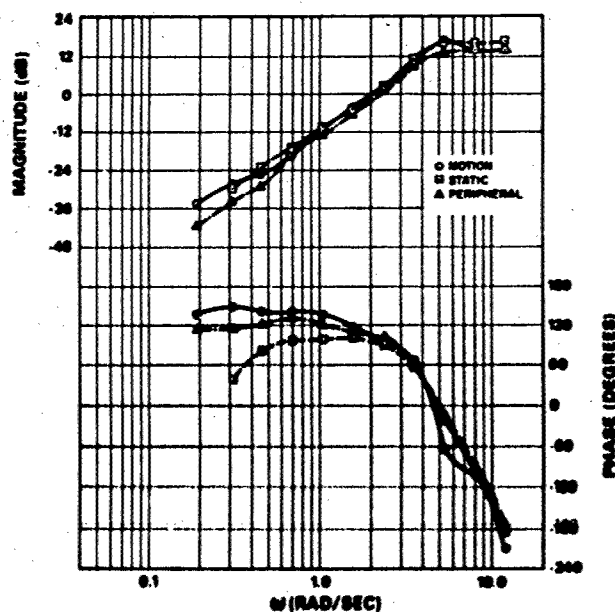


Fig. 5. Combined Man Describing Functions.

From these results we conclude that the peripheral display information has the same effect on the human operator control strategy as motion cues; namely, that he uses this plant rate information to improve his low frequency phase lead capabilities. It should also be added that the describing function phase values do indicate a greater phase lead improvement for the motion case over the peripheral case. This suggests that either the motion is a stronger stimulus than the peripheral display or that the linear acceleration component of the motion plays a role, though minor, in improving performance.

3. Modeling Effort No. 1

The frequency analysis results for both the static and motion conditions from experiment No. 1 were supplied to BBN for model matching using the optimal-control pilot-vehicle model. The results of this effort are reported in great detail in reference (12). A few of the principal results of the BBN effort are summarized below.

The significant effect of motion cues for target following is to improve low-frequency phase lead. Without motion cues present the human operator describing function exhibits what has been called low-frequency "phase droop." Therefore, the first thing done to the optimal-control model was to modify it to account for this phase droop. This was accomplished by modifying it to allow a different treatment of motor related pilot "noise." Specifically, the concept of "pseudo motor noise" was implemented to provide a model parameter related more directly to uncertainties about the control system as well as uncertainties about the pilot's control input. In addition, changes were made so that noise was injected on control rate as suggested in a previous study (10).

The focus of the modeling effort was to represent the effects of motion primarily by appropriate definition of the sensory variable assumed to be available to the pilot. Thus, static-mode tracking was modeled with a two-element "display" vector consisting of tracking error and error rate. In the case of motion tracking, the display vector was augmented to include quantities that would be provided by the pilot's motion-sensing capabilities; specifically, plant position (i.e., roll angle), plant rate, and plant acceleration.

With the optimal-control model modified, the data from experiment No. 1 was used to identify the model parameters. An iterative procedure was followed to arrive at a set of pilot-related parameter values that would explain the maximum amount of data with the minimum variation in parameters.

RESULTS

Comparisons of model and experimental frequency-response curves are provided in Fig. 6. In general, model response curves closely match experimental measures. Most importantly, the major effects of motion cues—the increase in low-frequency phase lead at low-frequencies—are mimicked by the model, as is the consistency of the midband frequencies between static and motion conditions.

4. Experiment No. 2

Since the optimal-control pilot-vehicle model has predictive capabilities, the next step was to ascertain how well it could predict pilot performance under different experimental conditions. A Multi-Axis Tracking Simulator (MATS) was used as the controlled vehicle for this experiment. Only the roll axis motion capabilities of the MATS were used. The simulator consisted of a single seat cockpit with a television monitor display and side-mounted force stick for vehicle control. The display of Fig. 3 was used. The roll axis system dynamics were identified and simulated on a hybrid computer. To test the capabilities of the optimal-control pilot-vehicle model and be able to compare our results with other motion cue experiments, we investigated the effects of two types of motion cues in this experiment. The first was target following as in experiment no. 1. The other was for motion cues resulting from the controlled vehicle being driven by disturbances. Both conditions were investigated with and without motion, making a total of four experimental conditions. The block diagram in Fig. 1 shows all conditions. For target following the disturbance input (ϕ) was set to zero and for the disturbance condition

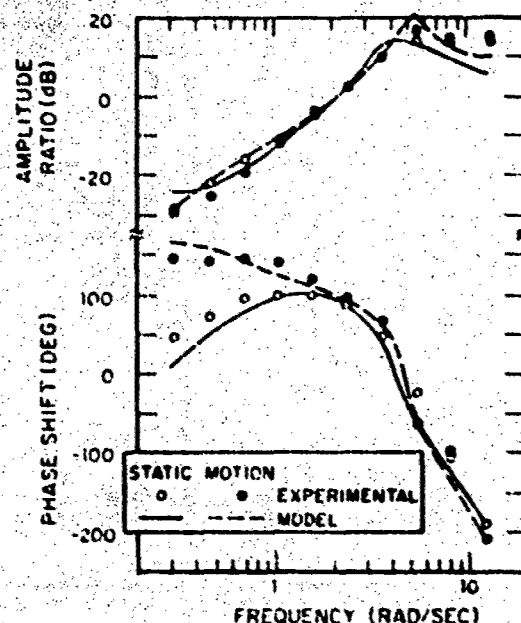


Fig. 6. Model and Experimental Data Comparison of Pilot Frequency Response.

the target input (ϕ_{TARGET}) was set to zero. The plant dynamics used for all conditions are given in Eq. (2).

$$\text{PLANT DYNAMICS} = \frac{K}{s(s+5)(s+20)} \quad (2)$$

With the vehicle to be controlled identified, the next step was to select task parameters for the experiment. The following design goals and constraints were considered: face validity, motion cue utilization, wide bandwidth response, and simulator motion limitations. Experimental parameters that we could adjust to meet these goals consisted of (1) RMS amplitude and spectral shape of the tracking input, (2) control gain and, (3) performance criterion. The input amplitude was adjusted to allow such response to be achieved with comfortable control forces. A second order noise process was considered for the tracking input and the critical frequency of the input spectrum was chosen to achieve the desired balance between measurement bandwidth and tracking difficulty. To keep RMS response rate and acceleration well below the physical limitations of the rotating simulator, as well as to encourage the test subjects to respond in a smooth manner, a performance criterion was defined as the weighted sum of mean-squared tracking error and mean-squared vehicle acceleration. That is,

$$C = \sigma_{\text{ERROR}}^2 + W \sigma_{\text{PLANT}}^2 \quad (3)$$

where C is the total "cost", σ_{ERROR}^2 the variance of the tracking error, and σ_{PLANT}^2 the variance of the acceleration of the vehicle or simulated vehicle in the absence of motion cues.

The immediate effect of introducing a penalty for vehicle acceleration was to limit the gain of the subject's response; the larger the weighting W , the lower the pilot gain. Pilot gain directly influenced overall man-machine system bandwidth, which in turn influenced roll rate and roll accelerations achieved during tracking.

Task parameters were selected in the following way. An initial set of parameters was chosen based on knowledge gained from previous experimental studies, and predictions of pilot-vehicle performance were obtained with the pilot-vehicle model. Task parameters were readjusted in an attempt to better meet the experimental constraints, and the system was reanalyzed. We iterated on this procedure until satisfied with the expected outcome of the experiment, as predicted by the optimal-control model. As a result of this iterative design process the following task parameters were selected. The force stick gain was adjusted to produce 10 degrees/second vehicle roll rate for one pound of force measured at thumb height on the control grip and the cost weighting W (Eq. 3) was set to 0.1. In addition, both the target and disturbance inputs were constructed from 13 sinusoids whose amplitudes were selected to simulate a second order noise process with bandwidths of 1.0 rad/sec for the target input and 2.0 rad/sec for the disturbance input. Input amplitude was adjusted to provide an RMS target input of 10 degrees and an RMS disturbance input of 14 deg/sec. With task parameters selected, the model was used to predict pilot-vehicle performance values which were saved for later comparison with experimental results. Six subjects were used for the experiment. One of the subjects was a licensed pilot and another student pilot.

RESULTS

Once subject training had been accomplished, data was collected for eight days for all subjects. Training was considered completed when subject performance as measured by total cost C for all conditions had reached asymptotic levels.

From the collected data various system parameter values were computed and averaged together across days and subjects. The experimental values include the mean and standard deviation resulting from averaging together the six subjects' results. Shown in Fig. 7 is a graphical comparison of predicted and experimental results for total cost (PERFORMANCE SCORE) and pilot input (RMS CONTROL FORCE). Experimental conditions are indicated on the abscissa of each graph; C indicates the Command (target following) condition, D indicates the Disturbance condition, M is for Motion and S for Static. These results indicate that the model could predict performance results quite accurately. The same trends were observed for other system parameters as reported in reference (13).

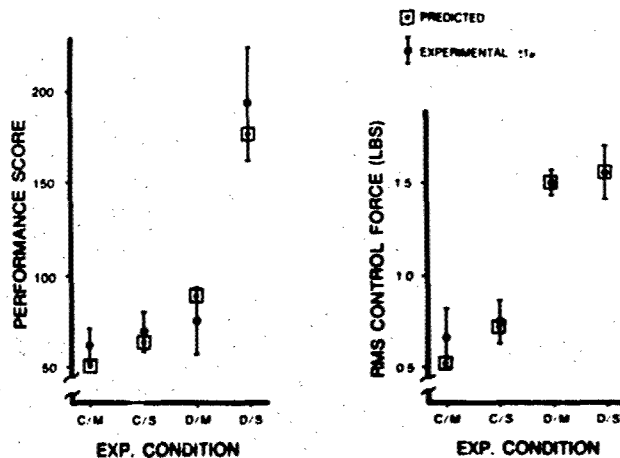


Fig. 7. Comparison Between Model Predictions and Experimental Results for Performance and Control Force.

As stated earlier the motion sensitive aspects of the model were developed for experimental conditions different from those investigated in this experiment and a different simulator with narrower bandwidth vehicle dynamics; experiment No. 1. These facts further emphasize the usefulness of the predictive capabilities of the model.

From the time history data frequency-response measures were computed. The results of the six subjects were averaged together. The average frequency-response measures presented in Fig. 8 show that motion-cue effects were qualitatively different for the two tasks. The two measures shown in the figure are amplitude ratio (i.e. pilot gain) and pilot phase shift.

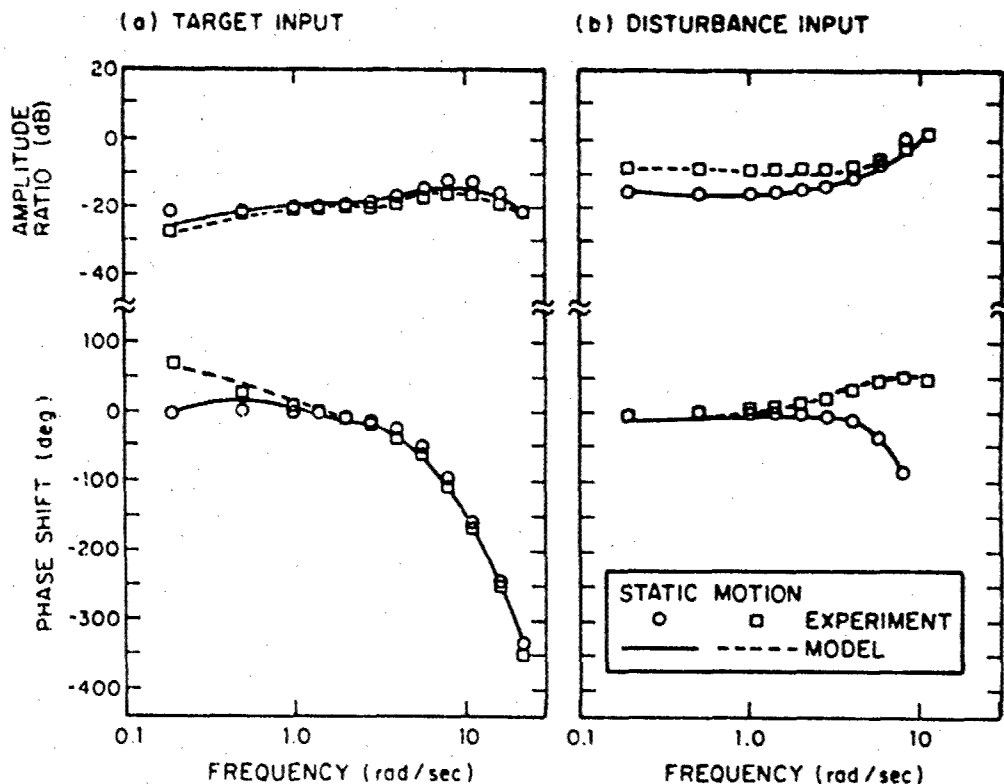


Fig. 8. Comparison of Model and Experimental Frequency Response.

The major influence of the motion cues in the target task was to induce a substantial phase lead at low frequencies. In the disturbance task, however, motion cues allowed the subjects to convert a high-frequency phase lag into a substantial phase lead and to increase amplitude ratio at low and mid frequencies. The effects of motion cues observed in the disturbance-regulation task agree with the effects reported by other researchers (2,3) who found that moving-base simulation allowed the pilot to reduce high frequency phase lag and to increase gain-crossover frequency and thereby, in many cases, lower his error score. The data from this experiment is analyzed in greater detail in reference (14).

5. Modeling Effort No. 2

Data resulting from experiment No. 2 was used to make further refinements to the motion sensitive optimal-control pilot-vehicle model. The results of this modeling effort are reported in great detail in reference (14). The revised optimal-control pilot-vehicle model developed in a preceding phase of this study was applied to the results of the experiment described above.

The treatment of motion cues was similar to that of the preceding modeling effort in that presence or absence of motion cues was represented by an appropriate definition of the sensory variable assumed to be available to the pilot. A three-element "display vector" consisting of tracking error, error rate, and (in one instance) error acceleration was used to model static-mode tracking. To model pilot response in moving-base tasks, we simply expanded this display vector to include position, rate, acceleration, and acceleration-rate of the vehicle; no other model parameters were changed to account for motion-static differences.

The scheme for identifying model parameters was similar to that described in (12). Parameter values were sought that would simultaneously provide a good match to performance scores, describing function, and remnant ratio. As in the preceding modeling effort, the primary goal of model analysis was to determine a straightforward and reliable procedure for predicting the effects of motion cues in a variety of control tasks. Therefore, we attempted to account for performance on all four tasks with the fewest variation in parameter values. Variations were made in only those parameters that could reasonably be expected to relate to the kind and quality of information provided to the pilot. Attentional parameters were the only model parameters that were varied across experimental conditions; all other parameter values were held fixed. The results of this modeling effort are shown in Fig. 8. Model outputs agreed quite well with experimental frequency-response measures, and major trends in the data were predicted. Specifically, inclusion of motion-related sensory information caused the model to predict an increase in low-frequency phase shift for the target task. For the disturbance task, the model correctly predicted large increases in low-frequency gain and high-frequency phase lead.

It is worthwhile to re-emphasize that the effects of motion cues have been accounted for solely by changes in model parameters related to the information availability and quality; other parameters have been kept fixed for the four experimental conditions.

6. Conclusions

Some of the conclusions that can be made as a result of the experiments and modeling effects performed in this research effort are summarized below.

The effects of motion cues on task performance and pilot response behavior are strongly dependent on the structure of the tracking task. The major effect of motion cues in a target-following task is to allow the pilot to generate low-frequency phase lead; in a disturbance-regulation task, the main effects are more phase lead (alternatively, less phase lag) at high frequencies accompanied by an increase in gain-crossover frequency.

Furthermore, in a target following or commanded motion condition the motion cues present will not have a significant impact on performance unless the vehicle being controlled is unstable or of high order. On the other hand the presence of disturbance type motion cues appear to have a significant effect on performance even for simply controlled or low order vehicle dynamics because of the alerting nature of the cues.

Because of the strong interaction between motion-cue effects and task structure, a pilot-vehicle model is required to extrapolate the results from one task to the next.

The "optimal-control" model for pilot-vehicle systems provides a task-independent framework for accounting for the pilot's use of motion cues. Specifically, the availability of motion cues is modeled by augmenting the set of assumed perceptual variables to include position, rate, acceleration, and acceleration rate of the moving vehicle.

As a result of our modeling effort we now have a predictive motion sensitive pilot-vehicle model for the roll axis. We are presently making use of this model and the knowledge gained from our experiments and others to investigate such things as visual-motion cue mismatch and motion simulator washout drive algorithms. By utilizing a manual control technological approach we plan to quantify the above effects on pilot control behavior and correlate the control behavior with subjective responses.

References

1. Ringland, R.F., R.L. Stapleford, and R.E. Magdaleno, "Motion effects on an IFR hovering task-analytical predictions and experimental results," NASA CR-1933, Nov., 1971.
2. Stapleford, R.L., R.A. Peters, and F. Alex, "Experiments and a model for pilot dynamics with visual and motion inputs," NASA CR-1325, May, 1969.
3. Shirley, R.S., "Motion cues in man-vehicle control," M.I.T., Cambridge, Mass., ScD Thesis, Jan., 1968.
4. Ringland, R.F., and R.L. Stapleford, "Experimental measurements of motion cue effects on STOL approach tasks," NASA CR-114458, Apr., 1972.
5. Van Gool, M.F.C., and H.A. Mooij, "A comparison of inflight and ground-based pitch attitude tracking experiments," Twelfth Annual Conference on Manual Control, NASA TM X-73, 170.
6. Junker, A.M., and C.R. Replegle, "Motion effects on the human operator in a roll axis tracking task," Aviation, Space and Environmental Medicine, Vol. 46, pp. 819-822, Jun., 1975.
7. Junker, A.M. and D. Price, "Comparison between a peripheral display and motion information on human tracking about the roll axis," Proceedings AIAA Visual and Motion Simulation Conference, 26-28 Apr., 1976.
8. Baron, S., D.L. Kleinman, et al., "Application of optimal-control theory to the prediction of human performance in a complex task" AFFDL-TR-69-81, Mar., 1970.
9. Kleinman, D.L., S. Baron and W.H. Levison, "An optimal-control model of human response, part 1: theory and validation," Automatica, Vol. 6, pp. 357-369, 1970.

10. Kleinman, D.L. and S. Baron, "Manned-vehicle systems analysis by means of modern control theory," NASA CR-1753, Jun., 1971.
11. Kleinman, D.L., S. Baron and W.H. Levison, "A control theoretic approach to manned-vehicle systems analysis," *IEEE Trans. on Auto. Control*, Vol. AC-16, No. 6, Dec., 1971.
12. Levison, W.H., S. Baron and A.M. Junker, "Modeling the effects of environmental factors on human control and information processing," AMRL-TR-76-4, AMRL, WPAFB, OH.
13. Junker, A.M. and W.H. Levison, "Use of the optimal-control model in the design of motion cue experiments," presented at the Thirteenth Annual Conference on Manual Control, Jun. 15-17, 1977, M.I.T., Cambridge, Mass., proceedings presently in press.
14. Levison, W.H. and A.M. Junker, "A model for the pilot's use of motion cues in roll axis tracking tasks," AMRL-TR-77-40, AMRL, WPAFB, OH.
15. Junker, A.M. et al., "A multiloop approach to modeling motion sensor responses," Eleventh Annual Conference on Manual Control, NASA TM X-62, 464, pp 645-655.
16. Ener, E.L., "A study of pilot performance during a glide-slope approach when rate information is supplied via the peripheral vision," AFIT Thesis GE-MA/74D-2, WPAFB, OH., Air Force Institute of Technology AD-A005284, Dec., 1974.
17. Levison, W.H., "Techniques for data analysis and input waveform generation for manual control research," BBN Technical Memorandum CSD-75-2, Cambridge: Bolt Beranek and Newman, Inc., Jan., 1975.
18. Curry, R.E., W. Hoffman and L. Young, "Pilot modeling for manned simulation," AFFDL-TR-76-124, AFFDL, WPAFB, OH.
19. McRuer, D.T. and E.S. Krendel, "Mathematical models of human pilot behavior," AGARDOGRAPH Report, AGARD-AG-188, Jan., 1974.

DISCUSSION

DR. H. JEX (USA)

How does the finding that the tilt cue was important in your experiments relate to the flight situation? Would those same cues be present in the flight case?

AUTHOR'S REPLY

As it turns out, this is why we wanted to explore this effect. When you are flying an aircraft and you bank, you don't feel yourself tilting, so I would say it is a false cue effect due to ground based simulation. It is a cue that we have to remove as far as physically sensing it.

REPORT DOCUMENTATION PAGE

1. Recipient's Reference	2. Originator's Reference AGARD-CP-253	3. Further Reference ISBN 92-835-0240-X	4. Security Classification of Document UNCLASSIFIED
5. Originator	Advisory Group for Aerospace Research and Development North Atlantic Treaty Organization 7 rue Ancelle, 92200 Neuilly sur Seine, France		
6. Title	MODELS AND ANALOGUES FOR THE EVALUATION OF HUMAN BIODYNAMIC RESPONSE, PERFORMANCE AND PROTECTION		
7. Presented at	the Aerospace Medical Panel's Specialists' Meeting held in Paris, France, 6-10 November 1978.		
8. Author(s)/Editor(s) Various Editor: Dr Ing. H.E. von Gierke*		9. Date June 1979	
10. Author's/Editor's Address Various	*Biodynamics & Bioengineering Division 6570th Aerospace Medical Research Laboratory (AFSC) Wright-Patterson AFB, OH 45433, USA		11. Pages 420
12. Distribution Statement	This document is distributed in accordance with AGARD policies and regulations, which are outlined on the Outside Back Covers of all AGARD publications.		
13. Keywords/Descriptors			
Biodynamics Stress (physiology) Humans Injuries		Acceleration (physics) Crash landing Aerial warfare Flight maneuvers	
14. Abstract			
<p>Rapid advance hampers wide knowledge and appreciation of models and analogues developed for the evaluation of human biodynamic response, performance and protection. The thirty papers presented at the Paris meeting of the Aerospace Medical Panel, November 1978, address this problem. Most cover whole body kinematic models for the prediction of body motion, as well as spinal, head-neck, and head injury models for the prediction of internal stress, strain and injury probability under escape, crash and windblast conditions. Some papers describe cardiovascular models of human response to acceleration and air-combat manoeuvres. A few illustrate applications for prediction of body motion, physiological response and injury probability under biodynamic stress, providing assistance in development of protective systems, crashworthiness and cockpit design.</p>			

<p>AGARD Conference Proceedings No.253 Advisory Group for Aerospace Research and Development, NATO MODELS AND ANALOGUES FOR THE EVALUATION OF HUMAN BIODYNAMIC RESPONSE, PERFORMANCE AND PROTECTION Edited by H.E. von Gierke Published June 1979 420 pages</p> <p>Rapid advance hampers wide knowledge and appreciation of models and analogues developed for the evaluation of human biodynamic response, performance and protection. The thirty papers presented at the Paris meeting of the Aerospace Medical Panel, November 1978, address this problem. Most cover whole body</p> <p>P.T.O.</p>	<p>AGARD-CP-253</p> <p>Biodynamics Stress (physiology) Humans Injuries Acceleration (physics) Crash landing Aerial warfare Flight maneuvers</p>	<p>AGARD Conference Proceedings No.253 Advisory Group for Aerospace Research and Development, NATO MODELS AND ANALOGUES FOR THE EVALUATION OF HUMAN BIODYNAMIC RESPONSE, PERFORMANCE AND PROTECTION Edited by H.E. von Gierke Published June 1979 420 pages</p> <p>Rapid advance hampers wide knowledge and appreciation of models and analogues developed for the evaluation of human biodynamic response, performance and protection. The thirty papers presented at the Paris meeting of the Aerospace Medical Panel, November 1978, address this problem. Most cover whole body</p> <p>P.T.O.</p>	<p>AGARD-CP-253</p> <p>Biodynamics Stress (physiology) Humans Injuries Acceleration (physics) Crash landing Aerial warfare Flight maneuvers</p>
<p>AGARD Conference Proceedings No.253 Advisory Group for Aerospace Research and Development, NATO MODELS AND ANALOGUES FOR THE EVALUATION OF HUMAN BIODYNAMIC RESPONSE, PERFORMANCE AND PROTECTION Edited by H.E. von Gierke Published June 1979 420 pages</p> <p>Rapid advance hampers wide knowledge and appreciation of models and analogues developed for the evaluation of human biodynamic response, performance and protection. The thirty papers presented at the Paris meeting of the Aerospace Medical Panel, November 1978, address this problem. Most cover whole body</p> <p>P.T.O.</p>	<p>AGARD-CP-253</p> <p>Biodynamics Stress (physiology) Humans Injuries Acceleration (physics) Crash landing Aerial warfare Flight maneuvers</p>	<p>AGARD Conference Proceedings No.253 Advisory Group for Aerospace Research and Development, NATO MODELS AND ANALOGUES FOR THE EVALUATION OF HUMAN BIODYNAMIC RESPONSE, PERFORMANCE AND PROTECTION Edited by H.E. von Gierke Published June 1979 420 pages</p> <p>Rapid advance hampers wide knowledge and appreciation of models and analogues developed for the evaluation of human biodynamic response, performance and protection. The thirty papers presented at the Paris meeting of the Aerospace Medical Panel, November 1978, address this problem. Most cover whole body</p> <p>P.T.O.</p>	<p>AGARD-CP-253</p> <p>Biodynamics Stress (physiology) Humans Injuries Acceleration (physics) Crash landing Aerial warfare Flight maneuvers</p>

<p>kinematic models for the prediction of body motion, as well as spinal, head-neck, and head injury models for the prediction of internal stress, strain and injury probability under escape, crash and windblast conditions. Some papers describe cardiovascular models of human response to acceleration and air-combat manoeuvres. A few illustrate applications for prediction of body motion, physiological response and injury probability under biodynamic stress, providing assistance in development of protective systems, crashworthiness and cockpit design.</p>	<p>ISBN 92-835-0240-X</p>	<p>kinematic models for the prediction of body motion, as well as spinal, head-neck, and head injury models for the prediction of internal stress, strain and injury probability under escape, crash and windblast conditions. Some papers describe cardiovascular models of human response to acceleration and air-combat manoeuvres. A few illustrate applications for prediction of body motion, physiological response and injury probability under biodynamic stress, providing assistance in development of protective systems, crashworthiness and cockpit design.</p>	<p>ISBN 92-835-0240-X</p>
<p>kinematic models for the prediction of body motion, as well as spinal, head-neck, and head injury models for the prediction of internal stress, strain and injury probability under escape, crash and windblast conditions. Some papers describe cardiovascular models of human response to acceleration and air-combat manoeuvres. A few illustrate applications for prediction of body motion, physiological response and injury probability under biodynamic stress, providing assistance in development of protective systems, crashworthiness and cockpit design.</p>	<p>ISBN 92-835-0240-X</p>	<p>kinematic models for the prediction of body motion, as well as spinal, head-neck, and head injury models for the prediction of internal stress, strain and injury probability under escape, crash and windblast conditions. Some papers describe cardiovascular models of human response to acceleration and air-combat manoeuvres. A few illustrate applications for prediction of body motion, physiological response and injury probability under biodynamic stress, providing assistance in development of protective systems, crashworthiness and cockpit design.</p>	<p>ISBN 92-835-0240-X</p>

AGARD

NATO OTAN

7 RUE ANCELLE · 92200 NEUILLY-SUR-SEINE
FRANCE

Telephone 745.08.10 · Telex 610176

DISTRIBUTION OF UNCLASSIFIED
AGARD PUBLICATIONS

AGARD does NOT hold stocks of AGARD publications at the above address for general distribution. Initial distribution of AGARD publications is made to AGARD Member Nations through the following National Distribution Centres. Further copies are sometimes available from these Centres, but if not may be purchased in Microfiche or Photocopy form from the Purchase Agencies listed below.

NATIONAL DISTRIBUTION CENTRES

BELGIUM

Coordonnateur AGARD - VSL
Etat-Major de la Force Aérienne
Quartier Reine Elisabeth
Rue d'Evere, 1140 Bruxelles

CANADA

Defence Scientific Information Service
Department of National Defence
Ottawa, Ontario K1A 0Z2

DENMARK

Danish Defence Research Board
Østerbrogades Kaserne
Copenhagen Ø

FRANCE

O.N.E.R.A. (Direction)
29 Avenue de la Division Leclerc
92 Châtillon sous Bagneux

GERMANY

Zentralstelle für Luft- und Raumfahrt-
dokumentation und -information
c/o Fachinformationszentrum Energie,
Physik, Mathematik GmbH
Kernforschungszentrum
7514 Eggenstein-Leopoldshafen 2

GREECE

Hellenic Air Force General Staff
Research and Development Directorate
Holargos, Athens, Greece

ICELAND

Director of Aviation
c/o Flugrad
Reykjavik

ITALY

Aeronautica Militare
Ufficio del Delegato Nazionale all'AGARD
3, Piazzale Adenauer
Roma/EUR

LUXEMBOURG

See Belgium

NETHERLANDS

Netherlands Delegation to AGARD
National Aerospace Laboratory, NLR
P.O. Box 126
Delft

NORWAY

Norwegian Defence Research Establishment
Main Library
P.O. Box 25
N-2007 Kjeller

PORTUGAL

Direcção do Serviço de Material
da Força Aérea
Rua da Escola Politécnica 42
Lisboa
Attn: AGARD National Delegate

TURKEY

Department of Research and Development (ARGE)
Ministry of National Defence, Ankara

UNITED KINGDOM

Defence Research Information Centre
Station Square House
St. Mary Cray
Orpington, Kent BR5 3RE

UNITED STATES

National Aeronautics and Space Administration (NASA)
Langley Field, Virginia 23365
Attn: Report Distribution and Storage Unit

THE UNITED STATES NATIONAL DISTRIBUTION CENTRE (NASA) DOES NOT HOLD
STOCKS OF AGARD PUBLICATIONS, AND APPLICATIONS FOR COPIES SHOULD BE MADE
DIRECT TO THE NATIONAL TECHNICAL INFORMATION SERVICE (NTIS) AT THE ADDRESS BELOW.

PURCHASE AGENCIES

Microfiche or Photocopy

National Technical
Information Service (NTIS)
5285 Port Royal Road
Springfield
Virginia 22151, USA

Microfiche

Space Documentation Service
European Space Agency
10, rue Mario Nikis
75015 Paris, France

Microfiche

Technology Reports
Centre (DTI)
Station Square House
St. Mary Cray
Orpington, Kent BR5 3RF
England

Requests for microfiche or photocopies of AGARD documents should include the AGARD serial number, title, author or editor, and publication date. Requests to NTIS should include the NASA accession report number. Full bibliographical references and abstracts of AGARD publications are given in the following journals:

Scientific and Technical Aerospace Reports (STAR)
published by NASA Scientific and Technical
Information Facility
Post Office Box 8757
Baltimore/Washington International Airport
Maryland 21240, USA

Government Reports Announcements (GRA)
published by the National Technical
Information Services, Springfield
Virginia 22151, USA



Printed by Technical Editing and Reproduction Ltd
Harford House, 7-9 Charlotte St, London W1P 1HD

ISBN 92-835-0240-X